MODULATORS OF DNA DAMAGE-INDUCED CELL DEATH IN *CAENORHABDITIS ELEGANS*

Dissertation

zur

Erlangung der naturwissenschaftlichen Doktorwürde

(Dr. sc. nat.)

vorgelegt der

Mathematisch-naturwissenschaftlichen Fakultät

der

Universität Zürich

von

Ralf Eberhard

von

Schänis-Maseltrangen SG

Promotionskomitee

Prof. Dr. Michael Hengartner (Vorsitz und Leitung der Dissertation)
Prof. Dr. Josef Jiricny
Prof. Dr. Ulrike Kutay
Dr. André Furger

Zürich, 2012

Summary

The formation and maintenance of tissues and organs mandate a fine-tuned balance between cell proliferation and cell loss. Apoptosis as one form of programmed cell death ascertains the timely and innocuous removal of superfluous, damaged, or potentially harmful cells. Disturbances leading to excessive or reduced apoptosis are at the basis of severe pathogenic processes like neurodegeneration or tumor growth. In my studies, I aimed at furthering our understanding of the genetically determined cell-death mechanism as well as its interactions with physiological or pathological tissue environments – knowledge that is needed for the elaboration of preventive or therapeutic strategies. Using the model organism *Caenorhabditis elegans*, I have characterised several novel determinants of the level of apoptotic death, particularly in response to DNA damage caused by ionizing irradiation. The key findings of this work: i) DNA-repair factors of homologous recombination (HR) are required for UV-C induced apoptosis. ii) *unc-119* regulates cell death and removal. This gene has been widely used as a transgene marker and potentially confounds findings of apoptosis research in *C. elegans*. iii) RNA polymerase I (transcription of rRNA) and other factors of ribosome biosynthesis modulate DNA damage-induced and constitutive cell death. This is likely mediated by Ras/MAPK signalling, that has manifold well-known effects in growth and development. We show a novel role for this signalling pathway in irradiation-induced apoptosis. iv) Besides these genetic determinants, the food type – i.e. for the nematode different types of bacteria – can largely influence the number of irradiation-induced or physiologic cell corpses. Many of our observations suggest a central effector that modulates the level of constitutive as well as of exogenously provoked apoptosis. v) In addition to DNA damage response, the p53 homolog CEP-1 is involved in developmental apoptosis as well as in non-irradiation-induced germ cell death, which blurs the current genetic distinction between DNA damage-induced and physiological apoptosis. Conclusively, the high evolutionary conservation of the proteins and mechanisms studied here should allow to transfer our observations in the worm *C. elegans* to the biology of the healthy and diseased human.

Zusammenfassung

Die Entwicklung und Aufrechterhaltung von Geweben und Organen erfordert eine fein regulierte Balance zwischen Zellerneuerung und Zellverlust. Apoptose, eine Form von programmiertem Zelltod, garantiert die rechtzeitige und saubere Beseitigung von überflüssigen, geschädigten oder potentiell schädlichen Zellen. Störungen mit vermehrter oder verminderter Apoptose liegen schwerwiegenden Krankheitsprozessen wie Neurodegeneration oder Tumorwachstum zu Grunde. Detaillierte Kenntnisse des genetisch festgelegten Zellsuizid-Programms in seiner Wechselwirkung mit Signalen aus dem physiologischen oder pathologischen Gewebskontext sind nötig für neue präventive oder therapeutische Ansätze. Im Rahmen dieser Arbeit habe ich mit Hilfe des Modellorganismus *Caenorhabditis elegans* verschiedene neue Faktoren charakterisiert, welche das Ausmass an Apoptose in der Keimbahn beeinflussen, insbesondere nach Schädigung des Erbgutes durch Bestrahlung. Folgende Haupterkenntnisse resultieren: i) DNA-Reparaturmoleküle der homologen Rekombination sind nötig für die Aktivierung von Apoptose nach UV-Bestrahlung. ii) Der seit Jahren häufig für Transgen-Selektion eingesetzte Marker *unc-119* reguliert Zelltod und -beseitigung; dies stellt zahlreiche Apoptose-Experimente in *C. elegans* in Frage, welche auf Transgenen basieren. iii) RNA Polymerase I (Transkription von rRNA) und zahlreiche weitere Faktoren der Ribosomen-Biogenese modulieren DNA-Schaden induzierte sowie physiologische Apoptose. Vermittlerin ist sehr wahrscheinlich die Ras/MAPK Signalachse, welche vielfache Wirkungen in Entwicklung und Wachstum hat. Wir zeigen eine bisher unbekannte Funktion für den Ras/MAPK Pathway in Bestrahlungs-induzierter Apoptose. iv) Neben den genetischen Determinanten beeinflusst der Nahrungstyp – für die Nematoden verschiedene Arten von Bakterien – die Zahl der physiologisch oder nach Bestrahlung sterbenden Zellen. Viele der Experimente weisen auf einen zentralen Effektor hin, der das Niveau sowohl von konstitutiver wie auch exogen provozierter Apoptose moduliert. Wir lockern die bestehende Abgrenzung der beiden Formen zudem durch unsere Beobachtung, v) dass das p53 Homolog in *C. elegans* auch in nicht-DNA-Schaden-induzierter und entwicklungsassoziierter Apoptose involviert ist. Die starke evolutionäre Konservierung der beschriebenen Proteine und Mechanismen sollte erlauben, unsere Beobachtungen im Fadenwurm *C. elegans* auf die Biologie des gesunden und kranken Menschen zu übertragen.

Acknowledgments

Nature and the evolution of life are so splendid that after half a billion years,
we are consciously looking for ourselves in the worm again.

I am grateful to everybody whom I can share this fascination with.

Die Entwicklung des Lebens ist so genial, dass wir uns nach einer
halben Milliarden Jahre mit bewusstem Geist wieder im Wurm suchen.

Vielen Dank an alle, mit denen ich diese Begeisterung teilen kann.

I would like to thank the many persons who kindly supported me and my projects during my PhD studies, who gave me advice, helped me with experiments, immersed in scientific discourses, and provided a motivating and cheerful working environment. Specifically, I acknowledge

Michael Hengartner for his generosity and for offering the basis in his lab for
'scientific freedom' and the development of critical minds.
André Furger, Josef Jiricny and Ulrike Kutay, who, as members of my thesis committee,
have followed my PhD projects and mentored me; and André for hosting me in his laboratory.
Susanna Bachmann, and the MLS PhD and MD-PhD Zurich programs.
Lilli Stergiou, who introduced me to the worm lab work and who I have highly
estimated in collaborations and as a friend.
Antje Beyer and Simon Hänni for support, inspiring meetings and vivid exchange of ideas.
Itay Nakdimon for the collaboration and other members of Alex Hajnal's lab for helpful inputs.
The semester course students Magda, Simon, Tobias, Lisa, Louisa, and Anina
for their inspired participation in the projects.
Michael Daube for his great assistance with experiments.
The former and current Hengartner lab members – researchers, students and administrators – for help, discussions, collaborations, and for the joyful atmosphere.

Additional persons will be mentioned in the thesis text; all others that are not named explicitly shall equally feel included in my acknowledgments.

Herzlichen Dank all meinen Freunden und meiner Familie.

In tiefer Verbundenheit zu Huy Leng und Jonay Tim.

Contents and structure

Structure of this work

First, I will give a general introduction to human cancer and the research fields of DNA damage response and apoptosis, and depict some overarching ideas and motivations for my studies. The second introductory chapter describes more specific aspects of apoptosis and DNA damage responses in *C. elegans*; the paper on the computational modelling of the *C. elegans* germ line can be read as an overview to the organ that presented the most important model system for my investigations.

Each topic will be introduced more profoundly and more specifically in the respective sections. Every chapter starts with a preface and an extended table of contents. Following this, the organisation of the chapters varies. The chapter *DNA damage repair pathways and apoptosis* is an assembly of two publications with introductions, discussion of additional experiments, and personal contributions. The chapters on *rpo-1b(op259)* form the most extensive part of this work. I characterised multiple facets of this mutation – biochemical implications, phenotypic traits, genetic interactions – and came to observations that were complementing or adjusting current concepts of germ cell apoptosis in *C. elegans*. Even though some of these novel findings apply to a more general context than to the mutant condition, they will be presented and discussed in these chapters. The first section, *Ribosome synthesis and DNA damage-induced apoptosis are reduced in rpo-1b(op259), a novel mutant of RNA polymerase I*, discusses the role of rRNA and ribosomal synthesis in apoptosis, the second section *rpo-1b(op259) links to p53, the Ras/MAPK pathway, and to the apoptotic core* characterises genetic aspects of apoptosis in *rpo-1b(op259)* and more generally of apoptosis regulation at its core.

In the chapter *unc-119 and apoptosis: novel functions for an omnipresent bystander*, a manuscript draft will describe the main findings. The final chapter *Food type influences apoptosis levels and vulval development* collects my contribution to a collaborative project that will eventually be merged into a manuscript together with concurrent discoveries in another model.

Since there are particular considerations for most experiments, they directly precede the findings; also, the results will usually be interpreted and discussed immediately in the context. The chapters will be concluded with a summary and additional discussion.

1 Introduction to apoptosis, DNA damage, and cancer

Apoptosis is a crucial mechanism in multicellular systems to neatly eliminate superfluous or potentially dangerous cells. As the superordinate term programmed cell death (PCD) implies, the dying and degradation processes follow a genetically and morphologically well-defined program. Failures in the apoptotic process – excessive or diminished death – contribute to devastating human diseases that have increasing prevalence worldwide: cancer, neurodegeneration, and immunological disorders. Inappropriate apoptosis can arise from genetic defects; and frequently, environmental factors are highly influential on the consequences for the organism. We use the nematode *C. elegans* as a convenient model to study apoptosis in a relatively simple intact organism. This system has proven highly valuable to uncover much of the genetic basis of PCD and it is still very proliferative in revealing novel aspects of apoptosis regulation. Damage to hereditary material that exceeds a cell's capacity for save repair is one of the situations when cells become inclined to apoptosis. In my PhD work, I investigated mechanisms and factors that are required for the apoptotic response upon DNA damage. For one thing, I was involved in studies addressing DNA repair pathways per se: the crosstalk of nucleotide excision repair (NER) and homologous recombination (HR); and the role of a novel factor involved in mismatch repair. Second, I examined a very basic cellular process – ribosome synthesis – for its connections with DNA damage responses and with apoptosis in general; nucleoli and ribosomes are increasingly acknowledged as a pivot system for homeostatic regulation and stress responses. During my studies, I have realised how much external conditions can modulate cell death levels; I characterised the significant impact of food type on DNA damage-induced apoptosis. Together, my findings extend the concept of apoptosis regulation at the core.

In this introductory chapter, I first embed apoptosis in a wider biological context and allude to its role in malignant processes. To demonstrate the relevance of neoplastic diseases for human health, I highlight some recent statistical data on global cancer epidemiology. Additionally, I introduce the concepts of DNA damage response – a constant challenge for cells and organisms, and with its potential to lead to apoptosis a mainstay of my research. Another section is dedicated to the usefulness of *C. elegans* as a model system for genetic research.

The next chapter *Apoptosis and reproduction in C. elegans* will give a more detailed description of DNA damage responses and the molecular mechanisms of apoptosis in *C. elegans*, and it comprises a manuscript that introduces the germ line of *C. elegans*, the tissue which formed the basic subsystem of my research.

Chapter 1

1.1 General context – biological perspective

Life is sustained by living and dying. Proliferation, maintenance and degradation in concert balance the delicate biological systems that have evolved along with the animate and inanimate nature. These systems are fundamentally conservative, and yet they have an amazing capacity to adjust to environmental changes and to compensate for internal disturbances.

Coordinate regulation of production and removal enables dynamic equilibria to establish on various biological levels. Inside a cell – the organising unit of living organisms – macromolecules are continually synthesized and decomposed. Besides the actual functions given by chemical composition and structure of these macromolecules, their abundance and turnover rates are major determinants for how they affect the complex network in which they interact. On the level of cellular conglomerates, cells contribute by their specialisation to the overall achievements, but their numbers and proportions are equally important for an optimal functioning. When, and where, and how many cells are formed and eliminated again is crucial for tissue homeostasis in multicellular organisms. Eventually, a healthy organism requires its partly autonomous constituents to suffice, to collaborate, but not to dominate. One might even carry this idea a level higher and think of a population as a super-assembly of individuals. As a whole, it is more resilient in a changing environment if it is not a static construct but formed by a steady state of self-renewal and decay.

Thanks to their dynamic build-up, biological systems are exceedingly robust and can cope with external and internal challenges to a great extent. There are risks associated with it, however. The dynamic constitution implies a progressive tendency: the building blocks have to be able to replicate, to grow, to expand – which means that they have a potential to over-proliferate, to over-grow, to over-expand, and to dispel other crucial components. This potential is particularly likely to be realised if the control mechanisms of a biological system are overwhelmed, for instance by disruptions due to chemical, physical or biological impacts from the outside. The consequences can be devastating: cancer develops, and ultimately it consumes the system. What this means for human health will be discussed in the following chapter *Human cancer*.

Organisms have very elaborate self-defence mechanisms: defence of the self and against the self. On several lines, a biological unit has to cope with external stimuli and interferences; structure and function are constantly at risk. Intricate protection and damage repair systems help to minimize adverse consequences. At some point, own components – cells for instance – can become potentially noxious. For the sake of the whole, such units are better removed timely; but not too early.

1.2 Apoptosis

Apoptosis is a form of programmed cell death. The concept of physiologic death of cells started to gain increasing interest with the notion that demise of cells was an important parameter in neoplastic growth. The first communications on physiological cell elimination in developing systems date back to the 19th century [For an overview on the origins of the theory, see (Lockshin 2001)]; in the 1920's already, plant biologists allegedly alluded to cell death as an active defence mechanism against infection (Jones 2001). John Saunders scrutinised and highlighted physiologically occurring cell death in the context of animal morphogenesis about half a century ago (Saunders 1966). Later, a similar form of cell death – with morphological characteristics well distinct from necrotic death – was found to be occurring in many different tumor tissues. In a landmark study, Kerr et al. proposed the term apoptosis to denote this form of cell death, which regulated tissue homeostasis in a variety of physiological and pathological conditions (Kerr 1972). Characteristic morphological features of apoptotic cell death were nuclear condensation, cell shrinkage and membrane blebbing. They reasoned that apoptosis had a conserved basis; the appearance of isomorphic cell death, in the fashioning of organisms and in tissue homeostasis for instance, suggested an inherently programmed phenomenon. It was also noted already that certain external stimuli could induce or inhibit apoptosis.

The precise description of the cell lineages in *C. elegans* by Sulston and Horvitz (Sulston 1977) established this organism as a leading model for apoptosis research: of the 1090 somatic cells that are formed in the developing nematode, 131 cells die by programmed cell death at a specific developmental stage. Soon, genetic mutants were found that had defects in apoptosis; these consolidated the idea of a genetically encoded death mechanism (Ellis 1986a). Many of the genes and mechanisms involved in apoptosis were henceforth discovered in the worm – observations that were readily transferrable to higher organisms thanks to the high evolutionary conservation of the apoptotic program.

1.2.1 Apoptosis in human diseases

The molecular bases of apoptosis have been characterised extensively in different biological systems [reviewed in e.g., (Hengartner 2000; Elmore 2007)]. It has been appreciated that apoptosis has crucial implications for the pathogenesis of human diseases. Prominently, apoptosis was linked to human cancer [reviewed in e.g., (Lowe 2000) or (Kaufmann 2000)]; evasion from apoptosis has been recognised as one of the hallmarks of tumor formation (Hanahan 2011, 2000). Both, too little or too much apoptosis can destabilise tissue homeostasis or control of the self; and inappropriate cleaning of apoptotic corpses can also trigger pathogenic mechanism. Excessive apoptosis is thought to substantially contribute to neurodegenerative diseases [molecular mechanisms are reviewed in (Krantic 2005)] or to degenerative processes following ischaemic events. Dysbalance of pro-death and pro-survival signals between immune cells can lead to autoimmune diseases; they can also result from impairment of programmed cell clearance. [The many implications of inappropriate apoptosis in human diseases have been reviewed, e.g., in (Fadeel 2005).]

A wealth of novel aspects of apoptosis has been described in the last two decades. Given the ample involvement in human disease, apoptotic pathways certainly have been addressed as therapeutic targets. Correcting inadequately regulated apoptosis, or inducing apoptosis to eliminate unwanted cells are

possible approaches to mitigate diseases for which there is no satisfactory treatment so far. To date, progress in the development of efficient therapeutics directly targeting apoptosis has been limited. Important advances have mainly been achieved with mimetics of the central BH3-domain regulators of apoptosis in the treatment of cancer (Chonghaile 2008; Richardson 2008; van Delft 2006); they might further exhibit synergistic activity with oncogenic kinase inhibitors (Cragg 2009). Apoptosis is one of the central mechanisms determining the effectiveness of current tumor treatment. Many of the treatments produce DNA damage that is supposed to induce replicative arrest or death preferentially of rapidly proliferating cells. Evasion from apoptosis is probably not only a hallmark of cancer, but also a significant cause of tumor resistance to treatment.

Altogether, apoptosis cannot easily be abstracted as an isolated cellular process. In treatment investigations, it should rather be considered as a mechanism that is embedded in a complex network regulating tissue homeostasis. Probably, apoptosis is often not simply cell suicide – at least, it is assisted suicide.

1.3 Human cancer

1.3.1 Cancer is a leading cause of death in humans

Cancer is very serious for the human; it is a highly prevalent disease and among the leading causes of death. Its significance has massively increased with the potent prevention and therapies of infection associated deaths and the increasing life expectancy during the 20th century. In the first decade of the 21st century, malignant neoplasms accounted for an estimated 13 % of all deaths worldwide. In countries of the so-called developed world, this number is significantly higher: about one quarter of all deaths are due to cancer. About 10 to 20 % of the world population will develop a malignant tumor in their lifetime; and every forth to third person in Europe. Collectively, malignant tumours already outrun heart diseases (20 % of deaths) and cerebrovascular insults (10 %) as the leading cause of death in developed countries. In the so-called developing countries, given the conditions prevailing for the majority of the populace (sanitation, access to health-care, population age structure) communicable diseases still amount to a high percentage of causes of death, keeping the relative levels of cancer-related deaths somewhat lower so far. A projection based on data from before 2002 predicts that cancers will have become the most frequent cause of death worldwide in 2030, starting to outnumber ischaemic heart diseases already around 2010 [(Mathers 2006), summary figure in (World Health Organization 2007)].

Worldwide, an estimated 12.7 million new cancer cases and 7.6 million cancer deaths occurred in 2008 (Ferlay 2010b). Simplified, one could thus state that 0.2 % of the world population developed, and 0.1 % died of, cancer in one year. The age-standardised rates (ASR) of new cancer cases of any location in the body (except for non-melanoma skin cancer) cumulated to approximately 182 per 100'000 persons per year (males: 204, females: 165). In Europe, the ASRs (per 100'000) were clearly higher: 433 new cancer cases for males and 294 for females, varying from 265 (Cyprus) to 523 (France) and from 199 (Greece) to 395 (Ireland), respectively. [For references, see *8.4 Cancer epidemiology resources*, where an overview for access to statistical data on human cancer worldwide is provided.]

1.3.2 Causes and mechanisms of cancer

Intense research has been invested to identify the causes and mechanisms of cancer. The understanding of the principles leading to malignant neoplasia has been advanced enormously in the last decades. Paradigms have evolved how cells become tumor cells and how tumor cells can develop to a malignant mass; they were described as hallmarks of cancer (Hanahan 2011) and form a widely accepted framework for current research on cancer. Many of the molecular pathways that permit and favour tumor growth and progression have been characterised in great detail. It has become common sense that cancer is an extremely complex, multifaceted and multifactorial disease; a disease that develops and progresses in an exchange of external stimuli and internal conditions.

1.3.3 Aetiology and prevention

The above numbers on incidence of cancer and mortality rates reveal that cancer has remained a highly lethal disease. Potent treatments have become available for a few cancer types; a majority of malignant

tumours, however, cannot be treated effectively and ultimately cannot be stopped from leading to death. The more, it is important to oppose cancer by other means, namely prevention. Learning about specific causes is key to early prevention: neoplasia might be avoided by treating or in turn preventing a driving condition, such as bacterial or viral infection or exposure to carcinogenic substances. Etiological and pathogenetic patterns have been identified for certain types of tumours, and many risk factors for tumor formation have been described to date. A wealth of environmental conditions have been linked to tumours in association studies. It is estimated that more than half of the cancer cases worldwide are potentially preventable (American Cancer Society 2011). Smoking is an established risk of high importance. Another large group of cancers is attributable to infections: worldwide, bacterial, viral and parasitic infections are judged to cause about 20 % of all cancers (Parkin 2006; de Martel 2009). Globally, and even more pointedly in countries with a modern Western life style, one group of risk factors prominently sticks out: diet or nutrition. It is currently thought that about 30 % of cancers in developed countries are accounted for by dietary factors (Key 2004, 2002). From an evolutionary perspective, the importance of food quantity and quality for cancer modulation is not so surprising when regarding the fact that energy supply is the motor of all living. It is to assume that nutrition and metabolic processes become particularly important in pathological conditions where basic regulation of homeostasis is altered. The role of food in cancer has become a major focus of research but remains very challenging to assess (Gonzalez 2010; Meyskens 2005; Miller 2010).

1.3.4 Association in humans and in model systems

In cancer research, it is often difficult or even impossible to distinguish causative, carcinogenic agents from factors that promote and modulate growth of a tumor. However, this distinction might also not be critical when aiming at a first-line offensive against manifestations of the disease. What is critical, though, is to distinguish causal relations of a putative risk factor with the disease from simple correlation or artifactual connections. For how new findings from studies and surveys eventually act on science, on society and on health politics, adequate communication is a major issue [see (Boffetta 2008) and ensuing discussions (Clapp 2009; Crosignani 2009; Cogliano 2010)].

Developing and performing studies to measure the influence of some suspect factor on tumours in humans is extremely demanding from biostatistical, economic and ethical perspectives. On the one hand, if performed meticulously, such studies can directly yield results of high biological relevance, since the subjects are not surrogate systems. On the other hand, observations made in such studies can be misleading; with the innumerable variables determining our being, it is very challenging to sort out real effects of single variables on the measured outcome; and interventional studies are rarely feasible in the human. It is here that model systems which can be readily used for experimental hypothesis testing become extremely helpful.

1.4 DNA damage responses

Integrity of the genome is essential to the functioning of a cell, to the health of an individual, and to the reproductive success of a species. The genome presents the templates for most proteins in a cell and carries much of the hereditary traits to the descendants of an organism. Genome integrity is continuously challenged; physical and chemical agents impact on cellular macromolecules and cause alterations that require stringent control. Threats come from outside and from inside: exogenous genotoxic substances and irradiation – naturally occurring or iatrogenic, that is, in the context of diagnostic procedures or of tumor treatment – but also endogenous reactive oxygen species (ROS) and by-products of cellular metabolism regularly introduce damage to the DNA. Further, DNA alterations can occur from replication errors or from 'spontaneous' chemical modification like deamination or depurination. Altogether, one mammalian cell has to cope with an estimated 10^5 DNA lesions per day arising from endogenous processes alone (Hoeijmakers 2009; Lindahl 1993). Life has evolved a complex molecular network to withstand such hazards and to efficiently balance potentially detrimental effects; stress response and more specifically DNA damage response systems help to preserve genetic stability.

Many factors of this network have been identified to date. They are commonly grouped into functional damage response and repair pathways that adequately master different types of DNA alterations, such as single strand breaks, double strand breaks, and misincorporated or modified bases. The long-standing mechanisms of repair comprise: mismatch repair (MMR) and base excision repair (BER) for mis-paired and chemically modified bases; nucleotide excision repair (NER) with its two branches transcription coupled repair (TCR) and global genome repair (GGR) for bulky lesions within one DNA strand; interstrand crosslink repair (ICL) for covalent links between the complementary strands; single strand break repair (SSBR); and two main modules for double strand break repair – homologous recombination (HR) and nonhomologous end joining (NHEJ); and direct repair (by e.g., photolyase or dealkylases) of chemical modifications on bases. [For a comprehensive review on repair pathways, see (Sancar 2004)]

The above number of endogenous DNA lesions indicates that the damage response systems are not just engaged upon some rare emergency following peak exposure to external mutagens, but that they constantly survey genome integrity. These damage response mechanism need to be controlled tightly – they are potent modifiers of DNA and could themselves pose a threat to the system if misregulated (Ciccia 2010). Regulation is extremely complex; a vast number of interdependent factors sense, signal, recruit, modify, and execute in an almost inscrutable manner to channel for the optimal repair pathway and guarantee minimal harm for the organism. Conceptually, damage response has been structured as a signal transduction pathway consisting of sensors, transducers, and effectors (Zhou 2000); attribution of damage response factors to one single category has become increasingly difficult with the acknowledgement of feedback loops on and between all levels [discussed in (Ciccia 2010)]. Also, the formally distinct repair pathways are very likely to interact on multiple levels and they play additional roles in mediating checkpoint responses such as cell cycle arrest or apoptosis, as will be elaborated in *3.2 NER and HR pathways act sequentially to promote UV-C-induced germ cell apoptosis in Caenorhabditis elegans*.

1.4.1 DNA damage in cancer development – and in cancer treatment

Selection of the repair mode is not just dependent on the type and load of damage, but it respects the current state of the affected cell: cell cycle stage and cell differentiation are integral parts of the decision (Essers 2006). These are equally decisive for weighting the best trade-off between maximal survival and maximal hereditary security, and thus for the cellular fate.

Checkpoints help to coordinate DNA repair with cell cycle progression, proliferation and survival. They relay cellular key responses upon DNA damage: slowdown or arrest of the cell cycle, repair of the lesions, transcriptional alterations, and, depending on the damage load and repair capacity, apoptosis (Zhou 2000). This classic quartet has more recently been extended by cellular senescence (permanent cell cycle withdrawal) (Zglinicki 2005) and by metabolic alterations. Malfunction of components in this response network can disinhibit the progression of damaged cells to abnormally proliferating clones, and it might unleash the development of abnormally growing tissue, eventually leading to cancer (Jackson 2009).

It is fascinating how reliably these survey mechanism must be at work. An adult human body consists of an estimated 10^{13} to 10^{14} cells; many of them have a high turnover (supposedly more than 90 % of all cells are replaced at least once a year; enterocytes or leukocytes at a rate of only a few days), rendering the total number of cells being generated during the lifetime of one individual to an incredibly high number. Considering the load of exogenous and endogenous DNA lesions, the number of mishaps allowing formation and growth of tumours seems remarkably small. It is not so surprising that this immense accomplishment happens at some cost, which might be aging (Hoeijmakers 2009).

DNA damage response and genome repair is of high interest for our understanding of tumor formation and tumor progression. Detailed knowledge on repair and signalling pathways and on principles of cellular responses is not less relevant for effective and save tumor treatment; most of the current tumor treatments involve induction of massive DNA damage.

The DNA repair pathways that were in the focus of my studies, namely the NER, HR and the FA pathways will be introduced in more detail in *3 DNA damage repair pathways and apoptosis*.

1.5 The nematode *C. elegans*

Caenorhabditis elegans has proven an extremely powerful genetic tool ever since it was chosen and established as a model organism by Sydney Brenner – initially mainly to study the genetic bases of the nervous system (Brenner 1974). Its small size and rapid generation cycle, together with its mostly hermaphroditic reproduction have made it one of the leading model systems to investigate genetic regulation of many aspects of life, and more recently to address universal principles of biology on a genomic scale. Key to its career in basic research was its cellular construction plan: all somatic cells follow a fixed lineage, which Sulston and Horvitz scrutinised and laid out in all detail (Sulston 1977). The versatile worm of around 1 mm length fulfils its tasks with a mere 959 somatic cells; but every cell is at its place, precisely integrated. When the embryo develops and cells divide, the pattern what they become and where they go is highly predictable, and reversely, the origins of each individual cell in the fully-grown animal are known. Thanks to this biology and its characterisation, *C. elegans* offered unique opportunities for developmental studies of intercellular crosstalk and of cell fate determination. In the cell pedigree, it became obvious that more than totally 959 somatic cells were generated during development; in fact, 1090 cells formed, of which 131 died again in the course – a specific 131 cells. Here, *C. elegans* was on the stage also for research on programmed cell death (Ellis 1986a).

1.5.1 *C. elegans* as a system to study the bases of human diseases

Given the high degree of evolutionary conservation of elemental biological processes, observations made in the worm can often be transferred to higher eukaryotes, including mammals. Reversely, the nematode can usually offer a system in which to study specific questions inferred from research in the latter. Genetic screens in *C. elegans* allow to search for novel factors involved in a biological process of interest; once the underlying genes have been identified, homologous molecular functions can often be inferred for the counterparts in higher organisms. Reversely, a known gene that attracted the attention as a factor associated with a human disease, for instance, might be studied more effectively in a more primitive system (provided it is conserved). Besides the genetic conservation, a suitable model would ideally present some degree of functional equivalence to the process being investigated; and it would hold some tools to allow for straightforward genetic manipulation.

The nine hundred fifty nine somatic cells of *C. elegans* probably compose a less complex system than the ten trillion cells defining a human body. Yet, when comparing the organisms on a cellular or subcellular level, the intricate networks that have established in hundreds of millions of years of evolution, resemble each other as if they were siblings. Furthermore, *C. elegans* comprises many different cell types dedicated to exert specific functions, and specialised tissues, which contribute to a whole living organism with an immense potential to reproduction and at the same time with great adaptability to the environment. For instance, it has contractile myocytes composing body muscles for movement, intestinal cells for digesting food, or neurons with high-speed signalling capacity for regulation and steering. Germ cells propagate the linage and give rise to the subsequent generation of worms. *C. elegans* thus offers itself as a multipurpose system to study many aspects of life in a relatively simple, but nonetheless comprehensive unit.

C. elegans has been used as a model for, and allowed insights into, basic processes of a great variety of human diseases. Many reviews have been written on specific areas in which research with *C. elegans* has proven beneficial [overview, e.g., (Silverman 2009)]. *C. elegans* is a well established model in research on stem cell biology (Joshi 2010a), aging (Johnson 2008; Brunet 2007), and cancer (Potts 2011). It has been used to study neurodegenerative disorders (Dimitriadi 2010) or also the basic mechanisms of obesity (Jones 2009)]. Increasingly, *C. elegans* is being evaluated as a tool for small molecular drug discovery (Artal-Sanz 2006) or for the characterisation of molecular action of new drugs (Kaletta 2006).

1.5.2 Genetics, genomics and genetic manipulation

The genome of *C. elegans* has been very well characterised. Sulston and Brenner characterised the DNA of *C. elegans* promptly (Sulston 1974) and realised that one haploid genome was just about 20 times the size of an *E. coli* genome. *C. elegans* was then the first multicellular organism to have its genome completely sequenced (1998). Not only the cell number of *C. elegans* is small considering the anatomical richness of the worm. The genome is very compact: it is only 100 Mio base pairs (3 billion base pairs in human), grouped on six chromosomes; yet it harbours almost 20'000 gene, which is probably not much less than the number of genes in the human genome (Finishing the euchromatic sequence of the human genome 2004).

The ease of handling of *C. elegans* and knowledge on the genome has stimulated the design of a variety of genetic screens. *C. elegans* can be mutagenised relatively easily, e.g., by chemical (ENU/EMS) or physical (UV-TMP) treatment (Jorgensen 2002). Due to the hermaphroditic self-fertilisation of the animal, newly introduced mutations are easily carried from one generation to the next. A wealth of genetic mutants isolated from forward genetic screens have become available to the *C. elegans* community, together with mutants obtained in more targeted approaches by accordingly specialised institutions, namely the Caenorhabditis Genetics Center (CGC) and the National BioResource Project (NBRP) in Japan (Mitani 2010). The advantages (from a geneticist view) of a hermaphroditic reproduction mode are supplemented by the availability of occasional males in the population that allow genetic transfer. Usually, mutations can be readily combined, and the genetic interaction of two or more factors can be assessed.

Forward genetic screens have been complemented by reverse genetic approaches. The expression of genes can be knocked down relatively specifically by RNAi, applicable in *C. elegans* by several means. In the simplest treatment, bacteria expressing dsRNA with a nucleotide sequence specific to the gene of interest are fed to the worms, which in many cases leads to the reduction of the according mRNA. Libraries with bacterial clones covering a high percentage of the *C. elegans* genome are available for ready treatment of *C. elegans*, and provide a setup for large-scale gene knockdown in reverse genetic screens, or for a first-line investigation of a gene of interest (Kamath 2003; Rual 2004a).

C. elegans is also amenable to genetic transformation. Genetic material can be introduced as dsDNA stretches or as plasmids and immediately be expressed in the transgenic animal. Originally, transformation was achieved by injection into the germ line rachis – a cylindrical structure to which all meiotic germ cells connect their cytoplasm – yielding progeny that carried extrachromosomal arrays of the transgene. Later, techniques became available to integrate transgenes so they would segregate in a

Mendelian manner. Most in use is ballistic transformation of *C. elegans* to directly create low-copy, integrated transgenes (Praitis 2001).

I will describe this last method in much more detail in *6 unc-119 and apoptosis: novel functions for an omnipresent bystander*. The bombardment of mutants with a selectable phenotype (Unc) to identify transgenic animals has been very convenient; tacitly, is has been assumed to work neatly. I will show that it does not always – not in apoptosis research at least.

2 Apoptosis and reproduction in *C. elegans*

C. elegans has become a favourite model system for basic biological processes thanks to its fixed cell lineage in the soma and thanks to the extraordinary spatiotemporal organisation of its germ line. Programmed cell death as a fate of a fixed 131 cells during development allowed to uncover the basic genetics of apoptosis regulation. In contrast to the fixed lineage of somatic cells, which are all post-replicative in the adult animal, germ cell proliferation proceeds into adulthood. It seems to be more stochastic, within the limits of a well predictable overall structure. The study of germ cell proliferation and differentiation in *C. elegans* helped to develop and validate concepts of stem cell maintenance and of germ cell fates. The cylindrical gonad has been dubbed a test tube for cell and developmental biology (Hubbard 2000).

I have studied apoptosis regulation mainly in the germ line context and occasionally confirmed or extended the findings in somatic cell death. Germ line structure and germ cell maturation were disturbed in many conditions that I studied – genetic and environmental – making it evident to me how manifold the influences, and how limited our understanding of superordinate connections and of driving forces in these processes were. A welcome approach to the complex interconnections of genetic regulation in time and space and varying environmental conditions was carried to me by Antje Beyer from Jasmin Fisher's research group in Cambridge. She was working on a computational model of the *C. elegans* germ line. This abstraction from the model system (itself a less complex environment than the mammalian counterpart) should help to develop and test hypotheses on the basic principles determining the fate of germ cells. We collaborated on the theoretical aspects of the model and in finishing the writing of a work that has recently been published , and which I add as a second part to this chapter.

The first part serves as an introduction to conserved aspects of apoptosis in *C. elegans* and to specific aspects of germ cell death. I present the DNA damage responses that can be studied in the gonad, and the genetics of DNA damage-induced apoptosis in *C. elegans*. Engulfment is an elemental process in apoptosis execution and is outlined here as well. The manuscript on the computational germ line model includes an overview on the organisation of the germ line, as well as references to several comprehensive reviews on the topic.

Chapter 2

2.1 Cell death in the soma and in the germ line

2.1.1 Programmed cell death in *C. elegans*

Apoptosis has been observed in multicellular systems from worm to human. The molecular principles driving apoptosis, and many of the involved genes have been well conserved in evolution and must represent an ancient program. *C. elegans* has been very productive in revealing basic mechanisms of apoptosis. Programmed cell deaths can easily be observed in living nematodes using Nomarski differential interference contrast (DIC) microscopy. In somatic development, exactly 131 cells are destined to die and undergo apoptosis at a predictable developmental stage (a high proportion affects neuronal precursors). In the germ line, the number of cells that die is less fixed, and the selection which cells undergo apoptosis is apparently stochastic. Somatic and germ cell death have different routes of induction, but they share the core effector mechanism.

2.1.2 The core apoptotic machinery

This apoptotic machinery is encoded by three known genes: *ced-3*, *ced-4*, and *ced-9*. Genetic screens for animals with an altered number of apoptotic corpses or with extra surviving cells first led to the isolation of *ced-3* and *ced-4* mutants (from Cell Death abnormal) that completely abolished cell death (Ellis 1986a). Michael Hengartner and colleagues then identified a dominant allele of *ced-9* that prevented developmental apoptosis, and cis-genic suppressor mutations that inverted the phenotype to increased cell death. They showed that *ced-9* was an inhibitor of apoptosis genetically upstream of *ced-4* and *ced-3* (Hengartner 1992). Eventually, *egl-1* was shown to be an essential pro-apoptotic gene for developmental cell death, genetically upstream of *ced-9* (Conradt 1998). This is the activation cascade as it stands today; EGL-1 is releasing CED-4 from inhibition by CED-9, thereby allowing CED-4 to oligomerize and activate CED-3. A very similar homologous cascade is conserved in mammalian cells; however, the worm seems to be more spartanic in the number of genes. Single genes in *C. elegans* unite the functions of several homologs from mammals (which makes the worm a preferred study system due to non-redundancy) – sometimes of homologs with opposite activity, i.e., pro- and anti-apoptotic (which makes the analysis of gene function thought-provoking, as this work exemplifies for instance).

CED-3 is the central caspase (cysteine-dependent aspartate-specific proteases) and the key effector molecule at the initiation of apoptotic degradation processes. While originally identified as a homolog of ICE1 (now caspase 1) (Yuan 1993), it is functionally most similar to the mammalian effector caspases caspase 3 and caspase 7. CED-3 is present in cells as an inactive zymogene, and it is activated by oligomeric CED-4, likely through auto-cleavage that is facilitated by induced proximity of CED-3 molecules on the CED-4 complex. The protease has numerous possible targets: proteins that are degraded specifically for the cell death execution process, and others that might be cleaved as a side effect of protease activation [approach to caspase substrates in (Timmer 2007)].

CED-4, similarly to its mammalian homolog Apaf-1 (Zou 1997), forms an oligomer and serves as a docking station for CED-3 once released from inhibitory binding to CED-9. The active CED-4 complex was recently demonstrated to be a homo-octameric assembly of differently conformed subunits [(Qi 2010), see details in *5.6.2 Structure of CED-9 and its binding partners*]. CED-4 was shown to translocate

from mitochondria to the perinuclear region upon apoptosis induction in *C. elegans* embryos (Chen 2000); newer observations however suggest that perinuclear localisation of CED-4 is not limited to cells undergoing cell death [(Pourkarimi 2011) and our own observations]. Interestingly, the *ced-4* locus was shown to code for two isoforms, one of which seemed to have anti-apoptotic effects (Shaham 1996a).

ced-4 and *ced-3* are essential for apoptosis in *C. elegans*; generally, loss-of-function mutations fully prevent programmed cell death. To my knowledge, only one instance has been described where apoptosis-like death could occur in the absence of functional CED-3 (Bloss 2003), an observation however that could not be confirmed by another group (Jagasia 2005). Yet, a current genetic screen in our laboratory supports the possibility of *ced-3*-independent apoptosis execution [internal communication by Sheng Zeng].

CED-9 is a critical switch for transmitting apoptosis-inducing signals to the execution phase. It is homologous to mammalian Bcl-2, an inhibitor of apoptosis (Hengartner 1994b). CED-9 is assumed to inhibit apoptosis by binding CED-4 and retaining it in the non-oligomerized inactive form, an interaction that is disrupted by EGL-1 (del Peso 2000; Yan 2004). CED-9 is required for preventing cell death in cells that are destined to survive by lineage (Hengartner 1992). Apparently, CED-9 also has a pro-apoptotic function beyond passively relaying pro-apoptotic signalling (Hengartner 1994a). The role and function of CED-9 and its interactions with CED-4 and EGL-1 will be discussed in more detail in *5.6 rpo-1b(op259) and CED-9*.

Several studies have indicated non-apoptotic roles of the core apoptotic factors in *C. elegans* and other organisms that are often conserved [reviewed in (Galluzzi 2008), Bcl-2 homologs in (Hetz 2008)].

2.1.2.1 Developmental cell death requires EGL-1

With few exceptions, programmed cell death in the soma depends on EGL-1 (Conradt 1998). The BH3-only protein EGL-1 can bind to CED-9, thereby inducing a conformational change in CED-9 that lowers affinity for CED-4 (Yan 2004; Fairlie 2006). EGL-1 expression is largely regulated by transcriptional control. The short CDS is flanked by cis-regulatory elements that reach unusually far upstream and downstream. Cell death specification of certain types of cells during development can be attributed to competition of transcriptional inhibitors and activators of *egl-1* [reviewed in (Peden 2008)].

Apoptotic priming other than by *egl-1* upregulation has been demonstrated for the tail-spike cell, in which transcriptional upregulation of *ced-3* is the main mechanism of apoptosis activation (Maurer 2007); in CEM neurons, *ced-3* transcription is upregulated in parallel with *egl-1* upregulation (Nehme 2010).

For controlled death of the Hermaphrodite Specific Neurons (HSN) in males, *eor-1*, a transcriptional target of EGF/Ras/MAPK signalling (Howard 2002; Rocheleau 2002), is required downstream of EGL-1 expression; loss of *eor-1* function can suppress the pro-apoptotic effect of EGL-1 overexpression in hermaphrodites, but cannot prevent excessive death of *ced-9(rf)* (Hoeppner 2004). This indicates that *eor-1* acts upstream of, or in parallel to, *ced-9*; which supposes – if not an inhibitory effect of EOR-1 on EGL-1 binding to CED-9 – a role for EOR-1 and for EGL-1 in apoptosis besides controlling CED-4 release from CED-9 by EGL-1 binding.

EGL-1 is involved in mitochondrial fragmentation, a process that precedes, and contributes to, apoptosis activation upstream of CED-3. EGL-1-induced mitochondrial fragmentation also requires functional CED-9, but is unlikely to be a result of EGL-1 binding to, and subsequent CED-4-release from, CED-9 (Jagasia 2005). [For a review on EGL-1, see (Nehme 2008), for a review on BH3-only proteins, (Giam 2008; Lomonosova 2008)]

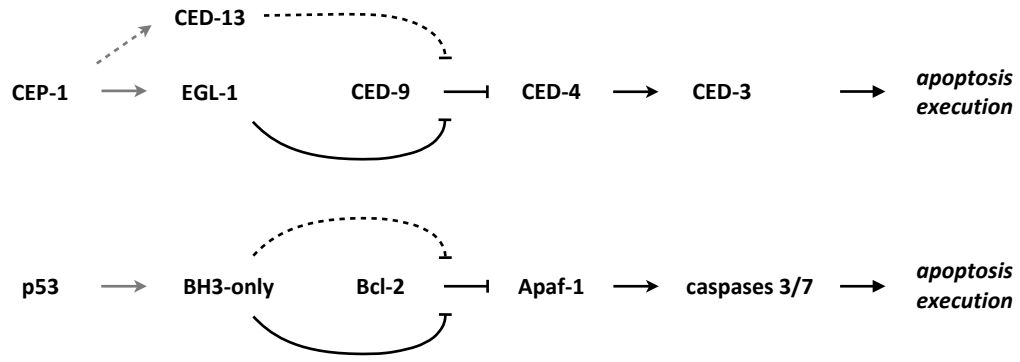

Figure 1 Basic model of apoptosis induction. The core apoptotic cascade from *C. elegans* (top) has a well-conserved correlate in mammals (bottom). In germ cells – upon stresses like DNA damage – CEP-1 transcriptionally upregulates EGL-1 and CED-13 expression. EGL-1, by binding CED-9, loosens the inhibitory binding of CED-9 to CED-4. The effect of CED-13 in CED-4 release and apoptosis induction is less significant. The same mechanism of EGL-1-induced release of CED-4 from CED-9 is thought to induce developmental cell death with cell specific activating mechanisms of EGL-1 transcription. A homologous cascade exists in mammalian cells. p53 activates BH3-only proteins (e.g., Noxa, Puma) that in turn act on Apaf-1 release, which in combination with cytochrome C activates effector caspases.

2.1.3 Constitutive (physiologic) germ cell apoptosis

In the germ line of adult hermaphrodites, cell deaths with the characteristic appearance of highly refractile discs can be observed by DIC microscopy (Gumienny 1999). Apoptotic germ cells seemingly detach from the syncytial germ cell rachis while condensing, and they are swiftly engulfed by the surrounding gonadal sheath cells. Approximately half the number of meiotic germ cells developing toward oogenesis is supposed to die by apoptosis at the exit from late meiotic pachytene stage. This constitutive, so-called physiologic, cell death is bound to oogenesis; it is spatially restricted to the gonad bend region, where alternatively to elimination by apoptosis, germ cells begin to grow rapidly into oocytes. Cell death events appear to be stochastic; which germ cells exactly will undergo apoptosis cannot be predicted so far. There is, however, some tendency for apoptotic corpses to appear in clusters.

The physiological role of the high rate of germ cell apoptosis is hypothetical. Cells of the according stage have just passed meiotic recombination and could have repair errors of endogenous DNA breaks, which would require elimination of the problematic cells. In the more favored 'nursing cell' model, cell death is a fate for temporarily required germ cells; more cells than needed for fertilization are produced initially, so they contribute to synthesis of cytoplasmic constituents and help supplying the rapidly growing oocytes; apoptosis would than timely remove supernumerous nuclei from the pool of advancing germ cells [reviewed in (Gartner 2008)].

2.1.3.1 Physiologic germ cell death is Ras/MAPK-dependent but *egl-1*-independent

The limited understanding of the physiological significance and the driving forces of constitutive germ cell apoptosis in *C. elegans* goes along with restricted knowledge on the molecular mechanisms determining cell death induction. Germ cell death requires the core apoptotic machinery consisting of CED-9, CED-4 and CED-3; whereas for some forms of germ cell apoptosis (e.g., irradiation-induced or infection-associated) the genetic requirements upstream of the core have been partially uncovered, it remains unclear how the cell deaths at baseline are regulated, and how pro- and anti-apoptotic signals are transduced to the core. Surprisingly, germ cell death can occur in the absence of EGL-1, in contrast to most somatic apoptosis. Also, the dominant gain-of-function mutation in *ced-9(n1950gf)*, which blocks developmental death, does not abolish germ cell apoptosis. However, loss of normal *ced-9* function massively increases germ cell death, indicating that CED-9 does play a central role as an inhibitor of apoptosis in the germ line as well (Gumienny 1999). Many of the experiments presented in this work should help to further specify constitutive germ cell apoptosis, with a focus on the role of CED-9.

Two regulatory pathways of global importance for cellular growth and proliferation have been associated with constitutive cell death. Ras/MAPK signaling is required for the exit of germ cells from meiotic pachytene and for maturation into oocytes (Church 1995). Reduced MAPK signaling also reduces germ cell death, which is linked to oogenesis; thus, constitutive germ cell apoptosis directly or indirectly depends on Ras/MAPK [discussed in (Gumienny 1999)]. A role for MAPK in regulating baseline levels was further suggested by the correlation of abnormally high MAPK activity and increased germ cell apoptosis in the *gla-3* mutant (Kritikou 2006). Another important regulatory influence on constitutive germ cell death was demonstrated for the Rb/DP/E2F complex homologs LIN-35/DPL-1/EFL-1; possibly, *dpl-1* (but not *lin-35*) regulates apoptosis induction through transcriptional regulation of the core apoptosis genes *ced-4* and *ced-3* (Schertel 2007). In the soma, these factors were suggested to promote cell death in a process downstream of, or in parallel to, CED-9 inhibition (Reddien 2007), which might also apply to the germ line.

2.1.4 Stress-induced germ cell death

Exogenous factors can increase the levels of germ cell apoptosis; several stressors that activate pro-apoptotic cascades have been identified – notably starvation, bacterial infection, and DNA damage response. The corresponding molecular pathways seem to employ activation mechanisms for the core apoptotic machinery that are not needed for constitutive apoptosis induction; EGL-1 is clearly required for the activation of apoptosis in response to infection or DNA damage, whereas it seems to be dispensable for constitutive germ cell apoptosis [reviewed in (Gartner 2008)]. *DNA damage-induced germ cell apoptosis* will be discussed below.

Several conditions can strongly increase the number of germ cells that undergo apoptosis; one could think of the total number of corpses under these conditions as an addition of stress-induced corpses to the constitutively dying cells. To my knowledge, however, it has not been shown whether 'physiologic' germ cell death indeed persists when stressors drive the number of dying cells above constitutive levels anyway.

2.1.5 DNA damage responses in *C. elegans*

Most of the DNA surveillance and damage response genes and pathways described in other organisms are conserved in *C. elegans*, and several new genes have been identified in this model by mutagenesis and RNA interference [for a comprehensive review on DNA damage response in *C. elegans*, see (Stergiou 2004)]. Many of these genes play diverse essential roles in DNA repair, cell cycle control, DNA replication, meiosis, mitosis, or apoptosis. The germline tissue of *C. elegans* is a versatile model to dissect the signalling network that links DNA damage as inflicted by chemical or physical agents to cellular key responses; DNA repair, transcriptional alterations, cell cycle arrest, cell death, and – as an integrated output – embryonic survival, can be studied in the context of a living organism. The transparency of the animal allows for efficient microscopic analysis of native worms or of fluorescently labelled products. Proliferation arrest of mitotic cells and apoptosis of damaged meiotic germ cells can be morphologically followed by DIC microscopy in two spatially separate areas of the germ line. DNA repair has been studied *in vivo* with fluorescently tagged markers of DNA lesions and of repair proteins. Also, transcriptional alterations can be tracked with *in situ* hybridisation or with transgenic markers.

2.1.5.1 Proliferating germ cells in the distal compartment arrest their cell cycle progression

Upon massive DNA damage, the mitotically dividing germ cells halt their cycle before the M-phase and are arrested until DNA damage has been repaired and the cell cycle can be resumed safely. Nuclear growth and cytoplasmic expansion meanwhile persist; morphologically, this becomes apparent as an enlargement of the germ cell nuclei and nucleoli (Gartner 2000). The concurrent reduction in the number of cells per distal gonad volume has commonly been used to measure the response. In mutants with defective cell cycle arrest response, the mitotic cells remain cycling (supposedly propagating damages of hereditary material (Harris 2006)); accordingly, the number of cells per volume does not decrease upon DNA damage.

2.1.5.2 Meiotic germ cells die in late pachytene

Few hours after worms have been treated with DNA damage inducing agents, the physiologically low number of germ cell corpses increases significantly and than rises gradually until about 36 hours after treatment. DNA damage-induced apoptosis is morphologically non-distinct from constitutive germ cell death and is restricted to the same gonadal compartment. It is not clear why only cells at this stage of the cell cycle undergo apoptosis in response to DNA damage. Whether it is due to inhibition of pro-apoptotic signals in other compartments of the gonad or due to restricted availability of pro-apoptotic cues and effectors in late meiotic pachytene has only been partially resolved.

2.1.5.3 Embryonic survival is reduced

Failure in properly controlling DNA damage – e.g., due to defective repair or abolished apoptosis – can lead to unhealthy or unviable progeny. Embryonic structure can be observed in retained or released eggs; viability of the embryos is usually assessed by counting the fraction of non-hatched eggs on a plate after a defined interval from DNA damage and egg-laying.

2.1.5.4 DNA damage responses in the soma

The soma of adult worms is surprisingly tolerant to different types of DNA damaging agents. In contrast to the proliferating and differentiating germ cells, somatic cells in the adult animal are all post-replicative and terminally differentiated (Sulston 1977), and therefore may be less susceptible to the detrimental effects of DNA lesions. Somatic cells do show some DNA repair activity, e.g., of UV lesions (Meyer 2007). In my experiments, I noted that young larvae are very sensitive to UV-irradiation and die or arrest growth at doses that are well tolerated by adults.

Specific somatic cells have been shown to die upon irradiation of larvae, by a cell death mode that is different from apoptosis (Weidhaas 2006a). Interestingly, the microRNA *mir-35* plays a role in irradiation-induced cell death downstream of CEP-1 activation both in the germ line and in the soma; mutants have decreased apoptotic germ cell response, but increased somatic non-apoptotic death (Kato 2009).

Although the gonad is the prime site of manifest stress responses, there is strong indication that the soma plays more than a bystander role in regulating these processes and in controlling homeostasis of the germ line (e.g., insulin signalling, hypoxia signalling (Sendoel 2010), cell-nonautonomous effect of *kri-1* (Ito 2010)). How much the soma modulates apoptosis levels and how much it can itself initiate or block apoptosis remains to be resolved.

2.1.6 DNA damage-induced germ cell apoptosis

Damage-induced apoptosis in the germ line of adult hermaphrodites shares the core apoptotic machinery with physiological demise of germ cells and with developmental death of somatic cells, but is seemingly distinct from these in its upstream factors. Checkpoint signalling and induction of apoptosis upon DNA damage involve many homologs of known repair and signalling molecules from mammals and are thought to follow a similar sequence of molecular events and similar regulation: DNA lesions are sensed, and signals are propagated by molecular transducers that in turn activate effectors of the DNA damage response [reviewed in (Stergiou 2004)].

2.1.6.1 Damage signalling and repair factors are required for apoptosis

The PI(3)K-like kinases ATM and ATL are critical transducers in mammalian cells [see *3.1.2 From sensors to effectors*]. Accordingly, mutants of *atm-1* (Garcia-Muse 2005; Stergiou 2007) and *atl-1* (Garcia-Muse 2005) have defective apoptosis induction in response to certain types of DNA damage. The tumor suppressor protein p53 is a key effector molecule for the induction of cell cycle arrest and apoptosis [e.g., (Zilfou 2009; Goh 2011)]. Its *C. elegans* homolog, CEP-1, is essential for DNA damage-induced germ cell death. Also, mutants of classical repair factors from various repair pathways have been shown to be defective for DNA damage-induced apoptosis. The 9-1-1 complex subunit mutants *hus-1* (Hofmann 2002) and *mrt-2* (Ahmed 2000), NER repair mutants (Stergiou 2007, 2011), or *clk-2(lf)* (Ahmed 2001) have minimal apoptotic DNA damage response. They all fail to properly activate CEP-1.

2.1.6.2 CEP-1 and EGL-1 are central for DNA damage-induced death

Dependency on CEP-1 has been a defining feature of stress-induced germ cell death in *C. elegans* (Schumacher 2001; Gartner 2000; Schumacher 2005b). Loss of *cep-1* function is thought to abolish any DNA damage-induced cell death. At the same time – what has been distinguished as 'physiologic' germ cell death – meiotic pachytene cells in *cep-1(lf)* mutants maintain the capability to die by apoptosis at a rate that corresponds to the constitutive level of germ cell death observed in non-treated wildtype worms. CEP-1 has been shown to exert its pro-apoptotic function mainly by transcriptionally activating the two pro-apoptotic BH3-only proteins EGL-1 and CED-13. EGL-1 presumably activates the core apoptotic machinery by binding to CED-9 and releasing CED-4, as in developmental cell death; the gain-of-function mutation *ced-9(n1950gf)*, which is thought to prevent EGL-1 binding to CED-9, abolishes DNA damage-induced death (Figure 1). In the germ line, loss of functional *egl-1* has a similar effect on apoptosis as loss of *cep-1*, i.e., normal levels of physiological cell death but defective DNA damage response. In contrast to *egl-1*, loss of *ced-13* function has only a mild effect on DNA damage-induced apoptosis; it is assumed to play a minor role in germ cell death (Schumacher 2005b).

It is intriguing that activation of the core apoptotic machinery apparently requires the same mechanism for the programmed death of somatic cells and for exogenously induced apoptosis of germ cells; transcriptional upregulation of EGL-1 to release CED-4 from CED-9 is employed by developmental programs and by stress responses. The non-dependence on EGL-1 of constitutive germ cell apoptosis is the more surprising. Germ cell apoptosis seems to have various regulatory inputs at the level of EGL-1 and CED-9. One part of my research addressed this interface. The functions of CEP-1, EGL-1 and CED-9 in constitutive and damage-induced germ cell apoptosis will be introduced and discussed in much more detail in *5.3 rpo-1b(op259) and CEP-1* and in *5.6 rpo-1b(op259) and CED-9.*

2.1.6.3 Pathways besides CEP-1 activation contribute to DNA damage-induced apoptosis

Even though CEP-1 activation is required for DNA damage-induced apoptosis, it is not sufficient. There is increasing evidence for pro-apoptotic signalling independent of, or in parallel to, CEP-1.

Several mutants have exhibited defective DNA damage response despite normally high activation of CEP-1, e.g., the pRb homolog *lin-35* (Schertel 2007), ubiquitin ligase *eel-1* (Ross 2011), the Sirtuin homolog *sir-2.1* (Greiss 2008), or the ceramide synthesis mutant *lagr-1* (Deng 2008).

Stress response pathways have been reported that activate apoptosis independently of CEP-1. Apoptotic response to arsenite depends on various MAP kinase (ERK/JNK/p38) cascades but not on *cep-1* (Pei 2008); and a very similar pattern was shown for copper (Wang 2009). MAP kinase pathways but not *cep-1* are also required for germ cell apoptosis induced by osmotic, oxidative, or heat shock stress, in a mechanism that involves ABL-1 (Salinas 2006).

2.1.6.4 Increased germ cell apoptosis with or without DNA damage

Many genetic conditions have been found that lead to increased cell death in the germ line of *C. elegans*. Some mutants presented with hypersensitivity to DNA damage, whereas others had increased apoptosis without exogenous activation, a phenotype described as Gla (Germ Line Apoptosis). Mutations have been distinguished that lead to excessive apoptosis through overactivation of CEP-1 from others that

cause increased apoptosis independently of CEP-1. These situations will be presented more comprehensively in *5.3 rpo-1b(op259) and CEP-1*.

2.1.7 IR and UV-C irradiation

DNA damage responses can be triggered relatively conveniently in *C. elegans*, with chemical substances that are applied to the agar plates on which the worms feed, or with irradiation that hits the worms almost uniformly given their small size. In most of my experiments, I used ionising radiation (X-ray) or UV-C irradiation to damage DNA, which have several advantages over chemical mutagens. Irradiation is non-toxic to the outside. The irradiation dose is better controlled than drug doses; drugs are mixed to plates, can be hard to dissolve and have local variations of concentration and might be inactivated; the routes how substances reach the cells of a worm are usually unknown and might happen with completely different kinetics. In contrast, irradiation is applied as a relatively short pulse (IR, approximately 20 min; UV-C, few seconds); and the worms are not exposed to the mutagenic agent before and after a reference time point.

Ionising and UV-radiation are biologically relevant mutagens for many organisms. Further, ionising irradiation at high doses is a frequently used therapeutic approach in the treatment of human cancer. Irradiation with IR or UV creates a spectrum of DNA lesions that also occur endogenously, and it provokes the activation of repair pathways that are also required to deal with physiological levels of DNA damage. Thus, irradiation represents a valid means to study molecular programs that are recruited beyond the rare situations of extreme irradiation exposure.

[Radiation biology of *C. elegans* has been reviewed in (Sakashita 2010)].

2.1.8 Engulfment of apoptotic cells

Removal of apoptotic corpses is an integral part of the apoptotic program. The disposed of material should be cleaned in an orderly fashion; failure of apoptotic cells to be engulfed by neighbouring cells or by specialised phagocytes can lead to autoimmune diseases in human [discussed in (Fullard 2009)]. The engulfment mechanism and engulfment genes are evolutionarily conserved and have been well studied in *C. elegans* (Reddien 2004). During somatic development, cells that die are rapidly engulfed by one of the neighbouring cells. In contrast, apoptotic germ cells are enclosed by protrusions of the large gonadal sheath cells, and incorporated and digested by these professional phagocytes; multiple dying cells are digested by only few sheath cells. Engulfment of apoptotic cells is an important biological process; further, it needs to be considered with every experiment on apoptosis levels *in vivo*, since reduced or enhanced engulfment can result in a similar increase or decrease in the cell corpse number as enhanced or reduced cell death. In fact, the first mutant genes that were found to affect cell death in *C. elegans* – *ced-1* and *ced-2*, with high levels of apoptotic corpses – were shown to be required for proper removal of apoptotic corpses (Hedgecock 1983).

In *C. elegans*, engulfment is carried by two main pathways converging on the small Rac GTPase CED-10 (Rac1); they have partly complementary, partly redundant activity (Kinchen 2005). Phenotypes from reduction of the function of one pathway are enhanced by simultaneous defects in the other; conversely, relieving negative regulation from one pathway can partly compensate for defects in the

other [reviewed in (Reddien 2004)]. CED-1 (CD91/LRP/SREC), CED-6 (hCED-6/GULP) and CED-7 (ABCA1) constitute one branch and together act in corpse recognition; CED-2 (CrkII), CED-5 (Dock180) and CED-12 (ELMO) are grouped in another branch of signal transduction toward activation of CED-10 in the engulfing cells. Several additional factors have been identified as regulators of engulfment through the CED-2/CED-5/CED-12 complex [summary in Figure S1 of (Neukomm 2011)]. Further, the tyrosine kinase homolog ABL-1 was shown to inhibit engulfment, likely by inhibiting ABI-1, a positive regulator of engulfment acting in parallel to both CED-1/CED-6/CED-7 and CED-2/CED-5/CED-12 (Hurwitz 2009).

Engulfment of apoptotic cells is more than an ultimate step to remove dead material; the dying and degradation processes in the apoptotic cell are coordinated with engulfment. It has been shown that intact engulfment is decisive for execution of cell death where other pro-apoptotic signals are weak (Reddien 2001; Neukomm 2011). So far, it has not been excluded that some of the known engulfment factors play an active role in apoptosis beyond their function in engulfment. Such an involvement might differ between germ cell death and developmental apoptosis of somatic cells, the context in which most of the engulfment mechanisms have been studied. In *6.2.2.6 unc-119 has distinct functions in germ cell death and removal,* I describe some findings that would support a role for *ced-2* in the dying of germ cells.

2.2 The germ line of *C. elegans* and germ line modelling

To help visualise the three-dimensional organisation of the distal gonad of *C. elegans*: it might well be likened to a corncob. The conical distal tip with small grains passes into a cylindrical structure where kernels of corn cover the circumference in a regular arrangement. The kernels would correspond to individual, well septated germ cell nuclei; the membrane almost completely envelops the unit, except for a gap at the base, where the germ cell connects to the rachis, the shared central cytoplasm.

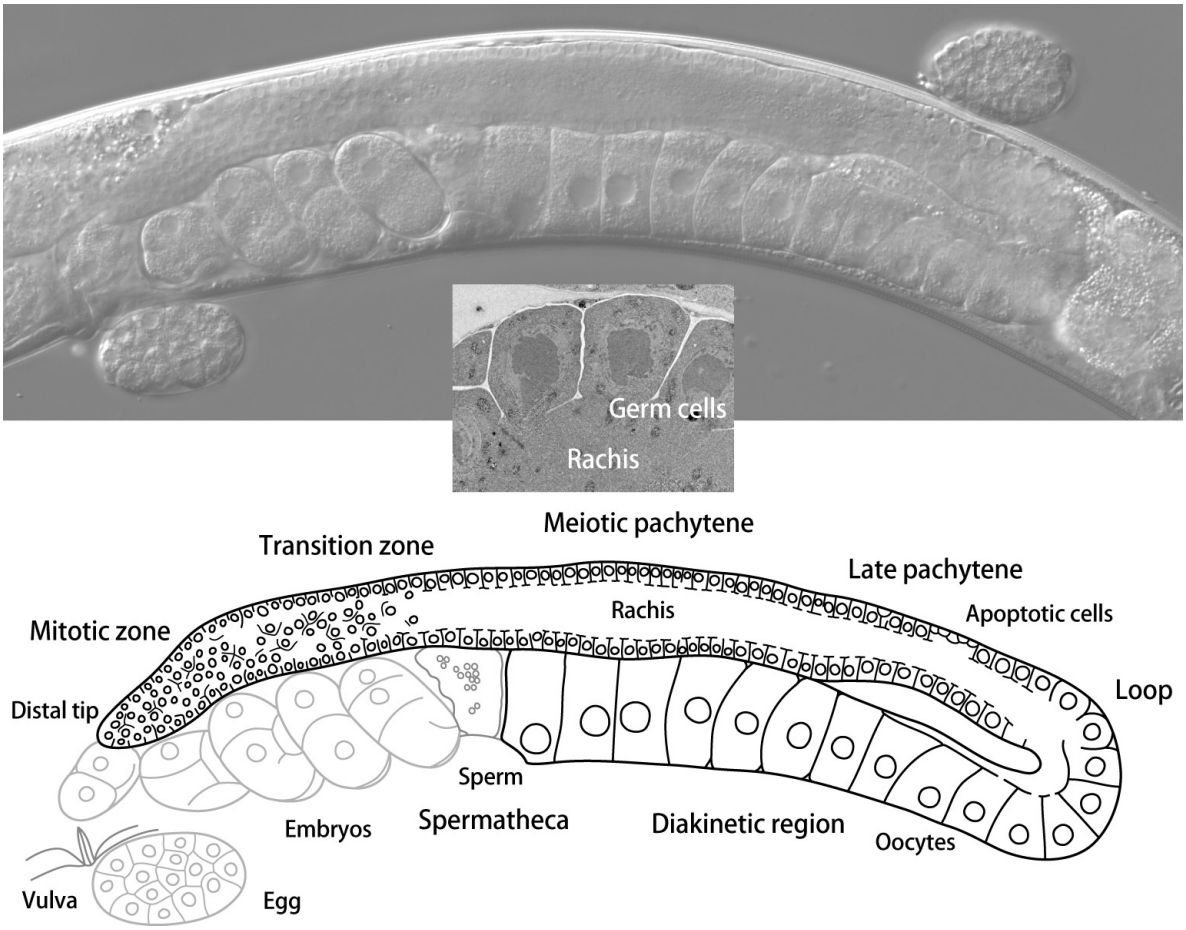

Figure 2 (Figure 1 from manuscript). The germ line of *Caenorhabditis elegans* by DIC (top), as a schematic (bottom), and in a cross section (transmission electron microscopy). The head of the worm is to the right, the posterior gonad to the left of the picture. Differential interference contrast (DIC) microscopy allows to observe live animals in any focal plane; here, an adult hermaphrodite is virtually dissected along a plane through the centre of the gonad tube. The germ cells in the meiotic pachytene region form a monolayer around a concentric inner tube, seen as a nuclei-free area in the longitudinal and cross sections (rachis). The limits of the transition zone and of the late pachytene stage within the meitoc pachytene region are not strictly defined by DIC. The oocytes in the loop have exited pachytene and begin the diakinetic stage of meiosis.

2.2.1 Manuscript, abstract and introduction

A Dynamic Physical Model of Cell Migration, Differentiation and Apoptosis in *Caenorhabditis elegans*

Antje Beyer[1], Ralf Eberhard[2,3], Nir Piterman[4], Michael O. Hengartner[2], Alex Hajnal[2], and Jasmin Fisher[5*]

[1]Department of Genetics, University of Cambridge, Cambridge, UK, [2]Institute of Molecular Life Sciences, University of Zurich, Zurich, Switzerland, [3]PhD Program in Molecular Life Sciences, Life Science Zurich Graduate School and MD/PhD Program, University of Zurich, Zurich, Switzerland, [4]Department of Computer Science, University of Leicester, Leicester, UK, [5]Microsoft Research, Cambridge, UK,

*corresponding author

Abstract The germ line of the nematode *C. elegans* provides a paradigm to study essential developmental concepts like stem cell differentiation and apoptosis. Here, we have created a computational model encompassing these developmental landmarks and the resulting movement of germ cells along the gonadal tube. We have used a technique based on Molecular Dynamics (MD) to model the physical movement of cells solely based on the force that arises from dividing cells. This novel way of using MD to drive the model enables calibration of simulation and experimental time. Based on this calibration, the analysis of our model shows that it is in accordance with experimental observations. In addition, the model provides insights into kinetics of molecular pathways within individual cells as well as into physical aspects like the cell density along the germ line and in local neighbourhoods of individual germ cells. In the future, the presented model can be used to test hypotheses about diverse aspects of development like stem cell division or programmed cell death. An iterative process of evolving this model and experimental testing in the model system *C. elegans* will provide new insights into key developmental aspects.

See full manuscript in Appendix A-325

Introduction

Since the early 1970s (1), the nematode *C. elegans* has been a widely studied model in biomedical research (reviewed in e.g. (2-5)). Through the worm's transparent body it is possible to trace any cell by light microscopy or to study gene expression and cellular development *in situ* (6). The fixed number of cells of the somatic cell lineages have been meticulously described (cf. (7)) and are invaluable for the genetic analysis of regulatory pathways in development (cf. (8)) or in neurobiology. The germ line of *C. elegans* allows for the observation of several essential developmental processes like stem cell proliferation, gametogenesis, and programmed cell death, also termed apoptosis. Importantly, these biological processes are spatially well resolved in this system, where germ cells mature in sequential steps along a tube-shaped gonad. It has therefore been extensively used in basic research (reviewed in

(9-12)). Other than the highly predictable development of somatic tissues, cellular events in the germ line seem to be very stochastic; consequently the underlying general mechanisms are little understood for some of these processes. This is particularly true for physiological germ cell apoptosis. Programmed cell death is a crucial developmental process that is found in many different species; aberrations in this program have important implications in complex diseases like human cancers (13) or neurodegenerative disorders (14). It is therefore key to gain fundamental understanding of its mechanisms. In this work, we propose a computational model of the germ line that is mainly based on physical properties and which aims to provide more insights into the previously mentioned developmental processes. With our model, we are able to test hypotheses about the causes and mechanisms of programmed cell death, among other developmental processes, and to highlight promising theories to be validated experimentally.

The *C. elegans* Germ line

The reproductive system of *C. elegans* has a symmetric structure with two Ushaped gonads extending from a single vulva, one anteriorly and one posteriorly. Our model considers the development from stem cells to mature oocytes within one gonad (see Fig. 1). Although the nuclei and their cytoplasm within the germ line are not completely encapsulated cells and thus are part of a syncytium, they are usually referred to as germ "cells". As the differential interference contrast (DIC) picture and the electron microscopy imaging in Fig. 1 indicate, the cytoplasmic membranes are not fully delimiting, leaving a connection of all cells to a common shared cytoplasm in the centre of the gonad tube, called rachis.

The mature hermaphroditic germ line can be divided into functionally different zones with specific developmental properties (15-18). At the distal most end of the gonadal tube the mitotic zone is located ("distal" here meaning farthest from the uterus), containing dividing stem cells and representing a stem cell niche. The potential of the mitotoic cell pool to divide is maintained by molecular signals – directly via activation of proliferation or, more likely, indirectly via inhibition of differentiation. Delta ligand from extrinsic sources (the distal tip cell) activates the Notch pathway, promoting a high Notch within the germ cells of this region. In the transition zone, where no external Delta ligand is presented, the Notch level gradually decays. When the germ cells are left without Notch, they complete the mitotic cell cycle, enter meiosis and start their differentiation into oocytes (16). A small transition zone in which mitotic and first meiotic cells are interspersed links to a seemingly well orchestrated meiotic pachytene region, where chromosomes undergo homologous recombination. At some point within the meiotic zone, the germ cells start growing at a low rate so that they have visibly increased their size by the time they reach the bend of the gonad and exit the pachytene stage of meiosis. In this loop region, the rachis is thinned to an eccentric tube, but still connecting the growing oocytes before they become proper cells with a fully closed membrane. Distal to the loop with the young oocytes, programmed cell death can be observed as part of normal oogenesis (19). Physiological apoptosis, the fate of about half of all germ cells, is considered to be restricted to this area of the gonad (11). Ras/MAPK activity is required for pachytene exit (20) and oocyte maturation; its absence also disables apoptosis (19). For our model, we premise that germ cells start accumulating Ras activity towards the end of the meiotic pachytene region, induced by an external Ras signal. If the Ras level surpasses a certain threshold in a germ cell, it starts to grow to become a fully grown oocyte filling the complete diameter of the tube when it reaches the proximal end of the gonad. We also assume here that the Ras level is decisive for germ cell death: it renders a cell capable for or insensitive to physiological apoptosis.

3 DNA damage repair pathways and apoptosis

In the introductory chapter *1.4 DNA damage responses*, I outlined the importance of DNA damage response mechanisms for genome integrity, for protecting cellular health and for preventing aberrant proliferation – and, it should be added, for tumor treatment. All organisms have to cope with and integrate environmental factors in their functioning; on the level of individual cells, adaptations can be provoked by external stimuli, and they happen in coordination with the surrounding tissue. This certainly also applies to DNA damage responses where pro-survival efforts are weighted against the need to avoid propagation of aberrant genetic material. The DNA damage response and repair systems are highly specialised and extremely well conserved. *C. elegans* offers a valuable model to study the genetic bases of DNA repair, and it has proven useful to characterise the role of DNA damage response factors for distinct cellular responses in a physiological tissue environment [see *2.1.5 DNA damage responses in C. elegans*].

I utilised this model in the context of two independent studies that were recently published. In the first study (Stergiou 2011), which was based on previous work from Lilli Stergiou and colleagues (Stergiou 2007), we assessed the role of two repair pathways – nucleotide excision repair (NER) and homologous recombination (HR) – for apoptosis induction in the *C. elegans* germ line. In the second project, Ataman Sendoel and me used the worm model to complement the characterisation by Josef Jiricny's group of a sensational novel repair factor in mammalian cells, FAN1 – a critical nuclease in interstrand crosslink repair (ICL) (Kratz 2010). Here, I outline the relevance of the three repair pathways for human disease and I refer to some work in *C. elegans*. (I additionally allude to an independent, hypothetical repair mode – RNA repair.) Detailed introductions and research questions are formulated in two the attached papers. I conclude the chapter with a description of my contribution to the published work and of additional experiments.

Chapter 3

3.1 Introduction to repair pathways

When cellular survey mechanisms encounter DNA lesions, a cascade of signalling events is precipitated that lead to recruitment of appropriate molecules, so repair is optimised for the chemical nature of the damage and for the cellular state. The repair network is composed of highly specialised factors that are subject to intricate, often mutual regulation. Remarkably, a high proportion of the so far known repair factors have been discovered by genetic linkage analyses of clinical syndromes. Hence, a lot of these genes carry the names of the associated syndrome: e.g., ATM/ATL (Ataxia teleangiectasia), XPA through XPG (Xeroderma pigmentosum), CSA/CSB (Cockayne syndrome), WRN (Werner syndrome), BLM (Bloom syndrome), NBS1 (Nijmegen breakage syndrome), SCKL2/SCKL3 (Seckel syndrome), or the 13 members of FANC (Fanconi anaemia).

These syndromes are all relatively rare by themselves. They present with a spectrum of different anomalies; however, there are some unifying aspects. Most syndromes are characterised by neurological defects and mental retardation; some involve growth defects and dysmorphisms; some lead to hematopoietic defects or to immunodeficiency. Many of the syndromes predispose to typical forms of cancers and/or lead to progeria (precocious aging) of certain organ systems (Jackson 2009). Often, the affected individuals are highly sensitive towards specific mutagens, such as UV light or chemotherapeutic drugs.

Other damage repair factors were found in association with hereditary cancer predisposition syndromes: e.g., BRCA1/BRCA2 mutations in familial breast cancer; or mutations in the mismatch repair factors MSH2/MSH6/MLH1/PMS2 underlying hereditary non-polyposis colorectal cancer (HNPCC) [reviewed in (Jiricny 2006)]. [For a summary table of syndromes caused by repair factor mutations see (Ciccia 2010).]

3.1.1 Gaps in the repair network

The many clinical syndromes in relation to the number of known repair factors reveal how delicate a system the DNA damage repair network is. Most of the syndromes arise from monogenetic disorders; that is, mutation of one gene is sufficient to destabilise the system; and many of the known repair factors lead to severe defects if mutated in human patients or in model organisms. This implies that these factors are non-dispensable and fulfil specific non-redundant functions, and that there is only limited capacity for correction.

Given the importance of DNA damage repair in tumor formation and in tumor treatment (Bartek 2007; Jackson 2009), it is important to know the players in detail. Discovery of ever novel repair molecules is an expression of the huge effort of the research community to identify as of yet unknown factors, but it is also a sign that the quest is not yet saturated and that the model of DNA damage repair factors is not yet complete. Further, it is of high interest how these factors act molecularly, how they act on DNA, how they interact physically with other damage response factors, and how they modify each other. The Discovery and characterisation of FAN1 has added another crucial member to the extensive network model of repair factors [see *3.3 Deficiency of FANCD2-Associated Nuclease KIAA1018/FAN1 Sensitizes Cells to Interstrand Crosslinking Agents*].

3.1.2 From sensors to effectors

A rough overview of the DNA damage response network is given in the general introduction on *DNA damage responses*. [The damage repair pathways have been reviewed multiple times, e.g., (Ciccia 2010) and very comprehensively in (Sancar 2004).]. The phosphoinositol-3-phosphate kinase PI(3)K-like kinases ATM and ATL are critical factors in the DNA damage response. They are recruited and activated rapidly after DNA damage has been sensed, and in turn regulate a variety of damage response proteins by phosphorylation (more than 500 target proteins of ATM/ATL were found to be phosphorylated upon DNA damage in two independent proteomic studies (Stokes 2007; Matsuoka 2007)). ATM is mainly activated by double strand breaks, whereas ATL is recruited to replication protein A (RPA)-coated single strand DNA. These kinases are central regulators of repair and signalling platforms that form around damage sites and that direct selection of the proper damage responses. Selection probably means favouring access and activation of certain factors over others (Ciccia 2010). Another central, extensively studied factor in the DNA damage response is the tumor suppressor protein p53. It is activated indirectly by ATM (via CHK2) in response to DSBs, for instance, and it has a splendid number of alternative activation streams [e.g., (Kruse 2009)]. p53 is decisive for the cellular responses – such as cell cycle arrest and apoptosis – which ensue in case of excessive damage, and which can be considered a general outcome of different types of lesions.

3.1.3 Crosstalk of repair modules and downstream effects

The density of the repair network, the irreplaceability of many repair factors, and the involvement of several factors in different repair pathways (e.g., RPA, ATM, XPF) suggests overlap and crosstalk between these pathways. For interstrand crosslink repair (ICL), it has been proposed that the Fanconi anaemia (FA) pathway feeds into homologous recombination [reviewed in (Moldovan 2009)]. In our study *3.2 NER and HR pathways act sequentially to promote UV-C-induced germ cell apoptosis in Caenorhabditis elegans*, we showed evidence for a link between the NER and HR pathways in response to UV-lesions.

Regarding the clinical syndromes caused by mutations in DNA repair factors, it is surprising that members of the same repair pathway can lead to heterogeneous patterns of clinical defects [particularly evident in NER, e.g., (Kraemer 2007)]. For some clinical presentations, there are reasonable molecular explanations (e.g., difference between TCR and GGR branches of NER [see following section]), while for others it is difficult to ascribe the heterogeneity to functional differences in repair. One hypothesis is that they arise from stage and tissue specific cellular effects downstream of faulty repair, which would suppose very specific integration of canonical DNA repair molecules not only in repair but also in cellular responses.

DNA damage is a constant threat to cells and organisms, but it also has become a therapeutic option. Most current cancer treatments besides surgical excision involve DNA damage. For this purpose, it is critical to have a detailed understanding of the multifaceted cellular damage response patterns.

3.1.4 Nucleotide excision repair

NER is specialised to remove bulky lesions that occur within and between bases of one DNA strand. The classical components of the NER pathway were identified based on patients with clinical syndromes

that characteristically involved hypersensitivity to sunlight, most prominently Xeroderma pigmentosum. Genetic analyses of cells from these patients revealed several complementation groups; seven of them were assigned the identifiers XPA to XPG. Analysis of other clinical syndromes with a similar spectrum of features, Cockayne syndrome (CS) and Trichothiodystrophy, yielded further repair factors. NER genes were also identified in rodent UV-sensitive cell lines; these were termed ERCCs (excision repair cross complementary groups) and partially overlap with the factors identified in human cells [reviewed in (Sancar 1996), summary table in (Hanawalt 2008)]. NER can be initiated from two distinct molecular complexes, depending on where in the genome the lesions occur. Damages that are recognised during gene transcription lead to activation of the transcription coupled repair (TCR) branch of NER, whereas lesions in non-actively transcribed regions of the genome are scanned for, and tackled by, the global genome repair (GGR) branch. The two streams converge on the excision machinery composed of nucleases and helicases [reviewed in (Hanawalt 2002), TCR in (Hanawalt 2008)]. A further important component for dealing with UV lesions in proliferating cells and for preventing genomic instability is Polη, a translesion synthesis DNA polymerase, which was found to be the genetic correlate of the Xeroderma pigmentosum variant XP-V [reviewed in (Cleaver 2005)].

UV radiation, a ubiquitous mutagen above ground, is a potent source for DNA lesions of the type that would activate NER. The predominant alterations caused by short wavelength UV (UVB/UVC) are cyclobutane pyrimidine dimers (CPDs) and pyrimidine-pyrimidone dimers (e.g., 6-4 PP). The patients with NER-associated syndromes tolerate UV light much less than healthy subjects. Besides light sensitivity, the pattern of defects is remarkably variable for different underlying mutations. Most patients present with some form of neurodevelopmental or neurodegenerative disorders; XP patients have a severe predisposition for cancer, whereas CS patients typically do not. Several syndromes include massively accelerated aging of the organism or of individual organ systems. The human syndromes have been precisely characterised and the effects of many mutations have been recapitulated in mice [reviewed in (Lehmann 2003)]. Specific involvement of the associated genes in either the TCR or GGR branches or in the trunk of the pathway might explain some of the differences between the syndromes; also, additional roles of some of the repair factors, e.g., in transcription, might contribute to the phenotypic diversity. Interesting models have been presented particularly for the delicate balance between carcinogenesis and aging [(Mitchell 2003) and (Diderich 2011; Hoeijmakers 2009)]. Yet, many of the current concepts for how repair mutants cause specific phenotypes and disease patterns base on theoretical considerations. They need further understanding of the cellular effects that result in response to DNA damage and from repair defects.

In *C. elegans*, several radiation sensitive mutants have been isolated (Hartman 1982) and classified as to their susceptibility to UV and IR irradiation and their repair capacities (Hartman 1989). One of the mutants with strongly delayed repair of photolesions, *rad-3* later turned out to be the XPA homolog. Recently, UV repair in *C. elegans* has been characterised in more detail. The capacity for repairing UV-induced lesions changes during the lifetime of the nematode. A recent study described the changing involvement of NER and chromatin remodelling factors in UV response during development (Lans 2010). Before, the nucleotide excision repair capacity had been shown to be declining in aging animals (Meyer 2007). Expression of UV damage repair factors seems to be generally low in somatic cells (Boyd 2010).

C. elegans NER mutants are hypersensitive to UV; irradiated adults produce a high percentage of inviable embryos, possibly an effect of abnormal repair in the germ line. Lilli Stergiou and colleagues characterised the genetic requirements for cellular UV responses in the germ line of *C. elegans*. They showed that not only the recognised mediators of DNA damage responses were necessary to induce germ cell apoptosis following UV-irradiation, but that this response also depended on repair factors of the NER. XPC-1 and XPA-1 were not less required than ATM-1 (at low UV doses), ATL-1 or CHK-2 (Stergiou 2007). The observation that repair factors themselves are somehow involved in signalling to effectors of DNA damage response was very stimulating for further investigations into this link. (Partial requirement for ATM-1 was also intriguing; even though not a novel notion [see (Matsuoka 2007; Stokes 2007)], it was surprising that ATM-1 should be involved in UV response, given its activation mainly by double strand breaks.) I joined Lilli's project when the NER was more and more evidently joining the homologous recombination pathway.

3.1.5 Homologous recombination

The homologous recombination repair machinery, like many NER factors, plays important roles in cell physiology besides coping with acute (exogenous) damage. It is central in the shuffling of genetic code between homologous chromosomes during meiotic recombination. The thorough understanding of homologous recombination has been promoted by, and feeding into, research both on its role in 'physiological' germ line processes and in DNA repair. In proliferating cells, replication, recombination and repair are closely linked processes; homologous recombination is deeply integrated into basic genome maintenance and its regulation is extremely fine-tuned [reviewed in e.g., (Heyer 2010)].

The main substrates of the HR machinery are DNA double strand breaks. DSBs can be highly toxic to the cell already in very small numbers, due to their deleterious effect on chromosome stability and due to the drastic cellular responses. Sealing of double strand breaks is urgent, yet should optimally reconstitute the integrity of the DNA sequence; HR and non-homologous end-joining repair (NHEJ) are two alternative mechanisms between which to decide. The decision is dependent on the cell cycle state; it has consequences for the repair result (NHEJ repair is usually not loss-less) and for the cellular DNA damage response [reviewed in e.g., (Pardo 2009)]. Failure in the regulation of the decision for and in the repair process of HR per se, and failure in activating appropriate cellular adaptation – with cell death as an option – lead to loss of genome integrity. This can induce and promote tumor formation and severely affect human health [the role of HR in human diseases, e.g., (O'Driscoll 2006)].

The homologous recombination machinery is recruited to DSBs occurring from acute impact on DNA structure, but it is also engaged in repair modalities of other types of damage, e.g., in ICL repair by the FA pathway, or in DNA replication-associated repair processes. We show that HR components are also recruited upon UV-irradiation, which is known to produce the classical substrates of NER. Visual HR markers in the germ line of *C. elegans* form foci following UV, a characteristic of DNA repair sites (Bekker-Jensen 2006), suggesting that NER substrates might be passed to HR in some instances.

HR and the handling of DSBs in *C. elegans* have been mostly studied in the gonad of *C. elegans*, where the spatiotemporal ordering of germ cell proliferation, progression through meiosis into gametes, and early embryogenesis, offers great opportunities for genetic and functional analysis of DNA DSB repair (Lemmens 2011).

3.1.6 Fanconi anaemia pathway

Crosslinks between the two complementary strands of DNA pose an insurmountable obstacle for the DNA replication machinery; the blocked replication fork needs to be resolved for the replication process to resume, and cell cycle progression has to be deferred adequately. The Fanconi anaemia (FANC) factors, representing genetic complementation groups that were found in patients with the eponymous syndrome, play a crucial role in initiating and regulating repair of ICLs [reviewed in (Moldovan 2009)]. The 13 known factors structurally and functionally cluster into two main components: the FA core complex (FANCA, B, C, E, F, G, L, and M), an ubiquitin ligase, is recruited close to the lesion and in a central step monoubiquitylates the FANCI-FANCD2 complex, which in turn assembles with FANCD1, N and J to license incision and subsequent processing of the damaged DNA. One of the nucleases that are activated by monoubiquitylated FANCI-FANCD2 is FAN1. Josef Jiricny's lab, in the study presented here, showed the relevance for this novel factor in ICL repair and characterised the biochemical activity of this nuclease (Kratz 2010). In agreement with our work, three other publications (MacKay 2010; Smogorzewska 2010; Liu 2010) simultaneously demonstrated the same function for FAN1 in mammalian cells and in *C. elegans* development (MacKay 2010). Further, loss of the chicken homolog in DT40 cells was shown to sensitise towards cross-linking agents (Yoshikiyo 2010). KIAA1018/FAN1 had been found independently in the list of interactors of mismatch repair proteins and by an shRNA screen for crosslink repair mutants. Physical association of FAN1 with mismatch repair proteins has been confirmed *in vitro* (Smogorzewska 2010).

Activity of the FA branch is mainly regulated by a series of ubiquitylation events. Ubiquitination is generally emerging as a key modification in regulating the complex interaction patterns of the DNA repair network. Several of the FANC homologs and FA pathway associated factors have been found and characterised in *C. elegans*, which therefore presents a useful model to study the cellular outcomes of FA mutants (Youds 2009). With regards to ubiquitylation events, a possible link between the ubiquitin ligase BRCA1, FA factors and cellular DNA damage checkpoints is HCLK2 (Collis 2007). This factor (which, at the beginning of my PhD, I had planned to investigate in detail) had originally been discovered in *C. elegans*; *clk-2* mutants have checkpoint defects in response to various damage types, including IR irradiation (Ahmed 2001). Besides or along with its function in DNA damage responses, *clk-2* has a considerable effect on nematode lifespan.

Ubiquitination is one form of protein modification by polypeptide tags; an alternative tag is the SUMO protein; interestingly one of the few annotated interactors of *C. elegans* FAN-1 is SMO-1, which physically interacted with FAN-1 in a Y2H screen [found in Wormbase WS200, referring to (Li 2004a)]. SMO-1 is the *C. elegans* SUMO homolog; it has been shown to be important for synaptonemal complex disassembly and bivalent formation during meiosis and for reproductive system development [see Wormbase entry (Gene Summary for smo-1)]. It is an intriguing possibility that FAN1 might also be recruited to sumoylated proteins, maybe in the context of DNA repair.

3.1.7 RNA damage and repair?

When, at the beginning of my PhD, I studied the literature on DNA damage responses, I was intrigued by the complexity of the safeguard mechanisms for the genome. It is astounding how many different

types of DNA lesions can be sensed and repaired impeccably. Repair and cellular responses seem to follow immediately once cells have been exposed to genotoxic agents. As to the germ line of *C. elegans*, cells visibly react with cell cycle arrest or apoptosis. These responses have been shown to involve and depend on multiple damage response genes, many of which are known DNA repair factors. It appeared to me that therefore, damage to DNA had been tacitly assumed to be the (only) initiator for these responses. Undoubtedly, the genome as a non-dispensable, non-replaceable core of life has to be treasured and is worth the immense effort and expenditure of the survey and repair machinery. But is it the only element to be protected so eagerly? And is it the only structure that would evoke the cellular responses? Probably, it is not. Proteins are the key executioners of cellular programs; synthesis errors or damage to proteins would readily lead to (partial) loss of their function or to aberrant activity and interactions, which might threaten cellular integrity immediately and turn cells unviable or potentially harmful. Thus, protecting the proteome is essential as well. Accordingly, cellular life has evolved intricate stress response and repair programs for protein disturbances, such as heat shock and unfolded protein response, or translation survey mechanisms. All cellular macromolecules are constantly subjected to endogenous and exogenous attacks and modifications. The treatments that are usually applied to provoke DNA damage (irradiation, chemical substances) in research and in therapeutic interventions are by no means specifically damaging DNA. Rather, they cause a broad spectrum of damages in all the exposed tissue. RNA is chemically similar to DNA (yet, less stable and usually not present in cells as a double strand of two complementary molecules). Likely, RNA suffers similar types and doses of lesions as DNA when cells are exposed to genotoxic agents [review and discussion in (Wurtmann 2008); several chemical substances were tested by (Fimognari 2008)]. Most cells have probably much more RNA than DNA (mammalian cells are assumed to have an RNA:DNA ratio of approximately 4:1).

I asked myself whether cells would worry about RNA damage or whether these abundant molecules would simply be turned over and replaced; I also wondered whether the cell would make sense of RNA in case of damage. Questions that seemed interesting to me:

- (How) does the cell survey RNA damage?
- Is RNA damage problematic for cells? – at high density for short-term function? – for long-term integrity of the cell?
- What happens to damaged RNA? Is it degraded, does it accumulate? Or is it repaired?
- Can DNA repair molecules also treat RNA? Are there even any dedicated RNA repair mechanisms?
- Is there signalling from RNA lesion recognition to cellular damage responses similar to DNA damage response? And can the response go so far as to induce apoptosis?
- Might the cell, if not repair RNA damage, at least extract information from it? Might damage in the abundant RNA be sensed as a measure for the level of momentary threat to the cell, or as a surrogate for the level of DNA damage? Could it evoke cellular stress responses?

Several RNA surveillance mechanisms have been characterised, e.g., nonsense mediated decay (NMD) of mRNAs [current review of RNA decay pathways, (Houseley 2009)]. However, I found only limited literature to the other questions; most of the ferreted publications were stating that RNA damage and

repair had been a scarcely addressed issue. Yet, the ones available were fostering my theoretical considerations.

A few reviews discussed the concept of, and first indications for, RNA repair (Brégeon 2005; Drabløs 2004; Krokan 2004). They also considered how RNA damage could be relevant in human health. So far, oxidative RNA damage has been shown to be associated with neurodegenerative diseases, where it might present a causing factor (Nunomura 2007, 2009); usually, damage to RNA is higher than damage to DNA in oxidative stress conditions (Li 2006).

Some molecules have been described with catalytic activities that would make them good candidates for RNA repair factors. RNA ligases that can heal and religate broken tRNAs have been found in bacteria (Martins 2004) and recently in eukaryotes (Nandakumar 2008). Most appealing to me was the discovery of RNA repair activity of the bacterial de-alkylating enzyme AlkB and of some of its mammalian homologs, human hABH3 (Aas 2003; Falnes 2004) and murine mAbh2/mAbh3 (Lee 2005). These enzymes can remove base-adducts from RNA directly by oxidative demethylation.

I planned to embark on the raft of RNA repair research and started to work with AlkB homologs as I will shortly describe below. Also attractive seemed the ribosomal protein S3, which has reported binding and repair capacity for different DNA base lesions (e.g. 8-oxoG), and which can induce apoptosis [see *4.1.4.3 DNA damage response might involve the nucleolus*]; its close interaction with RNA as part of the translation apparatus offered the interesting possibility of a link between RNA damage and cellular responses.

Up to now, evidence for cell cycle arrest or apoptotic response that would be directly induced by damaged mRNA is limited. Onconase, a cytotoxic RNase mainly cutting tRNA, had been in evaluation as a therapeutic molecule; it was shown to induce apoptosis in mammalian cells independently of p53 (Iordanov 2000). Recently, the NMD-factor SMG1 was shown to activate p53 – however, in response to DNA double strand breaks and not in response to exogenously oxidized RNA (Gewandter 2011).

RNA in DNA repair?

The numerous repair pathways indicate that cells have developed mechanisms to deal with chemically diverse damage types, often by employing excision and resynthesis of DNA from an optimally matching template. I guessed that cells might use yet more resources when protecting the hereditary code. In case of ambiguities about the pre-damage code in acutely damaged DNA, would it make sense to consult some instance that could know? If DNA breaks at a relaxed – e.g., actively transcribed – site and the ends become fuzzy, how to fill the gap if no sister strand is readily available? Possibly, not all potential templates are lost: RNA that had been transcribed before the damage occurred might still carry the due information.

Considering the theory that an RNA world preceded the DNA world (Poole 2005; Müller 2006) and the many instances of reverse transcription in biology (e.g., retroviruses, retro-transposons), it is not unlikely that a mechanism for RNA-templated DNA repair has evolved in at least some systems. Findings in plants that hint to reversion of genome-wide sequence changes by extra-genomic hereditary information [(Lolle 2005) with author replies, and (Xu 2007)], and recent evidence in yeast (Storici 2007) support such ideas.

3.1.7.1 Preliminary investigation: AlkB in direct repair of DNA and RNA

AlkB had long been recognised as a bacterial repair factor of alkylation damage in *E. coli*; bioinformatic prediction that AlkB defined a new family of 2-oxoglutarate- and iron-dependent dioxygenases suggested that it catalysed oxidative detoxification of alkylated bases (Aravind 2001); this was experimentally confirmed by two groups [(Trewick 2002; Falnes 2002), reviewed in (Jiricny 2002)]. Analysis of the substrate specificity of AlkB and of two of the human homologs revealed that AlkB and hABH3 preferentially acted upon ssDNA; and that they could also de-alkylate methylated RNA (Aas 2003; Falnes 2004). Similar activity was later demonstrated for Abh2 and Abh3 in mice (Lee 2005) and for viral AlkB (van den Born 2008). [Review on DNA and RNA repair by AlkB homologs (Falnes 2007) and short review of alkylation damage in (Kondo 2010).]

C. elegans has multiple, non-essential AlkB homologs

I set out to study the *C. elegans* homologs of human hABH1 to hABH8. I intended to test them for involvement in apoptosis induction upon treatment of the worms with genotoxic agents; possibly, they were required for the apoptotic response of germ cells upon MMS treatment. If so, I would use them as a starting point to find potential RNA repair activity. Some *C. elegans* orthologs of the human ABH1/4/6/7/8 had been identified by (Drabløs 2004), and I found two additional factors with high sequence similarity to CeABH1 and CeABH8 (Table 1). There seemed, however, not to be any *C. elegans* orthologs for human ABH2, ABH3 and ABH5. I prepared RNAi constructs to target the seven predicted AlkB homologs. Following a quest at the CGC, mutants became available later for the ABH4 and ABH7 homologs F09F7.7 and Y46G5A.35 (alleles *ok3133* and *ok3697*). So far, I have not carried the experiments beyond an initial analysis of viability and baseline levels of germ cell death; these did not obviously differ from wildtype.

In the meantime, the human AlkB homologs have attracted wide interest; the molecular mechanistics of some of the homologs have been characterised; other studies have shown association of ABH2, ABH3 and ABH8 with different types of cancer (Gao 2011; Tasaki 2011; Shimada 2009).

H. sapiens	Accession	*C. elegans*	Accession	% Identity	Comment
ABH1	Q13686	Y51H7C.4	NP_493970.1	28%	
		Y51H7C.5	NP_493969.3	27%	homology to Y51H7C.4
ABH2	Q6NS38				not identified
ABH3	Q96Q83				not identified
ABH4	Q9NXW9	F09F7.7a	NP_741141.1	32%	
ABH5	Q6P6C2				not identified
ABH6	Q3KRA9	B0564.2	NP_502522.1	36%	
ABH7	Q9BT30	Y46G5A.35	NP_001022442.1	36%	
ABH8	Q96BT7	C14B1.10	NP_497751.1	27%	protein contains putative methyl transferase domain
		C35D10.12	NP_498018.1	26%	best matching homolog of C14B1.10

Table 1 Putative *C. elegans* homologs of human ABH1 to ABH8. Similarity is calculated from an alignment of the human and *C. elegans* proteins (% Identity, BLOSUM62). Table is partially based on (Drabløs 2004); Y51H7C.5 and C35D10.12 were identified as best matching paralogs to Y51H7C.4 and C14B1.10, respectively, in Wormbase.

3.2 NER and HR pathways act sequentially to promote UV-C-induced germ cell apoptosis in *Caenorhabditis elegans*

3.2.1 Paper frontpage

Cell Death and Differentiation (2010), 1–10

www.nature.com/cdd

NER and HR pathways act sequentially to promote UV-C-induced germ cell apoptosis in *Caenorhabditis elegans*

L Stergiou[1,3,4], R Eberhard[1,2,4], K Doukoumetzidis[1] and MO Hengartner[*,1]

Ultraviolet (UV) radiation-induced DNA damage evokes a complex network of molecular responses, which culminate in DNA repair, cell cycle arrest and apoptosis. Here, we provide an in-depth characterization of the molecular pathway that mediates UV-C-induced apoptosis of meiotic germ cells in the nematode *Caenorhabditis elegans*. We show that UV-C-induced DNA lesions are not directly pro-apoptotic. Rather, they must first be recognized and processed by the nucleotide excision repair (NER) pathway. Our data suggest that NER pathway activity transforms some of these lesions into other types of DNA damage, which in turn are recognized and acted upon by the homologous recombination (HR) pathway. HR pathway activity is in turn required for the recruitment of the *C. elegans* homolog of the yeast Rad9-Hus1-Rad1 (9-1-1) complex and activation of downstream checkpoint kinases. Blocking either the NER or HR pathway abrogates checkpoint pathway activation and UV-C-induced apoptosis. Our results show that, following UV-C, multiple DNA repair pathways can cooperate to signal to the apoptotic machinery to eliminate potentially hazardous cells.
Cell Death and Differentiation advance online publication, 10 December 2010; doi:10.1038/cdd.2010.158

Eukaryotic cells possess several surveillance mechanisms that, upon sensing DNA damage, initiate signaling cascades that lead to response programs such as cell cycle arrest, DNA repair and apoptosis, to protect the organism against the introduction of new mutations. Disruption of such pathways results in increased genomic instability, a hallmark of most types of cancers.[1,2]

Genetic and biochemical studies have provided a thorough mechanistic understanding of the various repair processes initiated upon recognition of specific types of lesions. For example, the nucleotide excision repair (NER) pathway removes cyclobutane pyrimidine dimers (CPDs) and 6-4 photoproducts generated upon exposure to ultraviolet (UV-C) light, whereas the homologous recombination (HR) machinery repairs double-strand DNA breaks (DSBs) induced by treatments such as ionizing radiation (IR).[3]

Mutations in NER components underlie the syndromes xeroderma pigmentosum (XP), trichothiodystrophy or Cockayne syndrome. Patients are hypersensitive to sunlight and exhibit a variety of clinical features, including developmental defects, predisposition to skin cancer or internal tumors, neurological disorders and highly accelerated aging.[4] Studies in cell culture and mouse models,[5,6] as well as in yeast have led to the detailed molecular characterization of the NER factors.[3] Besides repair, many of these factors participate in the signaling network that ultimately balances cellular DNA damage responses between genome maintenance, senescence and death. Accordingly, loss of their function has consequences for DNA repair, cellular proliferation and survival.[6–8]

Simple model organisms are very useful to decipher complex DNA damage responses. In *Caenorhabditis elegans*, the effects of IR have been studied extensively.[9,10] We previously reported a genetic pathway that induces both apoptotic cell death of meiotic cells and cell cycle arrest of proliferating mitotic cells following UV-C treatment.[11] We identified several new genes required for these responses and genetically ordered them into a signaling pathway that overlaps with, but is distinct from the pathway(s) activated upon IR.

In this study, we investigate the molecular mechanism by which UV-C triggers apoptosis in the *C. elegans* adult hermaphrodite germ line. We show that lesions caused by UV-C are not pro-apoptotic *per se*; rather, they first require processing by the NER machinery before they can activate apoptosis. A fraction of UV-C lesions is likely transformed by NER into DNA intermediates that are substrates for the HR machinery. Activation of the latter, in turn, leads to recruitment of the *C. elegans* homolog of the yeast Rad9-Hus1-Rad1 (9-1-1) complex, activation of downstream checkpoint kinases

[1]Institute of Molecular Life Sciences, University of Zurich, Winterthurerstrasse 190, Zurich 8057, Switzerland and [2]PhD Program in Molecular Life Sciences, Life Science Zurich Graduate School and MD/PhD Program, University of Zurich, Zurich, Switzerland
*Corresponding author: MO Hengartner, Institute of Molecular Life Sciences, University of Zurich, Winterthurerstrasse 190, Zurich 8057, Switzerland. Tel: +41 44 635 3140; Fax: +41 44 635 6861; E-mail: michael.hengartner@imls.uzh.ch
[3]Current address: Pike Pharma, Schlieren-Zurich, Switzerland.
[4]These authors contributed equally to this work.
Keywords: apoptosis; *C. elegans*; HR; NER; UV-C
Abbreviations: UV-C, ultraviolet light C (254 nm); IR, ionizing radiation; CPDs, cyclobutane pyrimidine dimers; DSB, double-strand DNA break; NER, nucleotide excision repair; HR, homologous recombination; 9-1-1 complex, Rad9-Hus1-Rad1 complex (HPR-9/HUS-1/MRT-2 in *C. elegans*); XPA, XPB, XPD, XPF, XPG, xeroderma pigmentosum complementation group A, B, D, F, G; RPA-1, replication protein A large subunit homolog in *C. elegans*
Received 06.5.10; revised 07.9.10; accepted 20.9.10; Edited by E Baehrecke

See full paper in Appendix A-325

3.2.2 Additional experiments and observations

3.2.2.1 Repair kinetics of CPD lesions

In our studies of the cross-talk from the nucleotide excision repair (NER) pathway to homologous recombination (HR), we wanted to examine repair of UV-typical lesions in HR pathway mutants. We aimed at a system that would allow to quantitatively assess repair over time in different mutants, possibly at different conditions and treatments. Ideally, it should be applicable to testing different types of lesions. Importantly, it should imply a step to denature DNA, since many of the detection tools recognize this form only.

Specific antibodies are available for certain DNA lesions, such as an antibody detecting cyclobutane pyrimidine dimers (CPDs) (Torizawa 2000) or one specifically binding the pyrimidine (6-4) pyrimidone photoproducts (6-4 PP) (Yokoyama 2000). The Dot-Blot system is a means to transfer up to 96 samples synchronously onto a membrane that subsequently is incubated with a probe of interest. The resulting signals can be captured and measured in a rapid way thanks to the regular pattern of the 96-well format. I tried to establish an assay that would measure UV-C lesions in DNA from irradiated worms in this large-scale format. It should bring the following steps in a pipeline: irradiation of adult worms, collection at different time points after treatment, extraction of DNA, denaturation (Komatsu 1997), transfer by the Dot-Blot apparatus, and detection with lesion specific antibodies or with loading controls [see *8.2.7 Dot-Blot protocol for CPD lesions*]

The NER mutants *xpa-1(ok698)* and *xpg-1(tm1682)* have minimal repair

Initially, I tested the early time points after irradiation (0-2 hours); there was no clear trend, the normalized CPD signals were bouncing within about 20 % of the mean. We acknowledged that in correspondence with other systems that we mention in the paper, an extended time course of at least 12 hours would be more realistic to reliably detect CPD repair. One of the confounding factors to consider here was that over time, there was not only repair of CPD lesions, but also some degree of "CPD dilution"; DNA was being replicated in the developing embryos that continuously replaced advanced embryos with damaged genomes inside the adults (replication by stem cell proliferation is mostly halted by the UV-C-induced cell cycle arrest). Averaged over repeated experiments, we detected decay in the CPD signal intensity over time that was more rapid in wildtype N2 than in the NER mutants *xpa-1(ok698)* or *xpg-1(tm1682)*. Assuming a first order decay, the half time was approximately 15 hours for N2 (Figure 3), which was in the same order as the 11 hours we calculated from the immunofluorescence experiments.

Of note, the levels of initial CPD lesions were lower in *xpa-1(ok698)* mutants than in wildtype despite the same UV-C dose. We got a similar result with in-situ staining of CPDs in the germ line. If this were not due to experimental errors, this would indicate that *xpa-1(ok698)* mutants are less prone to form pyrimidine dimers upon UV-C. Possibly, the involvement of XPA-1 in transcription and maybe in chromatin structure conforms the DNA such that it is less prone to building the very CPD dimers upon UV-C.

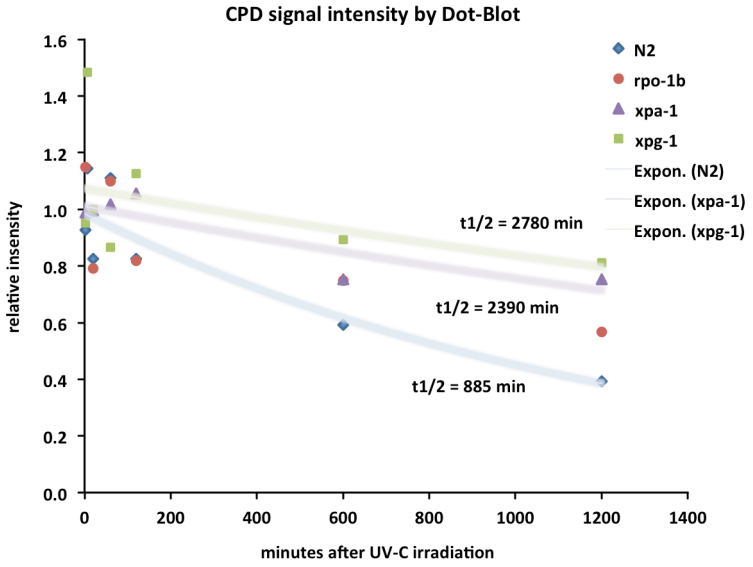

Figure 3 CPD levels in DNA extracted from adult worms (normalised to rDNA signal, see *8.2.7* Dot-Blot protocol for CPD lesions). N2 wildtype or NER mutant worms were irradiated with 200 J/m2 UV-C and dispersed to individual plates for collection at different time points after irradiation. Dots represent average relative intensity compared to the initial CPD signal (6 min post UV-C treatment). The trendlines assume an exponential decay of the signal intensity. N2 and *xpg-1*, 4 experiments for most timepoints; *rpo-1b* and *xpa-1*, one experiment.

3.2.2.2 Immunofluorescence for *in situ* detection of CPDs in the germ line

The Dot-Blot technique had allowed to approximate repair kinetics in wildtype adults and to demonstrate longer persistence of CPD lesions in NER mutants. However, the method required a considerable number of worms and determined CPD signals in whole animals only; to distinguish germ line specific repair from total repair, one would have to use a genetic background that causes a conditional lack of germ line tissue and indirectly calculate germ line specific repair by subtraction. Another hurdle would be imposed by the fact that HR mutants like *mre-11(ok179)* or *rad-54(ok615)* were homozygous sterile and therefore had to be balanced. For the experiment, huge numbers of homozygous worms would have to be selected manually from the balanced population.

We therefore decided to work out and optimize an immunofluorescence staining protocol that would allow to measure CPD lesion density in germ cells in situ, and to derive repair kinetics of this UV-C lesion in germ lines of different worm strains, as described in the above work.

3.2.2.3 Marker for DSBs

In our study, we demonstrated the involvement of the HR pathway upon UVC irradiation. We showed the formation of RAD-54 and RAD-51 foci in UVC-irradiated germ lines. One of the plausible theories was the conversion of UV-induced single-strand DNA lesions into intermediates that would in turn become substrates of the HR pathway components. Likely, these intermediates were DNA double strand breaks, since double strand breaks are the known targets of RAD-54 and RAD-51 binding. We were asked by reviewers to give (additional) evidence that the hypothesised intermediates were indeed DSBs. We assembled a candidate list of additional well-established DSB markers from mammalian systems, which comprised γH2AX, MDC1, 53BP1, BRCA1, MCPH1, NBS1, MRE11, RAD50, (Phospho-ATM). For none of the *C. elegans* homologs of these factors there were any worm-specific antibodies available,

nor reports that showed cross-reaction of antibodies to the mammalian proteins with the worm homologs. Based on the report on BRD-1, homolog of BARD1 which was also shown to bind DSBs (Boulton 2004b), we decided to build a transgenic YFP::BRD-1 to trace DSBs in live animals.

YFP::BRD-1 localises to chromatin

YFP::BRD-1 was nicely expressed in germ cells of more than two independent transgenic lines. Fluorescence was congruent with the chromatin pattern in meiotic pachytene cells (Figure 4). Some late meiotic pachytene cells and early oocytes had focally intense fluorescence. It seems that these foci are at the extremes of the condensed, linear chromosomes. While exciting by itself, the transgenic fluorescence pattern did not help to highlight sites of DNA DSB repair following irradiation. At 3 hours after IR, there was no obvious neo-formation of foci in germ cells; later time points did not show a difference, either.

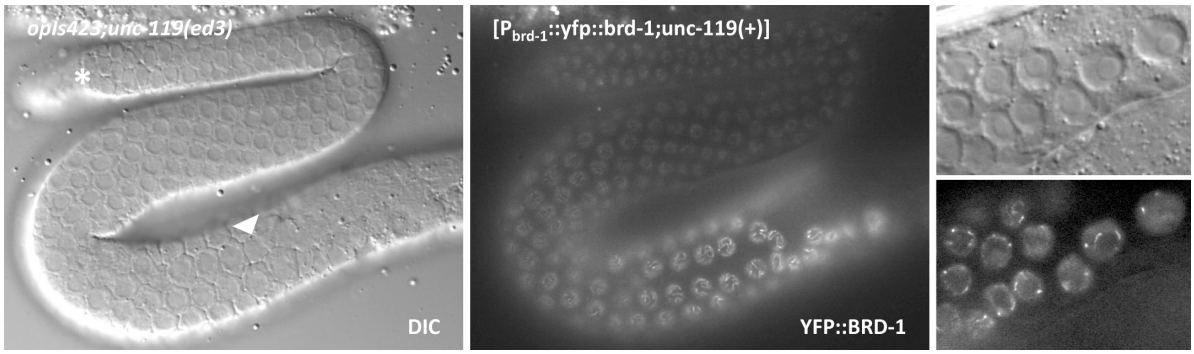

Figure 4 YFP::BRD-1 expression pattern in the dissected germ line of a non-irradiated adult worm. (*) distal end, (triangle) late meiotic pachytene cells. Small pictures show telomeric YFP-foci in late meiotic pachytene cells and oocytes of an intact adult worm.

Immunostaining for BRD-1

We doubted the absence of foci formation and wanted to double-check our observation with immunostaining of BRD-1. The antibody to BRD-1 (Boulton 2004b) did not work for us the way it was described; we got focal fluorescence in distal germ cells of non-irradiated animals; upon irradiation, there was no significant increase in the number of these foci.

Given that the two markers of BRD-1 did not distinguish IR irradiated from non-irradiated germ cells, we did not follow the strategy of DSB detection any further. Only, when we realised the importance of the transgenic background *unc-119(ed3)*/*unc-119(tg+)* for germ line phenotypes [see *6.2.1 unc-119 in transgenic lines*], we tested transgenic YFP::BRD-1 again in a line where *unc-119(ed3)* had been outcrossed; the fluorescence pattern did, however, not change.

3.3 Deficiency of FANCD2-Associated Nuclease KIAA1018/FAN1 Sensitizes Cells to Interstrand Crosslinking Agents

3.3.1 Paper frontpage

Cell

Deficiency of FANCD2-Associated Nuclease KIAA1018/FAN1 Sensitizes Cells to Interstrand Crosslinking Agents

Katja Kratz,[1,4] Barbara Schöpf,[1,4] Svenja Kaden,[1,4] Ataman Sendoel,[2] Ralf Eberhard,[2] Claudio Lademann,[1] Elda Cannavó,[1,5] Alessandro A. Sartori,[1] Michael O. Hengartner,[2] and Josef Jiricny[1,3,*]
[1]Institute of Molecular Cancer Research, University of Zurich
[2]Institute of Molecular Life Sciences, University of Zurich
[3]Department of Biology
ETH Zurich, Winterthurerstrasse 190, 8057 Zurich, Switzerland
[4]These authors contributed equally to this work
[5]Present address: Department of Microbiology, University of California, Davis, CA 95616-8665, USA
*Correspondence: jiricny@imcr.uzh.ch
DOI 10.1016/j.cell.2010.06.022

SUMMARY

Cytotoxicity of cisplatin and mitomycin C (MMC) is ascribed largely to their ability to generate interstrand crosslinks (ICLs) in DNA, which block the progression of replication forks. The processing of ICLs requires the *Fanconi anemia* (FA) pathway, excision repair, and translesion DNA synthesis (TLS). It also requires homologous recombination (HR), which repairs double-strand breaks (DSBs) generated by cleavage of the blocked replication forks. Here we describe KIAA1018, an evolutionarily conserved protein that has an N-terminal ubiquitin-binding zinc finger (UBZ) and a C-terminal nuclease domain. KIAA1018 is a 5′→3′ exonuclease and a structure-specific endonuclease that preferentially incises 5′ flaps. Like cells from FA patients, human cells depleted of KIAA1018 are sensitized to ICL-inducing agents and display chromosomal instability. The link of KIAA1018 to the FA pathway is further strengthened by its recruitment to DNA damage through interaction of its UBZ domain with monoubiquitylated FANCD2. We therefore propose to name KIAA1018 FANCD2-associated nuclease, FAN1.

INTRODUCTION

The *Fanconi anemia* (FA) pathway (Figure 1A) plays a key role in interstrand crosslink (ICL) metabolism in higher eukaryotes by coordinating S phase arrest and DNA repair (Moldovan and D'Andrea, 2009; Thompson and Hinz, 2009). Replication fork blockage activates the ataxia telangiectasia and RAD3-related (ATR) kinase (Pichierri and Rosselli, 2004), which phosphorylates members of the FA core complex (Meetei et al., 2003) composed of FANCA, B, C, E, F, G, L, and FAAP100. The activated complex then associates with FANCM-FAAP24, a DNA translocase (Gari et al., 2008), which activates the E3 ligase FANCL that subsequently ubiquitylates FANCD2-FANCI (Thompson and Hinz, 2009). The latter posttranslational modifications license the processing of the blocked replication fork (Figure 1A), which involves pausing of the fork, incision, lesion unhooking, translesion DNA synthesis (TLS), and homologous recombination (HR) (Moldovan and D'Andrea, 2009). FANCJ, a 5′→3′ DNA helicase, appears to be involved in the late stages of ICL repair (Bridge et al., 2005). Its action would give rise to 3′ flaps, preferred substrates of both endonucleases implicated in ICL processing to date, MUS81/EME1 and XPF/ERCC1.

Recently, several laboratories found interaction between FA proteins and polypeptides involved in mismatch repair (Peng et al., 2007; Zhang et al., 2002). Our analysis of the MLH1 interactome (Cannavo et al., 2007) identified FANCJ among the strongest interactors. Another strong MLH1 interactor was KIAA1018, a hypothetical protein predicted (Kinch et al., 2005; Kosinski et al., 2005) to contain a RAD18-like ubiquitin-binding zinc finger near its N terminus and a C-terminal endonuclease domain. Given the importance of ubiquitylation in the FA pathway (Moldovan and D'Andrea, 2009), and the fact that the putative endonuclease domain of KIAA1018 belongs to the same enzyme superfamily as those present in MUS81 and XPF, we asked whether KIAA1018 is related to FA and how mismatch repair (MMR) might be linked to this branch of DNA repair. Hence, we decided to characterize KIAA1018 and to study its role in DNA metabolism. We now show that KIAA1018 is a nuclease involved in the processing of mitomycin C (MMC)- and cisplatin-induced DNA damage, to which it is recruited by ubiquitylated FANCD2.

RESULTS

KIAA1018 Contains Evolutionarily Conserved Zinc Finger and Endonuclease Domains

Analysis of MLH1 and PMS2 interactomes (Cannavo et al., 2007) identified several peptides originating from the human *KIAA1018* open reading frame (ORF), which encodes a polypeptide of 1017

See full paper in Appendix A-325

3.3.2 Personal contributions and further experiments

Together with Ataman Sendoel, we addressed the role of the KIAA1018 homolog C01G5.8 in DNA damage response of the *C. elegans* germ line. We tested apoptosis and embryonic survival following treatment with cisplatin, or with IR or UV-C. Ataman had routinely worked with cisplatin and performed the cisplatin experiments, and I performed the irradiation experiments. I tested the C01G5.8*(tm423)* strain and did most of the genetic crosses; Ataman made the transgenic line expressing the GFP-tagged FAN-1.

3.3.2.1 *fan-1(tm423)* mutants and double mutants are viable

Josef Jiricny suggested that we try to confirm the observations on KIAA1018 from mammalian and avian cells in *C. elegans*. Luckily, a deletion allele of the KIAA1018 homolog in *C. elegans* was available from the NBRP (Mitani 2010). The allele C01G5.8*(tm423)* was annotated as being homozygous lethal, though; this would profoundly complicate studies of DNA damage-induced embryonic lethality and of germ line phenotypes. On the other hand, the C01G5.8 gene had not been found to be essential in large-scale RNAi screens for sterility or lethality. We detected that the strain in which the allele came was homozygous for *tm423* and that it was perfectly viable. The worms had no obvious defects and looked wildtype overall. Also, RNAi by feeding to C01G5.8 did not obviously affect animal health.

Some double mutants that we crossed for future analysis: *brc-1(tm1145); fan-1(tm423)*, *fcd-2(tm1298) fan-1(tm423)*, and *xpg-1(tm1682); fan-1(tm423)* were all viable. (It would be interesting to also test the double mutant with *clk-2*.)

3.3.2.2 cisplatin-induced germ cell apoptosis is blocked in *fan-1(tm423)*

Germ cell apoptosis is often altered in DNA repair mutants. In several loss-of-function conditions, DNA damage-induced apoptosis is abolished (e.g., *atm-1*, *atl-1*, *hus-1*, *mrt-2*, *clk-2*, *cep-1*); another group of mutants has increased baseline levels in the absence of exogenous DNA damage (*xpa-1*, *rad-54*, *brc-1*, *brd-1*, or the FANCJ homolog *dog-1*), with additional exogenous DNA damage-induced apoptosis being blocked (*xpa-1*, *rad-54*), normal (*dog-1*) or also increased (*brc-1*, *brd-1*) [overview and references in *5.3.1 The role of CEP-1 in DNA damage-induced apoptosis*]. We were interested in apoptosis levels of *fan-1(tm423)* at baseline, in response to irradiation and in response to the crosslinking agent cisplatin. Baseline apoptosis levels were similar to wildtype. Together with the low embryonic lethality of non-treated worms, this indicated that there was no massive increase in endogenous DNA lesions in *fan-1(tm423)*. In agreement with a role for *fan-1* in response to ICLs, DNA damage-induced apoptosis was selectively blocked upon cisplatin treatment [Ataman Sendoel]. This attributed a pro-apoptotic function to *fan-1*. Upon irradiation with IR, apoptosis was not different from wildtype, as had been the case for embryonic lethality. Interestingly, the apoptotic response to UV-C irradiation was not fully wildtype (Figure 5). The germ cell corpse number after irradiation increased initially, but dropped below wildtype at later time points. So far, we don't know the significance of this partial defect.

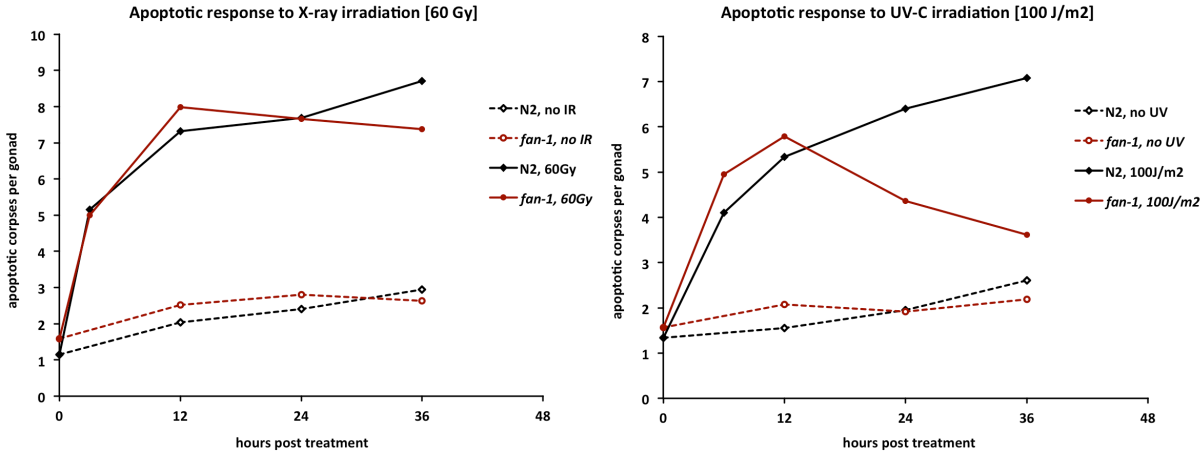

		no IR		30 Gy		60 Gy		120 Gy		no UV		100 J/m2	
		score	95% CI (n)	score	95% CI (n)	score	95% CI (n)	score	95% CI (n)	score	95% CI (n)	score	95% CI (n)
N2	0 h	1.15	±0.25 (60)							1.33	±0.25 (60)		
	3 h					5.15	±0.52 (20)					4.10	±1.33 (20)
	12 h	2.04	±0.40 (52)			7.69	±0.68 (67)			1.56	±0.24 (72)	5.33	±0.43 (60)
	24 h	2.41	±0.51 (59)	8.50	±1.55 (20)	8.71	±0.67 (68)	10.90	±1.35 (20)	1.95	±0.39 (59)	6.40	±0.78 (45)
	36 h	2.95	±0.61 (57)			8.72	±0.75 (58)			2.60	±0.52 (53)	7.08	±0.80 (52)
fan-1(tm423)	0 h	1.59	±0.22 (78)							1.57	±0.24 (60)		
	3 h					5.00	±0.75 (20)					4.95	±0.99 (20)
	12 h	2.53	±0.29 (78)			7.99	±0.76 (80)			2.07	±0.24 (67)	5.78	±0.78 (60)
	24 h	2.80	±0.37 (75)	7.50	±1.53 (20)	7.66	±0.66 (83)	9.30	±1.08 (20)	1.91	±0.26 (56)	4.36	±0.45 (53)
	36 h	2.63	±0.36 (73)			7.37	±0.64 (70)			2.19	±0.37 (53)	3.62	±0.42 (52)

Figure 5 Time courses of germ cell apoptosis in *fan-1(tm423)* mutants following irradiation with IR or UV-C. Data table shows average number of apoptotic corpses per gonad (score), 95% CI of the mean, and the total number (n) of worms scored for each condition.

3.3.2.3 Immunofluorescence staining of *fcd-2*

We planned to confirm epistasis of *fan-1* with the Fanconi anaemia pathway using an antibody to the FANCD2 homolog (Collis 2006). Normal formation of *fcd-2* foci would have indicated intact recruitment of the FANC complex to damage sites and would have made it unlikely that *fan-1* acted upstream. Possibly, if *fan-1* acted downstream of *fcd-2* in DNA repair, non-resolved lesions would persist as FCD-2 associated foci.

We failed to reproduce the immunofluorescence pattern that was reported for the anti-FCD-2 antibody and did not proceed with this approach.

4 Ribosome synthesis and DNA damage-induced apoptosis are reduced in *rpo-1b(op259)*, a novel mutant of RNA polymerase I

Based on a newly isolated mutant from a forward genetic screen, *op259*, I investigated the role of RNA polymerase I in germ cell apoptosis. Worms carrying a mutation in the gene coding for the β-subunit of RNA pol I (which we provisionally designated as *rpo-1b*) had been found to be deficient in DNA damage-induced germ cell death. RNA pol I is the transcription complex dedicated to synthesis of ribosomal RNAs.

Initially, I was attracted by the fact that an RNA processing machinery should link to apoptosis. I then became increasingly aware of the emerging role for the nucleolus and for ribosome synthesis in cellular homeostasis, which included adaptation to environmental changes and stress responses. Nucleoli were smaller in *rpo-1b(op259)* than in wildtype, and rRNA levels were preliminarily shown to be reduced. A then newly published study in mammalian cells demonstrated significant changes of RNA pol I transcription upon local irradiation of nucleoli, dependently on the DNA damage activated kinase ATM (Kruhlak 2007). This further motivated me to study the connection of rRNA synthesis and damage response in *C. elegans*, in the context of a whole organism. The *op259* mutation had pleiotropic effects, yet the worms were viable; therefore, the *rpo-1b(op259)* mutant offered a great means to investigate disturbances in the essential process of ribosome synthesis in a living system.

It was important to assess whether the observed phenotypes of *rpo-1b(op259)* resulted from a specific function of this particular RNA pol I subunit in the underlying molecular DNA damage response network, or whether they arose more generally as a consequence of altered transcription or processing of ribosomal RNA. Applying various methods, I quantified rRNA transcription and ribosomes, which were both reduced in the mutant. Further, I found differences in rRNA processing. Ribosomal RNA levels, and rRNA transcription and processing show some response to irradiation treatment of the worms; interestingly, the mutant responds differently to irradiation in several aspects. I found that other mutants of rRNA synthesis and processing factors reproduced the defect in the apoptotic response to irradiation, speaking for a wide involvement of ribosome synthesis in DNA damage response.

The work on *rpo-1b(op259)* is split into two chapters. This first part gives an introduction on rRNA and ribosome synthesis, and on the role of the nucleolus and of ribosomes in regulating various stress responses. I characterise the *op259* mutation; its effects on rRNA production; and the effects of alterations in ribosome synthesis on DNA damage-induced apoptosis. The second chapter describes the various phenotypes of the mutant and relates *rpo-1b(op259)* to key components of germ cell apoptosis; it further presents insights into general aspects of apoptosis regulation, which to discover *rpo-1b(op259)* has been very instructive for.

Chapter 4

4.1 Introduction to rRNA and ribosome synthesis

4.1.1 DNA-dependent RNA polymerases

Eukaryotic cells have three distinct polymerases to transcribe RNA from nuclear genomic DNA. RNA pol I transcribes the pre-rRNA, precursor for the 18S, 5.8S and 28S ribosomal RNAs. RNA pol II is responsible for mRNAs, most snRNAs and for microRNAs. RNA pol III transcribes all tRNAs, the ribosomal 5S rRNA, and other small RNAs. The polymerases have high substrate specificity, which is at least partly conferred by distinct promoter signals. The three polymerases are composites of several shared subunits with distinct, mostly paralogous factors (Table 7). Details are introduced in *4.6.1 RNA polymerase subunits and apoptosis*.

4.1.2 The nucleolus in health and disease

Aberrant nucleoli were among the first recognised hallmarks of cancer. The nucleolus is a prominent feature within the interphase nucleus and site of a very basic cellular process, rRNA synthesis and ribosome assembly. Hypertrophic and irregularly shaped nucleoli were reported to be characteristic of malignant cells already at the end of the 19th century (Montanaro 2008); these features gained increasing interest in tumor pathology and became an established prognostic marker for cancer progression. AgNORs – silver stained nucleoli (through strongly argyrophilic nucleolar components (Derenzini 2000)) – have a high prognostic value for several human neoplasias, sometimes excelling many other predictive factors for tumor growth, patient survival, or therapeutic response (Pich 2000). Large nucleoli and increased ribosome biogenesis form a common signature of proliferating cells; the increased demand for protein synthesis requires upregulation of ribosome production. It has therefore been challenging to explore whether nucleolar hypertrophy in cancer cells is a mere expression of rapid proliferation and consequently increased ribosome synthesis, or whether the enlarged nucleoli could play a causative role in tumor development (Montanaro 2008).

Given the long history of research on the nucleolus [short review in (Lo 2006)], revelations on the nucleolus as an integrative compartment for cellular proliferation, growth and death are relatively recent. By now, they have become vast and place the nucleolus at the crossroads of cellular metabolism, cell cycle regulation, growth control, cellular stress responses, aging, and cell death (Boisvert 2007). Many of the regulatory processes are associated with rRNA transcription and processing, with ribosome assembly, or with ribosomal proteins.

The nucleolus, organised by, and hosting ribosomal rRNA synthesis and ribosome assembly (Sirri 2008), is a central hub that has been approached from different angles. The major signalling pathways of cellular growth and proliferation have been shown to largely influence ribosomal synthesis [reviewed in e.g., (Ruggero 2003; Grummt 2003)]. On the other side, physiological or pathological changes in rRNA synthesis, nucleolar integrity, and ribosome synthesis affect cellular fate decisions; not only as a consequence of altered protein translation, but also more directly through regulatory signalling by these components [discussed below; articles and reviews, (Rubbi 2003a; Ruggero 2003; Montanaro 2008)]

4.1.3 Control of rRNA and ribosome synthesis by regulatory pathways

Synthesis of ribosomal RNA accounts for up to 75 % of total transcriptional activity in yeast (Rudra 2004); at least 50 % of the synthetic effort of rapidly proliferating eukaryotic cells is expended on ribosome production (Moss 2004). It is therefore not surprising that this process is tightly regulated and fully integrated into basic cellular signalling. Ribosomal synthesis rate has a large regulatory range and it responds to changes in cellular metabolism very quickly and flexibly [e.g., (Suthers 2007)]. Transcription by RNA pol I is probably the most rate-limiting step in the production of ribosomes (Chédin 2007; Laferté 2006a) and is the main target of signals activated by the metabolic state or cell cycle stage, either by direct effects on transcription or by epigenetic modifications (Grummt 2010).

Ribosomal RNA transcription is coordinated with cell cycle regulation and growth signals. The tumor suppressor Rb directly represses rRNA synthesis by inhibiting transcription initiation (Cavanaugh 1995). Another prime tumor suppressor, p53, can also inhibit rRNA transcription by blocking the assembly of transcription competent RNA pol I on the rDNA promoter (Zhai 2000). Growth factor signalling through the MAP kinase ERK activates rRNA transcription (Stefanovsky 2001). The oncoprotein Myc, a transcription factor that increases expression of ribosomal and nucleolar proteins [reviewed in (Ruggero 2003).], can also directly activate RNA pol I transcription. It coordinately regulates the three RNA polymerases to enhance ribosome synthesis [commented in (Oskarsson 2005)]. Similarly, mTOR regulates all three RNA polymerases to adjust protein biosynthetic capacity to nutrient availability (Mayer 2006). Further signals that report on the cellular metabolic status seem to impact on rRNA transcription initiation; e.g., hypoxia and the resulting cellular acidosis engage the ubiquitin ligase VHL (Von-Hippel-Lindau) to downregulate rRNA transcription (Mekhail 2006).

The nucleolus is a highly frequented platform during viral infection. Several viral components were shown to modulate ribosome synthesis, possibly favouring viral replication [reviewed in (Hiscox 2002), summary table in (Greco 2009)]. Also, *Mycobacterium tuberculosis* CarD was shown to be an essential regulator of rRNA transcription for bacterial persistence in the host cell (Stallings 2009). Cellular growth regulators and pathogenic organisms adjust the costly but potent basis of protein synthesis to the needs.

4.1.4 Control of cell fate by the nucleolus and ribosomes

The 21st century reviews the nucleolus under stress; it has emerged as a central regulatory component of cellular stress responses [reviewed in (Olson 2004), extended in (Mayer 2005; Boulon 2010)]. Nucleolar disruption has been considered a major hallmark of cellular stress; it occurs upon disturbances of rRNA and ribosome synthesis, but it is also an essential part of cellular response to many types of stress that are not primarily linked to ribosome synthesis [(Rubbi 2003b) and discussion in (Olson 2004)].

4.1.4.1 p53 is activated by nucleolar pathways

A key function is attributed to regulation of p53 stability by nucleolar integrity or nucleolar disintegration [reviewed in (Boulon 2010)]. Different nucleolus-mediated mechanisms are at work that collaboratively fine-tune p53 levels and localisation. p53 activity is regulated by innumerable posttranslational modifications (Kruse 2009). Very important in grading the effects of p53 is its turnover. Ubiquitination directs the protein to rapid degradation by the proteasome and keeps levels of p53 low in

non-stress conditions. A crucial ubiquitin ligase for, and negative regulator of, p53 is Mdm2. (Mdm2 is, however, not the only ubiquitin ligase for p53, and differential ubiquitination has other effects on p53 function besides degradation (Lee 2010a).) The interaction of Mdm2 with p53 is controlled by the tumor suppressor ARF ($p19^{ARF}$); ARF is a nucleolar protein. According to an initial model, ARF could be sequestered in the intact nucleolus, be released upon nucleolar breakdown and prevent the interaction of Mdm2 with p53 (Olson 2004). The interplay of ARF, Mdm2 and p53 with or without nucleolus has been refined, showing multiple regulatory loops. ARF further has p53-independent activity on rRNA transcription (Lessard 2010) and processing (Sugimoto 2003). An important binding partner and mutual regulator of ARF is the abundant nucleolar protein and oncogene B23/Nucleophosmin, which has itself broad implications on nucleolar stability and stress responses (Lindström 2011). The Mdm2–p53 interaction is also target of ribosomal proteins. Ribosomal proteins are released from the nucleolus following different types of stress and can mediate stabilisation of p53 (Deisenroth 2010); a prominent example is RPL11, which is released upon disturbances in ribosome synthesis (Hölzel 2010). An additional mechanism of p53 activation is employed by RPL26: it acts as a translational regulator by binding to p53 mRNA in mammals [reviewed in (Zhang 2009)].

A very recent publication demonstrated nucleolar involvement in p53 activation upon glucose starvation, via translocation of MYBBP1A from the nucleolar attachment to the nucleoplasm and facilitated interaction of p300 with p53 (Kumazawa 2011).

It is interesting to note that p53 was early found to be associated with ribosomes (Fontoura 1997) and to be covalently linked to 5.8S rRNA (Fontoura 1992). The significance of the latter has not been determined yet.

4.1.4.2 Ribosome synthesis defects affect cell survival and can be tumorigenic

Transcription, processing, and modification of rRNA involves an extensive set of factors, to some of which tumor predisposing diseases have been linked; e.g., Dyskeratosis congenita (pseudouridine synthase DKC1) or Diamond-Blackfan anaemia (ribosomal protein RPS19) [reviewed in (Ruggero 2003)]. The importance of balanced ribosomal proteins for tissue homeostasis was demonstrated in Zebrafish, where many ribosomal proteins proved to be haploinsufficient tumor suppressors (Amsterdam 2004). The mechanism of tumor formation following these disturbances is not yet understood.

Failures in rRNA and ribosome synthesis have been shown to induce apoptosis. For instance, depletion of the transcription initiation factor TIF-IA (see below) lead to nucleolar disruption, cell cycle arrest, or p53 mediated cell death in cultured cells and in a mouse model (Yuan 2005); in the nervous system, it caused apoptosis and neurodegeneration (Parlato 2008). In another study, Tat protein of human immunodeficiency virus caused processing defects at early steps of rRNA maturation and thereby induced protein synthesis shut-off and apoptosis (Ponti 2008). As already mentioned, various ribosomal proteins are directly involved in p53 activation, possibly when released upon nucleolar disintegration. Direct regulatory interaction with p53 was recently also shown for a processing component of the small ribosomal subunit, hUTP14a; its knockdown led to p53 stabilisation and cell cycle arrest, or to apoptosis (Hu 2011).

Positing that the intimate balance between RNA pol I transcription and growth-factor signalling is perturbed in most cancer cells, rRNA synthesis can be envisaged as a target for therapeutics in tumor

treatment (Drygin 2010). Some established anticancer drugs like 5-Fluorouracil (5-FU) or Mycophenolic acid act at least partially through disruption of rRNA synthesis (Ghoshal 1997; Sun 2007) or require ribosomal proteins for p53 activation (Sun 2008), respectively. New substances are being evaluated that selectively inhibit RNA pol I transcription. Interestingly, whereas CX-3543, a small molecule agent that disrupted chromatin structure of rDNA and thereby inhibited RNA pol I transcription, induced apoptosis in proliferating cells (Drygin 2009), another drug, CX-5461 inhibited the initiation stage of rRNA synthesis and induced both senescence and autophagy, but not apoptosis (Drygin 2011). The general transcriptional inhibitor actinomycin D did – at low doses when it preferentially blocks RNA pol I – induce apoptosis in post-mitotic, non-proliferating neurons (Kalita 2008).

Ribosome inactivating proteins (RIPs) are extremely potent toxins of plant or microbial origin (Stirpe 2006). Typically, they attack the active centre of ribosomes or translation factors, mostly factors of elongation. They can induce cell death with characteristics of apoptotic demise [reviewed in (Narayanan 2005)]. At least in some instances, apoptosis seems to involve mitochondrial cascades and is likely independent of translation inhibition (Sikriwal 2008).

4.1.4.3 DNA damage response might involve the nucleolus

DNA damage-induced apoptosis in mammalian cells has been suggested to involve nucleolar disruption as a mechanistical step, mostly according to the model of Rubbi and Milner discussed above (Rubbi 2003b); nucleolar events might significantly contribute to p53 stability and thus to cellular DNA damage response. Several factors associated with the nucleolus and ribosomes have been described that mediate DNA damage-induced apoptosis by alternative ways. For example, RPL26 and nucleolin regulate p53 translation by binding to the 5'UTR of p53 mRNA, with opposing effects; overexpression of RPL26 or knockdown of nucleolin increased the sensitivity of transfected cells to IR or to 5-FU-induced apoptosis, whereas knockdown of RPL26 or stable overexpression of nucleolin reduced the apoptotic response to IR (Takagi 2005). Another interesting link and an example of an extra-ribosomal function of a ribosomal protein are given by S3. RPS3 is possibly involved in pro-apoptotic signalling via activation of caspases 8 and 3 in immune cells (Jang 2004). It is a presumptive DNA repair endonuclease (base excision repair) that translocates to DNA damage sites following ERK mediated phosphorylation (Yadavilli 2007). Nuclear translocation of RPS3 is also stimulated by Akt-dependent phosphorylation; coincidentally, Akt prevents RPS3 from binding to, and synergistic effects with, E2F1 on apoptosis induction in neurons (Lee 2010b). E2F1 is an E2F family member with extraordinary pro-apoptotic activity upon DNA damage, via transcriptional upregulation of pro-apoptotic factors. Involvement in damage-induced apoptosis via E2F1 was also shown for the nucleolar protein RRP1B. RRP1B, itself a transcriptional target of E2F1, could bind coordinately with E2F1 to E2F1 targets and activate transcription of pro-apoptotic genes (Paik 2010).

Nucleolar disintegration in response to cell stress has mostly been proposed to happen upstream of p53 activation [(Rubbi 2003b) or, e.g., (Kalita 2008)]. However, analysis of the sub-cellular proteome localisation by spatial proteomics indicated that there were p53-independent but also p53-dependent protein translocation events in the nucleolus following DNA damage with etoposide (Boisvert 2010a). It seems a reasonable scenario that DNA damage primarily activates p53, which, given its regulatory

function on rRNA transcription, might contribute to the alterations in nucleolar composition and dynamics; such changes could reinforce p53 activity and foster cellular DNA damage responses.

4.1.4.4 RNA pol I transcription rate reacts to irradiation

How dramatically RNA pol I transcription can be affected by DNA damaging treatment has been demonstrated with quantitative *in situ* analysis of RNA pol I kinetics and transcription rates in mammalian cells (Kruhlak 2007). Irradiation of cells or even of individual nucleoli caused a rapid but temporary decline of RNA pol I assembly and rRNA synthesis in the affected compartment. The damage leads to inhibition of transcription initiation by RNA pol I, dependently on the PI(3)K kinase ATM. This is a very exciting mechanism how DNA damage signalling might touch on ribosome synthesis, possibly provoking nucleolar or ribosomal changes that affect cellular DNA damage responses like cell cycle arrest or apoptosis. The link from damage to cellular effects would go through RNA pol I.

4.1.5 Ribosomal RNA

The ribosome is an ancient molecular system; in all cellular species, it is composed of two subunits that both are large protein-RNA assemblies. Ribosomal RNA constitutes the backbone and also the functional centre of these macromolecular complexes. Structure and function of the ribosome have been described and depicted in great detail [(Taylor 2009a; Ben-Shem 2010), see (Armache 2010a) for localisation of rRNA or (Armache 2010b) for localisation of ribosomal proteins in the translating ribosome]. Eukaryotic ribosomes contain four rRNA species; the 18S rRNA in the small ribosomal subunit (SSU); and the 28S, the 5.8S and the 5S rRNA in the large subunit (LSU).

4.1.5.1 Eukaryotic rDNA is composed of repeats of co-evolving polycistronic units

The ribosomal RNA genes are organised very similarly in different eukaryotic species. Multiple tandem repeats of polycistronic rDNA units are collected in one (e.g., *S. cerevisiae* or *C. elegans*, see Figure 6) or several chromosomal regions (five in human) of a haploid genome (Lafontaine 2001). The units code for the 18S, the 5.8S and the 28S rRNA in this sequence and are transcribed by RNA pol I as one pre-rRNA. The 18S and 5.8S, and the 5.8S and 28S rRNA are separated by an internal transcribed spacer sequence (ITS1 and ITS2, respectively); external transcribed spacers (ETS) flank the 5' of 18S and the 3' of 26S rRNA. Between the pre-rRNA transcription units is an intergenic spacer (IGS); it is of variable length between species and contains regulatory elements for RNA pol I transcription. In yeast, the RNA pol III transcribed 5S rRNA genes are integrated in reverse orientation one in each IGS; in other eukaryotes, the 5S rDNAs are organised as a separate cluster. The number of rDNA units differs between evolutionary branches; yeast has approximately 140 repeats, the haploid human genome harbours about 400 repeat units. Conservation and evolution of the rDNA is challenging and must involve complex mechanisms of genome maintenance. The highly repetitive rDNA has sequences of high evolutionary conservation mixed with more variable regions (e.g., expansion segments within the mature rRNA); captivatingly, the individual rDNA units don't evolve separately, but remain largely as identical repeats [On the fascinating evolution of rDNA and gene conversion see e.g., (Eickbush 2007) and (Stage 2007)].

4.1.5.2 rRNA transcription rate is regulated by RNA pol I initiation

As described above, rRNA transcription as a major cellular process is under tight control of many signalling pathways [reviewed e.g., in (Grummt 2003)]. Much of the regulation of rRNA transcription and thus of ribosome synthesis rates happens at the level of transcription initiation by RNA pol I. In mammalian cells, the upstream binding factor (UBF) and the selectivity factor complex SL1 are crucial for RNA pol I loading on rDNA. Interaction of UBF and SL1 is inhibited by pRb binding to UBF (Cavanaugh 1995) or p53 binding to SL1 (Zhai 2000). The transcription initiation factor TIF-IA (conserved in yeast as Rrn3) is also essential for RNA pol I activity and for mediating growth-dependent control of rRNA transcription; TIF-IA binding defines the initiation-competent RNA pol I complexes. UBF and TIF-IA are subject to manifold regulatory phosphorylation by CK2, CDKs, and ERK kinases [reviewed in (Ruggero 2003) and (Cavanaugh 2002)]. For instance, rRNA transcription is dependent on, and is rapidly increased upon, phosphorylation of TIF-IA by the MAP kinase ERK (Zhao 2003b). [For a comprehensive overview on the mechanisms of RNA pol I transcription, see (Hannan 1998a) and (Paule 2000); the kinetics of RNA polymerases and particularly of RNA pol I have been assessed in (Dundr 2002).]

Overall rRNA transcription is controlled by two major strategies: an epigenetic state defines how many rDNA units are amenable to transcription; and the rate of RNA pol I transcription cycles largely determines the rRNA synthesis rate from a particular rDNA unit. In yeast and mammals, a considerable fraction of the rDNA is silenced in normal conditions (an estimated 50 %), but might be turned active and recruit the transcription machinery at increased cellular demand for ribosomes [reviewed in e.g., (Russell 2005)]. However, in exponentially growing *S. cerevisiae,* it has been shown that the integrated RNA pol I loading rate of the active rDNA units is a more important determinant for rRNA synthesis than the fraction of active rDNA genes (French 2003). Epigenetic regulation and heterochromatin formation, which involve the nucleolar chromatin remodelling complex NoRC, are important for the genetic stability of rDNA repeats and for structural integrity of the nucleolus [reviewed in (McStay 2008)].

Transcription by RNA pol I is coordinated with transcription by other polymerases; c-Myc (Oskarsson 2005) and mTOR (Mayer 2006) have been shown to modulate the activity of all three RNA polymerases in order to coordinately upregulate ribosome synthesis. Besides, increased RNA pol I transcription (e.g., by constitutive derepression) seems to entail upregulation of RNA pol II transcription specifically of ribosomal proteins, and of 5S transcription, likely in order to maintain the stoichiometric balance of ribosomal constituents [(Laferté 2006b), commented in (Michels 2006)]. Probably, rRNA transcription is a fine-tuned lever for ribosome synthesis and cellular homeostasis.

4.1.6 Ribosome synthesis

Ribosomes are assembled from rRNA and ribosomal proteins in separate pathways of small and large ribosomal subunit maturation [(Fatica 2002; Fromont-Racine 2003; Kressler 2010), nuclear export and cytoplasmic maturation (Zemp 2007)]. The 18S rRNA together with 33 canonical ribosomal proteins (in yeast) forms the 40S subunit; the 26S, 5.8S and 5S rRNAs combine with 46 ribosomal proteins to the 60S subunit. Numerous non-ribosomal factors (>200) and small nucleolar RNPs (snoRNPs, about 75) are required for the proper processing of ribosomal RNA and assembly of the ribosome (Kressler 2010).

Basically, rRNA has to be excised from the polycistronic transcripts and modified on some nucleotides, to be folded and to aggregate with ribosomal proteins; and the ribosomal subunits need to be exported from the nucleus to the cytoplasm. The maturation of small and large ribosomal subunits is separated early during pre-rRNA processing and channelled in two biosynthetic pathways. A number of rRNA processing and ribosomal synthesis factors are needed for both subunits, whereas others are involved specifically in the synthesis of either of the two (Fromont-Racine 2003).

Most of the known processes of ribosome assembly were revealed only in the last decade; much more research needs to be invested for a better understanding of the complex network driving ribosome assembly.

4.1.6.1 rRNA processing involves nucleolytic activity and base modifications

The processing of ribosomal RNA precursors has been studied relatively well, based on typical cleavage patterns of transcribed RNA *in vivo* and *in vitro*, and many of the relevant nucleases and processing factors have been identified; pre-rRNA is cleaved at specific sites in a mostly well-defined sequence of exo- and endonucleolytic events [for *S. cerevisiae,* e.g., (Fatica 2002)]. Firstly, the 5'-ETS is degraded, before the polycistronic transcript is cleaved within ITS1 and split into a fragment containing the 18S rRNA and one with the 5.8S and 25S rRNAs; the latter is further cleaved by two alternative routes to finally yield the two mature LSU rRNAs.

In addition to backbone cleavage, more than 100 nucleotides are modified in human rRNA: enzymatic isomerisation of uridines to pseudouridines and ribose 2'-hydroxyl-methylation are the most frequent modifications. These are assumed to mainly influence RNA conformation (Fromont-Racine 2003). The ribosomal subunits are exported to the cytoplasm at different degrees of maturation: the pre-18S rRNA has not been fully processed when the pre-40S particle is released from the nucleus (Zemp 2007)].

Transcription of rRNA, processing, and pre-ribosome assembly are not separate events but are interdependent and co-regulated [(Granneman 2005; Gallagher 2004); quantified and modelled in (Kos 2010)]. A mutation in yeast Rpa135 evidenced such a link between transcription by RNA pol I and efficient rRNA processing (Schneider 2007). The terminal knobs decorating the nascent pre-rRNA transcripts in Miller chromatin spreads represent the U3 snoRNA complex that is required for processing of the 18S rRNA, which indicates that processing is initiated co-transcriptionally; reversely, some of the UTPs (U-three proteins) of this complex are required for efficient rDNA transcription (referred to as t-UTPs), indicating regulation of transcription by the processing machinery [reviewed in (Granneman 2005)].

4.1.6.2 Ribosomal proteins are co-regulated

In rapidly growing yeast cells, transcription from ribosomal protein genes accounts for an estimated 50 % of RNA pol II transcription initiation events (Warner 1999). (Ribosomal proteins and RP mRNAs are very abundant and relatively short-lived compared with other proteins and mRNAs). The 80 ribosomal proteins are mostly represented at equimolar quantities, and synthesis of ribosomal proteins is expected to grossly be in stoichiometric balance with ribosomal RNA (Laferté 2006a; Rudra 2004; Mayer 2006). In eukaryotes, expression of ribosomal proteins is coordinated by gene regulatory networks and by posttranscriptional expression regulation [reviewed in (Perry 2007; Hu 2007)]. In mammalian cells,

mRNA levels of different ribosomal proteins are kept within narrow boundaries (mostly within a two-fold range). Efficient translation of ribosomal protein mRNAs is mediated by the 5' terminal oligopyrimidine (TOP) sequence, which is a ubiquitous feature in all vertebrate RP mRNAs (and which is also present in several other factors of the protein translation apparatus) (Meyuhas 2000).

An increasing number of extra-ribosomal functions for some of the ribosomal proteins is emerging, among which figure regulation of gene expression (Lindström 2009), stress response, and apoptosis. For example, as discussed above, the ribosomal protein S3 has endonuclease activity and acts in DNA damage response. Other ribosomal proteins have been shown to bind viral factors or to sequester regulatory factors like c-Myc or B23/NPM [so far known extra-ribosomal functions are summarised in (Warner 2009)]

4.1.7 The nucleolus

The nuclear nuclei are non membrane-delimited, prominent subcellular compartments that form around the nucleolar organiser regions (NORs) of eukaryotic chromosomes. NORs correspond to the loci of rDNA repeats. Nucleoli have long been recognised as the factories for ribosomes. In fact, many steps of ribosome biosynthesis occur in the nucleoli; and the nucleolar substructure as visualised by electron microscopy is largely determined by regions that probably represent different steps of ribosome synthesis. Transcription of rRNA by RNA pol I could be considered as the nucleating process around which the processing machineries and ribosome assembly factors organise; yet it is not sufficient for the maintenance of nucleolar morphology [discussed in e.g., (Raska 2006)]. The structure and organisation of the nucleolus remains a matter of debate. Likely, it is a highly dynamic composition of factors that form and maintain the structure through rapid association and dissociation with other nucleolar components [reviewed in e.g., (Hernandez-Verdun 2006) or (Pederson 2009)]. Accordingly, nucleolar morphology is linked to the cellular functional status and it can vary quickly along with the cell cycle or with external stimuli.

Transmission electron microscopy reveals two distinct nucleolar regions in most nucleoli: fibrous, electron-dense areas, called the dense fibrillar components (DFC), which are embedded in a pool of granules of the size of ribosomes, the granular component (GC). Often, a DFC encircles a third, less dense distinct region, namely the fibrillar centre (FC). RNA pol I can be found in the FCs and in the DFCs; ribosomal RNA is detected in the DFCs and the GC. Probably, the FCs represent areas of non-transcribed rDNA and of inactive RNA pol I (Raska 2006). Transcription is thought to happen at the interphase between the FC with the DFC, and the DFC is most likely the site of early rRNA processing steps. In the GC, ribosomal subunits are assembled and prepared for export. [Nucleolar structure and the structure-function relationship have been investigated for several decades. Some recent reviews: (Hernandez-Verdun 2006) and (Raska 2006), short overview on structure and composition (Shaw 2005), focus on RNA pol I activity (Prieto 2005); ultrastructural analysis of rRNA transcription and processing in (Biggiogera 2001; Koberna 2002; Huang 2002)]. Besides these canonical regions, several distinct substructures have been found in the nucleoli such as vacuoles, cavities or condensed chromatin.

Increasingly, the nucleolus has become acknowledged as a multifunctional cellular compartment that offers a platform for ribosome synthesis and linked processes (Boisvert 2007) and also for seemingly unrelated factors (Pederson 2009). Some of the established functions are maturation of non-nucleolar

RNAs or RNPs, the assembly of the signal recognition particle, or as already described above, cell cycle regulation, cellular stress response, or virus infection control [various reviews by M. O. Olsen (Olson 2000, 2004, 2009)]. Further, the nucleolus participates in the regulation of ubiquitin dynamics as evidenced by Mdm2 and VHL ubiquitin ligases (Mekhail 2005). A role for the nucleolus in telomere maintenance and aging was described early in yeast, and an exciting mechanism involving extrachromosomal rDNA circles was suggested (Sinclair 1997; Defossez 1998); Sirtuins, which regulate telomere length and rRNA transcription (Grob 2009; Ford 2006), and that presumably affect lifespan, are potentially important mediators.

In the past decade, characterisation of the nucleolar proteome has revealed numerous factors without previously known functional links to the nucleolus. Approximately 700 proteins were identified and their dynamics in the nucleolus assessed by a proteomic analysis of human nucleoli [(Andersen 2005), review in (Lam 2005)]. Another elaborate strategy called 'spatial proteomics' was used to determine the subcellular proteome localisation in response to external stimuli like DNA damage (Boisvert 2010b, 2010a). This and other approaches will allow to correlate nucleolar localisation of proteins with cellular functions, and will thus widen the known spectrum of proteins and cellular functions that are using the nucleolus.

4.1.8 Ribosome synthesis in *C. elegans*

Ribosome synthesis has mostly been studied in yeast and mammals (and rDNA in Drosophila). Much of the mechanistics and many of the factors involved have been well conserved in evolution, as would be expected for a most essential cellular process. Though, there are also significant differences. As already mentioned before, the intergenic spacers (IGS) of rDNA repeats are organised differently between yeast and mammals, with the yeast repeats hosting the 5S rRNA genes. Yeast has one genomic locus with approximately 140 repeats, the human genome has 5 loci on different chromosomes with a total of 400 repeats (Drosophila species have the rDNA locus on the X and Y chromosomes, totalling about 200 repeats) (Eickbush 2007).

Possibly reflecting the differences in the structure and base sequence of the IGS, the transcription initiation complex is different between yeast and mammals. In mammalian cells, UBF dimer binding to the promoter region and assembly with the SL1 complex (part of which is the TATA-box binding protein TBP) prepares for the transcription competent RNA pol I. In yeast, a protein similar to the HMG1-box protein, Hmo1p, can enhance rRNA transcription, but the initiation apparatus consists of a multisubunit upstream activating factor (UAF) associated with TBP, and a core factor complex (CF).

Both, mammalian and yeast core RNA pol I, bridge to their initiation complexes by the homologous TIF-IA/Rrn3 [reviewed in e.g., (Moss 2004) or (Grummt 2003)]. Also, the RNA pol I core complex components are highly conserved from yeast to human. Yeast, Drosophila and mammalian cells alike use no more than 50 % of the rDNA repeats for active transcription and show great flexibility in total rRNA synthesis rates (Moss 2004).

The ribosomal proteins are mostly conserved (78 RPs in yeast, 79 in mammals) (Warner 1999); a striking difference from the mammalian system is the duplication of most ribosomal protein genes in yeast.

Only few aspects of ribosome biogenesis have been investigated in *C. elegans*. The rDNA repeat number (Sulston 1974), the organisation of individual rDNA repeat units (Files 1981), the genomic locus (Albertson 1984), and the sequence and secondary structure of rRNA (Ellis 1986b) were all determined relatively early [see Figure 6]. *C. elegans* has one single locus of the RNA pol I transcribed gene repeats in the subtelomeric region of the right arm of chromosome 1 (LG I) (Albertson 1984). The rDNA locus is a tandem arrangement of approximately 55 repeat units of 7.2 kb length each (Files 1981). The rDNA genes are separated by a short intergenic spacer of only about 500 bp (the precise ends of the 5' and 3' external transcribed spacers in the pre-rRNA transcript of *C. elegans* have not been determined). The 5S rRNA is encoded by a locus containing approximately 110 repeats (Sulston 1974) of about 1 kb on the right arm of chromosome 5 (LG V) [(Nelson 1985) and (Nelson 1986)]. The repeats also contain the supposedly RNA pol II-transcribed SL1 trans-spliced leader gene, a short RNA element that is attached to the 5' end of the majority of mRNAs.

Transcription by RNA pol I in *C. elegans* has not explicitly been studied to date. Most but not all of the core subunits of RNA pol I that have been identified in yeast or mammals have obvious homologs in *C. elegans* (Table 7). It remains unresolved how the transcription initiation complex is composed in *C. elegans*. In a homology search, I could not identify any obvious homologs for the mammalian initiation factors UBF or Selectivity Factor 1 (SL1), nor were there clear homologs of UAF components from yeast. The transcription competence factor TIF-IA/Rrn3 has a homolog with C36E8.1, which is essential for animal growth and survival, as I found with the deletion mutant C36E8.1(*ok1714*). One factor has been identified in *C. elegans* that significantly affected rRNA transcription and nucleolar size, as well as cell size when mutated: NCL-1, homolog to Drosophila BRAT and a presumptive ubiquitin ligase, is a negative regulator of rRNA transcription (Hedgecock 1995; Frank 1998). Some groups have reported on rRNA processing in *C. elegans*. Saijou et al. characterised the major cleavage steps in pre-rRNA processing and described an 18S rRNA processing defect in animals with reduced *rbd-1*, the homolog of yeast Mrd1p (Saijou 2004). The group of Jane Hubbard isolated several candidates from a genetic screen to find regulators of germ line proliferation, which they found had mutations in genes coding for rRNA processing factors (Voutev 2006). The three genes identified in that screen, *pro-1* (Ipi3 in yeast), *pro-2* (Noc2) and *pro-3* (Sda1), and other processing factors that they tested (including *rbd-1*), were required for normal germ cell development; reduction of their function led to germ line tumor formation. *ncl-1* mutation could partially suppress the tumor phenotype. In that work, the pRb homolog *lin-35* was confirmed to be a negative regulator of rRNA transcription in *C. elegans*, according to the activity in mammals (Cavanaugh 1995); loss of *lin-35* function could also reduce tumor formation of the processing mutants. Another prominent nucleolar protein, *nst-1*, was linked to germ cell proliferation in *C. elegans* (Kudron 2008), as well as to CED-4-dependent cell- and body-size control (Chen 2008); the homologous nucleostemin family members are involved in stem cell renewal and different aspects of cell and tissue homeostasis, and have been shown to regulate p53 (Tsai 2009). As to rRNA modification and processing factors, a formerly unclassified small ncRNA, CeR-2, was recently characterised in *C. elegans* as a snoRNAs with unconventional processing activity, likely on the LSU rRNA precursor (Hokii 2010). An interesting dual function was detected for the RNA processing exonuclease *eri-1* (Eri1): one isoform performs 3' end processing of the 5.8S rRNA, a second isoform negatively regulates RNAi efficiency in both *C. elegans* and *Schizosaccharomyces pombe*.

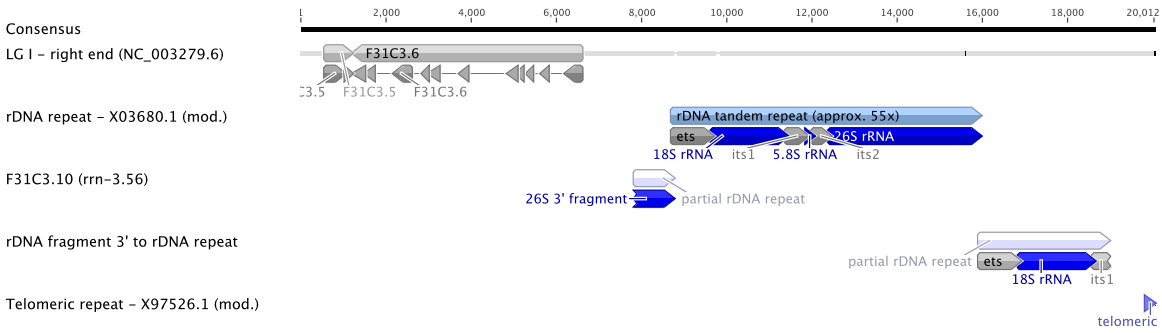

Figure 6 Right chromosomal end of LG I, comprising the multi-repeat rDNA locus. The approximately 55 tandem-repeat units of 7.2 kb are flanked by an incomplete unit both at their 5' and at the 3' end. They neighbour a Pol II transcribed gene and the LG I telomeric repeat $(TTAGGC)_n$, respectively.

C. elegans has well conserved homologs of the ribosomal proteins. They are present in single copies with a few exceptions: *rpl-11* and *rpl-25* have two genes, *rpl-11.1* and *rpl-11.2*, or *rpl-25.1* and *rpl-25.2*; RPL-11.1 is supposedly expressed specifically in the germ line. Also, *C. elegans* encodes two paralogs of the acidic ribosomal stalk protein P2.

The proposed link between nucleolar integrity and p53 stability and with apoptosis in mammals cannot be easily transferred to *C. elegans*. Whereas p53 is conserved as CEP-1, no homolog of the p53 ubiquitin ligase Mdm2 has been found in *C. elegans*. It is conceivable that sequence conservation is low and therefore the homolog has not been identified, or that alternative ubiquitin ligases regulate CEP-1 stability [see above, and (Lane 2010)]. Also, there is no *C. elegans* homolog of ARF, a crucial factor in mammals for stress response regulation via the nucleolus. Nor is there an obvious B23/NPM homolog. If the nucleolus plays a role in stress response in *C. elegans*, this would likely employ alternative mechanisms. Interestingly, some factors that have an influence on the nucleolus and on rRNA synthesis in mammals have been associated with apoptosis in *C. elegans*. For instance, the SIRT1 homolog *sir-2.1*, by homology a possible negative regulator of rRNA synthesis, was shown to be required for DNA damage-induced apoptosis, likely in a pathway parallel to *cep-1* (Greiss 2008). While ARF and Mdm2 homologs remain to be identified, EEL-1 was found as the ARF-BP1 homolog; this ubiquitin ligase promotes DNA damage-induced germ cell apoptosis (Ross 2011). Very excitingly, nucleolar factors were found to suppress innate immunity by inhibiting CEP-1: reduction of *nol-6* and other nucleolar factors increased resistance to pathogenic bacteria, dependently on *cep-1* (Fuhrman 2009).

Overall, ribosomal synthesis has not yet been exhaustively studied in *C. elegans*. Biochemical experiments to investigate the processes of rRNA synthesis and ribosomal assembly are challenging. However, *C. elegans* offers a great tool to study the connections from these elemental processes and the involved genes to various phenotypes on a cellular and organismal level. It could help to identify novel functions of the multifunctional nucleolus. The nucleoli in *C. elegans*, at least, are not hiding themselves from inspection; rather, they impose as prominent nuclear substructures in most cells (Figure 11).

4.2 Previous work on *rpo-1b(op259)* and initial motivation

Randall E. Hofmann et al. had performed a genetic screen for *C. elegans* mutants with defective cell cycle arrest response to ionising radiation (IR), and isolated the *op259* allele. Lilli Stergiou had continued the work on this mutant in her PhD Thesis (Stergiou 2006). They could map the mutation to a single base alteration in F14B4.3 (Figure 35), a missense mutation that leads to a Proline to Serine change in the N-terminal part of the second largest subunit (β-subunit) of RNA pol I. We provisionally designated the mutated gene as *rpo-1b*, the name that will be carried throughout this study. Randall and Lilli characterised several aspects of the *rpo-1b(op259)* mutant, which are shortly summarised here. *rpo-1b(op259)* mutants shared several features with mutants of classical DNA damage response factors. *rpo-1b(op259)* worms were defective for DNA damage-induced germ cell apoptosis upon IR or UV-C irradiation. The mutation suppressed the Gla phenotype (increased germ line apoptosis) of *rad-51* and *abl-1* (*cep-1*-dependent) but not of *gla-1* (physiologic cell death, *cep-1*-independent). Mutant phenotypes of *ced-6* (engulfment) and *ced-9* (core apoptotic machinery) were not suppressed. The pattern of irradiation-induced upregulation of EGL-1 and CED-13 transcripts (*cep-1* activation) was reminiscent of *atm-1* mutants. The apoptotic phenotype of *rpo-1b(op259)* mutants could be partially rescued by injecting the F14B4 cosmid into the germ line.

rpo-1b(op259) worms had a proliferation defect in the mitotic zone of the germ line and exhibited a Gro phenotype (slow growth). Embryonic lethality (unhatched larvae per eggs laid) raised from 20 % in untreated *rpo-1b(op259)* worms to 40 % upon IR (<5 % in wildtype worms). Synthetic lethality was observed with *hus-1* (9-1-1 complex) but not with *clk-2* (novel repair pathway). Mean lifespan of *rpo-1b(op259)* mutants was slightly reduced in comparison to wildtype.

Other important observations were the smaller size of germ cell and embryonic nuclei and nucleoli in *rpo-1b(op259)* animals and atypical nucleolar substructures. These concurred with reduced steady state levels of rRNA transcripts. An obvious explanation for the apoptotic defect seemed that *rpo-1b(op259)* could have reduced translation, which in turn might preclude efficient expression of pro-apoptotic factors in response to DNA damage. Inhibition of translation by cycloheximide treatment of wildtype worms indeed could block IR-induced apoptosis.

RPO-1B had the potential to be part of many different regulatory networks, both judged by its function as an RNA polymerase subunit and by the pleiotropic phenotypes of the *op259* allele. Various concepts and pathways for the integration of environmental conditions to metabolic activity and for stress response crossed at the nucleolus [see above]. It had been discussed as a regulating compartment for apoptosis (Olson 2004; Rubbi 2003b) and for tumor cell proliferation [for a review, see (Ruggero 2003)].

The observations in *rpo-1b(op259)* worms indicated abnormal ribosome biogenesis. Molecularly, this defect had been little characterised, and how it related to the defective DNA damage response was unclear. The role in apoptosis could be a specific characteristic of this polymerase subunit or even of the mutated site, and not be directly linked with the overall performance of RNA pol I. Alternatively, the anti-apoptotic effect could result from a more general alteration in transcriptional capacity of RNA pol I, and the consequences thereof.

To better understand why *rpo-1b(op259)* would lead to DNA damage response defects, I aimed at detecting possible molecular alterations of ribosome synthesis in *rpo-1b(op259)* mutants and at determining what element in the chain from rRNA transcription by RNA pol I to protein synthesis by ribosomes was most influential on apoptosis. I wanted to define genetically whether *rpo-1b* was integral part of already known damage response pathways, or whether apoptosis regulation by RPO-1B defined a novel mechanism. Ultimately, I wished to advance the understanding how disturbances of a core cellular process can revolt cellular responses to exogenous stimuli and how it affects tissue homeostasis.

4.3 Characterisation of the *rpo-1b(op259)* allele

4.3.1 *op259* affects the second subunit of RNA polymerase I

The core subunits of the DNA-dependent RNA polymerases are evolutionarily highly conserved (Bushnell 2003; Cramer 2002, 2000). This is particularly true for the catalytic, largest and second largest subunits (Cramer 2002). The eukaryotic α- (largest) and β- (second largest) subunits are functionally and structurally highly similar to the bacterial β and β' RNA polymerase subunits and to archeal A (A' + A'') and B (B' + B''). Sequence alignment of eukaryotic RNA polymerase I β-subunit proteins reveals a pairwise identity of amino acid residues between 40 and 50 % among representatives from yeast to human (Figure 8). (The homologs of the largest subunit also share about 40 to 45 % of residues.) Locally, identity is much higher in some critical protein regions such as the active site and interaction domains (Cramer 2001).

To deduce the relevance of the *op259* mutation, I scrutinised the mutated site in its sequence context and by inter-species comparisons. Alignment of the RPO-1B protein sequence with its homologs reveals that the P70S mutation affects a highly conserved residue at the beginning of a well-conserved stretch of amino acids that likely forms an alpha helix. This conservation holds true when comparing with diverse orthologous eukaryotic RNA pol I β subunits (Figure 8) as well as with the paralogs, i.e., the *C. elegans* β-subunits of RNA pol II and III (Figure 7).

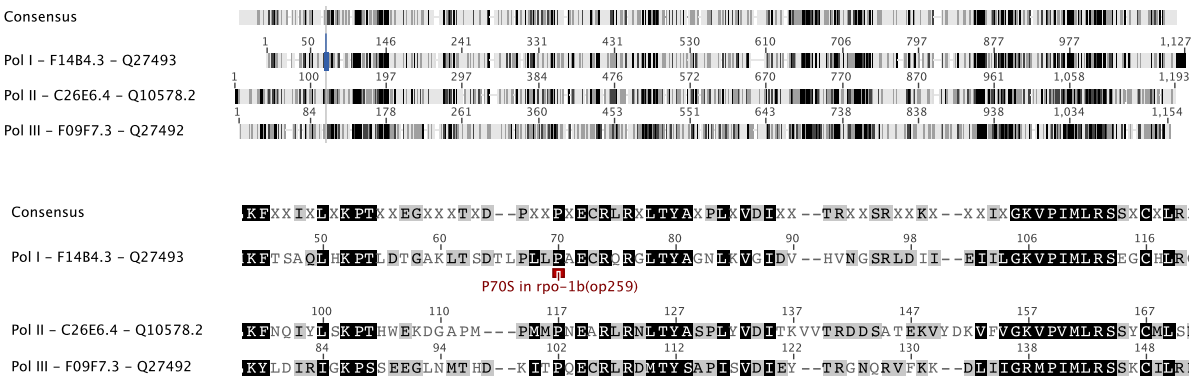

Figure 7 Sequence alignment of the *C. elegans* RNA polymerase β-subunits. P70 and subsequent amino acids are conserved between the paralogs. Full length protein (top) and region of the *op259* mutation (bottom).

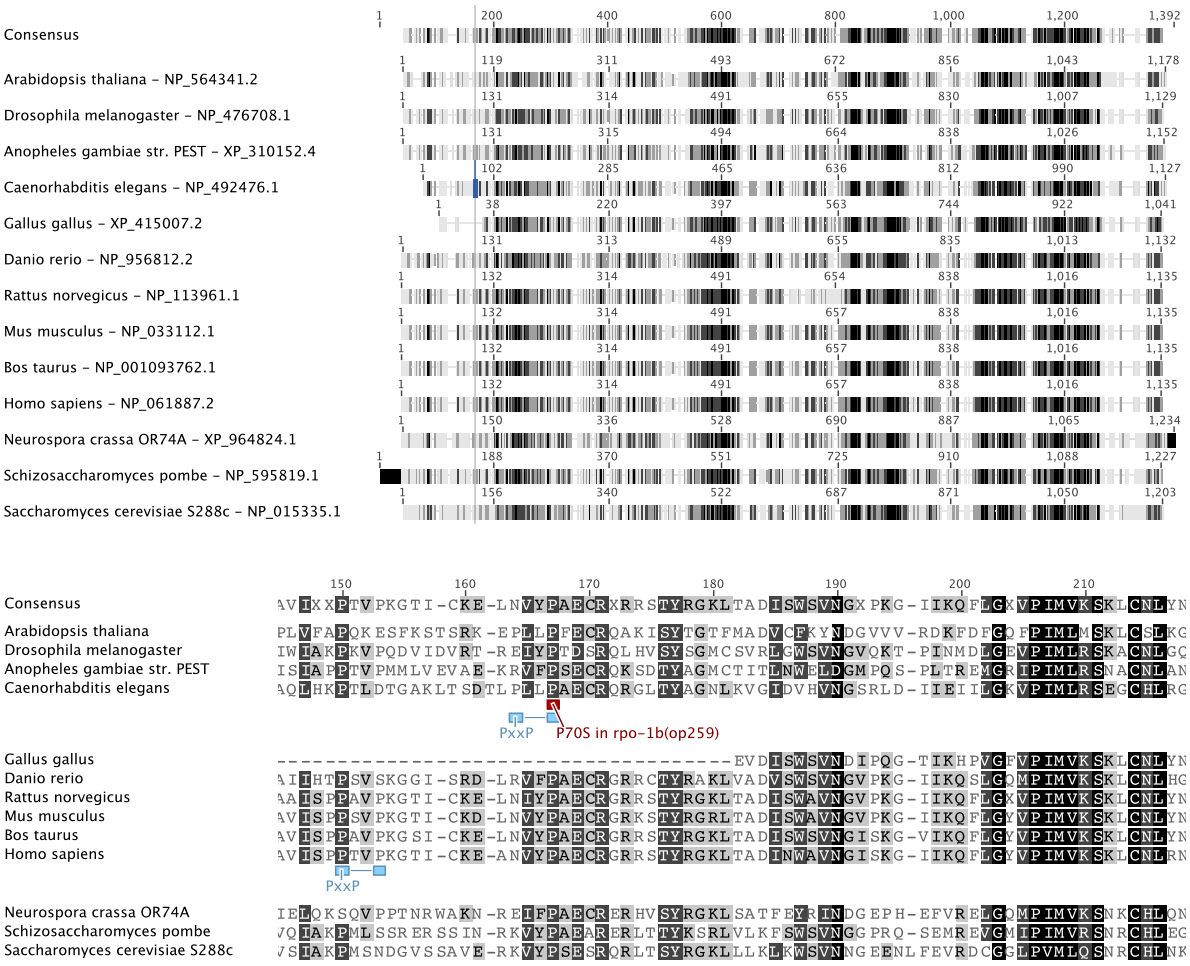

Figure 8 Sequence alignment of eukaryotic RNA polymerase I β-subunit proteins. The Proline mutated in *rpo-1b(op259)* (P70S) is conserved from yeast to human. Together with the Proline at 3 positions towards the N-terminus, P70 defines a predicted SH3-domain binding site (PxxP), a motif that in higher eukaryotic orthologs is also present nearby.

The high structural conservation between the three eukaryotic RNA polymerases I, II and III and the evolutionary conservation between different eukaryotic species should allow to infer the likely position of a protein region in a three-dimensional protein complex, once this has been modelled for a homologous equivalent. Yeast RNA pol II has been in the focus of structural analyses of RNA polymerases (Brueckner 2009) and of protein interactions within large multiprotein complexes (Ranish 2003b). The structural basis of transcription could be resolved to 2.8 Å from a crystal form of RNA pol II comprising the 12 core subunits (Cramer 2001). RNA pol I and RNA pol II share the subunits Rpb5, Rpb6, Rpb8, Rpb10, and Rpb12. The non-shared subunits A190/Rpb1, A135/Rpb2, AC40/Rpb3, AC19/Rpb11 and A12.2/Rpb9 have a sequence identity of about 20 %. Kuhn et al. assembled the complete structure of the 14-subunit RNA pol I at 12 Å using cryo-electron microscopy [(Kuhn 2007a), and reviews (Haag 2007; Werner 2009)]. The structure of the RNA pol I specific subunits A49 and A34.5 has been further detailed and is paralogous to the RNA pol II initiation factors TFIIF and TFIIE (Geiger 2010). Overall, the architectures of yeast RNA pol I and RNA pol II are very similar. Yeast Rpa135 has 26 % sequence identity with Rpb2 and 62 % of its amino acid residues localise in the same protein fold as their pairs in the homolog (Kuhn 2007a). Together, these analyses support the transferability of

sequence/position information from RNA pol II to RNA pol I. This should also apply to the transfer from an RNA polymerase complex in yeast to the ortholog in any other eukaryotic species, where conservation of sequence and function is even higher than between the three polymerases within one species. I thus aligned RNA polymerase β-subunits and identified the most likely homologous residue to the proline mutated in *rpo-1b(op259)* in the yeast RNA pol II β-subunit. The corresponding amino acid was represented in the structure model derived by X-ray diffraction, available as PDB entry 1|50.

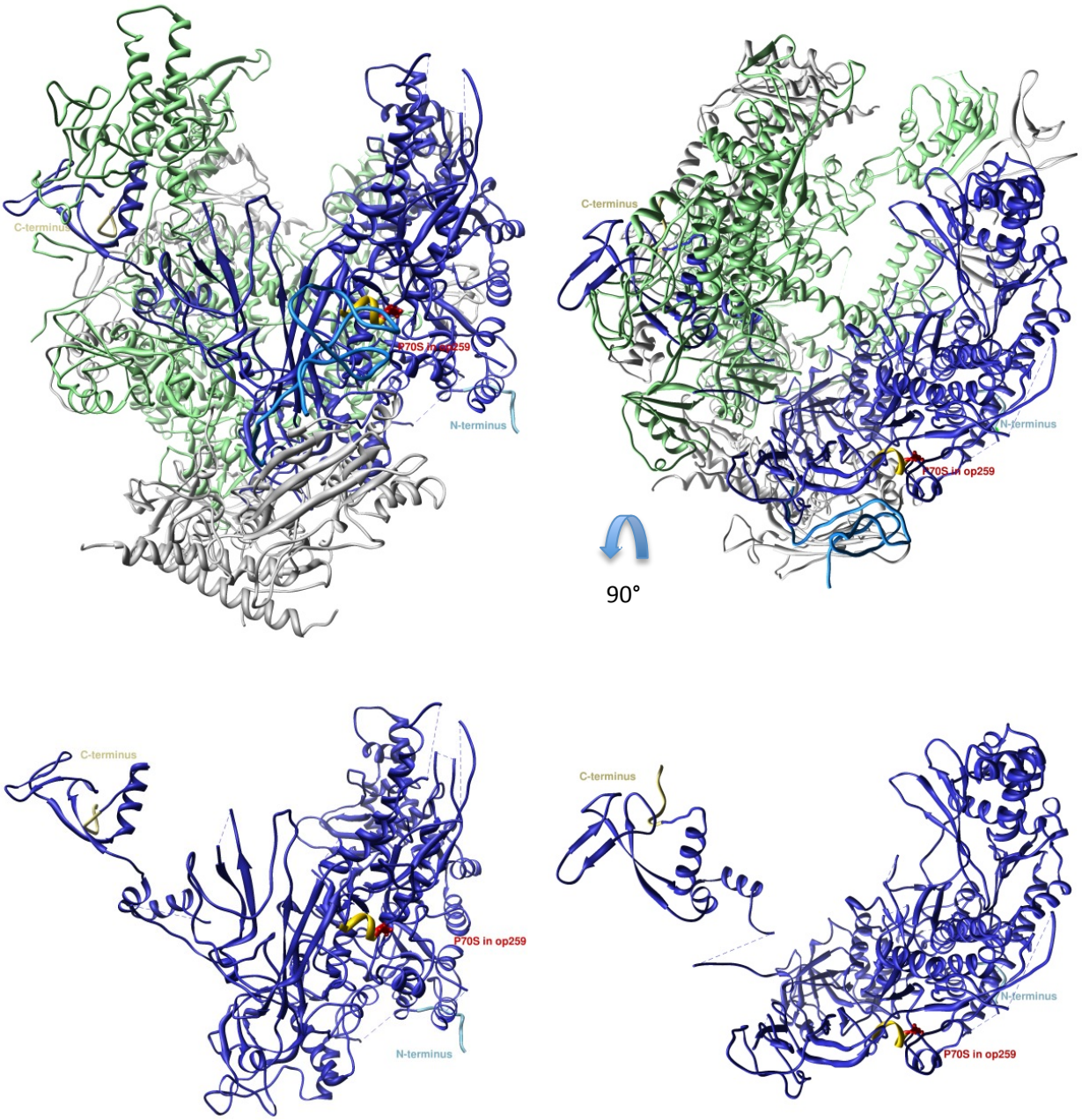

Figure 9 X-ray diffraction-based ribbon-and-band representation of yeast RNA pol II (top) and selectively of the β-subunit (bottom). The largest (green) and second largest (blue) subunits form the catalytic centre for nucleotide addition to the growing transcripts. The position corresponding to P70 in *C. elegans* RNA pol I (red) is at the beginning of a conserved α-helix (yellow), which localises toward the surface of the subunit and of the depicted RNA pol II core complex. Possibly, Rpb12 (cyan) is in close proximity to this region. Front view (left) and top view (right) according to (Cramer 2001). Rendering was done with UCSF Chimera Software (Pettersen 2004).

4.3.2 P70S hits a potential interaction site

In this crystal structure of the RNA pol II core complex from yeast, the mutated proline (P70S) maps to the beginning of a helix in a region that lies distant to the catalytic centre of the polymerase, towards an outer surface of the core complex (Figure 9); it could thus well be part of an interaction site for none-core components. Considering the linear amino acid sequence, the *op259* mutated site localises to a protein domain which in RNA pol II is predicted to form a protrusion (Cramer 2001). The proline is at the beginning of an alpha helix, nested in a domain that is supposed to interact with Rpb12.

A motif search by ScanSite (Obenauer 2003) predicted the proline mutated in *rpo-1b(op259)* to be part of a potential SH3 domain-binding site, more specifically for Src, Crk, Grb2, or Abl SH3 domains (low stringency settings). SH3 domains bind to proline rich sequences. Together with the proline at position 67, the proline at position 70 forms the consensus PxxP in RPO-1B. In the mutated protein P70S, this site is no longer presenting an SH3 binding motif. The predicted motif in RPO-1B only appeared at low stringency search settings; no such prediction was made for orthologs since only *C. elegans* has the preceding proline. Interestingly, however, the other metazoan homologs share a PxxP motif about 15 positions upstream that is missing in RPO-1B (Figure 8).

ABL-1 is a non-receptor tyrosine kinase known to regulate various aspects of cell proliferation and survival. In *C. elegans*, *abl-1* loss-of-function mutant worms have increased germ cell death and are hypersensitive to IR (Deng 2004). This is in agreement with the notion of a potent pro-survival activity of ABL in mammalian cells. As specified further in the text, *rpo-1b(op259)* can genetically suppress *abl-1(lf)*. *rpo-1b(op259); abl-1(ok171)* double mutants show only little germ cell apoptosis and no significant increase upon irradiation. It is therefore challenging to think of a possible mode of action if direct interaction of ABL-1 and RPO-1B at P70 were to regulate apoptosis.

4.3.3 Transgenic RPO-1B::YFP expression

I studied the cellular expression pattern of RPO-1B in several transgenic lines expressing YFP-tagged wildtype or mutant protein [see *5.9 rpo-1b(op259) transgenes and genetic background*]. Expression levels were variable between the strains. However, consistently, YFP::RPO-1B(P70S) had stronger cytoplasmic fluorescence than YFP::RPO-1B(wt). This was the case in the germ line as well as in somatic cells (Figure 10). We cannot tell at this point whether this is the result of reduced import into, or increased export from the nuclei. Altered protein localisation (e.g., cytoplasmic retention) offers a possible explanation for reduced transcriptional activity of RNA pol I in *rpo-1b(op259)*; alternatively, it might be linked to an rRNA processing defect [see *4.4.10 Summary of rRNA quantification methods*]. It is conceivable that cytoplasmic RPO-1B interferes with regulatory pathways for cell cycle control or apoptosis.

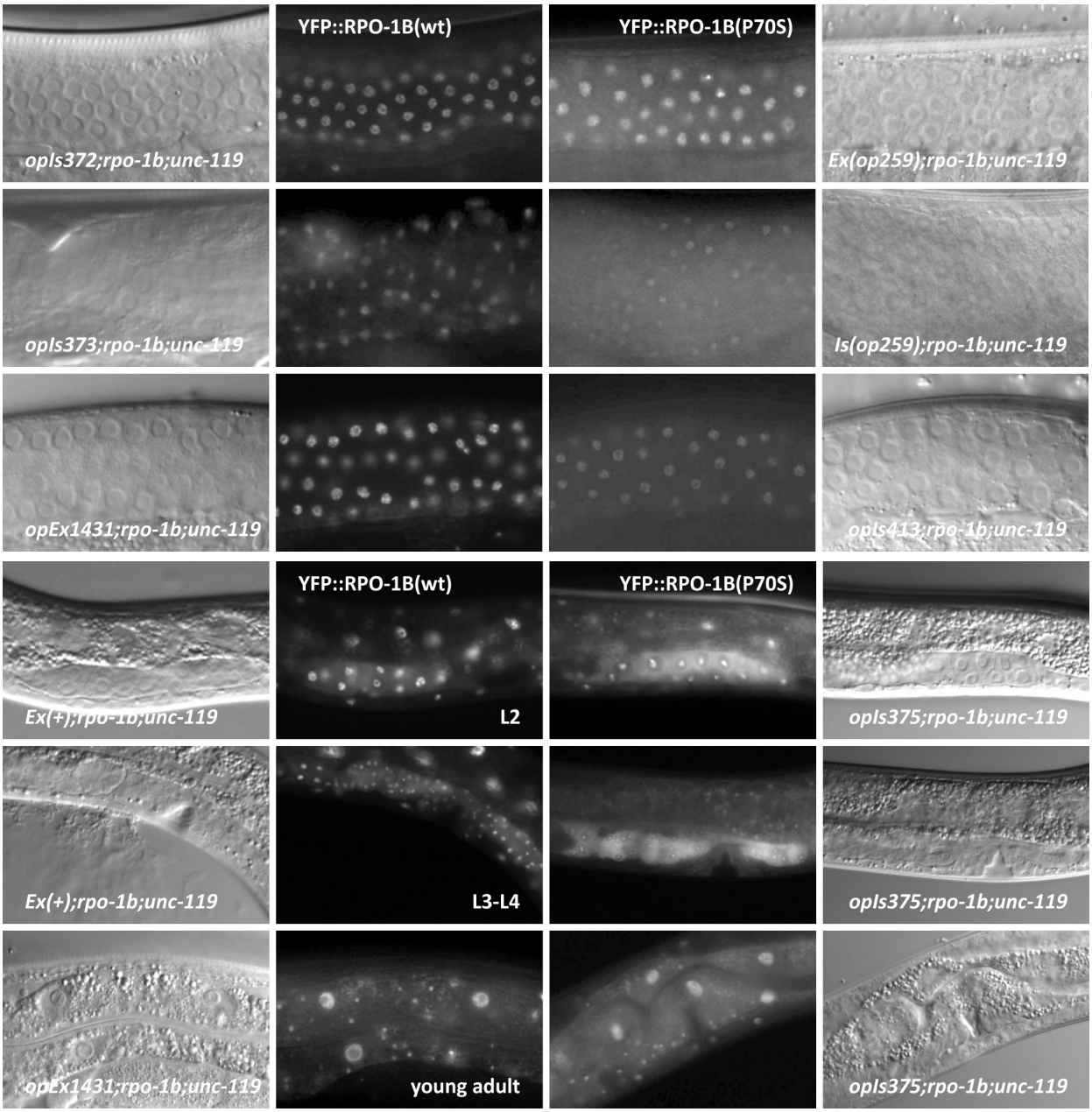

Figure 10 Mutant RPO-1B has an increased ratio of cytoplasmic versus nucleolar protein localisation. YFP::RPO-1B(P70S) spares the nucleoplasm, which makes cytoplasmic fluorescence clearly apparent. Meiotic pachytene region of the adult germ line (top) and somatic cells of the developing vulva and uterus, and intestinal cells (bottom). *opEx* and *opIs* are extrachromosomal and integrated transgenes, respectively; *Ex(+)* or *Ex(op259)* and *Is(op259)* are transgenes of wildtype or mutant RPO-1B for which the transgenic line has been lost before freezing.

4.4 rRNA and ribosome synthesis in *rpo-1b(op259)*

By its homology to the second largest RNA pol I subunit, RPO-1B is an essential factor for synthesis of rRNA and thus for most biological processes. Mutations in the well conserved transcription complex likely lead to alterations in the highly regulated rRNA synthesis process. From the essentiality of rRNA synthesis it is obvious that only mild effects of such mutations could be tolerated in a viable system. Loss of RNA pol I function would prevent growth and survival of an organism, and severe reduction of rRNA synthesis would probably soon result in exhaustion of a cell's capacity for protein synthesis. One would thus expect that a mutation in RNA pol I found in a viable organism could not be affecting net synthesis of rRNA too significantly. Conversely, alterations of transcription per se, i.e., transcription initiation, elongation or termination, will not necessarily lead to a strong phenotype: since ribosomal synthesis is highly regulated and responds to changes in cellular metabolism very quickly and flexibly (Suthers 2007), there must be great potential for up- or downregulation of this process. Production and turnover of ribosomes is controlled on various levels; alterations in the functioning of the rRNA transcription machinery might be compensated for by a multitude of concomitant or subsequent regulatory mechanisms of rRNA or ribosomal synthesis. (Certainly, there are limits to correction of a reduced rate of rRNA transcription due to defective RNA pol I; transcription by RNA pol I is probably one of the most rate-limiting steps in the production of ribosomes (Chédin 2007; Laferté 2006a), as is already introduced above in *4.1.5.2 rRNA transcription rate is regulated by RNA pol I initiation*). Conclusively, a mutation of RNA pol I in a viable system must either have only mild effects on transcription itself or its consequences must not exceed the compensatory mechanism.

4.4.1 *rpo-1b(op259)* mutants have small nucleoli

If a mutant organism largely compensates for defects in a core biological process on a gross phenotypic level, there might be multiple adaptations of function and structure at intermediate levels of biological organisation. *rpo-1b(op259)* animals are wildtype in many aspects. When looking at features that are likely linked to rRNA synthesis on a cellular level, however, one difference is very prominent: nucleolar size in DIC microscopy. The nucleoli are primarily the sites of rRNA transcription and of early steps of ribosome assembly. Changes in these processes might be reflected in nucleolar size and structure. The germ cell nucleoli, huge in relation to the nuclei or the germ cells, are smaller in *rpo-1b(op259)* animals (Figure 11). These smaller nucleoli might have led to the initial false positive pick of *op259* in the cell cycle arrest screen [see *5.2.2.1 rpo-1b(op259) do arrest proliferating germ cells upon DNA damage*]. When *op259* was mapped and found to affect a RNA pol I subunit, Lilli Stergiou and Randall Hofmann measured nucleolar size in different compartments of the germ line as well as in embryos. The diameter of the nucleoli as visualised by DIC was significantly reduced in all these cells. Taking the ratio of nucleolar diameter between mutant and wildtype to the three, the volume of the nucleoli is reduced by almost half in the mutant. Thus, the mutation in *rpo-1b(op259)* is certainly not without consequences for the cytological correlate of rRNA synthesis.

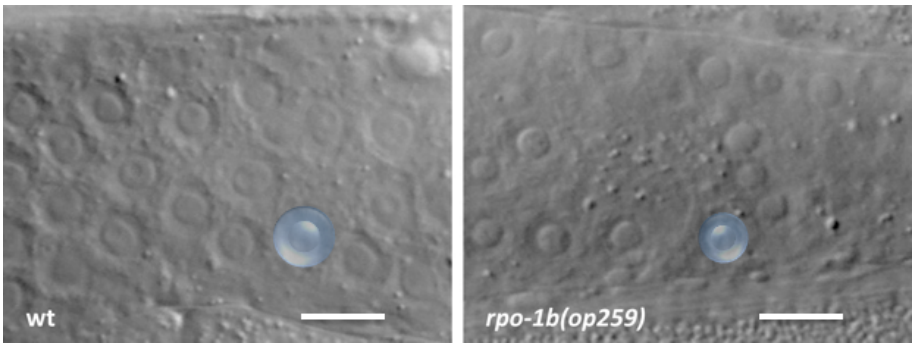

Figure 11 Nuclear and nucleolar size of germ cells in the late meiotic pachytene region. *rpo-1b(op259)* mutants have smaller than wildtype nucleoli (inner blue sphere) and nuclei (outer blue circle) by DIC microscopy.

4.4.2 Are rRNA synthesis and apoptosis connected?

To assess possible consequences of the *op259* mutation on RNA pol I activity, I decided to characterise various aspects of rRNA synthesis and ribosome biogenesis: transcription and processing of rRNA precursors, and levels of mature rRNA and of ribosomal proteins. Initially, the apoptotic defect of *rpo-1b(op259)* seemed to be specific for DNA damage response. Given the drastic regulation of rRNA synthesis in response to environmental changes (Ruggero 2003), I considered that such an adaptive process might be disturbed in *rpo-1b(op259)*. With the methods I applied to assess rRNA synthesis, I aimed at comparing *rpo-1b(op259)* to wildtype in a first step; in a further step, the response to DNA damage should be compared between the two.

4.4.3 Challenges of rRNA quantification

Since research on ribosome biogenesis in *C. elegans* was still in its infancy and not many methods for quantitative and qualitative analysis of rRNA had been used in the worm, I needed to search for according procedures in other systems and adapt them to *C. elegans*. One of the main challenges with all methods was the relative abundance of ribosomal RNA and protein. While mature ribosomal RNAs are easy to detect by most methods due to their supremely high abundance, their levels can hardly be normalised by any RNA that would approximate their order of magnitude. This is relevant because many methods have a very limited linear range for signal detection, and saturation is reached for rRNA signals long before other RNAs even pass the detection threshold. Ribosomal RNA is thought to constitute about 60 % of total cellular RNA in yeast (Warner 1999). A drop in the level of a single, much less abundant RNA, even if dramatic, would not notably affect relative measurements of other RNAs and can be neglected. However, changes in the levels of rRNA will significantly impact on the relative fraction any other RNA species occupies in the total RNA. Theoretically, if rRNA was reduced to half its amount, other RNAs would apparently be increased about 1.4-fold $[100/(100 - 0.5 \cdot 60)]$; rRNA itself would not be reduced from 60 % to 30 % of the total, but to only about 45 % $[30/(100 - 0.5 \cdot 60)]$.

4.4.4 Quantitative RT-PCR

4.4.4.1 Internal controls of RNA levels – are they robust?

Quantitative reverse transcription-PCR (qRT-PCR) has proven an accurate method to determine cellular levels of specific RNAs (Bustin 2002). However, it is not a quantitative analysis of absolute levels of a transcript, but gives relative numbers. Critical for reproducible measurements are therefore good internal controls in the samples, that is, endogenous transcripts with only little variation from one biological regimen to another of its class. The measurement for the transcript of interest can then be normalised by the levels of these controls. Often, so-called housekeeping genes fulfil this requirement and are used for normalisation: their products serve as a cell's basic constituents, such as structural proteins or key enzymes of metabolic pathways. The mRNA levels of these factors are supposed to be more or less stable between different samples. The validity of some of these normalisation factors for *C. elegans* has been addressed (Hoogewijs 2008). Careful selection is imperative and should consider the specific biological context. Might the levels of the controls not also be affected by biological differences between two samples, primarily or secondarily? Generally, a set of relatively independent controls rather than an individual factor can help to reduce this risk.

4.4.4.2 Competimers for rRNA reduce signal intensity

The controls need not be mRNA. In fact, other transcripts serving a more general and more basic process in a cell might give a more stable measure. Indeed, 18S rRNA levels were shown to be less dependent on developmental stage or tissue type than structural or metabolic factors often used as controls, like actin or GAPDH (Goidin 2001). Obviously, it does not serve when rRNA levels are expected to be subject to alterations themselves. Yet, in that study, they present a method how to apparently shift the order of magnitude of rRNA levels without simultaneously affecting the detection of other RNAs in the same sample: competitive primers are added to a qRT-PCR reaction (Figure 12). If a fraction of the specific primers is modified at the 3' end, such that they still anneal efficiently to the template but prevent elongation by the DNA polymerase, these competimers will continuously hide the majority of the cDNA to be measured by qPCR. Thus, only a fraction of the highly abundant template is accessible and amplification efficiency decreases, leading to lower signal. This brings the apparent levels of rRNA into the range of other transcripts in the same sample, allowing now relative quantification with parallel reactions that amplify normally (Figure 12).

I adopted this method to quantify mature ribosomal RNA in *C. elegans* by qRT-PCR and designed competimer primer sets for amplicons of all the RNA pol I transcribed rRNAs: the 18S, 5.8S and 26S (Figure 13).

For controls, I initially chose transcripts of the metabolic enzyme PGK-1 or of TBP-1, as well as of the ribosomal proteins S4 and L29. In further experiments, I included some of the transcripts shown to behave relatively stably in (Hoogewijs 2008), namely CDC-42, PMP-3, and Y45F10D.4. Martin Moser ran all the qPCR reactions mentioned in this study and assembled the quantitative data.

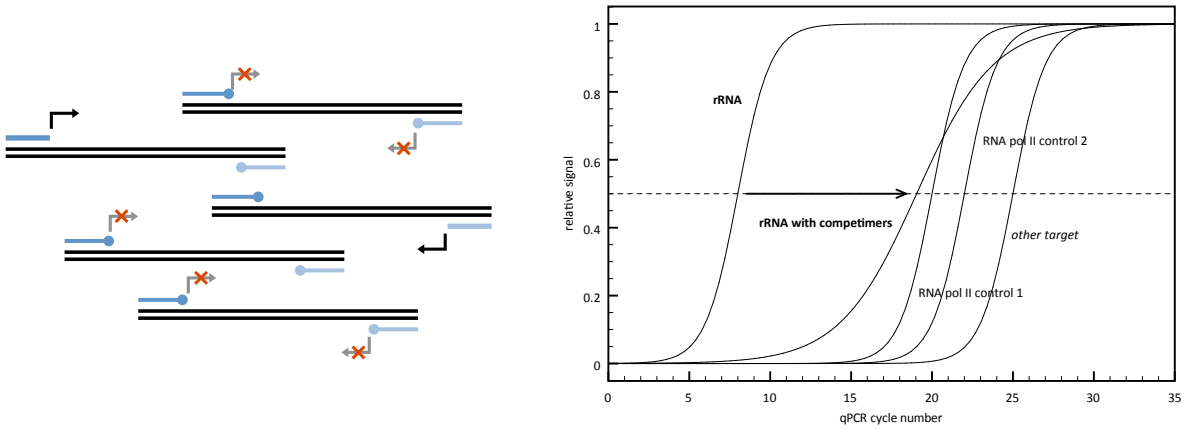

Figure 12 Primer competimer strategy to quantify abundant transcripts. Oligos with a 3'-modification compete with normal, extensible primers, and impede amplification of the so bound template. The specific template that remains accessible to the DNA polymerase is virtually reduced in an otherwise not diluted sample, and the amplification curve for the abundant transcript (rRNA) approximates the range of the internal controls.

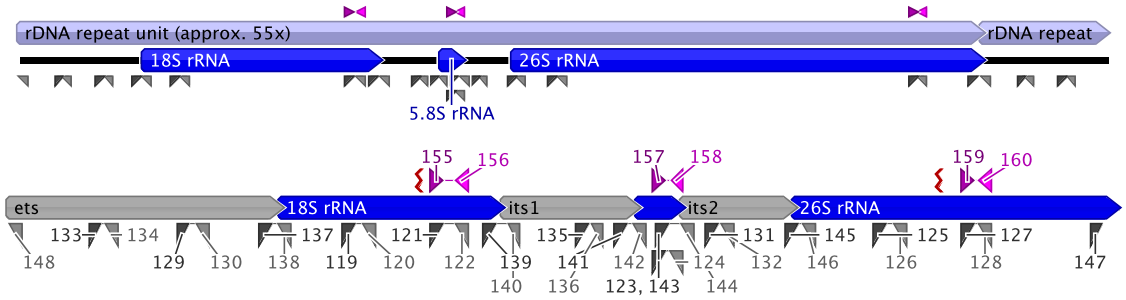

Figure 13 Overview of two adjoining rDNA repeat units with the position of the primers used for qRT-PCR (top) and detailed map with primer names (bottom; contractions within the rRNA are indicated as red flashes). Primer pairs cover regions within the mature rRNAs for quantification of rRNA levels, or they span putative processing sites within the transcribed spacers or between spacer and rRNA to measure levels of the short-lived pre-rRNAs. The primers in magenta represent the competimers, which were mixed to the extensible primers in a ratio of 3:1. The 5' and 3' ends of the pre-rRNA transcript are within the ets, but have not been precisely defined in *C. elegans*.

4.4.4.3 *rpo-1b(op259)* mutants have reduced rRNA

Ribosomal RNA was significantly reduced in *rpo-1b(op259)* mutants. On average, the relative levels of 18S, 5.8S or 26S were only about 70 % of N2 (Figure 14). The probes used in this qRT-PCR assay did not distinguish between mature rRNA and its precursors; since mature rRNA abundance exceeds by far its precursors, the values measured here can be supposed to represent mature RNA, however. To look at the short-lived precursor specifically, I used primers that anneal to the transcribed spacers ets, its1 or its2, and would thus only amplify the cDNAs of transcripts that have not yet been processed in the respective regions (Figure 13). Fully mature rRNAs would thus not overlay the signal from precursors. I specifically determined the levels of rRNA-precursors that still have the 5'ets, the transition from 18S to its1 (18S-i1), the its1, or the transition from 5.8S to its2 (5.8S-i2). Overall, precursor-rRNA levels were slightly reduced in *rpo-1b(op259)* mutants. The reduction was less significant than for total (mature) rRNA levels.

These observations are in agreement with the results from other methods to assess ribosomal synthesis as presented below.

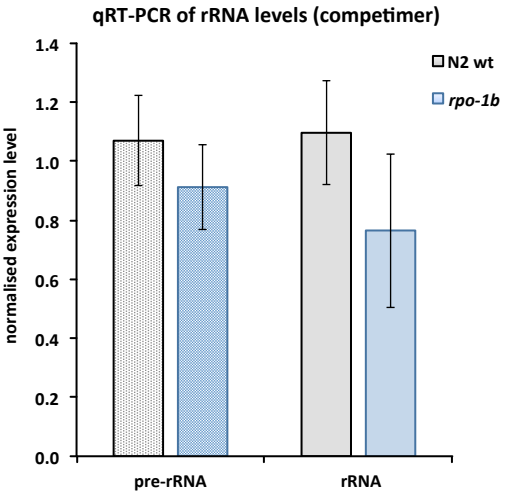

		wt		*rpo-1b(op259)*		*rpo-1b*/wt	t-test
		level	95% CI (n)	level	95% CI (n)	ratio	p-value
pre-rRNA	no IR	1.07	±0.15 (16)	0.91	±0.14 (8)	**0.85**	0.210
	60 Gy	1.02	±0.09 (11)	0.77	±0.21 (7)	**0.75**	0.027
	IR/no IR	**0.95**		**0.84**			
	t-test	0.597		0.271			
rRNA	no IR	1.10	±0.18 (20)	0.77	±0.26 (8)	**0.70**	0.055
	60 Gy	0.97	±0.14 (8)	0.42	±0.06 (5)	**0.43**	9.8E-05
	IR/no IR	**0.88**		**0.55**			
	t-test	0.398		3.6E-04			

Figure 14 rRNA quantification by qRT-PCR shows reduced levels of the mature transcripts in *rpo-1b(op259)* whole-worm RNA extracts. Levels of pre-rRNA and rRNA (competimer) were normalised to internal controls (Pol II transcripts) and related to one standard N2 wildtype sample in the according qRT-PCR set-up (multiple independent N2 wt samples per set-up explain values different from 1.0 and presence of error bars (95% CI)). The table compares levels without and with irradiation (columns), and between *rpo-1b(op259)* and wt at the respective conditions (rows). (n) indicates the number of samples tested for the according condition. There is a significant drop of the *rpo-1b*/N2 ratio upon IR irradiation, particularly for rRNA. This is most likely due to the strong reduction of the levels in *rpo-1b(op259)* after irradiation.

4.4.5 Nuclear run-on

I performed these experiments with the kind help from Helene Sharpe in André Furger's lab at the Department of Biochemistry, University of Oxford.

4.4.5.1 Freshly made transcripts are selectively labelled

The role of RPO-1B as a major subunit of RNA pol I suggests that rRNA transcription would be the first process to be affected by a mutation. I thus sought to determine whether and how transcription of rRNA would differ in *rpo-1b(op259)*.

In yeast, in cell culture systems, or in *in vitro* transcription systems, ongoing transcription can be assessed by run-on experiments. The system is provided with labelled nucleotides for a short time. An intact transcription machinery incorporates the labelled nucleotides into RNA that is being synthesised during this pulse. Newly synthesised RNA can then be assessed selectively by its label. If the pool of extracted RNA is hybridised to specific probes, the signal intensity allows to quantify transcription of any sequence of interest during the pulse, and thus to compare different transcripts within one sample. As this is a run-on and not a run-off, the sequences towards the 3' ends of the transcripts are not preferentially labelled. This allows even to compare transcription from different segments of one gene, when probes are used that specifically bind to a sub-sequence of a transcript. The labelled transcripts are fragmented before hybridisation to the probes; depending on the average fragment length and the probe length, transcription can be resolved down to some hundred nucleotides.

4.4.5.2 Extraction of functional nuclei by mechanical procedures

The bottleneck for using the run-on method with the worm obviously is the resistant, nearly impenetrable cuticle. Some drugs and substances that are ingested by the worm can readily be detected inside various tissues when presented in the agarose and/or the bacteria that *C. elegans* feeds on. However, the kinetics for nucleotides applied to the worm is not known; it would very likely prevent the rapid uptake into cells as required for a reasonably short pulse with labelled nucleotides. Alternatively to bringing the nucleotides into the tissues, the nuclei as the main cellular compartment for transcription could be extracted and incubated with labelled nucleotides. André Furger and his lab had been developing a method to extract functionally intact nuclei from live adult *C. elegans*. With mechanical rupturing of the resistant cuticle, the nuclei can be released and then be separated from most tissue fragments and cellular material by filtering steps and by differential centrifugation. The isolated nuclei are of good purity and remain transcriptionally active if maintained at favourable conditions. André Furger's group had been applying this method successfully to study transcription termination of RNA pol II transcripts.

4.4.5.3 Slot blot stripes for rRNA

Considering the high transcription rate of ribosomal RNA, this method should thus be sensitive enough to detect RNA pol I transcription already from a small amount of sample. I designed an assay that covered various regions of the polycistronic rRNA transcript (Figure 15) and would therefore not only allow to assess overall transcription efficiency by RNA pol I, but would also reveal if the mutant had a defect specifically in one aspect of transcription (processivity or transcription termination, for instance). Furthermore, I expected to detect differences in the processing of the normally short-lived rRNA precursors should there be any between *rpo-1b(op259)* and wildtype. Helen Sharpe kindly instructed and assisted me with probe preparation, nuclear extraction, run-ons and hybridisation experiments. We transcribed antisense RNA-probes from the linearized plasmids so they were of a well-defined length (Table 2). Efficient transcription and probe integrity were confirmed by gel electrophoresis. All antisense RNA-probes were transferred to a membrane on separate, standardised areas by the slot-blot technique and cross-linked by UV-C irradiation. In parallel, we extracted nuclei from worms that had been grown in liquid culture to a total of about 1 ml. The nuclei were purified and incubated for 20 min with radiolabelled uridines in excess along with non-labelled adenine, guanine, and cytosine. In control experiments, alpha-amanitin was added before this incubation step to slow down RNA pol II and III transcription. Immediately following the incubation with the labelled uridines, RNA was extracted by the hot-phenol method, and the purified RNA was fragmented to an average 300 nt long pieces that were then ready for hybridisation to the prepared membranes. The signals from individual slots representing the amount of labelled RNA bound to the specific probes were captured by phospho-imaging and quantified relative to each other.

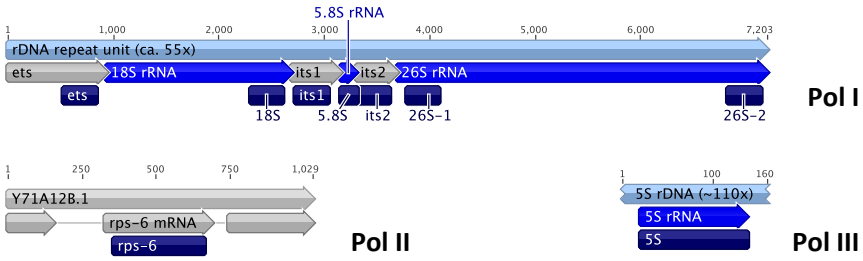

Figure 15 Position of the run-on probes on the pre-rRNA transcript and the Pol II and Pol III controls. The 5.8S and 5S rRNAs are shorter than 300 nt and are fully covered with the probe. The 5S rRNA is encoded in a repetitive region on chromosome 5 (LG V), with a repeat unit length of approximately 1 kb. The 5S early transcripts have not yet been investigated in *C. elegans*.

probe	accession	fw primer	rv primer	length*	GC%	U content**
ets	X03680.1	CACACTCCTATATGTGTCAGGG	GACCAATACCGCAACATCATTAGT	303	50.2	97
18S	X03680.1	CACGAGATTGAGCGATAACAGGTC	CGAAGTCGTTAAACCTCGAAGCG	301	51.2	81
its1	X03680.1	GATGCTCGACTGGCTTCACG	CCGAACCACGATCATCAAGACTAT	300	47.7	90
5.8S	X03680.1	CTAGCTTCAGCGATGGATCGGT	CAACCCTGAACCAGACGTACCA	151	51.0	39
its2	X03680.1	CTCAATGCCTTAGGCTTCTCTTCG	GACGAATCCCAGTATTCGAAAGGAG	300	49.0	90
26S-1	X03680.1	GTAACGGCGAGTGAAACGGGA	GTCCTTTGCAACTTTCCCTCACG	301	51.2	71
26S-2	X03680.1	CGAGAGGAACAGCGGGTTCAAA	GACCAAGAGACCAAGTCGTATGC	299	48.8	83
pGEM***				(128)	(59.4)	(25)
5S	X06102.1	GCTTACGACCATATCACGTTGAAT	AGCTTACAACATCCAGGATTCCC	119	51.3	30
rps-6	AL132902.4	GACAAGCAGGGATTCCCAATGAAG	GACGTATTTGGTGACATCGTCGTG	303	53.8	54
V2	U56966	Position 22220 - 22519		300	53.3	66
V3	U56966	Position 26894 - 27339		446	42.6	131

* Length of the specific target sequence (insert in pGEM-T easy).

** Uridine contents of the complementary sequence (T7 antisense transcripts).

*** Empty pGEM-T easy vector. Length of the SP6 transcript is indicated in parenthesis. (All SP6 transcribed probes contain these flanking sequences from the vector.)

Table 2 Primer pairs used for cloning of the run-on rRNA probes into the pGEM-T easy transcription vector and probe characteristics. U content is indicated for the T7 transcript (complementary to the probe and thus corresponding to the run-on transcript sequence).

4.4.5.4 Experiments and controls

Normalisation by probe loading amount

We spotted multiple membranes with the same set of antisense RNA-probes. To ascertain that the same amount of probe had been blotted to each membrane, we hybridised them with a labelled transcript complementary to a sequence that was present in almost all RNA probes on the blot: the specific RNA probes had been cloned as inserts in the common transcription vector pGEM-T Easy [Promega], and thus they contained common flanking sequence stretches from this plasmid (Table 2). The signals from this hybridisation was used to normalise the NRO signals by the amount of probe on each individual slot (Figure 16).

Normalisation by RNA pol II and RNA pol III transcription

The probes for the assessment of rRNA transcription and early processing comprised: probes to 18S and 5.8S, and two probes to 26S rRNA; a probe each to the 5'ets, to its1 and to its2; one probe to the

RNA pol III transcribed 5S; one probe to the RNA pol II transcript *rps-6* (*rps-6*) and two probes to vitellogenin (vit); finally, a short probe transcribed from the pGEM-T vector without any insert (Figure 15).

In the first experiment, we compared *rpo-1b(op259)* and N2. In a second experiment, we pre-incubated *rpo-1b(op259)* and N2 with or without α-amanitin to ascertain that the rRNA signals were from RNA pol I transcription. In a third experiment, we UV-irradiated *rpo-1b(op259)* and N2 worms or left them untreated. Thus, we had three NRO replicates of non-irradiated N2 and *rpo-1b(op259)*.

The signal intensities from the rRNA probes were very strong and clearly outweighed the signal of the RNA pol II transcripts (Figure 16). For each membrane, we calculated the signal ratios of the RNA pol I transcripts to the controls: either to 5S rRNA, to *rps-6*, to the geometrical mean of 5S and *rps-6*, or to a weighed average of 5S rRNA and all RNA pol II transcripts. The ratios varied slightly depending on the controls included, because: first, 5S rRNA was the only control for RNA pol III and maybe was not fully stable between experiments; second, the signals from the RNA pol II transcripts were in another order of magnitude than the signals from the highly abundant rRNAs, and it was not clear whether the weak and strong signals were in a linear range of signal intensity. Nevertheless, we would rely more on the relative values within one membrane than on differences of absolute signal intensities between different membranes.

In the control experiment with α-amanitin, the ratio of 5S rRNA to RNA pol I transcripts was reduced to about 50 %, showing that the RNA pol I signal is less affected by the drug than the RNA pol III signal, and therefore supporting that the signals are largely specific for the respective polymerases.

4.4.5.5 *rpo-1b(op259)* has reduced relative RNA pol I activity

For each probe of a sample, we calculated the ratio to 5S and *rps-6*, and we than compared these relative values between different samples. When grossly comparing relative RNA pol I transcription rates between *rpo-1b(op259)* and N2, there was no clear trend from the three experiments; only in one experiment *rpo-1b(op259)* had clearly lower RNA pol I transcript levels than wildtype over all probes. We chose two ways of how to perform a combined analysis of the three experiments; either, for each probe, the relative signal was compared between *rpo-1b(op259)* and N2 in all three experiments separately, and the mean of the three *rpo-1b(op259)* to N2 ratios was calculated (mean of ratios); alternatively, for each probe, the mean of the three *rpo-1b(op259)* samples was compared to the mean of the three N2 samples (ratio of means). The results of these calculations depended on whether averages (arithmetic mean) or the geometrical mean of individual ratios were considered. In the case of averages, the mean of ratios was only slightly below 1, whereas the ratio of means clearly indicated a reduced relative RNA pol I signal in *rpo-1b(op259)*. In the case of geometrical means, the mean of ratios and the ratio of means were identical and showed a reduction of the relative RNA pol I signals in *rpo-1b(op259)* to 50-70 % of wildtype (Figure 16 bottom).

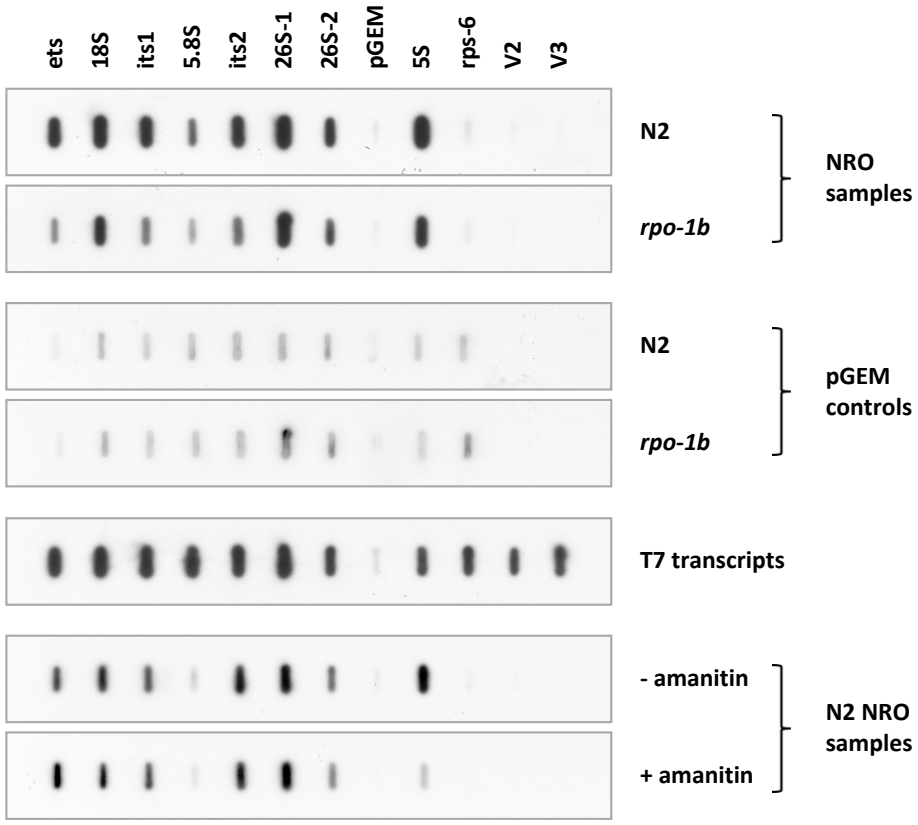

Figure 16 NRO analysis of relative RNA pol I transcription rate. Radiolabelled transcripts from extracted wildtype and *rpo-1b(op259)* nuclei (NRO samples); hybridisation of stripped blots with radiolabelled pGEM probe to control for equal probe transfer to the membranes (pGEM controls). Hybridisation with a mix of equal amounts of in vitro transcribed, radiolabelled sense transcripts to judge on binding affinity for each individual probe (T7 transcripts); V2 and V3 were on a variant vector and actually transcribed with SP6 polymerase). Pre-incubation without or with α-amanitin to block RNA pol II and RNA pol III transcription (N2 NRO samples).

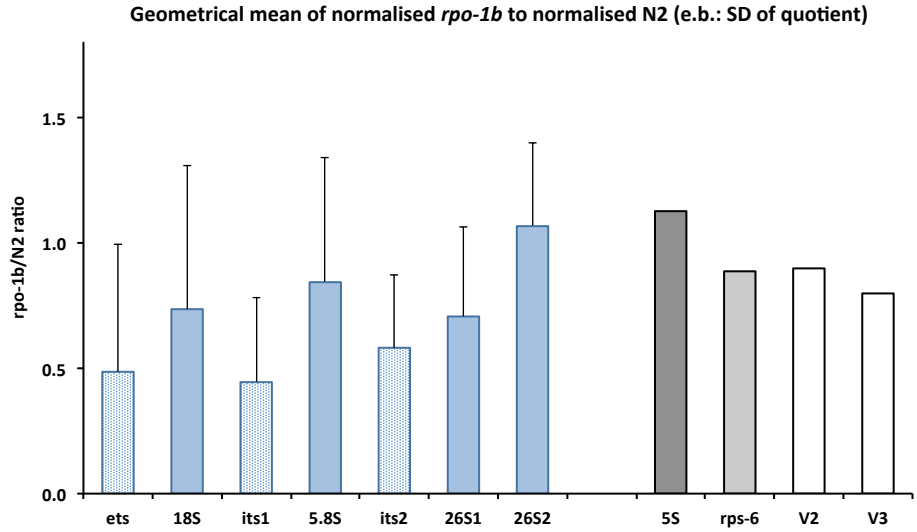

Figure 17 Relative NRO signal intensities in *rpo-1b(op259)* compared to wildtype. All signals were internally normalised by the geometrical mean of 5S and rps-6 signal intensity. For calculations see text. Analysis of three independent experiments.

pre-rRNA and rRNA vary differently

Independent of the analysis method, there was a striking pattern for the RNA pol I probes: across all experiments and for each individual experiment, the *rpo-1b(op259)*/N2 ratios for the pre-rRNA specific probes were lower than those for the 18S, 5.8S or 26S rRNA (Figure 16). This could indicate differential kinetics of transcription and processing between *rpo-1b(op259)* and N2.

Intriguingly, the 26S-2 probe gave a less reduced signal than the 26S-1 in all three comparisons of non-treated *rpo-1b(op259)* and N2. It cannot be easily judged whether this is on the account of a 26S-1 to 26S-2 gradient within wildtype or within *rpo-1b(op259)* samples, or within both, since no absolute levels can be measured by the NRO method. Anyway, the disparity is interesting with regards to the 26S-short rRNA that will be described and discussed in the according section *4.4.7 The 26S-short rRNA*. It could also indicate that at any given time point, more polymerase is active towards the 3' termini of the rRNA genes in the mutant, e.g., due to deceleration.

Of note, after UVC-irradiation the difference between relative 26S-2 and 26S-1 was reversed, so that in comparison of *rpo-1b(op259)* with N2, 26S-2 was more strongly reduced than 26S-1. The fact that here, a particular aspect of rRNA synthesis seems to respond differently in the mutant than in wildtype, hints at a possible link between irradiation response and this process; and at a role for *rpo-1b(op259)*. Due to missing replicates of the UVC-irradiation experiment, the significance of this observation is not yet substantiated.

4.4.5.6 Irradiation and RNA pol I transcription

The single experiment where we looked at DNA damage-induced changes of rRNA transcription revealed a very interesting difference between *rpo-1b(op259)* and N2. For non-irradiated animals, the ratio of RNA pol I transcripts to 5S rRNA was significantly lower in *rpo-1b(op259)* than in wildtype (*rpo-1b(op259)* ~20 % of N2). In animals that had been irradiated with 200 J/m^2 of UVC 2.5 hours before nuclear extraction, the Pol I to Pol III ratio dropped by 50 % in N2, but it remained almost unchanged in *rpo-1b(op259)*; this resulted in a milder difference of relative RNA pol I transcription between *rpo-1b(op259)* and N2 after irradiation (*rpo-1b(op259)* ~35 % of N2). For one thing, this experiment suggests that irradiation causes a shift in the ratio of RNA pol I to RNA pol III transcription in wildtype worms. Secondly, in *rpo-1b(op259)*, this relative RNA pol I to RNA pol III transcription rate seems not to change strongly upon irradiation.

Possibly, irradiation affects RNA pol III transcription

With qRT-PCR analysis, I had seen slightly lower levels of the short-lived precursor-rRNAs in *rpo-1b(op259)* than in N2, when normalised to housekeeping genes (Figure 14). Also, when related to 5S rRNA, these pre-rRNAs were lower in *rpo-1b(op259)*; this is consistent with the reduced relative RNA pol I transcription found in the NRO experiment.

Upon irradiation, pre-rRNAs did not show a trend to increase or decrease in relation to the RNA pol II control transcripts in wildtype. However, using the same controls, the levels of 5S rRNA tended to be increased 3 hours after irradiation. UV-C-irradiation reduced the ratio of RNA pol I transcripts to 5S rRNA in N2 by 40 %; a similar reduction could be observed after IR treatment of wildtype. Contrarily, in *rpo-1b(op259)*, pre-rRNA and also 5S rRNA levels remained almost unchanged after IR, and thus the

ratio remained constant. The trend was similar with qRT-PCR and NRO: wildtype worms had an increased 5S rRNA to pre-rRNA ratio 3 hours after irradiation; *rpo-1b(op259)* mutants had a higher ratio at baseline, but there was no response upon irradiation.

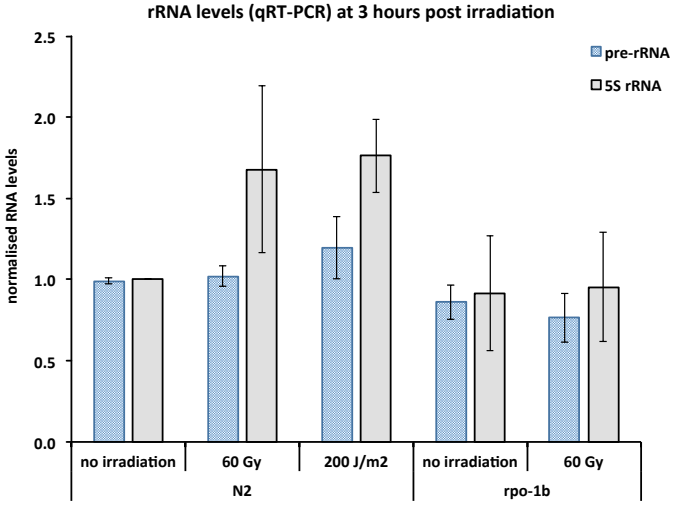

Figure 18 Levels of pre-rRNA and the RNA pol III-transcribed 5S rRNA in response to irradiation in wildtype and *rpo-1b(op259)* total RNA extracts. Normalised to RNA pol II control transcripts. Error bars 95% CI of the mean, 7 to 28 samples per condition.

These data indicate a possible implication of irradiation on the transcription rate of RNA pol III, more than on RNA pol I. Generally, precise quantification of the short (<119 nt), highly abundant 5S rRNA transcript is difficult with random-primed reverse transcription and qPCR; also, the total 5S rRNA levels as measured with this method might not reflect the transcription rate measured by NRO. While very exciting, these findings need verification by further replicates and/or by alternative methods.

4.4.6 Northern blot experiments

4.4.6.1 Processing of rRNA might be altered in *rpo-1b(op259)*

The qRT-PCR and NRO experiments were useful in quantifying transcription rates and levels of rRNA. They also indicated that *rpo-1b(op259)* might have an effect on rRNA processing. As described in *4.6.2.1 The processing mutant pro-2 shares phenotypes with rpo-1b(op259)*, *rpo-1b(op259)* shared several phenotypic aspects with *pro-2(na27)*; PRO-2 is the homolog of yeast Noc2p, a factor involved in nuclear export of pre-ribosomes (Milkereit 2001). The *pro-2* mutant had been shown to have processing defects of ribosomal RNA. Transcription of rRNA, processing, and pre-ribosome assembly are not separate events but are interdependent and co-regulated (Granneman 2005; Gallagher 2004); cotranscriptional processing and modification of rRNA was quantitatively assessed and modelled in great detail (Kos 2010). Of all things, a mutation in yeast Rpa135 evidenced the link between transcription by RNA pol I and efficient rRNA processing and ribosome assembly (Schneider 2007). This certainly supported the possibility of an effect of *rpo-1b(op259)* on rRNA and ribosomes beyond simple transcription of rRNA.

I sought to examine rRNA processing in *rpo-1b(op259)* mutants in more detail. The northern blot technique allows to assess levels of specific transcripts, and additionally it distinguishes RNAs by their length; it has been used among other methods to characterise the complex processing of the polycistronic precursor RNA for the 18S, 5.8S and 26S rRNAs in yeast and mammalian cells [reviewed in e.g., (Fatica 2002)]. Defects of certain early steps of rRNA processing can lead to accumulation of the pre-rRNA or to processing by alternative routes, eventually resulting in a characteristic pattern of processing intermediates. In northern blots, such intermediates show as aberrant bands of a certain size. For instance, *pro-1* mutants in *C. elegans* had been shown to differently process rRNA at the internal transcribed spacer its2, similar to yeast mutants of its homolog Ipi3 (Voutev 2006).

Northern blots might refine differences in rRNA transcription and processing between *rpo-1b(op259)* and N2. Alongside, I was interested whether irradiation of adult worms would influence rRNA transcription and processing at some steps; if so, I expected to reveal possible differences in this response between *rpo-1b(op259)* mutants and wildtype worms.

4.4.6.2 DIG labelled hybridisation probes

I used the same sequences that we had used for the NRO probes (Table 2) to generate antisense probes for northern blots. Instead of radioactive nucleotides, I used DIG (digoxigenin) to label the probes (Roche Applied Science). DIG labelled nucleotides can be incorporated into *in vitro* transcribed RNA and are detectable by a DIG-specific, alkaline phosphatase-coupled antibody. This is a sensitive method, allowing to work without radioactivity and to synthesise probes for multiple uses. I generated probes for the ribosomal RNAs 18S, 5.8S and two for 26S (26S-1 and 26S-2); and for the precursor sequences ets, its1 and its2. The probes its1 and its2 covered most of these internal transcribed spacers (Figure 15), such that processing intermediates that would retain the whole spacer or only a fraction at either end could be detected.

The probes for rRNA gave very strong signals of the expected size; the its2 pre-rRNA probe was sensitive enough to detect pre-rRNA intermediates of different sizes (Figure 19). Overall, the power of the DIG system was restricted by the fact that I was unable to strip the membranes once hybridised with a probe, and that I could therefore not easily test two different probes with overlapping signals on one membrane. I tried different strengths of the stripping procedure but always got residual signal in the subsequent detection, which would blend or overcome the specific signal of the second probe. Thus, I had to use separate membranes, or to step from the probe with a weak signal (its2) to the one with a strong signal (e.g., 26S-1) [see Figure 22].

I ran 200 to 800 ng of total RNA extracted from adult worms on denaturing agarose gels and blotted them on nylon membranes by passive transfer over several hours and UV-crosslinking. Hybridisation with the DIG labelled probes was at 68°C; this was followed by DIG detection using AP-coupled antibody and a chemoluminescent substrate, CPDstar, and exposure to a CCD camera.

4.4.6.3 pre-rRNA levels are not significantly reduced in relation to mature rRNA

For the its2 probe, one band of a size slightly larger than 26S rRNA was most prominent. Very likely, this band represents the intermediate following the scission in its1, which separates the 18S rRNA from the precursor RNA for the LSU rRNAs; this intermediate seemed much more abundant than the full-

length transcript (Figure 19). I used this band to approximate the ratio of pre-rRNA to mature 26S rRNA. A total of 20 samples of *rpo-1b(op259)* and of N2 were analysed on four independent blots with at least 3 samples each. Relative to the 26S rRNA signal detected with the 26S-1 probe, the pre-rRNA level in *rpo-1b(op259)* mutants was 95 % of wildtype (statistically not significantly different, p=0.33).

Northern blots hence did not demonstrate a decrease of pre-rRNA levels in *rpo-1b(op259)*. This, however, could be explained at least partly by a normalisation issue. Considering the overwhelming contribution of ribosomal RNA to total RNA [see *4.4.3 Challenges of rRNA quantification*], a drop of rRNA in a sample would increase the level of any other transcript, if the same amount of total RNA were to be loaded. In fact, the 26S rRNA bands were very steady between different genotypes. From the qRT-PCR results, one would expect a reduction of ribosomal RNA to 70 % of wildtype in *rpo-1b(op259)*. This means that about 1.2 to 1.4 times more of all non-ribosomal RNAs should fit into the same amount of total RNA. Despite almost equal signal intensity from pre-rRNA in *rpo-1b(op259)*, rRNA synthesis rates might in fact be reduced compared to wildtype; again, assuming a reduction of mature rRNAs to 70 % of wildtype, pre-rRNA levels are probably reduced by 20-30 % in *rpo-1b(op259)*. This is between the values calculated from the run-on experiments, which indicated a considerable reduction of pre-rRNA synthesis, and the minor reduction of pre-rRNA levels measured by qRT-PCR.

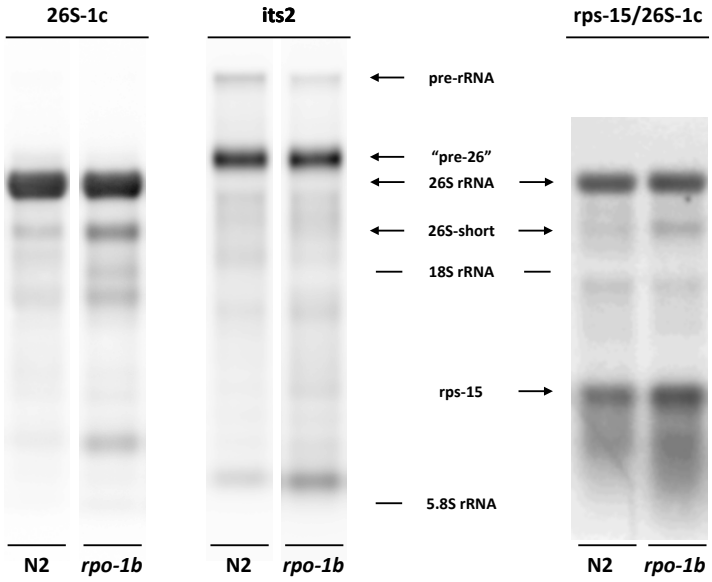

Figure 19 Hybridisation on northern blots of total RNA samples from wildtype and *rpo-1b(op259)* worms, with DIG-labelled probes complementary to sequences of the 26S rRNA (26S-01c, DNA oligonucleotide), the its2 of pre-rRNA (its2, 300 nt long antisense transcript), and to RPS-15 mRNA (rps-15, 300 nt long antisense transcript). An interesting side-observation of the experiment: the tail seen with the rps-15 probe was more pronounced with increasing growth temperature of the worms.

4.4.6.4 rRNA levels are reduced in comparison to mRNA

I used a probe to the mRNA of the ribosomal protein RPS-15 to assess the rRNA relative to an abundant RNA pol II transcript (Figure 19). Comparing lanes with equal amounts of total RNA, and similarly strong 26S rRNA signal, the signal from the *rps-15* probe was higher in *rpo-1b(op259)* than in wildtype (relative rps-15/26S signal ratio: *rpo-1b(op259)*/N2 = 1.49 (SD ±0.29) from three sample pairs [paired

t-test, p=0.17]) This supports the above notion and indicates that RNAs other than the bulk of mature rRNA are probably overrepresented in the *rpo-1b(op259)* samples.

4.4.6.5 *rpo-1b(op259)* have altered kinetics of irradiation-induced changes

With the its2 probe, there was a distinct band slightly larger than 5.8S rRNA (Figure 19); it likely corresponds to the 5.8S rRNA with an its2 tail, generated by processing of the 5.8S-26S rRNA intermediate, since a band of the same length can be detected with the 5.8S rRNA probe (Figure 21). The relative intensity of this band to the formerly described band at >26S rRNA (its2 probe) or to the 5.8S rRNA (5.8S probe) – direct internal controls – or to the 26S rRNA (26S-1 probe) was not constant. In at least three experiments, there was a moderate but consistent increase of this intermediate in samples from worms that had been irradiated (Figure 20). Related to 26S rRNA, the >5.8S signal peaked several hours after irradiation in N2 worms. Interestingly, the pattern of this transient increase of the >5.8S band also occurred in *rpo-1b(op259)*, but with seemingly accelerated kinetics. For the time points included, the relative signal intensity was maximal already at 30 min after irradiation.

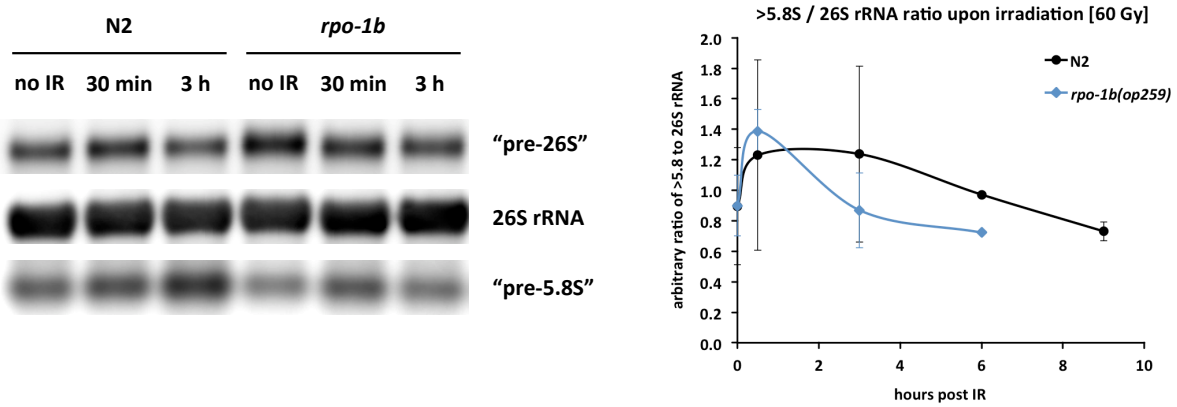

Figure 20 Time course of the >5.8S band intensity following IR irradiation in wildtype and *rpo-1b(op259)* worms. Detection was with the its2 ("pre-26S" and "pre-5.8S") and 26S-1 probes (26S rRNA). Error bars indicate SD of 3 samples (only 1 sample each at 6 hours).

4.4.7 The 26S-short rRNA

4.4.7.1 An uncharacterised, truncated rRNA species is prominent in *rpo-1b(op259)*

When separating total RNA in agarose gels and checking RNA quality by EtBr staining, I noticed a distinct band between the outstanding 26S and 18S rRNA bands (Figure 21). This product was more prominent in *rpo-1b(op259)* samples than in wildtype extracts. Given its high abundance – visible in EtBr gels – it likely represented some ribosomal RNA; either an intermediate of rRNA synthesis or a degradation product.

By its size, it might be an incompletely processed precursor to 18S rRNA, or a shortened 26S rRNA. In a first series of northern blots, I successively tested the 18S probe and the two 26S probes 26S-1 and 26S-2 (Figure 22). The 18S probe and the 26S-2 probe, that covers the 3' end of 26S rRNA, did not hybridise to the band of the according size; however, 26S-1, the 5' probe for 26S rRNA, gave a distinct band between the 26S rRNA and the 18S rRNA position. This band, as on EtBr gels, was more pronounced in *rpo-1b(op259)* than in N2 samples. Since it bound 26S-1 but not 26S-2, it was likely a

truncated version of 26S rRNA. I could not detect the band with the its2 probe; as this probe covers most of the internal transcribed spacer between 5.8S and 26S rRNA, the RNA was unlikely to contain much of the its2 upstream of 26S rRNA. To learn about the 3' end of this RNA species, I designed short oligo probes in the region of the presumptive end as approximated by the length of the product. The oligos were DIG-labelled and hybridised to the membranes at 55°C (Figure 22). I determined a pair of probes of which the first one (26S-01c, primer_206 in Figure 23) could detect the band, whereas the second (26S-07c, primer_212) gave no signal. Thus, the 3' end could be confined to 600 nt within the 3' end of the 26S rRNA.

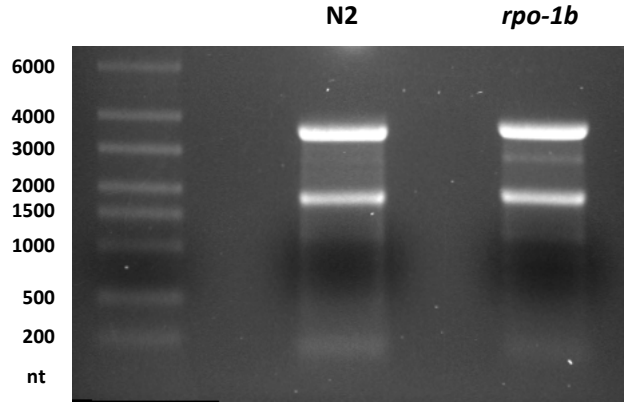

Figure 21 EtBr stained denaturing agarose gel with 800 ng of total RNA from wildtype and *rpo-1b(op259)* worms. An approximately 2.8 kb distinct band, running between the 26S and 18S ribosomal RNAs, is more prominent in *rpo-1b(op259)*. Later described as "26S-short rRNA".

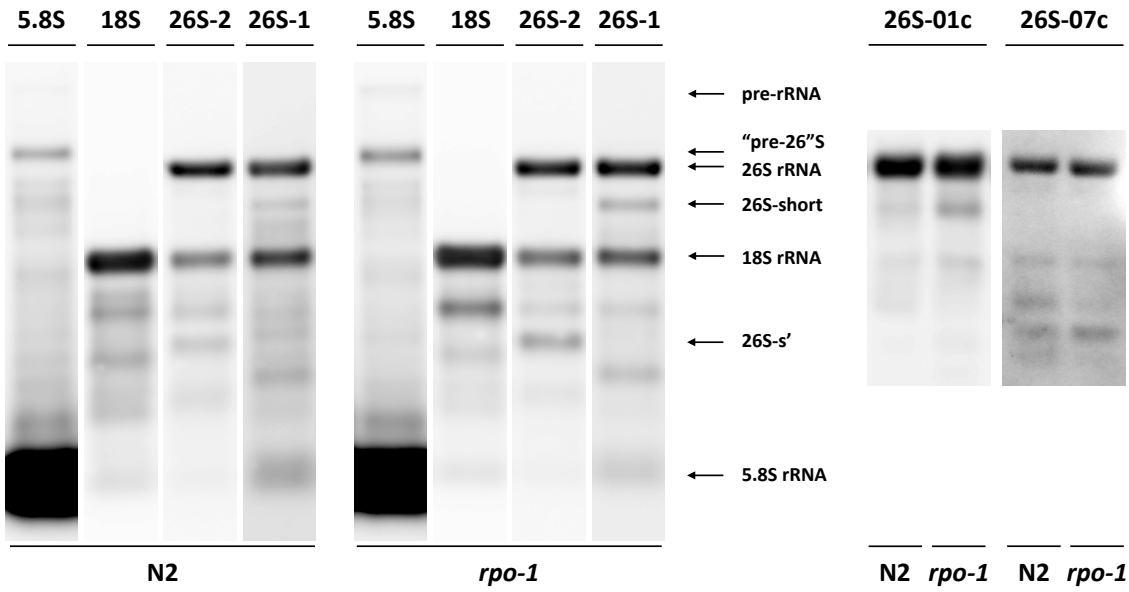

Figure 22 Sequential hybridisation with DIG-labelled RNA probes on total RNA extracts. Membrane stripping was not complete, as can be judged from the persistence of the 18S rRNA band. The 26S-short band can be detected with 26S-01c, but not with probe 26S-07c. The band labelled with 26S-s' is detected by the 26S-2 probe and is more pronounced in *rpo-1b(op259)*. Together with the size (~0.8-1 kb), this suggests that it could represent the counterpart of the 26S-short fragment, resulting from degradation of the full-length 26S rRNA.

4.4.7.2 Characterisation of the 26S-short rRNA sequence

RNA circularisation and reverse transcription

Simon Hänni in André Furger's lab coincidentally had observed the same band in RNA from nuclear extracts, where the corresponding rRNA species seems to be enriched (Figure 26). We collaborated to determine the precise sequence, particularly with regards to the 3' end. Truncated versions of 26S rRNA that are polyadenylated and supposedly targeted for degradation had been described in other species (Shcherbik 2010; Kuai 2004). It was therefore conceivable that the product in *C. elegans* stemmed from a homologous process. Simon Hänni suggested an approach that would possibly allow to assess the characteristics of the RNA species without cloning, and which indeed worked for us at the first attempt (West 2006). Shortly, total nuclear RNA – where the band was particularly prominent – was separated on agarose gels and the band between the 26S and 18S rRNA was excised, the RNA was extracted from the gel and circularised with RNA ligase. This was followed by reverse transcription with a specific primer, namely a primer that annealed to an RNA sequence within the region covered by the 26S-1 probe, close to the 5' end of 26S rRNA (primer_076). Reverse transcription should thus be initiated only from RNA with the according sequence, and in the case of RNA circles, extend across the former 5' end into the adjoining 3' end (Figure 23). The reverse transcripts would yield the templates for a PCR reaction with a pair of primers that should preferentially amplify the truncated 26S rRNA: the reverse primer_076 close to the 5' end, and a forward primer close to the presumptive 3' end of the truncated 26S rRNA (primer_191, complementary to the oligo primer_206, which had given a signal in northern blots, and which would bind maximally 600 nt upstream of the 3' end). With short enough an extension time during the PCR reaction, specifically the reverse transcripts from circularised truncated 26S rRNA and not from contaminating full length 26S rRNA should be amplified. We obtained a distinct PCR product of the expected size (<700 bp), which we sequenced.

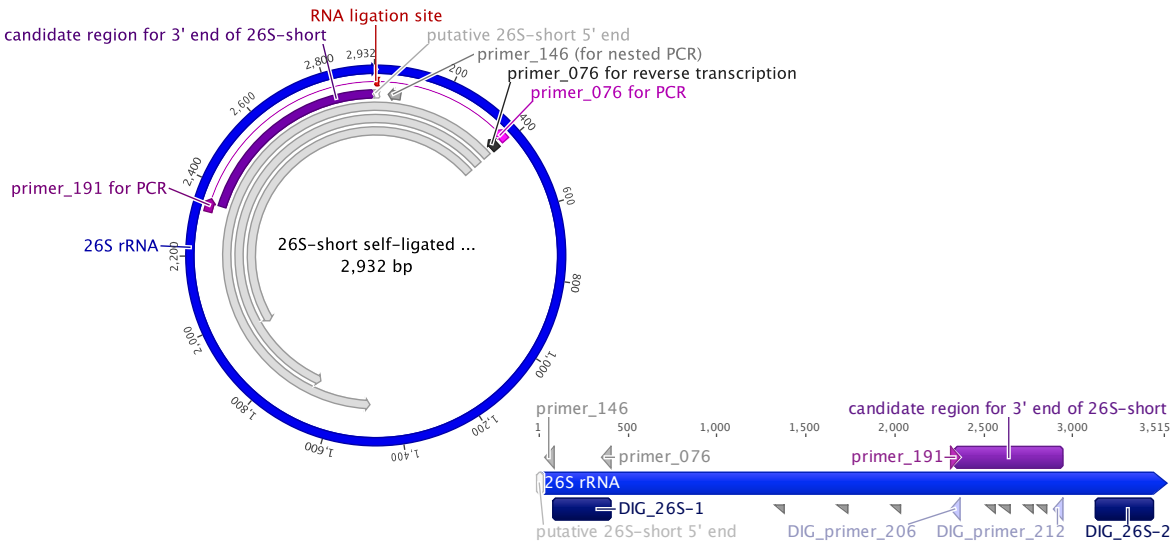

Figure 23 rRNA short fragment circularisation and reverse transcription. Position of the DIG probes that had narrowed the putative region of the 26S-short 3' end (no signal in northern blots with 26S-2 or primer_212, positive signal with 26S-1 or primer_206). Reverse transcription of the circularised RNA was performed with primer_076 and PCR with primers 191 and 076 was performed on the resulting reverse transcripts that reached from the 5' end directly into the 3' end of the circularised RNA.

The 3’ end is sharp and not polyadenylated

What would be expected if the short 26S rRNA band represented a precisely truncated but polyadenylated version of 26S rRNA is a mixture of reverse transcripts with poly-A stretches of supposedly variable length between the 3’ truncation position and the ligated 5’ start. By Sanger sequencing with the primer_191, one would find a single sequence down to the 3’ truncation site followed by some A’s that would flare into a sequence mix. Accordingly, with the primer_076, the reverse of the 26S 5’ sequence should be readable until the cutting site (canonical 26S rRNA 5’ start site?), transit into a short stretch of T’s and end in a non-readable mix of overlapping sequences. Surprisingly, we obtained no such signs of polyadenylation. There was a unique sequence read that abruptly changed into an overlap of two sequences; the two overlapping sequences could be resolved as the same sequence shifted by 1 nt. This was the case with both primers. Together, these analyses determined the 5’ and 3’ ends of the RNA species. The 5’ end is identical with the annotated start site of the 26S ribosomal RNA. The 3’ end is from a clear cut of the 26S rRNA sequence and is not carrying a poly-A tail. There seems to be one additional U in about half the product; since both the 5’ and 3’ end have an adjoining U in the pre-rRNA sequence, it can stem from alternative cutting at either end.

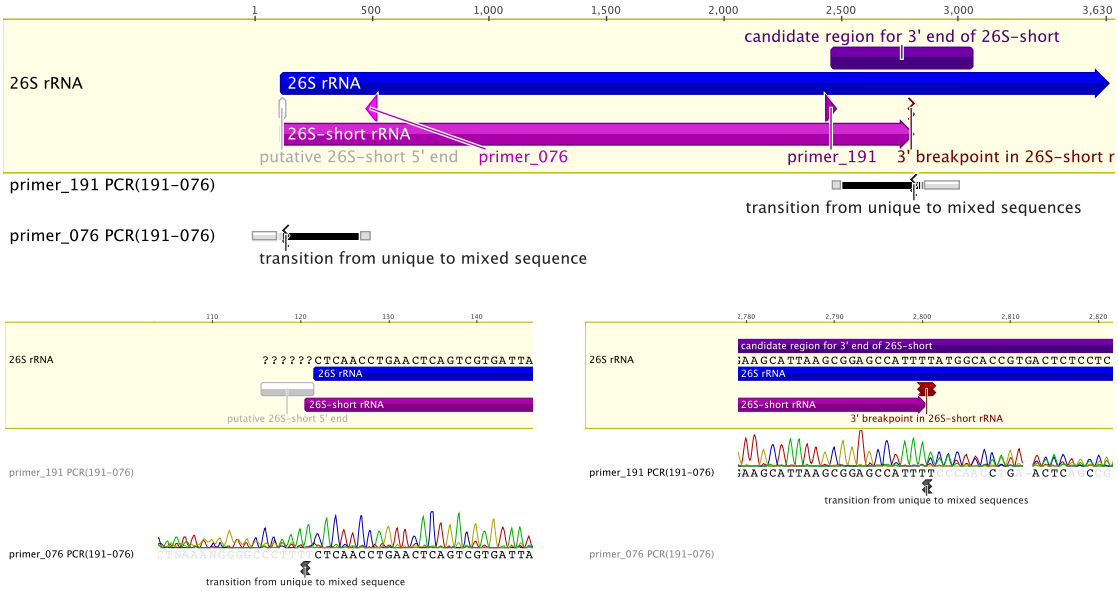

Figure 24 Definition of the precise 3’ end of the 26S-short rRNA by sequence alignment of the RT-PCR products from the circularised 26S-short rRNA fragment. Both sequencing directions give a breakpoint at the 5’ and 3’ ends of the 26S-short, respectively, with a transition from a unique sequence into an overlap of two identical sequences shifted by 1 nt. If dissected, the sequence corresponds exactly to the other end of the 26S-short. The overlap results from a T (U) that is present in approximately half the template.

Adapter ligation and sequencing confirm sharp ends

We used a second approach to confirm the findings and to assign the additional U to one of the ends. Again, the RNA band was excised and extracted from an agarose gel. Adapter RNA oligonucleotides were ligated to the ends of the isolated transcripts: first, RNA was ligated with an RNA oligonucleotide (RNA_SRA5Adpt) at the free 5’ ends. Consecutively, an oligonucleotide with a P5-phosphorylated 5’ end and an idT-modified 3’ terminus (RNA_SRA4Adpt) was ligated to the 3’ ends of the RNA. Two reverse transcription reactions were performed on the “capped” RNAs: one with the primer_076 to focus

on the 5' terminus of 26S rRNA, and one with a primer complementary to the RNA_SRA4Adpt adapter (rc_RT_GX1) to determine the 3' end and to read into more central parts of the truncated 26S rRNA.

PCR with primer_076 and a primer complementary to RNA_SRA5Adpt (rc-PCR_fw2) and subsequent sequencing with primer_076 revealed the precise 5' end of the truncated 26S rRNA. The majority of the transcripts had a U preceding the annotated start site of the 26S rRNA. We have not performed the reaction on the full-length 26 rRNA and can thus not state whether this represents a mis-annotation of the 5' end in the reference, or whether the truncated band has an extra nucleotide at its 5' terminus and is distinct from the full length 26S rRNA at this site as well. Ellis and colleagues acknowledged that defining the precise ends of the rRNAs was not possible at that time (Ellis 1986b).

PCR with the primers rc_RT_GX1 and primer_191, and sequencing with primer_191 confirmed the 3' end of 26S-short as a cut in the sequence 5'-CCAUUUUAUGG-3' (position 2830 of 26S rRNA, position 6372 in rDNA reference sequence), either after the second or the third U.

Further PCR reactions (primers_125/214 (1076 nt), primers_199/218 (675 nt), primers_201/060 (659 nt) were used to amplify the intermediate sequence between the 5' and 3' fragments. Sequencing confirmed the consensus 26S rRNA sequence, indicating that the 26S-short rRNA is a truncated 26S rRNA version that does not have further base sequence aberrations, and is therefore not likely to result from transcription of another locus than the rDNA repeats.

4.4.7.3 Truncated rRNA in *C. elegans* and in other species

The 26S-short truncation site is in a stem-loop structure

There have been several reports on well-defined 26S rRNA fragments in other species. In mammalian cells, bands corresponding to truncated 28S rRNA were observed in the context of apoptosis (Nadano 2000; Degen 2000; Samali 1997; Houge 1995) or of viral infection (Banerjee 2000). Houge et al. characterised a 28S rRNA fragment in myeloid leukaemia cells induced to undergo apoptosis (Houge 1993), and they fine-mapped the 3' terminus of the fragment to a 5'-GCGGUUCCGC-3' sequence in the variable region V13 (alternatively described as D8) (Houge 1995). This region is variable between species and is not conserved in *C. elegans*; it is about 20 nt upstream of the next stretch with considerable sequence similarity between human and *C. elegans*, which in turn is approximately 500 nt upstream of the 3' terminus of the 26S-short fragment in *C. elegans*. The 26S-short cutting site is in an evolutionarily more conserved sequence context, even though the very central bases (UU) are only present in fungi and many protozoa, but not in vertebrates. The cutting site is likely within the loop of a stem-loop structure that was already suggested with the first sequence analysis of the *C. elegans* rDNA locus (Ellis 1986b); it maps within the highly variable region D10 in that work. Taylor et al. recently published a detailed structure-analysis of the yeast ribosome (Taylor 2009b), where they also provided a model for the secondary structures in the rRNA constituents of the 60S ribosomal subunit. We tried to position the region that is homologous to the 3' end of the 26S-short fragment in this model. The sequence was around the nucleotide 2728 in the *S. cerevisiae* 26S rRNA, which could be found as position 2570 in the model. This position is within the loop of a stem-loop in ES31, an expansion segment (Taylor 2009b).

C. elegans has a partial rDNA repeat

Files and Hirsh characterised the rDNA locus as a multirepeat tandem array of about 55 of the polycistronic 7 kb long units (Files 1981). When digested with restriction enzymes with a single cutting site in the rDNA unit, the repeats were of uniform length except for a minor fraction (1 or 2 out of 55), which were longer than 7 kb and could be shown to represent two consecutive units with a 2.9 kb deletion including one restriction site. They attributed the deletion to the 18S rRNA coding region. Ellis et al., with a phage library sequencing approach (Ellis 1986b), did not reproduce this deletion, but they found another variant to the highly conserved repeat sequence. In a quest for sites where rDNA joins non-rDNA sequences, they found one clone with an abrupt transition from non-rDNA into the 3' region of the 26S rDNA; possibly, this transition represents the start of the multirepeat rDNA locus. The truncated rDNA sequence, annotated as *rrn-3.56* (F31C3.10) in Wormbase, intriguingly sets in precisely in the variable region D10, the region where the 26S-short rRNA sequence terminates; *rrn-3.56* reaches only 22 nt into the 3' terminus of 26S-short. This might be simple coincidence, but it fosters the speculation that there could be a counterpart to *rrn-3.56* in the *C. elegans* genome, one that terminates around D10 and that would give rise to a short 26S rRNA product if transcribed. The annotated transition of the rDNA locus into the telomeric end of chromosome I is in the internal transcribed spacer 1 (its1) of the rRNA repeat and thus not the candidate for such a transcript. Anyway, how the 3' terminus of a transcript from an interrupted rDNA sequence would be formed remains enigmatic.

4.4.7.4 26S-short rRNA in *rpo-1b(op259)*

The 26S-short rRNA appears more abundant in *rpo-1b(op259)*

I had noticed a difference in the relative abundance of the short versus the full length 26S rRNA between *rpo-1b(op259)* and N2. To determine whether there was also a qualitative difference, we performed all above reactions on both N2 and *rpo-1b(op259)* RNA extracts. However, there were no differences in the nucleotide sequence of the truncated 26S rRNA between wildtype and mutant.

We assessed the quantitative difference by various methods that relied on electrophoretic separation of RNA. Firstly, we determined the ratio of the intermediate band to the 26S rRNA band in EtBr stained agarose gels. Secondly, the same ratio was calculated from northern blots with probes complementary to the 5' terminus, that is, probes that hybridised to 26S rRNA and to the 3' truncated version (Table 3). Last, the RNA peak appearing between the 26S and the 18S rRNA peaks in the Bioanalyser [Agilent 2100 Bioanalyser] were quantified (Figure 26). The first and the second approach showed a highly consistent increase of the 26S-short band in *rpo-1b(op259)* mutants (more than 20 samples each of N2 and *rpo-1b(op259)* on 7 independent membranes). The intensity relative to the 26S rRNA was on average 1.4-fold higher in *rpo-1b(op259)* than in N2. Interestingly, there was a slight increase of the ratio 26S-short/26S upon IR irradiation of N2 (statistically not significant), and more strongly of *rpo-1b(op259)*, so that upon irradiation the ratio in *rpo-1b(op259)* was 1.5-fold that of N2.

	N2		*rpo-1b(op259)*		t-test
	ratio	**95% CI (n)**	**ratio**	**95% CI (n)**	**p-value**
no IR	0.95	±0.07 (13)	1.34	±0.12 (14)	1.20E-05
60 Gy	1.01	±0.11 (13)	1.51	±0.11 (11)	3.68E-06
t-test	0.29		0.08		

Table 3 26S-short to 26S ratio on northern blots of total RNA extracts (For the geometrical mean of the ratios of all N2 samples within one membrane, the value was arbitrarily set to 1). Comparison of non-irradiated with irradiated worms (columns) and of *rpo-1b(op259)* with wildtype samples (rows).

The 26S-short rRNA is not clearly bound to apoptosis

As mentioned above, truncated versions of ribosomal RNA had been described in other systems, often in the context of apoptosis. Possibly, the 26S-short band in *C. elegans* was a product of apoptotic degradation of nucleic acids. We therefore checked the RNA profile of *ced-3(n717)* mutants, where apoptotic decay is mostly supressed due to missing caspase activity. *ced-3(n717)* mutants also had the 26S-short band, at a similar intensity like wildtype worms (mean relative ratio of 0.99 ±0.15 SD, n=5). Furthermore, *ced-3(n717)* could not suppress the increase in *rpo-1b(op259)* (Figure 25). Thus, we think that the truncated 26S rRNA in whole worm extracts is not a product of apoptosis, for instance, of cells of the developing embryos that are carried by adult hermaphrodites.

Exosome dysfunction does not change 26S-short rRNA levels

The multi-exonuclease exosome has important functions in processing of ribosomal RNA [e.g., (Allmang 2000)]. I had observed that irradiation of adult worms led to an increase of a 5.8S-its2 fragment (Figure 20), very likely representing an incompletely processed precursor to the 5.8S rRNA. In other systems, exosome components are required for the removal of the its2 from the intermediate, and this is likely to be the case in *C. elegans* as well. I had seen different kinetics in the IR response between *rpo-1b(op259)* and wildtype, indicating that *rpo-1b(op259)* is relevant in this context. Could this difference and the increase of the 26S-short rRNA be a result of abnormal exosome function in *rpo-1b(op259)*? Of note, the exosomal component *exos-9* (homolog of yeast Rrp45) is a predicted interactor of RPO-1B (WBInteraction0050347). We examined an available mutant of *crn-3*, the homolog of the exosome component PM/Scl-100 in mammals (Rrp6 in yeast); as a cell death-related nuclease, it is also required for normal execution of apoptosis (Parrish 2003). If generation of the 26S-short rRNA involved the exosome, blocking normal exosome function might abolish this product. On the other hand, if the increase in *rpo-1b(op259)* was due to insufficient exosome activity, disturbing the exosome might reproduce an accumulation of the truncated 26S rRNA. Third, the increase in *rpo-1b(op259)* could be from excessive exosome activity, which would then be suppressed by the *crn-3* mutation. By northern blot analysis, the relative intensity of the 26S-short band in *crn-3(ok2269)* was not clearly different from wildtype (Figure 25). RNA from *rpo-1b(op259); crn-3(ok2269)* double mutants seemed to be more degraded overall (more smeary RNA lanes in agarose gels and more intense lanes with the its2 probe); the 26S-short band, however, was not significantly different from *rpo-1b(op259)*. The 26S-short rRNA band is therefore unlikely to be in direct connection with exosome function.

It is to mention that *rpo-1b(op259); crn-3(ok2269)* animals grew very slowly and had a low brood size. Thus, *rpo-1b(op259)* and *crn-3(ok2269)* have synthetic phenotypes in reproductive fitness.

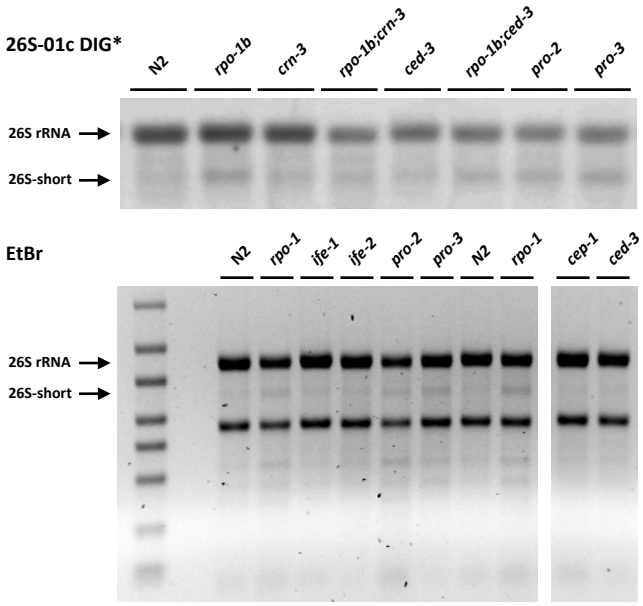

	normalised <26S/26S ratio	
	mean	95% CI (n)
N2	1.00	±0.07 (29)
rpo-1b(op259)	1.38	±0.11 (28)
pro-2(na27)	1.43	±0.22 (4)
pro-3(ar226)	1.45	±0.12 (4)
ife-1(ok1978)	1.04	±0.05 (4)
ife-2(ok306)	1.07	±0.02 (2)
cep-1(gk138)	0.98	(1)
cep-1 rpo-1b	1.11	(1)
gld-1(op236)	1.34	±0.35 (4)
gld-1 rpo-1b	1.77	±0.68 (4)
ced-3(n717)	0.99	±0.13 (5)
rpo-1b;ced-3	1.22	(1)
crn-3(ok2269)	0.76	(1)
rpo-1b;crn-3	1.24	(1)

Figure 25 26S-short band in total RNA extracts from exosome (*crn-3*), rRNA processing (*pro-2*, *pro-3*), and translation initiation factor (*ife-1*, *ife-2*) mutants, and of double mutant combinations of *rpo-1b(op259)*; northern blots (top) and agarose gels (bottom). *gld-1* is a negative regulator of the p53 homolog *cep-1* among many others and shows a strong apoptotic phenotype together with *rpo-1b(op259)* [see *gld-1(op236) rpo-1b(op259) animals have overly active CEP-1*]. Table indicates average of relative <26S/26S ratios, CI of the mean, and number of samples analysed by northern blot.

4.4.7.5 rRNA processing mutant *pro-2* is similar to *rpo-1b(op259)*

Besides *rpo-1b(op259)*, we looked at presumptive rRNA processing mutants on northern blots. Of the Pro mutants in *C. elegans*, mainly *pro-1(na48)* had been characterised on the level of rRNA synthesis (Voutev 2006). We wanted to determine whether the conditional sterility mutants *pro-2(na27)* and *pro-3(ar226)* also exhibited processing abnormalities, and whether *rpo-1b(op259)* shared with them, among other similarities [see *4.6.2.1*], the feature of increased 26S-short rRNA. With the probe its2, alterations in the relative intensities of rRNA intermediates were evident in *pro-2(na27)* and mostly in *pro-3(ar226)*. Also, the 26S-short to 26S rRNA ratio was about 1.4-fold that of wildtype (Figure 25). This strengthens the notion that *rpo-1b(op259)* and *pro-2(na27)* have very similar effects on rRNA, besides on germ cell development, and could be closely related mutants.

4.4.7.6 26S-short rRNA in nuclear extracts

Simon Hänni had observed the prominent 26S-short RNA peak in the Bioanalyser profile of RNA extracted from isolated intestinal nuclei. In that material, the peak had been much higher than in RNA extracts from whole worms. To determine whether the relative increase of the 26S-short rRNA was rather an effect of an altered ratio of nuclear versus cytoplasmic components in *rpo-1b(op259)* or of an actual increase in the mutant, we analysed whole worm and nuclear RNA extracts from *rpo-1b(op259)* and N2 with the Bioanalyser (Figure 26). First, the profiles reproduced the increase of 26S-short rRNA in *rpo-1b(op259)*; whole worm RNA extracts of adults and also of a larval worm pool had a higher according peak in *rpo-1b(op259)* than in N2.

In RNA from nuclei that had been isolated using the formerly presented nuclear extraction method [see *4.4.5 Nuclear run-on]*, the peaks were higher than in whole worm extracts, again speaking for at least some nuclei to be important hosts of the truncated 26S rRNA. The peak had been even higher in Simon's original profile. That RNA had been from intestinal nuclei that had undergone a further selection step by FACS; either the ensuing purification of the nuclei from non-nuclear material, or the selection of tissue specific nuclei must have risen the ratio of the 26S-short peak to the mature ribosomal RNAs. This fact supports that the provenance of the truncated rRNA could be nuclear. It becomes therewith unlikely that the truncated rRNA is a degradation product of 26S rRNA from mature cytoplasmic ribosomes.

In the RNA extracts from nuclei, the relatively higher levels of 26S-short rRNA in *rpo-1b(op259)* were not levelled to wildtype. It is difficult to judge which fraction of the RNA in the nuclear preparations was actual nucleoplasmic RNA, and which fraction was 'contaminating' cytoplasmic RNA. Yet, the experiments suggest that *rpo-1b(op259)* mutants have higher relative levels of the 26S-short rRNA than wildtype worms, also in their nuclei.

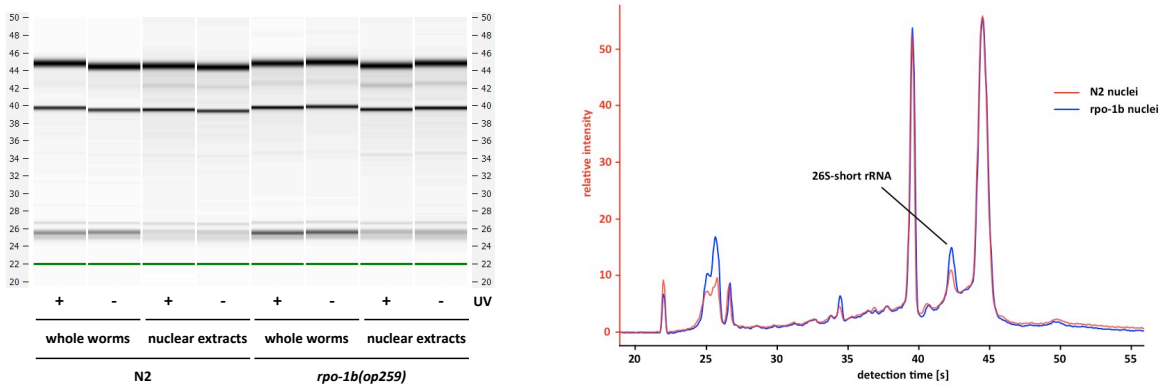

Figure 26 Bioanalyser profiles of total RNA isolated from whole worms (adult enriched) or from nuclear extracts. Left: lanes of RNA extracts from UV-C irradiated (+UV) or non-irradiated (-UV) animals. Right: the 26S-short rRNA peak is higher in *rpo-1b(op259)* than in wildtype, with the 18S and 26S rRNA peaks and the baseline being mostly overlapping. The peak at 34 s might correspond to the fragment detected with the 26S-2 rRNA probe in Figure 22.

4.4.7.7 26S-short rRNA in relation to mature 26S rRNA

I discussed before that care has to be taken when comparing northern blot signals between samples of N2 and *rpo-1b(op259)* due to the skewing effect of changes in the highly abundant rRNAs [*4.4.6.3 pre-rRNA levels are not significantly reduced in relation to mature rRNA*]. This certainly also applies to the Bioanalyser profile, which is strongly determined by the 26S and 18S rRNA peaks. This simple 'normalisation error' might alone be the reason why *rpo-1b(op259)* mutants seem to have a higher level of the truncated 26S rRNA. (Also, apparent nuclear enrichment of 26S-short rRNA could actually be a phenomenon of the stripping-off of cytoplasmic 26S rRNA.) The relatively stable increase of the 26S-short to 26S rRNA ratio by 40 % compared to wildtype fits well with the inverse of a reduction to 70 % of wildtype of the 26S rRNA. In fact, the ratio of 26S-short to the RNA pol II transcript *rps-15* was very similar between *rpo-1b(op259)* and wildtype (only small sample set; the overlap of the baseline curves in nuclear extracts (Figure 26) speaks against). Of course this does not undermine the relevance of all above observations and negate a difference between the mutant and wildtype; rather, it

indicates that the level of this truncated 26S rRNA is not closely related to the level of the RNA pol I transcribed, mature ribosomal RNAs.

4.4.7.8 Hypotheses on 26S-short rRNA

We could identify the 26S-short rRNA as a 3' truncated version of the 26S rRNA. The 26S-short rRNA fraction has a clean cut at a well-defined position within a presumptive loop structure and is not polyadenylated. The abundance of this fragment in relation to the 26S rRNA level is increased in the *rpo-1b(op259)* mutant as well as in mutants of rRNA processing. The fragment seems to be enriched in the nuclei. Besides the 26S-short band, there is a band stemming from the 26S rRNA 3' region and corresponding in size to the difference between 26S-short and the full-length 26S rRNA, which parallels the increase of 26S-short in *rpo-1b(op259)*. Possibly, 26S-short is a degradation product of the 26S rRNA. Such a degradation might happen with mature rRNA in ribosomes, or it could happen during transcription/processing of the pre-rRNA. Theoretically, it might represent a mechanism that adjusts 26S rRNA levels to 18S rRNA levels, before export of the large ribosomal subunit. *rpo-1b(op259)* has the same 18S/26S ratio as wildtype worms (Figure 26). It might have an rRNA synthesis defect predominantly affecting 18S rRNA and compensatorily degrade 26S rRNA to maintain the balance. Alternatively, the 26S rRNA might be degraded primarily, due to a processing defect for instance. Further, the 26S fragment itself could serve a specific purpose in the nucleoli or nuclei. Its abundance is very high and relatively stable within one worm strain.

4.4.8 *In vivo* assay for rRNA transcription rate

4.4.8.1 5-FU uptake into ribosomal RNA

All experiments so far were on a mixture of RNAs from all tissues. There might be cell type specific effects of the *rpo-1b(op259)* mutation on ribosomal RNA synthesis; somatic cells could be affected differently than germ cells. Many of the phenotypes of *rpo-1b(op259)*, particularly the DNA damage response defect, had presented in the germ line. To assess rRNA transcription specifically in the gonad, I adapted an *in vivo* assay from a cell culture system that uses the nucleotide analogue 5-Fluorouridine 5-FU (Kruhlak 2007). This ribonucleotide is substituted at position 5 of uridine with a fluorine; it is nevertheless efficiently incorporated into nascent RNA by the RNA polymerases. If applied in a pulse to cells, it can thereafter be visualised by indirect immunofluorescence using an anti-BrdU antibody, and it will reveal new transcripts. Since the absolute majority of transcriptional activity in a cell is committed to rRNA synthesis, a short pulse will primarily highlight transcription of ribosomal RNA. Interestingly, this method was used to show the effect of UV-irradiation on RNA pol I transcription (Kruhlak 2007). In mammalian cells, rRNA synthesis was strongly reduced shortly after focal irradiation with an UV-laser and returned to normal levels only several hours later; this response was dependent on the damage signalling kinase ATM. Such a link between irradiation, DNA damage response factors, and RNA pol I activity was exciting with regards to the link of RNA pol I and DNA damage-induced apoptosis in *rpo-1b(op259)*, and was a further motivation to apply the method in the worm.

4.4.8.2 Transcription in the germ line of *rpo-1b(op259)*

To create a system in *C. elegans* that can rapidly take up 5-FU from the medium, I extruded the germlines from adult animals and could thus overcome the impenetrable cuticle. I incubated the mostly intact dissected gonads with 5-FU for a short time (generally 20 min) before fixing and staining them. The signal predominantly localised to the nucleoli, confirming that the principle was working nicely, that 5-FU could be absorbed by the germ cells, and that it could be detected most strongly at the sites of early rRNA synthesis (Figure 27). I aimed at determining possible differences between wildtype and *rpo-1b(op259),* and how irradiation with IR or UVC would affect rRNA transcription.

Generally, the signal was not very homogenous within the dissected gonads, and there was considerable variation between individual gonads; some of the variation is likely due to unequal fixation/staining. In wildtype gonads, irradiation did not show an obvious effect on 5-FU incorporation, neither very shortly after treatment (e.g., 10 min, 30 min) nor at later time points (e.g., 2 hours, 6 hours); the inhomogeneity within and between gonads persisted, and there was no clear increase or decrease of the nucleolar signal intensity overall.

Similarly, comparison of the staining pattern and signal intensity of N2 and *rpo-1b(op259)* could not conclusively demonstrate or exclude a difference between the two. Also, irradiation did not obviously change the signal in *rpo-1b(op259)* at any of the post-treatment time points tested (Figure 28).

The adapted 5-FU method could highlight the large germ cell nucleoli, probably representing ongoing rRNA transcription. However, staining quality is variable. The 5-FU method was not accurate enough to reliably detect any presumably small differences between *rpo-1b(op259)* and wildtype with the available sample preparations; nor could it demonstrate a response of RNA pol I transcription to irradiation.

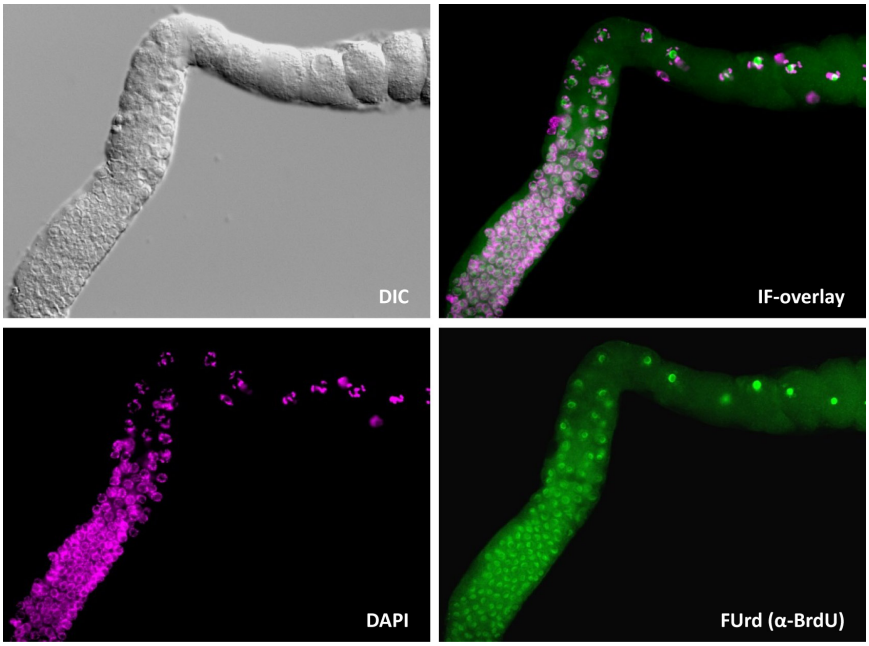

Figure 27 5-FU incorporation into nascent transcripts mainly highlights rRNA synthesis in the nucleoli. Chromatin (DAPI) encircles the central FUrd signal from the large germ cell nucleoli.

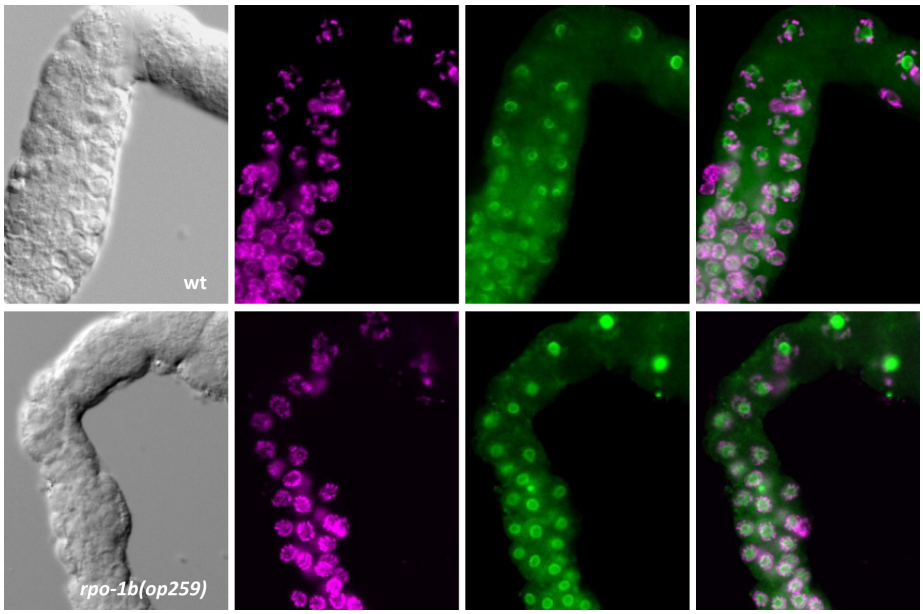

Figure 28 Transcription in the late meiotic pachytene region (zone of germ cell apoptosis) of wildtype and *rpo-1b(op259)* gonads. Both show a strong signal predominantly in the nucleoli (Pol I transcription) and a weaker signal where chromatin stains (Pol II/III). No obvious difference between mutant and wildtype in the pattern or intensity.

4.4.9 EM pictures

The small nucleoli found in *rpo-1b(op259)* germ cells might be the consequence of transcriptional alterations and merely indicate abnormal RNA pol I activity. Alternatively, the mutation could result in reduced nucleolar size due to a defect in rRNA transcription or a closely linked process that are relevant to nucleolar organisation, and secondarily, disturbed nucleolar architecture might impact on ribosome synthesis.

Theoretically, apparent reduction of nucleolar size could also be an artefact of DIC. Differences in optical density arising from changes in nucleolar/nuclear composition could lead to contrast changes at the interface between nucleoli and nucleoplasm, which in turn could shift the two-dimensional transition seen by DIC. Fluorescent microscopy in the FUrd experiments did not clearly reproduce the smaller nucleoli in *rpo-1b(op259)*.

To assess the ultrastructure of germ cells and their nucleoli, I performed electron microscopy at the Center for Microscopy and Image Analysis (ZMB) with the kind support of Andres Kaech and Theres Bruggmann. Besides the nucleoli, I compared ribosomes and mitochondria between wildtype and mutant worms. Electron microscopy pictures of germ cell nucleoli did not clearly show a reduction in nucleolar size in *rpo-1b(op259)*; these pictures have to be interpreted carefully, since the ultrasections are rarely central with regards to the nuclei. Some of the germ cell nuclei seem less spherical in the mutant than in wildtype, giving the appearance of a loose nuclear envelope. The density of cytoplasmic ribosomes was similar between mutant and wildtype. The number of mitochondria was not clearly different; however, their cristae were less well defined and less numerous in the mutant. Another difference between *rpo-1b(op259)* and N2 wildtype was the much higher density of lipid droplets in the mutant intestine. The high abundance of vitellogenins in *rpo-1b(op259)* as measured by quantitative proteomics (Table 6) is consistent with the significant increase of a lipid-storing compartment.

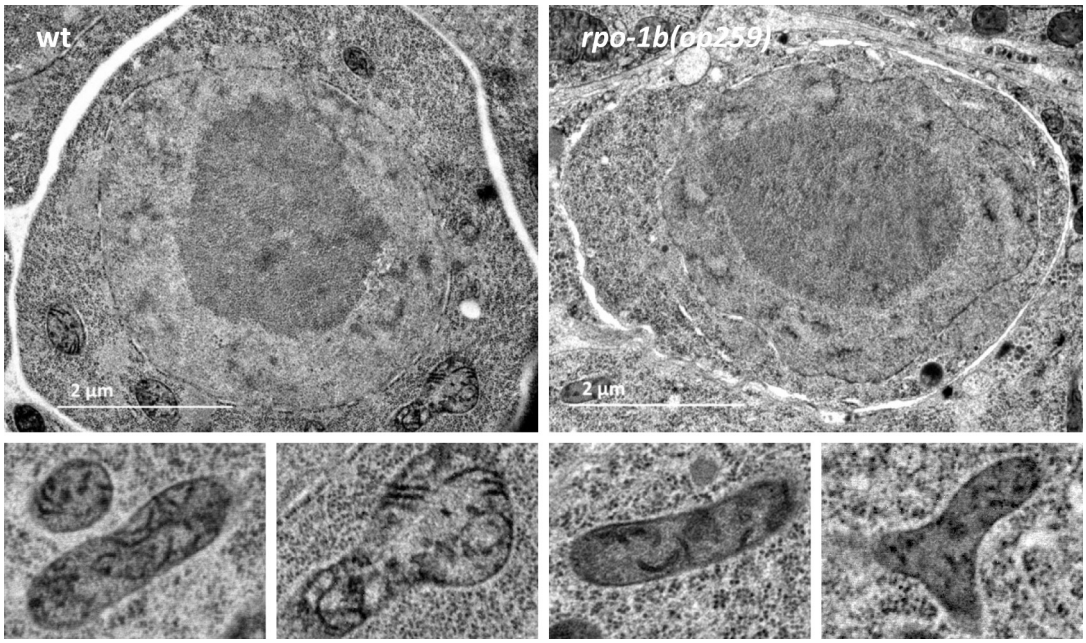

Figure 29 EM pictures of ultrathin cross-section through the worm gonad in the region of late meiotic pachytene cells. Germ cells, with prominent nucleoli surrounded by condensed chromosomes and the nuclear envelope, are not obviously dissimilar between wildtype and mutant. Mitochondria in the germ line of *rpo-1b(op259)* have fewer and less well defined cristae (mitochondria from two individual worms per strain).

4.4.10 Summary of rRNA quantification methods

Altogether, we have demonstrated a reduction of ribosomal RNA synthesis in *rpo-1b(op259)*. Nuclear run-on experiments have shown a decrease of the RNA pol I transcription rate relative to RNA pol II and RNA pol III activity. Furthermore, processing of the polycistronic pre-rRNA into mature ribosomal RNA seems to be altered in *rpo-1b(op259)*. Eventually, *rpo-1b(op259)* mutants have significantly reduced levels of mature 18S and 26S rRNA, as best evidenced by qRT-PCR. rRNA synthesis likely reacts to irradiation; the response of the mutant deviates from wildtype in several aspects.

In addition to the deviations in *rpo-1b(op259)* from wildtype, we detected and characterised an unconventional RNA of relatively high abundance, which has the nucleotide sequence of a 3'-terminally truncated, non-polyadenylated 26S rRNA, and which seems to be predominantly nuclear.

	pre-rRNA	rRNA	RPs	further observations
nucleolar morphology	⇣	⇣		reduced nucleolar size
NRO	↓↓	↓		
FUrd	n.q.	n.q.		
northern blot	↓	↓		26S-short rRNA band
qRT-PCR	↓	↓↓		
proteomics			↓↓	

Table 4 Summary of RNA quantification methods. Measured effects of the *rpo-1b(op259)* mutation on short-lived precursor rRNA (pre-rRNA) and on mature rRNA (rRNA) levels, as well as on ribosomal proteins (RPs) (all in comparison to wildtype). Reduced nucleolar size in germ cells was interpreted (dashed arrow) as surrogate of reduced ribosomal RNA. The FUrd in situ assay did not show an obvious difference between *rpo-1b(op259)* and wildtype and was not quantified (n.q.).

4.5 Proteomic profiles of *rpo-1b(op259)*

Quantitative or qualitative changes in transcription and processing of ribosomal RNA are likely to be reflected in the composition and the activity of ribosomes, and they will eventually influence translation. Analyses by qRT-PCR and northern blot had shown reduced levels of rRNA in whole worm extracts of *rpo-1b(op259)*. Some phenotypical aspects of the mutant could thus arise from altered protein expression. Interfering with translation regulation mechanisms often leads to alterations in protein expression that are confined to a subset of factors rather than being global [e.g., (Sonenberg 2009)]. For instance, ribosomal protein mRNAs themselves possess a sequence code in their 5' region that qualifies them for a cluster of collectively regulated, highly expressed transcripts (TOP mRNAs) (Meyuhas 2000).

Specificity for a restricted set of mRNAs was shown in *C. elegans* for isoforms of the translation initiation factor eIF4E (Song 2010; Henderson 2009; Dinkova 2005). Lifespan extension resulting from *ifg-1* inhibition (eIF4G homolog) was very recently shown to involve relative upregulation of stress response genes (Rogers 2011). Likewise, expression of some genes or groups of genes could be differentially affected in *rpo-1b(op259)* – on the background of a grossly wildtype translation. Theoretically, among the differentially expressed genes, there might be enrichment for factors with a known link to stress responses (Spriggs 2010).

4.5.1 2D-PAGE

In order to learn whether and how the *rpo-1b(op259)* mutation might affect protein expression, I chose to compare the proteomes of *rpo-1b(op259)* mutants and wildtype adult worms. (Evidently, the protein composition of worms is only an approximation to translation itself. Turnover of polypeptides is as relevant for measured protein levels as is synthesis.) Two-dimensional differential gel electrophoresis (2D DIGE) had been applied successfully to compare protein expression profiles at different developmental stages of *C. elegans* (Tabuse 2005). With the help from Sabine Schrimpf, we compared the protein patterns of *rpo-1b(op259)* mutant and wildtype worms in a pilot experiment using 2D gel electrophoresis. We separated equal amounts of protein extracts from whole worms by isoelectric focussing on IPS strips with gradients pH 4-7 and pH 6-11, and by subsequent gel electrophoresis in small acrylamide gels, which we then stained with Coomassie blue. In agreement with our hypothesis, the overall aspect of protein abundance was very similar in the two extracts. By visual comparison, we could identify individual spots on both gradient gels that had significantly different intensities between wildtype and mutant. MS analysis identified some prominent spots on the 2D gel as methionine sulfoxide-S-reductase MSRA-1 (higher in wildtype); and as adenylate cyclase F35D11.4, arginine kinase F46H5.3, vitellogenins, galectin LEC-2, and acidic 60S ribosomal subunit RPA-0 (increased in mutant). qRT-PCR showed only a moderate increase in the mRNA levels of the last two, indicating more significant regulation on a post-transcriptional level.

4.5.2 Mass spectrometry and spectral counting

The 2D gels strengthened our assumption that rather than having a global difference in translation, individual proteins or groups of proteins might be alternatively expressed in the mutant. For a more

comprehensive comparison of the mutant with the wildtype proteome, we performed mass spectrometric analysis, applying a label-free quantitation technique.

4.5.2.1 Preparation of non-labelled peptides

We used the same protein extracts that we had used for 2D gels: proteins from well-synchronised adult worms, the stage at which I observed most of the phenotypes and which had given a high protein yield. For the first mass spectrometry runs, the protein samples were not fractioned, e.g., by IP or size. We first tested time-dependent efficiency of proteolysis by trypsin; 3.5 hours was determined as the optimal duration for the digest of these worm samples. The proteins – extracted in Urea/Thiourea buffer and supplemented with CHAPS and DTT – were trypsin digested, and the resulting peptides were purified on an MCX cartridge; the high sample volume after elution (in 5 % formic acid/Methanol) was reduced by evaporation, and the concentrates were desalted with C18 ZipTips. Peptide concentration in the final samples was determined to ensure similar loading of the mass spectrometry column. With support from Bernd Roschitzki at the FGCZ, we determined protein levels by triplicate LTQ-FT runs of each sample and spectral counting.

4.5.2.2 Protein identifications in wildtype and *rpo-1b(op259)*

We could identify a total of 357 different proteins in at least one of the six runs; 342 in N2 samples and 343 in *rpo-1b(op259)*; that is 328 proteins that we could compare quantitatively since they had been detected at least once in both samples. For all identified proteins, a quantitative value was assigned by the Scaffold tool (Searle 2010), based on the relative representation in the peptide mix of proteotypic peptides for each protein. Alternatively to this analysis, we compared the average peptide signal intensity of the three best-detected peptides of a protein (mascot data): 373 different proteins were identified in total, 332 in N2 and 322 in *rpo-1b(op259)*.

Ribosomal proteins are significantly reduced in *rpo-1b(op259)*

Of the identified proteins, 70 were ribosomal; thus, most of the total 80 ribosomal proteins were represented and could be considered for quantitative analysis (Table 5). Strikingly, in the mutant, most ribosomal proteins were reduced to about 50-70 % of wildtype when we normalised by their fraction of the total in each sample. Collectively, ribosomal proteins formed 21.8 % of the total in N2, whereas in *rpo-1b(op259)* they represented a mere 14.2 % of total protein. Overall, the relative abundance of ribosomal proteins in *rpo-1b(op259)* was thus reduced to 65 % of N2. Looking at the small and large ribosomal subunits separately, SSU proteins were reduced to 69 % and LSU proteins to 0.62 % (t-test comparison between SSU and LSU, p=0.16). The relative abundances of individual ribosomal proteins ranged from $0.8 \cdot 10^{-4}$ to $0.9 \cdot 10^{-3}$ of total protein in the N2 sample and from $0.6 \cdot 10^{-4}$ (lowest threshold for protein detection) to $0.6 \cdot 10^{-3}$ in *rpo-1b(op259)*. On average, individual ribosomal proteins had a normalised ratio between *rpo-1b(op259)* and N2 of 0.66 (0.69 for SSU and 0.64 for LSU). Several other factors of protein synthesis were also reduced relatively in *rpo-1b(op259)*. In an assembly list of proteins that had been identified and quantified in multiple MS measurements of wildtype samples (compiled by Manuel Weiss), all ribosomal proteins together constituted approximately 19 % of the total.

Comparison of protein groups

For some groups of proteins, several members were represented and allowed a group comparison between *rpo-1b(op259)* and N2 (Figure 30). The highly abundant vitellogenins *vit-1* to *vit-6* had an average 1.25-fold higher relative fraction in *rpo-1b(op259)* than in N2, just about the inverse of the pool of ribosomal proteins. Some structural components of the cell and the chromatin were about equally abundant in *rpo-1b(op259)* and in N2 (Table 6).

An interesting group were the proteins identified as being mitochondrial by their Wormbase (WS200) annotations. Overall, the 31 mitochondrial factors had a ratio of 1.07 (SD ±0.44) between *rpo-1b(op259)* and wildtype; a subgroup of 8 proteins annotated with ATP synthetase activity, had an average ratio of only 0.77 (SD ±0.28), whereas the remaining factors had a ratio of 1.17 (SD ±0.44). Thus, there could be a slightly increased density of mitochondria in *rpo-1b(op259)* with significantly less ATP synthetase complexes (*rpo-1b(op259)*/N2 ratio of ATP synthetases to ratio of other mitochondrial proteins, 0.66, p=0.025). Interestingly, EM pictures of a small number of worms had shown altered mitochondrial morphology (less cristae) in the mutant (Figure 29).

In the 2D-gel analysis, one of the proteins identified from a spot that was markedly stronger in *rpo-1b(op259)*, was LEC-2. We looked for the galectins in the MS data: LEC-1 and LEC-2 had a ratio of 1.39; LEC-4, LEC-5, and LEC-9 had only been detected in *rpo-1b(op259)* at low levels. This indicates increased levels of galectins in *rpo-1b(op259)*.

Proteins with the most prominent measurable increase in *rpo-1b(op259)* comprised: F41C3.5 (serine carboxypeptidase (cathepsin A)), ratio *rpo-1b(op259)*/N2 of 4.16; *sodh-1* (alcohol dehydrogenase), 3.35; and *acp-6* (lysosomal and prostatic acid phosphatase), 3.79.

Vitellogenins

The increased abundance of vitellogenins (Table 6) was in agreement with previous biochemical experiments and with microscopic observations: in the 2D gel analyses, the vitellogenins were more prominent in the *rpo-1b(op259)* sample; in independent gel electrophoresis experiments, the vitellogenins had impressed as a strong silver stained band in protein extracts from the mutant. In *rpo-1b(op259)* mutants, more yolk accumulates in the cœlomic space of adult animals, as judged by DIC microscopy. In electron microscopy images, the gut had a higher density of lipid droplets, which might be enriched with the vitellogenins that are produced in this tissue.

One could argue that changes in the highly abundant vitellogenins between mutant and wildtype influence the relative fraction of all the other proteins and that we might therefore see a shift in the percentage of the total of other protein groups (Figure 30). However, this alone could not explain the relative changes of ribosomal proteins in comparison with other intracellular constituents.

Limitations of the analysis

These findings are revealing from a systemic point of view. Comparison of the proteomes permits to find tendencies in quantitative changes of major functional groups that are represented by many members. Abundances of individual proteins can significantly deviate from, or oppose, a group trend and might not necessarily reflect disturbances or adaptations of biological processes on a larger scale. Individual factors can be involved in various processes and might be regulated independently from other

players in a certain functional group. In addition, some of the individual measures can be subject to strong bias arising in the sample preparation or peptide detection and protein quantification. (This, however, might be tempered by analysing many biological replicates.)

Here, we have compared the proteomes of two worm strains based on just one biological sample. Nevertheless, we confidently assume that ribosomal proteins as a group are reduced in the *rpo-1b(op259)* sample in comparison to wildtype, even though a few members are not following the trend. Certainly, this trend itself could be due to sample processing; yet, wildtype and mutant samples were processed in parallel and a real difference in the biological specimen is thus very likely. With this onetime measurement, we can of course not exclude that biological variations between the two strains were caused by possible determinants like precise stage of the worms or slight differences in population density.

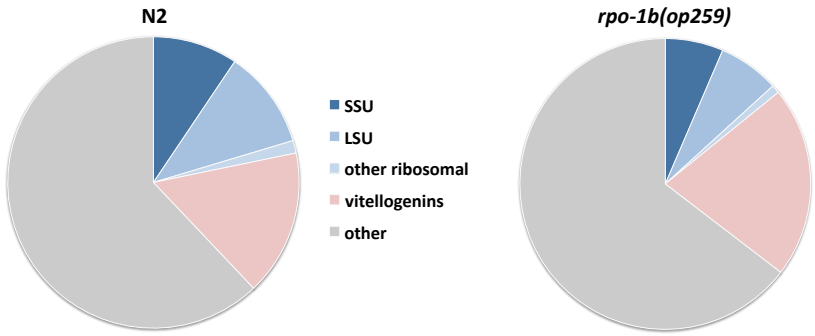

Figure 30 Relative abundance of ribosomal proteins and vitellogenins within all the identified proteins. Values were calculated from Scaffold 3 analysis [see text].

4.5.3 Conclusion: Ribosomes are reduced in *rpo-1b(op259)*

Ribosomal proteins are expected to grossly be in stoichiometric balance with ribosomal RNA (Laferté 2006a; Rudra 2004; Mayer 2006). Strikingly, the reduction in *rpo-1b(op259)* of ribosomal proteins to about two thirds of wildtype matches the reduction of mature rRNA levels very well. Those were repeatedly found to be only 70 % of wildtype [see *4.4.10 Summary of rRNA quantification methods*]. I thus assume that the amount of ribosomes is significantly reduced in adult *rpo-1b(op259)* mutant worms. It is intriguing how this mutant organism adapts to the disturbances in the very elemental process of ribosome and protein synthesis, and how it eventually preserves its viability and fertility.

Table 5 and Table 6 "Scaffold 3" and "Spectral counting" values are derived from the same triplicate LTQ-FS measurements of an N2 and an *rpo-1b(op259)* sample (see text); [ppm] is the relative abundance in a pool of many wildtype sample measurements (data from Manuel Weiss), which is included for comparison. For each protein group, the ratio of *rpo-1b*/N2 is calculated as ratio of the cumulative abundance of all group members (shaded), or as average of the *rpo-1b*/N2 ratios calculated for each individual protein.

Gene	Gene ID	# trx	Accession	Protein ID	Protein Accession	Scaffold 3 value (protein)			Spectral counting (peptides average)			[ppm]
						N2	rpo-1b	rpo-1b/N2	N2	rpo-1b	rpo-1b/N2	independent data
rpl-1	Y71F9AL.13	4	AC024200	Q9N4I4	RL10A_CAEEL	2.96	3.05	1.03	126913	72228	0.57	1486
rpl-2	B0250.1	2	Z81453	Q9XVF7	RL8_CAEEL	6.56	5.42	0.83	243649	102851	0.42	1874
rpl-3	F13B10.2	4		P50880	RL3_CAEEL	10.83	6.10	0.56	140834	85386	0.61	2910
rpl-4	B0041.4	2	AF000196	O02056	RL4_CAEEL	11.50	6.11	0.53	310387	134309	0.43	3055
rpl-5	F54C9.5	2	Z49967	P49405	RL5_CAEEL	11.81	9.49	0.80	232383	125139	0.54	3811
rpl-6	R151.3	2	U00036	P47991	RL6_CAEEL	5.25	4.40	0.84	261327	100560	0.38	2751
rpl-7	F53G12.10	5	AF003139	O01802	RL7_CAEEL	7.87	5.08	0.65	208559	137053	0.66	2587
rpl-7A	Y24D9A.4	2	AC006729	Q966C6	RL7A_CAEEL	5.57	2.04	0.37	100810	49172	0.49	1988
rpl-9	R13A5.8	2	AC006679	Q95Y90	RL9_CAEEL	6.56	3.39	0.52	132939	50035	0.38	2971
rpl-10	F10B5.1	2	Z48334	Q09533	RL10_CAEEL	7.54	5.42	0.72	72192	25049	0.35	2175
rpl-11.1	T22F3.4	2	U64844	Q94300	RL11_CAEEL	1.32	1.02	0.77				818
rpl-11.2	F07D10.1	2	U42845	Q19162	Q19162_CAEEL							832
rpl-12	JC8.3	3	Z82274	P61866	RL12_CAEEL	2.30	1.36	0.59	242208	111952	0.46	4272
rpl-13	C32E8.2	2	U88308	P91128	RL13_CAEEL	6.55	4.41	0.67	105487	45627	0.43	3029
rpl-14	C04F12.4	2	Z81461	Q9XVE9	Q9XVE9_CAEEL	2.63	2.71	1.03	157434	52794	0.34	3141
rpl-15	K11H12.2	2	U88168	P91374	RL15_CAEEL	5.57	2.37	0.43	147087	50868	0.35	2079
rpl-16	M01F1.2	3	Z46381	Q27389	RL13A_CAEEL	5.57	3.73	0.67	124665	54890	0.44	2481
rpl-17	Y48G8AL.8	2	AC025721	Q9BL19	RL17_CAEEL	6.56	3.39	0.52	98318	24080	0.24	2022
rpl-18	Y45F10D.12	2	AL021492	O45946	RL18_CAEEL	7.53	4.40	0.58	293021	88352	0.30	3464
rpl-19	C09D4.5	4	AF002196	O02639	RL19_CAEEL	5.90	4.07	0.69	192819	90972	0.47	2931
rpl-20	E04A4.8	3		O44480	RL18A_CAEEL	5.55	3.73	0.67	203682	97681	0.48	2775
rpl-21	C14B9.7	2	L15188	P34334	RL21_CAEEL	5.57	1.35	0.24	76894			2691
rpl-22	C27A2.2	3	U58760	P52819	RL22_CAEEL	4.59	2.71	0.59	93121	42031	0.45	2683
rpl-23	B0336.10	3	U32305	P48158	RL23_CAEEL	1.97	1.36	0.69				2219
rpl-24.1	D1007.12	2	AF003151	O01868	RL24_CAEEL	2.62	2.03	0.77	161785	59222	0.37	3878
rpl-24.2	C03D6.8	3	Z75525	Q17606	RLP24_CAEEL							67
rpl-25.1	F55D10.2	3	U40948	P48162	R23A1_CAEEL	4.59	3.04	0.66	175718	61594	0.35	1317
rpl-25.2	F52B5.6	4	Z75541	Q20647	R23A2_CAEEL	3.61	2.03	0.56	225494	69931	0.31	2250
rpl-26	F28C6.7	2	Z68315	Q19869	RL26_CAEEL	7.56	1.53	0.20	67230			1837
rpl-27	C53H9.1	2	AF003143	P91914	RL27_CAEEL	4.60	2.71	0.59	106464	46185	0.43	2587
rpl-28	R11D1.8	5	Z75547	Q21930	RL28_CAEEL	2.62	1.02	0.39	107892			2904
rpl-29	B0513.3	1	Z82256	O45226	O45226_CAEEL							1846
rpl-30	Y106G6H.3	1	AL032631	Q9XWS4	Q9XWS4_CAEEL	2.95	2.71	0.92	128042	72186	0.56	1252
rpl-31	W09C5.6	6	Z82077	Q9U332	RL31_CAEEL	1.97	1.36	0.69				992
rpl-32	T24B8.1	3	Z68338	Q22716	Q22716_CAEEL	5.24	2.71	0.52	116819	32510	0.28	2224
rpl-33	F10E7.7	4	U41264	P49180	RL35A_CAEEL	1.30	1.02	0.78	66671			1836
rpl-34	C42C1.14	2	CU457741	A3QMC5	A3QMC5_CAEEL							1852
rpl-35	ZK652.4	3	L14429	P34662	RL35_CAEEL	1.97	1.02	0.52	193610			4581
rpl-36	F37C12.4	2	U00033	P49181	RL36_CAEEL	2.29	1.02	0.45	75484			1814
rpl-37	C54C6.1	2	Z77131	P49622	RL37_CAEEL	1.46						138
rpl-38	C06B8.8	5	Z81463	O17570	RL38_CAEEL							1204
rpl-39	C26F1.9	2	U53148	P52814	RL39_CAEEL							
rpl-41	C09H10.2	3	Z50109	P48166	RL44_CAEEL							2747
rpl-42	C09H10.1	1	Z50109	Q17879	Q17879_CAEEL							10
rpl-43	Y48B6A.2	3	AL110490	Q9U2A8	RL37A_CAEEL	4.57	1.36	0.30				2363
rps-0	B0393.1	2	Z37983	P46769	RSSA_CAEEL	7.22	6.78	0.94	275075	122047	0.44	2582
rps-1	F56F3.5	1	Z32681	P48154	RS3A_CAEEL	7.55	5.42	0.72	178925	84405	0.47	2761
rps-2	C49H3.11	3	U42436	P51403	RS2_CAEEL	4.27	2.03	0.48	154593			2187
rps-3	C23G10.3	2	U39851	P48152	RS3_CAEEL	14.42	10.17	0.71	280750	130487	0.46	2806
rps-4	Y43B11AR.4	2	AC024780	Q9N3X2	RS4_CAEEL	12.47	4.74	0.38	256238	133878	0.52	2772
rps-5	T05E11.1	2	Z68751	P49041	RS5_CAEEL	2.29	1.69	0.74	67869			1349
rps-6	Y71A12B.1	1	AL132902	Q9NEN6	RS6_CAEEL	9.19	5.08	0.55	163745	75314	0.46	2374
rps-7	ZC434.2	2	Z75714	Q23312	RS7_CAEEL	4.28	3.39	0.79	264880	86884	0.33	2663
rps-8	F42C5.8	3	U40799	P48156	RS8_CAEEL	7.89	6.78	0.86	231794	124731	0.54	2449
rps-9	F40F8.10	2	Z69302	Q20228	RS9_CAEEL	6.56	1.70	0.26	148770			1863
rps-10	D1007.6	2	AF003151	O01869	O01869_CAEEL	7.23	5.42	0.75	129523	82740	0.64	2087
rps-11	F40F11.1	3	Z73426	Q20206	Q20206_CAEEL	5.25	3.39	0.65	124429	46625	0.37	2142
rps-12	F54E7.2	2	U00067	P49196	RS12_CAEEL	0.97	1.02	1.05				1079
rps-13	C16A3.9	2	U41534	P51404	RS13_CAEEL	2.62	1.70	0.65	120830	44313	0.37	2436
rps-14	F37C12.9	2	U00033	P48150	RS14_CAEEL	4.27	2.03	0.48	89547			1411
rps-15	F36A2.6	2	Z81077	Q9XVP0	RS15_CAEEL	6.89	5.08	0.74	71596	26959	0.38	2541
rps-16	T01C3.6	2	Z78413	Q22054	RS16_CAEEL	8.85	3.73	0.42	119320	34830	0.29	2508
rps-17	T08B2.10	2	AF000263	O01692	RS17_CAEEL	6.55	4.06	0.62	85464	45268	0.53	3255
rps-18	Y57G11C.16	3	Z99281	O18240	O18240_CAEEL	5.25	4.07	0.77	229648	70384	0.31	5374
rps-19	T05F1.3	2	Z81586	O18650	RS19_CAEEL	5.57	2.71	0.49	147395	55502	0.38	2329
rps-20	Y105E8A.16	2	AL132876	Q8WQA8	Q8WQA8_CAEEL	3.94	3.73	0.95	94955	39722	0.42	3428
rps-21	F37C12.11	2	U00033	P49197	RS21_CAEEL	2.97	2.04	0.69	16846			2664
rps-22	F53A3.3	4	AF025460	O17218	O17218_CAEEL	8.19	7.12	0.87	169516	66827	0.39	2417
rps-23	F28D1.7	3	Z70684	Q19877	RS23_CAEEL	2.95	2.03	0.69	162613	57104	0.35	2272
rps-24	T07A9.11	4	AF036706	Q1XFY9	Q1XFY9_CAEEL	3.61	3.39	0.94	94491	46831	0.50	2102
rps-25	K02B2.5	2	U41558	P52821	RS25_CAEEL	1.63	1.02	0.62	67406			2190
rps-26	F39B2.6	3	Z92834	O45499	RS26_CAEEL	2.30	2.03	0.88	222782	58333	0.26	1510
rps-27	F56E10.4	5	AF101312	Q9TXP0	RS27_CAEEL	2.62	2.03	0.78				167
rps-28	Y41D4B.5	2	AC024776	Q95Y04	RS28_CAEEL	1.97	1.02	0.52				2486
rps-29	B0412.4	2	U80953	P90983	P90983_CAEEL							824
rps-30	C26F1.4	2	U53148	Q18231	Q18231_CAEEL							244
rla-1	Y37E3.7	2	AC087079	P91913	RLA1_CAEEL	1.64	2.03	1.24				4566
rla-2	Y62E10A.1	3	AL132865	Q9U1X9	Q9U1X9_CAEEL	2.95	3.06	1.03	176682	135791	0.77	4936
rla-0	F25H2.10	2	Z79754	Q93572	RLA0_CAEEL	14.79	7.46	0.50	316473	143528	0.45	2936
rla-1/rla-2	C37A2.7	2	U97194	O01504	RLA2_CAEEL	4.27	2.37	0.56	87215	20649	0.24	3291
ubl-1 (rps-27a)	H06I04.4	2	AC006651	P37165	RS27A_CAEEL							629
ubq-2 (rpl-40)	ZK1010.1	2	Z82083	P49632	RL40_CAEEL							1547
					Trypsin	6.88	7.12	1.03	344622	246188	0.71	
					total all proteins	1694.85	1631.21		45258383	30051103		1000000
					Average			**1.00**			**0.69**	
					SD			**0.51**			**0.24**	
					95% confidence			**0.06**			**0.03**	
					total ribosomal	368.80	230.97		9539305	3615809		185919
					Average			**0.66**			**0.43**	
					SD			**0.21**			**0.11**	
					95% confidence			**0.05**			**0.03**	
					ribosomal/all	**0.218**	**0.142**	0.66	**0.211**	**0.120**	0.62	**0.186**
					rpo-1b/N2		**0.65**			**0.57**		
					small subunit	159.77	105.40		3968997	1433185		69272
					Average			**0.69**			**0.42**	
					SD			**0.19**			**0.10**	
					95% confidence			**0.07**			**0.04**	
					large subunit	185.39	110.65		4989938	1882657		98744
					Average			**0.62**			**0.43**	
					SD			**0.19**			**0.10**	
					95% confidence			**0.06**			**0.04**	
					SSU/all	**0.094**	**0.065**	0.69	**0.088**	**0.048**	0.61	**0.069**
					LSU/all	**0.109**	**0.068**	0.62	**0.110**	**0.063**	0.61	**0.099**

Table 5 Quantitative analysis of individual ribosomal proteins and of small and large ribosomal subunit components

Gene	Gene ID	# trx	Accession	Protein ID	Protein Accession	Scaffold 3 value (protein)			Spectral counting (peptides average)			[ppm]
						N2	rpo-1b	rpo-1b/N2	N2	rpo-1b	rpo-1b/N2	independent data
Vitellogenins												
vit-1	K09F5.2	1	U37430	P55155	VIT1_CAEEL	37.73	50.35	1.33	414594	378040	0.91	683
vit-2	C42D8.2	1	U56966	P05690	VIT2_CAEEL	50.53	81.35	1.61	417343	378040	0.91	1456
vit-3	F59D8.1	1	AC024137	Q9N4J2	VIT3_CAEEL	46.26	47.12	1.02	390771	267885	0.69	585
vit-4	F59D8.2	1	AC024137	P18947	VIT4_CAEEL	46.25	45.76	0.99	390771	267885	0.69	557
vit-5	C04F6.1	1	U42835	P06125	VIT5_CAEEL	44.61	47.45	1.06	390771	267885	0.69	706
vit-6	K07H8.6	1	AF047659	P18948	VIT6_CAEEL	48.88	74.53	1.52	262299	326308	1.24	2164
Structural proteins												
Actins												
act-4	M03F4.2	6	U64601	Q95ZL1	Q95ZL1_CAEEL	23.60	28.13	1.19	530522	509001	0.96	3903
act-5	T25C8.2	3	Z83241	O45815	O45815_CAEEL	19.02	20.68	1.09	248532	241396	0.97	1088
Tubulins												
tba-2	C47B2.3	3	Z99709	P34690	TBA2_CAEEL	6.54	8.13	1.24	141991	122101	0.86	813
tbb-2	C36E8.5	2	Z35597	P52275	TBB2_CAEEL	18.36	18.64	1.02	145668	121925	0.84	1183
Histones												
his-46	B0035.9	1	Z73102	P62784	H4_CAEEL	2.63	3.05	1.16	111791	70525	0.63	510
his-47	B0035.7	1	Z73102	P09588	H2A_CAEEL	5.57	5.76	1.03	151184	104880	0.69	279
his-48	B0035.8	1	Z73102	Q27876	H2B4_CAEEL	5.25	4.74	0.90	180294	143692	0.80	359
Mitochondrial proteins												
ATP synthetases												
asb-1	F35G12.10	2	Z46242	Q20053	Q20053_CAEEL	1.63	1.02	0.62				174
asb-2	F02E8.1	3	U53340	Q19126	Q19126_CAEEL	1.98	2.37	1.20		46270		660
asg-2	C53B7.4	2	U42830	Q18803	ATPL2_CAEEL	1.46	1.02	0.70				546
atp-2	C34E10.6	3	U10402	P46561	ATPB_CAEEL	29.22	31.18	1.07	348249	251687	0.72	5563
atp-3	F27C1.7	1	U80441	Q7JNG1	Q7JNG1_CAEEL	3.28	1.36	0.41	45536			1484
atp-4	T05H4.12	4	AF016452	O16517	O16517_CAEEL	1.97	1.02	0.52				2325
atp-5	C06H2.1	2	Z75526	Q17763	Q17763_CAEEL	5.57	3.73	0.67	93217	53384	0.57	1533
R04F11.2	R04F11.2	4	Z74475	Q21732	Q21732_CAEEL	0.98	1.02	1.03	22824	14923	0.65	1185
Other mitochondrial												
acdh-1	C55B7.4	6	AC006625	Q8IAB6	Q8IAB6_CAEEL	1.49	2.55	1.71	77523	67351	0.87	638
aco-1	ZK455.1	2	Z66567	Q23500	ACOC_CAEEL	1.63	1.69	1.04	41096	18009	0.44	840
aco-2	F54H12.1	1		P34455	ACON_CAEEL	5.57	5.08	0.91	68379	67150	0.98	1919
ant-1.1	T27E9.1	2	Z82059	Q86CZ9	Q86CZ9_CAEEL	22.96	23.72	1.03	420615	227863	0.54	2960
ard-1	F01G4.2	2	Z68341	Q19102	Q19102_CAEEL	1.97	2.03	1.03	39800	26089	0.66	435
cri-3	F59A2.3	2	Z34801	Q21018	CRI3_CAEEL	1.32	1.02	0.77				586
cts-1	T20G5.2	2	Z30423	P34575	CISY_CAEEL	4.25	2.70	0.64	88382	46472	0.53	1487
F23B12.5	F23B12.5	2	Z77659	Q19749	ODP2_CAEEL	4.60	3.05	0.66	46525	33250	0.71	641
fum-1	H14A12.2	1	AF025459	O17214	FUMH_CAEEL	1.32	1.52	1.15				1000
hsp-6	C37H5.8	1	U88315	P11141	HSP7F_CAEEL	3.93	5.42	1.38	69736	46543	0.67	1405
hsp-60	Y22D7AL.5	2	AC084153			9.84	6.78	0.69	126357	73860	0.58	2244
isp-1	F42G8.12	2	AF038618	O44512	O44512_CAEEL	1.96	1.69	0.86	61090	57022	0.93	523
LLC1.3	LLC1.3	2	Z82277	O17953	O17953_CAEEL	0.98	1.35	1.38				1000
mdh-2	F20H11.3	2	AF002197	O02640	MDHM_CAEEL	12.15	10.17	0.84	146186	120863	0.83	2425
nuo-5	Y45G12B.1	2		Q86S77	Q86S77_CAEEL	0.98	1.36	1.38				664
pccb-1	F52E4.1	2	U56964	Q20676	Q20676_CAEEL	1.31	2.04	1.55	14406	32291	2.24	808
phb-1	Y37E3.9	2	AC087079	Q9BKU4	PHB1_CAEEL	1.32	2.04	1.55		39153		1236
phb-2	T24H7.1	2	U28940	P50093	PHB2_CAEEL	2.30	1.36	0.59	43114			523
pyc-1	D2023.2	3	Z81052	O17732	PYC1_CAEEL	1.46	3.05	2.09	27481	19421	0.71	336
R05G6.7	R05G6.7	2	U58746	Q21752	VDAC_CAEEL	10.48	10.16	0.97	239732	115755	0.48	2489
sdha-1	C03G5.1	2	U41555	Q09508	DHSA_CAEEL	0.98	1.69	1.72		24035		595
T05H10.6	T05H10.6	3	Z47812	P52899	ODPA_CAEEL	0.99	1.01	1.02				480
Y37E3.17	Y37E3.17	1	AC087079	Q9BKT7	Q9BKT7_CAEEL	0.99	2.03	2.05				326
Galectins												
lec-1	W09H1.6	1	Z82081	P36573	LEC1_CAEEL	5.58	7.46	1.34	90815	88346	0.97	1528
lec-2	F52H3.7	1	Z66512	Q20684	Q20684_CAEEL	3.28	4.74	1.45	55856	48107	0.86	1019
lec-4	C44F1.3	1	Z49067	Q18625	Q18625_CAEEL		1.36			35630		358
lec-5	ZK1248.16	2	U29244	Q23426	Q23426_CAEEL		1.02					451
lec-9	C16H3.2	2	U67955	Q94169	Q94169_CAEEL		1.69					310
					total all proteins	1694.85	1631.21		45258383	30051103		1000000
					Average			**1.00**			**0.69**	
					SD			**0.51**			**0.24**	
					95% confidence			**0.06**			**0.03**	
					vitellogenins	274.26	346.56		2266550	1886042		6151
					Average			**1.26**			**0.85**	
					SD			**0.27**			**0.22**	
					95% confidence			**0.22**			**0.18**	
					vitellogenins/all	**0.162**	**0.212**	**1.25**	**0.050**	**0.063**	**1.23**	**0.006**
					structural proteins	80.96	89.13		1509982	1313520		8135
					Average			**1.09**			**0.82**	
					SD			**0.12**			**0.13**	
					95% confidence			**0.09**			**0.09**	
					structural/all	**0.048**	**0.055**	**1.09**	**0.033**	**0.044**	**1.18**	**0.008**
					mitochondrial	140.88	136.22		2020249	1381392		7581
					Average			**1.07**			**0.77**	
					SD			**0.44**			**0.41**	
					95% confidence			**0.15**			**0.19**	
					ATP synthetases	46.09	42.70		509827	366264		13470
					Average			**0.78**			**0.65**	
					SD			**0.28**			**0.08**	
					95% confidence			**0.20**			**0.08**	
					other mitochondrial	94.78	93.52		1510422	1015127		25557
					Average			**1.17**			**0.80**	
					SD			**0.44**			**0.45**	
					95% confidence			**0.18**			**0.23**	
					***mitochondrial*/all**	**0.083**	**0.084**	**1.07**	**0.045**	**0.046**	**1.11**	**0.008**
					ATP synthetases/all	**0.027**	**0.026**	**0.77**	**0.011**	**0.012**	**0.94**	**0.013**
					other mito/all	**0.056**	**0.057**	**1.17**	**0.033**	**0.034**	**1.15**	**0.026**
					galectins	8.86	16.27		146671	172083		3666
					Average			**1.39**			**0.92**	
					SD			**0.08**			**0.08**	
					95% confidence			**0.11**			**0.11**	
					galectins/all	**0.005**	**0.010**	**1.39**	**0.003**	**0.006**	**1.32**	**0.004**

Table 6 Groups of proteins with differential expression between *rpo-1b(op259)* and N2, and structural proteins.

4.6 rRNA transcription, the nucleolus, ribosomes, and translation as determinants for DNA damage-induced apoptosis

RPO-1B plays a role in apoptosis regulation [See *5 rpo-1b(op259) links to p53, the Ras/MAPK pathway, and to the apoptotic core* and Figure 31]. The previous chapter showed that ribosomal RNA and ribosomes are reduced in the *rpo-1b(op259)* mutant. Despite possible alterations in ribosome synthesis, the role of RPO-1B in apoptosis regulation might be an independent, specific characteristic of this second largest polymerase subunit or even of the mutated site, and might not be directly linked with the overall performance of RNA pol I as a transcription apparatus. Alternatively, the anti-apoptotic effect could result more generally from altered transcription by RNA pol I and its consequences on ribosome synthesis. If the effect of *rpo-1b(op259)* on apoptosis was more indirect in this sense, defective response to DNA damage should be phenocopied by altering the function of other RNA pol I core subunits or RNA pol I associated factors. Targeting factors further in the line from rRNA transcription to translation might also lead to the phenotype if the effect on apoptosis was regulated 'downstream' in that line. I thus assembled lists of genes that were annotated to be involved in rRNA synthesis in *C. elegans*, or that were the apparent worm homologs of interesting rRNA synthesis factors described in the literature.

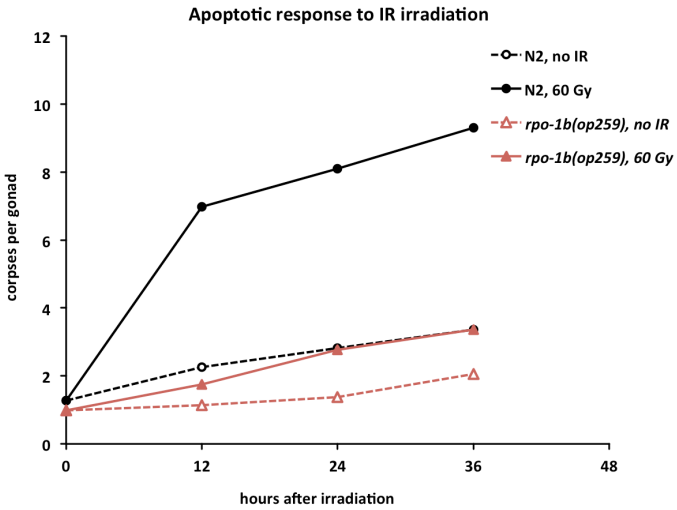

		N2		*rpo-1b(op259)*	
	post IR	score	95% CI (n)	score	95% CI (n)
no IR	0 h	1.27	±0.12 (224)	0.99	±0.23 (74)
	12 h	2.26	±0.19 (192)	1.13	±0.23 (60)
	24 h	2.82	±0.16 (619)	1.37	±0.22 (140)
	36 h	3.37	±0.32 (153)	2.05	±0.48 (60)
60 Gy					
	12 h	6.98	±0.35 (204)	1.75	±0.35 (60)
	24 h	8.10	±0.22 (831)	2.77	±0.31 (140)
	36 h	9.31	±0.55 (160)	3.37	±0.57 (60)

Figure 31 Time course of apoptotic response to IR irradiation in *rpo-1b(op259)* germ lines. The table indicates average number of apoptotic corpses per gonad, 95 % CI of the mean, and number of animals tested per condition.

4.6.1 RNA polymerase subunits and apoptosis

In a first approach, I evaluated RNA pol I, pol II, and pol III subunits. The *C. elegans* RNA pol II subunits have recently been named *rpb-1* through *rpb-12*, according to their homologs in yeast. Based on the table presented in (Cramer 2002), I considered *rpb-6*, *rpb-5*, *rpb-8*, *rpb-10*, and *rpb-11* to be shared among the three RNA polymerases. For the remaining RNA pol I and RNA pol III subunits, I manually searched for the best-matching worm homologs (Table 7). In several instances, homology was not obvious and unequivocal due to different nomenclature of the subunits in different phyla. I could not identify the orthologs of the smaller subunits A14/A43 (Rpb4/Rpb7 in RNA pol II) or of A34.5, member of the A49/A34.5 sub-complex that is specific to RNA pol I (with partial homology to RAP74/RAP30, an accessory sub-complex in RNA pol II) (Kuhn 2007b).

RNA polymerase I			RNA polymerase II			RNA polymerase III			
	Human	*S. cerevisiae*		Human	*S. cerevisiae*		Human	*S. cerevisiae*	Archeae
A190	POLR1A	RPA190	Rpb1	POLR2A	RPO21	C160	POLR3A	RPO31	A
A135	POLR1B	RPA135	Rpb2	POLR2B	RPB2	C128	POLR3B	RET1	B
AC40	POLR1C	RPC40	Rpb3	POLR2C	RPB3	AC40	POLR1C	RPC40	D
AC19	RPAC2		Rpb11	POLR2J	RPB11	AC19	RPAC2		L
A12.2		RPA12	Rpb9	POLR2I	(RPB9)	C11	POLR3K	RPC11	X
ABC27	POLR2E	RPB5	Rpb5	POLR2E	RPB5	ABC27	POLR2E	RPB5	H
ABC23	POLR2F	RPO26	Rpb6	POLR2F	RPO26	ABC23	POLR2F	RPO26	K
ABC14.5	POLR2H	RPB8	Rpb8	POLR2H	RPB8	ABC14.5	POLR2H	RPB8	-
ABC10β	POLR2L	RPB10	Rpb10	POLR2L	RPB10	ABC10β	POLR2L	RPB10	N
ABC10α	POLR2K	RPC10/RPB12	Rpb12	POLR2K	RPC10/RPB12	ABC10α	POLR2K	RPC10/RPB12	P
A14	POLR1D	RPC19	Rpb4	POLR2D	(RPB4)	C4	POLR3D	RPC53?	F
A43		RPA43	Rpb7	POLR2G	RPB7	C25	POLR3H	RPC25	E
A49	POLR1E	RPA49	RAP74	RAP74	TFG1				
A34.5		RPA34	RAP30	RAP30	TFG2				
C. elegans			*C. elegans*			*C. elegans*			
A190	Y48E1A.1		Rpb1	F36A4.7	*ama-1*	C160	C42D4.8	*rpc-1*	
A135	F14B4.3	*rpo-1b (inofficial)*	Rpb2	C26E6.4	*rpb-2*	C128	F09F7.3		
AC40	H43I07.2		Rpb3	C36B1.3	*rpb-3*	AC40	H43I07.2		
AC19	F58A4.9		Rpb11	W01G7.3	*rpb-11*	AC19	F58A4.9		
A12.2	C15H11.8		Rpb9	Y97E10AR.5	*rpb-9*	C11	Y77E11A.6		
ABC27	H27M09.2	*rpb-5*	Rpb5	H27M09.2	*rpb-5*	ABC27	H27M09.2	*rpb-5*	
ABC23	C06A1.5	*rpb-6*	Rpb6	C06A1.5	*rpb-6*	ABC23	C06A1.5	*rpb-6*	
ABC14.5	F26F4.11	*rpb-8*	Rpb8	F26F4.11	*rpb-8*	ABC14.5	F26F4.11	*rpb-8*	
ABC10β	Y37E3.3	*rpb-10*	Rpb10	Y37E3.3	*rpb-10*	ABC10β	Y37E3.3	*rpb-10*	
ABC10α	F23B2.13	*rpb-12*	Rpb12	F23B2.13	*rpb-12*	ABC10α	F23B2.13	*rpb-12*	
A14	n.i.		Rpb4	F43E2.2	*rpb-4*	C4	n.i.		
A43	n.i.		Rpb7	Y54E10BR.6	*rpb-7*	C25	ZK856.10		
A49	F23F1.9		RAP74	C01F1.1					
A34.5	n.i.		RAP30	Y39B6A.36					

Table 7 Eukaryotic RNA polymerase subunits. Common names (grey column) and the human and yeast names (upper block) of the subunits of the three polymerases (assembled from NCBI Homologene and literature comparison). Shared subunits are in blue or green. In *C. elegans*, the homologs of many Pol II subunits have been defined (assembled from Wormbase WS200 database entries and from BLAST searches). For the accessory subunits of the core transcription apparatus of RNA pol I, the *C. elegans* homologs remain to be identified (n.i.). "*rpa-1*" and "*rpa-2*" have already been attributed to other genes and unfortunately cannot be used to name the according subunits of RNA pol I.

4.6.1.1 Apoptotic defects are not induced by RNAi knockdown of other RNA pol I subunits

Considering the lack of viable mutants for most RNA polymerase subunits, I had to use RNAi to gradually knock down their levels. I chose the L3/L4 stage for initiation of RNAi by feeding, since by this stage, most of the somatic organs have been formed and the worms should get past the L4/adult molt despite knockdown of essential genes. The germ line has developed sufficiently to yield some oocytes and embryos in early adulthood even if the system is going to decay soon thereafter as a result of increasing RNAi effects. This should allow to assess germline apoptosis in at least a short time window also for deleterious knock-downs; this turned out to be the case except for some RNA pol II subunits.

I performed RNAi to those polymerase subunits for which we had a construct available in the Ahringer or ORFeome RNAi libraries. Surprisingly, knockdown did in several cases lead to defects in fertility and growth, but did not lead to defective DNA damage-induced apoptosis; an exception to this was the large subunit of Pol II. Importantly, RNAi to F14B4.3 did reduce germ cell apoptosis using these conditions (Figure 32). Where available, I repeated the experiment with RNAi clones from both libraries and could reproduce the same effects regarding fertility and apoptosis. Of note, not all RNA polymerase subunits tested seemed to be essential (Table 8). Consistently, knockdown of *rpb-12*, of *rpb-4*, of F23F1.9 (A49), of Y77E11A.6 (Rpb9 paralog C11), and of Y39B6A.36 (RAP30) did not strongly affect viability or

reproduction of the treated parental generation or their F1 progeny. This apparent non-essentiality of some subunits of a central macromolecular complex of life is rather unexpected. Even though RNAi treatment had a strong effect on fertility and viability for many subunits, it cannot be excluded that some of the genes were not knocked down efficiently. (I did not assess the efficiency of reduction of the according transcripts in the RNAi treated worms.) In addition, some subunits might be present at high abundance or have a much lower protein turnover rate than others. There are no mutant alleles available for the four genes that could prove or disprove non-essentiality.

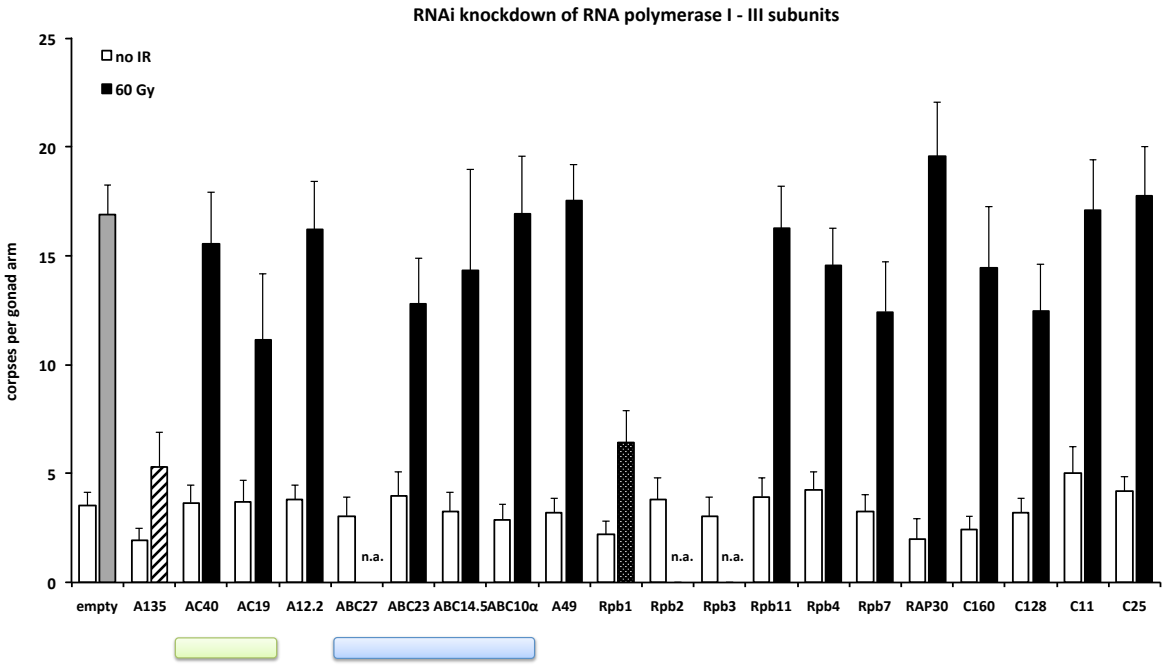

Figure 32 Apoptotic response to IR irradiation in the germ line of RNAi treated N2 worms. Synchronised L3 stage worms were transferred to RNAi bacteria, which often led to an apparent effect by the time the worms reached adulthood. For knockdown of the ABC27, Rpb2 and Rpb3 homologs and irradiation, germ line defects were so strong that scoring of apoptotic corpses was no longer possible. Shared subunits between Pol I and Pol III (green bar), and between all three polymerases (blue bar). Error bars represent 95% CI of the mean; see Table 8 for detailed numbers.

		# experiments		egg laying	hatching	larval development	Apoptosis, no IR		Apoptosis, 60 Gy	
POLR subunit	*C. elegans*	Ahr	ORF				score	95% CI (n)	score	95% CI (n)
	empty vector RNAi			normal	+	normal	3.56	±0.59 (88)	16.90	±1.35 (88)
A190	Y48E1A.1	0	0							
A135	F14B4.3	6	1	few eggs	+	larval arrest, or arrest at size of early stages	1.94	±0.55 (36)	5.31	±1.60 (36)
AC40	H43I07.2	7	0	few eggs	+	delayed growth / variably penetrant larval arrest	3.67	±0.82 (36)	15.53	±2.41 (36)
AC19	F58A4.9	1	0	delayed	+	delayed growth	3.70	±1.01 (20)	11.15	±3.00 (20)
A12.2	C15H11.8	6	1	delayed	+	normal to slightly delayed	3.83	±0.64 (36)	16.19	±2.22 (36)
ABC27	H27M09.2	0	1	some eggs	none	no larvae	3.06	±0.89 (16)		
ABC23	C06A1.5	6	1	normal	+	slightly delayed, some with germline defects	4.00	±1.10 (36)	12.81	±2.11 (36)
ABC14.5	F26F4.11	6	0	normal	(-)	delayed, sterile	3.25	±0.89 (20)	14.33	±4.63 (6)
ABC10β	Y37E3.3	0	0							
ABC10α	F23B2.13	6	1	(delayed)	+	normal	2.89	±0.72 (36)	16.92	±2.67 (36)
A14	n.i.									
A43	n.i.									
A49	F23F1.9	3	0	normal	+	normal	3.19	±0.71 (32)	17.53	±1.68 (32)
A34.5	n.i.									
Rpb1	F36A4.7	3	0	few eggs	(-)	delayed, arrest	2.21	±0.63 (33)	6.43	±1.46 (56)
Rpb2	C26E6.4	2	0	few eggs	(-)	early arrest	3.81	±0.99 (36)		
Rpb3	C36B1.3	1	1	few eggs	(-)	early arrest	3.03	±0.89 (32)		
Rpb11	W01G7.3	6	1	normal	(+)	slightly delayed, sterile	3.94	±0.85 (36)	16.25	±1.97 (36)
Rpb9	Y97E10AR.5	0	0							
Rpb4	F43E2.2	1	1	normal	+	normal	4.28	±0.78 (36)	14.58	±1.67 (36)
Rpb7	Y54E10BR.6	1	1	normal	(-)	early arrest	3.26	±0.80 (31)	12.44	±2.31 (32)
RAP74	C01F1.1	0	0							
RAP30	Y39B6A.36	1	0	normal	+	normal	2.00	±0.91 (16)	19.56	±2.48 (16)
C160	C42D4.8	1	1	some eggs	+	early arrest	2.43	±0.59 (35)	14.44	±2.82 (36)
C128	F09F7.3	1	1	some eggs	+	slightly delayed	3.22	±0.63 (36)	12.47	±2.12 (36)
C11	Y77E11A.6	1	1	normal	+	normal	5.03	±1.20 (36)	17.11	±2.31 (36)
C4	n.i.									
C25	ZK856.10	1	1	some eggs	+	slightly delayed	4.19	±0.65 (36)	17.78	±2.26 (36)

Table 8 RNAi knockdown experiments and observed effects on fertility, development, and apoptosis. # experiments indicates the number of independent experiments with the Ahringer (Ahr) and ORFeome (ORF) RNAi clones. Hatching: + normal, most embryos hatch; (+) several non-hatched eggs; (-) mostly non-hatched eggs. Number of apoptotic corpses per gonad with or without irradiation, 95 % CI of the mean, and total number of animals tested per condition.

4.6.1.2 Characterisation of the RNA pol I large subunit allele *ok2655*

ok2655 is a balanced deletion of Y48E1A.1

In the course of the RNAi experiments, a mutant worm strain RB2003 became available which was reported to have a deletion in the RNA pol I large subunit gene. At that point, the molecular details of the mutation had not been described. I determined the limits of the *ok2655* deletion which was annotated to be within the fifth intron and the sixth exon of Y48E1A.1. Supposedly, worms homozygous for such a mutation would not be viable. Indeed, I could also amplify the wildtype allele from the RB2003 strain by PCR, suggesting it was not homozygous for *ok2655*. Normally a loss-of-function allele of an essential gene is rapidly lost in a worm population; this was not the case for *ok2655*. I could repeatedly detect the allele in succeeding generations; I thus singled more slowly growing individuals, let them lay eggs, confirmed the presence of an *ok2655* allele, and analysed their F1 progeny. I was able to select a line that propagated the *ok2655* to all progeny. Nevertheless, a wildtype allele could also be detected in all of them. Seemingly, at least part of the *ok2655* allele is genetically balanced within the RB2003 strain. When I tried to cross the mutant allele into other strains, this balancing effect was lost and the *ok2655* allele disappeared rapidly in the progeny.

The deletion in Y48E1A.1*(ok2655)* might not necessarily abolish gene function completely, since of the coding sequence, it removes only a fragment of exon 6 at a length of 198 nt (a multiple of three). RT-PCR of a sequence spanning exons 5 to 7 (primers 178 and 188 in Figure 33) resulted in two products in the mutant line, one of approximately the wildtype length and one of a shortened transcript, corresponding to the deletion allele. Sequence analysis showed that the sequence deleted on exon 6 in *ok2655* was missing, but the remaining exon sequence was represented complete, indicating that the exon had not been fully skipped. However, 5' to the breakpoint in exon 6, not the 3' end of exon 5 was preceding, but an intronic sequence of 41 nucleotides had slipped in, exactly corresponding to the sequence from the breakpoint in intron 5 up to an alternative canonical splice acceptor (Figure 33). Together, this leads to 41 extra and 198 deleted nucleotides in the spliced transcript and thus to a frameshift in the Y48E1A.1*(ok2655)* coding sequence. In the resulting mutant protein – provided the remaining transcript is unchanged – the first 1330 of 1737 residues would be conserved, followed by 172 extra amino acids before the stop.

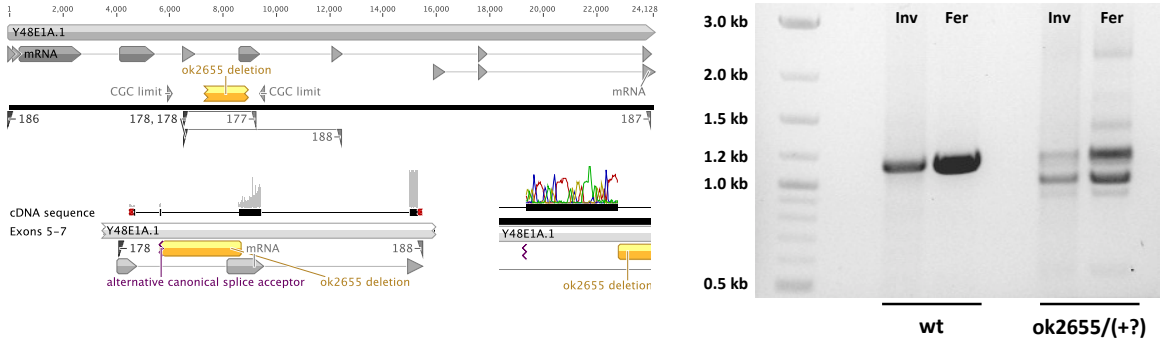

Figure 33 The deletion in Y48E1A.1*(ok2655)* removes part of exon six and leads to the use of an alternative canonical splice acceptor close to the beginning of the deletion within the preceding intron. The worm line analysed here propagates the deletion allele to all progeny and seems to maintain a wildtype copy as well. RT was performed on the same samples with random priming and with two different RT-polymerases (Superscript II from Invitrogen (Inv), or RevertAid H Minus from Fermentas (Fer)), and the PCR with primers 178 and 188. Sequencing of the 1.0 and 1.2 kb bands in the mutant yielded the splicing variant and the wildtype sequence, respectively.

Y48E1A.1*(ok2655)* mutants have an IR response defect

The internally balanced *ok2655* line derived from an individual of the RB2003 strain was growing more slowly than the average from the RB2003 worm population; the germ cell nucleoli appeared smaller than wildtype nucleoli. I tested the line for DNA damage-induced apoptosis. It was equally deficient as *rpo-1b(op259)* (Figure 34 and Figure 36). I crossed the *ok2655* allele into a proper genetic balancer strain with the *mT1* rearrangement balancing lethal mutations on chromosome II/III. Here, the internal balance of the line derived from RB2003 seemed to be lost, and propagation of *ok2655* became dependent on the presence of *mT1*. Heterozygous progeny from this balanced strain *ok2655*/*mT1* looked wildtype, and IR-induced apoptosis was not reduced. No RNAi clone for Y48E1A.1 had been present in either of the two libraries, so I could not readily predict and compare the effect of the deletion in the RNA pol I large subunit to a knockdown phenotype. The ambiguous results – the balanced strain that did not exhibit an apoptotic defect on one hand, and the line that propagated *ok2655* without a known balancer and had reduced DNA damage response on the other hand – make it difficult to conclude whether Y48E1A.1 is involved in IR-induced apoptosis in a similar way as *rpo-1b*.

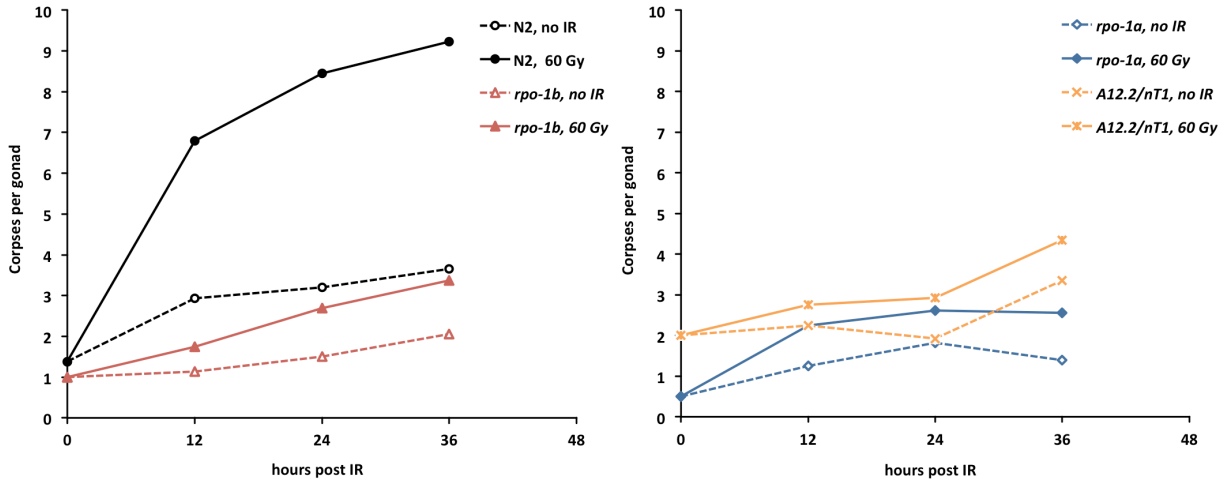

Figure 34 Time course of the apoptotic response to IR irradiation of RNA polymerase I mutants. *rpo-1b(op259)* "*rpo-1b*", Y48E1A.1*(ok2655)* "*rpo-1a*", and balanced strain with deletion in C15H11.8 "A12.2/nT1".

4.6.1.3 Two alleles affecting C15H11.8 cause an apoptotic defect

C15H11.8 codes for the *C. elegans* ortholog of A12.2, an RNA pol I associated factor that is similar to the transcription factor TFIIS. Two strains were available carrying mutations in this gene; however, both alleles do not affect C15H11.8 uniquely, but involve deletions in the flanking genes. *ok1531* in the strain VC1097 deletes the third (last) exon of C15H11.8 and part of *pas-1*, which codes for the regulatory subunit of the 20S proteasome core. *gk284* was reported to affect C15H11.8 and *rrbs-1*, a factor itself involved in ribosome biosynthesis. Whereas RNAi of C15H11.8 had only led to a slight growth delay in F1 larvae, both mutant alleles were lethal and had to be maintained by the genetic balancer *nT1*. Judged by the mutants, C15H11.8 could be an essential gene; however, the co-deletions in the flanking genes *pas-1* or *rrbs-1* could be lethal on their own. Interestingly, both mutant strains had a defect in IR-induced apoptosis even in heterozygous, i.e., balanced animals (Figure 34). RNAi to C15H11.8, however, had not resulted in an apoptotic defect. Conversely, *rrbs-1* knock-down led to reduced apoptosis (see also following section), thus the defect seen in the *gk284*/*nT1* mutant could well arise from the deletion of *rrbs-1* rather than of C15H11.8. *pas-1(RNAi)* did not have an obvious effect on germ line apoptosis, leaving it open whether the apoptotic defect in *ok1531*/*nT1* is rather to attribute to C15H11.8 or to *pas-1*.

4.6.1.4 A new allele of *rpo-1b*, F14B4.3*(ok1970)*, leads to apoptotic defect

ok1970 is a deletion in F14B4.3

A deletion strain for F14B4.3 was generated by the CGC during my project. This lethal *ok1970* allele of *rpo-1b* is balanced by the *hT2* balancer for chromosome 1. The 1241 bp deletion starts in intron 3 and removes exons 4 and 5 and most of exon 6.

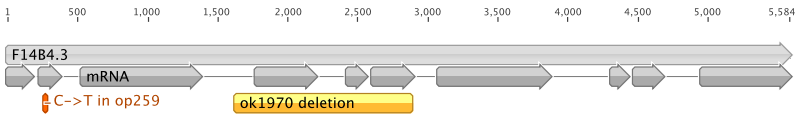

Figure 35 CDS of *rpo-1b* and available mutant alleles. Single base transition in *rpo-1b(op259)*, and deletion of a 1.2 kb genomic fragment in *ok1970*.

Anterior and posterior gonads have different apoptotic defects

Heterozygous animals exhibited a peculiar apoptotic phenotype: while IR-induced apoptosis was abolished completely, baseline apoptosis was increased in comparison to wildtype. When I dissected the apoptotic scores, it became evident that this increase was fully on the account of anterior gonads. Posterior gonads had only around 2 corpses on average – with or without irradiation – whereas in the anterior gonads, around 7 corpses could be observed by DIC, again with or without irradiation. Such a strong bias for the corpse number to one of the gonads has not been reported before, and we have not observed such a strong difference between anterior and posterior gonad in any other strain. (Worms grown on RNAi bacteria have a tendency for higher corpse numbers in the posterior gonad; see Figure 129.) To exclude that this was merely due to the balancer, I scored another mutant strain balanced by *hT2*; this strain only showed a slightly higher number of corpses in the anterior gonad, attributing the main effect to *ok1970*.

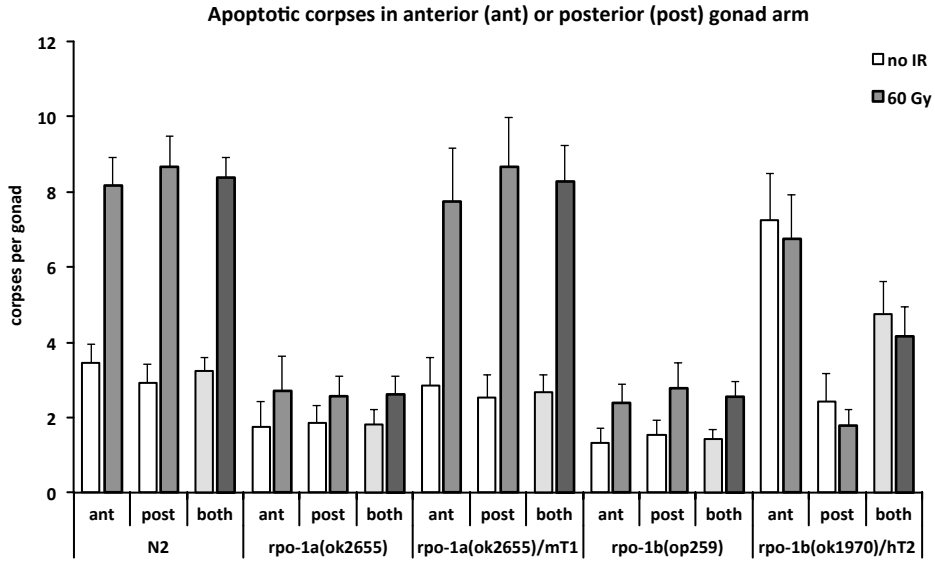

Figure 36 Germ line apoptosis in anterior (ant) and posterior (post) gonads 24 h after irradiation. *rpo-1a(ok2655)* (internally balanced derivative of RB2003) and *rpo-1b(op259)* have a lower level of constitutive apoptosis and defective IR response. The balanced *rpo-1b(ok1970)* strain has a strong anterior-posterior bias. Error bars indicate 95 % CI of the mean of at least 20 gonads.

4.6.1.5 Summary of RNA polymerase subunits and apoptosis

Collectively, I have observed altered germ cell apoptosis for mutants of the alpha- and beta-subunits of RNA pol I, whereas such an effect could not be demonstrated for the smaller subunits. The experiments also exemplify the difficulty of working with RNAi or balanced mutant strains. They demonstrate the immense value that non-lethal alleles of essential genes can add to the investigation of their roles in specific biological processes.

4.6.2 RNA processing factors and apoptosis

4.6.2.1 The processing mutant *pro-2* shares phenotypes with *rpo-1b(op259)*

rRNA processing and ribosomal assembly factors are critical for the maturation of the small 40S and the large 60S ribosomal subunits. There is a high number of factors involved specifically in the synthesis of either of the two subunits as well as factors needed for both (Fromont-Racine 2003). Worm homologs are often difficult to identify by database search due to missing annotation in the current genome data. Different nomenclature in the two prevailing model systems for ribosome synthesis – yeast and mammalian cells – further hamper the efficient identification of homologous worm genes. Research on ribosome synthesis has been relatively scarce in *C. elegans* so far. Interestingly, several conditional mutants of rRNA processing factors had been isolated from one genetic screen, based on their germline tumor phenotype (Killian 2004; Voutev 2006). These mutations were all mapped to genes that by homology were involved in ribosome synthesis. They lead to a Pro (proximal proliferation) phenotype at non-permissive temperature: ectopic, mitotically dividing cells in the proximal gonad grow to massive tumours in the adult animal. Intriguingly, *rpo-1b(op259)* presented a very similar phenotype when grown at 25°C. Germ cells have even smaller nucleoli than at 20°C; proximal to the often scarce oocytes, small germ cells resembling mitotic cells accumulate in the course and start growing to a bulky mass, that, in extreme cases, fills almost the whole diameter of the worm (Figure 44). This similarity brought me to look for apoptotic defects in the Pro mutants (Figure 37). One of two Pro mutants tested, *pro-2(na27)*, indeed failed to exhibit increased apoptosis upon IR at 20°C, similarly to *rpo-1b(op259)* [see Figure 34 for a comparison]. (In return, the similarities of *rpo-1b(op259)* to the Pro mutants supported the idea that *rpo-1b(op259)* could have an rRNA processing defect.)

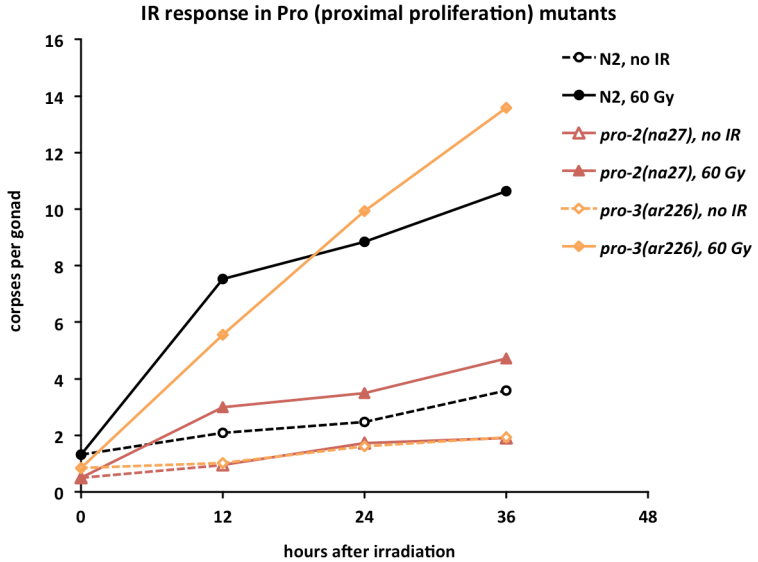

		N2		*pro-2(na27)*		*pro-3(ar226)*	
		score	95% CI (n)	score	95% CI (n)	score	95% CI (n)
no IR	0 h	1.31	±0.19 (100)	0.50	±0.27 (20)	0.85	±0.43 (20)
	12 h	2.10	±0.28 (100)	0.95	±0.27 (40)	1.03	±0.31 (38)
	24 h	2.48	±0.34 (120)	1.73	±0.31 (40)	1.63	±0.46 (40)
	36 h	3.59	±0.55 (56)	1.90	±0.30 (40)	1.93	±0.42 (40)
60 Gy	0 h						
	12 h	7.53	±0.60 (80)	3.00	±0.80 (40)	5.55	±0.97 (40)
	24 h	8.85	±0.61 (120)	3.50	±0.42 (40)	9.93	±1.58 (40)
	36 h	10.63	±0.99 (40)	4.73	±1.01 (40)	13.58	±1.92 (40)

Figure 37 Time course of apoptotic response to IR irradiation in gonads of rRNA processing mutants. The table indicates average number of apoptotic corpses, 95 % CI of the mean, and number of animals tested per condition.

4.6.2.2 RNAi knockdown of rRNA processing factors disturbs apoptosis

Using RNAi, I addressed the question whether failure in properly processing rRNA might more generally lead to changes in apoptosis. I tested several processing factors: U3 spliceosome subunits to assess early steps of 18S rRNA and thus SSU synthesis, and early and later factors of LSU maturation (Table 9). As for RNA polymerase subunits, I had to titrate RNAi conditions such that possible effects would become apparent without the germline having decayed already. For some RNAi knockdowns, I used the transgenic line *opIs110; unc-119(ed3)* that expressed Actin::YFP in gonadal sheath cells, which offered an additive means to score apoptotic corpses [see details in *8.2 Frequently used assays*]. (For some reason, apoptosis levels in the control RNAi condition were lower in this strain than in N2.) Most treatments had strong effects on germ line integrity, on fertility and on viability. IR-induced germ cell apoptosis was reduced in most cases (Figure 38). The effect was slightly less pronounced in processing factors of later steps of ribosome synthesis; for instance, *pro-2(RNAi)* and *pro-3(RNAi)* had weaker effects than knock-down of *lpd-7* or C18A3.3.

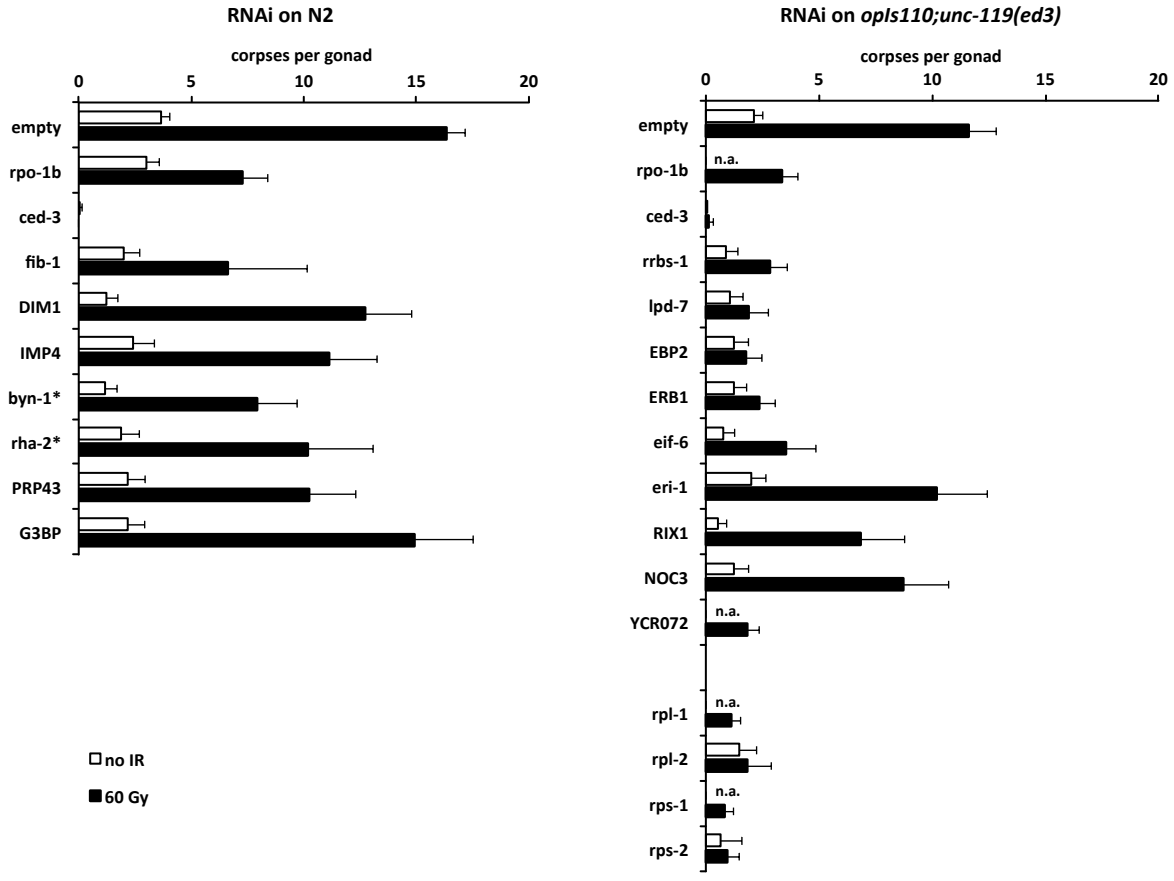

Figure 38 Apoptotic response to IR irradiation in the germ line of RNAi treated wildtype (N2) or *opIs110[P_{lim-7}::act-5::yfp; unc-119(+)]; unc-119(ed3)* worms. Synchronised L3 stage worms were transferred to RNAi bacteria, which often had an apparent effect by the time the worms reached adulthood. For gene annotations, see Table 9; *byn-1** and *rha-2** RNAi bacteria were contaminated with other, nonspecified target sequences. Error bars represent 95% CI of the mean.

4.6.2.3 Knockdown of ribosomal proteins abolishes germ cell apoptosis

To assess whether disturbing ribosomes by reducing individual ribosomal proteins would also impact on germ cell death, I picked *rps-1*, *rps-2* and *rpl-1*, *rpl-2* as representatives of the small and large subunit, respectively. The numbering of the ribosomal proteins in metazoa is mostly based on homology to the yeast proteins, but is not in full agreement with that system (Mager 1997). Anyway, it is not systematic as to molecular weight or functional groups. I considered these four targets as randomly tested ribosomal proteins. The effect on germ line appearance was very pronounced; germ cell contours became less clear and the phase contrasts in DIC changed around nucleoli and nuclei. The number of apoptotic corpses was reduced to very low levels in all four cases (Figure 38 and Table 9).

RNAi target	Gene	Yeast	Step	P-P	no IR		60 Gy		no IR, YFP halos		60 Gy, YFP halos	
N2					**score**	**95% CI (n)**	**score**	**95% CI (n)**	**score**	**95% CI (n)**	**score**	**95% CI (n)**
empty	*(none)*				3.64	±0.41 (148)	16.35	±0.82 (212)				
F14B4.3	*rpo-1b*	Rpa135			2.98	±0.60 (52)	7.25	±1.15 (52)				
ced-3	*ced-3*				0.05	±0.10 (20)	0.00	±0.00 (36)				
T01C3.7	*fib-1*	NOP1	nucleolar	x	2.00	±0.72 (16)	6.60	±3.55 (20)				
F32E10.6 ORF		(B23)	nucleolar		2.28	±0.73 (32)	19.75	±2.56 (16)				
F32E10.6 Ahr		(B23)	nucleolar		4.13	±0.77 (32)	20.19	±2.35 (16)				
E02H1.1		DIM1	SSU		1.25	±0.49 (16)	12.75	±2.04 (20)				
ZK795.3		IMP4	SSU		2.44	±0.93 (16)	11.15	±2.10 (20)				
F57B9.5	*"byn-1"*	ENP1	SSU		1.19	±0.51 (16)	7.90	±1.83 (20)				
C06E1.10	*"rha-2"*	ECM16	SSU		1.88	±0.82 (16)	10.20	±2.87 (20)				
F56D2.6		PRP43	both		2.19	±0.78 (16)	10.25	±2.06 (16)				
K08F4.2		G3BP	degrad.?		2.17	±0.76 (48)	14.91	±2.64 (32)				
opIs110;unc-119(ed3)												
empty	*(none)*				2.15	±0.36 (52)	11.63	±1.20 (76)	4.63	±0.97 (52)	11.66	±1.55 (62)
F14B4.3	*rpo-1b*	Rpa135					3.38	±0.71 (16)			6.00	±1.09 (16)
ced-3	*ced-3*				0.02	±0.04 (52)	0.14	±0.19 (76)	0.33	±0.24 (48)	0.07	±0.07 (68)
C15H11.9	*rrbs-1*	RRS1	5S incorp.		0.90	±0.54 (10)	2.86	±0.76 (56)	3.75	±2.12 (8)	4.73	±0.57 (48)
R13A5.12	*lpd-7*	NOP7	LSU	x	1.06	±0.58 (16)	1.90	±0.86 (20)	1.81	±0.78 (16)	3.75	±1.04 (16)
F32E10.6 ORF		(B23)	nucleolar				5.81	±1.65 (16)			10.00	±2.38 (16)
C18A3.3		EBP2	LSU	x	1.25	±0.63 (16)	1.75	±0.74 (20)	2.63	±1.20 (16)	2.75	±0.87 (16)
Y48B6A.1		ERB1	LSU	x	1.25	±0.55 (16)	2.35	±0.71 (20)	3.71	±1.29 (14)	5.31	±1.48 (16)
C47B2.5	*eif-6*	TIF6	LSU	x	0.75	±0.52 (16)	3.55	±1.31 (20)	3.06	±0.89 (16)	5.63	±1.07 (16)
T07A9.5	*eri-1*	ERI1	5.8S proc.		2.00	±0.67 (16)	10.20	±2.24 (20)	9.69	±2.66 (16)	12.56	±2.63 (16)
Y48A6C.4		RIX1	LSU	x	0.56	±0.36 (16)	6.85	±1.95 (20)	5.13	±1.90 (16)	5.94	±0.92 (16)
C37H5.5		NOC3	LSU		1.25	±0.66 (16)	8.75	±1.98 (20)	8.00	±1.67 (16)	8.31	±2.44 (16)
W07E6.2		YCR072	LSU	x			1.81	±0.54 (16)			6.31	±1.17 (16)
Y71F9AL.13	*rpl-1*		RP				1.13	±0.43 (16)			3.81	±1.32 (16)
B0250.3	*rpl-2*		RP		1.50	±0.76 (16)	1.85	±1.05 (20)	2.75	±1.28 (16)	2.56	±0.76 (16)
F56F3.5	*rps-1*		RP				0.81	±0.41 (16)			3.13	±0.89 (16)
C49H3.11	*rps-2*		RP		0.63	±0.98 (16)	0.95	±0.52 (20)	3.69	±1.69 (16)	3.06	±0.99 (16)

Table 9 Knockdown of rRNA processing factors and of ribosomal proteins. Factors are arranged according to an approximate chain of action on ribosomal small subunit (SSU) or large subunit (LSU) synthesis, or ribosome degradation. P-P indicates the factors for which a physical interaction has been predicted with RPO-1B (Wormbase WS200). For *opIs110; unc-119(ed3)*, corpses were scored by DIC and independently by the number of Actin::YFP halos forming from sheath cell protrusions around corpses (reporter *opIs110[P_{lim-7}::act-5::yfp; unc-119(+)]*). Blast search for the best matching homolog of the nucleolar protein Nucleophosmin/B23 yielded F32E10.6 (homology not confirmed). "*byn-1*" and "*rha-2*" RNAi clones were contaminated with other sequences. Average number of apoptotic corpses, 95 % CI of the mean, and total number of animals tested per condition.

4.6.3 Translation and apoptosis

So far, the loss of normal activity of RNA pol I subunits, of ribosomal rRNA processing and further ribosomal synthesis factors, and of ribosomal proteins had affected apoptosis. Finally, translation as the core function of ribosomes could be the critical step by which all the former disturbances impact on germ cell death. Interfering with ribosome synthesis at any step would likely have an effect on translation. To include the possibility that the defective apoptosis observed in *rpo-1b(op259)* is a result of altered translation, I tested whether inhibiting translation could reproduce the reduced IR response.

4.6.3.1 *ife-1* translation initiation mutants have apoptotic defect

eIF4E has been recognised as a central factor in translation initiation, and its aberrations have been associated with proliferative diseases (Fischer 2009). An early report on eIF4E in growth factor-restricted cell cultures had demonstrated a prohibitive effect of overexpression on apoptosis (Polunovsky 1996). *C. elegans* has five homologs of eIF4E, coded for by different genes *ife-1* to *ife-5* (Keiper 2000). They are preferentially expressed in either somatic tissue or in the germ line and have different affinities for cap-structures in the mRNA to be translated. The five homologs might help translation initiation of specific subsets of genes in specific tissues (Song 2010; Dinkova 2005). Likely, there is also some functional redundancy between the isoforms. *ife-3* is essential for viability; the available mutants of the other genes have variable, often conditional phenotypes, like meiotic defects at increased temperature. I tested the mutants of the five eIF4E isoforms for germ line apoptosis; *ife-1(ok1978)*, *ife-2(ok306)*, *ife-4(ok320)*, *ife-5(ok1934)*, and *ife-3(ok191),* which was balanced by *unc-34(e566)*. Specifically, *ife-1* mutants showed reduced apoptosis in response to IR, whereas the other mutants were not obviously defective (Figure 39). I confirmed the germline phenotype with two alleles, *ife-1(ok1978)* and *ife-1(bn127),* which I got from Brett Keiper (Henderson 2009). *ife-1(RNAi)* using the clone from the Ahringer library (Kamath 2003) did not phenocopy this defect, but rather increased germ cell apoptosis. Given the high degree of sequence conservation between the *ife* isoforms, it is unlikely that this RNAi treatment specifically targeted *ife-1*.

Contrarily to the *ife-1* mutant, and more in agreement with *ife-1(RNAi)*, specific knockdown of one isoform of *ifg-1*, the *C. elegans* eIF4G homolog, was reported to increase germ cell apoptosis; in case RNAi specifically targeted the longer isoform of *ifg-1* containing the eIF4E interacting domain, CED-4 expression was increased; animals became sterile or arrested as larvae when both isoforms were lost (Contreras 2008).

Interestingly, RPO-1B is predicted to interact not only with transcription factors; among the candidates for interaction are processing factors and several translation initiation/elongation factors (*eif-6*/eIF6, *iftb-1*/eIF2β, T04H1.2), as listed in Wormbase WS221 for F14B4.3.

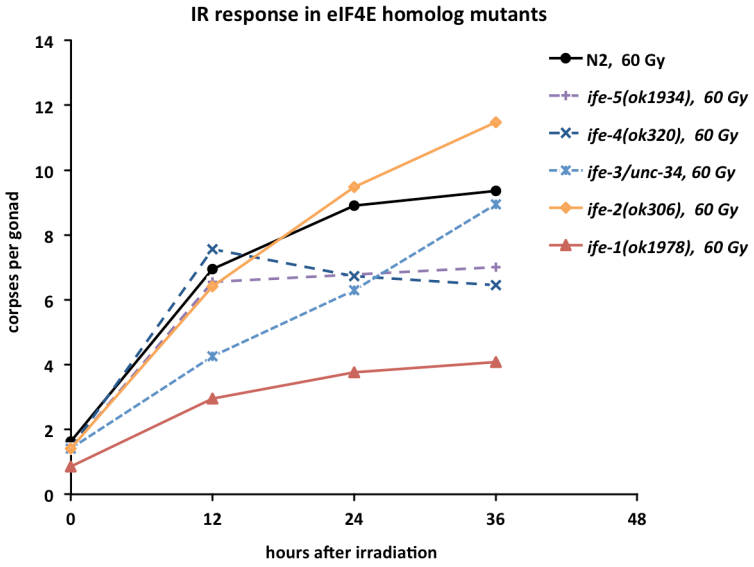

		N2		ife-1(ok1978)		ife-2(ok306)		ife-3(ok191)/+		ife-4(ok320)		ife-5(ok1934)		ife-1(bn127)	
		score	95% CI (n)	score	95% CI (n)	score	95% CI (n)	score	95% CI (n)	score	95% CI (n)	score	95% CI (n)	score	95% CI (n)
no IR	0 h	1.63	±0.21 (64)	0.85	±0.33 (20)	1.41	±0.25 (29)	1.41	±0.53 (20)	1.41	±0.62 (20)	1.41	±0.45 (20)		
	12 h	3.35	±0.56 (20)					2.35	±0.71 (20)	2.10	±0.72 (20)	1.90	±0.60 (20)		
	24 h	3.33	±0.69 (40)					2.90	±0.58 (40)	2.43	±0.60 (40)	2.12	±0.45 (52)	1.06	±0.26 (36)
	36 h	3.30	±0.83 (20)					2.95	±0.87 (20)	2.15	±0.84 (20)	1.25	±0.49 (20)		
60 Gy	0 h														
	12 h	6.94	±0.64 (64)	2.95	±0.32 (65)	6.42	±0.52 (48)	4.25	±0.79 (20)	7.55	±1.19 (20)	6.55	±1.67 (20)		
	24 h	8.91	±0.64 (88)	3.76	±0.44 (58)	9.48	±0.72 (52)	6.30	±1.33 (40)	6.73	±0.83 (40)			2.93	±0.55 (56)
	36 h	9.37	±0.89 (49)	4.07	±0.50 (41)	11.47	±1.94 (15)	8.95	±1.40 (20)	6.45	±1.26 (20)	7.00	±1.39 (20)		

Figure 39 Time course of apoptotic response to IR irradiation in eIF4E homolog mutants. The table indicates average number of apoptotic corpses, 95 % CI of the mean, and total number of animals tested per condition.

4.6.3.2 Chemical inhibition of translation prevents IR-induced apoptosis

We could also abolish IR-induced apoptosis by blocking translation with cycloheximide (CHX). Randy had observed this already and I confirmed the finding by transferring young adult worms to plates with different concentrations of CHX and irradiating them 6 hours later. Such an effect would be predicted by the assumption that DNA damage-induced apoptosis depends on transcriptional upregulation of the pro-apoptotic BH3-only factors and thus involves translation. More detailed results of the CHX experiments are discussed in the following chapter.

4.6.4 Cycloheximide and germ cell death

DNA damage-induced apoptosis is dependent on CEP-1 and EGL-1. The central mechanism involves CEP-1-induced transcriptional upregulation of EGL-1 (Derry 2001; Schumacher 2001). The appearance of apoptotic corpses several hours after exogenous DNA damage is in agreement with cellular responses beyond direct activation of pro-apoptotic cascades. For transcriptional upregulation of the BH3-only proteins EGL-1 and CED-13 to become effective, translation of the mRNA is most likely also part of the apoptotic response. DNA damage-induced apoptosis therefore can be assumed to be dependent on translation. We wanted to evaluate the possibility that the apoptotic defects in *rpo-1b(op259)* animals were a result of globally reduced translation in this mutant.

The bacterial toxin cycloheximide (CHX) can block translation in eukaryotic organisms; it has an immediate effect by directly interfering with translation elongation and has therefore been widely used in cell culture studies, and it has also been applied to inhibit translation in *C. elegans*. I administered different concentrations of cycloheximide in ethanol to agar plates with OP50; worms were transferred from normal plates to these drug-containing plates at a young adult stage.

4.6.4.1 Cycloheximide blocks IR-induced apoptosis

In a first series, wildtype N2 worms were tested on cycloheximide (0, 500, 1000 and 1500 µg/ml agar) for apoptotic response to irradiation. Young adults were exposed to CHX for 6 hours before they were irradiated, and were scored 12 or 16 hours later (Figure 40). At 500 µg/ml, most of the IR response seen in mock treated (0 µg/ml) animals was abolished, whereas baseline apoptosis was nearly unchanged. At higher doses, only few gonads could be assessed due to strong adverse effects of the drug on the organism; for those scored, IR-induced apoptosis was completely abolished and also the corpse number of non-irradiated animals was lower. Thus, IR-induced apoptosis is effectively – and preferentially – blocked by chemical inhibition of translation.

One of the early characterisations of CHX action in the cell had suggested an effect on transcription of rRNA and tRNA genes [(Gokal 1986), endorsed by (Matsui 1986)]; this effect had not reportedly been followed further. In principle, such an effect and not merely a block of translation could be underlying the apoptotic phenotype of CHX treated worms. CHX had been used in research of neuronal death, where it proved to be neuroprotective at very low doses [e.g., (Lobner 1996)]. One study showed that the neuroprotective effect of CHX involved upregulation of c-Fos, c-Jun and Bcl-2 at the mRNA and protein levels. Neuroprotection was maximal at 10-100 nM (approx. 3-30 ng/ml), concentrations that did not significantly lower protein synthesis (Furukawa 1997). Possibly, CHX also has effects on apoptosis in the worm that are independent of strong translation inhibition.

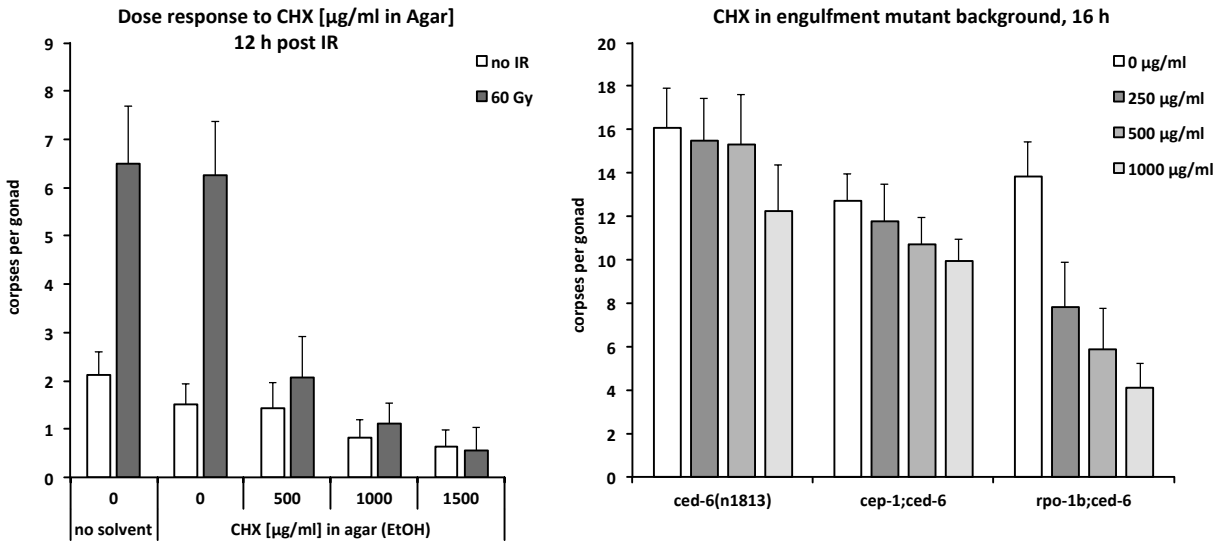

Figure 40 Left: Apoptotic response to irradiation in worms treated with different concentrations of cycloheximide (CHX) for 6 hours before irradiation. Right: Effect of CHX on constitutive cell death is strongest in *rpo-1b(op259)*, where constitutive cell death is *cep-1*-dependent [see Figure 68]; treatment on CHX was for 16 hours. Error bars represent 95 % CI of the mean.

4.6.4.2 Translation inhibition and apoptotic defects in *rpo-1b(op259)*

The effect on translation of the *op259* mutation is certainly much more subtle than that of chemical inhibition, since in the latter case, animals start degenerating soon after treatment. The worms look completely emaciated and the gonads shrink to thin tubes. The defective IR response in *rpo-1b(op259)* likely represents a more specific effect than just global reduction of translation. The doses we used to inhibit IR-induced apoptosis by CHX treatment are too high to guarantee survival of the animal, whereas *rpo-1b(op259)* animals have the apoptotic defect but remain grossly healthy (we have, however, not titrated the concentration of CHX).

I had seen that almost all apoptosis in *rpo-1b(op259)*, including the baseline apoptosis of non-irradiated animals, was dependent on *cep-1* and *egl-1 (see 5.3.3 Germ cell apoptosis in rpo-1b(op259); egl-1(lf))*. If, as it seems, all germ cell apoptosis in *rpo-1b(op259)* involves CEP-1-induced upregulation of EGL-1, this precludes that translation (of EGL-1) is generally not sufficient in the mutant to allow triggering of apoptosis.

I used the engulfment mutant *ced-6(n1813)* to increase the 'resolution' of the number of apoptotic corpses at baseline levels, that is, in the absence of exogenous DNA damage; dying germ cells are not removed but accumulate in the gonad. *ced-6(n1813)* mutants were shifted to CHX plates as young adults and the number of accumulated corpses was scored at a time point before a majority of the worms would show strong defects caused by CHX treatment (Figure 40). *ced-6(n1813)* mutants allowed to score in the range of about 15 corpses on average at this time point (whereas wildtype worms exhibited only about 2 corpses). In accordance with the previous experiments, 500 µg/ml CHX (that had inhibited IR-induced apoptosis) did not significantly block baseline apoptosis; also, the corpse number in non-irradiated *ced-6(n1813)* only weakly decreased with higher doses of CHX. This weak, gradual reduction in the number of accumulated corpses was not due to a CEP-1-dependent effect, since it could also be observed in *cep-1(gk138); ced-6(n1813)*.

Next, I tested *rpo-1b(op259); ced-6(n1813)*. Already at 250 µg/ml CHX, the number of corpses was reduced by almost half, and at 500 µg/ml it reached only 40 % of the mock-treated controls (Figure 40).

The strong response to CHX of baseline apoptosis in *rpo-1b(op259); ced-6(n1813)* is in agreement with the notion that in *rpo-1b(op259)* mutants, unlike in wildtype, 'physiological' germ cell apoptosis is dependent on CEP-1 (Figure 70). The effect of CEP-1-induced upregulation of EGL-1 transcription is likely blocked by chemical inhibition of translation, and consequently, baseline (non-IR-induced) apoptosis is strongly reduced in *rpo-1b(op259)*.

This does, however, not exclude that other mechanisms make *rpo-1b(op259)* hypersensitive for an apoptotic block by CHX treatment. For instance, *rpo-1b(op259)* mutants might be particularly sensitive to chemical inhibition of translation, e.g., due to a reduced capacity of the translational apparatus (numerically or structurally aberrant ribosomes), which would probably predispose to effects of chemical inhibition that become apparent in wildtype only at higher drug doses.

Cycloheximide blocks excessive apoptosis in *rpo-1b(op259); ced-9(n1653)*

In *C. elegans*, partial loss of the function of *ced-9*, the homolog of Bcl-2, increases germ cell death. I show genetically in this work that some of the excessive apoptosis is dependent on *cep-1* [see *5.6*

rpo-1b(op259) and CED-9]. I used cycloheximide to block translation-dependent apoptosis in the *ced-9(n1653)* mutant (Figure 41). (This experiment is mainly relevant in the context of the named chapter but is described here as it uses the same idea of blocking *cep-1*-mediated death by inhibition of translation with CHX.) There was a (statistically not significant) reduction of the corpse number in *ced-9(n1653)* at 12 hours of treatment. No such decrease was observed in *cep-1(gk138); ced-9(n1653)*. In *rpo-1b(op259); ced-9(n1653)*, the high corpse number was significantly reduced, indicating that much of the effect of *rpo-1b(op259)* on *ced-9(n1653)* mutants is translation-dependent. These findings are in agreement with the observation that some of the excessive death in *ced-9(n1653)* and most of the death in *rpo-1b(op259); ced-9(n1653)* is *cep-1*-dependent.

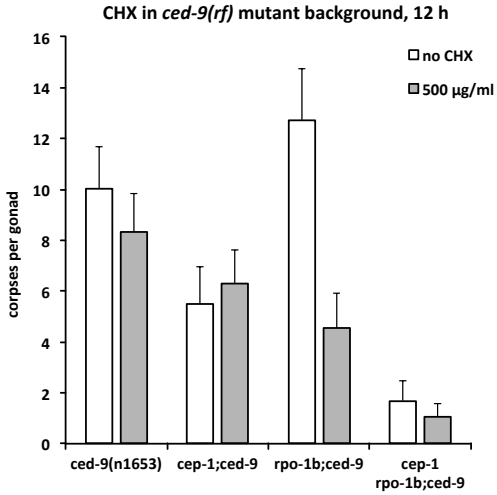

Figure 41 Suppression of excessive apoptosis of *ced-9(n1653)* with Cycloheximide (CHX). Worms were grown at 15°C until L4 stage, when they were exposed to CHX and transferred to 20°C for 12 hours. Error bars: 95 % CI of the mean.

4.6.4.3 Translation in *rpo-1b(op259)*

I considered to assess translation globally by metabolic labelling of newly synthesised proteins (Hansen 2007) or by a method using expression of a GFP protein and FRAP (fluorescence recovery after photobleaching) that would allow to quantify translation *in situ* (Kourtis 2009). Metabolic labelling of proteins by applying radioactive S-methionine in a pulse would allow to measure translation rates in whole animals. The accuracy of this method however seemed too low to detect the expectedly small differences in global translation in the mutant. Overall translation in all tissues would have to differ about twofold so the method would reveal a significant change. FRAP has several advantages: it does not require radioactivity; worms don't have to be perfectly staged; and translation can be assessed at the resolution of individual cells. Yet, considering that *rpo-1b(op259)* might affect translation only of a subset of transcripts, these changes might go undetected with the fluorescent GFP reporter. Instead of assessing translation directly, we chose the proteomics approach presented in *4.5 Proteomic profiles of rpo-1b(op259)* to compare global expression profiles between *rpo-1b(op259)* and wildtype.

Approximately, my experiments did not support global reduction of translation in *rpo-1b(op259)*; various fluorescent reporters that I tested in the *rpo-1b(op259)* background did not show grossly reduced expression. *rpo-1b(op259)* might have altered translation of a subset of proteins similar to *ife* mutants. Hypothetically, the BH3-only proteins are not normally upregulated upon stress due to specific

translation initiation defects. Supporting this, qRT-PCR experiments showed transcriptional upregulation of EGL-1 and CED-13 in *rpo-1b(op259)*, which, however, did not evoke increased germ cell death. Unfortunately, Western blot analysis to detect EGL-1 expression levels in *rpo-1b(op259)* failed. The *opIs56[P_{egl-1}::2xNLS::gfp::egl-1 3'UTR; unc-119(+)]* reporter indicated lower than wildtype EGL-1 expression in the late meiotic pachytene region, but aberrant expression in the distal mitotic region of *rpo-1b(op259)* upon irradiation (Figure 74). (This observation has to be interpreted carefully, since the reporter construct with only a relatively short 3'UTR for *egl-1* does not ascertain to represent the very physiological pattern of EGL-1 expression; EGL-1 transcription is regulated manifold by cis-elements in the promoter and especially in the genetic region far downstream of the coding sequence (Nehme 2008).)

4.6.5 Conclusion on ribosome synthesis and apoptosis

I show that knockdown or mutations of various genes involved in ribosome synthesis reduce germ cell apoptosis in *C. elegans*. Mutant alleles of the two large subunits of RNA pol I (but not knockdown of the other smaller subunits) lead to defective DNA damage-induced apoptosis. Most of the rRNA processing factors and ribosomal proteins that I have tested are necessary for wildtype apoptosis levels. Eventually, chemical inhibition of translation can also abolish irradiation-induced cell death. At this point, it is not possible to judge whether the block in apoptosis involves the same mechanisms in all these conditions. It is potentially of high relevance for tumor biology that changes in ribosome production go along with altered apoptosis levels. Often, cells in human tumours have aberrant nucleolar activity, which could influence how sensitive they are to endogenous and exogenous pro-apoptotic stimuli. We will see in subsequent chapters that genetic conditions which are frequently found in tumours – mutations in the p53 or Bcl-2 homologs for instance – can lead to diverse synthetic effects with the *rpo-1b(op259)* mutation.

4.7 Conservation between different biological systems

The proline mutated in *rpo-1b(op259)* is a highly conserved residue (Figure 8), and yet it results in a viable animal. This might serve as a starting point to study the implication of rRNA transcription or ribosome biosynthesis for the regulation of cell death in other systems, like yeast or mammalian cells. Yeast offers a well-established system for the analysis of rRNA transcription and processing. It also has well-studied checkpoint pathways, and basic cellular stress signalling is conserved. Even though yeast lacks an undisputed correlate of metazoan apoptosis, there has been increasing evidence for apoptosis-like pathways, and yeast is being established as a further important model organism for research on programmed cell death [reviewed in e.g., (Carmona-Gutierrez 2010)]. I was primarily interested in studying the effect of the amino acid change of RPO-1B(P70S) on rRNA transcription and processing in a parallel system that would be amenable to more convenient biochemical characterisation. David Schneider et al. had published on a RNA pol I β-subunit (RPA135) mutant in yeast, demonstrating a close link from rRNA transcription to rRNA processing (Schneider 2007). My observations of rRNA synthesis in *rpo-1b(op259)* mutants – slightly reduced transcription and abnormal processing – therewith had a sound correlate in yeast. Their Δrpa135 yeast strains, in which transgenic RPA135 could be readily tested for functionality, seemed a welcome system to compare and further analyse the effects of a mutation homologous to RPO-1B(P70S). First, the homologous mutation in yeast, RPA135(P123S), could be scrutinised for rRNA transcription or processing defects in that system. Such defects would most likely impact on growth or on temperature resistance. Possibly, one could then link specific biochemical alterations to cellular checkpoints and stress response pathways. In a collaboration, David Schneider produced mutant RPA135(P123S) by site-directed mutagenesis of an RPA135 expression plasmid and transfected Δrpa135 cells. Surprisingly, this strain did not exhibit any discernible phenotype on standard medium at optimal temperature (30°C). It grew at the same rate as wildtype, even at increased, often non-permissive temperature. The transgenic strain was further tested on 6-azauracil, a base analog that would reveal transcription elongation defects; again, the RPA135(P123S)/Δrpa135 strain was not different from wildtype. We did not continue the biochemical characterisation given there was no growth phenotype. Unfortunately, we thus miss the possibility of using yeast as a parallel system. The observation has shown that the residue, even though highly conserved, is not critical for basic RNA pol I function in yeast, in agreement with the observation in *C. elegans* that the mutation is not lethal and allows broadly normal animal development. Absence of a phenotype in yeast gives support to the idea that *rpo-1b(op259)* has a defect that involves specific interactions at the very level of RPO-1B, which are not conserved or less relevant for cellular homeostasis in yeast. It would be interesting to test a homologous mammalian system.

5 *rpo-1b(op259)* links to p53, the Ras/MAPK pathway, and to the apoptotic core

Genetic epistasis analysis of *rpo-1b* with the so-far known damage response network and particularly with *cep-1*, the *C. elegans* p53 homolog, pointed to interdependent roles. My experiments revealed a complex involvement of *rpo-1b* in setting the susceptibility of germ cells to apoptosis, beyond DNA damage signalling; furthermore, the *op259* mutation also affected programmed cell death in somatic development. For the *C. elegans* germ line, 'physiological' and 'stress-induced' cell death have been distinguished based on the minimal requirement for MAPK signalling or for *cep-1*, respectively, with the two entities sharing the core apoptotic machinery. Interestingly, the *rpo-1b(op259)* mutation rendered worms particularly sensitive to environmental factors and enhanced the phenotypes of several DNA damage- and apoptosis-associated mutants. It appeared to lead to misregulation of a core process involved in most apoptotic signalling. My observations suggest that *rpo-1b(op259)* regulates MAPK activity, which in turn modulates constitutive germ cell death; and that it also modulates the effects that CEP-1 has on apoptosis induction, likely at the level of the core apoptotic machinery. This would attribute the MAPK pathway a central function in determining the extent of germ cell apoptosis in *C. elegans*. In this context, I evaluated the genetic relationship of *rpo-1b(op259)* with the core inhibitor of apoptosis, the Bcl-2 homolog *ced-9*. *rpo-1b(op259)* enhanced the excessive apoptosis phenotype of a *ced-9* reduction-of-function allele, which resulted in temperature sensitive sterility. We used the link of sterility and apoptosis for genetic screens to find suppressors of excessive cell death in *rpo-1b(op259); ced-9(n1653)*, which would potentially reveal novel regulators of apoptosis. Eventually, I will analyse in this chapter the effects of RPO-1B transgenes; they were at the basis for findings on *unc-119*, which will constitute the next chapter.

Chapter 5

5.1 Phenotypic Characterisation of the *rpo-1b(op259)* mutant

rpo-1b(op259) mutant animals exhibit various phenotypes besides reduced irradiation-induced apoptosis that was in the focus of my studies. Some of these phenotypes that might or might not be in connection with the apoptotic phenotype are characterised here.

5.1.1 Developmental delay

5.1.1.1 *rpo-1b(op259)* have a prolonged replication cycle

The worm population of *rpo-1b(op259)* mutants expanded less rapidly than of wildtype worms. This might result from an extended duration of one generation-cycle and/or from a smaller brood size in *rpo-1b(op259)* mutants. I noticed that hatching from freshly laid eggs sometimes took longer; also, the L4 stage was reached some hours later; and the onset of egg laying was clearly delayed in *rpo-1b(op259)* worms. A full generation cycle at 20°C was at least 24 hours longer in *rpo-1b(op259)* than in wildtype.

5.1.1.2 Germ line maturation is most significantly delayed

I assessed the duration of the larval stages and of gonad maturation to see whether growth was globally delayed or whether some developmental steps were more significantly affected. I observed synchronised worm populations at 15°C, at 20°C, or at 25°C and estimated the time point when the majority of the population had passed a developmental stage (2 repetitions of the experiment). The developmental speed of N2 in my experiments (Figure 42) was slightly slower than in the reference cycle (Wood 1980). At all temperatures tested, *rpo-1b(op259)* worms were progressively more delayed over larval development, and at 20°C, they reached the L4/young adult molt about 12 to 16 hours later than N2. Most significantly delayed, however, was the progression from that stage to the appearance of the first eggs on the plate (Figure 42). Whereas in wildtype worms, embryos became visible within adult hermaphrodites at about 8 hours after L4 and the first eggs were laid at approximately 12 hours, in *rpo-1b(op259)* mutants, eggs appeared much later and were laid only starting about 30 hours after L4. I followed the development of the germ line in young adult *rpo-1b(op259)* by DIC imaging. After transiting the Christmas tree stage of vulval development, wildtype gonads first produce sperm and then switch the maturation of germ cells from spermatogenesis into oogenesis (Strome 2005). N2 wildtype germ lines soon produced the first oocytes, which were then fertilised by sperm stored in the spermatheca and then developed into embryos. In *rpo-1b(op259)* mutants, the switch from spermatogenesis to oogenesis seemed to be delayed. At 16 hours after L4, spermatogonia and sperm occupied the proximal gonad and no oocytes had developed. I think that slow maturation of the germ line in *rpo-1b(op259)* is the major impediment to normal developmental progression. It is possible that the delay in germ line development is not paralleled by a delay in somatic maturation. Interestingly, transcriptome comparison over time that was done to identify aging-associated groups of genes revealed two main components that diverged in certain mutant conditions. One component was strongly enriched for genes with high germ-line expression, the other for preferentially somatically expressed genes [personal, internal communication on the progress of a project that is part of PANACEA, ECAS Grant# 222936)]. There seem to be two aging kinetics that can be shifted relative to one another

in certain conditions; possibly, this separation is representing variable timing of germ line and somatic maturation.

In most of my experiments, I posited a germ line age that does not necessarily equal the somatic age, and I timed most experiments according to the germ line [*8.2.1 Timing of experiments*].

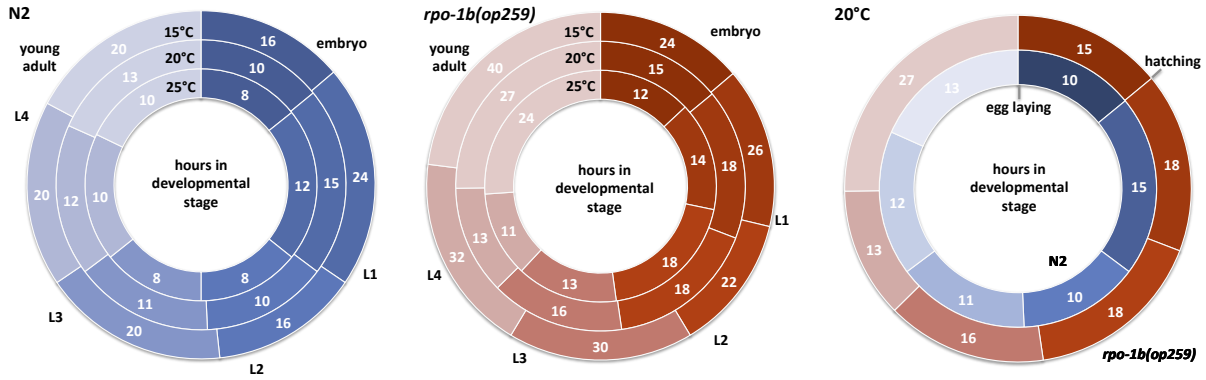

Figure 42 Reproductive cycle of wildtype and mutant worms grown at 15°C, 20°C, or 25°C. At 20°C, *rpo-1b(op259)* animals have a delay mostly on account of young adulthood. Young adulthood in *rpo-1b(op259)* at 25°C is approximated by rare escapers from temperature sensitive sterility.

5.1.2 Reduced reproduction

5.1.2.1 Egg laying rate of *rpo-1b(op259)* is reduced

Besides delayed germ line development and a prolonged replication cycle, a low rate of fertilisation seemed to contribute to the significantly slower expansion of the mutant worm population. The egg-laying rate of *rpo-1b(op259)* animals on the second day of egg-laying was only 2.3 eggs (SD ±0.41, n=78) per animal per hour, in comparison to 5.2 eggs (SD ±0.38, n=60) per wildtype worm. *rpo-1b(op259)* mutants had no clear signs of oocyte retention or stacking of embryos at this time point that would explain a lower output. (However, in the lifespan experiments shown in Figure 54, more *rpo-1b(op259)* than N2 animals had to be censored due to bagging, i.e., larvae hatching inside their mother.) Several determinants might be considered to account for a lower fertilisation/egg-laying rate in *rpo-1b(op259)*: generation of new germ cells by stem cell division could be reduced; germ cell progression might be delayed; and finally, excessive removal of germ cells before they arrive in diakinesis would also cause a drop in the rate of oocyte production.

5.1.2.2 Proliferation and/or progression of germ cells are slower

Apoptosis does not account for the reduced egg laying rate

The number of apoptotic germ cell corpses in *rpo-1b(op259)* was at level with or lower than in wildtype; therefore, increased subtraction of developing germ cells by cell death is an unlikely explanation for the lower rate of oocyte maturation and fertilisation. Unless *rpo-1b(op259)* mutants have significantly accelerated kinetics of apoptotic corpse removal, the low egg laying rate together with a low corpse number shift the blame further distal. The observation that *rpo-1b(op259); ced-4(n1162)* animals have not a higher and *rpo-1b(op259); ced-3(n717)* have even a lower egg laying rate than *rpo-1b(op259)*

single mutants corroborates a cell death defect rather than supporting high death combined with rapid engulfment.

The germ cell number is probably reduced

If germ cell progression were decelerated – at a constant rate of cell proliferation – one would expect increasing pressure and/or spatial expansion of the distal compartment over time. *rpo-1b(op259)* mutants have a somewhat thinner distal gonad than wildtype animals without obvious growth in aging adults; however, germ cells in *rpo-1b(op259)* have smaller nuclei and probably occupy less space than wildtype germ cells. Two of my observations would be in agreement with a delay in germ cell maturation and an expanding distal gonad (even though there are alternative arguments for both observations): first, the transition from late meiotic pachytene cells into diakinesis was more proximal in *rpo-1b(op259)* than in wildtype worms, giving the distal regions more room; second, when adult *rpo-1b(op259)* mutants were dissected and the gonads released, the distal ends tended to bulge, which is not the case in wildtype. Collectively, such adaptations in the mutant would probably not be sufficient to spatially compensate for the retention of the high number of germ cells that become fertilised as a surplus in wildtype. I think that *rpo-1b(op259)* mutants have a lower rate of germ cell proliferation; this could be due to a lower number of proliferating stem cells or due to a slower cycle of mitotic division; the data that will be presented in the section *5.2.2 Cell cycle arrest* support the latter idea. Whether there is an accompanying slowdown of germ cell progression and whether it would be a downstream phenomenon of reduced proliferation are questions that have not been addressed so far.

(The total number of progeny per animal and the duration of the reproductive lifetime would help to clarify some of the issues, as well as an assessment of the total number of germ cells per gonad at different stages of adulthood.)

5.1.2.3 Proliferation, apoptosis, gametogenesis, fertilisation: strong interdependence

It became obvious that apoptosis was but one aspect of germ cell production and turnover that differed between wildtype and *rpo-1b(op259)*. Certainly, the many facets of germ cell proliferation, progression and removal are strongly interconnected; few genetic mutants show selective alterations in one of these processes without consequences for the remaining. Of course, this makes investigation of underlying molecular mechanisms more challenging but also highly relevant in a wider context.

When studying a specific biological process of interest in the germ line, it seems advisable to also consider other features of the system. Yet, simply expressing a certain measure like the number of cell corpses in relation to one other parameter like the total number of germ cells is not necessarily more informative about molecular mechanisms than assessing unidimensional numbers; given the complexity of the system with its many interdependencies, most numerical connections are probably not linear. So far, the basic principles determining the biological system are not understood in enough detail to derive a comprehensive model of the germ line structure and germ cell development. The modelling approach that is presented in *2.2 The germ line of C. elegans and germ line modelling* will be a helpful means to advance the understanding of the main determinants of this system, and it might provide a set of rules that describe the numerical connection between different aspects of the germ line.

5.1.3 Temperature sensitive sterility at 25°C

The majority of *rpo-1b(op259)* mutant worms raised at 25°C in the growth rate studies had laid no eggs. At 20°C, the egg laying rate of *rpo-1b(op259)* had been reduced in comparison to wildtype, but fertility had been maintained. The mutation thus caused temperature sensitive sterility. When counting apoptotic corpses in the germ line of adult mutants, I had occasionally observed a germ cell differentiation disorder at 20°C. In a minor fraction of gonads, small cells resembling pre-diakinetic germ cells could be found intermittently with oocytes or between the most proximal oocyte and the spermatheca (Figure 43). The fraction of animals with such a defect increased considerably when the worms were grown at ambient temperature (21-22°C) rather than strictly at 20°C. I guessed that enhancement of this germ cell proliferation or maturation defect could be underlying the sterility phenotype at 25°C and examined germ line development in post-larval stages by DIC microscopy. Wildtype worms were inconspicuous; they developed the first few oocytes soon after L4 stage and laid the first few eggs less than 12 hours after L4 (Figure 44). Most *rpo-1b(op259)* mutants however did not switch to oogenesis by 18 to 24 hours after L4; often, a large proportion of the proximal gonad arm was filled with sperm. Only few animals developed some oocytes in the course. About half of all gonads already had some small cells most proximally, resembling immature germ cells. At later stages, some of these proximal cell clusters expanded to large masses of innumerable cells. In extreme cases, the cell masses grew to the whole diameter of the animal and seemed to occupy most of the mid-body volume. Another large fraction of gonads had a difficult to define clump of cells or cellular material in the proximal arm. A third major group of animals had proximal masses that were difficult to attribute to the confines of the germ-line or the uterus; the masses might have arisen from abnormally developing embryos. Overall, the spectrum of germ line abnormities was ample; most impressive were certainly the proximal proliferations and the hypercellular tumours that likely arose from them. I found evidence in the literature for a highly comparable phenotype (Killian 2004); in these studies, the proximal tumours were shown to be formed by ectopic, proliferating germ cells. Interestingly, the conditions that provoked this proximal proliferation phenotype (Pro) were mutations or RNAi knockdowns of genes involved in rRNA processing (Voutev 2006). (Apoptotic and other shared phenotypes of the *pro-2* mutant with *rpo-1b(op259)* are discussed in other chapters). In *rpo-1b(op259)*, DAPI staining of the tumours revealed a chromatin pattern that was in agreement with mitotic germ cells (Figure 46); normally, these are restricted to the distal tip region of the gonad. From the time course analysis of *rpo-1b(op259)* at 25°C, I derive that ectopic germ cells – proximal to oocytes and often proximal to sperm – develop into germ cell tumours that can grow to bulky masses (Figure 44). The germ cell-mass than clogs the proximal end of the gonadal tube and any advancement of oocytes. In some cases, the tumor mass evades from the confines of the gonad (Figure 47). I think that those animals that intermittently seem to have a normal germ cell and oocyte arrangement at 2 days post L4 (meiotic pachytene cells – oocytes – sperm – [uterus]) are the ones that give rise to the gonads with abnormal embryonic masses at later times.

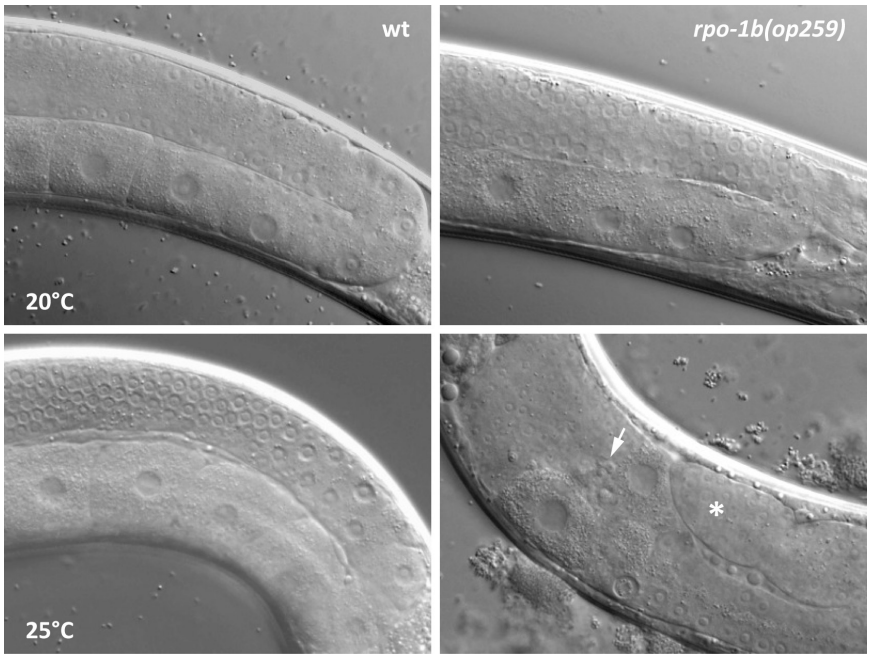

Figure 43 Proximal proliferation in *rpo-1b(op259)*. Worms were transferred as L1 to the indicated temperature. * distal tip region of the gonad; (arrow) sperm between oocytes and proximal germ cells.

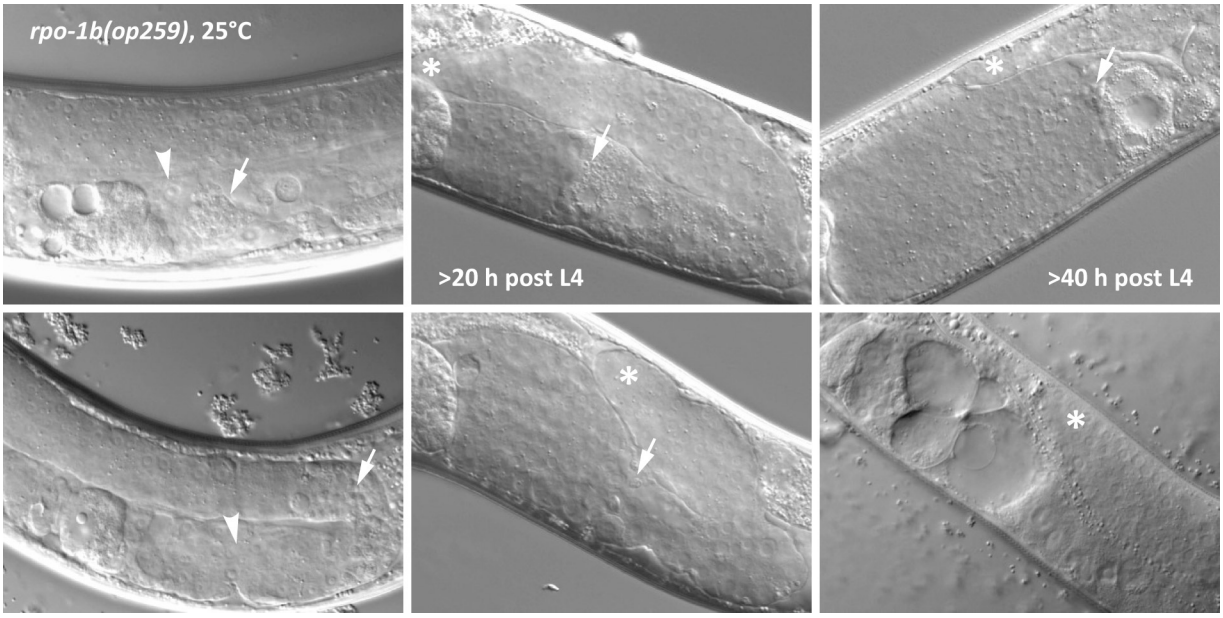

Figure 44 Tumor development starting from proximal proliferation. At early time points of post-larval development, few cells of the size of mitotic germ cells (arrowheads) become apparent in some worms, proximal to sperm (arrow); they continuously expand, so the region of spermatogenesis – or later, the most proximal oocyte – migrate further distal or are virtually consumed. About 2 days post L4, some gonads have grown into massive tumours probably arising from the proximal proliferation. Sometimes, large vacuoles form in the germ line of *rpo-1b(op259)* at 25°C. * distal tip of the gonad.

5.1.3.1 Germ line development and tumor formation

I tested whether sterility was an instantaneous consequence of increased temperature in post-larval gonads or whether high temperature was needed in larval stages for the tumor phenotype to arise in adults. When worms were shifted from the permissive 20°C to 25°C as freshly hatched larvae, all

animals were sterile as adults; when shifted only as L4, most animals produced some embryos and laid some viable eggs. The critical stage seemed to be L3; if shifted before, all animals were sterile; if shifted after, there was some fertility, and viable progeny could grow. Interestingly, this is the stage when the most proximal mitotic germ cells first start to enter into meiosis in wildtype worms (Crittenden 2006; Killian 2004). Developmental stage has repeatedly been found to be critical for germ cell proliferation phenotypes [(Pepper 2003; Waters 2010), Fig. 5 or Fig. 6, respectively; and (Bessler 2007)]. Most of the *rpo-1b(op259)* worms shifted at L4 carried some oocytes and embryos, but a high proportion developed germ line abnormalities that will be discussed as *The Gogo phenotype* in *5.1.4*. Most likely, the occurrence of islets of precocious, distal oocytes is a different phenomenon from the germ cell tumours that form proximally to gametes. In the developing tumours, the size and chromatin pattern of proximal nuclei resembles mitotic cells, whereas in the Gogo phenotype, the distal oocytes are adjoined by meiotic pachytene cells proximally and distally (Figure 46). I think that formation of the proximal tumours involves events in early germ line development and could be a result of spatiotemporal misfits of early germ cells and the signalling environment, as was suggested for the Pro mutant *pro-1(na48)* (McGovern 2009).

5.1.3.2 Apoptosis and germ cell tumours

rpo-1b(op259) – and, as is described in *4.6.2.1*, also *pro-2(na27)* – have abnormal germ cell apoptosis; the number of apoptotic corpses is reduced and response to DNA damage is minimal in *rpo-1b(op259)* at 20°C, despite apparently increased activity of the pro-apoptotic p53 homolog CEP-1. I was wondering whether abnormal apoptosis was contributory to the tumor phenotype in *rpo-1b(op259)*. First, I blocked apoptosis completely by mutation of *ced-3*; *rpo-1b(op259); ced-3(n717)* mutants grown at 25°C developed hypercellular proximal masses similarly to *rpo-1b(op259)*. Blocking apoptosis could therefore not abolish the tumor phenotype nor did it significantly increase the penetrance. Only, there was a higher fraction of worms with embryoid masses in comparison to *rpo-1b(op259)* single mutants.

gld-1(op236) is a conditional allele of the translational inhibitor GLD-1, a key player of the regulatory circuit of mRNA binding factors in the *C. elegans* germ line (Schumacher 2005a). loss-of-function mutants were reported to develop germ line tumours due to re-entry of pachytene cells into mitotic cell cycling, whereas the *gld-1(op236)* allele leads to a temperature sensitive increase of germ cell apoptosis, supposedly due to increased CEP-1 expression (at 20°C, germ cells are hypersensitive to irradiation; loss of *cep-1* function reportedly partially suppresses both hypersensitivity to IR and excessive cell death at 25°C). Subsequent chapters will show that *gld-1(op236)* reintroduces DNA damage-induced apoptosis in *rpo-1b(op259)*, to even a higher level than in wildtype [*5.3.2.2 gld-1(op236) inverts the apoptotic defect of rpo-1b(op259)*]. I guessed that restored or increased apoptosis in *gld-1(op236) rpo-1b(op259)* might suppress tumor formation of *rpo-1b(op259)* at 25°C. However, I observed the opposite: most gonads had hypercellular proximal tumours already in relatively young post-larval animals (Figure 45). *gld-1(op236)* alone, as already described, did not develop tumours; all animals at 25°C had complete decay of the proximal gonad but none had signs of proximal proliferation. One could see *rpo-1b(op259)* as a condition that evokes the *gld-1(null)* phenotype in *gld-1(op236)*; or *gld-1(op236)* as an enhancer of the proximal proliferation phenotype of *rpo-1b(op259)*.

gld-1(op236) reportedly has increased CEP-1 activity; I will show that *rpo-1b(op259)* also has increased CEP-1 activation; the double mutant *gld-1(op236) rpo-1b(op259)* has further enhanced CEP-1 activity levels. One possibility was that CEP-1 would support tumor formation in *rpo-1b(op259)*. I therefore tested *cep-1(gk138) rpo-1b(op259)* at 25°C: the double mutants had a more delayed germ line development but eventually formed proximal tumours similarly to *rpo-1b(op259)*. In summary, the tumours forming in *rpo-1b(op259)* are not dependent on CEP-1 or on apoptosis; and they are promoted by some condition caused by *gld-1(op236)*.

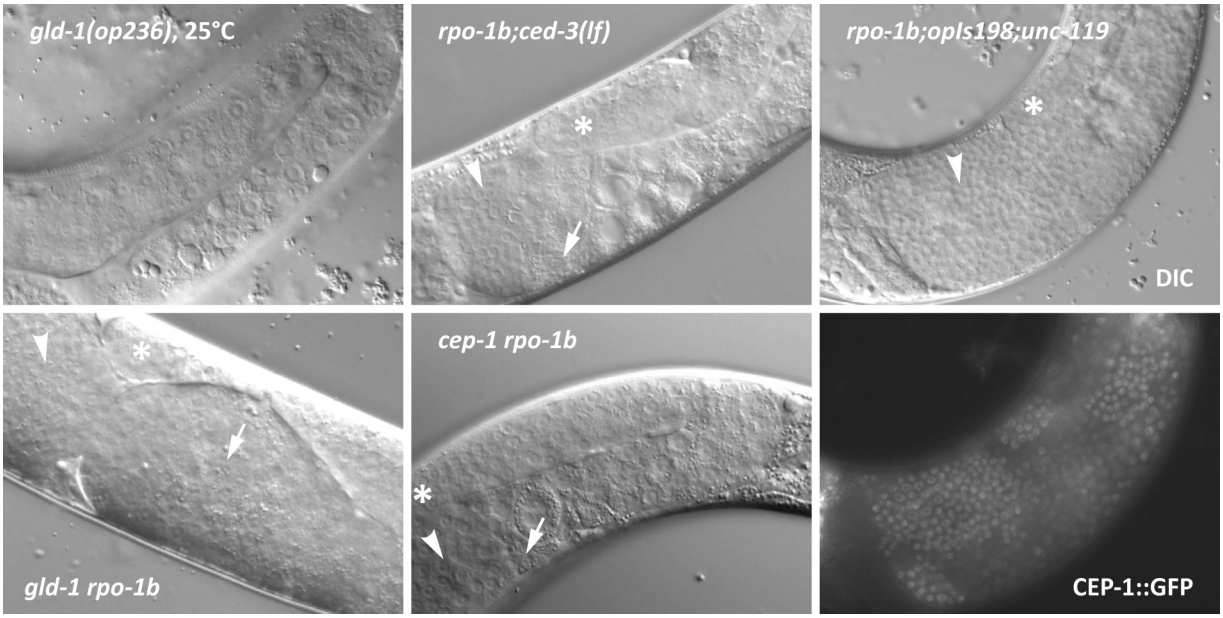

Figure 45 *gld-1(op236)* mutants have a decaying proximal gonad with aberrant cell death at 25°C. Conversely, *gld-1(op236) rpo-1b(op259)* have enhanced tumor growth. Tumor formation in *rpo-1b(op259)* is not suppressed by loss of *ced-3* or *cep-1* function. CEP-1::GFP is expressed in proximal tumor cells at regionally variable levels. * distal tip of gonad, (arrows) sperm, (arrowheads) proximal proliferation. *opIs198* is *[P_{cep-1}::cep-1::gfp; unc-119(+)]*.

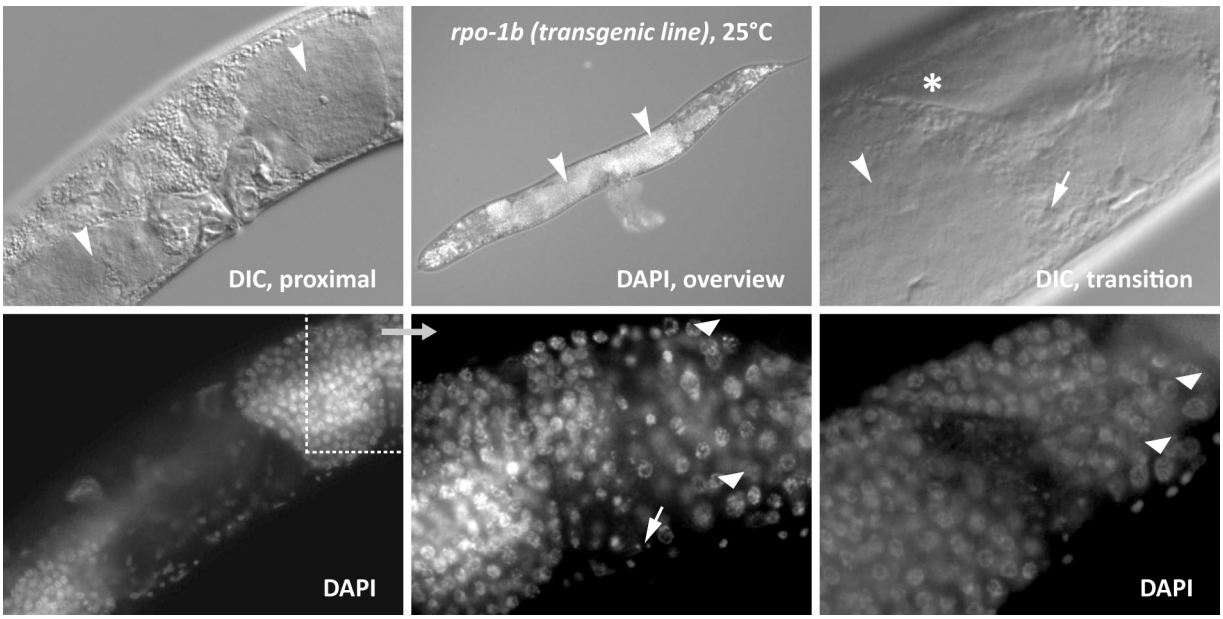

Figure 46 Tumor cells in proximal proliferation (arrowheads) have a chromatin pattern that is distinct from the "spaghetti bowl" pattern of meiotic pachytene cells (triangles) and that is consistent with mitotic germ cells. Three different animals grown at 25°C; * distal gonad end, (arrow) sperm.

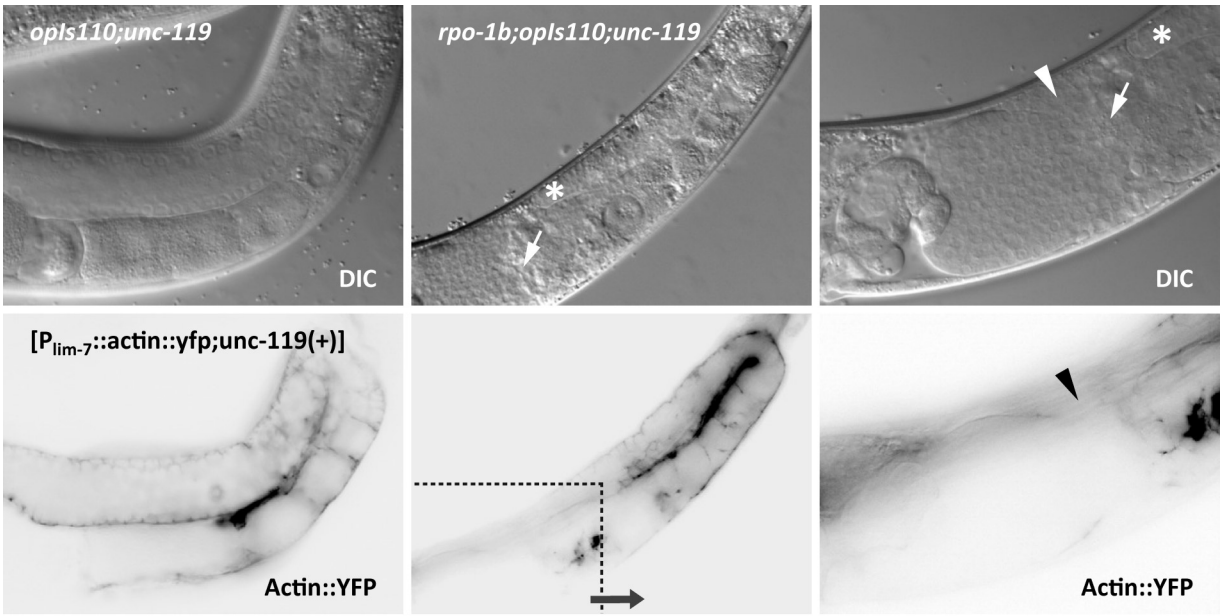

Figure 47 Penetration of the proximal tumor through the gonadal sheathing (thin black line). Actin::YFP from *opIs110[P_{lim-7}::act-5::yfp; unc-119(+)]* is expressed in gonad sheath cells. Example of an *rpo-1b(op259)* mutant worm grown at 25°C with evasion of cells from the proximal tumor (arrowhead). * distal gonad end, (arrow) sperm.

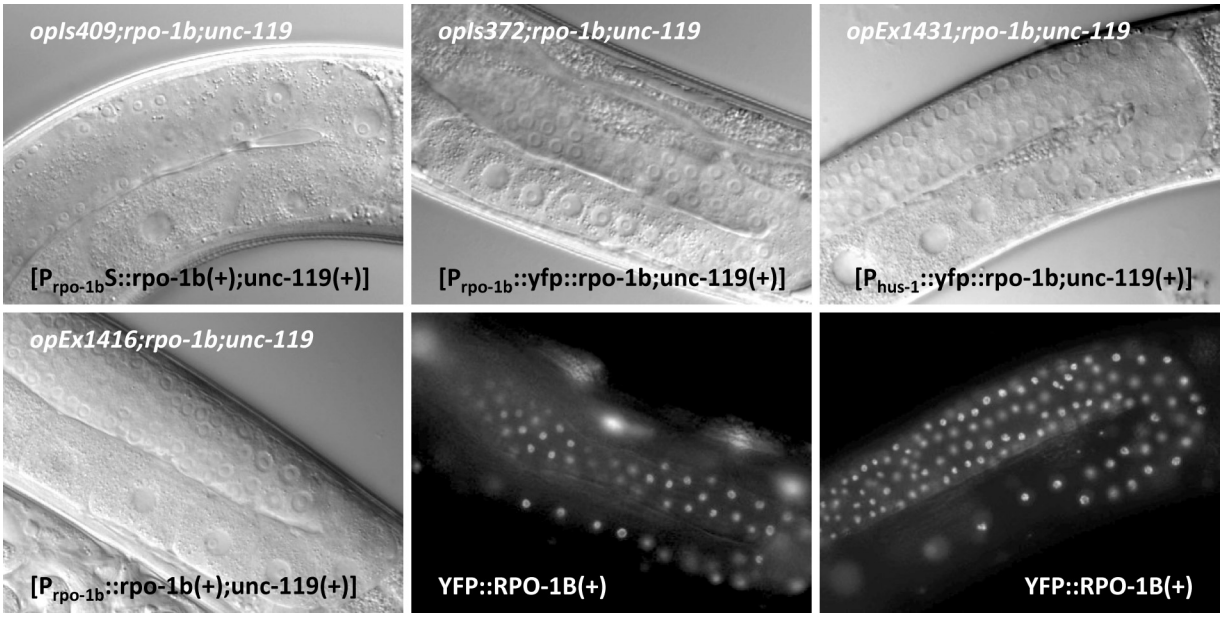

Figure 48 Rescue of the tumor phenotype at 25°C in transgenic lines expressing wildtype RPO-1B in an *rpo-1b(op259); unc-119(ed3)* background. P_{rpo-1b}S indicates short *rpo-1b(op259)* promoter (in contrast to long sequence reaching into upstream gene as used in promoter P_{rpo-1b}). [See chapter *rpo-1b(op259) transgenes and genetic background.*]

5.1.3.3 Germ cell proliferation and tumours

Release from Notch signalling is required in germ cells of the distal region for them to exit from mitotic cycling and transit into meiotic germ cell maturation [e.g., (Joshi 2010b)]. Constitutive activation of this signalling pathway causes cells to remain dividing while progressing along the gonad tube, so that eventually, the whole gonad will be filled with mitotic germ cells. A conditional gain-of-function allele of *glp-1*, the Notch receptor in mitotic germ cells, causes a very weak phenotype at permissive

temperature of 15°C; however, it was shown to evoke a synthetic germ cell hyperproliferation phenotype in conjunction with a mutation of *him-17*, that in turn was acknowledged to affect efficacy of the GLP-1/Notch signalling pathway (Bessler 2007). With such a rationale, I tested the double mutant *rpo-1b(op259); glp-1(ar202)* at various temperatures for germ line tumours. At 25°C, the spectrum of germ line abnormities resembled that of *rpo-1b(op259)*. At 20°C, a small fraction of *rpo-1b(op259); glp-1(ar202)* animals exhibited proximal proliferation. At 15°C, none of the double mutant animals as none of the *rpo-1b(op259)* animals had abnormal germ cell arrangement; there is thus no obvious synthetic effect of *rpo-1b(op259)* and *glp-1(ar202)*.

5.1.3.4 Sterility suppression of *rpo-1b(op259)* in genetic screens

The sterility of *rpo-1b(op259)* mutant hermaphrodites grown at 25°C, which correlated with disorganised germline tissue and germ cell tumours, lent itself as a relatively simple means to screen for suppressors of these abnormities. If the phenotypes of *rpo-1b(op259)* were not due to an absolutely limiting loss of transcription competent RNA pol I, a genetic screen could help to identify functional interactors of RPO-1B, be they regulators of rRNA synthesis on the one hand, or more specific germ line differentiation factors on the other hand. Suppression of sterility at 25°C would offer a strong criterion to select against in a high throughput forward genetic screen.

With students of the BIO323 genetics course 2009 (Magdalene Adamczyk, Simon Schäfer, and Tobias Strassfeld), we initiated a forward genetic screen with EMS mutagenesis of *rpo-1b(op259)* adults. Mutagenised F1 animals were aliquoted in small batches to individual plates and the freshly hatched L2 larvae were shifted to the restrictive temperature (25°C). The screen however failed due to instable temperature conditions in the incubator that we used for selection of suppressors from the F2 generation; sterility was not fully penetrant and possible candidates had not been enriched for before all plates were overpopulated.

With the help from Cathy Zheng, I performed a second screen where we used the mutagenic effect of the *Mos1* transposon; this approach should allow to map potential candidate genes very rapidly by inverse PCR of the digested genome so the sequences flanking the integrated *Mos1* can be identified [(Williams 2005) and *5.7.5* Forward genetic screen using the *Mos1* transposon]. We crossed the transposable element into *rpo-1b(op259)* and mobilised it by heat-shock treatment according to a recent protocol (Boulin 2007). The selective conditions in the F2 generation were harsh enough to suppress fertility of *rpo-1b(op259)* almost completely. Several rounds of mutagenesis and selection did, however, not yield any suppressor of the sterility phenotype of *rpo-1b(op259)* at 25°C. Possibly, transposition efficiency was lower in *rpo-1b(op259); Mos1* than what had been achieved by other groups; we tested for the insertion rate of the *Mos1* transposon after heat-shock in a control experiment and found less than 10 % of the F1 to have integrated the transposon. Besides the low mutagenic rate of the *Mos1* transposon, adverse effects of potential candidate mutations might have prevented reproduction. Likely, the tumor phenotype of *rpo-1b(op259)* would be rescued by mutations of regulatory factors that are themselves critical for animal health; *Mos1* mutagenesis is prone to disrupt genes and create more deleterious effects than missense mutations, disfavouring generation of weak reduction-of-function alleles that would be more compatible with survival.

In *5.7 Genetic screens to find suppressors of apoptosis*, another forward genetic screen will be discussed that might reveal mutations that can compensate for defects in *rpo-1b(op259)*.

5.1.4 The Gogo phenotype

In my studies with *rpo-1b(op259)*, I repeatedly observed a germ line phenotype that I termed Gogo. Various conditions or treatments could provoke this phenotype of irregular germ cell maturation. In which way some of these determinants influence the Gogo phenotype will be detailed in the according chapters. Here, I characterise the phenotype, summarise the influential conditions, and describe some further investigations.

5.1.4.1 Different conditions lead to Gogo

dpl-1(n3643)

Most prominently, the Gogo phenotype arose in a double mutant of *rpo-1b(op259)* and *dpl-1(n3643)* [see *5.5.1.1 dpl-1(n3643) and rpo-1b(op259) show synthetic phenotypes*]. In a high percentage of adult gonads, oocytes appeared precociously in the distal arm, interspersed between germ cells in meiotic pachytene (Figure 49). Often, these oocytes had a high number of associated cellularised germ cells, likely representing apoptotic corpses. Sometimes, the group of cells with ectopic maturation appeared as an islet in the sea of apparently normal early pachytene nuclei in the distal gonad; this will be described as "distal islet". Sometimes, oocytes of the diameter of the gonad tube completely separated the smaller pachytene cells into two or occasionally more regions; I derived the name of the GOGO phenotype from the resulting succession of Germ cells – Oocytes – Germ cells – Oocytes along the gonad.

Temperature shift

In rare cases, *rpo-1b(op259)* mutant animals grown at standard conditions (20°C, OP50 on NGM agar plates) also exhibited distal oogenesis. At slightly higher temperatures, the fraction of *rpo-1b(op259)* animals presenting distal islets or a full Gogo increased considerably. When *rpo-1b(op259)* mutants were grown at 25°C starting at early larval stages, the Pro phenotype dominated in post-larval animals. However, if the worms were shifted from 20°C to 25°C only at the L4 stage, a high proportion of adults had distal oocytes (Figure 49).

Food type

I noticed that also the food type was influential on the penetrance of ectopic oogenesis in *rpo-1b(op259)*. Worms fed on HT115 bacteria were more likely to exhibit distal oocytes at 20°C than worms fed on the standard OP50 (*5.5.1.3 lin-35(RNAi) and dpl-1(RNAi) enhance IR-induced Gogo*, Table 11). Wildtype worms did not have the phenotype, neither on OP50 nor on HT115 (or empty vector control RNAi conditions).

lin-35(RNAi)

The Gogo phenotype could also be enhanced by interfering with RB complex components. As mentioned above, the *dpl-1(n3643)* mutation was very strong in evoking distal oocytes. *rpo-1b(op259); dpl-1(n3643)*, *rpo-1b(op259); dpl-1(RNAi)* and *lin-35(RNAi) rpo-1b(op259)* had significantly higher penetrance of distal islets and Gogo than *rpo-1b(op259)* or *rpo-1b(op259); empty(RNAi)*, respectively. RNAi to *dpl-1* or *lin-35* did not produce any of these phenotypes in N2. In *rpo-1b(op259); dpl-1(n3643)*, more than 70 % of all 2 day old adults had a Gogo

phenotype (Figure 51). Penetrance was significantly lower when worms were grown at 15°C instead of 20°C: approximately 10 to 20 % of all gonads had distal oocytes at >72 hours post L4.

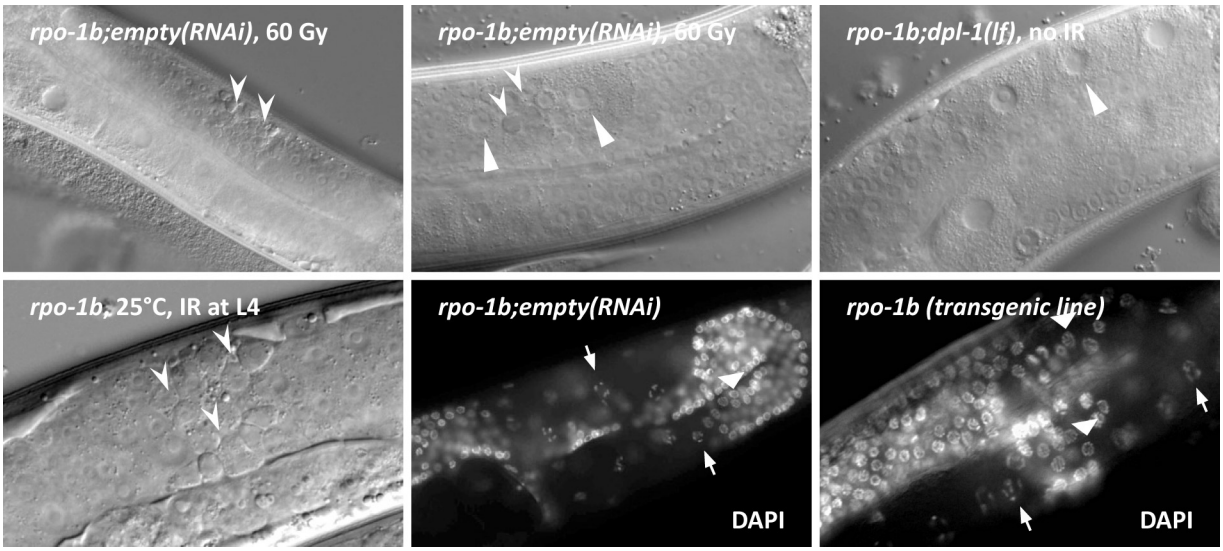

Figure 49 *rpo-1b(op259)* mutants are prone to distal oocytes (indicator) and associated corpses (arrowheads). Distal and proximal oocytes with condensed chromosome pairs (arrows) are preceded by nuclei with the "spaghetti bowl" pattern of late meiotic pachytene cells (triangles).

5.1.4.2 Irradiation enhances Gogo

IR treatment was a potent enhancer of the ectopic germ cell maturation phenotype in most conditions. About 5 % of *rpo-1b(op259)* worms at 20°C developed a clearly visible distal oogenesis phenotype after irradiation, in contrast to only about 1 % of non-irradiated animals. I mentioned before that food type was relevant for the Gogo and distal islet phenotypes in *rpo-1b(op259)*. This was particularly pronounced in the response to irradiation. Around 20 % of the gonads showed a phenotype when *rpo-1b(op259)* worms were fed on empty vector RNAi bacteria (Figure 51). Irradiation and HT115 seem to collaboratively promote distal oogenesis in *rpo-1b(op259)*.

rpo-1b(op259) mutants had disturbed germ cell apoptosis; they had presented with a low level at baseline and a much weaker increase of the corpse number than wildtype after irradiation. Surprisingly, the sites of ectopic oogenesis were often accompanied by a high number of cellularised cells resembling apoptotic corpses. Further, irradiation significantly increased cell death at these sites, to corpse numbers that outrange by far irradiation-induced apoptosis in wildtype. This is in line with two observations discussed also in other chapters of this work: first, cells in *rpo-1b(op259)* mutants are not in principle unable to execute the apoptotic program; second, *rpo-1b(op259)* mutants are not incapable to induce cellular changes in response to irradiation; third, there are conditions in which *rpo-1b(op259)* enhances rather than blocks net cell death [e.g., *5.6 rpo-1b(op259) and CED-9*].

A high corpse number was achieved in the distal region of *rpo-1b(op259); dpl-1(n3643)* gonads upon irradiation. Most of the distal islets or oocytes in non-treated animals were associated with less than 5 cell corpses. However, at 24 hours after irradiation, almost all distal oocytic structures were preceded or surrounded by more than 5, and about 50 % by significantly more than 10 corpses.

Similarly, IR treatment led to a high number of corpses in distal islets of *rpo-1b(op259)* mutants that were irradiated and shifted from 20°C to 25°C as L4 larvae. Non-irradiated, temperature-shifted worms mainly developed distal oocytes; in irradiated and temperature-shifted *rpo-1b(op259)*, of the 30 to 40 % of gonads with distal islets, almost all had a cluster of corpses without any large oocyte (Figure 49).

Large cells have chromatin pattern of oocytes and possibly Ras/MAPK activation

Hoechst staining of germ lines extruded from adult *rpo-1b(op259); dpl-1(n3643)* or DAPI staining of irradiated, RNAi treated worms revealed a chromatin staining in the nuclei of enlarged cells that was consistent with maturing oocytes: pairs of diakinetic chromosomes (Figure 49 and Figure 52). This supports that the large distal cells are most likely oocytes and not some trans-differentiated cells.

In a later chapter, implications of the Ras/MAPK pathway on germ cell apoptosis will be discussed (*5.5 rpo-1b(op259) and the Ras/MAPK pathway*). Immunostaining of activated (double phosphorylated) MPK-1 in germ lines reveals high intensity in the late pachytene region and in the most proximal oocytes of wildtype gonads. The distal regions of mitotic and early meiotic pachytene cells normally show no activated MPK-1. In *rpo-1b(op259); dpl-1(n3643)*, I observed positive ppMPK-1 signal in presumptive distal clusters of ectopic germ cell maturation and apoptosis, indicating that MPK-1 is activated in these regions (Figure 50).

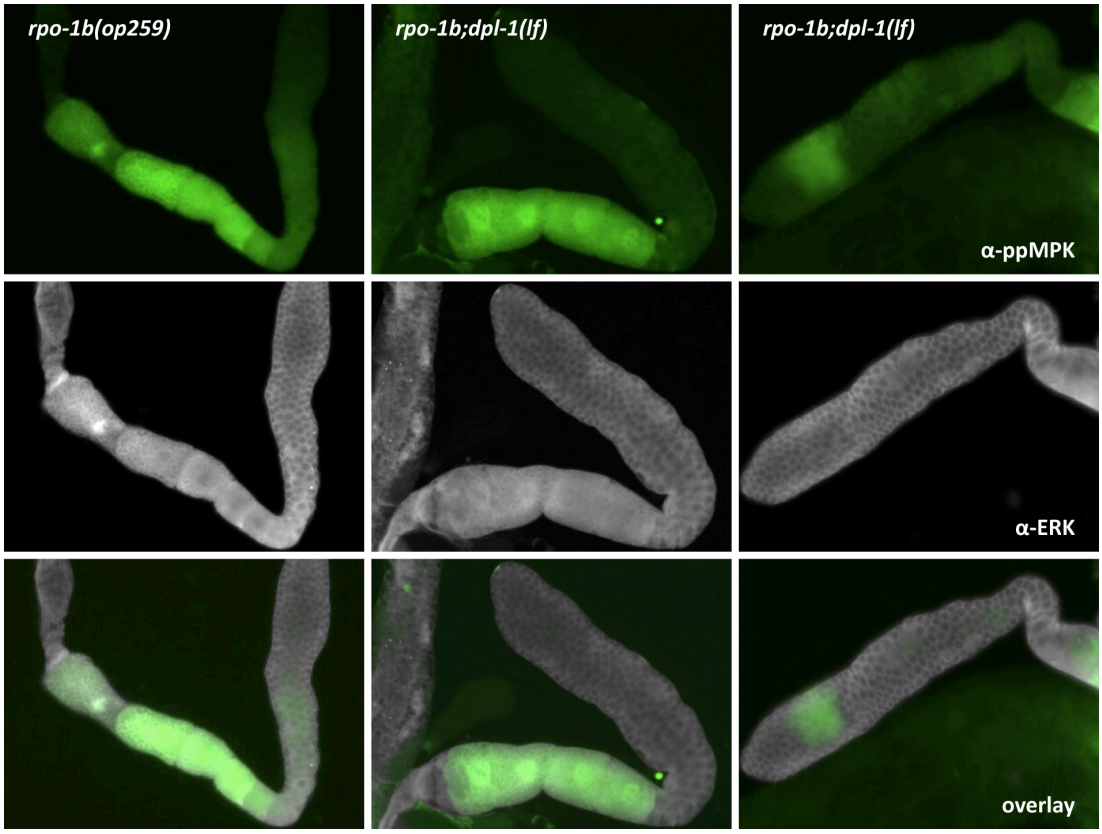

Figure 50 Ectopic MPK-1 activation in distal region of *rpo-1b(op259); dpl-1(n3643)*. Gonads were extruded from adults (at 24 hours post L4) and immunostained with an antibody specifically detecting double phosphorylated MPK-1 (ppMPK). The specificity of the anti-ERK antibody for MPK-1 could not be clearly confirmed, nevertheless, the signal serves as internal standard and to highlight germ line cytoplasm. Signal intensity in *rpo-1b(op259)* was generally lower than in wildtype [see Figure 92]. The gonads of a *rpo-1b(op259)* animal and of two *rpo-1b(op259); dpl-1(n3643)* animals are shown. One of these latter has a patch of strong signal in the distal gonad (in the absence of obviously large cells).

5.1.4.3 Apoptosis to Gogo

Distal oocytes are not dependent on apoptosis

There are alternative explanations for the association of corpses with ectopic maturation of germ cells in the distal gonad: either, premature cell death facilitates oogenesis, or precocious oogenesis evokes cell death in neighbouring cells, or both processes occur independently with or without a common cause. I addressed the first possibility by treating *rpo-1b(op259)* mutants with *ced-3(RNAi)* to prevent apoptotic death. Like in *empty(RNAi)* treated worms, about 20 % of the gonads of *rpo-1b(op259); ced-3(RNAi)* developed distal oocytes after irradiation; these were, however, not accompanied by corpses (Figure 51). This observation confirmed that the high number of cellularised cells in distal islets were indeed apoptotic; and it demonstrated that distal oogenesis is most likely not dependent on apoptosis. It should be mentioned that sites of ectopically maturing germ cells in the distal gonad were more difficult to spot without any corpses highlighting those, and that the percentage of abnormal gonads could be more easily underestimated in this situation. Gonadal sheath cell markers also supported the apoptotic nature of the distal corpses (Figure 53).

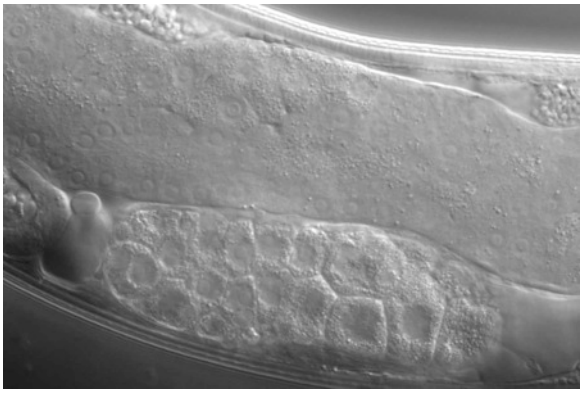

	no IR		60 Gy	
rpo-1b(op259)	% with Gogo	95% CI (n)	% with Gogo	95% CI (n)
(OP50)			6%	±0.07 (103)
empty	3%	±0.03 (116)	20%	±0.07 (212)
dpl-1 [ORF]	16%	±0.02 (60)	64%	±0.20 (135)
lin-35 [Ahr]			40%	±0.24 (71)
ced-3 [ORF]			24%	±0.07 (64)

Figure 51 Distal oocytes in *rpo-1b(op259); ced-3(RNAi)*. Distal islets are not suppressed by inhibition of cell death with *ced-3(RNAi)*. The effectiveness of the RNAi treatment is apparent from the small oocyte pattern in the proximal gonad and from the absence of corpses. The distal oocytes are not surrounded by small cellularised cells typically seen in control conditions, which evidences that these latter are apoptotic corpses. Table: RNAi treatment of *rpo-1b(op259)* mutants starting at L1 stage with the indicated RNAi bacterial clones from the ORFeome [ORF] or Ahringer [Ahr] libraries; fraction of gonads with distal islets / Gogo (average of at least three experiments), 95 % CI of the mean, and number (n) of worms considered over all experiments.

Loss of *cep-1* function reduces the Gogo phenotype

Irradiation-induced apoptosis requires the p53 homolog CEP-1. In *C. elegans*, CEP-1 activates the apoptotic machinery in response to signalling from DNA damage recognition factors. The experiments described before had demonstrated that irradiation promotes cell death in distal regions of the gonad. It was likely, although not evident, that these cell deaths were mediated by CEP-1. Analysis of the CEP-1::GFP pattern in gonads with ectopic oocytes confirmed high levels of CEP-1 expression in germ cells distal to the distal oocytes, supporting the idea of a CEP-1 mediated process. Additionally, with the transcriptional reporter *opIs56[P_{egl-1}::2xNLS::gfp::egl-1 3'UTR; unc-119(+)]*, I detected significant EGL-1 expression in distal oocytes and preceding cells, which speaks for CEP-1 activation (Figure 52). I used the temperature shift experiment (irradiation and shift from 20°C to 25°C at L4 stage) to

assess whether IR-induced corpses in the distal compartment depended on CEP-1. Indeed, *cep-1(gk138) rpo-1b(op259)* double mutants had only very few distal islets with corpses. Thus, like normo-topic apoptosis in the gonad bend region, IR-induced ectopic cell death in the distal compartment of *rpo-1b(op259)* was dependent on *cep-1*.

Apoptosis was reduced; but also distal oogenesis was strongly reduced in *cep-1(gk138) rpo-1b(op259)*. Thus, *cep-1* seems to be a critical factor for the induction of ectopic oogenesis. Since loss of *cep-1* function prevented the formation of distal islets in non-irradiated animals as well, this effect seems not to be linked to irradiation. This does of course not exclude that DNA damage signalling could be involved in provoking distal apoptosis and possibly oogenesis. (We need to confirm the findings in *cep-1(gk138) rpo-1b(op259)* with repeated experiments.)

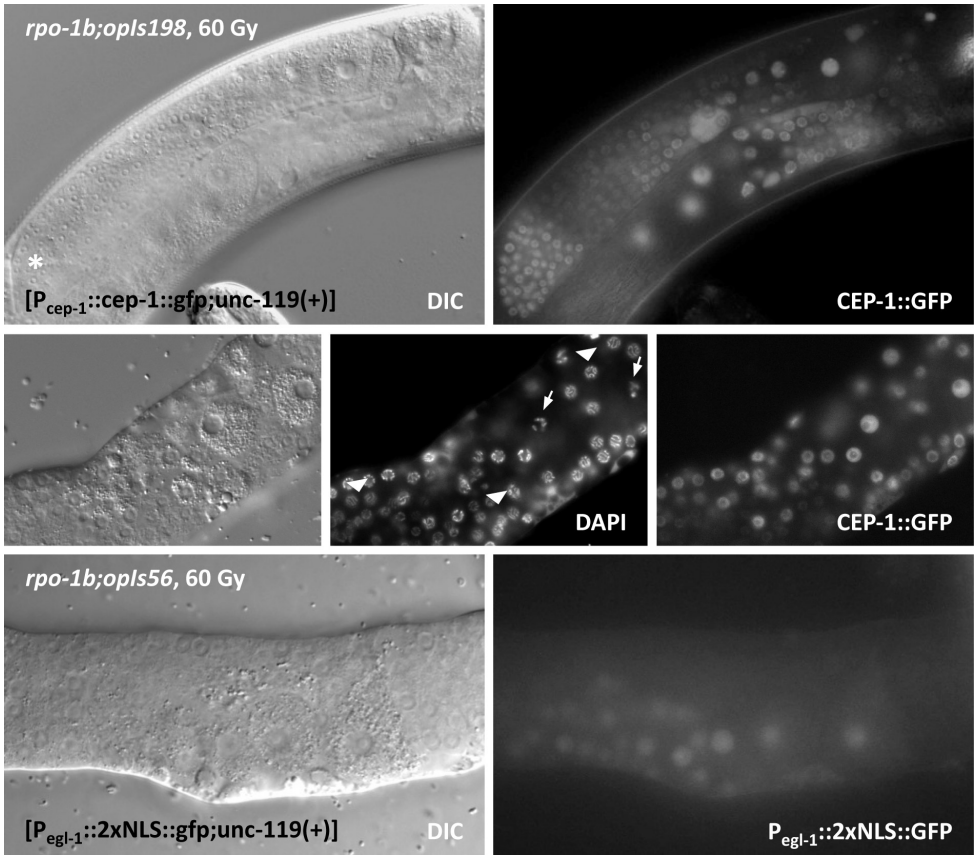

Figure 52 Distal oocytes express CEP-1 and have high expression of a transcriptional EGL-1 reporter. (Top): Both pre-oocytic regions have germ cells with high nuclear CEP-1::GFP fluorescence. The levels in the germ cells directly proximal to the distal oocytes are equally low as in transition zone cells; this is in agreement with two waves of progressing germ cells. (Middle): The large distal cells exhibit a chromatin pattern typical for oocytes (DAPI staining of dissected gonad) and are interspersed with cells in late meiotic pachytene (triangles). (Bottom): egl-1 expression is increased in the islet cells, indicating increased CEP-1 activation.

Interestingly, *rpo-1b(op259); dpl-1(n3643)* had massively increased levels of EGL-1 and CED-13 transcripts by qRT-PCR, indicative of CEP-1 overactivation; already without irradiation, the mRNA levels in the double mutant were comparable to irradiated wildtype worms, and irradiation further boosted the levels. *dpl-1(n3643)* also had a stronger increase than wildtype in response to irradiation. Possibly, *rpo-1b(op259)* creates a condition in the distal germ line that makes cells prone to ectopic maturation, via a mechanism that is activated by CEP-1.

I also assessed EGL-1 and CED-13 transcript levels in worms grown on RNAi bacteria, another condition that could significantly rise the percentage of worms with a Gogo phenotype. The levels were indeed higher than on OP50 bacteria, with or without irradiation.

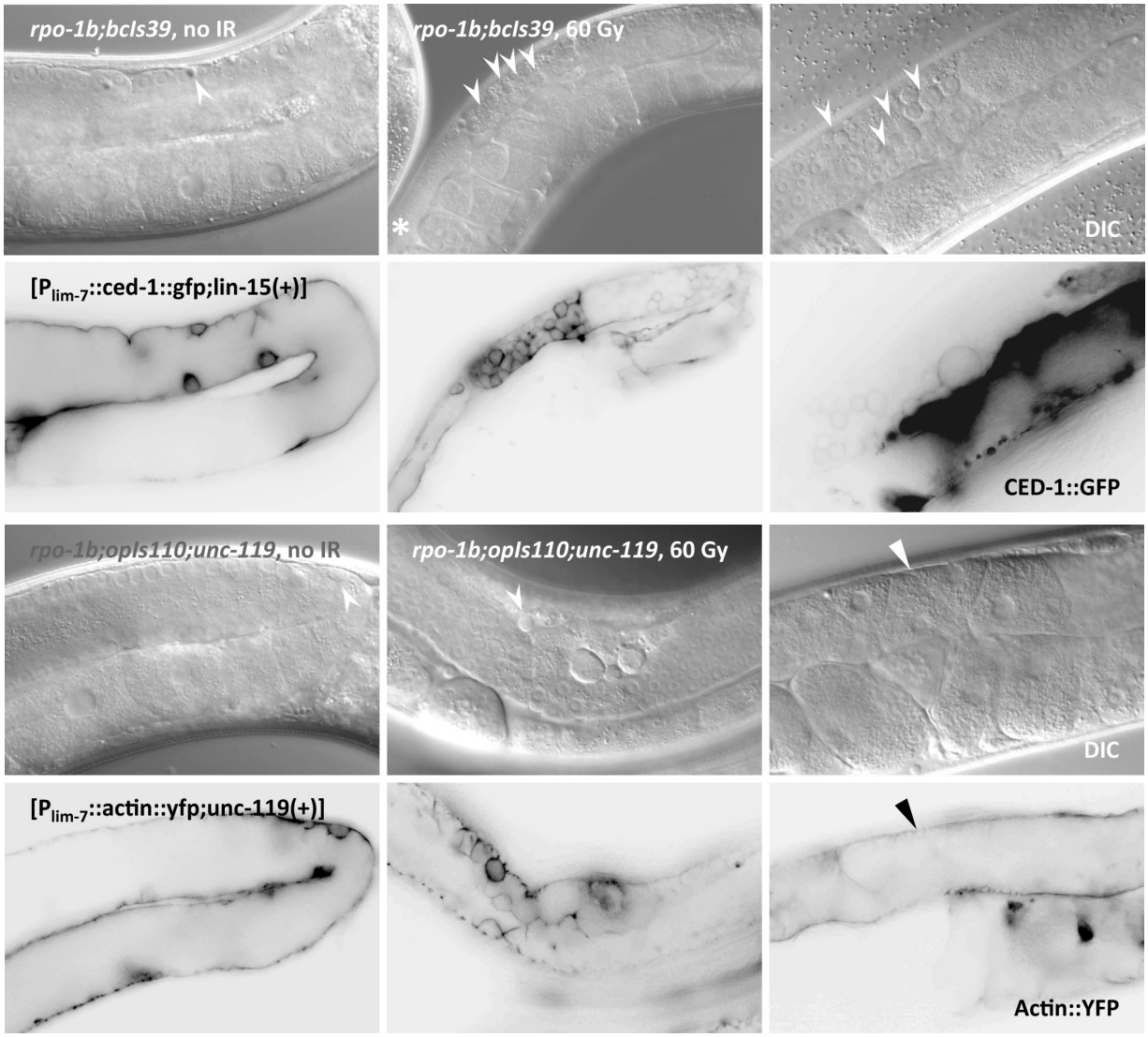

Figure 53 Cellularised cells in the neighbourhood of distal oocytes are wrapped by sheath cell protrusions typical for apoptotic corpses. CED-1::GFP and Actin::YFP form halos around the presumptive corpses (arrowheads). The sheath cells form a continuous lining of the gonad tube in the region of ectopic oocytes (indicator). Images from occasional Gogo phenotype observed in irradiated *rpo-1b(op259)* animals at 20°C.

5.1.4.4 Various influences drive a similar phenotype

In some cases of RNAi treated and irradiated, and in temperature shifted and irradiated *rpo-1b(op259)* worms, distal corpses appeared in the absence of considerably large oocytes. It so becomes unlikely that ectopic cell death is induced solely by neighbouring mature oocytes. More probably, both, transition from late pachytene into oogenesis and germ cell apoptosis, are primed by a condition that is met in *rpo-1b(op259)* already before the gonad bend. An ectopic signal might be presented to germ cells in the distal arm that permits both oogenesis and apoptosis. Factors like irradiation, food type specific cues or mutation of regulatory genes might promote such a signal or facilitate the reaction to it. Alternatively, spatial progression of germ cells along the gonad could be slowed down in *rpo-1b(op259)* (e.g., due to a

reduced proliferation rate in the distal compartment) and some cells might have passed a decisive developmental age before they reach the gonad bend.

These are just a few possible hypotheses that the germ line model presented in *2.2 The germ line of C. elegans and germ line modelling* might allow to test in the future.

N2 develop Gogo at extreme conditions

I had occasionally observed the Gogo phenotype in other mutants at some conditions. Here, I identified several environmental conditions that promoted the formation of distal islets and the Gogo phenotype. The abnormal organisation of germ cell development was characteristic but probably not specific for *rpo-1b(op259)* and might even arise in wildtype if the promoting conditions were carried to an extreme. In fact, the gonads of N2 worms that had accidentally been grown at temperatures above 25°C were disorganised to a large part into a Gogo arrangement. This indicates that *rpo-1b(op259)* might more broadly lower the threshold for temperature sensitive germ line phenotypes.

RPO-1B transgenes in the *rpo-1b(op259); unc-119(ed3)* background

I observed an increased penetrance of the distal islet and Gogo phenotypes in several transgenic lines of *rpo-1b(op259)*. Some transgenes of tagged RPO-1B in *rpo-1b(op259); unc-119(ed3)* were associated with a high fraction of germ lines showing distal islets, and that comprised large numbers of corpses. This led us to look at the control strain *rpo-1b(op259); unc-119(ed3)*. (The suppressive effect of *unc-119(ed3)* on germ cell apoptosis will be discussed in *6 unc-119 and apoptosis: novel functions for an omnipresent bystander*.) I showed that mutation of *unc-119* strongly reduced IR-induced apoptosis and that it had a stabilising effect on excessive germ cell death in *rpo-1b(op259); ced-9(n1653)*. Possibly, *unc-119(ed3)* would also improve germ line integrity of *rpo-1b(op259)* in situations that otherwise cause ectopic maturation. Indeed, irradiated *rpo-1b(op259); unc-119(ed3)* grown on HT115 had much less distal islets than *rpo-1b(op259)*. I have not further investigated how the transgenes enhance distal islets and ectopic apoptosis: through abnormal function of transgenic RPO-1B or due to overexpression of transgenic UNC-119, or by a combined or unrelated mechanism.

5.1.5 Life span

C. elegans has been a leading model organism to show what a marked influence reduced metabolic turnover can have on life span (Vanfleteren 1999; Lakowski 1998). Caloric restriction has been recognised early as a potent means to extend average life span of a worm population (Klass 1977; Hosono 1989). Recently, conditions that entail lower rates of protein synthesis have been demonstrated to increase life span (Pan 2007; Syntichaki 2007a; Hansen 2007). In these studies, knockdown of certain initiation factors of translation or of ribosomal proteins could considerably prolong adult life. *C. elegans* has five isoforms of the homologous eukaryotic translation initiation factor eIF4E, *ife-1* through *ife-5*. Their binding affinities to differently capped 5' ends of mRNAs varies (Ruszczyńska-Bartnik 2011), and they are supposed to be active in different tissues: the isoforms *ife-2* and *ife-4* in somatic cells; and the isoforms *ife-1*, *ife-3* and *ife-5* mostly in the germ line (Keiper 2000). In an assessment of the eIF4E homolog mutants, knockdown of *ife-2* but not of the other *ife* isoforms extended lifespan (Syntichaki 2007b); the *ife-2(ok306)* mutant was longer-lived than wildtype worms, possibly due to reduced translation and

increased resistance to oxidative stress. Another study demonstrated effects on lifespan of RNAi treatment to the eIF2β-homolog *iftb-1* and to the homolog of mammalian eIF4G, *ifg-1* (Hansen 2007). Reports on lifespan in the mutant of the ribosomal S6K homolog *rsks-1* are contradictory between these two studies. Overall, reduced translation seems to correlate with lifespan extension. Given the effects of the *rpo-1b(op259)* mutation on ribosome synthesis [see *4.4 rRNA and ribosome synthesis in rpo-1b(op259)* and *4.5* Proteomic profiles of *rpo-1b(op259)*], it seemed possible that *rpo-1b(op259)* had a reduced rate of translation (however, we have not confirmed this directly). We tested whether *rpo-1b(op259)*, accordingly to other conditions of restricted translation, would cause an extension of the mean adult lifespan.

Often, fluorodeoxyuridine (FUDR) is used for lifespan studies to prevent the production of progeny that would afflict scoring of survival [see the studies on lifespan]. This seemed a bit improper to me since there were other studies showing that the germ line was an important regulator of adult lifespan (Mukhopadhyay 2007). I renounced the drug and transferred the adult worms onto fresh plates every two days so they would always be clearly distinguishable from the progeny. To decide on death I assessed pharyngeal pumping activity, head movements and reaction to touch. An initial experiment done by Randall Hofmann had shown a slight reduction of the mean lifespan of *rpo-1b(op259)*. The second experiment started with 120 worms per genotype; I tested *rpo-1b(op259)*, N2, and *ife-2(ok306)* animals. I realised that more *rpo-1b(op259)* than N2 animals had to be censored by about 5 days of adulthood due to bagging and internal hatching of larvae. The Kaplan-Meier survival curve for *rpo-1b(op259)* was shifted to the left, indicating a median survival of 2 days less than wildtype. In agreement with the literature, *ife-2(ok306)* lived slightly longer than N2. Thus, *rpo-1b(op259)* does not fall into a group with the lifespan extending mutants of translation regulation.

It is remarkable that mutants of the preferentially germ line-active *ife-1* isoform had a similar defect in IR-induced apoptosis as *rpo-1b(op259)*, but not the *ife-2(ok306)* mutant (this is discussed in the chapter *4.6.3.1 ife-1 translation initiation mutants have apoptotic defect*). Mutation and knockdown of the somatic *ife-2* increased lifespan whereas knockdown of *ife-1* by RNAi was reported not to increase lifespan. (I should have included the *ife-1* mutants in my lifespan assay since, as I later realised, the apoptosis phenotype of *ife-1(RNAi)* was opposite to that of the mutant, that is, hypersensitivity to irradiation.) The phenotype of *rpo-1b(op259)* resembles *ife-1(ok1978)* more than *ife-2(ok306)*. It is possible that *rpo-1b(op259)* has differential effects on translation between the post-replicative somatic cells and the synthetically highly active, growing germ cells. Should there be a link between apoptosis, lifespan and reduced translation in *rpo-1b(op259)* and in *ife-1(ok1978)*, the germline would likely be the prime tissue to study [see also discussion in (Tavernarakis 2007)].

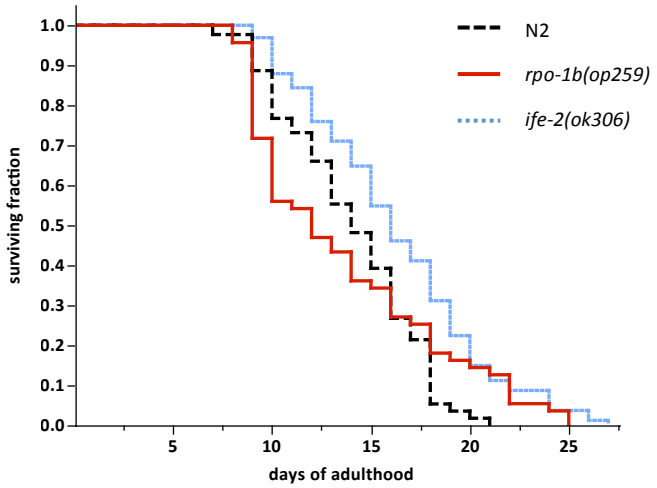

	N2	*rpo-1b*	*ife-2*
# failed	58	57	82
# censored	63	63	38
Mean survival [d]	14.02	13.67	16.29
Std Error	0.44	0.66	0.48
Median survival [d]	14	12	16
Lower 95% confidence	13	10	15
Upper 95% confidence	16	14	18
χ^2 Wilcoxon (N2)		0.171	0.0016

Figure 54 Life span is slightly reduced in *rpo-1b(op259)*, and not prolonged as in the translation initiation mutant *ife-2*. The experiment was started with 120 young adult animals per strain. χ^2 testing was in comparison to N2.

5.1.6 Males

rpo-1b(op259) have a higher fraction of males than wildtype in a normal population (approximately 1 to 5 % at 20°C in comparison to approximately 0.2-1 %). This might indicate an increased rate of chromosomal non-disjunction in meiotic germ cells of the mutant. Certainly, the availability of males made genetic crosses more convenient. Usually, I crossed males of *rpo-1b(op259)* (or mutant combination) with hermaphrodites of the other genotype of interest.

5.1.7 Body size elongation

rpo-1b(op259) L4 larvae appeared slightly shorter and thinner than same stage N2 animals; in contrast, adult *rpo-1b(op259)* mutants grew larger than wildtype. Deviations from wildtype body length have been described in a number of worm mutants [summarised in (Mörck 2006)]; some were also named after the phenotype of long (Lon) or small (Sma) body size. Molecularly, TGFβ and insulin signalling are key pathways for regulation of growth and body size (Patterson 2000; So 2011a). Generally, two underlying phenomena have been considered for changes in body volume: hyper-/hypocellularity or increased/decreased cellular volume. Among the cell-size regulatory proteins figure CED-4, and two factors that are closely linked to protein synthesis: *nst-1*, homolog of the p53 interacting nucleolar factor nucleostemin, and the homolog eIF2B, a translation initiation factor. Chen et al. described the interrelationship of these factors, and they further characterised *tfg-1(RNAi)* as a condition leading to reduced cell size (Chen 2008). While *rpo-1b(op259)* shared the small size at larval stage with these mutants, it clearly differed from them in aging adults. At three days of adulthood, *rpo-1b(op259)* mutants exceeded wildtype worms in body length. For some reason, this was particularly pronounced in several transgenic lines (*rpo-1b(op259); unc-119(ed3)* with integrated transgenes) or in the double mutant condition *gld-1(op236) rpo-1b(op259)*. I quantitatively assessed body dimensions on images taken of adult worms with a photographic camera on a dissecting-scope. With ImageJ Software (Abramoff 2004), the length was integrated along the central axis and the diameter was determined in the post-pharyngeal region; the volume was approximated by assuming a cylindrical body shape.

rpo-1b(op259) animals at 4 days post L4 were 20 % larger than wildtype worms, mainly on account of an increased length. (The transgenic lines even reached 150 to 180 % of the wildtype volume). I looked for morphological correlates of the increased length by DIC microscopy. *rpo-1b(op259)* animals had an extended distance from the U-turns of the gonads to the tail and to the pharynx; intestinal cells that were often extremely rich in granular lipid droplets, filled the gap. Also, the cœlomic space was distended by large circumscript, mobile elements that had the appearance of lipid drops in DIC imaging. Much more lipids seemed to be accumulating in transgenic *rpo-1b(op259)* animals.

ced-4(lf) mutants are significantly shorter than wildtype animals as larvae and also as adults. I performed epistasis analysis of *rpo-1b(op259)* with *ced-4(n1162)* (Figure 55). At L4, *rpo-1b(op259)* mutants were smaller than N2 and *ced-4(n1162)* mutants were smaller than *rpo-1b(op259)*. The double mutant *rpo-1b(op259); ced-4(n1162)* was of the length of *ced-4(n1162)*, indicating that there was not a synthetic effect of *rpo-1b(op259)* towards even smaller body size. *rpo-1b(op259)* had a growth spurt in early adulthood so it was longer than wildtype at 2 days post L4. *ced-4(n1162)* grew only as much as wildtype, preserving a significant size difference to adult N2. The double mutant *rpo-1b(op259); ced-4(n1162)* behaved like *rpo-1b(op259)*, with considerable post-larval growth, so it compensated for the size difference it had had with N2 at L4. *rpo-1b(op259)* was thus epistatic to *ced-4(n1162)* in determining post-larval body length. From this experiment, one can conclude that larval and adult body sizes are not strictly correlated; they seem to be determined by different processes. The boosting effect *rpo-1b(op259)* has on adult body length is not dependent on the growth regulator *ced-4*. CED-4 is apparently more relevant for larval growth; *ced-4(n1162)* mutants are significantly smaller than wildtype as L4, but they show a similar size increase from L4 to 3 day-old adults.

Interestingly, other than the reported mutants of cell size regulation – *nst-1*, *tfg-1*, or eIF2B – *rpo-1b(op259)* changes from too small to too big. It seems to affect at least two different components of body size control. The association of massive post-larval growth with lipid accumulation in intestinal cells and intercellular space lets speculate that these components drive expansion of the organism. (High lipid content in *rpo-1b(op259)* is further evidenced by increased vitellogenin detection by Gel electrophoresis and mass spectrometry (Figure 30), and by a higher density of electron dense cytoplasmic droplets in electron micrographs of cross-sections through intestines.) For larval growth, it can not be guessed easily whether *rpo-1b(op259)* and *ced-4(n1162)* act on the same lever.

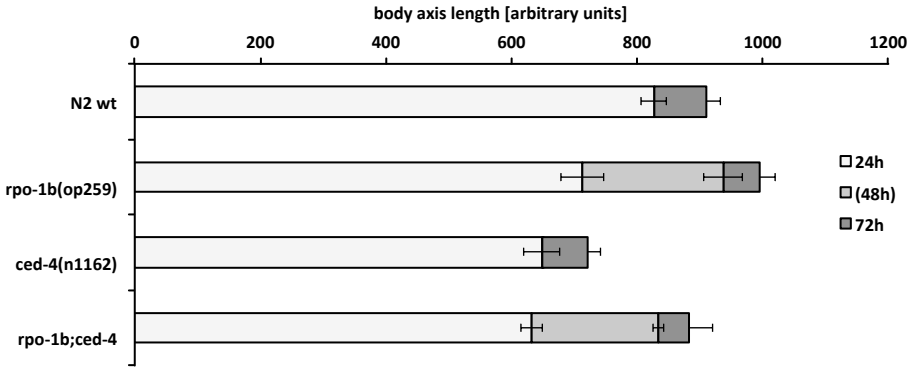

Figure 55 Body-size control by *rpo-1b(op259)* and by *ced-4(n1162)* seems to involve two different mechanisms. The post-larval increase in body-length of *rpo-1b(op259)* is not suppressed by loss of *ced-4* function. Error bars represent 95 % CI of the mean of the measured lengths along the central body axis at the respective time points post L4 stage (at 24 and 72 hours, and additionally at 48 hours for mutants with *rpo-1b(op259)*).

5.2 DNA damage responses in *rpo-1b(op259)*

5.2.1 Apoptosis

5.2.1.1 *op259* mutants have low response to irradiation

Defective irradiation-induced germ cell apoptosis was the main feature that led me to study the *rpo-1b(op259)* mutant; the superordinate motivation was to ascertain that, and to understand why, the point mutation in the second larges subunit of RNA pol I would alter the number of apoptotic corpses that arise in the *C. elegans* germ line upon irradiation. The apoptotic defect in response to irradiation was the reference for most of my work. Randall Hofmann and Lilli Stergiou had characterised the low level of germ cell corpses following IR irradiation of adult worms. They had performed a time course experiment, counting apoptotic corpses in the gonad by DIC microscopy at various time points after irradiation. Wildtype worms show a dose-dependent increase in the number of apoptotic cells over time, reaching a plateau at about 36 hours after irradiation and at a dose of 60 to 120 Gy. *rpo-1b(op259)* mutants had only a very moderate increase at all doses tested, indicating that there was a defect presenting in a wide range of damage load. I confirmed the reduced apoptotic response to IR irradiation in multiple experiments (Figure 31). I also performed a dose-response experiment with UV-C irradiation, a mutagen that causes different types of DNA lesions than IR. Similarly to IR, UV-C did increase the corpse number in a dose-dependent manner in wildtype but provoked only a weak response in *rpo-1b(op259)* mutants (Figure 56). [See Figure 66 for DIC images of corpses in irradiated wildtype and *rpo-1b(op259)* gonads.]

For the planning of forthcoming experiments, it was important to assess the nature of the mutation; whether *rpo-1b(op259)* was dominant or recessive with regards to apoptosis; whether *op259* was a null or a hypomorphic allele; and whether it was temperature sensitive. RNAi and temperature shift experiments demonstrated that *op259* was a weak allele of the essential *rpo-1b* gene and that it had a temperature sensitive sterility phenotype [see *5.1.3 Temperature sensitive sterility at 25°C*]. I assessed the apoptotic IR response in *rpo-1b(op259)*/*rpo-1b(+)* heterozygous animals; to that end, I selected normally crawling F1 progeny from a cross of N2 or *rpo-1b(op259)* males with Dumpy hermaphrodites (caused by *dpy-5(e61)* on LG I) and irradiated them as young adults. The apoptotic IR response in the *dpy-5(e61) +/+ rpo-1b(op259)* heterozygotes was intermediate between *rpo-1b(op259)* and the control *dpy-5(e61)/+* animals; however, the counts were not very stable. *rpo-1b* might be slightly haploinsufficient or the mutant allele could be exerting a weak dominant effect.

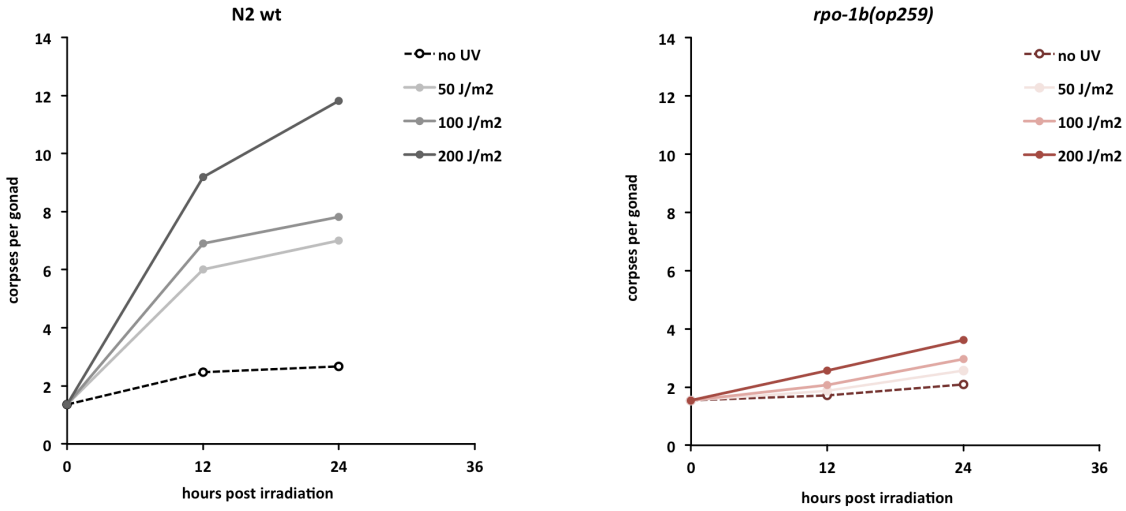

		no UV		50 J/m2		100 J/m2		200 J/m2	
	post IR	score	95% CI (n)	score	95% CI (n)	score	95% CI (n)	score	95% CI (n)
N2	0 h	1.35	±0.26 (83)						
	12 h	2.47	±0.39 (59)	6.00	±1.20 (16)	6.91	±0.74 (32)	9.20	±1.46 (10)
	24 h	2.67	±0.41 (88)	7.00	±1.07 (5)	7.81	±1.20 (32)	11.81	±1.79 (26)
rpo-1b	0 h	1.54	±0.31 (35)						
	12 h	1.71	±0.70 (7)	1.87	±0.38 (15)	2.08	±0.41 (13)	2.56	±0.34 (9)
	24 h	2.08	±0.56 (12)	2.56	±0.51 (16)	2.96	±0.40 (47)	3.61	±0.78 (18)

Figure 56 Time course and apoptotic dose-response to UV-C irradiation in *rpo-1b(op259)* mutants. The table indicates average number of apoptotic corpses per gonad, 95 % CI of the mean, and number of animals tested per condition.

5.2.1.2 RNAi knockdown of F14B4.3

When a novel candidate from a genetic screen can be mapped to a gene, the mutation has to be linked causally to the phenotype. In a first line, already available alleles of the candidate gene are examined for the phenotype; additionally or alternatively, RNAi is usually applied to see whether knockdown of the candidate gene can phenocopy the feature of interest. Third, a transgenic wildtype protein should be able to rescue the defects of non-dominant alleles. No other allele for F14B4.3 was available when I started the investigations on *rpo-1b(op259)*. Later, a deletion allele was generated by the CGC, *ok1970*, which had to be maintained by a chromosomal balancer and could not be tested as a homozygote [see *4.6.1.4 A new allele of rpo-1b, F14B4.3(ok1970), leads to apoptotic defect*]. I tested the effect of RNAi knockdown of *rpo-1b*. Two bacterial clones were available in the Ahringer and ORFeome libraries for RNAi by feeding (Kamath 2003; Rual 2004b). When I tried to grow N2 worms on F14B4.3 clones starting as L1 larvae, the animals were delayed and were completely sterile; only a very rudimentary gonad had developed when the worms reached post-larval stages. I therefore transferred the larvae at different developmental stages to RNAi so they would reveal some effects of RNAi treatment, without having the phenotype of a strong loss of F14B4.3 function. A developmental time point between L3/L4 larval molts turned out to be optimal to preserve germ cell proliferation and progression. I irradiated the young adults and scored apoptosis 24 hours post irradiation. Whereas worms grown on control RNAi conditions (empty vector RNAi clone) showed a strong increase of the cell corpse number, F14B4.3*(RNAi)* treated animals had only few germ cell corpses (Figure 57). This supported that *rpo-1b(op259)* was causally involved in the apoptotic defect of *op259*.

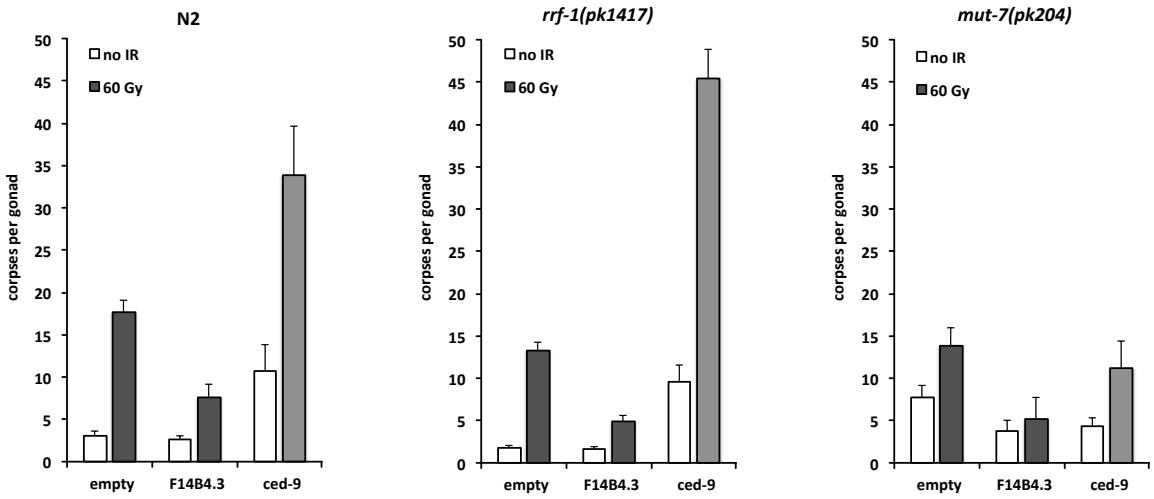

		empty(RNAi)		F14B4.3(RNAi)		ced-9(RNAi)		gla-3(RNAi)	
		score	95% CI (n)	score	95% CI (n)	score	95% CI (n)	score	95% CI (n)
N2	no IR	3.05	±0.64 (40)	2.64	±0.44 (36)	10.67	±3.18 (46)	17.23	±3.00 (100)
	60 Gy	17.68	±1.45 (80)	7.67	±1.47 (36)	33.88	±5.81 (16)	49.75	±3.86 (32)
rrf-1	no IR	1.73	±0.32 (88)	1.61	±0.34 (56)	9.65	±1.96 (20)	10.28	±3.02 (32)
	60 Gy	13.25	±1.07 (88)	4.86	±0.80 (56)	45.45	±3.44 (20)	45.19	±4.78 (16)
mut-7	no IR	7.77	±1.44 (64)	3.81	±1.22 (16)	4.30	±1.00 (20)	5.22	±1.50 (32)
	60 Gy	13.88	±2.06 (52)	5.13	±2.55 (16)	11.20	±3.21 (20)	10.25	±1.97 (16)

Figure 57 Knockdown of *rpo-1b* in the whole animal (N2), or specifically in the germ line (*rrf-1*) or in the soma (*mut-7*) affects germ cell apoptosis. *ced-9* and *gla-3* were included as controls for supposedly germ cell autonomous genes in apoptosis regulation. The table indicates average number of apoptotic corpses, 95 % CI of the mean, and number of animals tested per condition.

Apoptotic defect can be induced by germ line specific knockdown of *rpo-1b*

I used RNAi further to differentiate whether the reduction in the number of apoptotic corpses was more likely due to a cell- or tissue-autonomous effect in the germ line, or whether the soma was contributory to the changes. Two mutant strains have been commonly used to assess tissue-specific requirements for genes of interest: *rrf-1(pk1417)*, carrying a mutation in the RNA-directed RNA polymerase RdRP (QDE-1) homolog, which selectively abolishes RNAi effects in somatic cells (Sijen 2001); and *mut-7(pk204)*, a mutation in the RnaseD homolog which affects the RNAi machinery specifically in the germ line (Ketting 1999). Knock-down of genes that are relevant in somatic tissues but not in the germ line should not produce an effect in the *rrf-1(pk1417)* mutant but in *mut-7(pk204)*. Inversely, a phenotype due to loss of gene activity in the germ line can be evoked in *rrf-1(pk1417)* but not in *mut-7(pk204)*. I performed RNAi to F14B4.3 on *rrf-1(pk1417)* and *mut-7(pk204)* animals. The two strains had slightly different levels of germ cell corpses on *empty(RNAi)*, but they both responded to irradiation with a significant increase of the corpse number. F14B4.3*(RNAi); rrf-1(pk1417)* had a much weaker response to irradiation, confirming that reduction of *rpo-1b* gene product specifically in the germ line did affect germ cell apoptosis. Interestingly, the response was also limited in irradiated F14B4.3*(RNAi); mut-7(pk204)* in comparison to irradiated *empty(RNAi); mut-7(pk204)*. This indicates that reduction of RPO-1B in the soma ultimately also contributes to a reduced number of irradiation-induced germ cell corpses. It is not fully excluded, however, that *mut-7(pk204)* is leaky for some RNAi

knockdown on the non-germline specific F14B4.3 and that therefore, the effect seen in the germ line actually results from germ line knockdown.

5.2.2 Cell cycle arrest

rpo-1b(op259) had stood out in a screen for mutants with disturbed cell cycle arrest response to irradiation. In wildtype worms, proliferating germ cells in the distal compartment of the germ line halt their mitotic cell cycle and are arrested before the M-phase until irradiation-induced DNA damage has been repaired. Nuclear growth and cytoplasmic expansion meanwhile persist; morphologically, this becomes apparent as an enlargement of the germ cell nuclei and nucleoli [(Gartner 2000) and Figure 74]. The concurrent reduction in the number of cells per distal gonad volume has commonly been used to measure the response. In mutants with defective cell cycle arrest response, the mitotic cells remain cycling, supposedly propagating damages of hereditary material (Harris 2006); accordingly, the number of cells per volume does not decrease upon DNA damage.

5.2.2.1 *rpo-1b(op259)* do arrest proliferating germ cells upon DNA damage

In several mutants of DNA damage response, defective cycle arrest in the mitotic region and defective apoptosis of late pachytene meiotic cells are correlated [*hus-1*, *mrt-2*, *clk-2* (Stergiou 2004), *atm-1* (Stergiou 2007)]. The apoptotic defect in *rpo-1b(op259)*, which had been found secondarily, therefore had led to little doubt on the cell cycle arrest defect. Nevertheless, when we studied nuclear and nucleolar size in *rpo-1b(op259)*, we realised that germ cells in the distal region were markedly different from wildtype (Figure 76). Could a smaller cellular volume have led to a deceptively high number of cells per volume? I decided to examine irradiation response in the distal compartment of *rpo-1b(op259)* in more detail and used chromatin staining of dissected gonads. With this, there was an obvious difference between irradiated and non-irradiated *rpo-1b(op259)* germ lines (Figure 60). The uniform pool of nuclei in the distal compartment of non-irradiated worms was interspersed with larger nuclei shortly after irradiation; at 6 hours, almost all nuclei had significantly enlarged chromatin staining. I realised why the cells in the mitotic compartment of *rpo-1b(op259)* could be mistaken as non-responsive to DNA damage-induced cell cycle arrest by DIC imaging. Normal mitotic cells are small and have a small nucleolus, both in wildtype and in *rpo-1b(op259)*. Upon irradiation of wildtype worms, the nucleoli of arrested cells enlarge massively, contributing to a large part to the increase of total nuclear diameter; this is easily visible by DIC; and it shows as a thickened, enlarged chromatin ring in Hoechst stained cells. In *rpo-1b(op259)*, the nucleoli grow only little, and the total nuclear diameter of arrested cells remains far below wildtype so that the increase can be missed by DIC; with chromatin staining, the ring has a somewhat enlarged radius but mainly is thickened; therewith, it is clearly distinct from normal mitotic cells. I also saw a significant enlargement of the nucleoplasm of arrested mitotic cells with the CEP-1::GFP reporter in *rpo-1b(op259)* (Figure 77). Thus, mitotic germ cells in *rpo-1b(op259)* do show a response to irradiation; the isolation of *rpo-1b(op259)* from the cell cycle arrest screen had been based on a false positive identification.

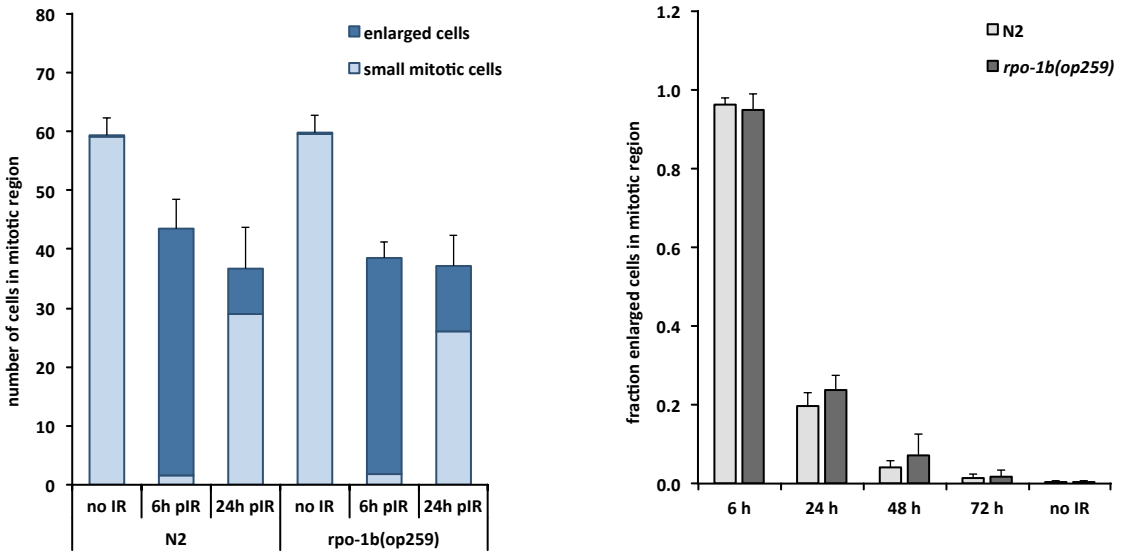

Figure 58 Cell cycle arrest is induced normally in *rpo-1b(op259),* as judged from the reduction in the number of total mitotic cells (left) and steep increase of the fraction of enlarged cells at 6 hours post irradiation. Re-entry is slightly delayed in *rpo-1b(op259)*; more cells remain enlarged at later time points. Error bars indicate 95 % CI of the mean of at least 12 gonads.

5.2.2.2 *rpo-1b(op259)* have slightly delayed kinetics in distal germ line

I assessed and compared the kinetics of the cell cycle arrest response between *rpo-1b(op259)* and wildtype. Based on the appearance of crescent shaped chromatin staining representing cells in transition from replication cycles to meiotic division (Figure 59), I defined the borders of the mitotic compartment and counted the number of nuclei in a cross section of the flattened distal gonad (this number is lower than the total number of cells in the three-dimensional conical tube of that region, which was estimated to be around 250 (Maciejowski 2006)). In wildtype worms, already six hours after irradiation almost all nuclei were enlarged. After 24 hours, 20 % of the mitotic cells were still enlarged, probably representing a fraction that had not been released from arrest yet. This percentage decreased to less than 5 % at 48 hours and to less than 1 % at 72 hours (Figure 58). It is not certain whether all formerly arrested cells had restarted cycling at these later time points; occasionally, enlarged nuclei with the chromatin pattern of mitotic cells could be found further proximal in the germ line, possibly cells that left the distal compartment in an arrested state. The fraction of arrested cells in the mitotic region appears to follow a first order decline, with an approximate half-time of 10 to 11 hours (depending on whether the time point of irradiation or the six hour time point is chosen as the reference in an exponential fit model).

In *rpo-1b(op259)*, the same high percentage of cells as in wildtype was enlarged at 6 hours after irradiation. The fraction also decreased significantly over time, however at a rate of decline that was slightly lower than wildtype; the half-time of a fitted exponential function was between 11 and 12 hours. Thus, the kinetics of cell cycle arrest response is similar between *rpo-1b(op259)* and N2. Possibly, re-entry into cell division cycles is slightly delayed in *rpo-1b(op259)*; this would be interesting to correlate with the division rate of mitotic cells in the two strains.

5.2.3 DNA damage repair

5.2.3.1 Repair is activated in *rpo-1b(op259)*

Some of the known mutants with defective DNA damage responses have mutations in genes that are involved in DNA damage repair (Stergiou 2004, 2007; Lemmens 2011). It was therefore conceivable that the defect in irradiation-induced apoptosis of *rpo-1b(op259)* went along with altered DNA repair. I used the transgene *opIs257[P_{rad-54}::rad-54::yfp 3'UTR; unc-119(+)]* to observe germ line expression of RAD-54::YFP. We had characterised and used this reporter in our studies on UV-C repair. Shortly, RAD-54 is involved in homologous recombination at sites of DNA double strand breaks; it participates in meiotic recombination, and it is also recruited to repair sites when DNA has been damaged exogenously; upon irradiation, RAD-54::YFP forms foci on germ cell chromatin. The reporter would reveal defects in DNA damage repair. After exogenous DNA damage, no foci would form if the repair process were not induced properly. In worms without exogenous damage, an increased foci number would indicate accumulation of endogenous damage – as the result of excessive damage formation, or of defective repair activity.

I assessed the foci number in late meiotic pachytene cells and in mitotic cells of the distal tip region. In the region of late pachytene cells, where germ cells can undergo programmed death, all cells should have completed meiotic recombination and therefore, the expected number of RAD-54::YFP foci is low. Without irradiation, the foci number was equally low (less than 0.5 foci per nucleus) in *rpo-1b(op259); opIs257* as in *opIs257*. This indicated that *rpo-1b(op259)* does not have an increased number of non-repaired DNA damages and that it is probably not basically defective in DNA damage repair. I next scored the number of foci three hours after irradiation with IR. Again, *rpo-1b(op259)* responded very similarly to wildtype, with an increase to approximately 3.5 foci per nucleus. This confirmed that *rpo-1b(op259)* mutants are not principally defective in recruiting RAD-54, and that the former observation of low basic foci numbers is likely not a result of missing recruitment of RAD-54. It further demonstrated that, other than the apoptotic response of germ cells, induction of DNA damage repair is likely not defective in *rpo-1b(op259)* mutants.

For the distal germ line compartment, I combined the foci scoring with analysis of cell cycle arrest. Above, I described the changes of nuclear size and of chromatin staining in the mitotic region of irradiated wildtype and *rpo-1b(op259)* worms. As to RAD-54::YFP, non-irradiated wildtype worms had very few foci in the mitotic zone; upon irradiation, the number strongly increased (Figure 60). Here, I noticed a strong association of RAD-54::YFP foci with enlarged cells; this could somehow be expected considering that the enlarged cells were those arrested in the cell cycle, likely due to unrepaired DNA damage.

I scored the number of mitotic cells, the fraction of enlarged cells, and the number of RAD-54::YFP foci in the distal compartment of wildtype and *rpo-1b(op259)* gonads upon irradiation. For the counting, gonads were extruded from adult worms and stained with Hoechst; the fluorescent images depict slightly more than a simple axial cross-section through the gonads, as these were flattened by the preparation.

Judged by the chromatin pattern, the total number of mitotic cells decreased after irradiation; both wildtype and *rpo-1b(op259)* showed a continuous reduction from the irradiation time point to 6 hours

and from 6 hours to 24 hours after irradiation (Figure 60). The total number of RAD-54::YFP foci per distal gonad peaked at 6 hours and was again lower at 24 hours; at 6 hours, *rpo-1b(op259)* had a lower total number of foci, and at 24 hours it was higher than wildtype. From these few sampling time points, it seemed that *rpo-1b(op259)* had a temporally shifted, i.e. delayed, repair response to irradiation, with a slower formation but longer persistence of the repair foci. However, I mentioned before that the foci were mainly found in enlarged cells; deviations in the absolute number of arrested cells per distal compartment would therefore affect the number or foci considerably. I therefore normalised the foci number to the number of enlarged cells. Here, the number of RAD-54::YFP foci per large mitotic cell doubled from about three at 6 hours to six at 24 hours. This was similar for *rpo-1b(op259)* and wildtype.

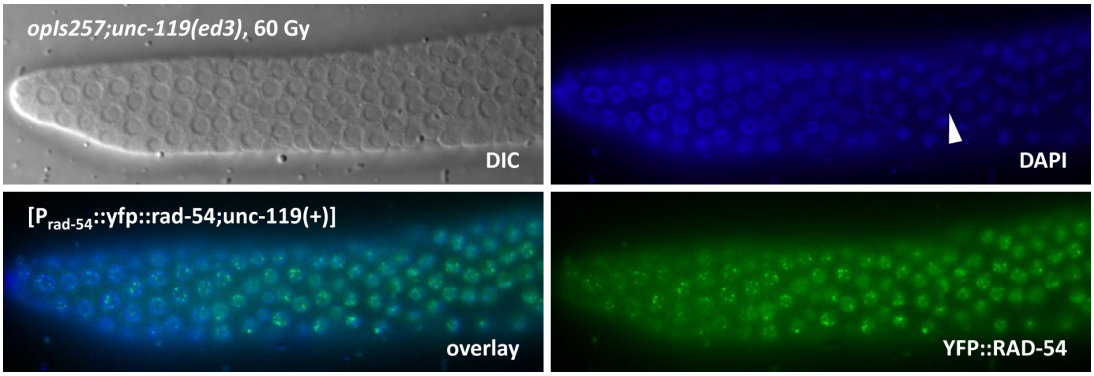

Figure 59 Upon DNA damage, mitotic germ cell nucleoli and nuclei enlarge, and YFP::RAD-54 forms foci in chromosomal regions of arrested mitotic cells. (Indicator) shows crescent-shaped chromatin pattern in early transition zone. Wildtype background, 12 hours after irradiation.

5.2.3.2 Signs of repair endure longer in *rpo-1b(op259)*

The maximum average was thus not reached at 6 hours but only at 24 hours; the cells that remained in arrest through to 24 hours had more foci than an average arrested mitotic cell at the earlier time point (Figure 60). This observation is different from the kinetics observed in meiotic cells, as we described it in our study on UV-C response [see chapter *3.2*]. Meiotic pachytene cells had shown a plateau in the number of foci per nucleus at three hours after irradiation with UV-C or with IR irradiation. It is however not clear whether the apparently higher number of foci in arrested mitotic cells at 24 hours signifies de-novo formation after the 6 hour time point or is due to a selection process of the cells with already higher numbers at the 6 hour time point. A high number of foci in a minor fraction of cells at 6 hours might be concealed in the group mean. At least, the majority of cells had left mitotic arrest at 24 hours; this was probably following complete resolution of the repair foci since virtually none of the re-cycling cells maintained a RAD-54::YFP focus. Overall, the resolution of RAD-54::YFP foci likely precedes exit from cell cycle arrest; the fraction of cells that remain arrested through to later time points are probably the ones that have not yet managed to complete repair. In summary, *rpo-1b(op259)* mutants have slightly delayed appearance of repair foci and exit from cell cycle arrest. This delay in DNA damage response kinetics in the mitotic zone would be in agreement with a generally prolonged cell cycle in *rpo-1b(op259)* mutants.

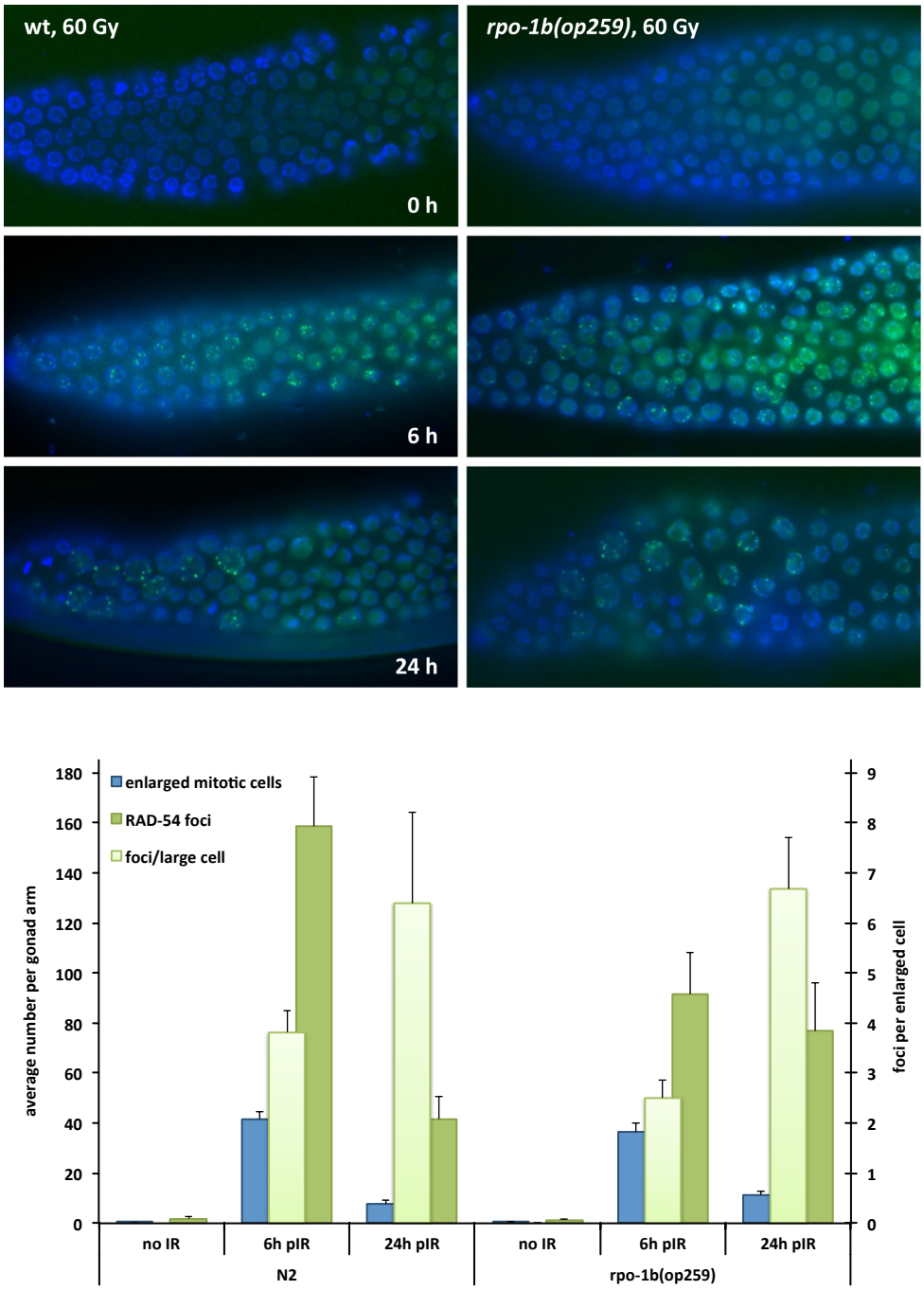

Figure 60 *rpo-1b(op259)* mutants have a slight delay in the appearance of RAD-54::YFP foci upon irradiation. Enlargement of nuclei and formation of YFP-foci in the mitotic compartment (panel). The average number of foci per enlarged cell rises more slowly in *rpo-1b(op259)*. Error bars represent 95% CI of the mean from at least 12 animals.

5.2.4 Interaction with DNA damage signalling factors

rpo-1b(op259) animals had defective apoptotic response to IR and UV-C. Cell cycle arrest could be induced, and recruitment of repair factors was similar to wildtype. I assessed the genetic interaction of *rpo-1b(op259)* with DNA damage repair and signalling factors in animal health and in apoptosis induction. For an introduction to the factors considered here see *2.1.6 DNA damage-induced germ cell apoptosis*.

5.2.4.1 *cep-1(lf) rpo-1b(op259)* mutants are thin

Interactions of *rpo-1b(op259)* with the central DNA damage response factor *cep-1* will be extensively discussed in *5.3 rpo-1b(op259) and CEP-1*. *cep-1* and *rpo-1b* are very closely linked on chromosome I (1.0 cM); Randall Hofmann had constructed a double mutant of the loss-of-function allele *cep-1(gk138)* with *rpo-1b(op259)*. Whereas *cep-1(gk138)* animals look wildtype, *cep-1(gk138) rpo-1b(op259)* double mutant larvae were smaller and thinner than *cep-1(gk138)* or *rpo-1b(op259)* animals, and the adults were thin and long. The onset of egg-laying was more delayed than in *rpo-1b(op259)* and the egg laying rate was reduced. The germ line was thinner than in *rpo-1b(op259)*; however, germ line integrity was more robust.

5.2.4.2 *hus-1(lf) rpo-1b(op259)* mutants are strongly Him

HUS-1 is the *C. elegans* homolog of a 9-1-1 complex subunit; it is required for irradiation-induced apoptosis and signals through CEP-1 activation (Hofmann 2002); the 9-1-1 complex is also involved in telomere maintenance, which is particularly interesting with regards to the subtelomeric location of the rDNA repeat region. We crossed the double mutant of the linked genes *hus-1* and *rpo-1b* (6.5 cM). *hus-1(op244) rpo-1b(op259)*, like *cep-1(gk138) rpo-1b(op259)*, had less progeny than *hus-1(op244)* or *rpo-1b(op259)*. *hus-1(op244)* have a high incidence of males (Him) (more than *rpo-1b(op259)*), and the fraction of males rose above 20 % in the *hus-1(op244) rpo-1b(op259)* double mutant. The synthetic effect might indicate a collaborative function on chromosome segregation; however, I have not excluded the possibility of somatic sexual differentiation defects. Germ line health of *hus-1(op244) rpo-1b(op259)* was mostly intact. The double mutant had only very few germ cell corpses, with or without irradiation. Interestingly, *hus-1(op244)*, *rpo-1b(op259)* and *hus-1(op244) rpo-1b(op259)* behaved very similarly in the context of *ced-9* and *gla-3* RNAi [see *5.6.10.2 ced-9(RNAi) facilitates apoptotic IR response of hus-1(op244)* and *5.6.11.3 hus-1(op244) mutants show strong IR response on gla-3(RNAi)*].

5.2.4.3 *atm-1 rpo-1b(op259) have excessive* CEP-1 activation

ATM and ATL are first line transducers of DNA damage responses in mammalian cells [see *3.1.2 From sensors to effectors*]. Mutants of *atm-1* have defective apoptosis induction in response to IR and UV-C irradiation (Garcia-Muse 2005; Stergiou 2007). ATM was shown to mediate the shutdown of RNA pol I transcription upon irradiation of mammalian cells [(Kruhlak 2007), see *4.1.4.3 DNA damage response might involve the nucleolus*]. Randall Hofmann had constructed the double mutant *atm-1(gk186) rpo-1b(op259)*. The animals were of the size of *rpo-1b(op259)*, growth and maturation was less delayed than in *cep-1(gk138) rpo-1b(op259)* or *hus-1(op244) rpo-1b(op259)*. The germ lines were less intact than in *rpo-1b(op259)*. Surprisingly, whereas both *atm-1(gk186)* and *rpo-1b(op259)* have only little apoptotic response to IR, *atm-1(gk186) rpo-1b(op259)* had almost wildtype levels of irradiation-induced germ cell death. ATM-1 is supposed to contribute to DNA damage-induced apoptosis by *cep-1*-dependent signalling; not explicably by this model, the mRNA levels of EGL-1 and CED-13, transcriptional targets of CEP-1, were increased in the double mutant of *atm-1(gk186) rpo-1b(op259)* (very significantly in non-irradiated animals) beyond the high levels of *rpo-1b(op259)* (see later chapters), speaking for strongly enhanced CEP-1 activation in this constellation.

5.2.4.4 *rpo-1b(op259)* suppresses hypersensitivity of *abl-1(lf)* for IR-induced apoptosis

Loss-of-function mutants of the ABL kinase homolog *abl-1* have increased germ cell death and are hypersensitive to irradiation, by a mechanism that depends on *cep-1* (Deng 2004). Germ line health of *rpo-1b(op259); abl-1(ok171)* was intact; regarding apoptosis, *rpo-1b(op259)* did fully suppress the *abl-1(ok171)* loss-of-function effects, and the response to irradiation was minimal.

5.2.4.5 *rpo-1b(op259)* has synthetic effects with several repair mutants

The double mutants of *rpo-1b(op259)* with the BRCA1 homolog *brc-1(lf)* had extremely high embryonic lethality; plates of adult populations were full with eggs that mostly failed to hatch. *brc-1(tm1145)* mutants are hypersensitive to irradiation-induced apoptosis (Boulton 2004a). In *rpo-1b(op259); brc-1(tm1145)*, baseline apoptosis was low and irradiation caused a slightly higher level of corpses than in *rpo-1b(op259)*, but remained below wildtype. In agreement with an effect downstream of CEP-1 activation, *rpo-1b(op259)* is epistatic to *brc-1(tm1145)* regarding IR induced cell death.

clk-2(mn159) is a temperature sensitive mutant of a DNA damage signalling molecule with so far little defined functions; it has DNA damage checkpoint defects, among which a failing cell cycle arrest response and defective IR-induced apoptosis. The double mutant *rpo-1b(op259); clk-2(mn159)* grew very poorly. Apoptosis scoring has not been done yet.

A screen for synthetic effects of combinations of DNA damage response mutants had indicated genetic interaction of *rpo-1b(op259)* with the Ku80 NHEJ repair factor homolog *cku-80* [Andrew Fraser, personal communication to Michael Hengartner]. Interestingly, DNA-PK subunits had been found in association with the RNA pol I transcription intiation complex (Michaelidis 2002). I could not produce an effect with *cku-80(RNAi)* knockdown on *rpo-1b(op259)* mutants regarding animal health or irradiation-induced apoptosis.

5.3 *rpo-1b(op259)* and CEP-1

5.3.1 The role of CEP-1 in DNA damage-induced apoptosis

CEP-1 is the *C. elegans* homolog of the mammalian p53 family of tumor suppressor proteins. p53 is a key player in adjusting cell cycle progression and cell survival in response to exogenous or endogenous cellular stress. Abnormal p53 function has been implicated in many cancer types; it is one of the most frequently mutated and one of the most extensively studied factors associated with tumor formation and progression. Its connections to the nucleolus are introduced in *4.1.4 Control of cell fate by the nucleolus and ribosomes*.

The distinction of *cep-1*-dependent and *cep-1*-independent germ cell apoptosis is introduced in *2.1.6 DNA damage-induced germ cell apoptosis*. Loss-of-function mutations of *cep-1* are thought to abolish any DNA damage-induced cell death while leaving constitutive germ cell apoptosis intact. CEP-1 is assumed to exert its pro-apoptotic function mainly by transcriptionally activating the two pro-apoptotic BH3-only proteins EGL-1 and CED-13 (Schumacher 2001; Gartner 2000; Schumacher 2005b). EGL-1 in turn presumably activates the core apoptotic machinery by binding to CED-9 and by releasing CED-4; the gain-of-function mutation *ced-9(n1950)*, which was shown to prevent EGL-1 binding *in vitro* (del Peso 2000; Yan 2004), abolishes DNA damage-induced death. Loss of functional *egl-1* has a similar effect on germ cell apoptosis as loss of *cep-1*, i.e., defective DNA damage response but normal levels of physiological cell death. Transcriptional upregulation of EGL-1, probably to release CED-4 from CED-9, is employed by developmental programs in somatic cells and by stress responses in germ cells; the non-dependence on EGL-1 of constitutive germ cell apoptosis is the more surprising.

5.3.1.1 Increased germ cell apoptosis is often mediated by CEP-1

For novel mutants of germ cell apoptosis, it has been decisive to categorise their effects as *cep-1*-dependent or -independent. Conditions that lead to increased levels of apoptosis can be tested relatively easily: combining the mutant with *cep-1(lf)* abolishes excessive cell death if it is mediated by CEP-1 activation. This way, many genetic conditions with hypersensitivity to DNA damage or with increased apoptosis in the absence of exogenous activation have been characterised.

Most mutants that are hypersensitive to DNA damaging agents in terms of apoptosis have been shown to involve CEP-1 for the excessive response. (It should be considered that dependence on CEP-1 in this instance does not necessarily mean overactivation of CEP-1, since DNA damage-induced apoptosis in wildtype also requires CEP-1.) Mutants that have enhanced *cep-1*-mediated DNA damage response (with or without having significantly increased constitutive cell death) comprise: the tyrosine kinase *abl-1(lf)* (Deng 2004), the translational regulator *gld-1(rf)* (Schumacher 2005a), the ubiquitin ligase SCF^{fsn-1} loss-of-function (Gao 2008), the DNA repair and signalling factors *brc-1(lf)* and *brd-1(lf)* (Boulton 2004a), the arginine methyltransferase *prmt-5(lf)* (Yang 2009), the FANCJ homolog *dog-1(lf)* (weak effect) (Youds 2007), and the AKT homolog *akt-1(lf)* (but not *akt-2(lf)*) (Quevedo 2007).

An increasing number of mutants have been identified that, without exogenous DNA damage, exhibit excessive germ cell apoptosis: the Gla mutants *gla-1* (isogenic to *cpb-3*, the CPEB1 homolog) and *gla-3(lf)* (Kritikou 2006), the p38 MAPK homolog *pmk-3(lf)* (Lettre 2004), factors of an RNA binding

complex *cgh-1(lf)* and *car-1(lf)* (Boag 2005), *abl-1(lf)*, the DNA repair factors *rad-50(rf)* (Lettre 2004), *rad-51(lf)*, *xpa-1(lf)* and *xpc-1(lf)* (Stergiou 2007, 2011), the FANCD2 homolog *fcd-2(lf)* (Lee 2007a), *dog-1(lf)*, the hypoxia inducible factor *hif-1(lf)* (Sendoel 2010) and the Pax group transcription factor *pax-2(lf)* (Park 2006). In a fraction of those, aberrant cell death has been shown to depend on *cep-1* function, indicating a possible activation of DNA damage response or cell stress signalling in the mutant condition. Suppression by *cep-1(lf)* was demonstrated for *abl-1*, *rad-51*, *rad-50*, *xpa-1*, *hif-1*, and partially for *pax-2*.

5.3.1.2 Gla mutants have increased apoptosis independently of *cep-1*

Other mutants have been shown to exhibit increased baseline apoptosis independently of *cep-1*: *gla-3(lf)*, *cpb-3(lf)*, *pmk-3(lf)* (Lettre 2004), *cgh-1(lf)* and *car-1(lf)* (Boag 2005), only partial *cep-1*-dependence in *pax-2(lf)* (Park 2006). Genetically, they were therefore placed in pathways that act in parallel to, or downstream of, DNA damage/stress response signalling [summarised in (Gartner 2008)]. For instance, the marked enhancing effect of *gla-3(lf)* on baseline apoptosis could not be suppressed by *cep-1(lf)* (Kritikou 2006).

5.3.1.3 DNA damage response mutants often fail to activate CEP-1

When, in contrast to increased apoptosis, germ cells show no or only reduced response to DNA damage, the genetic relationship of the mutant factors to *cep-1* cannot be easily determined by a double mutant with *cep-1(lf)*. CEP-1 activation levels have been assessed instead, to differentiate whether mutants are irresponsive to DNA damage due to a failure of properly activating CEP-1 or whether they have normal CEP-1 activation and are defective due to an effect downstream of it. Two approaches are common: either, phosphorylated CEP-1 is detected to evidence activated protein, or transcript levels of the EGL-1 and CED-13, direct transcriptional targets of CEP-1, are measured to indirectly assess protein activity. This way, several mutants with reduced DNA damage-induced apoptosis were shown to lack normal CEP-1 activation; mostly, these mutations affected genes involved in DNA damage repair: the kinases *atm-1* (Garcia-Muse 2005; Stergiou 2007) and *atl-1* (Garcia-Muse 2005), the 9-1-1 complex subunits *hus-1* (Hofmann 2002) and *mrt-2* (Ahmed 2000), the novel damage signalling and repair factor *clk-2* (Ahmed 2001), nucleotide excision repair factors (Stergiou 2007, 2011), and supposedly the growth inhibitor *ing-3* (Luo 2009); a special case is an uracil-DNA glycosylase *ung-1* mutant, where apoptosis levels and CEP-1 activation were dependent on the type of cell stress (more than wildtype following IR and less than wildtype following paraquat treatment) (Skjeldam 2010).

5.3.1.4 Pathways besides CEP-1 activation contribute to DNA damage-induced apoptosis

Even though CEP-1 activation is required for DNA damage-induced apoptosis, it is not sufficient. There is increasing evidence for pro-apoptotic signalling in parallel to CEP-1.

Several mutants exhibit defective DNA damage response despite normally high activation of CEP-1; e.g., the Rb homolog *lin-35(lf)* (Schertel 2007), the ARF-BP1 homolog ubiquitin ligase *eel-1(lf)* (Ross 2011), the Sirtuin *sir-2.1(lf)* (Greiss 2008), or the ceramide synthesis mutant *lagr-1(lf)* (Deng 2008).

Further, stress response pathways have been reported that can increase apoptosis independently of CEP-1. Apoptotic response to arsenite (Pei 2008), to copper (Wang 2009), and partly to cobalt (Chong 2009)

depends on various MAPK cascades (ERK/JNK/p38), but not on *cep-1*. Also, MAP kinase pathways but not CEP-1 are required for germ cell apoptosis induced by osmotic, oxidative, or heat shock stress (Salinas 2006); interestingly, the mechanism was shown to involve ABL-1, which itself influences CEP-1.

In summary, there must be pathways that activate germ cell apoptosis in response to DNA damage and cell stress downstream or in parallel to *cep-1*.

5.3.2 The *cep-1(gk138) rpo-1b(op259)* double mutant

5.3.2.1 *rpo-1b(op259)* mutants have increased CEP-1 activity

rpo-1b(op259) mutants do not raise the number of germ cell corpses upon irradiation as strongly as wildtype animals. Accordingly, we wanted to test whether CEP-1 is being insufficiently activated; we determined the levels of EGL-1 and CED-13 transcripts by qRT-PCR. When calculating the transcript levels 3 hours after irradiation relative to the levels without irradiation, *rpo-1b(op259)* mutants indeed seemed to fail to induce CEP-1 activity upon DNA damage (Figure 61). However, when EGL-1 and CED-13 transcript levels were normalised by control transcripts and all normalised levels were expressed in comparison to non-irradiated wildtype, it became evident that irradiated *rpo-1b(op259)* animals reached the same levels as irradiated wildtype. To my surprise, the levels of non-irradiated *rpo-1b(op259)* animals instead were significantly higher than those of the non-irradiated wildtype reference. I confirmed that the increased EGL-1 and CED-13 transcript levels were dependent on CEP-1: in *cep-1(gk138) rpo-1b(op259)*, as in *cep-1(gk138)* animals, they were reduced below wildtype.

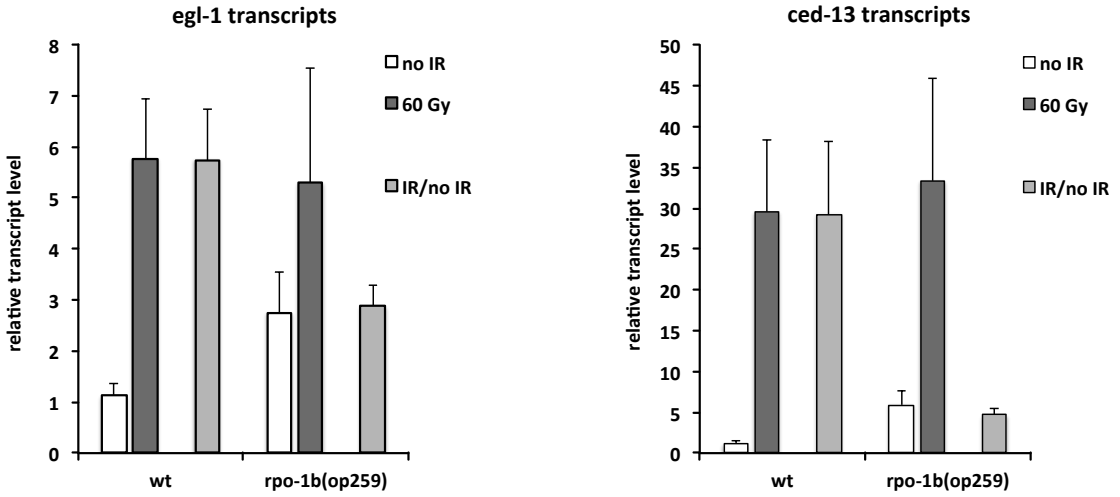

Figure 61 Surrogate markers of CEP-1 activity are increased in non-irradiated *rpo-1b(op259)*. qRT-PCR measurements of total worm RNA at 3 hours post treatment. Usually, more than one non-irradiated wildtype sample was included per qRT-PCR setup, which explains a value different from 1.0 and the error bar for the reference. Error bars represent 95 % CI of the mean.

Thus, *rpo-1b(op259)* presented a new situation: it failed to have wildtype levels of IR-induced apoptosis despite apparently normal CEP-1 activation. At the same time, non-irradiated animals had increased levels of CEP-1 activity without a consequential increase in the number of dying cells. Two overlapping effects seem to be in play in *rpo-1b(op259)*. First, an increase in CEP-1 activity does not ensue increased germ cell death, that is, responsiveness to CEP-1 is apparently lower than in wildtype. Second,

a so far unknown process seems to activate CEP-1 in non-irradiated *rpo-1b(op259)* mutants. Genetically, *rpo-1b* thus acts as an inhibitor of *cep-1*, but it is also involved in a process feeding into the apoptotic cascade downstream of *cep-1*.

These considerations base on the assumption that increased transcript levels mean increased transcription in the germ line tissue. One should be aware that the measured levels are integrated values from whole animals. Thus, the increase in qRT-PCR does not necessarily reflect an increase in the specific cells that were going to undergo apoptosis. I have not so far excluded that CEP-1 activation could be disorganised and maybe abolished in meiotic pachytene cells despite an overall increase; there are some arguments and experimental indications speaking for and against. EGL-1 and CED-13 transcripts in adult animals are mainly on account of non-somatic tissue; *ced-13* transcription reportedly is very low in *glp-4(bn2)* mutants without a germ line (Schumacher 2005b); irradiation response of *ced-13* transcript levels was also dependent on the germ line. This indicates that the increased levels detected in non-irradiated *rpo-1b(op259)* most likely stem from the gonad (germ cells or gametes or embryos!). Also, *rpo-1b(op259)* mutants do show a significant response to IR, which is thus most likely linked to the gonadal tissue. The CEP-1::GFP reporter [described in *5.3.4 CEP-1 and EGL-1 reporter in germ cells*] is restricted to germ cells in adults (Schumacher 2005a); in my experiments, it did not glow in somatic cells of adult wildtype animals apart from a few head neurons. This pattern was not obviously different in *rpo-1b(op259),* and no additional tissue had significant fluorescence, which further supports the germ line as the relevant tissue for increased CEP-1 activity.

The EGL-1 reporter *opIs56[P_{egl-1}::2xNLS::gfp::egl-1 3'UTR; unc-119(+)]* indicated lower than wildtype EGL-1 expression in the late meiotic pachytene region, but aberrant expression in the distal mitotic region of *rpo-1b(op259)* upon irradiation (Figure 74). (This observation has to be interpreted carefully, since the reporter construct with only a relatively short 3'UTR for *egl-1* does not ascertain to represent the very physiological pattern of EGL-1 expression, and it has the usual limitations of a transcriptional reporter; also, the signal was generally weak in the meiotic region and did not clearly increase upon irradiation of wildtype animals. Additionally, the signal in the meiotic region was not dependent on CEP-1, since in *cep-1(lf)* mutant animals, it appeared at the same intensity as in wildtype worms.)

Further, as will be described in *5.3.2.4 cep-1(gk138) and rpo-1b(op259) have synergistic effects on apoptosis,* loss of *cep-1* or *egl-1* function can suppress residual cell death in *rpo-1b(op259)*, indicating that CEP-1 is active in promoting germ cell apoptosis and therefore unlikely to be strongly reduced in the late meiotic pachytene region of the germ line.

5.3.2.2 *gld-1(op236)* inverts the apoptotic defect of *rpo-1b(op259)*

As a genetic approach to the (mis-)functioning of *cep-1* in *rpo-1b(op259)*, I increased *cep-1* activity by a partial loss-of-function allele of *gld-1*. Among many other targets, GLD-1 was shown to bind to, and repress translation from, CEP-1 mRNA in the germ line. The point mutation *gld-1(op236)* leads to derepression of some targets and to ectopic expression of the respective proteins including CEP-1 (Schumacher 2005a), without evoking the full loss-of-function phenotype that ends in germ cell tumours and sterility. Mutant *gld-1(op236)* could restore IR-induced apoptosis in *rpo-1b(op259)*; the corpse number was already high without irradiation and increased massively upon IR (Figure 62 and Figure 65). Without irradiation, the corpse number even exceeded the one in *gld-1(op236)* single mutants, which is

by itself higher than wildtype. Thus, whereas *rpo-1b(op259)* mutants have reduced cell death, this mutation enhances excessive cell death of *gld-1(op236)*. In some gonads of *gld-1(op236) rpo-1b(op259)*, all proximal germ cells were cellularised and the germ line seemed to disintegrate completely after irradiation (a phenotype that, depending on the knockdown conditions, also arises with *gld-1(RNAi)*). The germ lines of *gld-1(op236) rpo-1b(op259)* exhibited multiple defects besides increased apoptosis, altogether reminiscent of double mutants of *rpo-1b(op259)* with *gla-3(lf)* or with *lip-1(zh15),* that are described in sections of *5.5 rpo-1b(op259) and the Ras/MAPK pathway*.

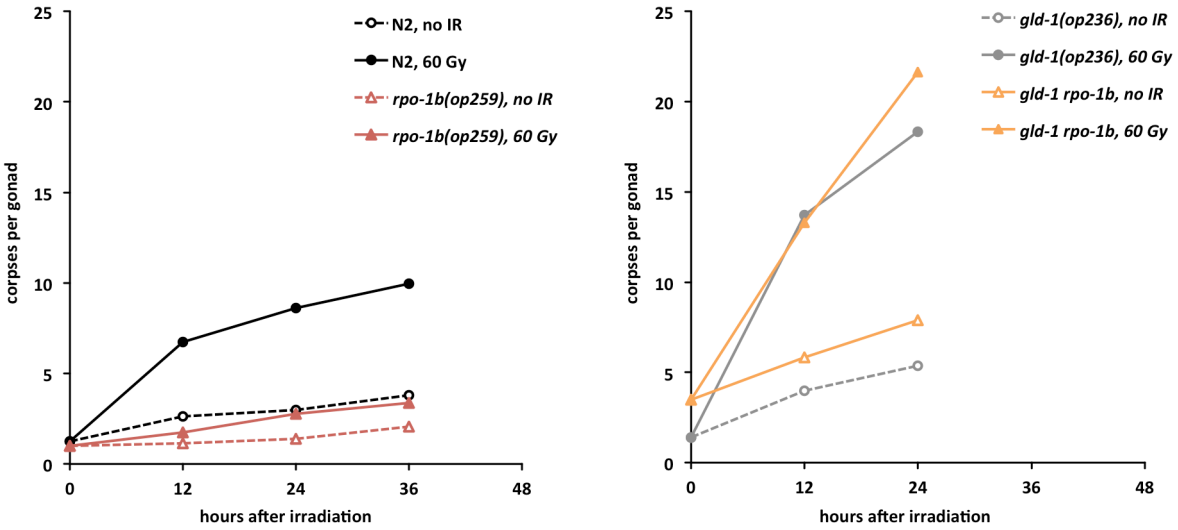

Figure 62 Time course of apoptotic response to IR in *gld-1(op236) rpo-1b(op259)*. For statistics, see Figure 68.

gld-1(op236) rpo-1b(op259) animals have overly active CEP-1 like *rpo-1b(op259)*

There were mainly two possible explanations for excessive cell death in *gld-1(op236) rpo-1b(op259)*. First, it could arise from increased CEP-1 signalling due to loss of translational inhibition together with the additive effect of the *rpo-1b(op259)* mutation on CEP-1 activity levels. This would also imply that *rpo-1b(op259)* mutants were sensitive to CEP-1 activity once high enough; transcript levels of EGL-1 and CED-13 might be significantly higher in the double than in *rpo-1b(op259)*, which could eventually be enough to surpass a threshold of non-responsiveness to *cep-1* activity. Second, CEP-1 might not be the main initiator of increased death in *gld-1(op236) rpo-1b(op259)*; additional factors that are normally regulated directly or indirectly by GLD-1 could be aberrantly expressed and become highly relevant in the context of *rpo-1b(op259)*.

qRT-PCR analysis of EGL-1 and CED-13 transcripts did not confirm increased levels in *gld-1(op236)* at baseline or upon IR (Figure 63). In *gld-1(op236) rpo-1b(op259)*, the transcript levels behaved similarly as in *rpo-1b(op259)*. Here, however, other than in *rpo-1b(op259)* with wildtype *gld-1*, the corpse number increased along with increased CEP-1 activity. The discomposure of the gonad indicates that other processes are disturbed considerably in the double mutant, which could render cells prone to apoptosis. Likely, the effect of *gld-1(op236)* on apoptosis in *rpo-1b(op259)* is mediated in parallel to CEP-1 activation; it sensitises *rpo-1b(op259)* to the effects of the latter.

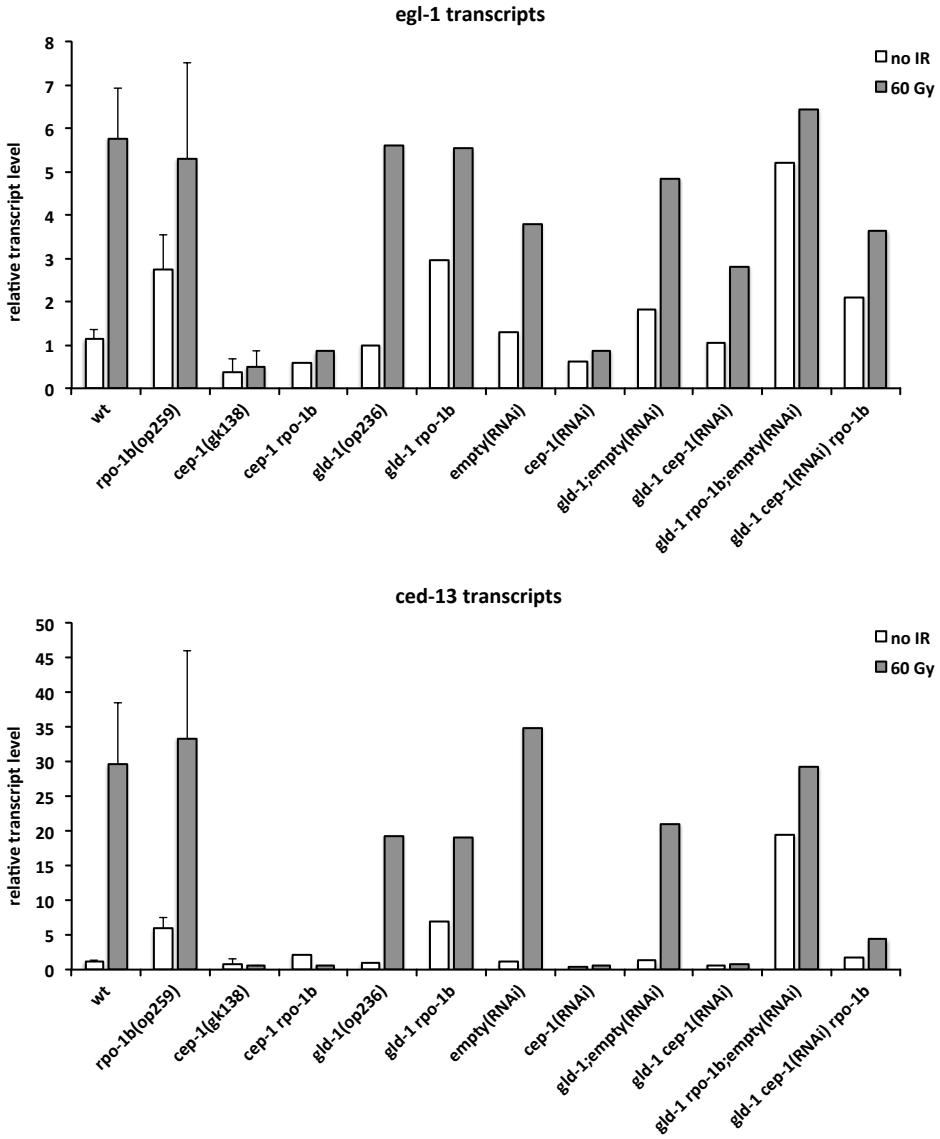

Figure 63 CEP-1 activity in *gld-1(op236) rpo-1b(op259)* as measured by of EGL-1 and CED-13 transcript levels 3 hours post irradiation (internally normalised and related to non-irradiated wildtype). Note the higher baseline levels in *gld-1(op236) rpo-1b(op259)* on RNAi bacteria than on OP50. Error bars represent 95% CI of the mean of different samples; only one experiment (triplicate measurements per sample) was performed for conditions without error bar.

cep-1(RNAi) partially suppresses apoptosis of *gld-1(op236) rpo-1b(op259)*

Unfortunately, I could not build the triple mutant *gld-1(op236) cep-1(gk138) rpo-1b(op259)* to address the above hypothesis since these three genes are very closely linked. *cep-1(RNAi)* was not fully proficient to suppress IR-induced apoptosis in the first treated generation of wildtype worms and gives only an approximation to the effect of a loss-of-function mutant (even though EGL-1 and CED-13 transcript levels are reduced considerably (Figure 63)). In my experiment, *cep-1(RNAi)* reduced the number of excessive corpses both in *gld-1(op236)* and in *gld-1(op236) rpo-1b(op259)* (without suppressing them completely), indicating that CEP-1 is required for at least some of the increased apoptosis (Figure 64 and Figure 67). Again, this does not rule out that additional pro-apoptotic mechanisms are promoted by *gld-1(op236)*.

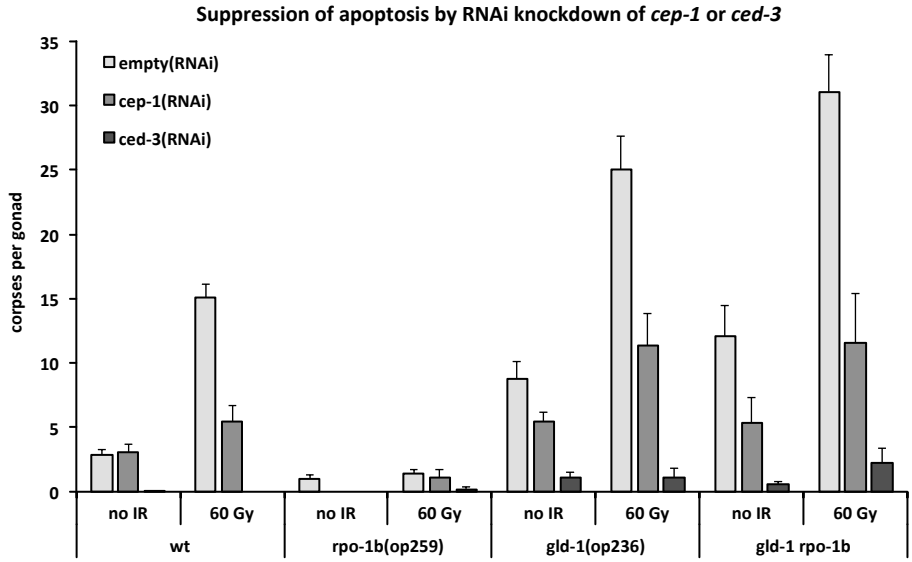

Figure 64 Germ cell apoptosis in RNAi-treated *gld-1(op236) rpo-1b(op259)* at 18 hours after irradiation. *cep-1(RNAi)* can partly suppress increased death in irradiated and non-irradiated animals; *ced-3(RNAi)* confirms that the corpses are apoptotic. Apoptosis levels in *gld-1(op236)* and *gld-1(op236) rpo-1b(op259)* fed on RNAi bacteria are significantly higher than on OP50. Error bars represent 95% CI of the mean.

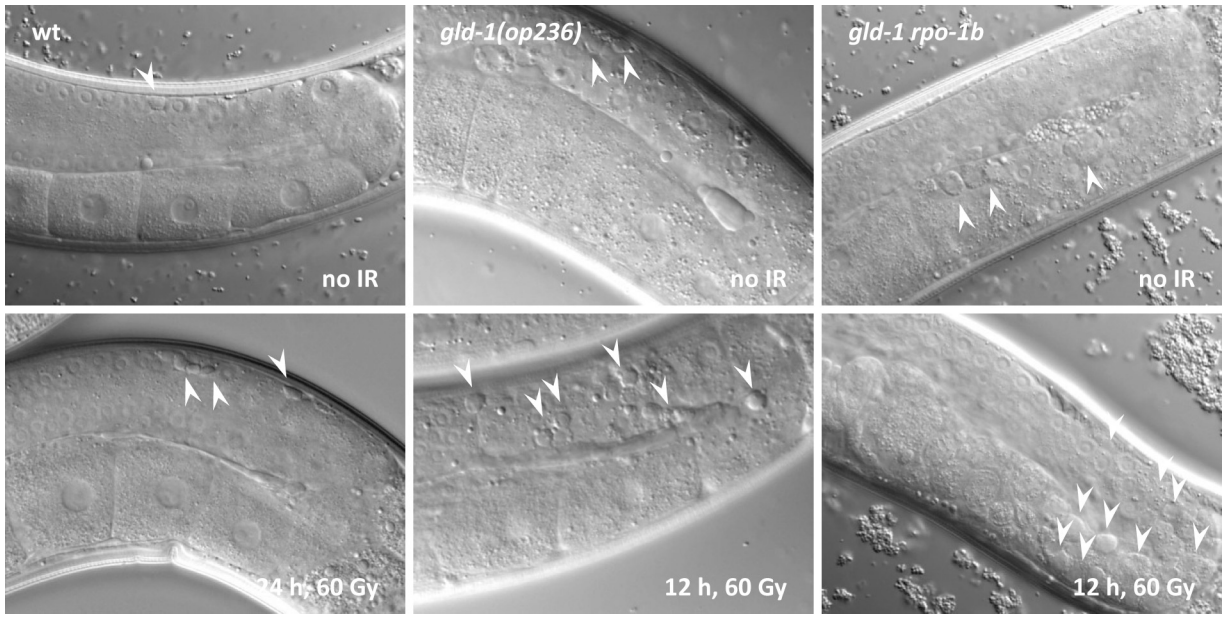

Figure 65 Apoptotic corpses following IR irradiation. *gld-1(rf)* restores apoptosis (arrowheads) in *rpo-1b(op259)*, and *rpo-1b(op259)* further enhances increased IR response of *gld-1(rf)*. Often, the proximal gonads in the double mutant decay after irradiation.

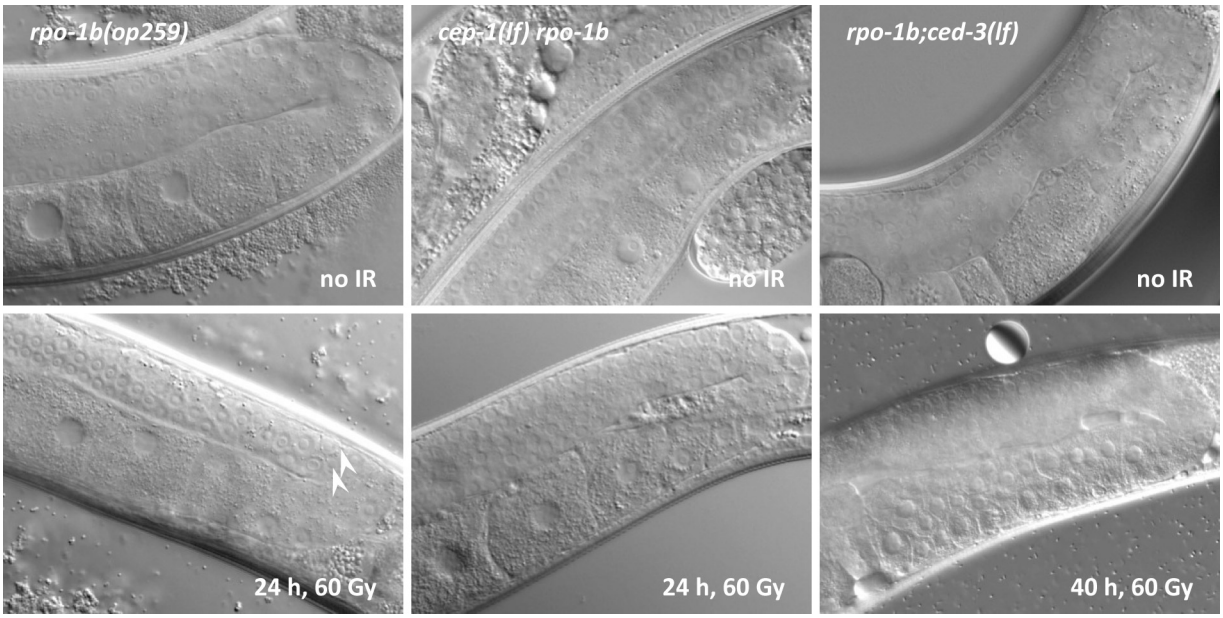

Figure 66 Weak apoptotic response (arrowheads) to IR in *rpo-1b(op259)* is further reduced by *cep-1(gk138)*. *ced-3(n717)* fully abolishes cell death; a small oocyte phenotype is often found in the *rpo-1b(op259); ced-3(n717)*. A similar phenotype has been found in double mutants of *ced-3(n717)* and RNA binding factors (Boag 2005).

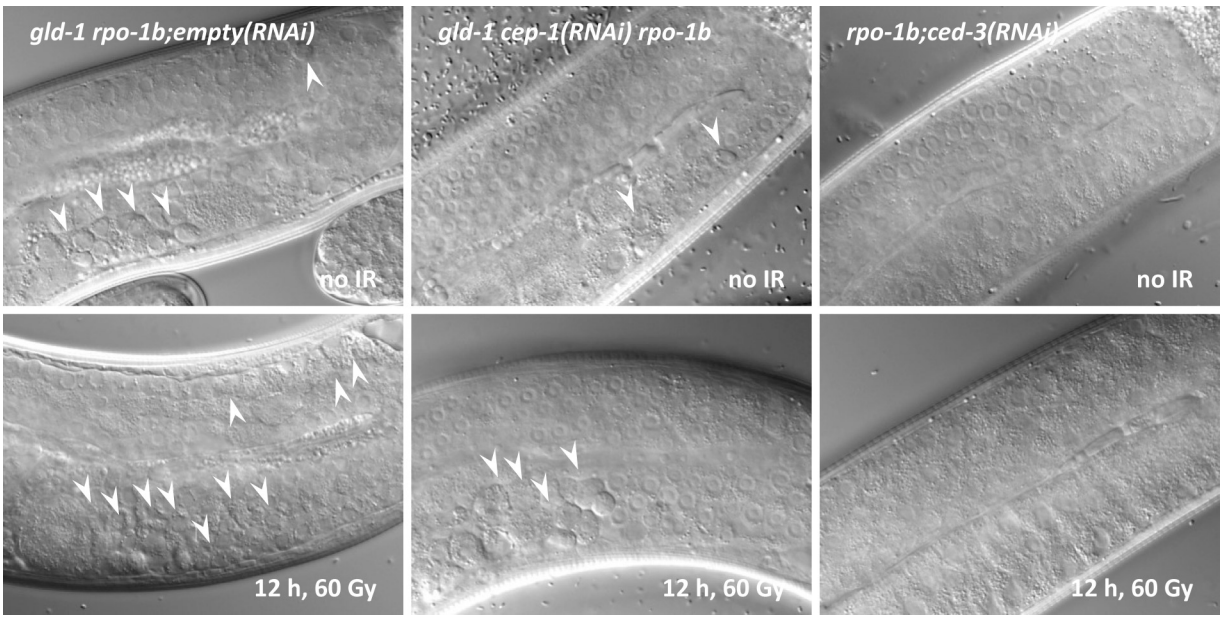

Figure 67 Proximal decay in *gld-1(op236) rpo-1b(op259)* is enhanced in RNAi conditions as compared to OP50 food. *cep-1(RNAi)* partly, and *ced-3(RNAi)* fully suppresses the excessive corpse number. However, germ line health is not fully restored.

5.3.2.3 Model: Germ cell apoptosis in *rpo-1b(op259)* is reduced downstream of *cep-1*

It is to resolve why *rpo-1b(op259)* does not have higher than wildtype numbers of corpses at baseline despite increased EGL-1 and CED-13 transcript levels. As delineated above, *rpo-1b(op259)* mutants do have some baseline apoptosis and low levels but not complete absence of IR-induced corpses. This observation would fit with a model where CEP-1 activation is achieved but is ineffectively transmitted into pro-apoptotic effects. Genetic combination with *gld-1(op236)* demonstrated that germ cell death

and its enhancement by irradiation are not principally blocked in *rpo-1b(op259)* but can be evoked, supposedly by counteracting constraints in *rpo-1b(op259)* for effective CEP-1 signalling.

It is conceivable that *rpo-1b(op259)* affects an apoptotic mechanism downstream of CEP-1. Genetically, *egl-1* is directly downstream of *cep-1*, and several other known pro-apoptotic cues converge at the level of EGL-1 or CED-9; it is likely that such other stimuli are not transmitted equally well in *rpo-1b(op259)*. One would then expect a more general reduction in the number of corpses, also at non-DNA damage conditions. In principle, germ cell apoptosis in non-irradiated *rpo-1b(op259)* could be a summed result of reduced baseline apoptosis and some death arising from the increased (but ineffectively transmitted) CEP-1 activation. This way, a reduction of "physiological" death in *rpo-1b(op259)* could be concealed by the effect of increased EGL-1 and CED-13.

5.3.2.4 *cep-1(gk138)* and *rpo-1b(op259)* have synergistic effects on apoptosis

Most apoptosis is abolished in *cep-1(gk138) rpo-1b(op259)*

To study this issue in more detail, we built and analysed the double mutant *cep-1(gk138) rpo-1b(op259)*. Loss of *cep-1* function strongly reduced the transcript levels of EGL-1 and CED-13 in *rpo-1b(op259)*, confirming that the high levels in non-irradiated animals were dependent on, and thus likely resulting from transcriptional activation by, CEP-1 (Figure 63). The findings for germ cell apoptosis were compelling: without or with irradiation, *cep-1(gk138) rpo-1b(op259)* double mutants had extremely few corpses, far less than either *cep-1(gk138)* or *rpo-1b(op259)* (Figure 68).

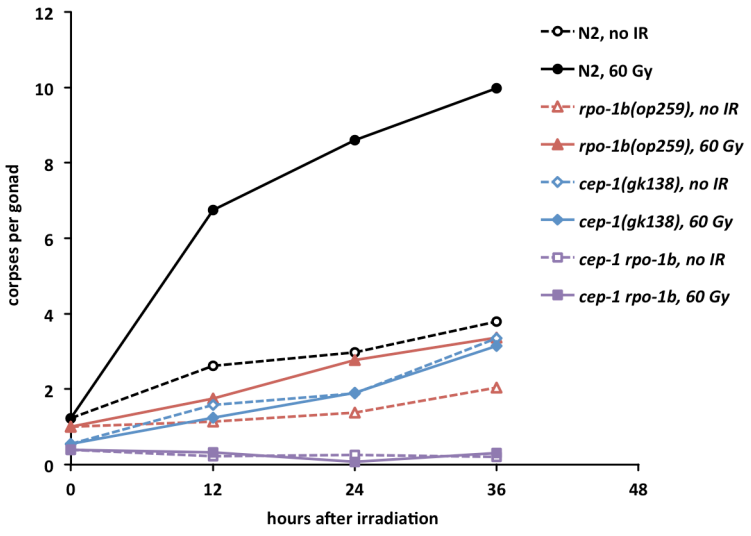

		N2		*rpo-1b(op259)*		*cep-1(gk138)*		*cep-1 rpo-1b*		*gld-1(op236)*		*gld-1 rpo-1b*	
	post IR	score	95% CI (n)	score	95% CI (n)	score	95% CI (n)	score	95% CI (n)	score	95% CI (n)	score	95% CI (n)
no IR	0 h	1.23	±0.20 (100)	1.00	±0.28 (60)	0.55	±0.26 (40)	0.40	±0.26 (20)	1.40	±0.33 (20)	3.48	±0.57 (40)
	12 h	2.62	±0.26 (100)	1.13	±0.23 (60)	1.58	±0.44 (40)	0.23	±0.15 (40)	3.98	±0.64 (40)	5.82	±0.89 (40)
	24 h	2.97	±0.20 (428)	1.37	±0.22 (140)	1.89	±0.30 (96)	0.25	±0.15 (40)	5.38	±0.86 (40)	7.90	±0.97 (40)
	36 h	3.80	±0.39 (80)	2.05	±0.48 (60)	3.35	±0.57 (40)	0.20	±0.18 (20)				±1.65 (20)
60 Gy													
	12 h	6.75	±0.49 (100)	1.75	±0.35 (60)	1.25	±0.36 (40)	0.33	±0.16 (40)	13.70	±1.31 (20)	13.28	±1.50 (40)
	24 h	8.61	±0.27 (524)	2.77	±0.31 (140)	1.90	±0.26 (136)	0.08	±0.08 (40)	18.33	±1.61 (60)	21.65	±2.72 (40)
	36 h	9.98	±0.80 (80)	3.37	±0.57 (60)	3.15	±0.55 (40)	0.30	±0.21 (20)				

Figure 68 Time course of apoptotic irradiation response in *cep-1(gk138) rpo-1b(op259)* germ lines. Table indicates average number of apoptotic corpses per gonad, 95 % CI of the mean, and number of animals tested per condition.

The *ced-6(n1813)* engulfment mutant background accentuates the difference

Yet, numerical resolution of germ cell corpses around baseline levels might not be sufficient for distinguishing two strains, the more as the inter-individual variation within one strain is relatively high. To improve this resolution, I crossed *cep-1(gk138)*, *rpo-1b(op259)* and *cep-1(gk138) rpo-1b(op259)* into a *ced-6* mutant background. *ced-6(n1813)* animals have a strong defect in engulfment – that is, removal – of apoptotic germ cells by the gonadal sheath cells, leading to accumulation of dead cells. Thus, the cumulative number of cells having undergone apoptosis rather than just a steady state level of dying cells can be assessed by DIC optics (Figure 69). *ced-6(n1813)* mutants accumulate approximately 40 corpses in 24 hours. Upon irradiation, this rate rose dramatically so that at 24 hours post IR more than 100 cells could be found per gonad (the cell number can only be approximated at such high levels). In agreement with the observation for *cep-1(gk138)* and wildtype, *cep-1(gk138); ced-6(n1813)* animals had almost the same levels as *ced-6(n1813)* without irradiation; but *cep-1(gk138); ced-6(n1813)* did not respond to IR. Also for *rpo-1b(op259)*, observations in the wildtype and engulfment mutant background were consistent. Without irradiation, somewhat less cells accumulated in *rpo-1b(op259); ced-6(n1813)* than in *ced-6(n1813),* and there was only a weak increase after irradiation. Definitely, *cep-1(gk138) rpo-1b(op259)* had a massively reduced corpse number; almost no corpses accumulated in non-irradiated or in irradiated animals (Figure 70).

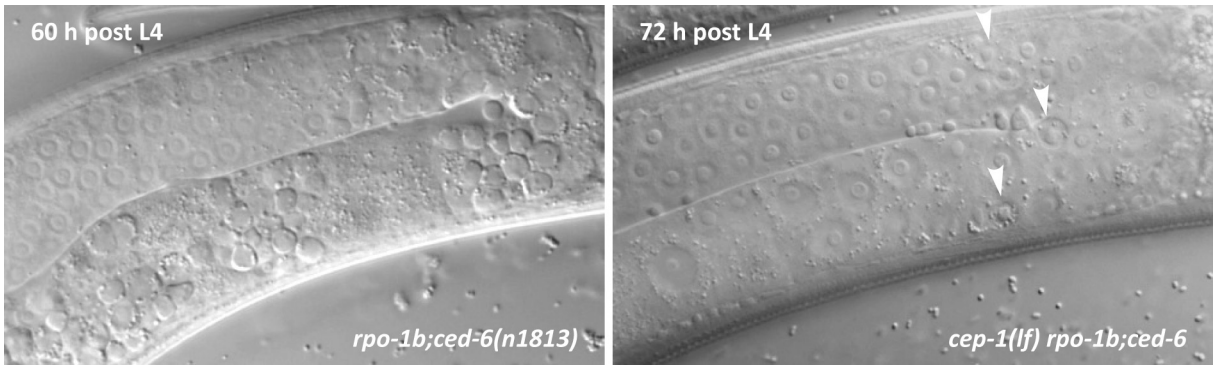

Figure 69 *cep-1(gk138)* prevents accumulation of a high number of corpses in *rpo-1b(op259); ced-6(n1813)*. Whereas the gonads of adult double mutants are loaded with corpses, only few (arrowheads) can be found in the triple mutant.

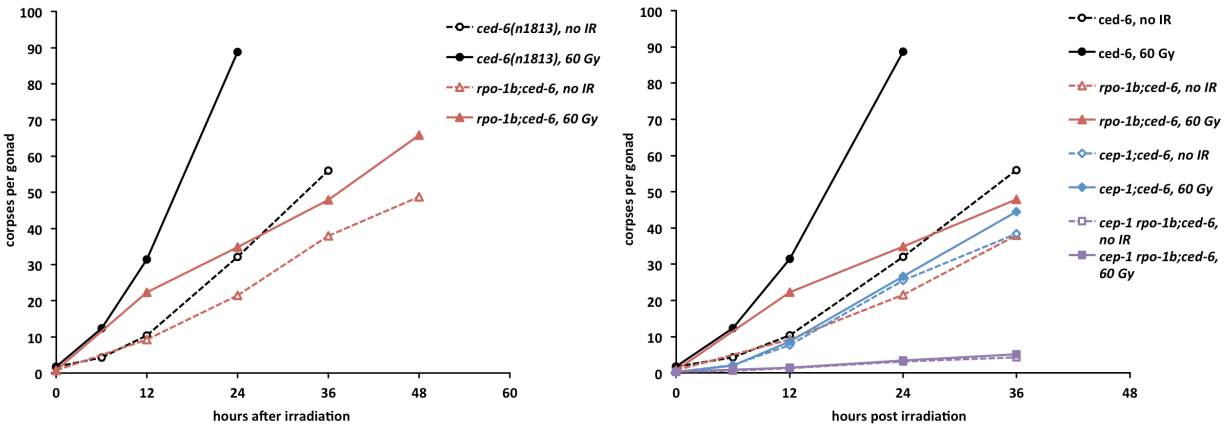

		ced-6(n1813)		*rpo-1b(op259);ced-6*		*cep-1(gk138);ced-6*		*cep-1 rpo-1b;ced-6*	
	post IR	**score**	**95% CI (n)**	**score**	**95% CI (n)**	**score**	**95% CI (n)**	**score**	**95% CI (n)**
no IR	**0 h**	1.67	±0.37 (60)	0.70	±0.55 (20)	0.23	±0.15 (40)	0.31	±0.15 (80)
	6 h	4.29	±0.82 (86)			2.17	±0.75 (36)	0.55	±0.30 (20)
	12 h	10.42	±1.11 (96)	9.29	±1.54 (83)	7.71	±0.96 (56)	1.25	±0.33 (80)
	24 h	32.10	±2.36 (60)	21.52	±1.76 (77)	25.58	±2.61 (40)	3.17	±0.44 (100)
	36 h	56.00	±3.55 (20)	38.01	±2.81 (76)	38.35	±4.17 (40)	4.25	±0.73 (60)
	48 h			48.75	±5.06 (40)				
	60 h							5.65	±1.48 (20)
60 Gy	**0 h**								
	6 h	12.32	±1.40 (56)			1.97	±0.74 (20)	0.85	±0.56 (20)
	12 h	31.41	±1.63 (76)	22.29	±4.88 (20)	8.66	±1.12 (56)	1.48	±0.63 (40)
	24 h	88.75	±6.59 (20)	34.83	±2.52 (76)	26.68	±2.67 (40)	3.47	±0.65 (60)
	36 h			47.92	±3.03 (76)	44.45	±4.33 (40)	5.05	±1.11 (40)
	48 h			65.78	±4.66 (40)				

Figure 70 Time courses of corpse accumulation in engulfment mutant background. Constitutive apoptosis of *rpo-1b(op259)* is blocked by loss of *cep-1* function. Note that an immense number of corpses are reached in irradiated *ced-6(n1813)* already at 24 hours after irradiation. Table indicates average number of apoptotic corpses per gonad, 95 % CI of the mean, and total number of animals tested per condition.

5.3.2.5 Model: *rpo-1b* and *cep-1* are mutually dependent for cell death

In combination, *rpo-1b(op259)* and *cep-1(gk138)* abolish virtually all germ cell apoptosis. One can look at this effect from several perspectives. *rpo-1b(op259)* prevents baseline apoptosis, so far termed 'physiological' cell death of *cep-1*. Normal function of *rpo-1b* is thus required for physiological levels of germ cell apoptosis in *cep-1(gk138)* and maybe in general for *C. elegans*. Turning the perspective, *cep-1(gk138)* does not only suppress the moderate levels of IR-induced death, but it eliminates any considerable cell death events in *rpo-1b(op259)* gonads. One could thus state that all germ cell apoptosis in *rpo-1b(op259)*, including "physiological" cell death, is *cep-1*-dependent; or that *rpo-1b(op259)* lost the capacity for physiological apoptosis and replaced it by *cep-1*-induced death. Overall, these observations support a model where *rpo-1b(op259)* mutants have a generally reduced responsiveness to apoptotic cues, and "physiological" cell death is almost completely abolished. For some reason, the mutants simultaneously have increased CEP-1 activity in the absence of exogenous DNA damage; this high baseline CEP-1 activity as well as the wildtype-like increase after irradiation is only weakly transponded into cell death events in *rpo-1b(op259)*.

5.3.3 Germ cell apoptosis in *rpo-1b(op259); egl-1(lf)*

Both, *cep-1* and *egl-1* loss-of-function mutants are defective for DNA damage-induced germ cell death, but they retain the capacity for 'physiological' apoptosis [see *2.1.6.2 CEP-1 and EGL-1 are central for DNA damage-induced death*]. If germ cells do not principally require EGL-1 to die, there must be alternative ways how the core apoptotic machinery can be stimulated and eventually CED-3 caspase can be activated. In *rpo-1b(op259)*, not only DNA damage-induced apoptosis but also germ cell death in non-irradiated animals is *cep-1*-dependent. This might or might not be mediated by the classical axis CEP-1→EGL-1⊣CED-9 that mediates IR-induced death; in *rpo-1b(op259)*, other pro-apoptotic factors activated by CEP-1, such as CED-13 or as yet unknown molecules, could become more obviously relevant than in wildtype worms. Also, CEP-1 itself might directly act on the core apoptotic machinery; several observations from homologs in other species suggest physical interaction of CEP-1 with mitochondria and the core apoptotic machinery, independently of its transcriptional activity (Schuler

2005). To largely exclude a mechanism that would bypass EGL-1, I tested *rpo-1b(op259); egl-1(n3082)* for apoptosis. Like *cep-1(gk138) rpo-1b(op259)*, these animals had very low baseline apoptosis and they did not respond to irradiation. Thus, germ cell death in *rpo-1b(op259)* is dependent on both *cep-1* and *egl-1*.

5.3.3.1 Model: *rpo-1b(op259)* reduces apoptosis downstream of EGL-1 expression

One could argue that the surrogate *egl-1* (and *ced-13*) transcript level does indeed represent increased CEP-1 activity in *rpo-1b(op259)*, but that it does not ascertain high EGL-1 protein levels in the cells where needed for apoptosis induction. In fact, reduced responsiveness to CEP-1 signal in irradiated and non-irradiated animals could be the result of abnormal translation of the EGL-1 message in *rpo-1b(op259)* [see discussion in *4.6.4.3 Translation in rpo-1b(op259)*]. Unfortunately, Western blot analysis to directly detect EGL-1 expression levels failed due to lack of a suitable antibody.

The argument alone, however, would not explain why baseline apoptosis is abolished as well; this is assumed to be *egl-1*-independent in wildtype and would not be expected to be reduced solely due to insufficient EGL-1 translation. It is therefore likely that *rpo-1b(op259)* affects apoptosis regulation at a step that follows downstream of EGL-1 expression.

5.3.3.2 *cep-1(gk138); egl-1(n3082)* double mutants preserve baseline apoptosis

The above argument would ensue the following consideration: *cep-1* mutants do have baseline apoptosis; *egl-1* mutants do have baseline apoptosis; does this really signify that 'physiological' germ cell death is distinct from any pro-apoptotic signalling that does involve EGL-1, such as DNA damage signalling or apoptosis induction in somatic development? Or are the mutants just not revealing involvement of *egl-1* and possibly even of *cep-1* in 'physiologic' germ cell apoptosis? CEP-1 and EGL-1 could have complementary and partially redundant function in activating physiologic germ cell death. Possibly, *cep-1* mutants express enough EGL-1 to guarantee baseline apoptosis without transcriptional activation by CEP-1. And *egl-1* mutants might activate apoptosis by compensatory binding to CED-9 of other pro-apoptotic factors like *ced-13*; or even by the hypothetical transcription-independent pro-apoptotic activity of CEP-1 (Schuler 2005). To evaluate this possibilities, I crossed a *cep-1(lf); egl-1(lf)* double mutant. These animals seemed equally healthy as both single mutants; like both single mutants, *cep-1(gk138); egl-1(n3082)* animals were defective for IR-induced apoptosis (1.80 ±0.54 corpses per gonad (n=20)), but they maintained a baseline level of constitutive apoptotic germ cell corpses (1.90 ±0.55 (n=20)). Thus, 'physiologic' germ cell death can happen in the simultaneous absence of both functional CEP-1 and EGL-1.

Conclusively, I suggest that *rpo-1b(op259)* reduces germ cell apoptosis at a level downstream of *cep-1* and of *egl-1*.

The question why *rpo-1b(op259)* mutants should have increased *cep-1* activity without exogenous DNA damage will be addressed in the following section and in the section on the *rpo-1b(op259); ced-9(n1653)* suppression screen [see *5.6.6.3 A genetic screen will help to identify activators of apoptosis*].

5.3.4 CEP-1 and EGL-1 reporter in germ cells

I considered that high CEP-1 activity in *rpo-1b(op259)* might arise from overexpression or ectopic expression of CEP-1 in the germ line. Such a difference might become apparent with the translational reporter CEP-1::GFP from the transgene *opIs198[P_{cep-1}::cep-1::gfp::cep-1 3'UTR; unc-119(+)]*. It is normally expressed in the distal tip region (i.e., mitotic zone) of the germ line and in the region of late meiotic pachytene cells and oocytes, whereas the transition zone and the early pachytene region has very weak GFP fluorescence, a pattern in agreement with immunofluorescence experiments (Schumacher 2005a). GLD-1 can bind to *cep-1* mRNA and is required to inhibit translation of *cep-1* in the germ line where appropriate; loss of normal GLD-1 function can lead to misexpression of *cep-1* in the early pachytene region at restrictive temperature settings, presumably the cause of increased apoptosis in this condition. In my experiments, the *rpo-1b(op259)* mutation had enhanced this increased apoptosis phenotype of *gld-1(op236)* and aggravated its unhealthy germ line appearance (Figure 62 and Figure 65). I tested for CEP-1::GFP expression in wildtype, in *rpo-1b(op259)*, in *gld-1(op236)* and in *gld-1(op236) rpo-1b(op259)* animals. At 20°C, *rpo-1b(op259)* had no obvious differences from wildtype in CEP-1::GFP expression levels, and the germ line expression pattern closely resembled wildtype (Figure 71).

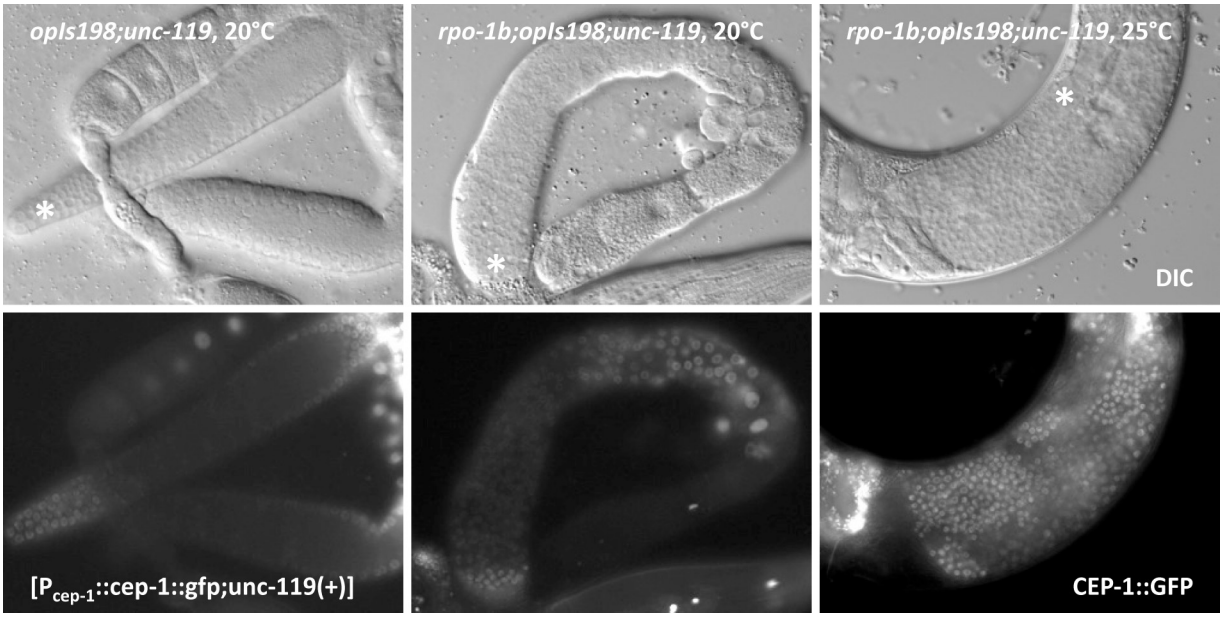

Figure 71 CEP-1::GFP has a wildtype pattern in *rpo-1b(op259)* at permissive temperature, with fluorescence in mitotic nuclei of the distal gonad (*) and in the late meiotic pachytene region as well as in oocytes. At 25°C, the proximally proliferating cells have (variably) high levels of CEP-1::GFP expression.

5.3.4.1 *gld-1(op236)* and *rpo-1b(op259)* synthetically provoke ectopic expression of CEP-1::GFP

gld-1(op236) grown at 20°C did not exhibit significant ectopic CEP-1::GFP expression, consistent with former observations (Schumacher 2005a). However, the germ lines of the double mutant *gld-1(op236) rpo-1b(op259)* often had much less restricted nuclear CEP-1::GFP with only weak differences between the mitotic and the early pachytene regions (Figure 72). The much more diffuse germ line pattern went along with disordered germ cell maturation as judged from DIC microscopy and

from DAPI staining: the borders between the zones were much less distinct; there was no clear transition zone and only a short stretch of meiotic pachytene cells. The effect could be significantly enhanced with IR irradiation. Thus, *rpo-1b(op259)* itself had no strongly increased or ectopic CEP-1 expression, but it enhanced the effects of *gld-1(op236)*. The high CEP-1::GFP protein levels correlate with the high CEP-1 activity in the double mutant as assessed by EGL-1 and CED-13 transcript levels. Again, it is not clear whether *rpo-1b(op259)* further increases CEP-1 protein levels of *gld-1(op236)* germ cells, which could then lead to abnormal germ cell maturation and excessive apoptosis; or whether *rpo-1b(op259)* and *gld-1(op236)* synthetically evoke a germ cell maturation defect that does not primarily involve *cep-1*. In this case, ectopic CEP-1::GFP expression could be the result of spatially disorganised germ cell maturation and not directly of regulation by *rpo-1b(op259)* and *gld-1(op236)*. I wonder whether this could not also be the case for CEP-1::GFP in the *gld-1(null)* mutant background, which has abnormal germ cell progression (Schumacher 2005a).

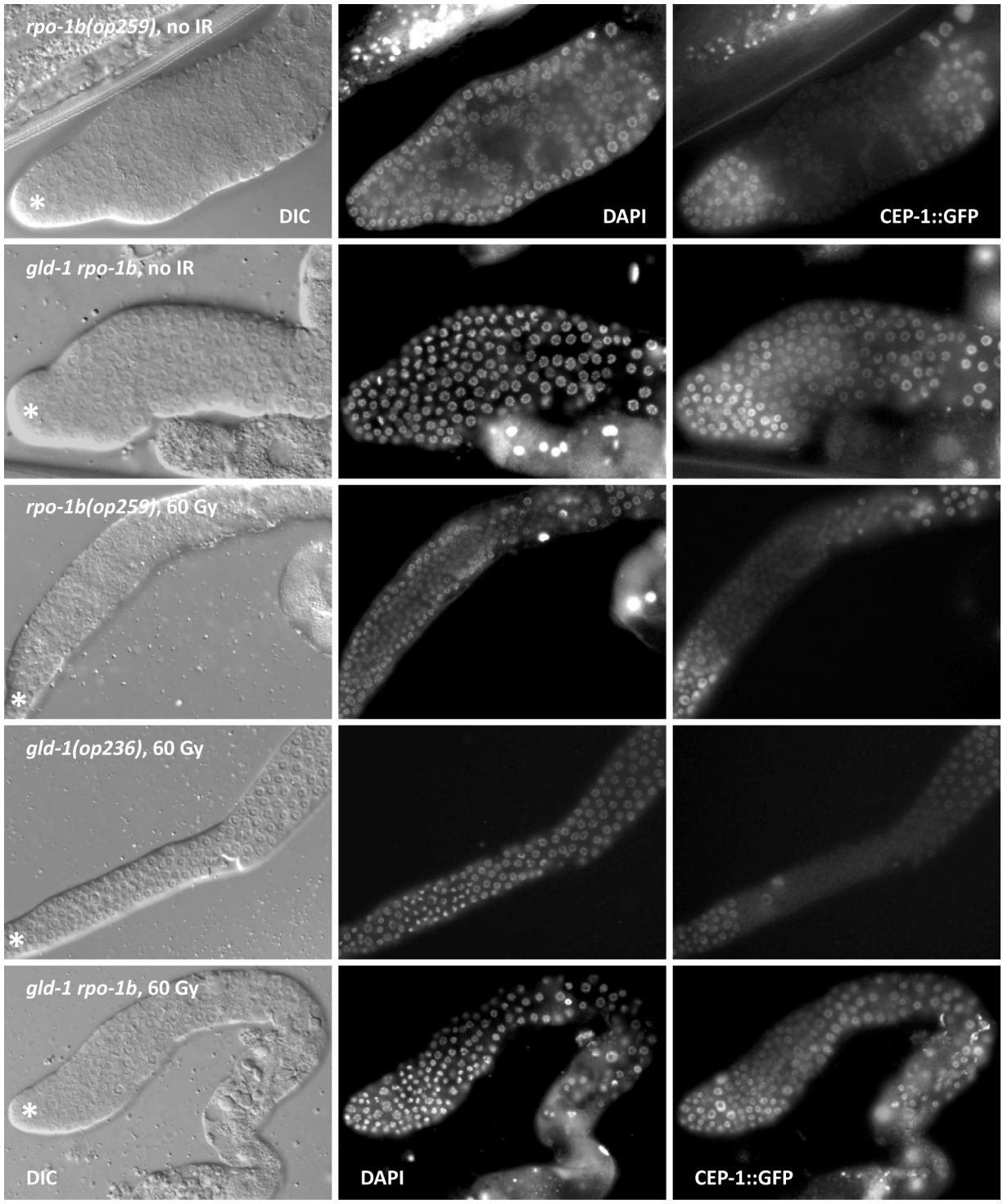

Figure 72 High ectopic CEP-1::GFP expression in non-irradiated and irradiated *gld-1(op236) rpo-1b(op259)* germ lines. Gonads extruded from adult worms grown at 20°C, 24 hours post irradiation. * indicates distal tip with mitotic region.

5.3.4.2 A transcriptional EGL-1 reporter shows altered expression pattern in *rpo-1b(op259)*

I tested the transcriptional EGL-1 reporter *opIs56[P_{egl-1}::2xNLS::gfp::egl-1 3'UTR; unc-119(+)]* in *rpo-1b(op259)* mutant. In the late meiotic pachytene region, the signal was weaker in *rpo-1b(op259)* than in wildtype animals. (The signal was generally weak in the meiotic region and did not clearly increase upon irradiation of wildtype animals. *cep-1(lf)* did not abolish the signal.) Surprisingly, I detected high expression in the distal mitotic region of *rpo-1b(op259)* gonads upon irradiation

(Figure 74), which I did not see in wildtype background. The reporter construct with only a relatively short 3'UTR for *egl-1* does not ascertain to represent the very physiological pattern of EGL-1 expression, and it has the usual limitations of a transcriptional reporter. I have not yet confirmed the finding with an independent method.

To see whether the high ectopic CEP-1 levels in *gld-1(op236) rpo-1b(op259)* would possibly be paralleled by EGL-1 induction, I tested the transcriptional reporter in this double mutant background. Irradiated *gld-1(op236)* had a similar pattern like wildtype. In contrast, irradiated *gld-1(op236) rpo-1b(op259)* had strong and ubiquitous expression in the germ line (Figure 73). Again, germ cell maturation as judged by chromatin staining was highly abnormal. Expression was also increased in meiotic pachytene cells of non-irradiated animals.

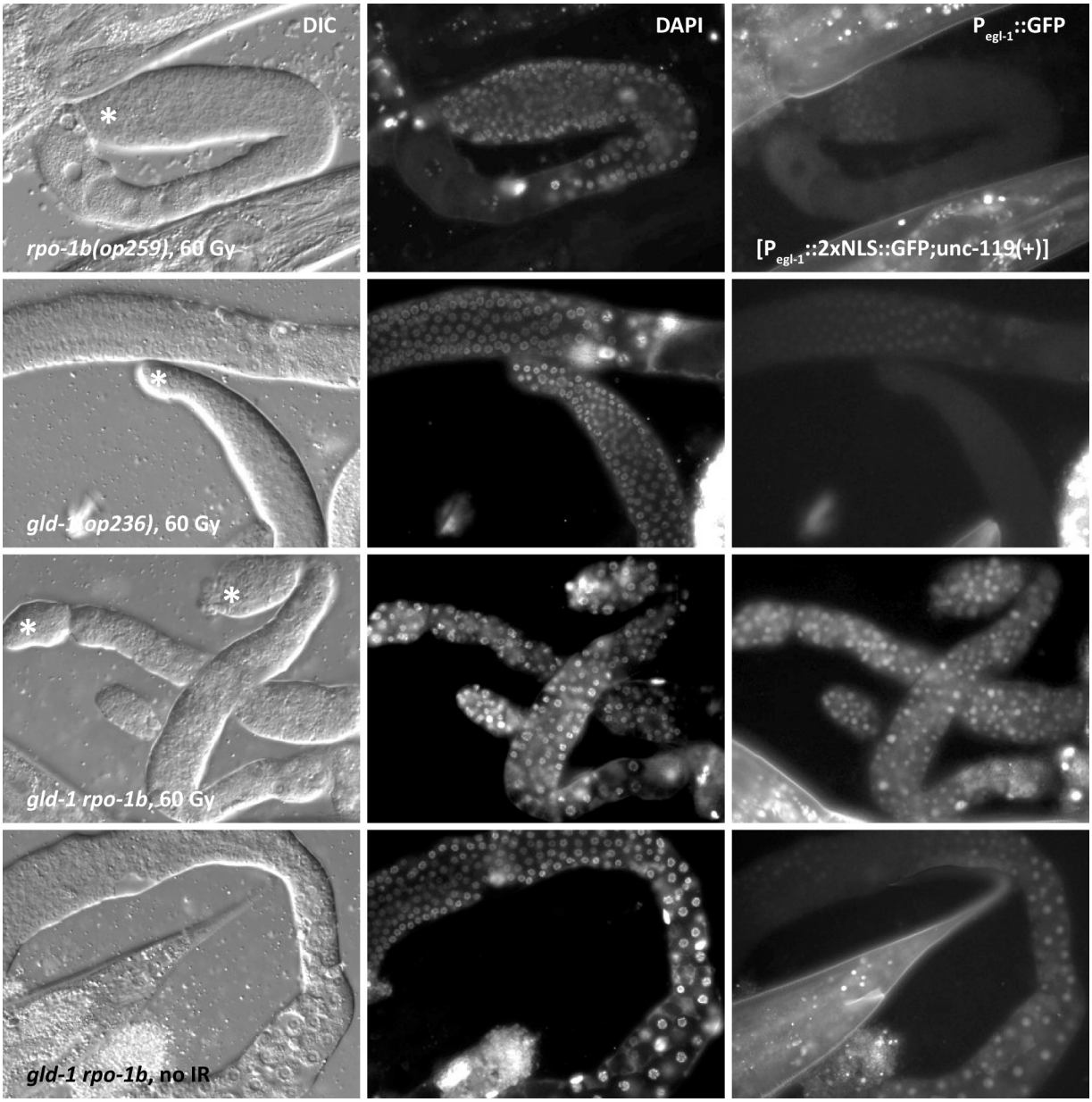

Figure 73 Ectopic expression of a transcriptional reporter for EGL-1 in *gld-1(op236) rpo-1b(op259)*. The effect is enhanced at 24 hours post irradiation. (*) distal gonad region.

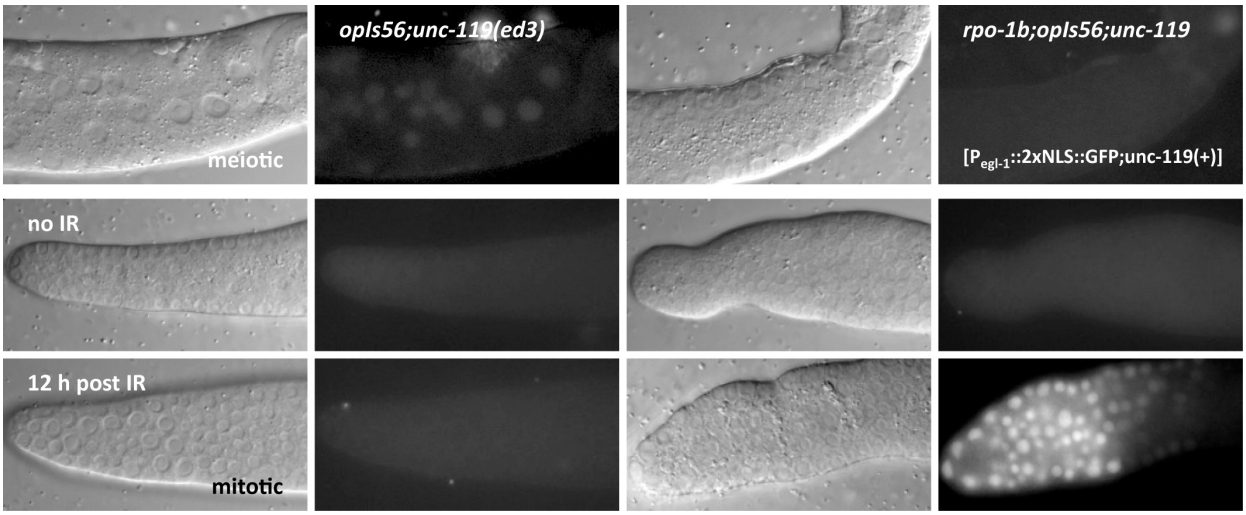

Figure 74 In the meiotic pachytene region, EGL-1 expression is lower than wildtype in *rpo-1b(op259)*. Conversely, there is a strong increase of fluorescence in the mitotic region of *rpo-1b(op259)*. The observations in wildtype – no significant change neither in mitotic nor in meiotic region upon irradiation – contrast with previous reports on this reporter transgene.

5.3.4.3 CEP-1::GFP localises to nucleolar substructure

The CEP-1::GFP reporter revealed an interesting difference when comparing *rpo-1b(op259)* to wildtype worms at a subcellular level. A high proportion of meiotic pachytene cells in *rpo-1b(op259); opIs198* gonads had a focal GFP fluorescence in the nucleoli. These dots corresponded to a nucleolar body seen in DIC images. We had observed that these nucleolar substructures were often enlarged in germ cells of the late meiotic pachytene region of *rpo-1b(op259)* mutants; conversely, mitotic cells in the distal region of irradiated *rpo-1b(op259)* worms had less of these structures than the corresponding wildtype. This was intriguing considering the role of *rpo-1b(op259)* for nucleolar structure on one hand, and the mechanisms that were suggested for the regulation of CEP-1 by nucleolar integrity (Rubbi 2003a) on the other hand.

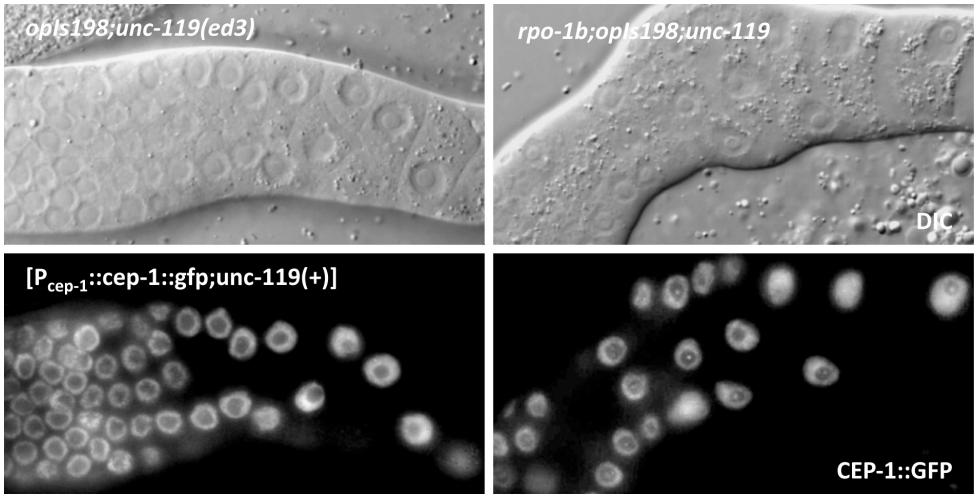

Figure 75 CEP-1::GFP-positive nucleolar dots in meiotic pachytene cells and oocytes are pronounced in *rpo-1b(op259)* germ lines.

Nucleolar substructures are larger in pachytene cells of *rpo-1b(op259)*

I counted the fraction of germ cells in the CEP-1::GFP-positive compartment of meiotic pachytene that had a GFP-positive nucleolar dot, with or without irradiation (Figure 75). Clearly, *rpo-1b(op259)* germ cells had more and often larger CEP-1 positive dots than wildtype (Figure 77). There was no significant difference between irradiated and non-irradiated worms, neither in wildtype nor in *rpo-1b(op259)* mutant worms.

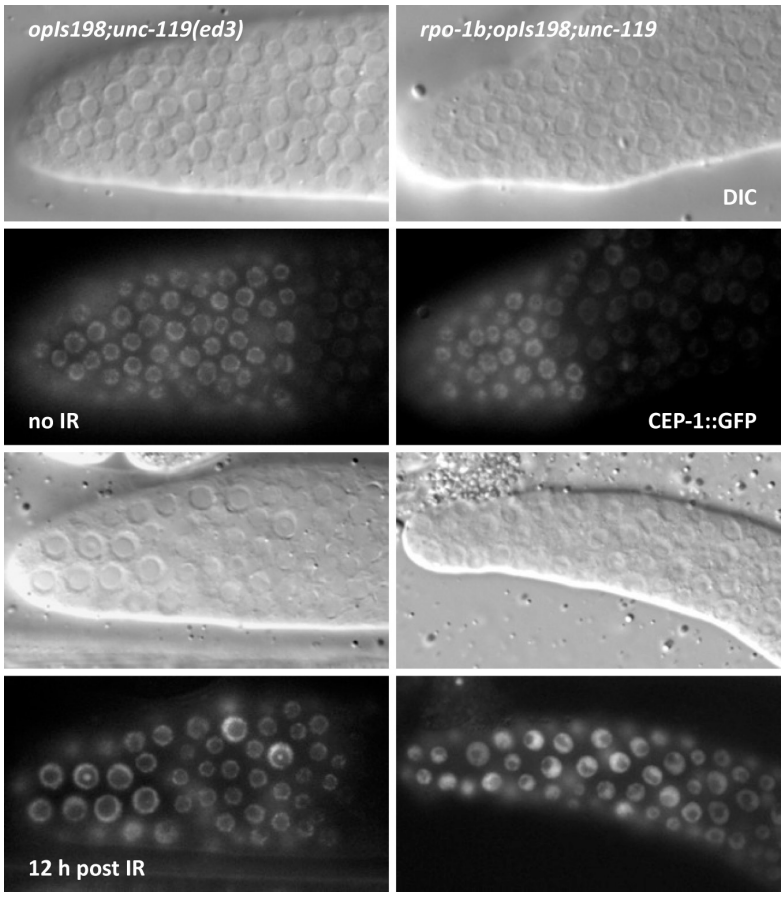

Figure 76 CEP-1::GFP-positive nucleolar dots become prominent in mitotic germ cells upon irradiation, but are not apparent in *rpo-1b(op259)*.

Nucleolar dots increase upon IR in wildtype mitotic cells but not clearly in *rpo-1b(op259)*

I also assessed the percentage of mitotic cells with a CEP-1::GFP nucleolar substructure. Without irradiation, *rpo-1b(op259)* and wildtype gonads had equally low numbers. After irradiation, the fraction increased in wildtype, but remained low in *rpo-1b(op259)* (Figure 77). The nucleolar dots were strongly associated with mitotic cells that were enlarged due to the cell cycle arrest in response to DNA damage (Figure 76). The difference between *rpo-1b(op259)* and wildtype cannot mainly be explained by a reduced fraction of enlarged cells in *rpo-1b(op259)*. In fact, these cells often had a small nucleolus in an enlarged nucleus, imposing as a small blank in a large GFP fluorescent area, whereas in wildtype, arrested cells had large nuclei and large nucleoli with large nucleolar substructures. In mitotic cells of *rpo-1b(op259)*, the nucleoli thus do not respond to irradiation in a wildtype manner; they do not increase their volume and they often do not develop a visible nucleolar dot. It is interesting that this does happen in wildtype. The nucleoli could be enlarging due to increased rRNA synthesis or decelerated ribosomal

maturation upon DNA damage; growth of the nucleoli might entail the growth of nucleolar substructures. Alternatively, the nucleolar substructures could be growing as part of the DNA damage repair or cell cycle arrest response and thus be driving the expansion of the nucleoli. In the meiotic region, cells did not show a significant increase of nucleolar dot number upon IR; concurrently, there was no significant increase in nucleolar size. If appearance or enlargement of the nucleolar substructures were part of a general DNA damage response independently of the cell cycle stage, one would expect an increase of their size and number in meiotic cells as well. Possibly, such an increase subtly happens in early meiotic pachytene cells before they start expressing CEP-1::GFP and can be assessed by presence of GFP-positive nucleolar foci.

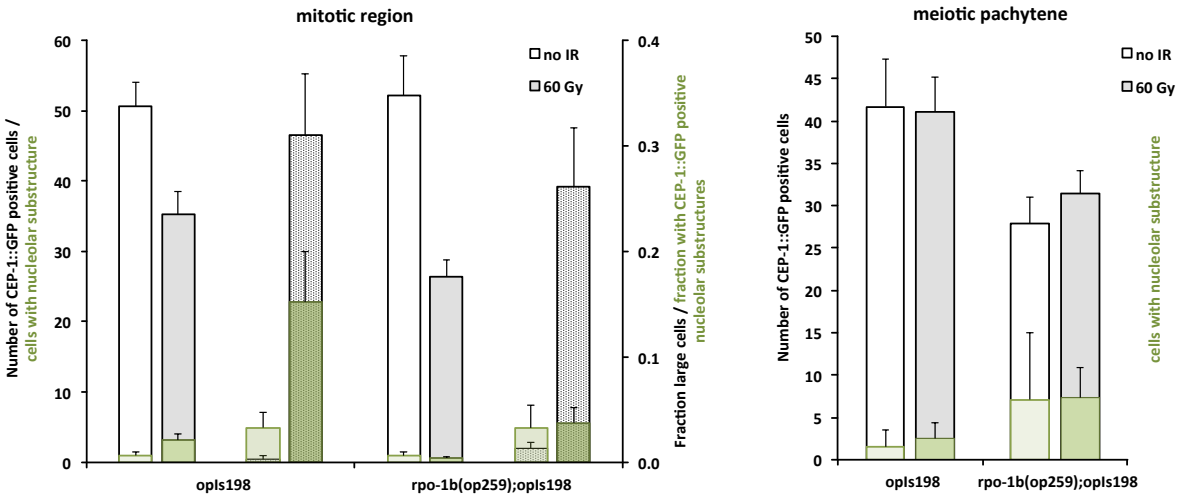

Figure 77 Mitotic region: less dots upon IR in *rpo-1b(op259)* mutant, which is not due to a reduced cell number or a reduced fraction of enlarged cells. Number of CEP-1-positive cells and number of nucleolar substructures per gonad (left bars); fraction of enlarged mitotic cells and fraction of mitotic cells with nucleolar substructures (right bars). Meiotic pachytene: more nucleolar dots in *rpo-1b(op259)* mutants, no irradiation response. Nuclei were counted in dissected gonads; error bars represent 95 % CI of the mean.

Is CEP-1 a regulator of nucleolar dots?

Could these nucleolar dots be a result of altered CEP-1 activity? And might numerical and structural changes in *rpo-1b(op259)* represent adjustments of RNA pol I regulation by CEP-1? In *cep-1(gk138)* mutants, I could detect nucleolar dots similar to wildtype (by DIC), which indicated that their formation is not dependent on CEP-1 (*cep-1* is arguably not required for the cell cycle arrest response). Further, *cep-1(gk138)* did not abolish the increased size of nucleolar dots in meiotic cells of *rpo-1b(op259)* mutants, either; thus, the size of these dots is unlikely to be subject to CEP-1.

Are nucleolar dots the sites of RNA pol I regulation by CEP-1?

Activated p53 has been shown to repress RNA pol I transcription by directly interfering with the assembly of a competent transcriptional machinery on the rRNA promoter, by disrupting the interaction of UBF with SL1 [(Zhai 2000), see *4.1.3 Control of rRNA and ribosome synthesis by regulatory pathways*]. I have not been able to identify homologs of the RNA pol I auxiliary factors SL1 and UBF in *C. elegans*. Nevertheless, one idea to consider here was that CEP-1 could be regulating RNA pol I from within the nucleolar dots and that aberrations in these structures would cause misregulation, which might explain

some of the phenotypes of *rpo-1b(op259)*. I had found YFP::RPO-1B not to localise to the whole nucleolus but to patches within the nucleoli that often showed confluence to a ring around a central hollow; the site where a nucleolar dot was usually apparent by DIC (Figure 78). YFP::RPO-1B, presumably as part of the RNA pol I complex on ribosomal DNA, thus spared the nucleolar substructures, the sites of focal CEP-1::GFP. Therefore, the nucleolar compartment is unlikely to be the site of direct regulation of RNA pol I by CEP-1.

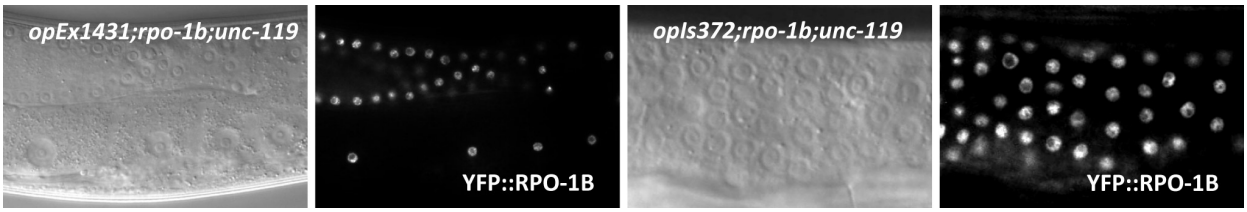

Figure 78 Nucleolar dots are spared by YFP::RPO-1B. Apoptotic region of two transgenic lines expressing tagged wildtype RPO-1B; *opEx1431[P_{hus-1}::yfp::rpo-1b (genomic)::rpo-1b 3'UTR; unc-119(+)]* (including oocytic nucleoli) and *opIs372[P_{rpo-1b}::yfp::rpo-1b (genomic)::rpo-1b 3'UTR; unc-119(+)]* (higher magnification).

5.3.5 The nucleolar cavities

What are these nucleolar bodies? They appear as round, mostly central structures by DIC; they occur within germ cell nucleoli and can also be seen in other cells with large nucleoli, like intestinal or hypodermal cells. Sometimes, within these bodies, there is a further, mobile substructure resembling a pinball. In germ cells, the nucleolar CEP-1::GFP foci precisely colocalise with these bodies. Various reporters of other proteins have a similar, target-like nuclear pattern; we have seen nucleolar foci for instance with RPA-1, TYR-2, CED-3 or phosphorylated MPK-1 markers. YFP::RPO-1B in the nucleoli, presumably as part of the RNA pol I complex on ribosomal DNA, spared these nucleolar substructures.

Are these structures relevant for the core function of nucleoli, the synthesis of ribosomal RNA? Or are they important interfaces for nuclear and nucleolar factors in the regulation of stress responses? Or do they represent mere speckles of entrapped nucleoplasm that do not have any functional relevance?

Interestingly, recent publications described similar structures in the nucleoli of mammalian cells. They contained p53 and other stress response factors and they were responsive to proteasome inhibiting drugs (Latonen 2011; Karni-Schmidt 2008). In agreement with my observations described above, p53 was shown to localise to intranucleolar regions that were distinct from the sites of ribosome production (Krüger 2010).

Theoretically, the nucleolar substructures in the *C. elegans* germ line could be important for CEP-1 activity regulation. The mitotic region of *rpo-1b(op259)* has increased *egl-1* expression upon irradiation, at reduced size/number of the nucleolar dots. In the meiotic pachytene (irradiated or non-irradiated), it is the inverse. The compartments could be retaining CEP-1 from activation, by mechanisms that are discussed in [*4.1.4.1 p53 is activated by nucleolar pathways*]

5.3.5.1 Electron microscopy indicates indenting nucleoplasm

I looked at electron microscopy images of germ cell cross-sections to find a possible correlate of the dots seen by DIC microscopy. Indeed, some of the wildtype germ cell nucleoli had contiguous areas of

lower density, often towards the centre. However, on occasional sections, these areas seemed confluent with the nucleoplasm (Figure 79). I therefore think that the central dot-like structures seen by DIC are in fact nucleolar compartments that are communicating with the nucleoplasm.

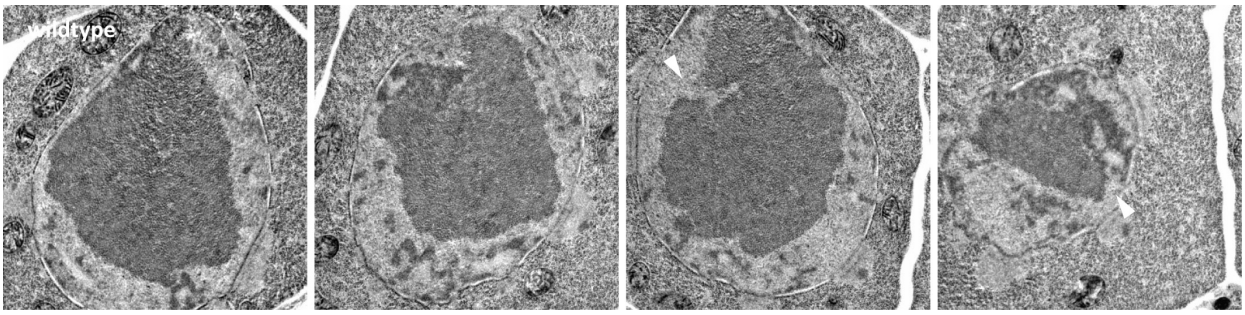

Figure 79 Electron microscopy pictures of meiotic germ cell nuclei in wildtype show different degrees of indentations (arrowhead) into the nucleoli that are of the density of the nucleoplasm.

5.3.6 Conclusions on *rpo-1b(op259)* and CEP-1

The p53 group of proteins in mammals, homologous to CEP-1, play key roles in cell cycle regulation and cell death induction in response to DNA damage. Mutation or misregulation of p53 has been found to be one of the most frequent causative factors of tumor growth and progression. In the last decade, several studies have highlighted the role of various nucleolar factors in the regulation of p53 activity. Less is known about the regulation of this central tumor suppressor in *C. elegans* and very few links have been made to the nucleolus. My data show that CEP-1 is critical for germ cell death in the mutant of RNA pol I both in the presence or absence of exogenous DNA damage. On the other hand, RPO-1B is required for CEP-1 to effectively induce apoptosis. CEP-1 activity overall seems to be increased in *rpo-1b(op259)* mutants. Concomitantly, we see differences between *rpo-1b(op259)* and wildtype gonads in nucleolar substructures that become particularly apparent in the mitotic region after irradiation; CEP-1 localises to these substructures. Intriguingly, EGL-1 expression as an indicator of CEP-1 activity is increased in the mitotic region of the *rpo-1b(op259)* germ line. It seems an attractive hypothesis that *rpo-1b(op259)* affects nucleolar structure and function and thereby modulates CEP-1 activation, similarly to p53 regulation in mammalian cells. I think that the interconnection of RNA pol I and CEP-1 in apoptosis regulation can become highly relevant in tumor progression, where abnormal rRNA synthesis and p53 mutations are likely to occur simultaneously, and in tumor treatment. My data show minute apoptosis levels in double mutants of *cep-1(lf) rpo-1b(op259)*, both without and with exogenous DNA damage.

	constitutive apoptosis		irradiation response (ΔIR)		post irradiation levels	
	(+)	*rpo-1b(op259)*	(+)	*rpo-1b(op259)*	(+)	*rpo-1b(op259)*
wt	→	(↓)	→	↓	↑	→
cep-1(lf)	(↓)	↓↓	×	×	(↓)	↓↓
egl-1(lf)	(↓)	↓↓	×	×	(↓)	↓↓
gld-1(rf)	→	↑	↑	↑↑	↑↑	↑↑↑

Table 10 Summary of the effect *rpo-1b(op259)* has in mutants of central factors of DNA damage-induced germ cell apoptosis. Levels of apoptotic cell corpses in non-irradiated worms are indicated as increased ↑, or reduced ↓ in comparison to wildtype levels →. ΔIR indicates the incremental effect of irradiation on apoptosis levels, in relation to the effect in wildtype animals →; mutants with *cep-1(lf)* or *egl-1(lf)* show no change after irradiation ×. The post-irradiation levels are again in relation to the levels in non-irradiated wildtype animals. *cep-1(lf)* and *egl-1(lf)* had slightly lower levels than wildtype in my experiments (↓).

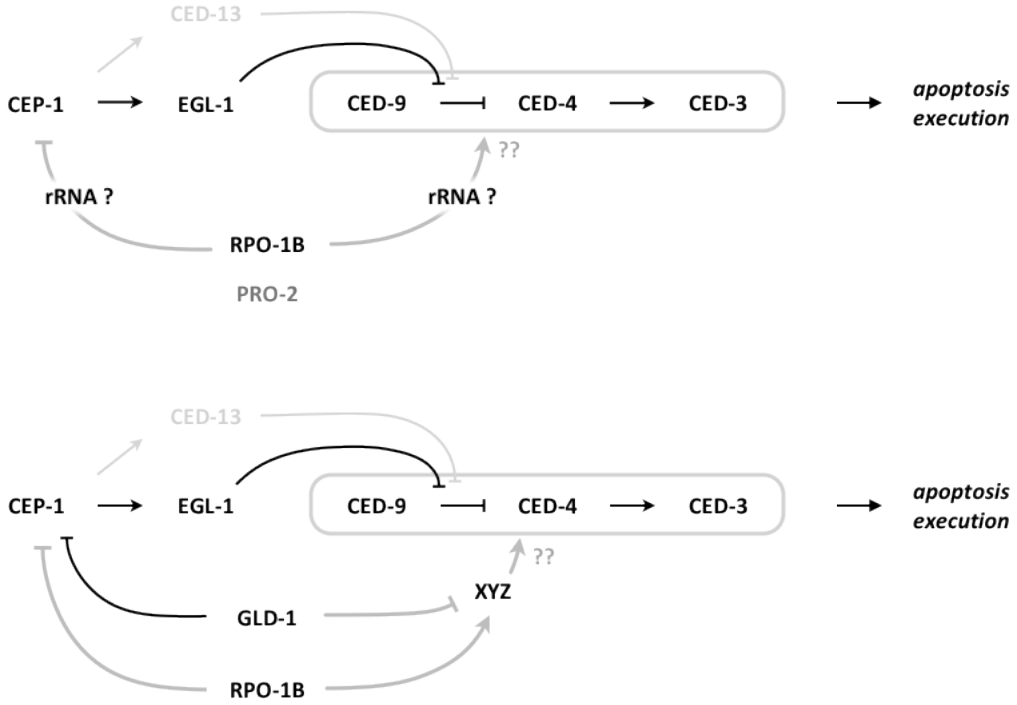

Figure 80 Model for the genetic interaction of RPO-1B with CEP-1. CEP-1 activity is increased in *rpo-1b(op259)*, but this does not result in increased germ cell apoptosis; rather, apoptosis is reduced. RPO-1B likely has a permissive effect on apoptosis at the level of the core apoptotic machinery (the precise level of action is not defined, indicated by ??) downstream of EGL-1 expression. Possibly, the modulatory effect of RPO-1B on apoptosis is via rRNA synthesis, as mutation of the rRNA processing factor *pro-2* leads to very similar phenotypes as *rpo-1b(op259)*. GLD-1, a known inhibitor of CEP-1, likely has other inhibitory effects on the cell death cascade downstream of EGL-1, as the synthetic effect of *gld-1(rf)* with *rpo-1b(op259)* suggest, a constellation in which *rpo-1b(op259)* enhances cell death. This could be via a hypothetical factor XYZ on which both RPO-1B and GLD-1 act. Reduction of normal pro-apoptotic XYZ activity by *rpo-1b(op259)* would be compensated for by *gld-1(rf)*, and increased CEP-1 activity could effectively lead to increased cell death. Black lines indicate established links. CED-13 is thought to play a minor role in germ cell apoptosis and is weakly shaded in this figure and in subsequent figures. The other grey arrows stand for novel, partly hypothetical links.

5.4 Cell death and cell removal in the germ line and in the soma

5.4.1 Developmental cell death in embryos / L1 larvae

The above experiments demonstrate that *rpo-1b(op259)* affects various aspects of germ cell death and that it likely acts on core aspects of the apoptotic program. I tested whether *rpo-1b(op259)* also influenced apoptosis of somatic cells. I used two systems to assess developmental cell death occurring at a late embryonic/early larval stage.

5.4.1.1 *rpo-1b(op259)* animals have less corpses in L1 heads

Mutants of genes required for engulfment of apoptotic cells accumulate non-removed corpses in the heads of L1 stage larvae. This becomes a sensitive tool to detect conditions with reduced pro-apoptotic capacity. *ced-6(n1813)* mutants have approximately 20 non-removed corpses shortly after hatching. I scored the heads of *rpo-1b(op259); ced-6(n1813)* animals: the number of apoptotic corpses was reduced to 13 per animal on average (Figure 81). This clearly demonstrated an effect of *rpo-1b(op259)* on somatic apoptosis.

Possibly, *rpo-1b(op259)* reduced cell death per se; alternatively, the reduced number of corpses could be an effect of improved engulfment (e.g., release from negative regulation); a further alternative was that *rpo-1b(op259)* modulated the kinetics of cell death or of engulfment. So far, I have not distinguished between these possibilities in embryos / young larvae.

5.4.1.2 Developmental cell death in *rpo-1b(op259)* does not depend on *cep-1*

In the germ line, combining *rpo-1b(op259)* with *cep-1(lf)* abolished apoptosis almost completely. Even in the *ced-6(n1813)* engulfment mutant background, very few corpses accumulated. I showed that baseline germ cell death, which in wildtype worms does not depend on CEP-1, required functional CEP-1 activity in *rpo-1b(op259)*. Like physiologic germ cell death, somatic cell death had been assumed not to depend on CEP-1. The experiment described in *5.6.8 CEP-1 and CED-9 in developmental cell death* shows that at least in certain genetic constellations, *cep-1* is involved in somatic death. I scored corpse accumulation in L1 heads of *cep-1(gk138) rpo-1b(op259); ced-6(n1813)* to test whether *cep-1(gk138)* and *rpo-1b(op259)* also blocked apoptosis synthetically in this system. First, *cep-1(gk138); ced-6(n1813)* had very similar levels as *ced-6(n1813)*, in agreement with the notion that CEP-1 is not obviously required for developmental death (Figure 81). Also, the cell corpse number of *cep-1(gk138) rpo-1b(op259); ced-6(n1813)* was not different from *rpo-1b(op259); ced-6(n1813)*. Somatic cell death in *rpo-1b(op259)* thus did not become dependent on CEP-1.

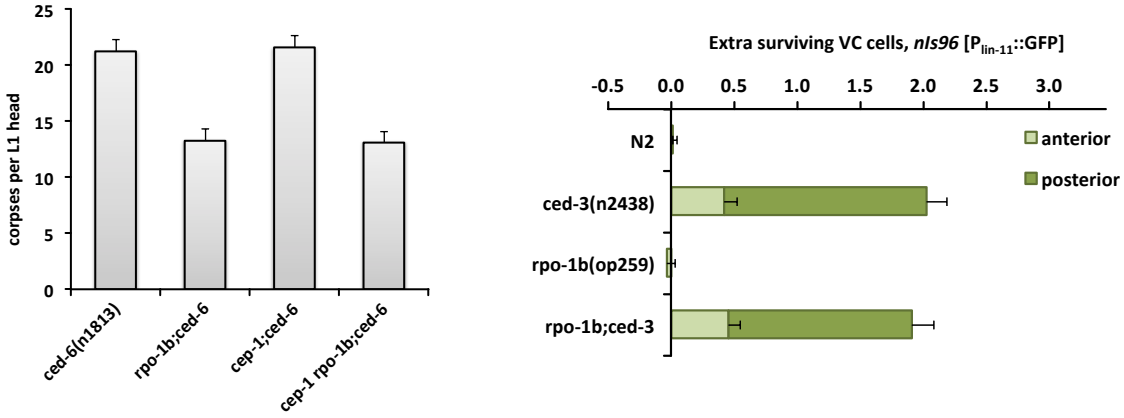

Figure 81 *rpo-1b(op259)* has less corpses accumulating in the heads of L1 stage larvae. The remaining death is not dependent on *cep-1*. Normal number of extra surviving neurons in the ventral cord does not support reduced death. In the Ventral Cord system, the number of GFP positive cells is counted that exceeds the 6 cells normally destined to survive, anterior (maximal 2) or posterior (maximal 4) to the vulva. Error bars represent 95 % CI of the mean.

5.4.2 Developmental death in ventral cord Pn.aap cells

This assay, used to demonstrate the final rather than a transitory state of somatic death during development, will be presented in *5.6.7 ced-9(n1653) in developmental cell death*. It did not show a significant difference of extra surviving cells between *ced-3(n2438)* and *rpo-1b(op259); ced-3(n2438)* (Figure 81); this would speak for different kinetics in cell death and removal rather than reduced apoptosis in the course of development. However, the experiments showed a clear rise in the number of extra cells when comparing *rpo-1b(op259); ced-9(n1653); ced-3(n2438)* with *ced-9(n1653); ced-3(n2438)* (Figure 103). At least in that condition, *rpo-1b(op259)* mutants seem to lack some pro-apoptotic component.

5.4.3 Engulfment pathways in *rpo-1b(op259)*

Different kinetics of cell death and removal could be contributory to the low corpse number in *rpo-1b(op259)* germ lines. Theoretically, the number of apoptotic events could be normal – or, as high CEP-1 activity and increased corpse numbers in the *ced-9(n1653)*, *gld-1(op236)* or *lip-1(zh15)* background would suggest, even increased in *rpo-1b(op259)*. Accelerated removal and degradation of apoptotic cells might decrease the steady state level of dying cells. Also, there could be morphological alterations in apoptotic corpses of *rpo-1b(op259)* that concealed them from identification by phase contrast microscopy.

5.4.3.1 IR-induced apoptosis in *rpo-1b(op259); ced-6(n1813)* is reduced

Analysis of *rpo-1b(op259)* in the *ced-6(n1813)* mutant background indicated that the corpse number relative to the *rpo-1b(+)* control was not significantly higher when engulfment was blocked, and the increase upon IR was, in comparison to the overwhelming response in the wildtype control, very moderate (Figure 70). More corpses would be expected if *rpo-1b(op259)* had more cell death or normal IR response, unless *rpo-1b(op259)* had an enhancing effect on engulfment that would still be at work in

the *ced-6(n1813)* mutant (e.g., by a mechanism involving an alternative branch of engulfment signalling, see *2.1.8 Engulfment of apoptotic cells*).

5.4.3.2 CED-1::GFP and Actin::YFP halos highlight dying cells

To get a better idea how *rpo-1b(op259)* affected death and removal of germ cells, I used two fluorescent markers that were expressed in the gonad sheath cells and highlighted apoptotic corpses idling at certain stages of engulfment. *bcIs39[P_{lim-7}::ced-1::gfp; lin-15(+)]* encodes a transgenic CED-1::GFP expressed under the sheath cell specific P_{lim-7} promoter; CED-1::GFP clusters at membranes that contact apoptotic cells early during corpse recognition and highlights dying cells with a fluorescent halo. *opIs110[P_{lim-7}::act-5::yfp; unc-119(+)]* codes for Actin::YFP, also under the sheath cell specific promoter; as a central component of cytoplasmic restructuring and of incorporation of the dying into the engulfing cell, tagged Actin becomes visible as ring-like fluorescence around apoptotic corpses (Figure 82).

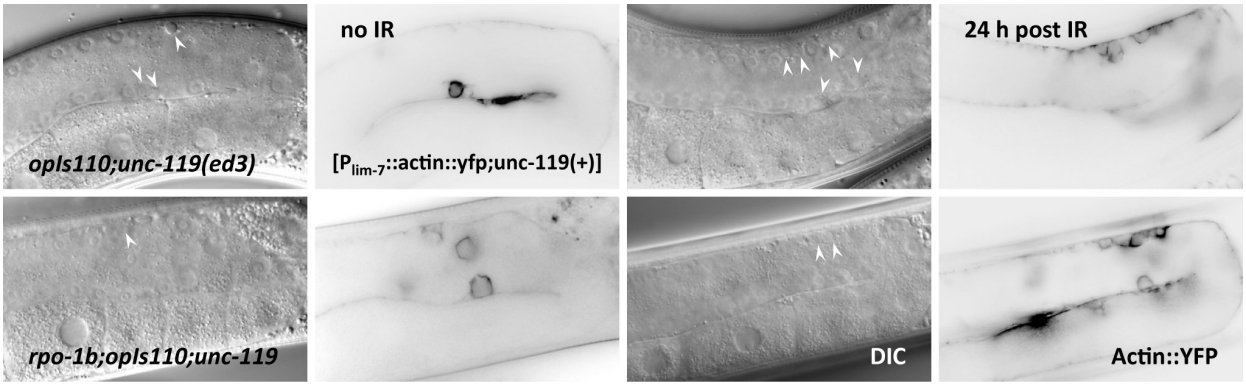

Figure 82 Actin::YFP-halos (*opIs110[P_{lim-7}::act-5::yfp; unc-119(+)]*) in *rpo-1b(op259)* are more numerous than corpses visible by DIC (arrowheads).

CED-1::GFP highlights less apoptotic cells in *rpo-1b(op259)*

rpo-1b(op259); bcIs39 had less apoptotic germ cell corpses by DIC than the strain *bcIs39*, with or without irradiation (Figure 83); the number of GFP-halos was also lower in *rpo-1b(op259)* than in wildtype. The ratio of halos per gonad to DIC corpses per gonad was comparable. Consistently, these counts indicated a decrease in the number of dying cells rather than enhanced engulfment. This is in agreement with the notion of reduced cell death in *rpo-1b(op259)* mutants.

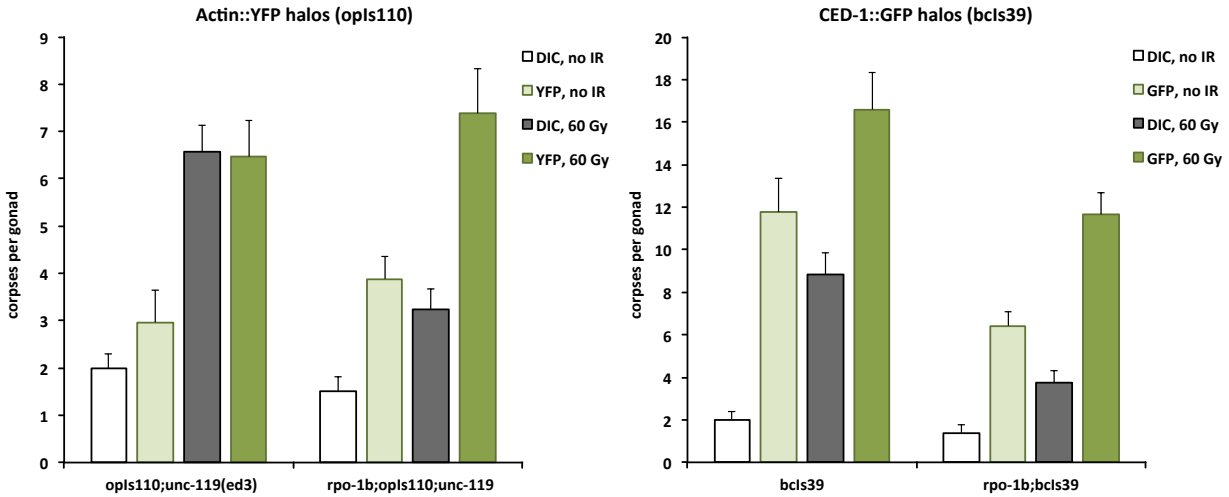

Figure 83 Halo numbers of Actin::YFP or CED-1::GFP in *rpo-1b(op259)* are divergent. Number of corpses were scored by DIC or by fluorescent halos (scored independently, not necessarily on the same individuals). Heterozygosity for *unc-119(ed3)* has not been excluded in *rpo-1b(op259); opIs110*. Error bars represent 95 % CI of the mean.

opIs110 highlights more corpses in *rpo-1b(op259)* but might be erroneous

Actin::YFP was divergent. Again, *rpo-1b(op259); opIs110* had less corpses than the control strain judged by DIC imaging. However, the number of Actin::YFP halos was very similar between the two (Figure 83). Thus, relatively more cells had an Actin::YFP wrapping in *rpo-1b(op259)*. At first sight, this could indicate that the number of apoptotic cells is underestimated by DIC in *rpo-1b(op259)*. During our studies of the role of *unc-119*, we would learn, however, that any results from the transgenic reporter *opIs110* should be interpreted with restraint [see *6.2.2.7 Actin cytoskeleton in engulfing sheath cells is influenced by unc-119*]; the counts may be confounded by the background combination of *unc-119(ed3)* and *unc-119(tg+)* on the *opIs110* transgene construct. (The control strain in this experiment was *opIs110; unc-119(ed3)* from which I had derived the cross-progeny with *rpo-1b(op259)*; we later realised that *opIs110* animals have very different numbers of YFP-halos than *opIs110; unc-119(ed3)* (Figure 120).)

5.4.4 Morphology of apoptotic cells

Germ cell corpses in *rpo-1b(op259)* often have an abnormal appearance by DIC microscopy, that is, not the classical aspect of refractile discs. That these corpses are indeed apoptotic cells is evidenced by the defining feature that they are suppressible by *ced-3(lf)* (Figure 66). The corpses in *rpo-1b(op259)* are often larger than in wildtype, more granular, and they often retain what imposes like the nucleolus. This deviation from wildtype corpses increased in situations of enhanced apoptosis like in the *rpo-1b(op259); ced-9(n1653)* double (Figure 98); or it became very prominent in combination with mutants that do themselves alter the aspect of apoptotic germ cell corpses. These mutants such as *gld-1(op236)*, *lip-1(zh15)*, *gla-1(RNAi)* or *gla-3(RNAi)* sometimes have large corpses especially after irradiation, when the number of apoptotic cells rises dramatically. Also, the corpses in association with distal islets were often enlarged and not as unruffled as classical corpses (Figure 49). The obvious morphological deviation might result from differences or failure in the execution of cellular demise

and/or from differences of engulfment and degradation processes in the engulfing gonadal sheath cells. Interestingly, the aspect of corpses in the engulfment mutant *rpo-1b(op259); ced-6(n1813)* was not very different from *ced-6(n1813)* or wildtype, despite the high number. Whether this means that corpse morphology becomes symptomatic downstream of the initial steps of engulfment remains unanswered.

The seemingly altered kinetics of nuclear and nucleolar breakdown might be a result of aberrant rRNA synthesis and nucleolar composition and could be in connection with the presumable role of nucleolar disruption in cellular stress responses, which is discussed in *4.1.4 Control of cell fate by the nucleolus and ribosomes*.

5.4.5 The core apoptotic factors in *rpo-1b(op259)* mutants

5.4.5.1 Transcript levels of *ced-9* are slightly reduced in *rpo-1b(op259)*

Given that *rpo-1b(op259)* seemed to modulate apoptosis induction downstream of *egl-1*, I considered that altered expression of core apoptotic genes might underlie the apoptotic germ cell defects. Some instances have been described where apoptosis correlated with transcriptional changes of *ced-9*, *ced-4*, or *ced-3*. In developmental death of the tail-spike cell, transcriptional upregulation of *ced-3* is the main mechanism of apoptosis activation (Maurer 2007); in CEM neurons, *ced-3* transcription is upregulated in parallel with *egl-1* upregulation (Nehme 2010). Decreased germ cell apoptosis in the Rb complex mutants *lin-35* or *dpl-1* involved derepression of *ced-9* transcription in the germ line, or reduced transcriptional activation of *ced-4* and *ced-3*, respectively (Schertel 2007). The pro-survival factors PAX-2 and EGL-38 limit germ cell apoptosis, probably by upregulating *ced-9* transcription (Park 2006). I extracted RNA from complete adult wildtype and *rpo-1b(op259)* mutants to compare transcript levels of *ced-9*, *ced-4*, and *ced-3*. The transcript levels of *ced-3* and *ced-4* were very stable between the two, excluding a strong effect of *rpo-1b(op259)* on transcription of these core pro-apoptotic factors. Conversely, *ced-9* transcript levels were moderately, but consistently decreased in *rpo-1b(op259)* whole worm RNA extracts (t-test, p=0.012 (10 samples each)). This reduction was similar to the situation in *pax-2(lf)* (Park 2006)). Possibly, reduced *ced-9* expression is a component of the high level of germ cell apoptosis observed in *rpo-1b(op259); ced-9(n1653)*; I have, however, not examined the protein levels of CED-9.

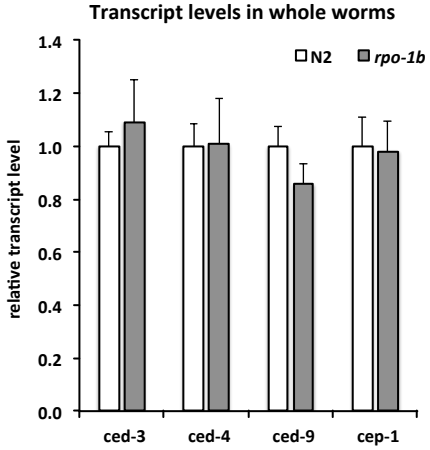

Figure 84 Expression levels of core apoptotic factors in *rpo-1b(op259)* are similar to wildtype. *ced-9* mRNA has a statistically significant decrease in *rpo-1b(op259)* as compared to wildtype to animals. Error bars represent 95 % CI of the mean.

5.4.5.2 Protein expression pattern of CED-4 is not different in *rpo-1b(op259)*

I guessed that in *rpo-1b(op259)* mutants, CED-4 or CED-3 expression could be mis-regulated on a post-transcriptional level. Possibly, the proteins were not sufficiently expressed in the germ line; if this was the cause of reduced apoptosis, transgenic expression of fluorescently tagged protein would either reveal comparatively lower protein levels in *rpo-1b(op259)* or – if transgenic overexpression concealed the protein difference between *rpo-1b(op259)* and wildtype, one might expect a rescue of the apoptotic phenotype. I used a CED-4::GFP (*opIs219*) reporter line (Zermati 2007) that exhibits perinuclear fluorescence. Expression is weak in somatic cells of adults but is pronounced in all germ cells of the meiotic pachytene region and in oocytes. This expression pattern did not obviously differ in *rpo-1b(op259)* (Figure 85 and Figure 86).

Due to the newly detected influence on apoptosis of the transgene selection marker *unc-119(ed3),* I compared apoptosis levels of *opIs219; unc-119(ed3)* and *rpo-1b(op259); opIs219; unc-119(ed3)*, and of *opIs219* and *rpo-1b(op259); opIs219* animals. Indeed, *opIs219; unc-119(ed3)* seemed to be defective for IR-induced apoptosis, whereas *opIs219; unc-119(+)* had slightly stronger response than wildtype worms (Figure 116). This confirmed the relevance of the *unc-119* background in transgenic lines [see *6.2.1.9 unc-119 can confound experiments of germ cell death at the level of the core apoptotic machinery*]. *rpo-1b(op259); opIs219* (but not *rpo-1b(op259); opIs219; unc-119(ed3)*) had an increase of the germ cell corpse number upon irradiation, indicating that transgenic CED-4 might compensate partially for the apoptotic defect of *rpo-1b(op259)* (provided the increase is not an effect of transgenic *unc-119(tg+)*). The observation that *rpo-1b(op259); opIs219* has reduced IR-induced apoptosis in comparison to the *rpo-1b(+)* control despite apparently similar CED-4 levels and distribution indicates that CED-4 is not normally activated in *rpo-1b(op259)* or has a limited effectiveness.

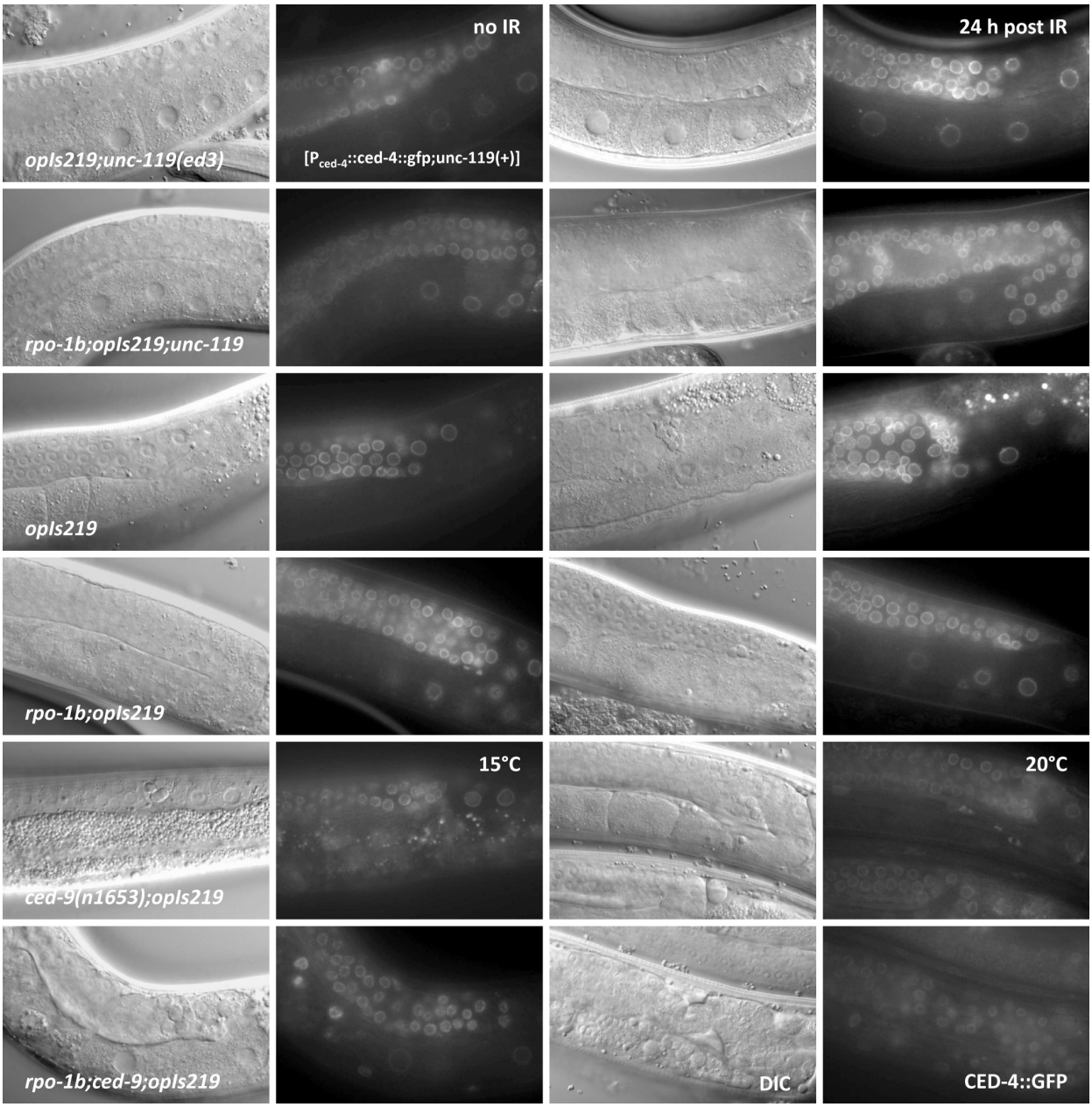

Figure 85 CED-4::GFP expression in meiotic germ cells. Perinuclear signal intensity in the late meiotic pachytene region increases slightly upon irradiation (all at 20°C). *ced-9(rf)* mutant germ cells have a weaker CED-4::GFP signal.

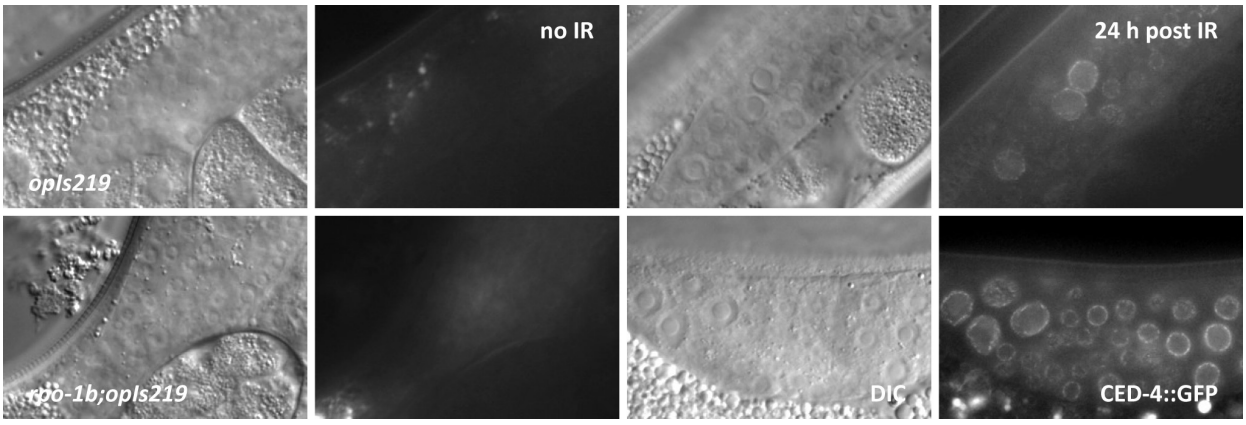

Figure 86 CED-4::GFP expression in mitotic germ cells of the distal gonad. Increase of nuclear size and of CED-4::GFP signal upon irradiation. The intensity of non-enlarged cells appears higher in *rpo-1b(op259)*.

ced-9(n1653) mutants have increased CED-4 levels in somatic cells

I tested CED-4::GFP expression in the *ced-9(n1653)* mutant background, where apoptosis was increased and where *rpo-1b(op259)* further enhanced excessive germ cell apoptosis. The perinuclear CED-4::GFP pattern in germ cells looked wildtype, except for an overall weaker signal (Figure 85). Interestingly, *rpo-1b(op259); ced-9(n1653)* animals but also *ced-9(n1653)* mutants alone had discernible perinuclear fluorescent signal in somatic cells at 20°C or at 15°C. Possibly, *ced-9(n1653)* has an influence on CED-4 protein levels in the germ line and in the soma.

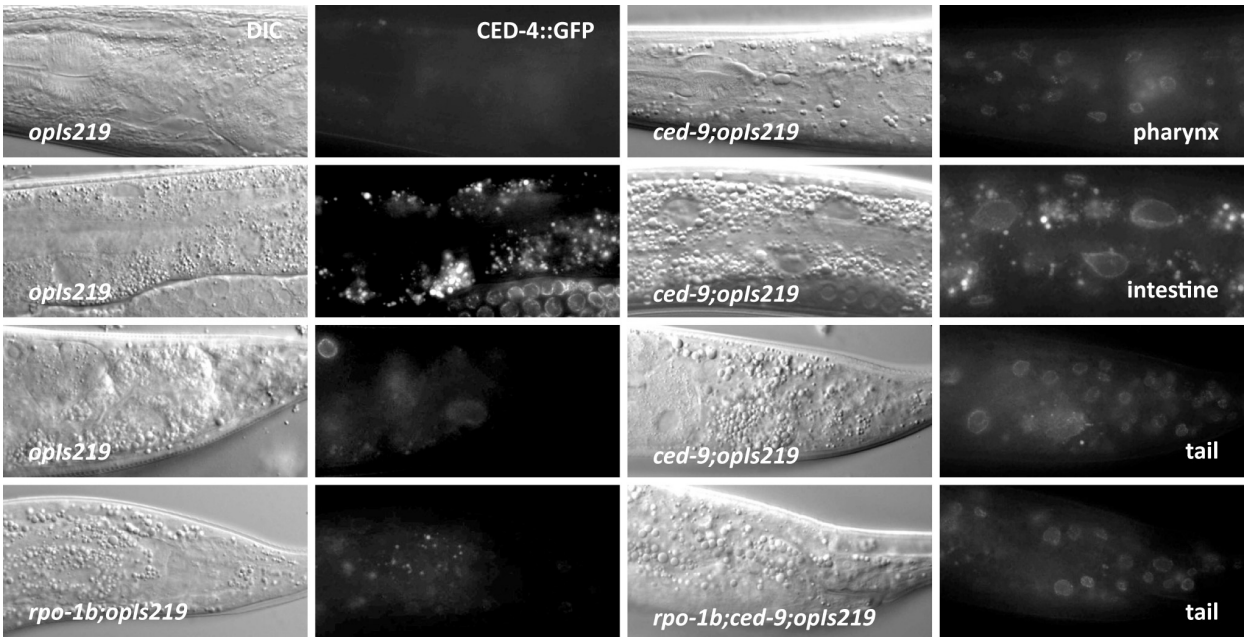

Figure 87 Somatic CED-4::GFP expression is increased in *ced-9(n1653)*. Several tissues show increased perinuclear signal.

5.4.5.3 Protein expression pattern of CED-3 is not different in *rpo-1b(op259)* gonads

Lei Xiong had produced transgenic lines expressing CED-3::GFP in an *unc-119(ed3); ced-3(n717)* mutant background. I outcrossed *unc-119(ed3)* from the background and tested one line (transgene *opIs461*) more extensively for CED-3 expression and rescue of the *ced-3(n717)* apoptosis defect. *opIs461; ced-3(n717)* or *opIs461; unc-119(ed3); ced-3(n717)* animals had close to wildtype levels of germ cell apoptosis upon irradiation (here, the *unc-119(ed3)* in the background did not clearly block IR-induced apoptosis). GFP fluorescence was detectable in mitotic cells, weakly in nucleo-/cytoplasm of late meiotic pachytene germ cells, and most prominently in oocytic nuclei (Figure 88). It was interesting to find highest CED-3 at this location; CED-3 is attributed a role in oocyte maturation besides apoptosis execution (Andux 2008; Hasegawa 2006). The CED-3::GFP expression pattern did not clearly differ in *rpo-1b(op259); ced-3(n717)*, indicating that *rpo-1b(op259)* does not have strongly abnormal CED-3 protein levels. Possibly, *rpo-1b(op259)* animals have somewhat higher CED-3 levels in the distal gonad.

Together, the apoptotic defects in *rpo-1b(op259)* are not likely to result mainly from CED-4 or CED-3 mis-expression.

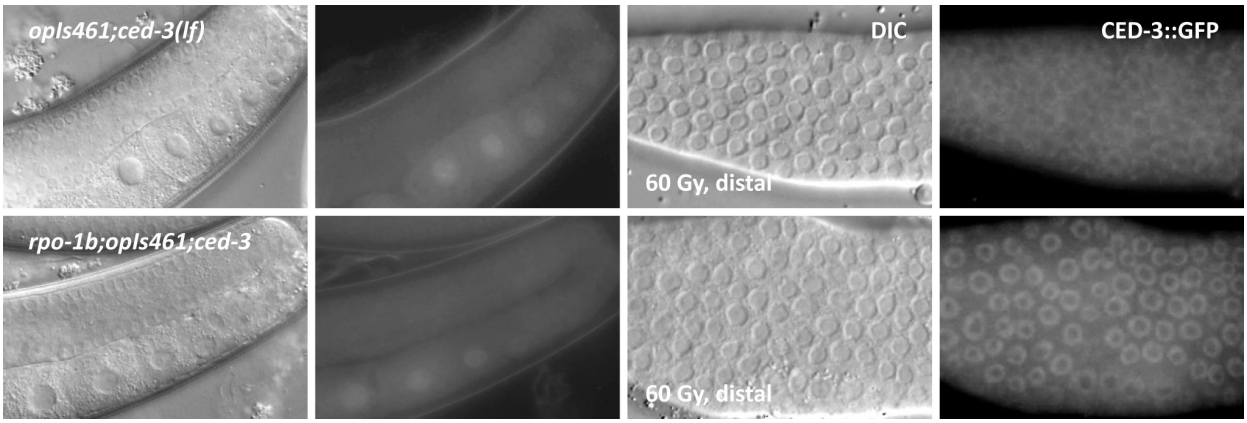

Figure 88 CED-3::GFP expression in oocytic nuclei and in mitotic germ cell nuclei is similar between *rpo-1b(op259)* and wildtype. *opIs461* is *[P_{ced-3}::ced-3 (genomic)::gfp::ced-3 3'UTR; unc-119(+)]*. Transgenes were in the *ced-3(n717)* loss-of-function background.

5.4.6 Autophagy in *rpo-1b(op259)*

Autophagy, the process of cell-internal degradation of proprietary material, links starvation and various stress responses in *C. elegans* (Sigmond 2008). It is intertwined with apoptotic and other cell death programs, and can by itself be a pathway of cell death induction [discussed in e.g., (Erdélyi 2011)]. Since *rpo-1b(op259)* might present to the cells a condition that resembles starvation, I planned to test *rpo-1b(op259)* mutants for alterations in autophagy. The integrated transgene *buIs1* gives stable expression of the autophagy reporter GFP::LGG-1 (Erdélyi 2011). In case autophagy has been induced, LGG-1 – the *C. elegans* Atg8/LC3 homolog – localises to distinct granules representing early autophagosomes in hypodermal cells, among others, of the developing larvae (Meléndez 2008). I crossed the reporter into *rpo-1b(op259)*; the mutant had a punctate fluorescent pattern in hypodermal cells, indicating many more autophagic vacuoles than described for wildtype worms with the original, extrachromosomal reporter (Meléndez 2003). However, the control strain *buIs1* had equally high numbers of puncta, even without exogenous autophagy induction. The transgenic reporter also behaved unexpectedly in that the dominant Roller phenotype conferred by the transgene marker *rol-6(su1006)* was occasionally lost from animals that still expressed GFP tagged protein. I have not further pursued the autophagy phenotypes of *rpo-1b(op259)*.

5.5 *rpo-1b(op259)* and the Ras/MAPK pathway

MAPK signalling pathways are central regulators of cell proliferation and growth. Vulval development in *C. elegans* has been an effective system for the study of cell fate determination by the EGFR/Ras/ERK axis, in crosstalk with other major developmental pathways [review of RTK/Ras/MAPK in *C. elegans* (Sundaram 2006)]. The Ras/ERK pathway has multiple implications in germ cell progression and oocyte maturation (Church 1995; Lee 2007c). It is required for constitutive germ cell death (Gumienny 1999) and might increase apoptosis if upregulated [(Schouest 2009) or (Kritikou 2006)]. I have assessed genetic interactions of *rpo-1b(op259)* with factors of the EGFR/Ras/ERK axis and with factors that are known to modulate MPK-1 (ERK) activity in somatic systems of *C. elegans*. The experiments have revealed a novel function for Ras/ERK in regulating germ cell apoptosis: it does not only permit 'physiological' germ cell death, but it also modulates apoptotic response following IR irradiation; decreased MPK-1 activity seems to abolish IR response, increased activation enhances the number of corpses following irradiation. The results further show that *rpo-1b(op259)* mutants have decreased MPK-1 activation in the germ line, possibly a reason why they do not have normal apoptotic IR response.

In vulval development, the EGFR/Ras/ERK signalling cascade has been deciphered in much detail (Sternberg 2005). The EGF homolog LIN-3 is released from the anchor cell to locally bind to LIN-23 (EGFR) on vulval precursor cells. The signal is transmitted by SEM-5 (Grb2) and LET-341 (Sos) to the Ras homolog LET-60. Via LIN-45 (Raf) and MEK-2 (MEK), the ERK homolog MPK-1 is phosphorylated. Activated (double phosphorylated) MPK-1 regulates transcription of a large set of target genes. This axis is positively and negatively regulated at various levels. LIN-15A and LIN-15B are supposed to modulate signalling upstream of LIN-23; GAP-1 is a negative regulator of LET-60. A crucial regulatory element of MPK-1 activation in vulval precursors is lateral inhibition of neighbouring cells by Notch signalling; the phosphatase LIP-1 is positively regulated by Notch and transmits inhibitory signals to MPK-1, which it inactivates by dephosphorylation (Berset 2001). Other major signalling pathways have been shown to impact on Ras/MAPK signalling to determine vulval development: TGFβ signalling, and the Rb complex. *lin-35*, the Rb homolog, was found in a screen for synMuv (synthetic Multivulva) genes (Lu 1998); it belongs to class B of the two redundant groups of genes, synMuv A and synMuv B, that negatively regulate vulval induction. The DP and E2F transcription factor homologs DPL-1 and EFL-1, that act in a complex with LIN-35, have also been assigned an inhibitory role on MAPK signalling in vulval development (Ceol 2001) and in embryonic development (Page 2001). The mechanism of how they regulate MPK-1 activity in these instances has not been discovered. In the germ line, the phosphatase LIP-1, partly redundantly with PUF RNA binding proteins, restricts MAPK activity [(Hajnal 2002) and (Lee 2007b)]. A recent study demonstrated transcriptional regulation of LIP-1 expression by DPL-1 in the germ line, providing a possible link from the Rb complex to MAPK activity (Lin 2008).

My approach to the MAPK pathway started with the role of Rb complex homologs in *rpo-1b(op259)*. Loss of *dpl-1* function, besides causing a new germ line phenotype that I termed Gogo, enhanced IR-induced apoptosis in *rpo-1b(op259)*; so did *lip-1(lf)* or *let-60(gf)*, two conditions that lead to increased Ras/MAPK signalling.

After writing this work, I got aware of the details of a newly published study on the novel role of the MAPK pathway in irradiation-induced germ cell death (Rutkowski 2011). Their way to the involvement of the Ras/MAPK signalling and ours come from different angles; yet, most of our findings overlap.

5.5.1 RB complex homologs *lin-35* and *dpl-1*

Candidates for genetic interaction with *rpo-1b* in regulating germ cell development comprised the Rb complex homologs *lin-35*, *dpl-1* and *efl-1*; besides coordinating cell cycle-dependent transcription, the Rb complex regulates MAPK activity and other crucial pathways, and it has repeatedly been shown to control rRNA transcription (Hannan 2000; Cavanaugh 1995; Ciarmatori 2001). With the rationale that loss of normal *lin-35* function might disinhibit rRNA synthesis, Voutev et al. (Voutev 2006) investigated whether *lin-35(rf)* could compensate for the reduction of maturing rRNA in *pro-1* mutant animals, and whether this would suppress tumor formation [see *5.1.3.1 Germ line development and tumor formation*]. Indeed, *lin-35(n745)* was able to suppress the proximal proliferation phenotype of the Pro mutant *pro-1(na48)*. The Rb complex thus might regulate rRNA synthesis in *C. elegans* and play a role in the development of germ cell tumours in rRNA synthesis mutants.

I sought to determine whether mutations in Rb factors would also influence the conditional tumor and sterility phenotype of *rpo-1b(op259)*. This would endorse the similarity of *rpo-1b(op259)* with the Pro mutants and favour the hypothesis that at least part of the germ line phenotypes of *rpo-1b(op259)* are caused by altered rRNA synthesis. Further, if the apoptotic defect in *rpo-1b(op259)* were a consequence of reduced rRNA synthesis, inhibiting RB complex function might restore normal apoptosis by compensating for this reduction. Yet, conflicting with this hypothesis, *lin-35* and *dpl-1* mutants had been shown to be defective for DNA damage-induced apoptosis on their own (Schertel 2007).

5.5.1.1 *dpl-1(n3643)* and *rpo-1b(op259)* show synthetic phenotypes

I aimed to test the double mutant *lin-35(lf) rpo-1b(op259)* for germ line proliferation and for DNA damage-induced apoptosis. However, *lin-35* and *rpo-1b* are closely linked; even repeated crossing and self-fertilisation did not yield the double mutant. This could be the result of the close linkage or due to adverse effects on viability of the combination.

The E2F-like protein DPL-1, homolog of the mammalian DP, is required for normal oogenesis and has distinct pro-apoptotic functions (Schertel 2007). *dpl-1*, like *lin-35*, is a synMuv class B gene (Harrison 2006) (that is, it is involved in the regulation of vulval development by Ras signalling), and *dpl-1* mutants resemble *lin-35(lf)* in many respects (more than *efl-1*, a homolog of mammalian E2F (Kirienko 2007)). I could construct the double mutant *rpo-1b(op259); dpl-1(n3643)*, which presented with striking phenotypes. The slight Dumpy phenotype of *dpl-1(n3643)* was enhanced, maturation of adults was protracted, and a high fraction of eggs remained unhatched. The germ line architecture was strongly perturbed in adult animals: *rpo-1b(op259); dpl-1(n3643)* exhibited a novel phenotype with ectopic oogenesis [see *5.1.4.1 Different conditions lead to Gogo*]. Oocytes appeared precociously in the distal arm of the gonad, interspersed between germ cells in meiotic pachytene (Figure 49). Often, these oocytes had a high number of associated cellularised germ cells, most likely representing apoptotic corpses. Irradiation could further enhance this effect. Such a phenotype had not been described for *dpl-1,* and I could not provoke it by irradiating *dpl-1(n3643)* mutants with IR.

5.5.1.2 *lin-35(RNAi)* and *dpl-1(RNAi)* disagree from mutant phenotypes

Due to non-availability of the *lin-35(rf) rpo-1b(op259)* double mutant strain, I chose RNAi treatment as an alternative to compare effects of loss of *dpl-1* with *lin-35*. In contrast to the apoptotic defect reported for *lin-35(n745)* mutants (Schertel 2007), *lin-35(RNAi)* of N2 animals did not result in reduced IR response (Figure 89). For *dpl-1*, the incongruence was even more pronounced: whereas *dpl-1(n3643)* animals showed defective IR response [(Schertel 2007) and our observations], *dpl-1(RNAi)* treated N2 worms accumulated a rapidly rising number of corpses in the proximal gonad one day after irradiation. The marked difference in the apoptotic response between RB mutants and the according RNAi treatment is difficult to interpret: for one thing, *lin-35* was itself shown to be involved in RNAi mechanisms and its loss enhances RNAi sensitivity (Lehner 2006; Ouellet 2007). As studied and discussed in more detail in the section *7 Food type influences apoptosis levels and vulval development,* feeding worms on RNAi bacteria rather than on OP50 has a significant effect on cell death levels, which complicates the interpretation of the above results. Very hypothetically, factors of the Rb complex might themselves be involved in the mechanisms determining food-dependent apoptosis levels, and their loss could boost such differences. At least, *dpl-1(n3643)* had a significantly increased apoptotic response on *empty(RNAi)* compared to OP50, and *dpl-1(n3643)*/*dpl-1(RNAi)* had a strong apoptotic IR response (Table 11).

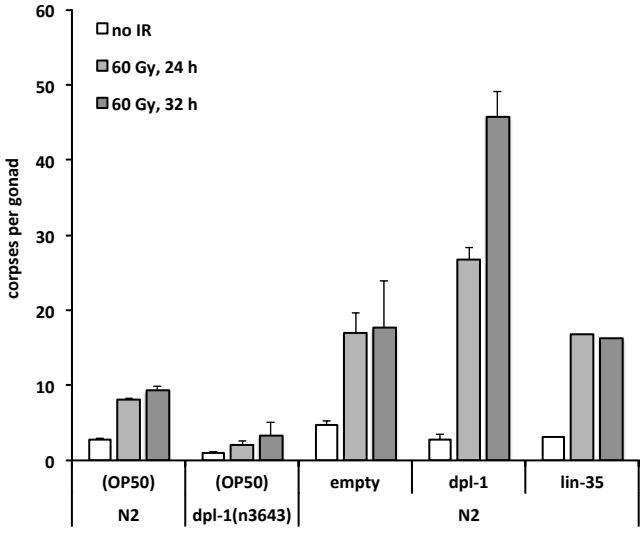

Figure 89 Apoptotic response to irradiation in *dpl-1(RNAi)* treated animals strongly contrasts with the apoptotic defect in *dpl-1(n3643)*. OP50 bacteria were grown on NGM agar plates; 'empty' stands for control RNAi vector, dpl-1 is ORFeome RNAi clone, lin-35 is from Ahringer library. Error bars represent 95 % CI of the mean.

5.5.1.3 *lin-35(RNAi)* and *dpl-1(RNAi)* enhance IR-induced Gogo

Apoptotic response in *rpo-1b(op259); dpl-1(RNAi)* animals could not be scored unambiguously: up to two thirds of the adult gonads showed the germ cell differentiation phenotype already observed in *rpo-1b(op259); dpl-1(n3643)*, that is, distal oogenesis with associated corpses. This phenotype, however, was not unique to *dpl-1(RNAi)*; 40 % of the gonads of *lin-35(RNAi)* treated *rpo-1b(op259)* mutants also exhibited this phenotype after irradiation. Since neither *dpl-1* or *lin-35* mutations alone nor RNAi treatment to *dpl-1* or *lin-35* on N2 had provoked this phenotype, it might be inherent to *rpo-1b(op259)* mutants. Indeed, a fraction of IR treated *rpo-1b(op259)* animals exhibited this phenotype

one day after irradiation. Of note, this fraction rose from about 5 % to 20 % when worms were fed on empty vector RNAi bacteria rather than on OP50 (Figure 51 on page 136). Reduction of *dpl-1* or *lin-35* seems to boost the penetrance of a phenotype in *rpo-1b(op259)* that is also enhanced by differences in the food regimen. These factors might thus regulate a process which integrates environmental cues like food type, and which is disturbed in *rpo-1b(op259)*. Collectively, irradiation, RNAi bacteria and reduction of *dpl-1* push the mutant system into a similar pattern of disturbed germ line organisation. (Additionally, shifting of L4 stage *rpo-1b(op259)* mutants to 25°C led to a similar phenomenon. See *5.1.4.1 Different conditions lead to Gogo*)

		no IR		60 Gy, 24 h		60 Gy, 32 h	
	RNAi target	score	95% CI (n)	score	95% CI (n)	score	95% CI (n)
N2	(OP50)	2.84	±0.16 (647)	8.10	±0.22 (831)	9.31	±0.55 (160)
	empty	4.73	±0.25 (690)	17.02	±0.51 (731)	17.65	±1.79 (40)
	dpl-1	2.81	±0.48 (68)	26.80	±2.63 (56)	45.78	±6.18 (27)
	lin-35	3.07	±0.66 (56)	16.75	±1.56 (56)	16.33	±3.45 (12)
	mpk-1			5.25	±2.10 (20)		
cep-1(gk138)	(OP50)	1.89	±0.30 (96)	1.90	±0.26 (136)	3.15	±0.55 (40)
	empty	2.56	±0.44 (108)	2.98	±0.51 (96)		
	dpl-1	3.44	±1.04 (16)	2.94	±1.10 (16)		
dpl-1(n3643)	(OP50)	0.94	±0.49 (16)	2.00	±0.62 (16)	3.25	±0.96 (28)
	empty	1.76	±0.90 (34)	6.07	±1.56 (58)		
	dpl-1	1.67	±0.80 (9)	13.39	±2.86 (28)		
rpo-1b(op259)	(OP50)	1.43	±0.21 (152)	2.77	±0.31 (140)	3.37	±0.57 (60)
	empty	0.80	±0.17 (164)	1.66	±0.28 (200)	1.19	±0.72 (16)
	dpl-1*	0.75	±0.33 (36)	4.67	±1.55 (36)		
	lin-35	1.83	±0.63 (40)	3.10	±1.17 (40)		
let-60(n1046gf)	(OP50)	1.98	±0.40 (56)	19.53	±1.96 (60)		
	empty			31.20	±2.22 (20)		
	mpk-1			4.75	±1.60 (20)		

Table 11 Apoptotic irradiation response at 24 and 32 hours after irradiation in adult worms grown on OP50 or on RNAi bacteria; 'empty' stands for control RNAi vector. (*dpl-1**) corpses of *rpo-1b(op259); dpl-1(RNAi)* were only scored in animals without distal oocytes; distal oocytes were typically associated with a high number of corpses. Average number of apoptotic corpses per gonad, 95 % CI of the mean, and number of animals tested per condition.

5.5.2 The MPK-1 phosphatase LIP-1

rpo-1b(op259) mutants show some germ line features reminiscent of reduced MAP kinase activity: exit from meiotic pachytene and the appearance of the first large oocyte is topically shifted from just distal to the gonad bend in wildtype to the proximal arm of the gonad in *rpo-1b(op259)*; and baseline levels of germ cell apoptosis are reduced. The synthetic effect with *dpl-1* regarding the distal oogenesis phenotype is also a possible hint to abnormal MAP kinase pathway activity: as mentioned before, *lin-35* and *dpl-1* had been found to be synMuv class B genes, which suggested a role in the regulation of Ras/MAPK activity in somatic development. In fact, LIN-35 acts with DPL-1 and EFL-1 to antagonise Ras signalling (Ceol 2001). Additionally, DPL-1 and EFL-1 regulate the transcriptional programs required for ovulation and fertilisation in the germ line (Chi 2006, 2009). It was demonstrated that DPL-1 acts in germ cell development by promoting expression of the MPK-1 phosphatase LIP-1 (Lin 2008). (DPL-1 thus acts in a circular relation with the Ras/MAPK pathway, since it is itself targeted by MAP kinase activity.) LIP-1, by regulating MPK-1 activity, is an important regulator of oocyte maturation

(Hajnal 2002) and also of the extent of germ cell proliferation (Lee 2006); redundantly with PUF RNA binding proteins, it also prevents excessive germ cell apoptosis (Lee 2007b).

Possibly, some of the disturbances in *rpo-1b(op259); dpl-1(lf)* and also in *rpo-1b(op259)* resulted from alterations in MAPK activity. Given the above mentioned germ line features, I posited the hypothesis that *rpo-1b(op259)* mutants have too little Ras/MAPK pathway activation. Hypothetically, the massive effects of reducing DPL-1 in *rpo-1b(op259)* arise from reduced transcriptional *lip-1* activation and consequently derepresses MPK-1 activity.

5.5.2.1 *lip-1* regulates sensitivity to IR-induced apoptosis

I wondered whether removing LIP-1 phosphatase in *rpo-1b(op259)* would phenocopy some of the germ cell development disorders of *rpo-1b(op259); dpl-1(n3643)*, and specifically, whether it would also increase sensitivity to IR-induced apoptosis. Indeed, *rpo-1b(op259); lip-1(zh15)* double mutants had increased germ cell death already without irradiation and they were highly sensitive to IR (Figure 90 and Table 12). Also, *lip-1(zh15)* mutants had increased baseline apoptosis in comparison to wildtype. Surprisingly, *lip-1(zh15)* animals were equally hypersensitive to IR. These observations thus revealed a novel role for *lip-1* in limiting excessive cell death. They further defined *lip-1* as epistatic to *rpo-1b(op259)* in terms of IR-induced germ cell apoptosis.

5.5.2.2 *lip-1(zh15)* does not provoke Gogo

rpo-1b(op259); lip-1(zh15) animals had increased apoptosis, but unlike *rpo-1b(op259); dpl-1(n3643)*, they did not show distal oocytes. Possibly, in *rpo-1b(op259)* mutants, *dpl-1* regulates germ cell sensitivity to apoptosis via a pathway involving *lip-1*, and, in another functional branch, it affects the position in the germ line where germ cells are rendered capable to develop into oocytes or go into apoptosis. It is not fully excluded that ectopic oogenesis is overlaid by other germ line defects of *rpo-1b(op259); lip-1(zh15)*. The gonads looked overall very unhealthy; often, the proximal gonad had only few oocytes, and apoptotic corpses were larger than in wildtype or *rpo-1b(op259)* worms: defects that were all further pronounced after irradiation. This was not only true for *rpo-1b(op259); lip-1(zh15)*: *lip-1(zh15)* showed similar defects, as had already been described before (Hajnal 2002). Further, I saw a similar phenotype in other double mutant conditions of *rpo-1b(op259)* [see *5.4.4 Morphology of apoptotic cells*].

5.5.3 Model: Ras/MAPK pathway activity sensitises for IR-induced apoptosis

LIP-1 is the major phosphatase for MPK-1 in the regulation of vulval development. MPK-1 had further been recognised to play a role in physiological germ cell death (Gumienny 1999). It is required for germ cell progression from meiotic pachytene to diakinesis. In its absence, germ cells can't exit the pachytene stage and thus do not form oocytes nor become susceptible to apoptosis. It thus seemed intuitive that *lip-1* mutants could have increased baseline apoptosis, assuming that in the absence of the phosphatase, activated MPK-1 would remain phosphorylated and thus in its active state. Yet, the notion that the Ras/MAPK could also play a role in DNA damage-induced apoptosis had been somewhat defeated by the distinction of physiological cell death – the sphere of MAPK signalling – and stress-induced cell death with its key player CEP-1. Increased baseline apoptosis and hypersensitivity to IR-induced cell

death in *lip-1* mutants points towards a model in which increased Ras/MAPK pathway activity generally levers the susceptibility of cells to pro-apoptotic cues.

5.5.3.1 *mpk-1(rf)* blocks IR-induced apoptosis

I tested *mpk-1(ga111)* mutants for apoptotic IR response. This allele is supposed to cause a temperature sensitive germ line defect; at 20°C, oocytes can develop and viable progeny is produced; at 25°C, many germ cells show the *mpk-1* loss-of-function pachytene-exit defect and brood size is reduced. In our experience with other genes and alleles, temperature sensitivity is often rather gradual, and subtle defects might occur at lower temperatures already. I therefore scored apoptosis at 20°C, where germ cell progression into oocytes did still occur. Indeed, *mpk-1(ga111)* animals had low levels of 'physiological' germ cell death and they did not respond normally to IR (Table 12), emphasising a role for MPK-1 in DNA damage-induced cell death. I confirmed the finding with RNAi knockdown of *mpk-1*, which reproduced the apoptotic defect (Table 11).

5.5.4 The Ras homolog *let-60*

Gain-of-function mutations of *let-60*, the *C. elegans* Ras homolog, cause hyperactivation of MPK-1. If in *lip-1* mutants, reduced MPK-1 dephosphorylation was responsible for IR hypersensitivity, *let-60(gf)* animals might be equally hypersensitive to IR-induced apoptosis due to constitutively enhanced MPK-1 activation. We tested the *let-60(n1046gf)* mutant allele, which has a reportedly weak germ line phenotype (Lee 2007b) and leaves germline architecture grossly intact.

5.5.4.1 Gain of *let-60* function increases germ cell apoptosis

Indeed, the cell corpse number after irradiation was significantly higher in *let-60(n1046gf)* than in wildtype animals (Figure 90 and Table 12). Together, hypersensitivity for germ cell apoptosis in both *lip-1(zh15)* and *let-60(n1046gf)* on the one hand and low apoptosis levels in *mpk-1(rf)* on the other hand strongly speak for a decisive role of the Ras/MAPK pathway in this process.

5.5.4.2 Increased MPK-1 activation can restore IR-induced apoptosis in *rpo-1b(op259)*

The above observation that loss of *lip-1* function suppresses the apoptotic defect of *rpo-1b(op259)* suggests that LIP-1 mediates the reduction of cell death. If it is Ras/MAPK activity that is critical for germ cell death in *rpo-1b(op259)*, other situations of increased Ras/MAPK activity might also compensate for reduced apoptosis in *rpo-1b(op259)*. Indeed, *let-60(n1046gf)* could suppress the apoptotic defect of *rpo-1b(op259)*, rising IR-induced cell death up to levels of irradiated wildtype (Figure 90 and Table 12). As mentioned before, *let-60(n1046gf)* had exhibited higher than wildtype response to IR. Thus, *let-60* is not fully epistatic to *rpo-1b(op259)*; conversely, *rpo-1b(op259)* seems to suppress most of the excessive cell death of *let-60(n1046gf)*. These observations are consistent with reduced Ras/MAPK activity in *rpo-1b(op259)* that can be compensated for by *let-60(n1046gf),* and vice versa.

5.5.4.3 Hypothesis: *rpo-1b(op259)* acts upstream of *lip-1*

Whereas *rpo-1b(op259)* partly suppressed IR hypersensitivity in *let-60(n1046gf)* gain-of-function mutants, *rpo-1b(op259); lip-1(zh15)* exhibited the high levels of apoptosis of *lip-1(zh15)*. If

rpo-1b(op259) reduced MPK-1 activity independently of *lip-1* and this reduction was responsible for the apoptotic defect, one would expect some reduction also of the excessive apoptotic response of *lip-1(zh15)* by *rpo-1b(op259)*. (This needs to be tested with e.g., *mpk-1(rf); lip-1(zh15)* or *let-60(rf); lip-1(zh15)*.) These considerations support a model where *rpo-1b(op259)* causes a reduction of MPK-1 activation by high LIP-1 activity. qRT-PCR did not show a significant increase of *lip-1* mRNA levels in whole worm extracts of *rpo-1b(op259)* worms. This does not preclude a local increase of *lip-1* transcription in the germ line, e.g., by high *dpl-1* activity (Lin 2008); and it does not exclude expression changes on a post-transcriptional level. To determine LIP-1 protein levels in the germ line and to relate *rpo-1b(op259)* and *lip-1* more precisely, one would have to perform immunofluorescence with a depleted anti-LIP-1 antibody (a first staining with the crude serum gave strong background signal) or use a transgenic reporter for LIP-1 expression.

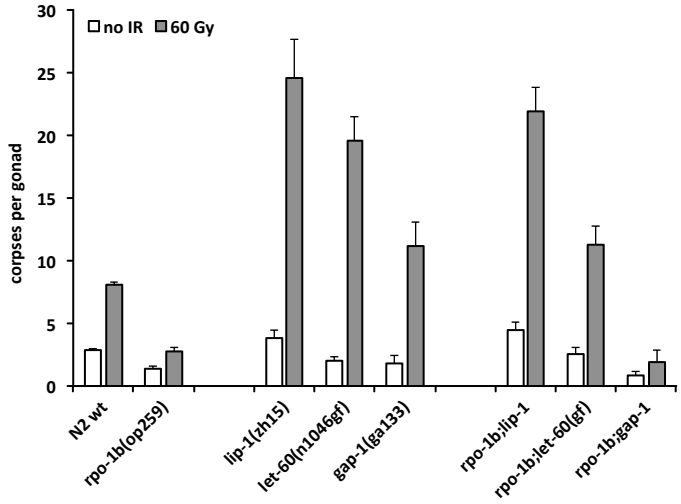

Figure 90 *lip-1(lf) and let-60(gf)* increase apoptotic IR response of *rpo-1b(op259)*. *lip-1* is epistatic to *rpo-1b(op259)* regarding IR response. Error bars represent 95 % CI of the mean.

5.5.5 Ras/MAPK in somatic development of *rpo-1b(op259)*

5.5.5.1 *rpo-1b(op259)* suppresses *let-60(gf)* effects in somatic development

lip-1(zh15) and *let-60(n1046gf)* both restored IR-induced cell death in *rpo-1b(op259)*. The observation that these mutations by themselves lead to excessive cell death indicated the potential of high MAP kinase activity to increase germ cell apoptosis. In *rpo-1b(op259)*, over-activation of the Ras/MAPK pathway either compensates for reduced MPK activation, or it overcomes other functional disturbances in apoptosis regulation. The other way, *rpo-1b(op259)* might reduce enhanced death of *let-60(gf)* in a Ras/MAPK-independent manner.

Vulval development in *C. elegans* has been an extremely valuable model for dissecting central developmental signalling cascades, such as the Notch and ERK/Ras/MAPK pathways, which act mostly antagonistically in this system. (Sternberg 2005). For Ras/MAPK, overactivation leads to excessive induction of vulval precursor cells in larval stages and to multiple vulvae (Muv phenotype) in the adult animal. If, however, in the absence of MAP kinase signal, no precursors are induced properly, no vulva

is formed and the adults stay vulvaless (Vul) (Sternberg 1986). Classically, the Ras gain-of-function mutation *let-60(n1046gf)* hyperactivates MPK-1 and has extra inductions of vulvae; this is quantified as an increased vulval induction index of about 4.2 rather than 3 (which means no extra inductions) for wildtype [*8.2 Frequently used assays*].

We used this system to refine genetic relations of *rpo-1b(op259)* and *let-60(n1046gf)*. Regarding IR-induced apoptosis, the double mutant *rpo-1b(op259); let-60(n1046gf)* had an intermediate phenotype between *rpo-1b(op259)* and *let-60(n1046gf)*. As discussed above, hyperactive MAPK might overcome defective apoptotic mechanisms in *rpo-1b(op259)* that are not directly related to Ras/MAPK; in this case, *rpo-1b(op259)* would likely not change the effect of *let-60(n1046gf)* on vulval development. However, if *rpo-1b(op259*) negatively acted on MAPK, it would possibly also counteract *let-60(n1046gf)* in the somatic system. Indeed, the double mutant strain *rpo-1b(op259); let-60(n1046gf)* had only few animals with extra vulvae and an average vulval induction index of 3.1, suggesting that *rpo-1b(op259)* can potently suppress *let-60(n1046gf)* in this setting (Figure 91).

lip-1 mutants do not exhibit a Muv phenotype by themselves. Only when *lip-1(zh15)* is combined with mutations that lead to overactivation in the Ras/ERK branch, *lip-1(zh15)* can lead to synthetic effects in vulval development (Berset 2001). *rpo-1b(op259); lip-1(zh15)* had innocuous vulval numbers.

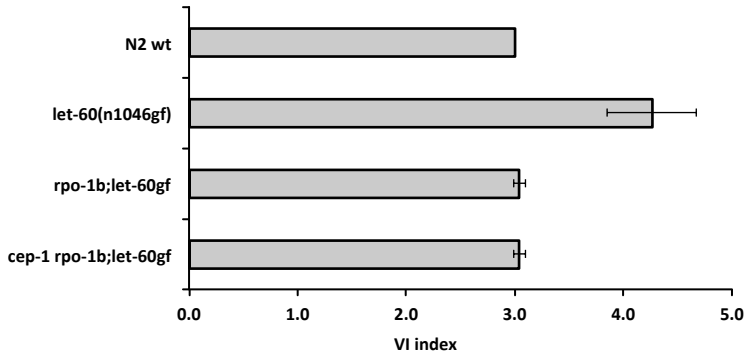

Figure 91 *rpo-1b(op259)* suppresses excessive vulval induction of *let-60(n1046gf)*. Assay description see *8.2 Frequently used assays*; error bars indicate 95 % CI of the mean (N2 wildtype was not assessed here, reference value is 3.0, corresponding to normal induction of one vulva).

5.5.5.2 MPK pathway effector *lin-1* is epistatic to *rpo-1b(op259)* in vulval induction

Obviously, *rpo-1b(op259)* does not have a full block of MPK-1 activity. Strong alleles of *mpk-1* are lethal, and conditional mutants of *mpk-1* become sterile at non-permissive temperature due to abnormal germ cell maturation. Also, no Vul phenotype has been observed in *rpo-1b(op259)*. Likely, *rpo-1b(op259)* mutants have reduced activity of the Ras/MAPK pathway but they (at least partly) retain the capacity to integrate signals that lead to enhanced activation.

Suppression of extra vulval inductions in *rpo-1b(op259); let-60(n1046gf)* placed *rpo-1b(op259)* epistatically to *let-60(n1046gf)*, but it did not allow to position the influence of *rpo-1b(op259)* genetically with regards to MPK-1 activation. *rpo-1b(op259)* could be acting downstream of *mpk-1* and disturbing a more general cellular process like proliferation, differentiation or migration, which would entail an incapacity to form extra vulvae. To rule out the possibility of such an effect that would prevent any extra inductions, I tested whether *rpo-1b(op259)* would also suppress the strong Muv phenotype of

lin-1(n304). In its non-phosphorylated state, LIN-1 acts as a negative regulator of transcription of genes that regulate vulva formation (Jacobs 1998; Miley 2004); it is a direct target of, and inhibited by, MPK-1 kinase activity. Loss of *lin-1* function thus mimics Ras/MAPK overactivity downstream of *mpk-1* and leads to transcriptional de-repression. All animals of *rpo-1b(op259); lin-1(n304)* had a high number of extra vulvae, indicating that the effect of *rpo-1b(op259)* is at the level or upstream of *mpk-1*.

5.5.6 *In situ* detection of activated MPK-1 in the germ line

The experiments so far suggested that MPK-1 activity might be reduced in *rpo-1b(op259)*. Further, analysis of apoptosis in *rpo-1b(op259)* and in mutants of the MAP kinase signalling pathway had indicated that this pathway might be relevant for DNA damage-induced apoptosis. To test the levels of activated MPK-1 in situ, we performed immunofluorescence analysis on dissected gonads. Antibody staining *in situ* might reveal differences in the protein levels of activated MPK-1, and it would also show deviant expression/activation patterns. A commercially available antibody to di-phosphorylated ERK (MAPK-YT) (Yung 1997) was shown to specifically bind to the homologous di-phosphorylated MPK-1 in *C. elegans* as well (Miller 2001). MAPK-YT has been reported to detect high ppMPK-1 levels in the most proximal oocytes and distinct accumulation in the region of late pachytene cells, whereas the distal gonad does not significantly bind the antibody (Page 2001). Together with students from the BIO323 genetics course 2010 (Lisa Haldemann, Louisa Müller, and Anina Schneider), we adapted an immunostaining protocol so as to combine fixation with paraformaldehyde, freeze-cracking, and methanol fixation. Blocking and antibody incubations were in serum from goat, the host species of the secondary antibodies. We stained with MAPK-YT and also with an antibody for total ERK (cross-reacts with MPK-1), and we included an anti-DNA antibody to have a control for antibody staining that was independent of protein expression. To test for specificity of the MPK-1 antibodies, we applied the immunofluorescence protocol to *mpk-1(ga111)* reduction-of-function mutants and to *mpk-1(RNAi)* treated worms. In both cases, loss of MPK-1 function was not very severe since most animals showed only minute phenotypes at the stage of analysis. Accordingly, the ppMPK-1 signal was reduced in some animals but not completely absent (Figure 94). It therefore remained difficult to subtract background from MPK-1 specific signal, particularly for the total ERK antibody, which in contrast to MAPK-YT did not stain distinct germ line regions. Staining here was uniform; the nuclei were mostly spared, the signal appeared to be concentrated at the plasma membrane (this particular staining was fainter in the controls). In gut cells, the total MPK-1 antibody stained nuclei in full congruence with MAPK-YT.

5.5.6.1 *rpo-1b(op259)* mutants have reduced levels of activated MPK-1 in the germ line

For wildtype worms, we got the signal pattern as described before for ppMPK-1: strong staining of the most proximal oocytes, with even stronger signal in the large oocytic nuclei; and cytoplasmic staining in the pre-oocytic meiotic pachytene (Figure 92). In *rpo-1b(op259)*, this signal was clearly reduced (with some variation between individuals). Thus, *rpo-1b(op259)* mutants have reduced levels of activated MPK-1 in the region of late pachytene, where germ cells start maturing into oocytes or become apoptotic.

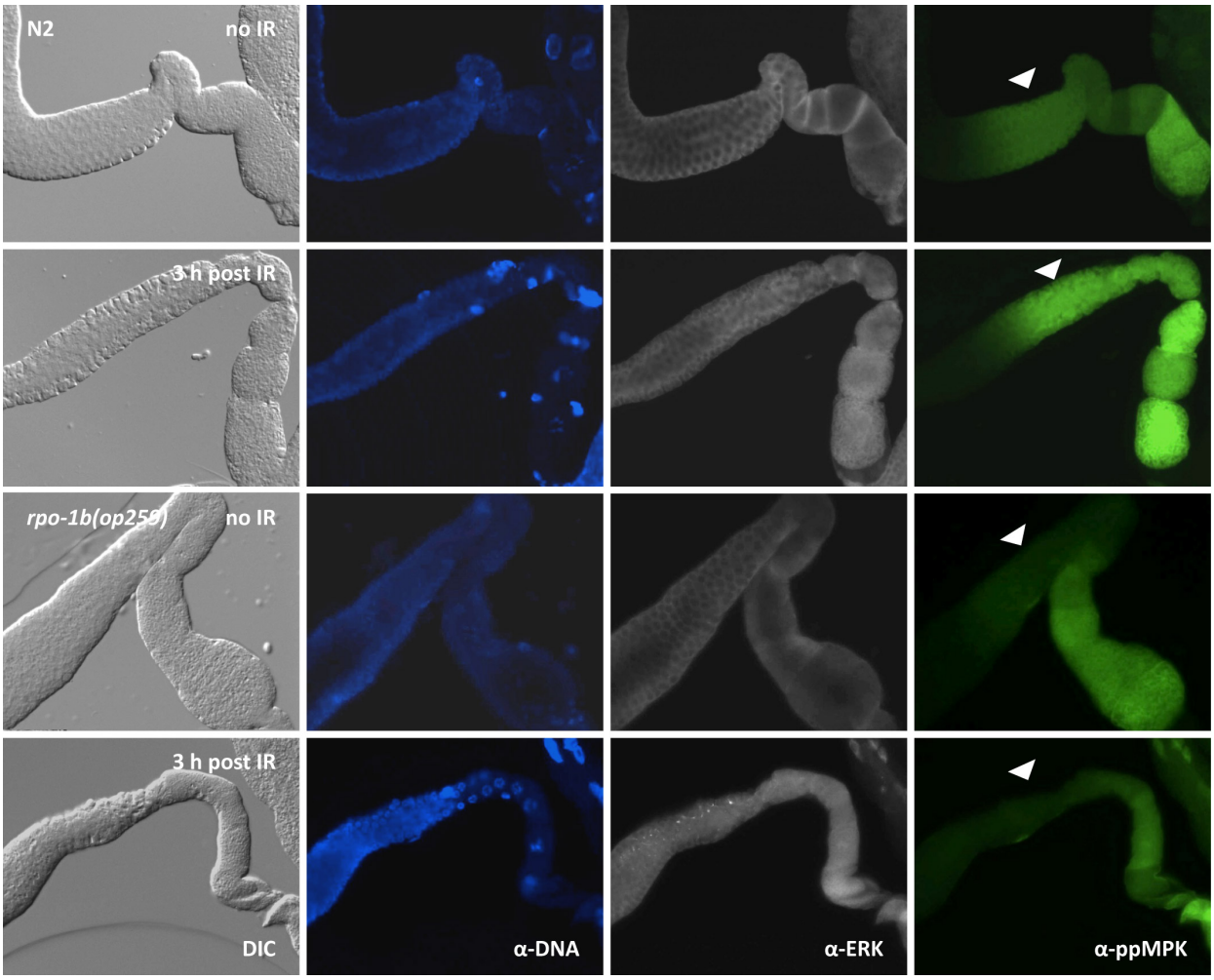

Figure 92 ppMPK-1 levels in the late meiotic pachytene region (triangle) are reduced in *rpo-1b(op259)* and don't increase upon irradiation as in wildtype. The specificity for MPK-1 of the cytoplasmic signal with anti-ERK is not clear. anti-DNA antibody was added as an additional control for staining.

We tested *let-60(n1046gf)* animals. The signal intensity was slightly higher than in wildtype (Figure 93). *let-60(n1046gf)* did also moderately increase the ppMPK-1 levels in *rpo-1b(op259)*, which endorsed the notion that *rpo-1b(op259)* is not fully epistatic to *let-60(n1046gf)* in the germ line and that it does not fully prevent activation of MPK-1.

In *lip-1(zh15)*, the ppMPK-1 signal was clearly lower than in wildtype (Figure 93). This is against the expectation that loss of *lip-1(zh15)* would allow accumulation of activated MPK-1, and it is not in agreement with the observation of increased ppMPK-1 in (Hajnal 2002). As such, the absolute levels of activated MPK-1 seem to correlate little with the apoptotic irradiation response. It is conceivable that not only the static absolute levels are relevant but also the relative active fraction of MPK-1 or gradients within the germ line. As mentioned already, *lip-1(zh15)* gonads are generally much less healthy than wildtype, which could have implications for steady state levels of core signalling networks.

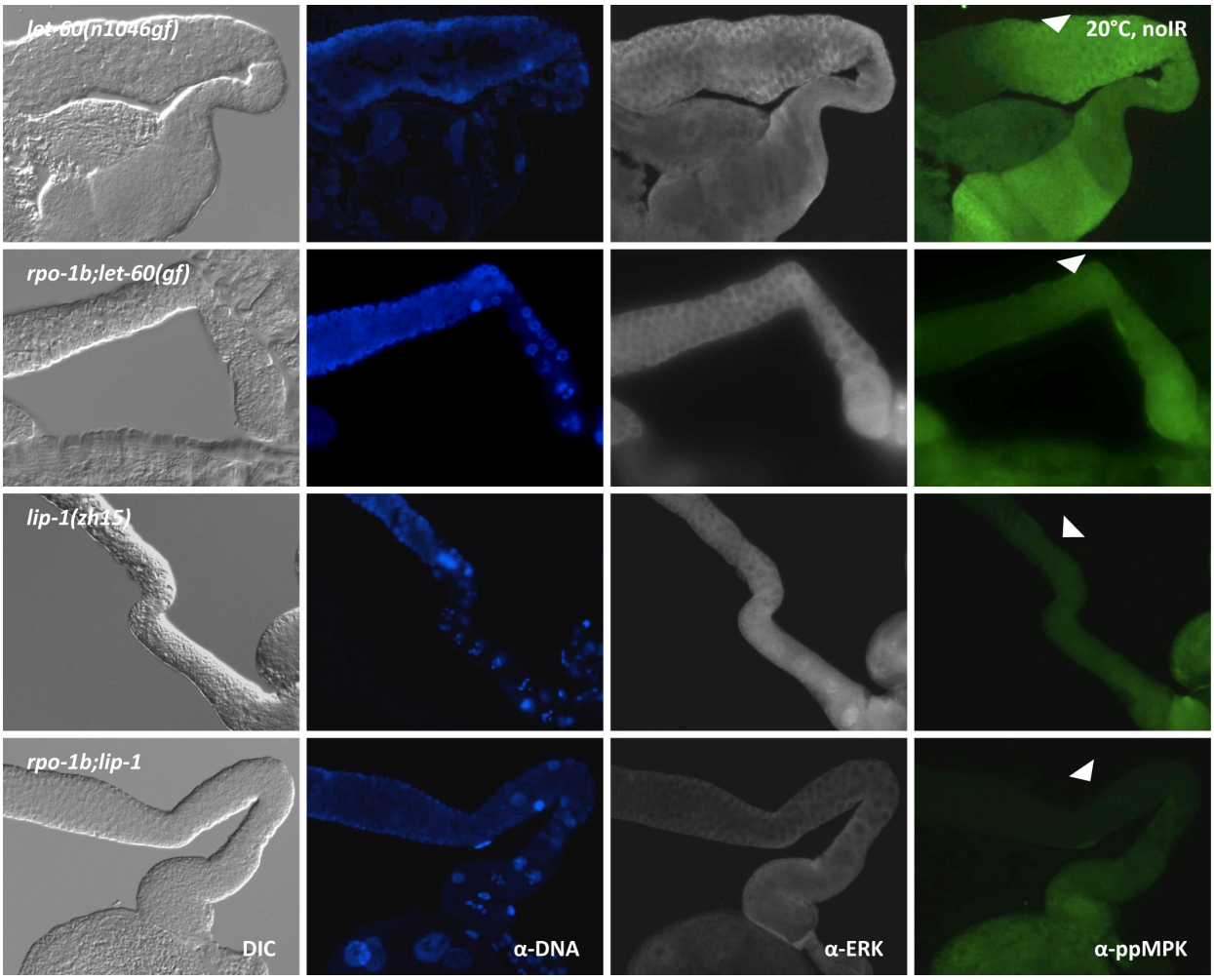

Figure 93 ppMPK-1 signal of *rpo-1b(op259)* is partly restored by *let-60(n1046gf). lip-1(zh15)* has a weaker signal than wildtype in the late meiotic pachytene region (triangle) and in oocytes.

5.5.6.2 Irradiation increases activated MPK-1 in wildtype gonads

We had detected a role for MAPK signalling in DNA damage-induced apoptosis. *mpk-1(rf)* and *rpo-1b(op259)* had only weak IR response; on the other side, elevating MAPK activation by genetic mutations had a potentiating effect on apoptosis levels, most significantly following irradiation. We wondered whether the role of MAPK pathway activity was solely to facilitate apoptosis independently of the pro-apoptotic cue, or whether the pathway might actually be recruited by irradiation responses. We therefore examined the effect of irradiation on MPK-1 levels at a defined time post treatment. In independent experiments using fluorescently tagged DNA repair proteins, we had evaluated that already three hours after setting DNA damage these proteins reached a plateau in the number of newly formed nuclear foci [see chapter *3.2*]. We thus chose this time point for the analysis of MPK-1; it is also between immediate effects of irradiation and the occurrence of the first few damage-induced corpses. Three hours after irradiation, the ppMPK-1 signal in the late pachytene region was indeed stronger in IR treated wildtype worms than in non-treated controls (Figure 92). We also saw an increase in *let-60(n1046gf)* animals. Thus, irradiation leads to an increase of activated MPK-1 in mid-late meiotic pachytene at an early time point after treatment.

rpo-1b(op259) mutants did not significantly respond to irradiation, and signal intensity remained lower than in non-irradiated wildtype worms. However, irradiated *rpo-1b(op259); let-60(n1046gf)* animals had somewhat higher ppMPK-1 than non-irradiated controls.

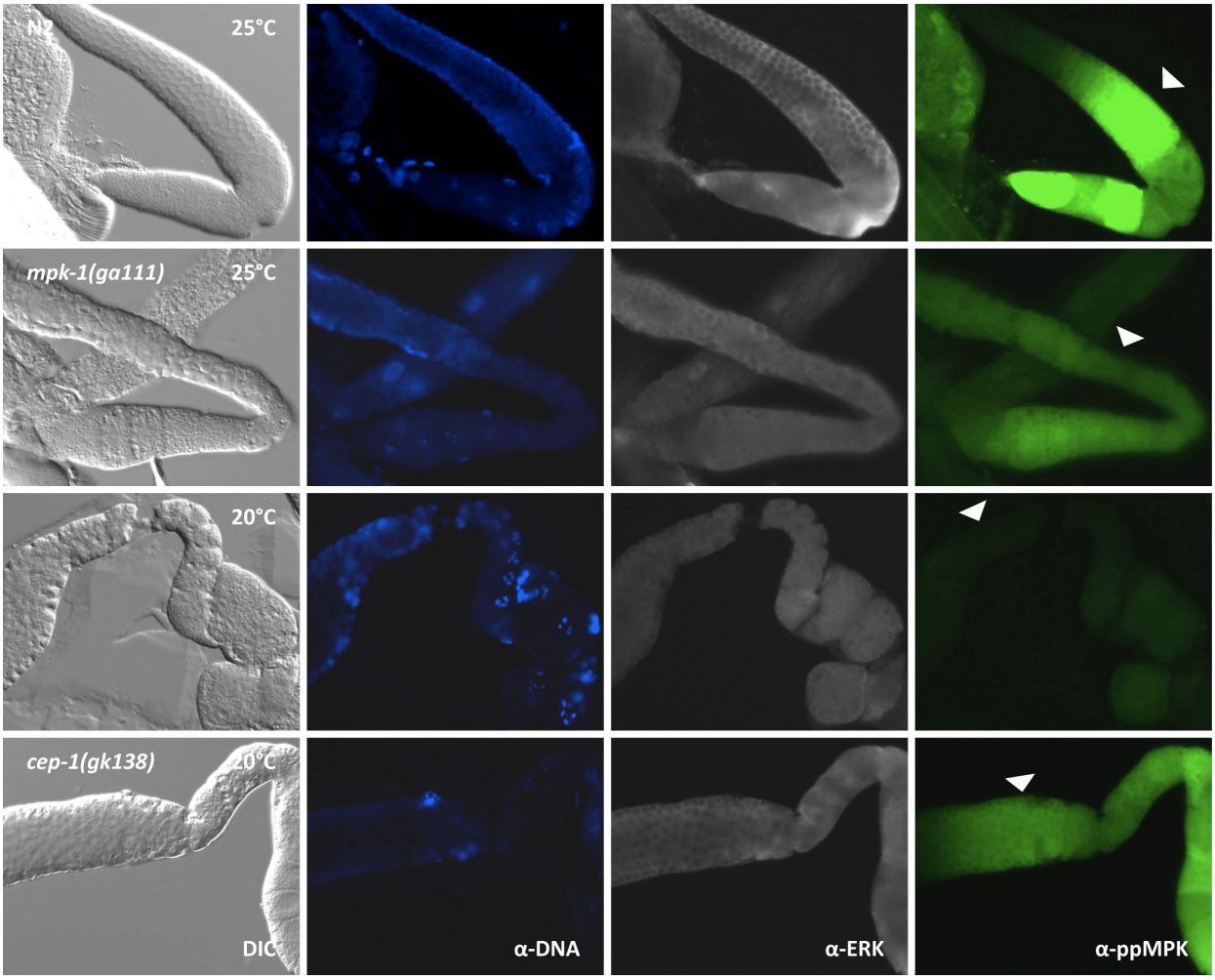

Figure 94 Control experiments for ppMPK-1 signal. *mpk-1(ga111)* mutants at 25°C have lower signal intensity than the variably high signal from wildtype in the meiotic pachytene region (triangle). Also at 20°C, the signal is reduced in this temperature sensitive strain.

5.5.7 MAPK pathway and CEP-1

5.5.7.1 IR-induced death in *lip-1(zh15)* is partially dependent on *cep-1*

So far, DNA damage-induced apoptosis was thought to be fully dependent on CEP-1, the *C. elegans* p53 homolog, via its activating function on transcription of the BH3-only proteins EGL-1 and CED-13. One would thus expect the IR-induced excessive germ cell death in Ras/MAPK pathway mutants to also be dependent on *cep-1*. Alternatively, the hypersensitivity to IR could be mediated by another pathway with no or only partial dependence on *cep-1*. To evaluate this hypothesis, I tested whether *cep-1(lf)* could suppress excessive cell death of *lip-1(lf)* mutants.

cep-1(gk138); lip-1(zh15) had normal levels of germ cell apoptosis at baseline. Other than what is typically observed when CEP-1 is missing, the number of corpses in this double mutant increased moderately upon IR, to about the levels of irradiated wildtype (Figure 95). Thus, the apoptotic response

to irradiation in *lip-1* is not fully dependent on *cep-1*. There appears to be a *cep-1*-independent feed of DNA damage response signalling into the apoptotic machinery in the *lip-1(zh15)* mutant condition. This response, however, was completely blocked by *rpo-1b(op259)*, i.e., no additional corpses arose upon irradiation of *cep-1(gk138) rpo-1b(op259); lip-1(zh15)*.

I had also observed *cep-1*-independent IR response in *gla-3(RNAi) cep-1(gk138)*, where irradiation could increase germ cell apoptosis (Table 18).

Interestingly, loss of functional EGL-1 was capable to suppress apoptosis of *lip-1(zh15)* more completely, but not of *rpo-1b(op259); lip-1(zh15)*.

5.5.7.2 *cep-1(gk138)* animals have normal ppMPK-1

We considered the possibility that CEP-1 regulates Ras/MAPK activity. It might modulate the pathways leading to MPK-1 activation in normal conditions or after DNA damage. Immunofluorescence with the MAPK-YT antibody did not show a clear difference of activated MPK-1 levels in *cep-1(gk138)* mutants in comparison to wildtype; signal intensity was robust in untreated *cep-1(gk138)* (Figure 94) and showed a wildtype increase upon irradiation.

5.5.7.3 Ras/MAPK does not overactivate CEP-1

Given the high level of IR-induced cell death in *lip-1(zh15)* and *let-60(n1046gf)*, it was conceivable that CEP-1 could have been excessively activated upon DNA damage. Hypothetically, CEP-1 might be overactivated when MPK-1 signalling is increased. Due to the lack of means to directly assess activated CEP-1, expression levels of the surrogates EGL-1 and CED-13 were measured by qRT-PCR. In both mutants, transcript levels were similar to wildtype without or 3 hours after irradiation.

The different apoptotic response of Ras/MAPK pathway mutants to IR is unlikely to result from significant changes of CEP-1 activation upon DNA damage at relatively early time points after irradiation. Supporting this, at least *lip-1(zh15)* sensitised to apoptotic IR response in the absence of functional CEP-1 (see above).

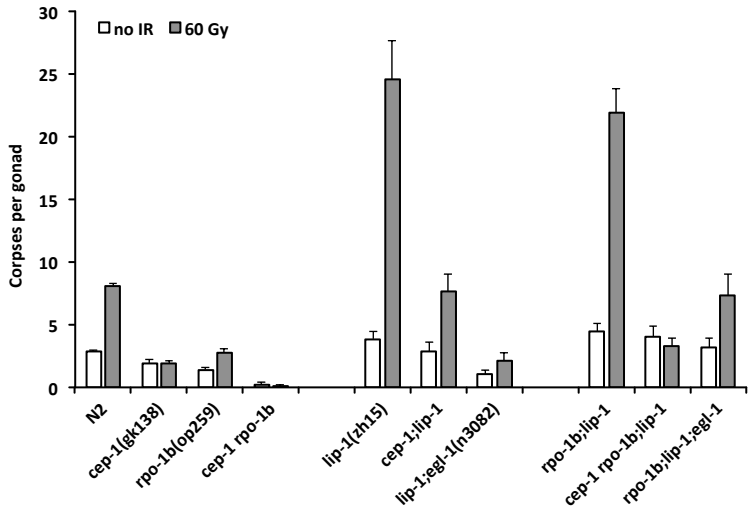

Figure 95 Loss of *cep-1* function does not fully suppress IR-induced apoptosis in *lip-1(zh15)*. Apoptotic germ cell corpses at 24 hours post irradiation; error bars represent 95 % CI of the mean.

5.5.8 Other factors with altered Ras/MAPK signalling

5.5.8.1 *gap-1(ga133)* does not rescue IR defect of *rpo-1b(op259)*

Further mutants of the ERK/Ras/MAPK pathway are available that act upstream of *let-60* and lead to pathway hyperactivation. GAP-1 is a GTPase-activating protein presumably acting as a negative regulator of LET-60 (Hajnal 1997). *gap-1(ga133)* mutants show synthetic effects on vulval induction with other synMuv genes but not on their own. I also tested *gap-1(ga133)* for IR sensitivity. The levels of IR-induced germ cell death were slightly higher than wildtype (Figure 90 and Table 12). *gap-1(ga133)* could however not rescue the apoptotic defect of *rpo-1b(op259)*.

5.5.8.2 *gla-3(RNAi)* restores apoptosis in *rpo-1b(op259)* to wildtype levels

The chapter *5.6.11.2 gla-1(RNAi) and gla-3(RNAi) to rpo-1b(op259) enhance apoptosis levels only after IR* elaborates the effects of *gla-3(RNAi)*. Disregarding morphological alterations of germ cells and structural changes of the gonad, *gla-3(RNAi) rpo-1b(op259)* animals have similar apoptosis levels like *control(RNAi)* treated wildtype worms (with or without irradiation) (Table 18), whereas *gla-3(RNAi)* in wildtype leads to increased death. Superficially, one could consider this a rescue of the apoptotic defects of *rpo-1b(op259)* by *gla-3* knockdown. *gla-3* mutants have been shown to have increased Ras/MAPK activity both in vulval development and in the germ line (Kritikou 2006); possibly, this compensates for a reduction of pathway activity in *rpo-1b(op259)*.

	wildtype background				*rpo-1b(op259)* background			
	no IR		60 Gy		no IR		60 Gy	
	score	95% CI (n)	score	95% CI (n)	score	95% CI (n)	score	95% CI (n)
wt	2.84	±0.16 (647)	8.10	±0.22 (831)	1.43	±0.21 (152)	2.77	±0.31 (140)
cep-1(gk138)	1.89	±0.30 (96)	1.90	±0.26 (136)	0.25	±0.15 (40)	0.08	±0.08 (40)
dpl-1(n3643)	0.94	±0.49 (16)	2.00	±0.62 (16)				
lip-1(zh15)	3.87	±0.55 (54)	24.58	±3.11 (50)	4.42	±0.68 (92)	21.88	±1.99 (74)
cep-1;lip-1	2.85	±0.80 (40)	7.67	±1.40 (58)	4.06	±0.84 (64)	3.28	±0.61 (60)
lip-1;egl-1(n3082)	1.05	±0.33 (40)	2.13	±0.59 (39)	3.19	±0.72 (36)	7.32	±1.68 (37)
let-60(n1048gf)	1.98	±0.40 (56)	19.53	±1.96 (60)	2.58	±0.45 (55)	11.22	±1.50 (55)
gap-1(ga133)	1.80	±0.66 (20)	11.17	±1.89 (18)	0.80	±0.39 (20)	1.91	±0.98 (35)
mpk-1(ga111)	0.94	±0.39 (17)	2.25	±1.07 (20)				
hs::mpk-1 -HS	1.14	±0.47 (28)	1.91	±0.52 (32)	0.57	±0.40 (14)	1.06	±0.55 (16)
hs::mpk-1 +HS	0.62	±0.22 (60)	1.09	±0.38 (43)	0.57	±0.57 (14)	0.36	±0.26 (14)
lin-15(n309)	0.50	±0.39 (20)	1.25	±0.60 (20)	0.80	±0.42 (20)	0.40	±0.22 (20)
pmk-1(km25)	0.72	±0.32 (36)	3.36	±0.74 (59)	1.20	±0.36 (40)	1.35	±0.38 (40)

Table 12 Apoptotic response to irradiation in mutants with presumptive MAPK overactivation or reduction. Most mutants were also tested in an *rpo-1b(op259)* background. Average number of corpses per gonad, 95 % CI of the mean and total number of animals scored per condition.

5.5.8.3 Abnormal IR response in mutants with supposedly high MPK-1 pathway activity

I tested two other worm strains that show signs of increased MAPK signalling in vulval development. *lin-15* is a negative regulator of EGFR (LIN-23 in *C. elegans*) activation; loss of the two isoforms *lin-15a* and *lin-15b* in the *lin-15(n309)* mutant leads to a highly penetrant Muv phenotype (Clark 1994; Huang 1994). The mechanism of *lin-15* function is not known in detail; transgenic mosaic studies suggested synthesis of the proteins from hypodermal cells (Herman 1990), and further experiments

demonstrated an anchor cell-signal independent effect on vulval induction, that was genetically upstream of EGFR/*lin-23* (Clark 1994). It has not been studied what effect *lin-15* has on germ line Ras/MAPK signaling. I tested *lin-15(n309)* for irradiation-induced apoptosis. Contrarily to my expectations of similarity with *let-60(n1046gf)*, I found extremely low levels of germ cell apoptosis without and with irradiation (Figure 96 and Table 12). The gonads were thin and had much less germ cells than wildtype.

I was interested in the effects that a direct increase of MPK-1 would have on germ cell apoptosis. The transgene *gaIs36[hsp16-41::mpk-1(+) EF1a-D-mek(+); unc-30(+)]* codes for heat-shock promoter-driven *mpk-1*, the activity of which is enhanced by the Drosophila homolog of MEK (MAPKK for ERK). The transgene integration site is linked to mutant *him-5* (Lackner 1998). I heat-shocked *gaIs36* worms at L1 or L4 stage to induce MPK-1 expression and irradiated as usual. MPK-1 overexpression in this strain did not, as expected from the previous experiments, increase irradiation response, but rather lowered germ line apoptosis to very low levels (Figure 96 and Table 12). The transgene does not only lead to somatic MPK-1 overactivation effects upon heat-shock treatment, but already induces the characteristic tail blips in worms grown at 20°C. For the germ line, the apoptotic defect and morphological deviations from wildtype did not vary considerably between induced versus non-induced animals, and resembled the phenotype in *lin-15(n309)*. It is possible that the transgene does not evoke germ line expression, since it has been derived from an originally extrachromosomal array. We have to measure ppMPK-1 levels in situ to judge on MAPK pathway activity in the germ lines of *lin-15(n309)* and of the strains carrying *gaIs36*. It is an attractive possibility that the balance between somatic and germ cell Ras/MAPK activity determines apoptosis levels.

5.5.8.4 Mutants of the p38 MAPK *pmk-1* have reduced IR response

The p38 MAPK homolog *pmk-1* has been implicated in infection-induced germ cell death [see *7.2.1.8 Food type sensitivity does not depend on classical infection signaling*]. I tested whether this pathway might also play into irradiation-induced apoptosis. *pmk-1(km25)* animals had reduced apoptotic corpse numbers without or with irradiation (Figure 96 and Table 12).

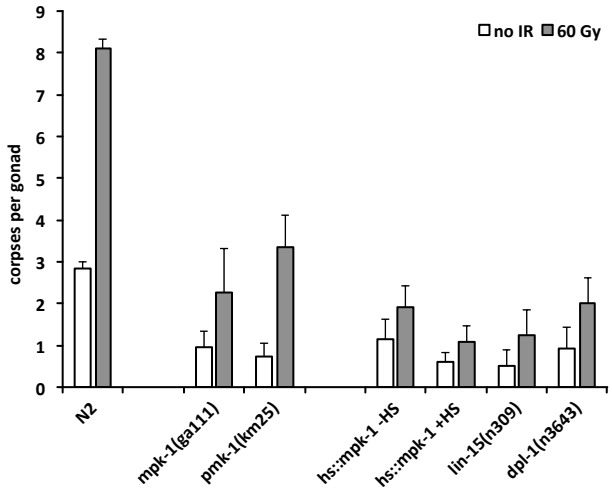

Figure 96 Mutants/transgenic lines with supposedly increased MPK activation have reduced IR-induced apoptosis. Apoptotic germ cell corpses at 24 hours post irradiation; error bars represent 95 % CI of the mean.

5.5.9 Conclusions on *rpo-1b(op259)* and Ras/MAPK activity

In summary, our genetic analyses demonstrated a functional relevance of the Ras/MAPK pathway in the regulation of IR-induced germ cell death. Mutations leading to MPK-1 overactivation increased the apoptotic corpse number upon irradiation. Conversely, in the *mpk-1(ga111)* weak reduction-of-function mutant, IR-induced apoptosis was reduced. *rpo-1b(op259)* mutants have reduced DNA damage-induced apoptosis. We found that the *rpo-1b(op259)* mutation significantly reduced the Ras/MAPK gain-of-function effect of *let-60(gf)* in vulval development. *In situ* staining confirmed decreased levels of activated, that is, di-phosphorylated, MPK-1 in *rpo-1b(op259)* mutant gonads. A causal link between reduced MPK-1 activity in *rpo-1b(op259)* and impaired IR response was again suggested by genetic experiments. These showed an increase of IR-induced apoptosis in *rpo-1b(op259)* when mutations were introduced that lead to hyperactivation of MPK-1. I therefore propose that a certain level or fraction of activated MPK-1 is required for a wildtype apoptotic response to DNA damage, and that in *rpo-1b(op259)* mutants, this level is not reached. Consequently, *rpo-1b(op259)* animals have fewer corpses than wildtype upon irradiation. This happens in spite of normally increased CEP-1 activity, a hallmark of DNA damage response; even more, in non-irradiated animals, CEP-1 activity is higher in *rpo-1b(op259)* than in wildtype. I showed in [*5.3 rpo-1b(op259) and CEP-1*] that constitutive germ cell death in *rpo-1b(op259)* is slightly reduced and fully dependent on *cep-1* function. In wildtype worms, Ras/MAPK, but not CEP-1 activity is acknowledged to be required for constitutive death; accordingly, I detected clearly reduced baseline apoptosis in the *mpk-1(ga111)* mutant. *rpo-1b(op259)* mutants, in the absence of functional CEP-1, have minimal baseline apoptosis, which is in agreement with significantly reduced MPK-1 activity. Collectively, these findings support a model in which CEP-1 and MPK-1 collaboratively establish the level of germ cell apoptosis. The MAPK pathway is therewith not only necessary for constitutive 'physiological' germ cell death, but is more generally critical for how sensitive cells are towards further pro-apoptotic signals (Figure 97). Ras/MAPK activity is possibly a master regulator of germ cell apoptosis in *C. elegans*.

Interestingly, irradiation increases MPK-1 activation in the meiotic pachytene region of wildtype gonads soon after treatment. Whether this increase has a consequence or is even essential for an efficient irradiation response cannot be clearly concluded from our result so far. Neither is it obvious that it is part of the DNA damage response. Other damages besides DNA lesions that also result from IR irradiation might activate the Ras/MAPK pathway, which could then be integrated as an additional stress-signal and render cells prone to death. Our observations indicated that CEP-1 is not required for MPK-1 activation, as ppMPK-1 levels in *cep-1(lf)* mutants were at least as high as in wildtype. Weidhaas et al. presented a somatic tissue model for IR-induced reproductive cell death in *C. elegans*; in this system, reduction of Ras/MAPK pathway activity did increase the sensitivity of dividing cells to irradiation-induced necrotic death (Weidhaas 2006b). An intact DNA damage response network was protective for cell survival, genetically upstream of Ras/MAPK. Theoretically, Ras/MAPK activity could, in addition to its permissive effect on germ cell apoptosis (and/or when above a certain threshold level), also entail cytoprotective measures to limit cell death. Maybe intact DNA damage signalling activates such an effect.

The restoration of apoptosis in *rpo-1b(op259)*, which has reduced levels of activated MPK-1, by mutations that enhance Ras/MAPK pathway activity is likely due to compensation of this reduction downstream of RPO-1B function. It is conceivable that there is a circulatory relationship of *rpo-1b(op259)* and Ras/MAPK. Mammalian ERK and RSK were shown to activate RNA Pol I activity by phosphorylation of TIF-1A (Zhao 2003a). Increasing Ras/MAPK pathway activation might partly compensate for rRNA synthesis defects in *rpo-1b(op259)* and thereby taper effects of *rpo-1b(op259)* on apoptosis. We need to determine rRNA transcript levels in sufficient replicates of double mutant worm samples to conclude on this.

The observation that Ras/MAPK pathway activity determines irradiation-induced apoptosis levels, and that this regulation is critically influenced by *rpo-1b(op259)* is potentially of high relevance for how tumours respond to therapeutic irradiation treatment. Changes in Ras/MAPK and in rRNA synthesis are very frequently found in proliferative diseases. *C. elegans* has proven valuable for studying cellular responses in a tissue context. The germ line as a model system within an intact organism allows to investigate the combinatorial effects that disturbances in basic cellular processes and pathways can have on cellular outcomes. It is to exploit this model further to understand the interactions in more detail.

	constitutive apoptosis		irradiation response (ΔIR)		post irradiation levels	
	(+)	*rpo-1b(op259)*	(+)	*rpo-1b(op259)*	(+)	*rpo-1b(op259)*
wt	→	(↓)	→	↓	↑	→
cep-1(lf)	(↓)	↓↓	×	×	(↓)	↓↓
ced-9(rf)	↑↑	↑↑↑	↑	n.d.	↑↑↑	n.d.
gld-1(rf)	→	↑	↑	↑↑	↑↑	↑↑↑
gla-1(rf)	↑↑	↑↑↑	n.d.	n.d.	n.d.	n.d.
lip-1(lf)	(↑)	↑	↑	↑↑	↑↑	↑↑↑

Table 13 Summary of the effect *rpo-1b(op259)* has in mutants with increased baseline apoptosis levels or enhanced irradiation response. Levels of apoptotic cell corpses in non-irradiated worms are indicated as increased ↑, or reduced ↓ in comparison to wildtype levels →. ΔIR indicates the incremental effect of irradiation on apoptosis levels, in relation to the effect in wildtype animals →; mutants with *cep-1(lf)* show no change after irradiation ×. The post-irradiation levels are again in relation to the levels in non-irradiated wildtype animals. *cep-1(lf)* and *egl-1(lf)* had slightly lower levels than wildtype in my experiments (↓), non-irradiated *lip-1(lf)* slightly higher levels (↑). Irradiation response was not determined (n.d.) in *gla-1(rf)* mutant combinations and in *rpo-1b(op259); ced-9(rf)*.

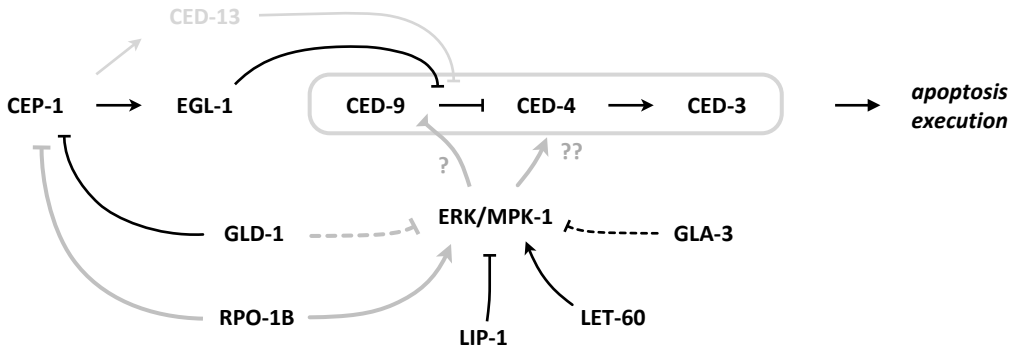

Figure 97 Model for the genetic interaction of RPO-1B with the Ras/MAPK pathway. CEP-1 activity is increased in *rpo-1b(op259)*, but this does not result in increased germ cell apoptosis; rather, apoptosis is reduced. RPO-1B likely has a permissive effect on apoptosis at the level of the core apoptotic machinery. As described in Figure 80, the precise level of action, downstream of EGL-1 expression, is not defined (indicated by ??). Likely, the modulatory effect of RPO-1B on apoptosis is via the Ras/MAPK pathway. *lip-1(lf)* and *let-60(gf)*, well-established activators of MPK-1, and *gla-3(rf)*, that was also shown to increase MPK-1 activation, sensitise germ cells to constitutive apoptosis as well as to CEP-1-induced death. All these mutations restore high germ cell apoptosis levels in *rpo-1b(op259)*. The next chapter will describe the combinatorial effect of *rpo-1b(op259)* and *ced-9(rf)*, which points to CED-9 as a critical factor for apoptosis modulation by *rpo-1b(op259)*. Given the similarity of *rpo-1b(op259); ced-9(rf)* with *rpo-1b(op259); lip-1(rf)* or *gla-1(rf) rpo-1b(op259)*, it is conceivable that the MAPK pathway acts on CED-9 (?, see next chapter). In Figure 80, I suggested an inhibitory effect of GLD-1 on the hypothetical factor XYZ. This factor might in fact be the Ras/MAPK pathway. In a published list of the transcriptome that co-precipitated with GLD-1, MPK-1 mRNA showed a significant enrichment in the pulldown vs. the control sample [see Supplementary Tables in (Wright 2010)]. Black lines indicate established links.

5.6 *rpo-1b(op259)* and CED-9

I had found that the *rpo-1b(op259)* mutation inhibits germ cell apoptosis downstream of *cep-1* and *egl-1*. Fitted into the current genetic models for programmed cell death in *C. elegans*, *rpo-1b* would then affect apoptosis at the level of the core apoptotic machinery or downstream of it. I therefore addressed the core apoptotic machinery for genetic relationship with *rpo-1b*. During these investigations, I undisclosed several new aspects of the genetics of *ced-9*. In this section, I will give an introduction on CED-9 and on structure-function analyses of the core apoptotic machinery. The findings on genetic relation of *rpo-1b(op259)* and *ced-9* will be presented and eventually lead to novel connections of CED-9 with CEP-1 and EGL-1.

5.6.1 CED-9 – the core inhibitor of apoptosis

At the core of apoptosis, three molecular components have been recognised to be indispensable in *C. elegans* non-disputably. CED-3, the effector caspase, is activated by CED-4 (Shaham 1996b), which is normally withheld by CED-9 in a quiescent state and which is released and activated upon pro-apoptotic signalling. CED-9 thus becomes a central angle point, allowing rapid disinhibition of the apoptotic execution cascade. Initially, *ced-9* was identified based on its protective function on cell death (Hengartner 1992). Gain of *ced-9* function prevents deaths of cells normally destined to die during development, whereas loss of *ced-9* function leads to extra cell death (Hengartner 1994a). This anti-apoptotic function of *ced-9* is consistent with the role of mammalian Bcl-2, which was identified to be its functional homolog (Hengartner 1994b). Pro- and anti-apoptotic signals are weighted by interactions of the interrelated Bcl-2 family proteins, for which the mammalian genome offers several members (Youle 2008); the *C. elegans* repertoire is more limited with CED-9 and the BH3-only proteins EGL-1 and CED-13. CED-9 might unite the functions of several mammalian homologs in one factor.

ced-4 and *ced-3* are essential for apoptosis in *C. elegans*; generally, loss-of-function mutations fully prevent programmed cell death. One instance has been described where apoptosis-like death occurred in the absence of functional CED-3 (Bloss 2003), an observation however that could not be repeated by another group (Jagasia 2005). A current genetic screen in our laboratory supports the possibility of *ced-3*-independent apoptosis execution [internal communication by Sheng Zeng].

5.6.1.1 CED-9 is at the interface of pro-apoptotic signalling and the core machinery

CED-9 is the decisive factor at the interface of pro-apoptotic signalling and the release of CED-4 for activation of the effector caspase CED-3; loss of CED-9 leads to massive, uninhibited cell death and presumably detaches the core machinery from upstream signalling. *ced-4*, *ced-3* and the cell death execution machinery are epistatic to apoptosis induction and to *ced-9*; loss of CED-3 or CED-4 blocks apoptosis independently of whether inhibitory CED-9 is present or not.

In contrast, loss of the function of pro-apoptotic factors that act upstream of *ced-9* – and that would normally activate apoptosis by inhibiting *ced-9* – are expected not to suppress apoptosis arising from reduction or loss of *ced-9* function.

5.6.1.2 The role of *ced-9* in physiological germ cell death is poorly defined

ced-9 mutants have been used to separate 'physiological' germ cell death from stress-induced apoptosis on a genetic level (Gartner 2008). DNA damage signalling for instance activates apoptosis mainly by upregulation of EGL-1, which binds to CED-9 and thereby disinhibits CED-4; the gain-of-function mutation *n1950* in CED-9, supposed to preclude EGL-1 binding and release of CED-4 from CED-9, prevents propagation of such pro-apoptotic signals to the execution machinery. Physiological germ cell apoptosis however is not prevented by loss of *egl-1* function or by the gain-of-function mutation *ced-9(n1950)* (Gumienny 1999); induction of 'physiological' germ cell death is therefore transmitted to the core apoptotic machinery via other mechanisms that might or might not even involve CED-9. Nevertheless, germ cell death occurring in *ced-9* reduction- or loss-of-function mutants has so far not been clearly distinguished from, or has even been equaled to, uninhibited physiological apoptosis.

5.6.1.3 The temperature sensitive *ced-9(n1653)* mutant is a viable approach to *ced-9* function

ced-9 temperature sensitive mutants have been very helpful in studying apoptosis. Whereas *ced-9* loss-of-function mutants die as larvae or become sterile due to excessive cell death, conditional mutants have moderately increased cell death at lower temperatures and only exhibit a strong phenotype at temperatures above 20°C. The *ced-9(n1653)* allele is supposed to be hypomorphic, with a temperature sensitive effect on apoptosis. It had originally been identified in a genetic screen for missing HSN neurons (Desai 1988), where it had led to an egg laying defect; this defect was later found to be due to aberrantly dying cells (Hengartner 1992). Programmed cell death was blocked in *ced-9(n1653)*/*ced-9(n1950gf)* trans-heterozygotes (Hengartner 1992), which indicated that *n1653* did not have dominant pro-apoptotic effects over the (dominant) anti-apoptotic gain-of-function allele *n1950*. Thus, *n1653* was suggested to cause excessive apoptosis by partial loss of CED-9 anti-apoptotic function, possibly by weakened interaction with CED-4 (Yan 2004). This allele therefore seemed highly valuable to study apoptosis regulation at the level of the core apoptotic machinery, including the very level of CED-9 itself. [See restraints in the following sections]

5.6.2 Structure of CED-9 and its binding partners

The interactions within the core apoptotic trio and of CED-9 with EGL-1 have been assessed *in situ* as well as biochemically and structurally [structure of CED-9 in (Yan 2004) and (Woo 2003), binding of CED-9 to CED-4 dimers in (Yan 2005), structure of the CED-4 octamer and of CED-3 nesting in (Qi 2010)]. According to the latest model, two CED-3 molecules are brought into close proximity in a hutch of the CED-4 apoptosome. The CED-3 dimer then probably undergoes auto-cleavage. The active CED-4 complex was shown to be a homo-octameric assembly of differently conformed subunits (Qi 2010), which revised the former assumption of a tetrameric CED-4 complex (Yan 2006). The CED-4 apoptosome is an assembly in rotation symmetry of four CED-4 dimers that are in turn the congregate of two isomers, CED-4a and CED-4b, which are distinct in the conformation of the N-terminal CARD domain. This basic dimer was also suggested as the structure that is withhold by CED-9; in the inhibitory complex, CED-9 binds the CED-4a subunit (Yan 2005). Somewhat in disagreement with this 1:2 stoichiometry, another *in vitro* study suggested a 2:2 heterotetrameric complex of CED-4 and CED-9

(Fairlie 2006). The studies on CED-4 release from CED-9 agree that EGL-1 binding to CED-9 potently disrupts the CED-9·CED-4 complex. EGL-1 binds to a fold in CED-9 that is opposite from the CED-4 binding interface; this binding leads to a significant conformational change of CED-9, thereby lowering the affinity for CED-4 (Yan 2004). The second known BH3-only protein in *C. elegans*, CED-13, was shown to also cause CED-4 release *in vitro*, even though less efficiently, in accordance with a lower CED-9 binding affinity than EGL-1 (Fairlie 2006).

5.6.2.1 CED-9 can regulate apoptosis without direct mitochondrial attachment

CED-4 was shown to translocate from mitochondria to nuclear membranes upon apoptosis induction in *C. elegans* embryos; overexpression of EGL-1 could induce this translocation; CED-9 was required for mitochondrial retention of CED-4 (Chen 2000). Newer observations however suggest that perinuclear localisation of CED-4 is not limited to cells undergoing cell death; for instance, we detected perinuclear accumulation of a CED-4::GFP reporter in all meiotic germ cells independently of exogenous apoptotic stimuli. Interestingly, Apaf-1/CED-4 was shown to have a non-apoptotic role in the DNA damage checkpoint upstream of Chk1 kinase activation (Zermati 2007); this might explain 'constitutive' localisation of CED-4 away from mitochondria. Mitochondrial localisation seems not to be essential for anti- and pro-apoptotic effects of CED-9. It was shown that transgenic CED-9 protein lacking the C-terminal transmembrane domain could mostly compensate for loss of *ced-9* function in somatic cell death regulation. This did of course not exclude an additional role of CED-9 at the mitochondria, in cell death or in other cellular processes (Tan 2007). Interesting interactions of CED-9 with mitochondrial proteins have been demonstrated that are relevant in apoptosis regulation. CED-9 is required for DRP-1 mediated mitochondrial fragmentation that happens upstream of CED-3 activation in developmental apoptosis of somatic cells (Jagasia 2005). The adenine nucleotide transporter (ANT) homolog WAN-1 (or ANT-1.1) localises to mitochondria and can form a complex with CED-9 and CED-4; it is required for efficient apoptosis in somatic and in germ cells (Shen 2009; Zhivotovsky 2009). Recently, a novel function for CED-9 was shown in association with lipid membranes, which it could remodel (Tan 2011).

5.6.2.2 Amino acid substitutions in CED-9*(n1950)* and CED-9*(n1653)* affect EGL-1 or CED-4 binding

ced-9(n1950) is a dominant inhibitor of developmental cell death (Hengartner 1992). One study in a heterologous expression system (human embryonic kidney cells) specifically characterised the effect of the G169E amino acid substitution in *ced-9(n1950)* on EGL-1 and CED-4 binding. EGL-1 could no longer disrupt the CED-4·CED-9(G169E) complex; it did bind to mutant CED-9, although with lower affinity than to wildtype CED-9 (del Peso 2000). G169E was modelled to result in a local bulge within the EGL-1 biding grove of CED-9 that would sterically clash with EGL-1 and therefore weaken EGL-1 binding to mutant CED-9 [(Yan 2004), (no data shown)]. Parrish et al. had demonstrated earlier a 4-fold reduction of EGL-1 binding affinity by the G169E substitution, and re-establishment of efficient binding to mutant CED-9 by second-site mutations in EGL-1. Only the second-site mutant EGL-1 but not EGL-1(wt) could displace CED-4 from CED-9(G169E); CED-9 affinity for CED-4 itself was unaffected by the G169E substitution (Parrish 2000). The inferred model states that EGL-1 binding to CED-9 is required for CED-4 release, and that G169E prevents EGL-1 binding, CED-4 release and therefore apoptosis induction. However, it is difficult to explain why such a modification would render the mutant

protein a dominant inhibitor of apoptosis. Theoretically, the available wildtype CED-9 protein in a *ced-9(n1950)*/*ced-9(+)* heterozygous cell should be able to bind EGL-1 and to normally release some CED-4. One possible explanation is that CED-4 in conjunction with CED-9 act as active inhibitors of apoptosis. Jagasia et al. showed that *ced-9(n1950)* but not loss of EGL-1 could block DRP-1-induced mitochondrial fragmentation, emphasising that different mechanisms from EGL-1-induced CED-4 release are involving CED-9 in apoptosis regulation, which are disturbed in the G169E mutant (Jagasia 2005).

The point mutation in *ced-9(n1653)* affects the residue Y149, which is near the beginning of the BH1 domain (Woo 2003) and in the alpha-helical structure α4 that apparently adjoins the EGL-1 binding grove in CED-9 (Yan 2004). The authors attribute a structural role to the residue, also concluding from the poor solubility of the Y149N mutant protein. They found reduced CED-4·CED-9 interaction of CED-9(Y149N) *in vitro* (using an N-terminally truncated CED-9); the consequences for EGL-1 binding were not addressed, however. In a motif search performed at ScanSite (Obenauer 2003), I found that the Y149 defines a potential target site for the Src type kinases. The tyrosine residue is however not conserved as a phosphorylation target in the human homologs of CED-9 [Figure 1 in (Woo 2003)].

5.6.2.3 The core apoptotic machinery conserves its inscrutable regulation

Detailed analysis of structure and structure-function relationship of BH3 domain proteins has facilitated the development of small molecular drugs to target apoptosis at its core (Chonghaile 2008; Richardson 2008; van Delft 2006). *C. elegans* offers a welcome tool for the study of the core apoptotic processes due to the relatively modest number of caspases and BH domain proteins. CED-9 and its interactions with EGL-1 on the one hand and CED-4 on the other hand have been carefully dissected. Nevertheless, the precise mechanisms how and when CED-4 is released and what other events than EGL-1 or CED-13 binding to CED-9 regulate CED-4 activation remains largely open. The effects of loss of *egl-1* function and of the point mutations in *ced-9* cannot be fully explained by the current understanding of structural changes. Germ line apoptosis occurring independently of EGL-1 suggests that there are either molecules with similar structure and redundant function, or that there are alternative routes to disrupt the CED-9·CED-4 complex. The occurrence of constitutive death in the *ced-9(n1950)* mutant, together with the observed incapacity of EGL-1 (and supposedly of redundant factors) to disrupt CED-4 binding to CED-9(G169E), favours the idea of alternative means how to release or otherwise activate CED-4. This could be by binding of other factors (such as for instance the ANT homolog WAN-1 (Shen 2009)) or by posttranslational modifications on CED-9 that might induce conformational changes, or by altered turnover of CED-9 protein; eventually, effects downstream of or in parallel to CED-9 are conceivable.

5.6.3 The *rpo-1b(op259); ced-9(n1653)* double mutant

rpo-1b(op259) mutants were defective for IR-induced apoptosis; if *rpo-1b(op259)* affected DNA damage signalling per se, *ced-9(n1653)* could be expected to increase cell death irrespective of this upstream block in apoptosis induction. However, I had discovered that in *rpo-1b(op259)* animals without exogenous DNA damage, baseline apoptosis must be different from the *cep-1* and *egl-1*-independent physiological germ cell death in wildtype animals: almost all germ cell death was abolished in *rpo-1b(op259)* mutants when functional CEP-1 was lost. Regarding this defect in 'physiological'

germ cell apoptosis, it was possible that *rpo-1b(op259)* blocked cell death at the level of or downstream of *ced-9*. We built the *rpo-1b(op259); ced-9(n1653)* double mutant to test whether *rpo-1b(op259)* would suppress excessive apoptosis caused by the presumptive *ced-9* reduction-of-function allele.

5.6.3.1 *rpo-1b(op259); ced-9(n1653)* have excessive germ cell corpses

To our great surprise, apoptosis of *ced-9(n1653)* was not reduced, but strongly enhanced. At 20°C, young adult animals rapidly started accumulating a lot of cell corpses; cell death increased and eventually all germ cells decayed so that none progressed to oocytes (Figure 98). The effect was less pronounced at 15°C, but still, *rpo-1b(op259); ced-9(n1653)* gonads had significantly higher numbers of corpses than *ced-9(n1653)*, which at this temperature had only a mild increase of cell death. When the double mutant worms were grown at increased temperature, most animals failed to give rise to embryos and became sterile. The sterility was unlikely to be a mere consequence of alterations in early germ line development: *rpo-1b(op259); ced-9(n1653)* worms lost fertility even when they were shifted to increased temperature only at late L4 stage, whereas when kept at 15°C they maintained a low rate of oocyte production and fertilisation. Before, the *rpo-1b(op259)* mutation seemed to regulate cell death negatively downstream of EGL-1 translation. In combination with *ced-9(n1653)*, however, it could strongly enhance the pro-apoptotic condition. This suggests that *rpo-1b(op259)* disturbs apoptosis by a molecular mechanism at the level of CED-9.

Corpses have uncommon morphology but are apoptotic

Germ cell corpses in *rpo-1b(op259); ced-9(n1653)* were different from the classical refractile discs observed by DIC in *ced-9(n1653)*: the proximal gonads were filled with cellularised germ cells that were usually larger and more granular than normal corpses and that often retained the shades of the nucleolus (Figure 98). This appearance was reminiscent of corpses in *gld-1(op236) rpo-1b(op259)*, *gla-1(op234) rpo-1b(op259)* and *rpo-1b(op259); lip-1(zh15)*, or in irradiated *gld-1(op236)*, *gla-3(RNAi)* and *lip-1(zh15)* mutants – all conditions with strongly enhanced germ cell death. To confirm that these cell corpses in *rpo-1b(op259); ced-9(n1653)* were indeed apoptotic, we crossed the strain with the *ced-3* loss-of-function allele *n717*, as dependency on CED-3 is a defining characteristic of apoptotic cell death. *ced-3(n717)* could fully suppress formation of the abnormal corpses in *rpo-1b(op259); ced-9(n1653)*, confirming the apoptotic nature of these deaths.

5.6.3.2 Loss of *ced-3* function suppresses sterility of *rpo-1b(op259); ced-9(n1653)*

ced-3(n717) partly restored fertility of *rpo-1b(op259); ced-9(n1653)* at 20°C, although the brood size remained very low. *rpo-1b; ced-9; ced-3(n717)* germ lines developed relatively healthy oocytes in young adult stages (Figure 98); at increasing age, oocytes did not reach normal size any more and started stacking in more than one row in the proximal gonad; eventually, the worms did not produce viable embryos any more. This phenomenon is known for *ced-3* mutants at certain conditions, i.e., high age (Andux 2008), or in combination with Gla mutations (Boag 2005). *rpo-1b(op259); ced-3(lf)* animals were already more strongly prone to exhibit this phenotype (Figure 51) and had much less progeny on average than *rpo-1b(op259)* or *ced-3(n717)* mutants alone. *ced-9(n1653)* seemed to enhance it even further. Although *ced-3(n717)* introduces additional health deficits in *rpo-1b(op259); ced-9(n1653)* germ lines,

it can suppress excessive cell death; and very likely by preventing apoptosis it restores fertility in otherwise sterile animals at 20°C.

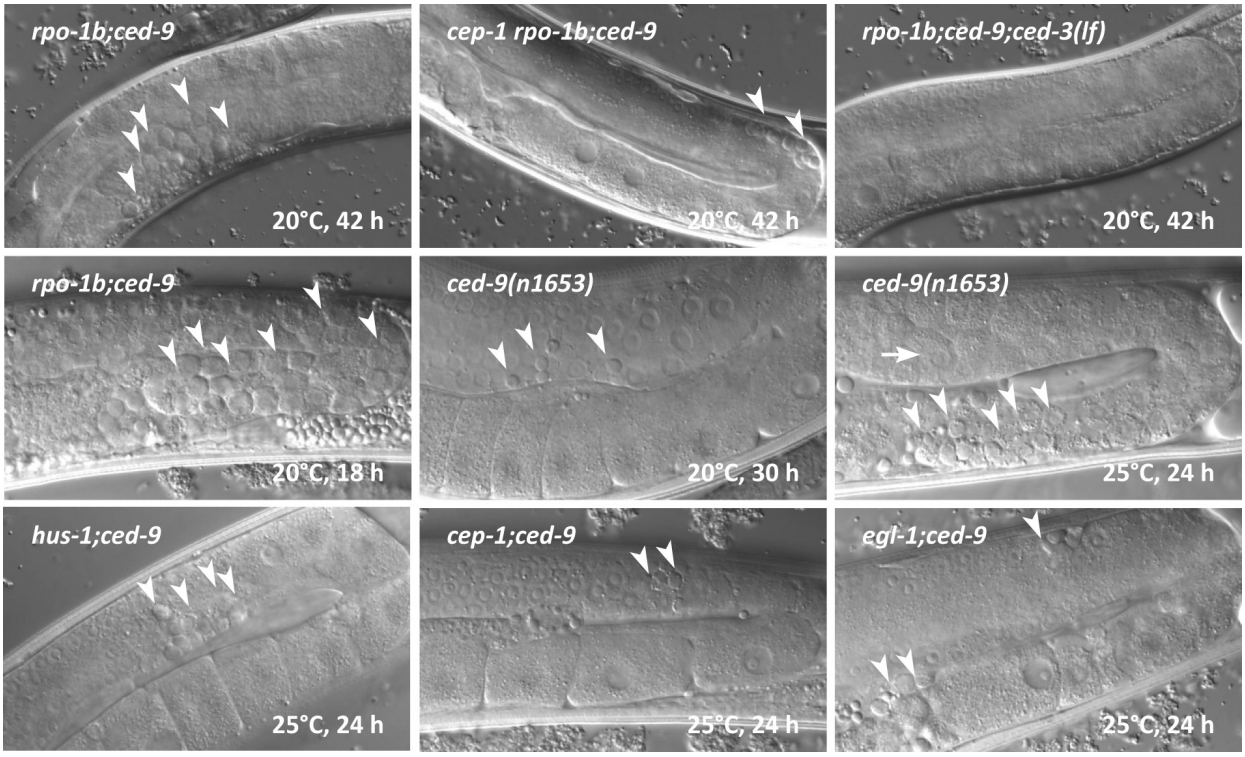

Figure 98 Excessive cell death in *rpo-1b(op259); ced-9(n1653)*. A large number of corpses (arrowheads) accumulate at the proximal end of the germ line already in young adults at 20°C. *ced-9(n1653)* mutants alone had a similar phenotype at 25°C. *cep-1(lf)* and *ced-3(lf)* can suppress sterility.

5.6.3.3 *ced-9(n1653)* can restore apoptosis in *cep-1(gk138) rpo-1b(op259)* or *rpo-1b(op259); egl-1(n3082)*

I showed that *cep-1(gk138) rpo-1b(op259)* or *rpo-1b(op259); egl-1(n3082)* had almost no germ cell death. In the current model of germ cell apoptosis, *cep-1(gk138)* or *egl-1(n3082)* would block stress-induced death and *rpo-1b(op259)* would consequently be blocking physiological germ cell death. There remained the possibility that these constellations brought about an impediment to apoptosis not directly related to apoptosis induction, like germ line differentiation or cell death execution defects. *ced-9(n1653)* had commonly been used to evaluate whether apoptosis execution in a mutant with defective pro-apoptotic signalling was principally possible. To test this, I built the triple mutants *cep-1 rpo-1b; ced-9* and *rpo-1b; ced-9; egl-1*. *ced-9(n1653)* could restore germ cell apoptosis in *cep-1(gk138) rpo-1b(op259)* and in *rpo-1b(op259); egl-1(n3082)* to some degree, which demonstrated that there was not a complete block of apoptosis execution downstream of *ced-9*.

5.6.3.4 Loss of *cep-1* or *egl-1* function suppresses excessive death and sterility of *rpo-1b(op259); ced-9(n1653)*

Considering that with mutant CED-9 protein the core apoptotic mechanism is unleashed from the signalling axis CEP-1→EGL-1⊣CED-9, one would expect similarly high levels of cell corpses for the triple mutants *cep-1(gk138) rpo-1b; ced-9* and *rpo-1b; ced-9; egl-1(n3082)* as for

rpo-1b(op259); ced-9(n1653). To my surprise, loss of *cep-1(gk138)* or of *egl-1(n3082)* reduced the highly excessive number of germ cell corpses of *rpo-1b(op259); ced-9(n1653)* (Figure 99). At 15°C, the germ lines particularly of *cep-1 rpo-1b; ced-9* looked much more healthy than of *rpo-1b(op259); ced-9(n1653)*; at 20°C, not all germ cells died, and oocytes and embryos developed in place (Figure 98). Intriguingly, this also ascertained some viable progeny, which we deployed in a genetic screen that will be described later in *5.7 Genetic screens to find suppressors of apoptosis*.

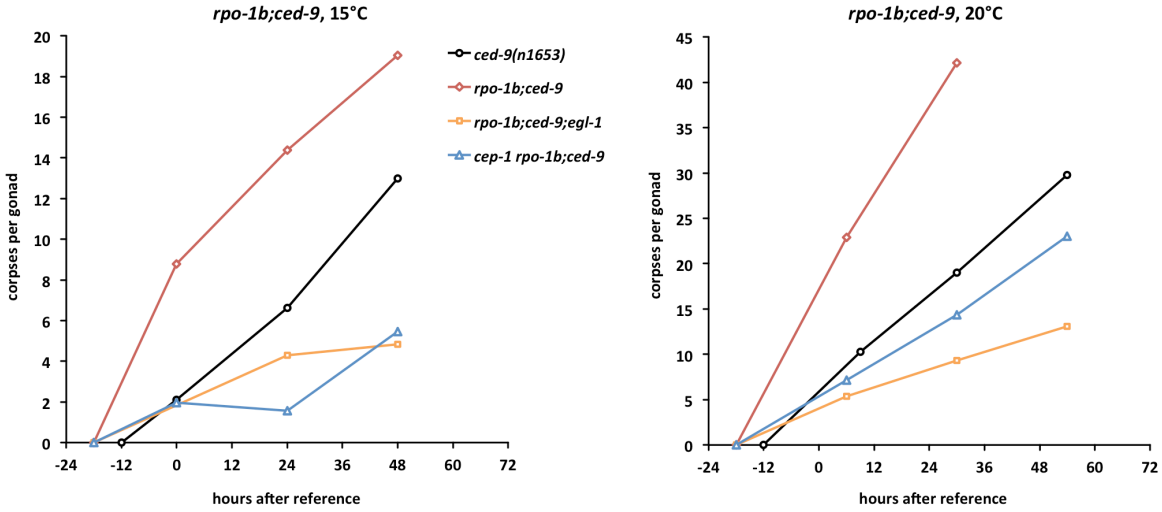

Figure 99 Cell death is increased in *rpo-1b(op259)* by *ced-9(n1653)*, in a *cep-1* and *egl-1*-dependent manner. Time course with shift from 15°C to indicated temperature at L4 stage. The reference time point was adjusted to the developmental speed of the respective mutants. Statistics see Table 15.

5.6.3.5 Conclusion: *ced-9(n1653)* mutants are responsive to pro-apoptotic cues

These findings were relevant from two perspectives. First, loss of CEP-1 or of EGL-1 could suppress a high fraction of germ cell death in non-irradiated mutants; an indication of significant CEP-1 activity that was consistent with the observation of increased EGL-1 and CED-13 mRNA levels in untreated *rpo-1b(op259)* mutants (Figure 61).

Second, the findings demonstrated that the *rpo-1b(op259); ced-9(n1653)* mutant was permissive to CEP-1 and EGL-1 pro-apoptotic signalling. This could specifically be due to an effect *rpo-1b(op259)* likely had at the level of CED-9; but it was also possible that *ced-9(n1653)* mutants could generally still transmit pro-apoptotic signals. I irradiated *ced-9(n1653)* mutants to test whether they were responsive to DNA damage-induced apoptosis (Figure 102). Indeed IR treatment could further increase the already high number of corpses of *ced-9(n1653)*, suggesting that the *ced-9(n1653)* mutation does not eliminate propagation of specific apoptotic signalling to the core apoptotic factors.

5.6.4 *pro-2(na27)* and CED-9

5.6.4.1 The rRNA processing mutant *pro-2(na27)* and *rpo-1b(op259)* have similar effects on *ced-9(n1653)*

I had studied the rRNA processing mutant *pro-2(na27)* due to its similarity with *rpo-1b(op259)*. Both mutants have defective apoptosis in the germ line; both seem to block IR-induced death downstream of

EGL-1 and CED-13 upregulation. They share another germ line defect: the proximal proliferation phenotype at increased temperature. Since both RPO-1B and PRO-2 are involved in early steps of ribosome synthesis, it is likely that the shared phenotypes of *rpo-1b(op259)* and *pro-2(na27)* are a consequence of alterations in this process. I was wondering whether the implications of *rpo-1b(op259)* on apoptosis regulation at the level of *ced-9* might also be a shared feature with *pro-2(na27)* and thus in more likelihood the result of disturbed rRNA synthesis. Indeed, *pro-2(na27); ced-9(n1653)* double mutatns were similar to *rpo-1b(op259); ced-9(n1653)* animals. Excessive apoptosis of *ced-9(n1653)* at 20°C was strongly enhanced (Figure 100) and most animals had only few progeny (Table 17); however, the defect slightly improved in older animals, when some normal oocytes were formed and a few embryos could develop. Like in *rpo-1b(op259); ced-9(n1653)*, *cep-1(gk138)* could significantly reduce the number of corpses in *pro-2(na27); ced-9(n1653)*. The number of apoptotic cells in *cep-1(gk138); pro-2(na27); ced-9(n1653)* was lower than in *ced-9(n1653)* or in *cep-1(gk138); ced-9(n1653)*. I think that the apoptotic phenotypes of *rpo-1b(op259)* and *pro-2(na27)* are very similar in many aspects and suggest that they have a common underlying mechanism.

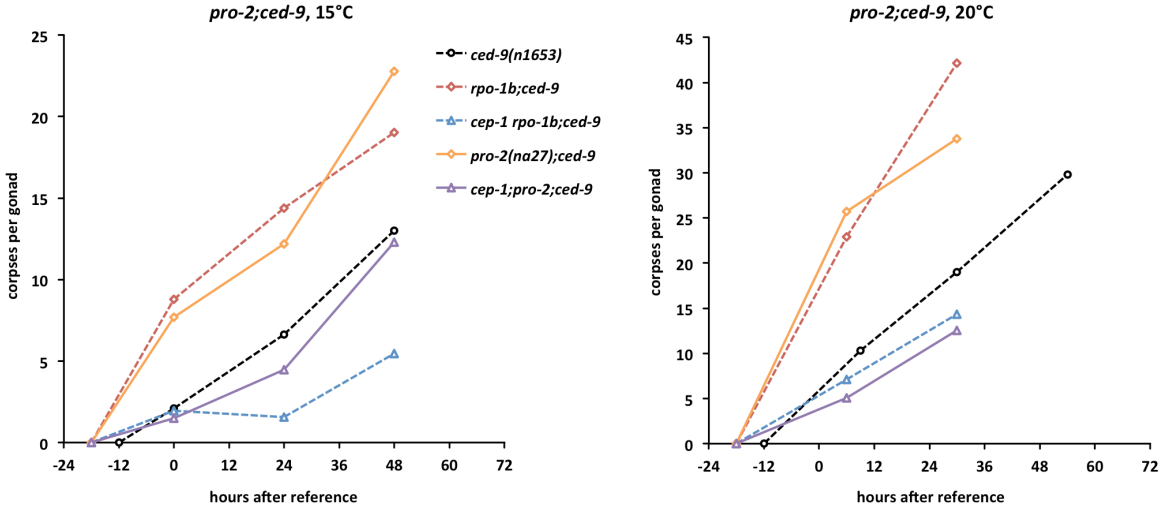

Figure 100 *pro-2(na27)* is similar to *rpo-1b(op259)* in combination with *ced-9(n1653)*. The high corpse number is also strongly reduced by cep-1(gk138). Time course as in Figure 99.

5.6.5 *ced-9*, *cep-1* and *egl-1*

5.6.5.1 Corpse numbers in combinations of *rpo-1b(op259)*, *ced-9*, *cep-1*, and *egl-1*

To elucidate the interplay of *rpo-1b(op259)*, *ced-9* and *cep-1*, I scored the number of germ cell corpses at different temperatures in the following mutant combinations:

ced-9(n1653)

ced-9(n1653) mutants, in agreement with previous observations (Gumienny 1999), had progressively increasing corpse numbers over time. At 15°C, the increase was moderate, reaching around 10 corpses per gonad 48 hours after the reference time point; at 20°C, about 20 corpses were present already at 24 hours (Figure 99 and Table 14); at 25°C, all germ cells became apoptotic soon after the temperature shift (Figure 98), which made the mutants sterile (Table 17).

rpo-1b(op259); ced-9(n1653)

rpo-1b(op259); ced-9(n1653), as described already, had massively higher numbers of corpses (Figure 99 and Table 15). The levels of *rpo-1b(op259); ced-9(n1653)* at 15°C resembled those of *ced-9(n1653)* at 20°C; at 20°C, germ cells would occasionally develop into oocytes in very young adults but became all apoptotic in aging animals.

cep-1(gk138); ced-9(n1653)

Interestingly, *cep-1(gk138); ced-9(n1653)* were not indifferent from *ced-9(n1653)* as would have been expected if germ cell death of non-irradiated animals were independent of CEP-1 and EGL-1. Instead, *cep-1(lf)* reduced the number of corpses (Figure 101 and Table 14); slightly at 15°C, more noticeably at 20°C, and most significantly at 25°C. It could even suppress the sterility phenotype of *ced-9(n1653)* at 25°C (Figure 98 and Table 17), as will be further discussed in later sections.

cep-1(gk138) rpo-1b(op259); ced-9(n1653)

cep-1 rpo-1b; ced-9 had very low numbers at 15°C; and also at 20°C the average corpse number was lower than in *ced-9(n1653)* mutants (Figure 99 and Table 15). It was also below that of *cep-1(gk138); ced-9(n1653)*. This indicates that *rpo-1b(op259)* requires functional CEP-1 to provoke an enhancement of the *ced-9(n1653)* effect; without CEP-1, *rpo-1b(op259)* mutation reduces the number of corpses of *ced-9(n1653)*.

ced-9(n1653); egl-1(n3082)

egl-1(n3082) strongly reduced the number of cell corpses in *ced-9(n1653)* germ lines (Figure 101 and Table 14); it reduced apoptosis at 15°C, at 20°C and at 25°C, and suppressed sterility of *ced-9(n1653)* at 25°C (Table 17). Lei Xiong had built a double mutant of *ced-9(n1653)* with the deletion allele *egl-1(ok1418)*, which we also examined for germ cell apoptosis; it suppressed excessive apoptosis equally well as *egl-1(n3082)*. Increased cell death in *ced-9(n1653)* thus largely depends on functional *egl-1*.

rpo-1b(op259); ced-9(n1653); egl-1(n3082)

rpo-1b; ced-9; egl-1 had equally low levels as *ced-9(n1653); egl-1(n3082)* (Figure 99 and Table 15). *egl-1(n3082)*, like *cep-1(gk138)*, could suppress sterility of *rpo-1b(op259); ced-9(n1653)* at 20°C (Table 17).

		ced-9(n1653)		*ced-9;egl-1(n3082)*		*cep-1(gk138);ced-9*		*hus-1(op244);ced-9*	
		score	**95% CI (n)**	**score**	**95% CI (n)**	**score**	**95% CI (n)**	**score**	**95% CI (n)**
15°C	**0 h**	2.10	±0.56 (40)			1.36	±0.45 (36)		
	24 h	6.63	±1.47 (40)	3.69	±0.98 (16)	5.93	±1.04 (40)	6.25	±1.69 (20)
	48 h	13.00	±1.96 (60)	3.86	±0.90 (36)	7.20	±1.41 (40)	11.20	±2.69 (20)
20°C	**9 h**	10.30	±1.24 (133)	4.76	±0.79 (66)	9.68	±2.02 (56)	10.47	±2.26 (36)
	30 h	19.01	±1.35 (100)	6.67	±1.80 (48)	16.52	±1.91 (60)		
	54 h	29.81	±4.19 (16)	6.58	±1.80 (24)	25.55	±3.07 (20)		
25°C	**12 h**	44.24	±3.33 (17)	20.80	±3.62 (50)	10.41	±2.56 (59)	35.31	±3.85 (16)
	36 h	sterile		16.71	±4.31 (14)	22.56	±3.21 (18)	sterile	

Table 14 Apoptotic corpses in *ced-9(n1653)* are strongly suppressed by loss of *egl-1* function at 20°C. Average number of corpses per gonad, 95 % CI of the mean and total number of worms scored per condition.

		ced-9(n1653)		*rpo-1b(op259);ced-9*		*rpo-1b;ced-9;egl-1(n3082)*		*cep-1(gk138) rpo-1b;ced-9*	
		score	**95% CI (n)**	**score**	**95% CI (n)**	**score**	**95% CI (n)**	**score**	**95% CI (n)**
15°C	**0 h**	2.10	±0.56 (40)	8.78	±2.13 (40)			1.95	±0.64 (40)
	24 h	6.63	±1.47 (40)	14.39	±2.37 (36)	4.30	±1.43 (30)	1.58	±0.55 (40)
	48 h	13.00	±1.96 (60)	19.03	±2.44 (40)	4.84	±2.33 (25)	5.45	±1.22 (44)
20°C	**6 h**	10.30	±1.24 (133)	22.91	±2.68 (35)	5.38	±0.85 (48)	7.14	±1.23 (80)
	30 h	19.01	±1.35 (100)	42.14	±3.16 (28)	9.33	±1.39 (64)	14.33	±1.24 (120)
	54 h	29.81	±4.19 (16)	sterile		13.06	±3.25 (32)	23.02	±2.18 (56)

		hus-1(op244) rpo-1b;ced-9		*atm-1(gk186)) rpo-1b;ced-9*		*rpo-1b;ced-9 unc-119(ed3)*		*rpo-1b;ced-9;ced-3(n717)*	
		score	**95% CI (n)**	**score**	**95% CI (n)**	**score**	**95% CI (n)**	**score**	**95% CI (n)**
15°C	**0 h**								
	24 h	7.03	±1.05 (58)	14.13	±2.30 (32)				
	48 h	7.98	±1.63 (41)			3.30	±1.13 (20)		
20°C	**6 h**	7.84	±1.01 (81)	23.78	±2.82 (37)	4.79	±1.70 (19)		
	30 h	14.88	±1.82 (60)	37.69	±3.50 (16)	7.56	±1.18 (77)	0.00	(32)
	54 h	16.30	±2.29 (20)	sterile					

		pro-2(na27);ced-9		*cep-1;pro-2;ced-9*	
		score	**95% CI (n)**	**score**	**95% CI (n)**
15°C	**0 h**	7.68	±2.18 (22)	1.50	±1.88 (4)
	24 h	12.20	±2.80 (20)	4.45	±1.60 (33)
	48 h	22.77	±2.65 (35)	12.31	±3.40 (39)
20°C	**6 h**	25.68	±3.39 (38)	5.10	±1.31 (42)
	30 h	33.75	±4.88 (16)	12.57	±3.42 (37)
	54 h	37.71	±5.23 (7)	37.06	±6.72 (17)

Table 15 Excessive germ cell apoptosis in *rpo-1b(op259); ced-9(n1653)* and in *pro-2(na27); ced-9(n1653)* and suppression by loss-of-function mutations of pro-apoptotic factors. Average number of corpses per gonad, 95 % CI of the mean, and total number of worms scored per condition.

5.6.5.2 Increased apoptosis in *ced-9(n1653)* is dependent on EGL-1 and enhanced by CEP-1

rpo-1b(op259) enhances apoptosis in *ced-9(n1653)* dependently on *cep-1*

In summary, these data show that increased germ cell death in *ced-9(n1653)* involves *cep-1* and *egl-1*. *rpo-1b(op259)*, that in a *ced-9* wildtype background reduces apoptosis, does enhance the increased cell death of *ced-9(n1653)*, dependently on *cep-1* and *egl-1*. The presumptive reduction-of-function mutant *ced-9(n1653)* is not irresponsive to *cep-1* and *egl-1* signalling. Rather, it seems that germ cells in *ced-9(n1653)* mutants are particularly sensitive to these factors; even without exogenous stress, *cep-1* and *egl-1* are relevant for apoptosis.

Excessive apoptosis in *ced-9(n1653)* is not 'physiological'

Considering the independence of 'physiological' germ cell apoptosis from CEP-1 and EGL-1, it was surprising that cell death in *ced-9(n1653)*, which in former models was assumed to correspond to unleashed physiological death, could be significantly reduced by loss of *cep-1* or *egl-1* function. Possibly, the basic levels of EGL-1 present in non-damaged germ lines are sufficient to provoke cell death in *ced-9(n1653)*; loss of *egl-1* function almost completely cut the increase of apoptotic cells in *ced-9(n1653)*. With or without exogenous DNA damage, EGL-1 transcription seems to be maintained mainly by CEP-1, since *cep-1* loss-of-function mutants have generally reduced *egl-1* transcript levels; this would then explain why loss of CEP-1 could also reduce apoptosis in *ced-9(n1653)*.

5.6.5.3 CEP-1 activity is increased in *ced-9(n1653)*

Alternatively to apoptosis being a mere result of increased sensitivity to CEP-1/EGL-1, it could in fact be an increase of CEP-1 activity that drove enhanced cell death in *ced-9(n1653)*. To test for this possibility, I measured EGL-1 and CED-13 transcript levels in *ced-9(n1653)* mutants at different temperatures. At 15°C and at 20°C, levels of EGL-1 and CED-13 were significantly increased in *ced-9(n1653)* as compared to wildtype (Table 16). This increase is likely due to CEP-1 activity, since *cep-1(gk138); ced-9(n1653)* animals have low levels.

The egg laying defect of *ced-9(n1653)* could be confounding the qRT-PCR data of EGL-1 and CED-13 transcript; *ced-9(n1653)* animals tend to harbour a lot of eggs and thus of developing embryos; for *egl-1*, the transcripts from retained eggs in some of the mutants might account for the increase to some extent; however, suppression by *cep-1(gk138)* would speak for germ cell provenance, since in cells of the developing embryo, EGL-1 transcription should be *cep-1*-independent. (For *ced-13*, transcripts from the germ line and transcripts of embryos arising from them have not been clearly distinguished in the experiments that compared animals with or without germ line (Schumacher 2005b).) Again a caveat is that *cep-1(gk138)* also suppresses the Egl phenotype considerably [see *5.6.6.4 hus-1(op244) and cep-1(gk138) but not egl-1(n3082) rescue the Egl phenotype of ced-9(n1653)]*. We minimised the risk by measuring transcript levels in *ced-9(n1653); ced-3(n717)* animals, that do not have the strong Egl phenotype either. Although reduced in comparison to *ced-9(n1653)*, *ced-9(n1653); ced-3(n717)* had clearly higher EGL-1 and CED-13 transcript levels than wildtype. It is therefore unlikely that the increase seen in *ced-9(n1653)* is solely due to embryo retention. Also, this experiment shows that the increase happens independently and thus likely upstream of CED-3 and is not itself a result of more apoptotic corpses.

ced-9(n1653) have some CEP-1-independent, EGL-1-dependent apoptosis

ced-9(n1653) animals at 20°C have a high number of corpses; this is reduced in *cep-1(gk138); ced-9(n1653)*, but still clearly above wildtype; and it is even more strongly reduced by *egl-1(n3082)*. Altogether, it appears that *ced-9(n1653)* mutants do have some CEP-1-independent increase of apoptosis; additionally, CEP-1 activity is stimulated by an unknown mechanism, which further enhances germ cell death.

I am testing with a triple mutant *cep-1(gk138); ced-9(n1653); egl-1(n3082)* whether death promotion by CEP-1 and EGL-1 could be happening in parallel.

CEP-1 activity in *ced-9(n1653)* is not further enhanced by *rpo-1b(op259)*

As described in former paragraphs, *rpo-1b(op259)* mutants have increased CEP-1 activity. I considered that this increase might explain the enhancement by *rpo-1b(op259)* of excessive apoptosis of *ced-9(n1653)*. In support of this idea, I had seen strong dependence on *cep-1* for excessive apoptosis in *rpo-1b(op259); ced-9(n1653)*. To assess whether *rpo-1b(op259)* had a measurable effect on CEP-1 activity also in *ced-9(n1653)*, I determined EGL-1 and CED-13 transcript levels in *rpo-1b(op259); ced-9(n1653)* and in *cep-1 rpo-1b; ced-9*. Interestingly, levels in *rpo-1b(op259); ced-9(n1653)* were not above *ced-9(n1653)* and not clearly above *ced-9(n1653); ced-3(n717)* (caution: *rpo-1b(op259); ced-9(n1653)* animals are not Egl); also the

levels were in the range of *rpo-1b(op259)*. From these data, the enhancement of apoptosis in *ced-9(n1653)* cannot simply be explained by *rpo-1b(op259)*-induced upregulation of CEP-1 activity.

	15°C					20°C					25°C				
	egl-1		ced-13			egl-1		ced-13			egl-1		ced-13		
	level	SD	level	SD	n	level	SD	level	SD	n	level	SD	level	SD	n
wt	1.04	0.27	1.18	0.24	2	1.07	0.25	1.07	0.22	13	1.07	0.03	1.61	0.22	2
rpo-1b(op259)	4.35		9.73		1	2.32	1.34	6.10	4.44	9					
egl-1(n1084 n3082)						2.06		3.26		1					
cep-1(gk138)						0.53		1.22		1					
hus-1(op244)						3.19		2.53		1					
cep-1 rpo-1b						0.60		2.13		1					
hus-1 rpo-1b						1.96		2.13		1					
rpo-1b;ced-3(n717)						1.09		13.22		1					
ced-9(n1653)	5.87	3.20	8.92	2.97	3	5.62	0.25	22.22	20.37	2	4.12	1.63	21.02	21.77	2
ced-9;egl-1	6.28	4.03	6.36	6.97	2	7.65		3.00		1					
cep-1;ced-9	0.66		0.91		1	1.06		2.15		1	2.09		1.55		1
hus-1;ced-9	4.21	0.40	3.11	1.30	2	3.10		1.50		1					
ced-9;ced-3(717)						2.00		7.09		1					
ced-9(n2812)/qC1	2.59		2.66		1						3.65		6.12		1
ced-9(n2812);ced-3	1.06		3.34		1						2.01		26.42		1
rpo-1b;ced-9	2.92		6.41		3	2.38		5.91		1					
rpo-1b;ced-9;egl-1	3.68		5.87		1	3.03		8.08		1					
cep-1 rpo-1b;ced-9	3.16		2.26		1	2.40		1.76		1					
hus-1 rpo-1b;ced-9	2.63		2.77		1	1.49		2.03		1					
atm-1 rpo-1b;ced-9	3.51		9.02		1	2.39		10.56		1					

Table 16 Transcript levels of the CEP-1 targets EGL-1 and CED-13 in *ced-9(n1653)* mutants, at increasing temperature. Double mutants with *ced-9* were shifted to the indicated temperature as L4 and worms were collected at 20 to 36 hours post L4 (depending an temperature and mutant condition). Internally normalised levels were related to one wildtype (wt) control at 20°C in each experiment; SD standard deviation and n number of replicates are indicated. Note that for most conditions, only one worm culture was sampled.

5.6.5.4 Conclusion: CED-9 is critical for modulation of apoptosis by *rpo-1b(op259)*

It is intriguing that the inhibiting effect of *rpo-1b(op259)* on apoptosis can be overcome by the mutation in CED-9. *ced-9(n1653)* seems to render germ cells more sensitive to CEP-1 and EGL-1 and/or to increase their activity levels; possibly in such a way that the blocking effect of *rpo-1b(op259)* would be dominated. The fact that the block in apoptosis is not only relieved, but even reversed to an enhancement in *ced-9(n1653)* suggests that CED-9 itself is a critical factor for how *rpo-1b(op259)* limits germ cell apoptosis; in the *ced-9(n1653)* mutant, this regulation might be lost or disturbed.

5.6.6 Modes of hyperactivation of apoptosis in *ced-9(n1653)*

5.6.6.1 *hus-1(op244)* weakly suppresses excessive apoptosis and sterility

We speculated on mechanisms for CEP-1 activation in *ced-9(n1653)*. Might it involve other factors of DNA damage response? If *ced-9(n1653)* somehow provoked DNA damage signalling and this was causing increased apoptosis, loss of such factors would reduce excessive cell death. HUS-1 is the *C. elegans* homolog of a 9-1-1 complex subunit; it is required for irradiation-induced apoptosis and signals through CEP-1 activation (Hofmann 2002). We tested the loss-of-function allele *hus-1(op244)* in *ced-9(n1653)* and in *rpo-1b(op259); ced-9(n1653)*. Indeed, *hus-1(op244)* slightly reduced the number of apoptotic corpses in *ced-9(n1653)* (Figure 101) and in *rpo-1b(op259); ced-9(n1653)* (Table 15); it could also weakly suppress sterility of *rpo-1b(op259); ced-9(n1653)* at 20°C (Table 17). Analysis of EGL-1 and CED-13 transcripts showed lower levels in *hus-1(op244); ced-9(n1653)* and *hus-1 rpo-1b; ced-9*

than in *ced-9(n1653)* and in *rpo-1b(op259); ced-9(n1653)*, respectively. Thus, HUS-1 possibly mediates some of the CEP-1 activity and of apoptosis in *rpo-1b(op259); ced-9(n1653)*.

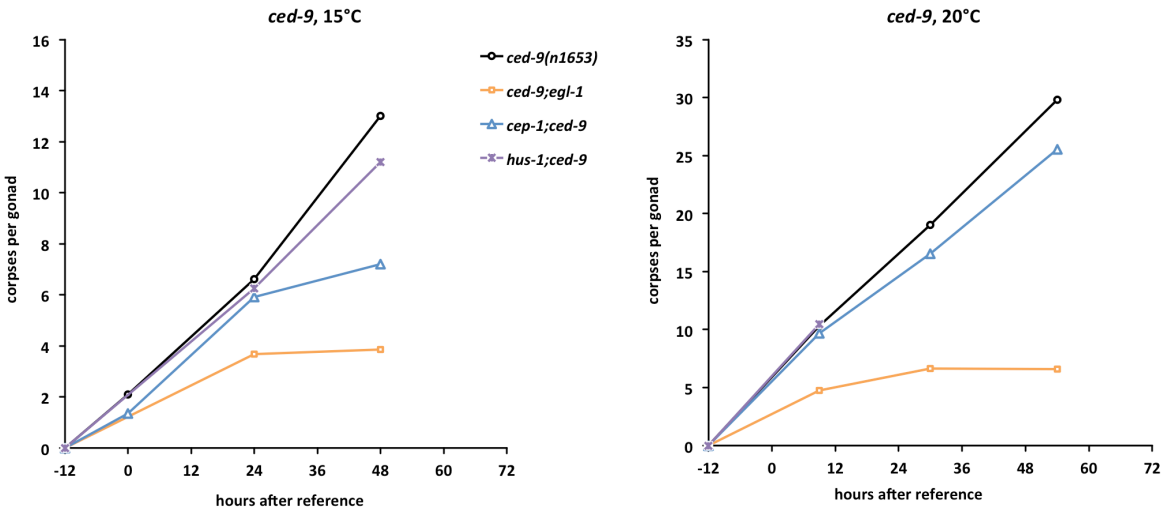

Figure 101 Strong suppression of excessive death of *ced-9(n1653)* by loss of *egl-1* function, and decrease of cell death levels by *cep-1(gk138)*. Time course as in Figure 99; statistics in Table 14.

5.6.6.2 Suppression of apoptosis can suppress sterility

We quantitatively assessed suppression of sterility of *ced-9(n1653)* and *rpo-1b(op259); ced-9(n1653)* at 25°C and 21°C, respectively, by mutant factors for which he had detected a reduction of apoptosis (Table 17). It was likely that these factors mainly increased fertility by suppression of excessive germ cell death; however, as the example of *ced-3(lf)* showed, the mutations with the strongest suppression of apoptosis do not necessarily improve fertility most significantly.

ced-3(n717), *egl-1(n3082)*, *cep-1(gk138)* and partly also *hus-1(op244)* restored fertility; relatively, the effects in *ced-9(n1653)* did not parallel those in *rpo-1b(op259); ced-9(n1653)*. In *ced-9(n1653)*, *cep-1(gk138)* was most potent; its suppressive effect was significantly stronger than *ced-3(n717)* or *egl-1(n3082)*. In *rpo-1b(op259)*, *egl-1(n3082)* was more potent than *cep-1(gk138)*. *hus-1(op244)* weakly restored fertility in *rpo-1b(op259); ced-9(n1653)*, but not in *ced-9(n1653)*. We also tested the reduction-of-function allele *ced-3(n2438)* in *ced-9(n1653)*; it improved fertility slightly better than the strong loss-of-function allele *ced-3(n717)*.

It remains to be determined how the *ced-3(n717)*, *ced-3(n2438)*, *egl-1(n3082)*, *cep-1(gk138)* and *hus-1(op244)* mutations themselves influence fertility at 21°C and at 25°C.

	15°C -> 25°C at L4	
	total eggs	95% CI (n)
N2 wt	106	±10.91 (8)
ced-9(n1653)	3	±1.29 (72)
ced-9;egl-1	21	±3.54 (34)
cep-1;ced-9	73	±10.54 (36)
hus-1;ced-9	5	±1.61 (42)
ced-9 unc-119	21	±2.35 (15)
ced-9;ced-3(n717)	19	±3.90 (32)
ced-9;nIs96	5	±3.73 (24)
ced-9;ced-3(n2438);nIs96	29	±4.05 (16)

	15°C -> 21°C at L4	
	total eggs	95% CI (n)
rpo-1b;ced-9	2	±1.65 (64)
rpo-1b;ced-9;egl-1	92	±10.07 (35)
cep-1 rpo-1b;ced-9	36	±7.79 (40)
hus-1 rpo-1b;ced-9	14	±6.00 (40)
atm-1 rpo-1b;ced-9	3	±1.13 (72)
rpo-1b;ced-9 unc-119	67	±4.50 (40)
pro-2;ced-9	23	±5.90 (81)
cep-1;pro-2;ced-9	28	±8.34 (24)

Table 17 Restoration of fertility in *ced-9(n1653)* mutants. One (N2 wt, *cep-1(gk138); ced-9(n1653)*) to five L4 stage worms were transferred as groups to individual plates and shifted to the indicated temperature. The number of viable progeny was counted 72 (25°C) or 96 (21°C) hours later and the average per worm was calculated for a plate. Table indicates average number of eggs per worm, 95 % CI of the mean and total number of worms scored.

5.6.6.3 A genetic screen will help to identify activators of apoptosis

We used sterility as a surrogate for excessive apoptosis in *rpo-1b(op259); ced-9(n1653)*. With a genetic screen for suppressors of sterility, we might identify the pathways that are relevant for apoptosis induction in *ced-9(n1653)*. Possibly, such a screen would reveal the factors and mechanisms that lead to activation of CEP-1. Three screening approaches that followed this aim will be described in *5.7 Genetic screens to find suppressors of apoptosis*.

5.6.6.4 *hus-1(op244)* and *cep-1(gk138)* but not *egl-1(n3082)* rescue the Egl phenotype of *ced-9(n1653)*

ced-9(n1653) mutants have an egg-laying defect (Egl) that presumably results from aberrant cell death of the Hermaphrodite Specific Neurons (HSN) (Desai 1989). Mutants of the core apoptotic factors *ced-4* or *ced-3* can suppress HSN cell death and hence the Egl phenotype (Yuan 1993). Interestingly, both *rpo-1b(op259)* and *cep-1(gk138)* could also suppress the Egl phenotype of *ced-9(n1653)*; whereas *ced-9(n1653); egl-1(n3082)* were equally Egl as *ced-9(n1653)*. *egl-1(n3082)* had been identified as an intragenic suppressor (Conradt 1998) of *egl-1(n1084)* – itself a dominant mutation that leads to release of EGL-1 transcription from inhibition in HSN neurons and thus to apoptosis (Ellis 1986a). If the Egl phenotype in *ced-9(n1653)* mutants is indeed a result of aberrant HSN apoptosis, suppression by *cep-1(gk138)* but not by *egl-1(n3082)* indicates that CEP-1 can contribute to cell death in *ced-9(n1653)* mutants; by a route that does not require *egl-1(n3082)* activation. Loss of HUS-1, that is supposed to act through *cep-1(gk138)* in germ cell apoptosis, did also suppress the Egl phenotype of *ced-9(n1653)*, indicating that the DNA damage response factor HUS-1, too, can contribute to somatic cell death in *ced-9(n1653)*. The interplay of CED-9 and of DNA damage response factors in developmental apoptosis of somatic cells will be further considered in *5.6.7 ced-9(n1653) in developmental cell death*.

5.6.6.5 Conclusion: *cep-1* and *egl-1* – more than two successors in a linear pathway

I have shown that in *ced-9(n1653)* mutants, *cep-1* and *egl-1* are highly involved in activating germ cell apoptosis even without exogenous DNA damage. *cep-1(gk138)* and *egl-1(n3082)* both suppressed

excessive cell death of *ced-9(n1653)* to some extent; however, loss of *egl-1* function had a more pronounced effect on apoptosis suppression than *cep-1(gk138)* at 15°C and at 20°C. Conversely, *cep-1(gk138)* was significantly more beneficent for fertility of *ced-9(n1653)* at 25°C. Also, as described in the former section, *cep-1(gk138)* and *egl-1(n3082)* were different in their effect on the Egl phenotype.

Loss of these two genes is clearly not equivalent in *ced-9(n1653)*, even though *cep-1* and *egl-1* are assumed to act in a linear pathway in germ cell apoptosis, with CEP-1 directly activating EGL-1 transcription. The stronger suppression of apoptosis in *ced-9(n1653); egl-1(n3082)* than in *cep-1(gk138); ced-9(n1653)* might be explained by complete dependence on EGL-1 for CEP-1 to be effective; and 'leaky' EGL-1 transcription in the absence of CEP-1 might be sufficient to maintain the levels of death seen in *cep-1(gk138); ced-9(n1653)*. Alternatively, CEP-1 could have *egl-1*-independent effects on germ cell apoptosis. One could consider CED-13, the second known pro-apoptotic BH3-only protein; it was shown to be relevant, yet of lower importance than EGL-1, in DNA damage-induced germ cell apoptosis (Schumacher 2005b); its transcription is strongly activated by CEP-1 upon irradiation. If CED-13 was partly redundant with EGL-1, it might compensate for *egl-1(n3082)* and permit increased cell death in *ced-9(n1653)*. As I have shown above, *cep-1(gk138)* suppresses both EGL-1 and CED-13 transcript levels and would thus block both redundant factors; it would then be surprising that the corpse number is still higher in *cep-1(gk138); ced-9(n1653)* than in *ced-9(n1653); egl-1(n3082)*.

5.6.6.6 *cep-1(gk138)*, but not *egl-1(n3082)* blocks apoptotic IR response in *ced-9(n1653)*

I had shown that *ced-9(n1653)* mutants could respond to irradiation with an additional increase in cell death. Next, it should be characterised whether DNA damage-induced apoptosis in this instance also depended on *cep-1* and *egl-1*. Irradiation of *cep-1(gk138); ced-9(n1653)* did not alter the number of corpses, confirming that the IR response in *ced-9(n1653)* mutants involves and fully depends on *cep-1(gk138)*. However, other than in a *ced-9* wildtype background, *egl-1(n3082)* did not fully block IR-induced apoptosis (Figure 102). This supports the idea that in *ced-9(n1653)* mutants, other factors than EGL-1 can transduce DNA damage-induced germ cell death. Whether these are activated by CEP-1 or whether it is CEP-1 itself cannot be concluded from the analysis so far; despite the increase seen in *ced-9(n1653); egl-1(n3082)* after irradiation, the number of corpses does not exceed the one in *cep-1(gk138); ced-9(n1653)* and might thus be attained independently of *cep-1(gk138)*.

Altogether, it is intriguing that with the mutation in CED-9, DNA damage-induced apoptosis becomes at least partly independent of EGL-1, but still fully depends on CEP-1. This is in surprising agreement with the observations of the Egl phenotype.

5.6.8 CEP-1 and CED-9 in developmental cell death will discuss the role of *cep-1* and *ced-9* in somatic apoptosis. In that context, I show that CEP-1, contrary to former assumptions, has a pro-apoptotic effect; and loss of *cep-1* function enhances the partial incapacity of *ced-9(n1653)* to promote normal cell death.

I am building the triple mutant *cep-1(gk138); ced-9(n1653); egl-1(n3082)* to test whether CEP-1 has some EGL-1-independent effects on apoptosis and whether the EGL-1-independent IR-induced apoptosis requires CEP-1.

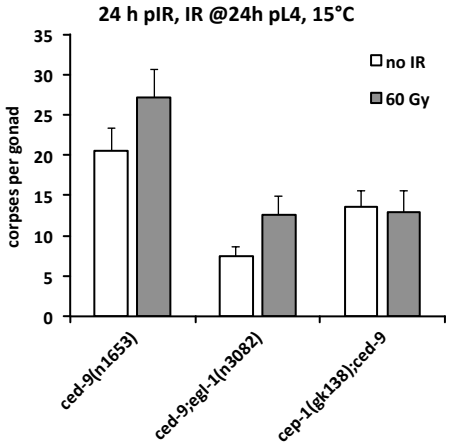

Figure 102 Apoptotic response to irradiation in *ced-9(n1653)* mutants is not fully blocked by *egl-1(n3082)*. Error bars indicate 95 % CI of the mean.

5.6.7 *ced-9(n1653)* in developmental cell death

I showed above that *rpo-1b(op259)* not only disturbed programmed cell death in the germ line, but that the number of apoptotic cells was also affected in somatic development. *rpo-1b(op259)* significantly reduced the number of cell corpses accumulating in the heads of freshly hatched engulfment mutants (Figure 81). I wanted to learn whether *rpo-1b(op259)* would affect somatic death at later stages of development; additionally, I aimed at finding possible implications of *rpo-1b(op259)* on *ced-9(n1653)* in somatic apoptosis.

I therefore used the well-established transgenic marker *nIs96[P_{lin-11}::gfp; lin-15(+)]* for ventral cord Pn.aap cells [see *8.2 Frequently used assays*]. In wildtype larvae, only six out of the 12 ventral cord Pn.aap neurons that are generated during development survive; the other six are removed by programmed death. In a *ced-3* loss-of-function situation, none of the cells can undergo apoptosis and 12 cells remain. With the transgene *nIs96*, all surviving Pn.aap cells are highlighted by a GFP reporter expressed under the P_{lin-11} promoter, starting at the L3/L4 stage. This system can reveal both pro-apoptotic and anti-apoptotic conditions if set to a sensitized state: reduction of *ced-3* function causes some (approximately 2) of the cells normally destined to die to survive. Loss of pro-apoptotic cues further increases, and loss of anti-apoptotic cues reduces the number of extra surviving cells.

5.6.7.1 *ced-9(n1653)* has more extra surviving Pn.aap cells

Wildtype animals had no extra cells; *rpo-1b(op259)* mutants too had none but the six default cells (Figure 81). In the *ced-3(n2438)* background, on average two cells did not die; this was almost unchanged in *rpo-1b(op259); ced-3(n2438)*.

The only known *C. elegans* Bcl-2 homolog CED-9 is considered to be the core inhibitor of apoptosis [see introduction on page 202]. However, besides its role as an anti-apoptotic factor, it has been assigned some pro-apoptotic activity as well (Hengartner 1994a). In the absence of normal CED-9, some cells that should die during development are not eliminated properly. I confirmed the requirement for CED-9 in the Pn.aap system: *ced-9(n1653)* mutants occasionally had an extra surviving neuron (Figure 103). This was more pronounced in the sensitized *ced-3(n2438)* background: at 15°C, the number of extra

surviving cells rose from 1.5 per animal in *ced-3(n2438)* to 3 on average in *ced-9(n1653); ced-3(n2438)*. At this point, it cannot be concluded whether *ced-9(n1653)* has lost some pro-apoptotic activity of CED-9 or whether this allele has some gain-of-function aspects overlaid to the apparent reduction of gene function.

5.6.7.2 *rpo-1b(op259)* strongly enhances the pro-apoptotic defect of *ced-9(n1653)*

Next, I investigated the influence of *rpo-1b(op259)* upon this effect of *ced-9(n1653)*. *rpo-1b(op259); ced-9(n1653)* animals often had one to two extra cells, and in *rpo-1b; ced-9; ced-3(n2438)* almost all six extra neurons survived (Figure 103). (Interestingly, *rpo-1b(op259)* favoured survival of posterior cells slightly more than of anterior cells.) Thus, in this system again, *rpo-1b(op259)* seems to augment defects of the *ced-9(n1653)* mutant. In the germ line, it had been loss of anti-apoptotic activity of CED-9, here it was a defect in pro-apoptotic activity of CED-9 that *rpo-1b(op259)* apparently enhanced.

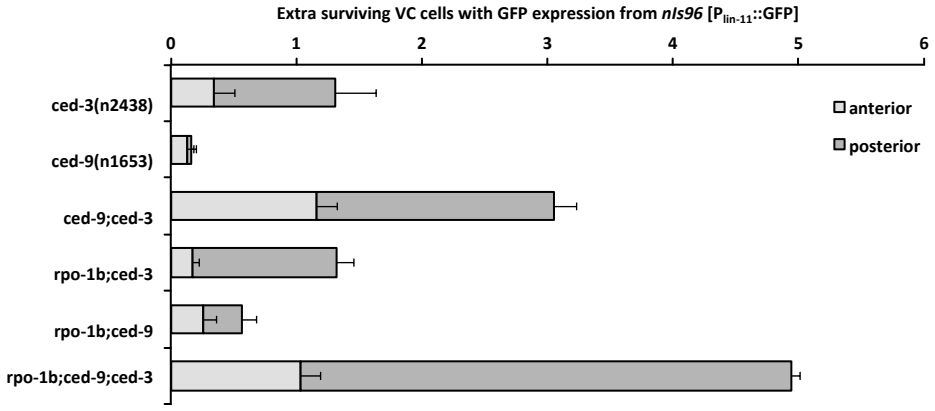

Figure 103 *ced-9(n1653)* increases number of extra surviving ventral cord neurons, which is strongly enhanced by *rpo-1b(op259)*. Extra cells anterior (max. 2) and posterior (max. 4) to the vulva were assessed separately at L4 stage in worms at 15°C. Error bars indicate 95 % CI of the mean.

5.6.8 CEP-1 and CED-9 in developmental cell death

5.6.8.1 CEP-1 can influence somatic apoptosis

CEP-1 had been considered to induce germ cell death upon DNA damage but not to be involved in developmental apoptosis of somatic cells (Schumacher 2001). The observation that *cep-1(gk138)* could suppress the Egl phenotype of *ced-9(n1653)* [*5.6.6.4 hus-1(op244) and cep-1(gk138) but not egl-1(n3082) rescue the Egl phenotype of ced-9(n1653)*], itself probably a result of HSN neuron apoptosis, pointed to a possible implication of CEP-1 in somatic cell death. I used the Pn.aap assay to study *cep-1(gk138)* in combination with *ced-9(n1653)*. In a *ced-3* wildtype background, *cep-1(gk138)* had no extra cell survival; however, in *ced-3(n2438)*, more cells could survive when CEP-1 activity was lost (Figure 104). I therefore conclude that CEP-1 can support apoptosis in somatic cells.

5.6.8.2 *ced-9(n1653)* and *cep-1(gk138)* have additive effects on extra cell survival

Excessive cell death in germ lines of *ced-9(n1653)* is partly *cep-1*-dependent; I wondered whether in the somatic system, loss of CEP-1 would make a difference to *ced-9(n1653)*. Strikingly, apoptotic removal of extra Pn.aap was almost completely abolished in *cep-1(gk138); ced-9(n1653)*.

The anti-apoptotic effect on Pn.aap cells seen in *ced-9(n1653)* is therefore not equivalent to the loss of CEP-1. Possibly, the *ced-9(n1653)* mutation leads to a weak gain of CED-9 inhibitory activity that still responds to EGL-1 binding; reduced EGL-1 through loss of CEP-1 function (if CEP-1 acts by this mechanism in the soma) would further reduce activation of the core apoptotic machinery. Or, CED-9 has some pro-apoptotic function that is lost in *ced-9(n1653)*; at the same time, disinhibition of CED-4 still depends on EGL-1 binding. Alternatively, *cep-1* has some pro-apoptotic function that is not plainly upstream of *ced-9* and might not involve *egl-1* activation.

Whatever the mechanism, *cep-1* and *ced-9* are synergistically required for developmental apoptosis of the Pn.aap neurons.

EGL-1 has clearly been associated with developmental apoptosis (Conradt 1998); it is essential for most programmed cell deaths. How it is regulated depends on the cell type (Nehme 2008). It would be desirable to define the role of *egl-1* in Pn.aap cell death and to see whether *egl-1(lf)* has a similar synthetic phenotype with *ced-9(n1653)* as *cep-1(lf)* has; however, I have not been able to cross the reporter *nIs96* into *egl-1* mutants, likely due to close linkage of the transgene and *egl-1*.

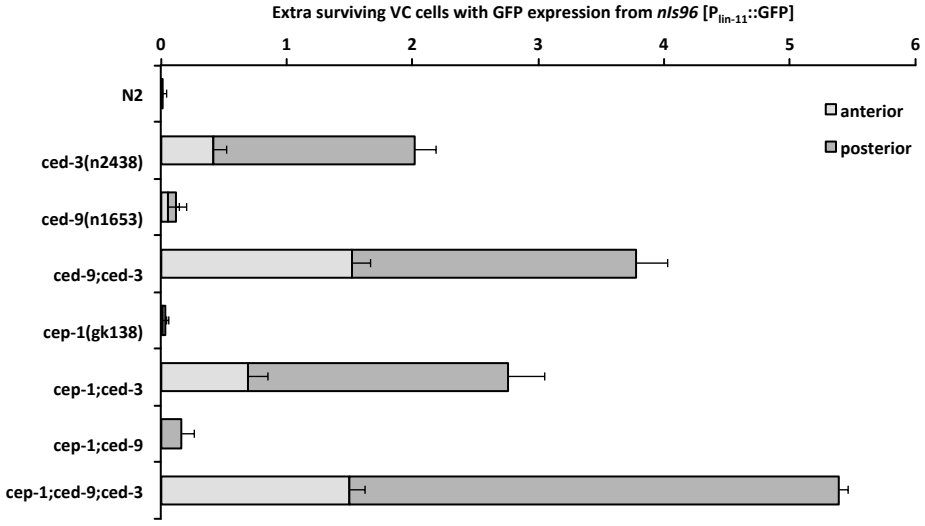

Figure 104 *cep-1* is involved in somatic cell death. Extra cells anterior (max. 2) and posterior (max. 4) to the vulva were assessed separately at L4 stage in worms at 20°C. Error bars indicate 95 % CI of the mean.

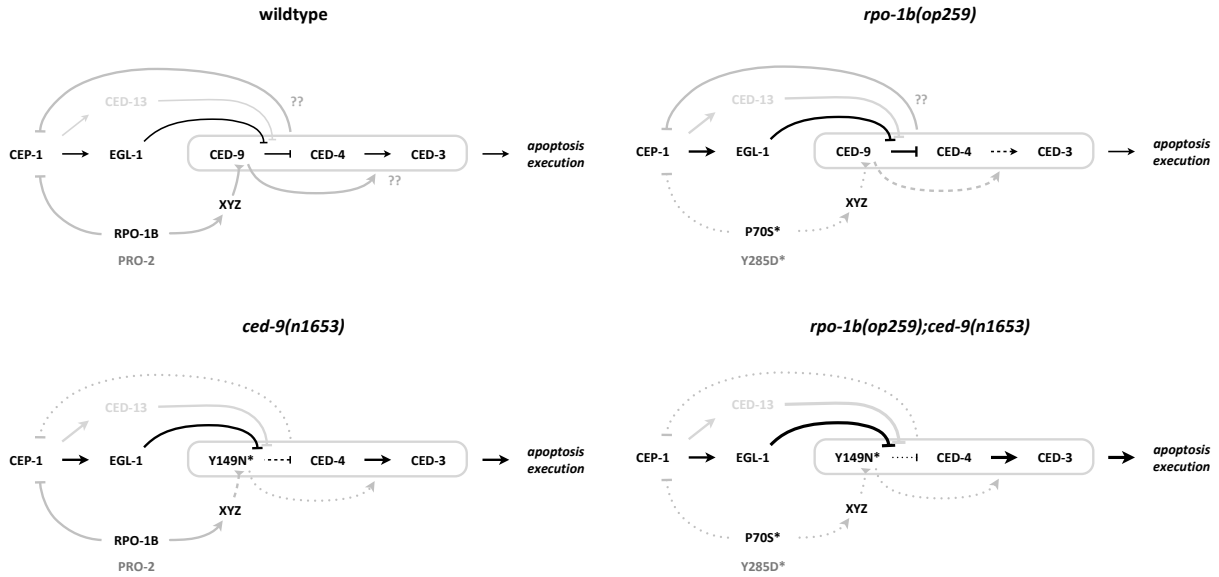

Figure 105 Model for CED-9 functions in apoptosis regulation and the effects of the *ced-9(n1653)* Y149N and the *rpo-1b(op259)* P70S mutations*. Wildtype CED-9, besides inhibiting the apoptotic cascade, seems to have some promoting function on apoptosis at least in somatic cell death (provided the abnormal survival of cells in *ced-9(n1653)* mutants is not an inhibitory gain-of-function effect). The inhibitory action from around CED-9 to CEP-1 is derived from the observation of increased CEP-1 activity in the CED-9 mutant condition. CEP-1 activity is increased in *rpo-1b(op259)*, which leads to increased cell death once the CED-9(Y149N) mutation overcomes a loss of pro-apoptotic stimuli occurring in *rpo-1b(op259)*. Arguable EGL-1-independent effects of CEP-1 on the core apoptotic machinery are not considered in this model. Black lines indicate established links (the effect of CED-13 is supposed to be minor, light grey). The other interactions shown in grey are suggested by this study. Thin lines indicate normal effect, thickened lines an increased action in the mutant condition, dashed and dotted lines indicate that the effect weakened. *pro-2(na27)* showed similar effects as *rpo-1b(op259)* in combination with *ced-9(n1653)* and *cep-1(lf)*, suggesting that it is altered rRNA synthesis that causes the apoptotic defects seen in *rpo-1b(op259)*.

5.6.9 RNAi knockdown of *ced-9*

The *ced-9(n1653)* allele exhibited ambiguous apoptotic phenotypes. It might not be a simple reduction-of-function variant of CED-9 but it could have more specific alterations. To test whether quantitative reduction of *ced-9* expression would reproduce the effects of *ced-9(n1653)* mutation, I applied *ced-9(RNAi)* to the various mutant strains that had been tested in combination with *ced-9(n1653)*. Lei Xiong had cloned an RNAi construct targeting *ced-9* since none had been available in the RNAi clone libraries (Lei had used the genomic sequence of *ced-9*, limited by the ends of the ORF).

5.6.9.1 *ced-9(RNAi)* confirms dependence of excessive cell death on *egl-1(n3082)*

In N2 worms at 20°C, *ced-9(RNAi)* increased the number of apoptotic corpses to about 20 per gonad at 32 hours after the reference time point (Figure 106). The increase was reduced in *cep-1(gk138)* and more significantly in *egl-1(n3082)*, almost down to wildtype levels.

hus-1(op244); ced-9(RNAi) animals had lower levels than *cep-1(gk138); ced-9(RNAi)*; for some reason, *hus-1(op244); empty(RNAi)* also had much lower levels than wildtype*; empty(RNAi)* or *cep-1(gk138); empty(RNAi)*.

5.6.9.2 *ced-9(RNAi)* does not increase apoptosis in *rpo-1b(op259)*

I also tested *ced-9(RNAi)* on *rpo-1b(op259)*. Opposite to *rpo-1b(op259); ced-9(n1653)* where *rpo-1b(op259)* enhanced the high level of germ cell apoptosis, *rpo-1b(op259)* responded very weakly to *ced-9(RNAi)*, that is, with only a minute increase of the corpse number (Figure 106). Thus, for *rpo-1b(op259)*, the effects on *ced-9(n1653)* and on *ced-9(RNAi)* strongly contrasted; I considered various possibilities.

Possibility: *rpo-1b(op259)* mutants are insensitive to RNAi knockdown.

The *ced-9(RNAi)* was able to cause the expected phenotype in N2, thus the clone can principally increase apoptosis. We checked the RNAi clone sequence and realised that there was a sequence element within a *ced-9* intron that corresponds to a *C. elegans* repeat sequence present in multiple non-exact copies throughout the genome and in non-transcribed or non-translated regions of a multitude of genes. These could theoretically lead to an off-target RNAi effect that becomes relevant in *rpo-1b(op259)*.

rpo-1b(op259) could have a general alteration of RNAi sensitivity. *rpo-1b(op259)* likely has some implications with factors and pathways that were shown to influence RNAi efficiency, such as *lin-35* [see *5.5.1 RB complex homologs lin-35 and dpl-1*] or nuclear exosome components [see *4.4.7.4 26S-short rRNA in rpo-1b(op259)*]. I used a set of RNAi clones on *rpo-1b(op259)* that are commonly used to detect genetic mutants with altered RNAi sensitivity (*pos-1*, *mom-2*, *ces-1*, *unc-22*). So far, I have not found a global difference of RNAi effects between N2 and *rpo-1b(op259)*.

Possibility: enhancement of cell death is specific for the *ced-9(n1653)* allele.

I have already discussed the hypothesis that *rpo-1b(op259)* impacts on apoptosis at the level of *ced-9*. A selective alteration of CED-9 by the *ced-9(n1653)* mutation could lead to gain- or loss-of-function aspects that become particularly significant in *rpo-1b(op259)*; the actual *ced-9* reduction-of-function phenotype might be one that maintains the blocking effect of *rpo-1b(op259)* on germ cell apoptosis.

(Another interference that can never be excluded for sure is a variation in the genetic background of the mutant strain that leads to pro-apoptotic effects beyond the partial loss of *ced-9* function. *rpo-1b(op259); ced-9(n1653)* and possibly also the *ced-9(n1653)* strain might harbour mutations that are not present in the *ced-9(RNAi)* condition, and that might activate CEP-1 and thus boost germ cell death.)

Possibility: RNAi conditions counteract the effects of *ced-9(rf)*.

I observed that feeding *rpo-1b(op259)* on HT115 rather than on OP50 affected germ cell differentiation. This might be relevant in combination with *ced-9(rf)*; RNAi bacteria might improve germ line health in *rpo-1b(op259); ced-9(n1653)*.

I addressed the latter two possibilities with RNAi knockdown of *ced-9* in the double mutant *rpo-1b(op259); ced-9(n1653)*. *rpo-1b; ced-9; empty(RNAi)* had similarly high corpse numbers as *rpo-1b(op259); ced-9(n1653)* on OP50, which does not support the last explanation. *rpo-1b(op259); ced-9(n1653)*/*ced-9(RNAi)* had a slightly lower corpse number than the control RNAi treated worms at 6 hours post reference (15.6 ±3.51 vs. 22.9 ±3.44 (average ±95% CI, n=16)); this indicates the possibility that *ced-9(n1653)* has some dominant pro-apoptotic effect in *rpo-1b(op259)*, which can be reduced through reduction of CED-9(Y149N) expression by RNAi.

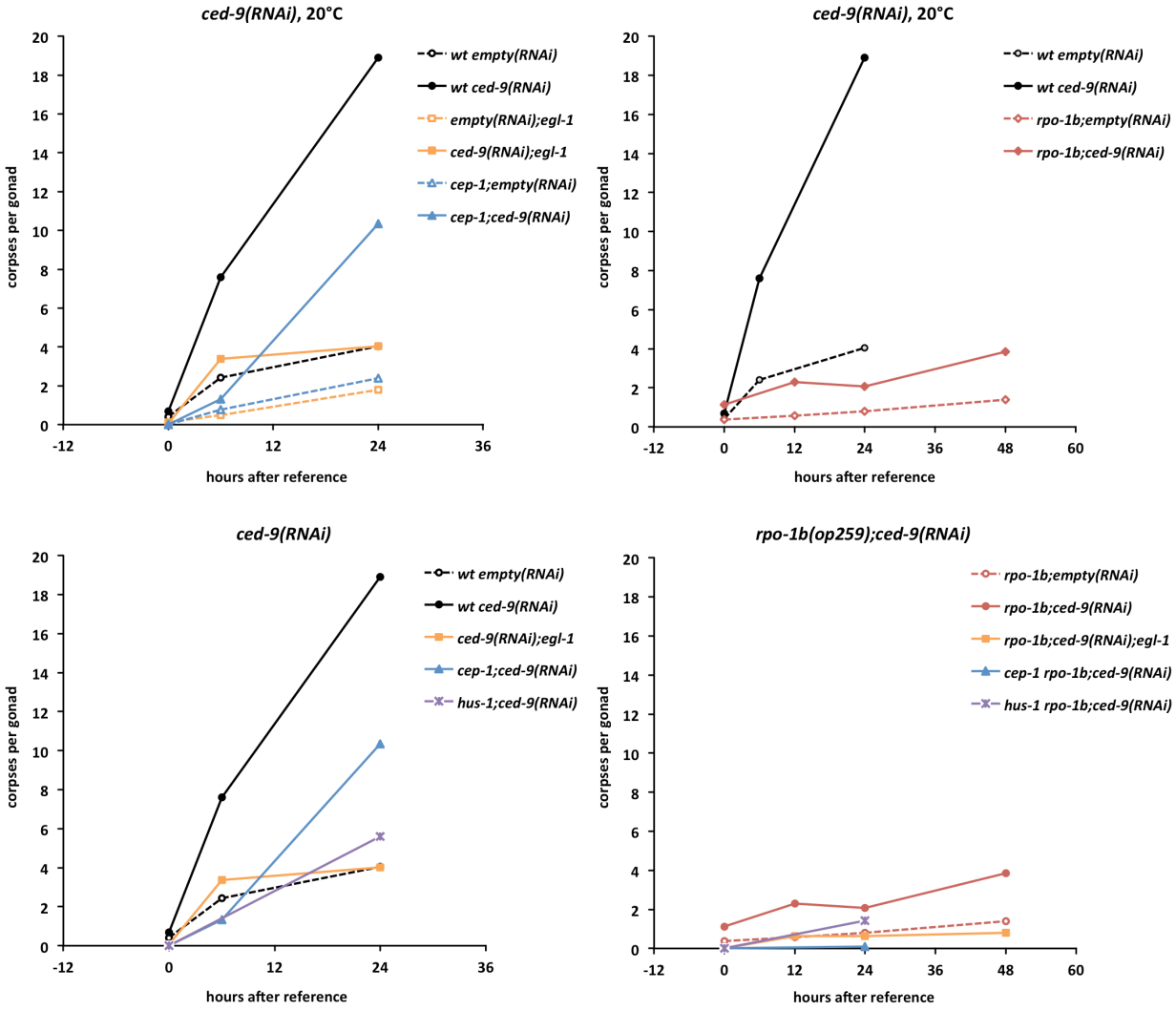

		wt		egl-1(n3082)		cep-1(gk138)		hus-1(op244)	
		score	95% CI (n)	score	95% CI (n)	score	95% CI (n)	score	95% CI (n)
empty(RNAi)	0 h	0.41	±0.18 (56)	0.13	±0.17 (16)			0.25	±0.24 (20)
	6 h	2.42	±0.43 (52)	0.50	±0.54 (16)	0.78	±0.29 (36)		
	24 h	4.05	±0.51 (148)	1.78	±0.56 (32)	2.40	±0.77 (52)	0.43	±0.18 (40)
ced-9(RNAi)	0 h	0.69	±0.43 (16)	0.06	±0.12 (16)				
	6 h	7.60	±0.72 (52)	3.38	±1.04 (16)	1.32	±0.48 (56)		
	24 h	18.91	±1.54 (124)	4.03	±0.85 (32)	10.36	±1.73 (76)	5.60	±1.20 (20)

		rpo-1b(op259)		rpo-1b;egl-1		cep-1 rpo-1b		hus-1 rpo-1b	
		score	95% CI (n)	score	95% CI (n)	score	95% CI (n)	score	95% CI (n)
empty(RNAi)	0 h	0.38	±0.30 (16)						
	12 h	0.56	±0.59 (16)	0.19	±0.20 (16)	0.10	±0.13 (20)		
	24 h	0.80	±0.21 (128)	0.13	±0.17 (16)	0.23	±0.16 (40)	0.25	±0.24 (20)
	48 h	1.40	±0.74 (52)						
ced-9(RNAi)	0 h	1.13	±1.12 (16)						
	12 h	2.31	±1.19 (52)	0.63	±0.43 (16)				
	24 h	2.07	±0.56 (68)	0.63	±0.30 (16)	0.10	±0.20 (20)	1.43	±0.52 (40)
	48 h	3.86	±1.39 (32)	0.81	±0.37 (16)				

Figure 106 *ced-9(RNAi)* does not considerably increase cell death in *rpo-1b(op259)*. Time course of apoptotic corpse number in RNAi treated worms (starting at L1), grown at 20°C. Reference is 12 hours post L4 for wildtype and 24 hours for *rpo-1b(op259)*. Table indicates apoptotic corpses in *ced-9(RNAi)* (starting at L1) treated worms. Average number of corpses per gonad, 95 % CI of the mean and total number of worms scored per condition.

5.6.10 *ced-9(RNAi)* and irradiation

I tested irradiation response in the *ced-9(RNAi)* treated strains N2, *cep-1(gk138)*, *hus-1(op244)*, *rpo-1b(op259)* and in *cep-1(gk138) rpo-1b(op259)* and *hus-1(op244) rpo-1b(op259)*. The corpse number of *ced-9(RNAi)* treated N2 at 20°C increased upon irradiation (Figure 107 and Table 18); such a DNA damage-induced increase was blocked in *cep-1(gk138); ced-9(RNAi)*, consistently with the observations in *ced-9(n1653)* mutants (Figure 102).

5.6.10.1 *ced-9(RNAi)* and irradiation provoke *cep-1*-dependent cell death in *rpo-1b(op259)*

ced-9(RNAi) had not reproduced the effect of the *ced-9(n1653)* mutation in *rpo-1b(op259)*; the corpse number remained low in *rpo-1b(op259); ced-9(RNAi)*, in accordance with a suppressive effect of *rpo-1b(op259)* on apoptosis. Due to this low number of corpses, *rpo-1b(op259); ced-9(RNAi)* was amenable for scoring of IR-induced cell death. Surprisingly, irradiation strongly elevated the number of apoptotic cells in *rpo-1b(op259); ced-9(RNAi)*. The finding points at different things: *ced-9(RNAi)* can restore IR-induced apoptosis in *rpo-1b(op259)*; this also implies that the *ced-9(RNAi)* clone is not without effect in *rpo-1b(op259)*; therefore, the low corpse number in *rpo-1b(op259); ced-9(RNAi)* is likely due to a suppressive effect of *rpo-1b(op259)* on *ced-9(RNAi)*-induced death.

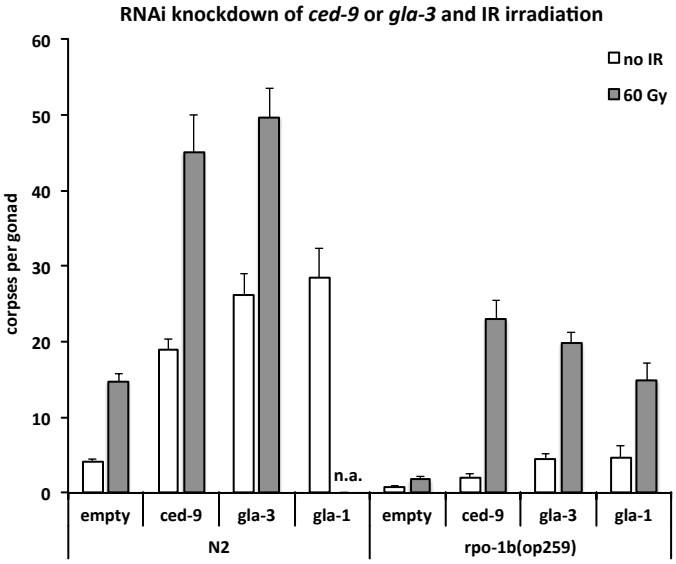

Figure 107 Apoptotic response to IR in RNAi (starting at L1) treated *rpo-1b(op259)* and wildtype worms at 24 hours post irradiation. Only irradiation can provoke the expected effects of *ced-9* or *gla-3* knockdown in *rpo-1b(op259)*. Error bars represent 95 % CI of the mean.

To confirm that the irradiation-induced increase of cell death involved *cep-1*, I irradiated *cep-1(gk138) rpo-1b(op259); ced-9(RNAi)* worms (Table 18). Animals without irradiation had almost no corpses; and irradiation could not significantly increase this number, indicating that the IR response in *rpo-1b(op259); ced-9(RNAi)* involves CEP-1.

5.6.10.2 *ced-9(RNAi)* facilitates apoptotic IR response of *hus-1(op244)*

hus-1(op244) has been shown to be necessary for DNA damage-induced apoptosis (Hofmann 2002); I confirmed this with apoptosis in *hus-1(op244); empty(RNAi)*, which did not respond to irradiation.

However, with *ced-9(RNAi)* treatment, *hus-1(op244)* mutants showed increased cell death upon irradiation. Thus, apoptosis induction upon irradiation is no longer fully dependent on HUS-1 in *ced-9* knockdown conditions. This could indicate *hus-1*-independent activation of CEP-1 in these conditions; or release from blocked pro-apoptotic effects in parallel to *cep-1*. Irradiation might not be enhancing DNA damage-induced apoptosis but increase the low response of *hus-1(op244)* to *ced-9(RNAi)*. I have not yet tested this further, e.g., with *hus-1(op244) cep-1(gk138)* (difficult to construct due to close linkage).

		empty(RNAi)		*ced-9(RNAi)*		*gla-3(RNAi)*		*gla-1(RNAi)*	
		score	**95% CI (n)**	**score**	**95% CI (n)**	**score**	**95% CI (n)**	**score**	**95% CI (n)**
N2	**no IR**	4.05	±0.51 (148)	18.91	±1.54 (124)	26.14	±2.91 (64)	28.55	±3.89 (40)
	60 Gy	14.76	±0.96 (136)	45.06	±4.90 (36)	49.75	±3.86 (32)		
rpo-1b(op259)	**no IR**	0.77	±0.20 (144)	2.18	±0.60 (120)	4.43	±0.82 (96)	4.68	±1.54 (40)
	60 Gy	1.64	±0.35 (148)	23.09	±2.43 (56)	19.81	±1.47 (96)	14.92	±2.20 (37)
cep-1(gk138)	**no IR**	2.40	±0.77 (52)	10.36	±1.73 (76)	18.57	±2.92 (76)		
	60 Gy	1.97	±0.49 (36)	12.43	±2.05 (60)	27.82	±3.80 (56)		
hus-1(op244)	**no IR**	0.43	±0.18 (40)	5.60	±1.20 (20)	2.35	±0.84 (20)		
	60 Gy	0.55	±0.26 (40)	13.90	±2.99 (20)	18.55	±2.76 (20)		
cep-1 rpo-1b	**no IR**	0.18	±0.12 (60)	0.10	±0.20 (20)	1.63	±0.39 (60)		
	60 Gy	0.40	±0.19 (60)	0.85	±0.52 (20)	3.83	±1.12 (59)		
hus-1 rpo-1b	**no IR**	0.25	±0.24 (20)	1.43	±0.52 (40)	2.90	±1.20 (40)		
	60 Gy	0.45	±0.36 (20)	12.63	±3.69 (40)	17.10	±3.26 (40)		

Table 18 *hus-1(lf)* and *rpo-1b(op259)* do not suppress *ced-9(RNAi)* effects upon IR. *hus-1(op244)*, *rpo-1b(op259)*, and *hus-1(op244) rpo-1b(op259)* show very similar response both with *ced-9(RNAi)* and *gla-3(RNAi)*. Average number of corpses per gonad at 24 hours post irradiation, 95 % CI of the mean and total number of worms scored per condition.

5.6.11 Gla mutants, RNAi and irradiation

I planned to test how other conditions that had been described to increase germ cell death independently of DNA damage signalling would affect apoptosis in *rpo-1b(op259)*. In genetic screens, two mutants, *gla-1* and *gla-3*, had been isolated that have elevated germ line apoptosis (Gla) without exogenous damage. Their function in apoptosis has not been characterised in full detail. *gla-1* is syngenic with *cpb-3*, the *C. elegans* homolog of human CPEB1; it is required for germ cell progression and oocyte maturation (Hasegawa 2006). *gla-3* is required for exit from meiotic pachytene of developing oocytes; it has likely some negative effect on Ras/MAPK signalling (Kritikou 2006). Mutations in *gla-1* or *gla-3* lead to increased germ cell death that is *cep-1*-independent and has therefore been considered 'physiological' apoptosis (Lettre 2004). I tested the *gla-1(op234) rpo-1b(op259)* double mutant; for *gla-3*, I was limited to RNAi since *gla-3* and *rpo-1b* are very closely linked and I could not get a double mutant.

5.6.11.1 *rpo-1b(op259)* enhances Gla of *gla-1(op234)*

gla-1(op234) animals have a high number of apoptotic corpses, but the worms remain fertile at 20°C. *gla-1(op234) rpo-1b(op259)* mutants, however, had extremely little progeny at 20°C; this was likely due to massive germ cell death: similarly to *rpo-1b(op259); ced-9(n1653)*, germ cells in the region of late meiotic pachytene were all cellularised – likely apoptotic – and no normal size oocytes developed (we did not assess this quantitatively). Thus, *gla-1(op234) rpo-1b(op259)* was a further instance besides *gld-1(op236) rpo-1b(op259)* (Figure 62), *rpo-1b(op259); lip-1(zh15)* (Figure 90) and

rpo-1b(op259); ced-9(n1653) (Figure 99) where *rpo-1b(op259)*, rather than blocking apoptosis, clearly enhanced a Gla phenotype.

5.6.11.2 *gla-1(RNAi)* and *gla-3(RNAi)* to *rpo-1b(op259)* enhance apoptosis levels only after IR

RNAi to *gla-1* had a strong effect in N2: at 24 hours of adulthood, the gonads harboured approximately 25 corpses on average (Figure 107 and Table 18). After irradiation, the number rose to very high levels, so that – given also significant morphological alterations of the germ cells and gonads – it could not be counted any more. The effect of *gla-1(RNAi)* in *rpo-1b(op259)* was strikingly similar to the effect of *ced-9(RNAi)*: non-irradiated animals had only a weak increase to about 5 corpses per gonad. However, *gla-1(RNAi)* made *rpo-1b(op259)* animals responsive to irradiation-induced apoptosis.

gla-3(RNAi) had very similar effects on apoptosis as *gla-1(RNAi)* in many respects. Germ cell death was increased to about 25 corpses per gonad in non-irradiated *gla-3(RNAi)* treated N2 worms; upon irradiation, this number rose massively, to 50 corpses on average. Again, in *rpo-1b(op259)* mutants, *gla-3(RNAi)* was little effective in increasing the corpse number when the worms were not irradiated (Figure 108). IR treated *gla-3(RNAi) rpo-1b(op259)* gonads, however, reached levels in the range of irradiated wildtype worms at *control(RNAi)* conditions (Figure 107 and Table 18).

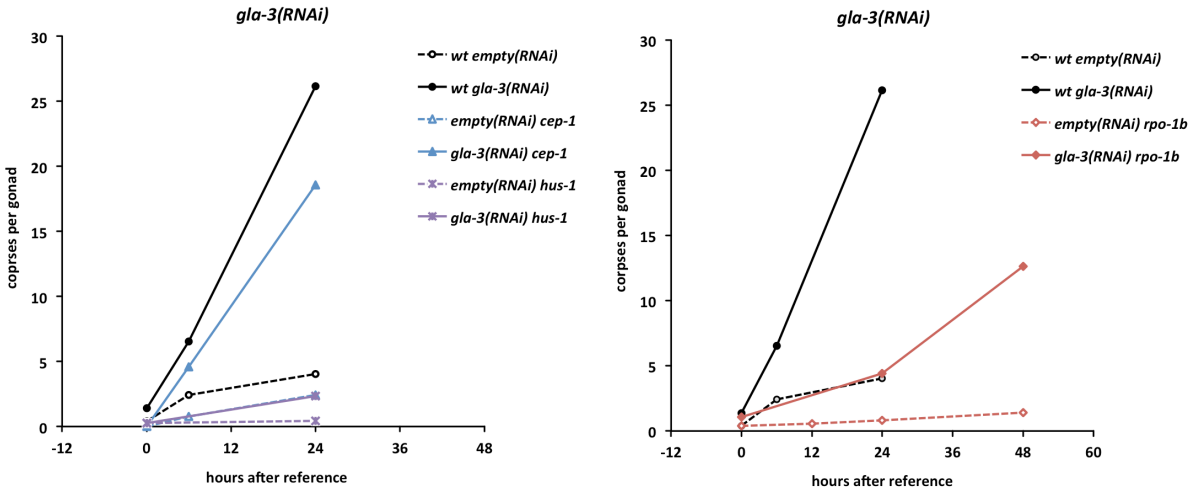

Figure 108 Time course of apoptotic corpse number in *gla-3(RNAi)* treated worms (starting at L1), grown at 20°C. Reference is 12 hours post L4 for wildtype and 24 hours for *rpo-1b(op259)*. *gla-3(RNAi)* does not considerably increase cell death in *hus-1(op244)* whereas the increase is nearly that of wildtype in *cep-1(gk138)* mutants. *rpo-1b(op259)* exhibits a low response at early time points.

5.6.11.3 *hus-1(op244)* mutants show strong IR response on *gla-3(RNAi)*

I treated *hus-1(op244)* animals with *gla-3(RNAi)*; interestingly, mutation of *hus-1* seemed to suppress the Gla phenotype of *gla-3(RNAi)* even though it is thought to act upstream of *cep-1* in apoptosis induction. On the other hand, the apoptotic response of *gla-3(RNAi) hus-1(op244)* to IR was very pronounced; like *ced-9(RNAi)*, *gla-3(RNAi)* makes *hus-1(op244)* dispensable for irradiation-induced apoptosis. Unlike in *ced-9(RNAi)* worms, in *gla-3(RNAi)* worms *cep-1* is partly dispensable as well.

5.6.11.4 *gla-3(RNAi)* evokes partly *cep-1*-independent apoptotic IR response

It is interesting that *gla-3(RNAi)* does not only increase baseline apoptosis, but that it can also enhance the effect of irradiation on the corpse number. Loss of GLA-3 was shown to increase germ cell death independently of *cep-1* (Kritikou 2006). If the enhanced response of *gla-3(lf)* to IR is not due to strongly activated CEP-1, other mechanisms must be in play that sensitise germ cells both to baseline apoptosis and to DNA damage-induced death.

I wondered whether irradiation might provoke enhanced apoptosis in *gla-3(RNAi)* by mechanisms other than CEP-1 activation. Indeed, loss of *cep-1* function could not fully suppress IR-induced apoptosis in *gla-3(RNAi)* treated worms. Upon irradiation, the number of corpses in *gla-3(RNAi) cep-1(gk138)* was clearly increased (Table 18), indicating that there must be *cep-1(gk138)*-independent effects on apoptosis induction in IR response. It should be noted that irradiation also enhanced disturbances of the germ lines in *gla-3(RNAi) cep-1(gk138)*. I have met a similar situation – that is, increased cell death upon irradiation in the absence of functional CEP-1 – in *lip-1* mutants [see *5.5.7.1 IR-induced death in lip-1(zh15) is partially dependent on cep-1*]. *lip-1* is a negative regulator of MPK-1 activity, which is also a presumptive function of *gla-3*.

5.6.12 Conclusions on *rpo-1b(op259)* and CED-9

The *ced-9(n1653)* reduction-of-function allele reversed the effect *rpo-1b(op259)* had on germ cell apoptosis levels. The low levels in the *rpo-1b(op259)* single mutant turned into an enhancement of the *ced-9* reduction-of-function phenotype, leading to excessive apoptosis and eventually to sterility in *rpo-1b(op259); ced-9(n1653)*. This effect was transmitted by functional CEP-1 and EGL-1; in the absence of either one, cell death was reduced and fertility restored. I show that loss of *cep-1* or *egl-1* function reduces aberrant cell death also in *ced-9(n1653)* mutants and rescues temperature sensitive sterility. This is against the expectation, as these two genes have been thought to be involved specifically in DNA damage induced cell death in the germ line. Additionally, I demonstrate a pro-apoptotic effect of CEP-1 in somatic cell death, in parallel with a pro-apoptotic effect of CED-9. I further show that *ced-9(n1653)* animals have increased CEP-1 activity, indicating that disturbances in the core apoptotic machinery can lead to activation of 'upstream' factors. Whether it is a specific defect in mutant CED-9 that makes its function dependent on (extra-activated) CEP-1 or whether CEP-1 plays a partly redundant role in activation of developmental cell death and of germ cell death that is independent from exogenous damage, remains unresolved. Loss of *cep-1* function reduces death in both situations where either loss of anti- or pro-apoptotic CED-9 function prevails. It is conceivable that CEP-1 activates pro-apoptotic cues in parallel to CED-9.

The *ced-4* locus was shown to code for two isoforms, one of which had pro- and the other had anti-apoptotic effects in development (Shaham 1996a). If both isoforms were regulated by CED-9, 'constitutive' release of pro-apoptotic CED-4 in *ced-9(n1653)* would explain increased germ cell apoptosis. In other cells, aberrant release of inhibitory CED-4 isoforms might be more relevant. Interestingly, I found that fluorescence intensity of a CED-4::GFP reporter (Zermati 2007) was increased in somatic cells of *ced-9(n1653)*, whereas the intensity in germ cells was slightly lower than in wildtype (Figure 87). The role of CED-4 protein localisation and its translocation upon apoptosis induction seems to vary between somatic cells and germ cells (Pourkarimi 2011) and deserves further study.

Finally, I see it a possibility that CED-9 has some promoting function in cell corpse engulfment. It is surprising that the number of corpses increases massively over time in *ced-9(rf)* gonads, similar to engulfment mutants. If cell removal were unperturbed, this would presume that the pro-death effect increases significantly over time. A role of CED-9 for efficient engulfment could explain accumulation of corpses in the germ line as well as the extra survival of somatic Pn.aap cells; engulfment promotes cell death in this system. The recently discovered lipid remodelling function of CED-9 (Tan 2011) is a hypothetical link to membrane activity required for engulfment. It is intriguing that loss of *unc-119* function, which we identified to result in enhanced cell corpse engulfment [*6.2.2 The function of unc-119(ed3) in apoptosis*], can restore fertility in *ced-9(n1653)*, and even more potently in *rpo-1b(op259); ced-9(n1653)*.

The persistence of constitutive germ cell apoptosis in *egl-1(lf)* mutants suggest that it either happens independently of EGL-1 and CED-9, i.e., by other means of activating CED-4 and/or CED-3, or that the capacity of CED-9 to regulate CED-4 is modulated by additional factors besides EGL-1 binding. *rpo-1b(op259)* suppresses EGL-1-independent germ cell death and thus likely interferes with such an additional activation mode. Mammalian pro-survival CED-9 homologs are regulated by protein turnover rates. Phosphorylations on specific residues of MCL1 were shown to target it for ubiquitin ligases and for degradation; various MAP kinases were active on MCL1 and influenced survival in mammalian cell cultures (Wertz 2011). Such regulatory mechanisms have not been studied in detail for CED-9 in *C. elegans*. Interestingly, the *ced-9(n1653)* mutation affects a potential phosphorylation residue, Y149. This site is predicted a target of Src type kinases. It is an intriguing possibility that this very site is the target for the regulatory input which is disturbed in *rpo-1b(op259)*. Loss of this site in *ced-9(n1653)* would detach apoptosis regulation from this input stream, preserving the effect of EGL-1-induced CED-4 release; this could explain why the anti-apoptotic effect of *rpo-1b(op259)* is relieved in the double mutant, but sensitivity to EGL-1 is not. How relevant this potential phosphorylation is for CED-9 function and regulation remains to be determined.

In an *rpo-1b(+)* background, *ced-9(RNAi)* provokes a similar defect as the *ced-9(n1653)* mutation, that is, an increase in germ cell corpse numbers. In *rpo-1b(op259)*, *ced-9(RNAi)* and *ced-9(n1653)* contrasted; *ced-9(RNAi)* did not lead to increased corpse numbers. Surprisingly, irradiation appeared to trigger the pro-apoptotic effect of *ced-9* knockdown. According to our model presented in *5.5 rpo-1b(op259) and the Ras/MAPK pathway*, *rpo-1b(op259)* lacks sufficient activation of the core apoptotic machinery due to missing Ras/MAPK activity; this might still be limiting in conditions of reduced CED-9 protein levels (but not with mutated CED-9 in *ced-9(n1653)*). The chapter *5.1.4 The Gogo phenotype* showed how RNAi bacteria and irradiation collaboratively affect the Gogo germ cell differentiation phenotype in *rpo-1b(op259)*. If, as suggested in the model in Figure 124, RNAi bacteria and irradiation positively regulate MAPK pathway activity, these might eventually compensate for the reduction in *rpo-1b(op259)* and facilitate the pro-apoptotic effect of reduced CED-9 levels. The similarity of *ced-9(RNAi)* with RNAi knockdown of *gla-3* – increased baseline apoptosis and hypersensitivity to irradiation-induced apoptosis in wildtype background and only an apparent effect in *rpo-1b(op259)* post irradiation – suggests that they act in a common pathway for apoptosis regulation.

	ced-9(n1653) mutation				RNAi knockdown			
constitutive apoptosis	**(+)**	***rpo-1b(op259)***	***ced-9(n1653)***	***rpo-1b;ced-9***	***empty(RNAi)***	***rpo-1b(op259); empty(RNAi)***	***ced-9(RNAi)***	***rpo-1b(op259); ced-9(RNAi)***
wt	→	↓	↑↑	↑↑↑↑	(↑)	↓	↑↑	→
egl-1(lf)	(↓)	↓↓	↑	↑	→	↓↓	→	n.d.
cep-1(lf)	(↓)	↓↓	(↑↑)	↑↑	→	↓↓	(↑↑)	↓↓
hus-1(lf)	→ (*)	↓	(↑↑)	↑↑↑	↓	↓↓	(↑)	→

irradiation response (ΔIR)	**(+)**	***rpo-1b(op259)***	***ced-9(n1653)***	***rpo-1b;ced-9***	***empty(RNAi)***	***rpo-1b(op259); empty(RNAi)***	***ced-9(RNAi)***	***rpo-1b(op259); ced-9(RNAi)***
wt	→	↓	(↑)	n.d.	(↑)	↓	(↑↑)	↑↑
egl-1(lf)	×	×	→	n.d.	→	n.d.	→	n.d.
cep-1(lf)	×	×	×	n.d.	→	↓↓	(↑↑)	×
hus-1(lf)	× (*)	n.d.	(↑↑)	n.d.	↓	↓↓	(↑)	↑

post-irradiation levels	**(+)**	***rpo-1b(op259)***	***ced-9(n1653)***	***rpo-1b;ced-9***	***empty(RNAi)***	***rpo-1b(op259); empty(RNAi)***	***ced-9(RNAi)***	***rpo-1b(op259); ced-9(RNAi)***
wt	↑	→	↑↑↑	n.d.	(↑)	↓	↑↑↑↑	↑↑
egl-1(lf)	(↓)	↓↓	↑↑	n.d.	→	↓↓	→	n.d.
cep-1(lf)	(↓)	↓↓	(↑↑)	n.d.	→	↓↓	(↑↑)	↓↓
hus-1(lf)	→ (*)	n.d.	(↑↑)	n.d.	↓	↓↓	(↑)	(↑↑)

Table 19 Summary of the effects of the *ced-9(n1653)* allele and of *ced-9(RNAi)* treatment. The effects of mutant and knockdown vary considerably in *rpo-1b(op259)* and in combinations with loss-of-function mutations of DNA damage response genes. Levels of apoptotic cell corpses in non-irradiated worms are indicated as increased ↑ or reduced ↓ in comparison to wildtype levels →. ΔIR indicates the incremental effect of irradiation on apoptosis levels, in relation to the effect in wildtype animals →; mutants with *cep-1(lf)* or *egl-1(lf)* show no change after irradiation ×. The post-irradiation levels are again in relation to the levels in non-irradiated wildtype animals. Non-irradiated *cep-1(lf)* and *egl-1(lf)* had slightly lower levels than wildtype in my experiments (↓), RNAi treated wildtype worms slightly higher (↑) levels than worms grown in standard conditions (OP50 bacteria). (↑↑) is a gradation between ↑ and ↑↑. Irradiation response was not determined (n.d.) in some mutant combinations; (*) for *hus-1(lf)* is the observation described in the literature (not determined here).

5.7 Genetic screens to find suppressors of apoptosis

Forward genetic screens to isolate new players in a biological process of interest have been performed in *C. elegans* almost since its establishment as a model organism. With a well-designed setup, genetic screens can yield candidates within short time and with reasonable effort (Jorgensen 2002). The advancement of powerful mapping techniques has allowed to accelerate the identification of the relevant genes in a candidate mutant strain. We combined classical EMS mutagenesis and sterility based candidate selection with mapping by whole genome sequencing after repeated outcrossing.

5.7.1 Temperature sensitive sterility of *ced-9(n1653)* and of *rpo-1b(op259); ced-9(n1653)*

ced-9 mutants had been used in genetic screens to isolate suppressors of sterility at 25°C [personal communication by Michael Hengartner]. Mostly, what the screens had yielded were alleles of *ced-3*, which did suppress apoptosis and thus sterility. In our current experiments, we realised that mutations of factors supposed to be genetically upstream of *ced-9* could also suppress sterility of *ced-9(n1653)*; these genes could therefore be expected to figure among the candidates of a well-saturated genetic screen. We were interested in the molecular pathways that lead to activation of CEP-1 and EGL-1 in *ced-9(n1653)* and more particularly in *rpo-1b(op259); ced-9(n1653)* mutants. We saw that *rpo-1b(op259); ced-9(n1653)* animals also had temperature sensitive sterility, which was at least partly due to increasingly excessive apoptosis at higher temperatures. So far, the mutant factors that suppressed sterility in *ced-9(n1653)* were all capable to suppress sterility of *rpo-1b(op259); ced-9(n1653)* as well.

5.7.2 Selection of sterility suppressors of *rpo-1b(op259); ced-9(n1653)*

We conceived a novel genetic screen with *rpo-1b(op259); ced-9(n1653)* that would base on the convenient selection criterion of fertility versus sterility. In a classical F2 selection approach, *rpo-1b(op259); ced-9(n1653)* grown at the permissive temperature would be mutagenised as adults, the F1 progeny would be split and F2 worms would be shifted to restrictive conditions. If a critical gene had acquired a mutation, the homozygous fraction of F2 animals would successfully proliferate and the new candidate could be selected based on survival and amplification of the population at otherwise non-permissive conditions.

5.7.2.1 Some suppressor genes might be activators of CEP-1

Candidates selected from the screen might help to resolve the intricate regulation of apoptosis at the level of CED-9. We primarily aimed at identifying the pathways that lead to *cep-1* activation in *ced-9(n1653)* (and in *rpo-1b(op259)*). In this screen, there were of course several scenarios how a candidate mutation could suppress sterility. We were expecting to find among the candidate mechanisms and genes:

Possibility: Suppression of the core apoptotic pathway

- Mutations of genes that act downstream of *ced-9(n1653)* in programmed cell death and that block or reduce all apoptosis (e.g., *ced-4*, *ced-3*).
- Mutations that affect CED-9 regulation (e.g., kinases, degradation pathways)

- Mutations of genes that participate in CEP-1 activation in *rpo-1b(op259); ced-9(n1653)* (e.g., *cep-1* itself). It is difficult to predict whether the *rpo-1b(op259)* and the *ced-9(n1653)* mutation differentially activate CEP-1 and which influence would dominate in the double; factors of two different paths might show as separate candidates.
- Mutations that break the signalling from *rpo-1b(op259)* to the core apoptotic machinery (e.g., Ras/MAPK pathway? [see *5.5 rpo-1b(op259) and the Ras/MAPK pathway*]).

Possibility: Indirect effects on apoptosis

- Mutations that compensate for effects of *rpo-1b(op259)* on rRNA. If disturbances in rRNA synthesis and ribosome assembly caused by the *rpo-1b(op259)* mutation are relevant for apoptosis or for germ line defects in *rpo-1b(op259); ced-9(n1653)*, increasing or decreasing synthesis or turnover of rRNA or ribosomes might counteract the effect of *rpo-1b(op259)* in this constellation.
- Mutations of germ line differentiation genes that alter germ cell development programs and prohibit cell death (often, such defects lead to sterility by themselves).

5.7.3 Forward genetic EMS screen with *rpo-1b(op259); ced-9(n1653)*

Together with students of the BIO323 genetics course 2009 (Magdalene Adamczyk, Simon Schäfer, and Tobias Strassfeld), we performed ethyl methane sulfonate (EMS) mutagenesis on *rpo-1b(op259); ced-9(n1653)* animals and screened the progeny of about 4500 F1 worms, i.e., approximately 9000 haploid genomes, for suppressors of sterility. The screening procedure was hampered by the extremely slow growth and low progeny number of *rpo-1b(op259); ced-9(n1653)* at permissive temperature, which led to extensive fungal contamination.

5.7.3.1 First screen yielded 18 candidates

We split the F1 worms into 152 pools of about 30 animals each and shifted the F2 to the selective temperature of 21°C; of the 152 plates, 18 had continuous growth of the worm population over at least 4 generations. We considered each population one independent suppressor line (according to a poisson distribution, 17 out of 18 lines are expected to be the progeny of one single candidate) and attributed the candidate alleles the designations *op514* to *op531*.

Degree of suppression is variable between the candidates

Fertility and growth were very variable between the 18 strains. Some lines had a considerable brood and amplified rapidly, others were reproducing at a rate just above a minimum to maintain the population. Some lines had a generation cycle almost as short as wildtype, others were much delayed in growth and needed almost one week to pass one cycle. With regards to apoptosis, some had a strong suppression or nearly complete abolition of germ cell death; others reduced the levels enough so most animals could produce some oocytes and embryos, but the corpse number was as high as, or higher than, in *ced-9(n1653)*. Germ line integrity was also variable; several lines had healthy looking gonads; some had a *ced-3*-like arrangement of small oocytes; one line showed high penetrance of the distal oocyte phenotype also seen in *rpo-1b(op259); dpl-1(n3643)*. Interestingly, there was one candidate strain that,

besides suppression of *rpo-1b(op259); ced-9(n1653)* sterility, had a strong Unc phenotype that was very similar to that of *unc-119* mutants.

5.7.3.2 Candidate genes segregate with sterility suppression phenotype

We wanted to identify the relevant mutations by applying a recently probed method for direct mutation mapping using repeated outcrossing and whole genome sequencing (Zuryn 2010). This approach is based on the idea that by repeated outcrossing of the candidate allele into the original strain, most of the mutagenised genome is ultimately replaced by homologous recombination with the original genome, except for the locus carrying the suppressing mutation and the genomic region closely linked to it. Full genome sequencing of the outcrossed candidates would then reveal regions with a significant enrichment of homozygous de-novo mutations. Nucleotide changes from the reference genome that are common to all candidates can be readily subtracted from consideration since they most likely represent polymorphisms in the original strain.

Repeated outcrossing from EMS-induced polymorphisms

With Michael Daube, we prepared the candidates accordingly. Males from the original *rpo-1b(op259); ced-9(n1653)* strain were crossed into the candidates and the males of the cross progeny were again crossed into *rpo-1b(op259); ced-9(n1653)*; the resulting F1 progeny was singled out and F2 animals were shifted to the restrictive temperature to select for worms that supposedly were again homozygous for the candidate mutation. We repeated the procedure to get the multiply outcrossed lines that we amplified for isolation of genomic DNA.

5.7.3.3 Whole genome sequencing delimits a few candidate mutations

Full genome sequencing by the SOLiD 4 system [Applied Biosystems] of a pool of 8 candidates by Microsynth AG resulted in an average coverage of 15 to 20-fold. 98 to 99 % of the genome had at least one mapped read, leaving 1 to 2 % uncovered; a large fraction of the polymorphisms called by an analysis that required a minimum coverage of 1-fold and a minimum variant frequency of 0.5 were in scarcely covered regions (1 to 5-fold) [mapping and polymorphism searches performed either with Bioscope Software and Biomatters Geneious 5.3; or with CLCBio Genomic Workbench]. As one could expect, numerous variations from the *C. elegans* reference sequence were present all over the genome in all 8 candidates. An even higher number of single nucleotide polymorphisms appeared in some but not all of the strains at variable frequency; this indicates that the original *rpo-1b(op259); ced-9(n1653)* strain was not highly isogenetic and that the population carried multiple alleles at many loci, even though the *rpo-1b(op259); ced-9(n1653)* strain had been inbred for many generations after the cross. We were not able to identify genomic regions in most of the strains with a significant enrichment of unique, homozygous single nucleotide polymorphisms that are typical for EMS-induced mutations. Therefore for us, mapping by finding peaks of de-novo mutations that are linked to the relevant suppressor allele did not work out. However, the list of homozygous, protein-relevant SNPs was limited to less than 20 for most candidate strains, for some strains to less than five. Two of the 8 strains contained two different missense mutations in *ced-4*, which likely form the relevant alleles for suppression of apoptosis and sterility. Yet, there was no significant enrichment of homozygous mutations around the *ced-4* locus that would have pointed to this region. One other strain had a mutation in *ced-3*, which we interpreted as

further validation for the screening approach of linking apoptosis and sterility suppression. We are analysing the sequencing results of the remaining strains and confirming SNP calls by classical Sanger sequencing. For all candidates, we had derived two suppressor lines from the F1 of the last outcrossing step. Relevant mutations will have to be confirmed in both lines and in the non-outcrossed candidate strain.

5.7.4 *ced-9(n1653) unc-119(ed3)*

I found that *unc-119* could suppress sterility of *ced-9(n1653)*. *ced-9(n1653) unc-119(ed3)* and *rpo-1b; ced-9 unc-119(ed3)* were fertile at 25°C and 21°C, respectively [see *6.2.2.11 unc-119(ed3) suppresses excessive apoptosis and sterility in ced-9(n1653) mutants*]. *unc-119(ed3)* could improve the brood size of *rpo-1b(op259); ced-9(n1653)* very significantly (Table 17). Apoptosis was strongly reduced in *ced-9(n1653) unc-119(ed3)* in comparison to *ced-9(n1653)* (Figure 121), and the corpse number in *rpo-1b; ced-9 unc-119(ed3)* was reduced at least as much as in *rpo-1b; ced-9; egl-1(n3082)* (Table 15). It was interesting that one candidate from the EMS screen had an Unc phenotype very much resembling *unc-119(ed3)*; whether the candidate gene falls into a functional group with *unc-119* remains to be determined.

5.7.5 Forward genetic screen using the *Mos1* transposon

In parallel to EMS mutagenesis, I tried another mutagenesis and candidate mapping approach to find suppressors of *rpo-1b(op259); ced-9(n1653)*. The *Mos1* transposon is a heterologous mobile element from Drosophila that, by integrating into one of the innumerable genomic target sites in *C. elegans*, can disrupt host genes. It has been used for the generation and selection of mutants of interest (Duverger 2007) and is has been applied successfully for efficient identification of novel genes in forward genetic screens [e.g., in (Yook 2007) or in a screen based on selection by survival in our laboratory (Butschi 2010)]. The mobile element is delivered to the strain of interest as a plasmid together with a transgenic heat-shock inducible transposase. Upon heat-shock, the *Mos1* integrates into random reception sites in the *C. elegans* chromosome, which can have a mutagenic effect. The integration locus can be readily identified by circularisation of restriction digested genomic DNA and PCR amplification from the *Mos1* sequence.

5.7.5.1 All 5 candidate strains have lost the *Mos1* transposon

I generated the transgenic *rpo-1b(op259); ced-9(n1653); [Mos1 plasmids]* strain, and together with Cathy Zheng, we mutagenised transgene positive adults by heat-shock activation, grew the F1 at the permissive temperature of 15°C, and shifted the F2 to the restrictive temperature. From multiple rounds of mutagenesis and candidate selection from the F2 generation, we isolated 5 strains that were fertile at 21°C. Unfortunately, in none of these candidates the *Mos1* transposon was detectable any more and therefore, the integration sites could not be identified. It is a known drawback of the method that the transposons are mobilised again, often leaving but a mutagenic scar at the integration site. The mutagenesis method was laborious and little efficient in *rpo-1b(op259); ced-9(n1653)*; it involved manual selection of *Mos1* plasmid positive animals for heat shocking. Regarding the small brood of *rpo-1b(op259); ced-9(n1653)* and the additional noxious effect of the heat shock, few F1 arose from

these adults, such that a high number of animals had to be selected and treated. Together with the high rate of 'escaping' *Mos1*, this led us not to further pursue the *Mos1* strategy.

5.7.6 Reverse genetic screen using RNAi

RNAi is a fast and often efficient means to knock down genes in *C. elegans*. Genome wide RNAi knockdown using libraries that contain the constructs for targeting more than 90 % of the genes of the *C. elegans* genome have been used widely in *C. elegans*. Initially, gene functions were assessed in a rather unbiased approach in wildtype N2 [e.g., (Fraser 2000; Sönnichsen 2005), overview in (Lee 2004)] or in RNAi sensitised strains (Simmer 2003). With the availability of comprehensive bacterial libraries for RNAi by feeding (Kamath 2003; Rual 2004a), the knockdown technique has been increasingly applied in reverse genetic screens; it has been very successful in identifying many novel genes involved in a great variety of phenotypes and molecular pathways.

5.7.6.1 *ced-3(RNAi)* can improve low fertility

Linkage of apoptosis and fertility in *rpo-1b(op259); ced-9(n1653)* make this mutant a convenient system to search for novel genes involved in cell death regulation or maybe in synthesis of ribosomes. We wanted to further exploit the great advantage this mutant provides for candidate selection and planned a reverse genetics approach. Together with Erica Bogan and a summer school student, we evaluated the most suitable assay conditions for large scale RNAi testing on *rpo-1b(op259); ced-9(n1653)*. Sterility was not as penetrant in RNAi conditions as on OP50 bacteria at 21°C; this might complicate the selection of truly positive candidates. However, knockdown of *ced-3* by RNAi improved fertility of *rpo-1b(op259); ced-9(n1653)* noticeably in comparison to control treated worms (grown in liquid bacterial cultures with empty vector). Like the loss-of-function allele *ced-3(n717)*, *ced-3(RNAi)* could thus suppress sterility of *rpo-1b(op259); ced-9(n1653)*. (The phenomenon that at RNAi conditions *rpo-1b(op259); ced-9(n1653)* worms are somewhat less sterile will be discussed in *7 Food type influences apoptosis levels and vulval development*.) We tested one 96-well plate out of the Ahringer RNAi clone library (the one that also contained *ced-3(RNAi)*) for possible candidates. In addition to *ced-3(RNAi)*, fertility was significantly increased by 2 other RNAi clones: targeting Y45F10B.9, a predicted E3 ubiquitin ligase, and B0564.10, the homeobox domain containing factor *unc-30*. We have not yet confirmed the validity of these findings and not yet correlated it with germ cell apoptosis.

5.7.6.2 A photometric system allows large scale analysis of population growth

Gino Poulin and Mark Elvin at the Faculty of Life Sciences at University of Manchester recently established an automated large-scale approach to measure survival and proliferation of worm cultures photometrically. They set up the appropriate conditions for a screen in *rpo-1b(op259); ced-9(n1653)* and compared food consumption between worms in control RNAi bacteria and in *ced-3* or *cep-1* RNAi clones. After culturing the worms for 10 days, food consumption increased promptly in *ced-3(RNAi)* or *cep-1(RNAi)* but not in the controls. Thus, the screening system should principally be able to distinguish suppressors from non-suppressors. Similarly to the forward genetic screen, the slow growth of *rpo-1b(op259); ced-9(n1653)* and the generally low brood size set the limits to the power of this approach. Nevertheless, this screen setup should provide a great tool to search for further candidates that

contribute to cell death in *C. elegans*. A preliminary screen with about 200 selected genes from apoptosis pathways and of central developmental programs revealed *ced-3*, *ced-4* and *cep-1* as top candidates (Figure 109) and showed weaker suppression with knockdown of about a dozen other genes. The set of genes included in this screen was biased to major signalling pathways and to known factors of apoptosis regulation. Very interestingly with regards to our findings in *5.5 rpo-1b(op259) and the Ras/MAPK pathway*, several of the genes that led to some suppression of sterility when knocked down in *rpo-1b(op259); ced-9(n1653)* have been described to directly or indirectly regulate Ras/MAPK activity. We will have to confirm an effect on germ line apoptosis in these conditions and check, what the effect is of a knockdown in the *rpo-1b(op259)* and *ced-9(n1653)* single mutants.

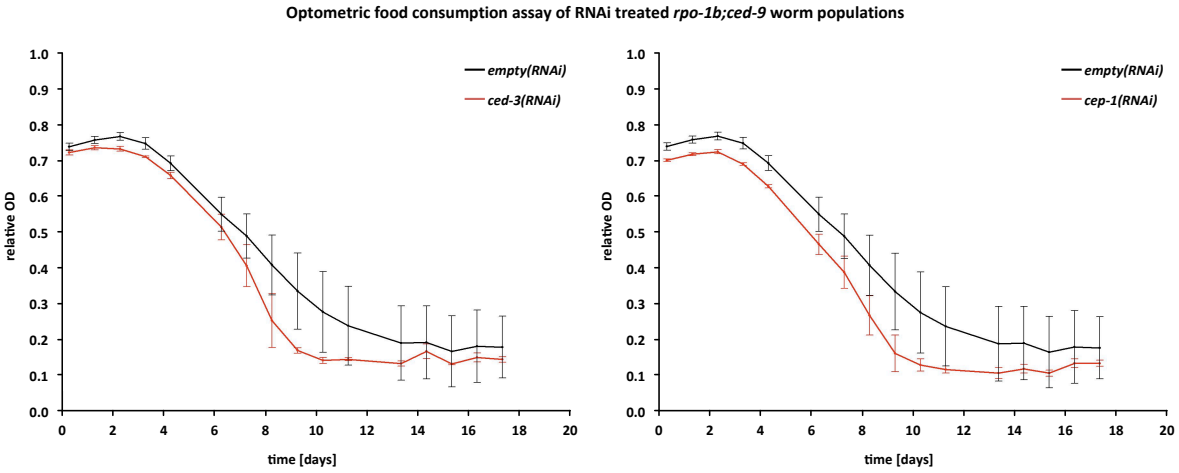

Figure 109 *ced-3(RNAi)* or *cep-1(RNAi)* improve slow culture expansion of *rpo-1b(op259); ced-9(n1653)*. Bacterial density changes were assessed as surrogate of worm population growth in an automated screening system.

5.8 Physical interactions of RPO-1B with other proteins

RPO-1B has several predicted interactions with rRNA processing and translation initiation factors and with factors of other physiological processes that are possibly affected in *rpo-1b(op259)* mutants [see interaction list for F14B4.3 summarised in Wormbase]. Many of these interactions had been inferred from yeast two-hybrid (Y2H) studies or were predictions based on observations in other biological systems. The Y2H system or *in vitro* association of isolated proteins, even though highly valuable to test direct binding of two factors, would however not reveal more indirect binding partners of a protein of interest. Careful extraction of a protein of interest from its physiological environment potentially co-extracts relevant binding partners, of the protein itself or of a protein complex that the protein is part of. The amino acid substitution in mutant RPO-1B, P70S, possibly disrupts a specific interaction of RPO-1B involving this position, or it could more indirectly be altering the context of RPO-1B, e.g., by destabilising the RNA pol I complex. Both should be reflected in changes of the interacting proteome. Even though there might be differences in the binding partners of the wildtype and mutant RPO-1B protein version or in the RNA pol I complexes, the apoptotic defects of *rpo-1b(op259)* would not necessarily be reflected therein. Still, successful pull-down experiments would undoubtedly help to characterise regulation und (mis-)functioning of *rpo-1b* in *C. elegans*.

5.8.1 RPO-1B transgenic lines

5.8.1.1 TAP-tagged RPO-1B(wt) and RPO-1B(P70S)

The successful study of macromolecular complexes by quantitative proteomics has been exemplified with the analysis of an RNA pol II preinitiation complex (approximately 70 subunits) using isotope coded affinity tag (ICAT) reagents and mass spectrometry (Ranish 2003a). I cloned a TAP::RPO-1B fusion construct and its '*op259* counterpart' carrying the P70S mutation. Comparison of the two interactomes should allow to identify differential interaction partners and to define interactions with potentially functional relevance for *rpo-1b(op259)* phenotypes. We might also learn on DNA damage response related modulation of RNA pol I by comparing RPO-1B co-precipitates from worms exposed to various conditions.

The generation of the transgenic lines and evaluation of the transgenes is described in *5.9 rpo-1b(op259) transgenes and genetic background*. I created lines with the TAP::RPO-1B(wt) or (P70S) transgene in an *rpo-1b(+); unc-119(ed3)* background and used them to perform affinity pull-downs. I used gentle conditions to purify TAP::RPO-1B and interacting factors by protein-G coupled sepharose from freeze-cracked adult worms. Andreas Frei analysed the co-precipitated proteins by mass spectrometry; unfortunately, there was massive background signal in the spectra and RPO-1B itself was not detected in the protein mix. The resulting protein identifications were thus not telling for differences between wildtype and *op259* variants.

5.8.1.2 YFP-tagged RPO-1B(wt) and RPO-1B(P70S)

Other protein tags have been used successfully to precipitate proteins of interest by high affinity interactions. I considered pull-down experiments with an YFP-tag and the anti-GFP antibody (YFP is a sequence variant of GFP that is also recognised by the antibody); besides offering the epitope for

immunoprecipitation, the fluorescent tag would serve to confirm correct cellular protein expression patterns and localisation in subcellular compartments *in vivo*. I got several transgenic lines which, however, did not show stable germ line expression of YFP::RPO-1B. Therefore, I left this approach.

5.8.2 Custom-made antibody to RPO-1B

With an antibody to RPO-1B, immunochemical detection, co-immunoprecipitation, and *in situ* staining of endogenous RNA pol I should be possible. Transgenic expression of tagged protein had not rescued some of the defects of *rpo-1b(op259)* or had even introduced new defects, likely due to overexpression; and it would not easily allow to assess quantitative differences of RPO-1B itself or of the RNA pol I complex. No commercial antibody was available for the β-subunit of RNA pol I neither in *C. elegans* nor in other eukaryotic species. One antibody had been used successfully in yeast and was characterised precisely as to its recognition site on Rpa135 (Klinger 1996); unfortunately, the epitope was not conserved in *C. elegans* RPO-1B.

5.8.2.1 Antibody design

We therefore decided for the generation of a new custom-made antibody by Genovac (Genovac); to be clear about the epitopes, I chose a two-peptide immunisation protocol. For the selection of the target sequences, I scrutinised the peptides that were judged as good targets by a prediction algorithm of Genovac; there should be minimal similarity of the sequences with the homologous second largest subunits of RNA pol II and RNA pol III or any other worm protein; and ideally, the epitope should map on the surface of the RNA pol I complex. I determined the structural context of the candidate sites based on the structure model of the related yeast RNA pol II. Finally, I chose one peptide of 15 residues starting at position 237 from the N-terminus, and one peptide of 18 residues starting 64 upstream of the C-terminus. Five rats were immunised (rat serum was supposed to give less background signal on *C. elegans* than rabbit for instance) and bled, and the sera collected separately. The antibody from one serum was affinity-purified on the peptides used for immunisation.

5.8.2.2 Immunological detection

I tested all sera, the purified antibody, and the serum from a pre-immunised rat on worm extracts from N2 and from *rpo-1b(op259)*. In a first set of testing, the antibody seemed not to detect the target protein on Western Blot.

However, with appropriate conditions in indirect immunofluorescence staining of extruded gonads, the purified antibody yielded a nucleolar pattern likely to represent RPO-1B. (Besides, there was distinct and strong granular, perinuclear staining in meiotic germ cells and intense staining of two distinct dots in the posterior pole of early embryos). RNAi knockdown of F14B4.3 in N2 worms starting at L4 stage reduced the nucleolar staining (without reducing the perinuclear dots). Since the antibody seemed to have some affinity for RPO-1B, I used it to coat beads for pull-down of RPO-1B from N2 and *rpo-1b(op259)* worm samples.

Immunoprecipitation with this custom-made anti-RPO-1B antibody has not yielded pure enough and specific samples, as concluded by staining of electrophoresis gels and mass spectrometric fingerprinting of some differential protein bands. I have not so far repeated this method.

5.9 *rpo-1b(op259)* transgenes and genetic background

Rescue of mutant phenotypes by the transgenic wildtype copy of a candidate gene is a most accepted evidence for the causal link of genotype and phenotype. I aimed at restoring irradiation-induced apoptosis in *rpo-1b(op259)* by introducing transgenic RPO-1B(wt); besides, I planned to use the transgenes for further protein analysis such as immuno-co-precipitation [see *5.8 Physical interactions of RPO-1B with other proteins*]. The transgenes would probably have to be expressed in the germ line for sufficient function. [The issues of germ line expression have been reviewed in (Merritt 2010)]. The rescue efforts were hampered by the transgene-transgenic background situation. This section will delineate my initial evaluations of the non-rescue cases; the following chapter *6 unc-119 and apoptosis: novel functions for an omnipresent bystander* demonstrates that disturbed apoptosis is an inherent problem of the transgene selection system. Analysis of the transgenes for RPO-1B did thus not primarily advance the understanding of its involvement in cell death but it lead to the discovery of a formerly neglected function of *unc-119* in apoptosis regulation.

5.9.1 The backbone of transgenes

When I planned the rescue experiments for *rpo-1b(op259)*, I decided to use the well-established microparticle bombardment method to transform *rpo-1b(op259); unc-119(ed3)* double mutants. As outlined in *6.1.2 Transgenesis in C. elegans*, *unc-119(lf)* and the wildtype allele on the transformation plasmid serve as phenotypic selection marker to isolate transgenic animals. I cloned transformation plasmids based on the vector *pLN022yfp* [plasmid from Lukas Neukomm], which harbours, in its backbone, the *unc-119* gene sequence that was originally used in an *unc-119* rescuing construct pDP#M0016 (Maduro 1995). The transformation plasmid is designed to facilitate cloning by the use of rare restriction sites, which generally allows to insert long sequences that are not otherwise fragmented by the restriction enzymes. This system, termed Lazyboy, is modular in that it has different eight-base palindromes flanking the genomic fragments to be cloned, such as the promoter, the ORF, tags, and the 3'UTR, that can thus be exchanged individually by using the corresponding rare cutting enzymes.

5.9.2 YFP- and TAP-tagged RPO-1B

I wanted to express fluorescently labelled RPO-1B for localisation studies and TAP-tagged protein for co-immunoprecipitation experiments. Optimally, tags should be neutral to a protein's intrinsic function. In *C. elegans*, no research either on RPO-1B or on any of its paralogs, i.e., the beta subunits of RNA pol II or RNA pol III, had been published. From the literature, I inferred that an N-terminally tagged RPO-1B might be functional, since homologous proteins had been successfully expressed in yeast (Schneider 2007) and mammalian cells (Hannan 1998b). I thus cloned several constructs, placing the genomic ORF with a tag at its 5' end between the endogenous promoter and 3'UTR regions of *rpo-1b*: 1a) YFP::RPO-1B(wt), the genomic wildtype allele of *rpo-1b* with the coding sequence for the Yellow Fluorescent Protein; 2a) TAP::RPO-1B(wt), with the coding sequence for the 192 residue Tandem Affinity Purification (TAP) tag; and 1b) YFP::RPO-1B(P70S) and 2b) TAP::RPO-1B(P70S) with the genomic *op259* mutant allele. In repeated bombardments – at least three per construct – I obtained several transgenic lines that I identified based on restoration of the crawler phenotype. As expected,

some of them were inheriting the crawling phenotype to all progeny, whereas others failed to propagate the rescue to all offspring, representing integrated or extrachromosomal transgenes, respectively.

5.9.3 YFP::RPO-1B shows distinct nucleolar localisation

I found several lines that had, at least transiently, expression of YFP-tagged protein with nucleolar localisation. Only few lines had significant germ cell fluorescence. In germ cells and in somatic cells, YFP::RPO-1B could be detected in distinct nucleolar regions, sparing the prominent nucleolar dots described in *5.3.4.3 CEP-1::GFP localises to nucleolar substructure* (Figure 78). Interestingly, the mutant transgenes expressing YFP::RPO-1B(P70S) had consistently higher cytoplasmic levels than the wildtype transgenes, in the germ line as well as in somatic cells (Figure 10). This is indicative of significant cytological consequences of the *rpo-1b(op259)* mutation.

I observed condensation of YFP::RPO-1B to a bright nucleolar focus in apoptotic cells (Figure 110). These foci appeared already in early corpses, when chromatin morphology was still intact. Localisation to foci was not prevented by the P70S mutation.

I did not observe obvious changes of YFP::RPO-1B fluorescence intensity or distribution at different time points following irradiation with IR or UV-C that would have reproduced the observations from mammalian cells [(Kruhlak 2007), see *4.1.4.4 RNA pol I transcription rate reacts to irradiation*].

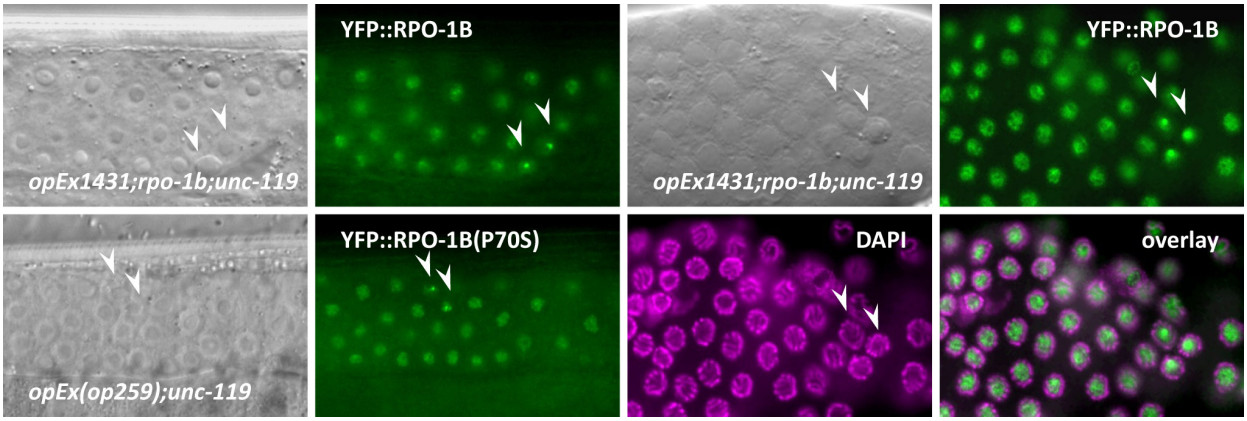

Figure 110 YFP::RPO-1B condenses into nucleolar foci in early apoptotic corpses. Transgenes *opEx1431[P_{hus-1}::yfp::rpo-1b (genomic)::rpo-1b 3'UTR; unc-119(+)]* in *rpo-1b(op259); unc-119(ed3)* background and *opEx(op259)[$P_{rpo-1b::}$yfp::rpo-1b(op259) (genomic)::rpo-1b 3'UTR; unc-119(+)]* in *rpo-1b(+); unc-119(ed3)*. DAPI staining of an extruded gonad reveals intact chromatin pattern in cells with foci, indicating a relatively early stage of apoptotic degradation.

5.9.4 RPO-1B transgene functionality

5.9.4.1 Most transgenes seem to enhance phenotypes of *rpo-1b(op259)* or introduce novel defects

The transgenes either ought to rescue the *rpo-1b(op259)* phenotypes (if coding for wildtype RPO-1B) or not to rescue it (in case of *op259*). I tested all transgenic lines for rescue of the apoptotic defect. Tagged mutant and wildtype transgenes alike could not restore normal apoptotic IR response (Table 21). Rather, new defects were often introduced into the germ line structure and the worms exhibited small brood

size, increased body length, and massive accumulation of what were likely cœlomic lipids in aging adults.

5.9.4.2 Rescue of the apoptotic IR-response defect in one line

I could eventually get a rescue of the apoptotic defect by a non-tagged transgene expressing RPO-1B(wt) from a short promoter (approximately 1 kb, up to the beginning of the annotated neighbouring gene in reverse genomic orientation). There was no rescue with the corresponding *rpo-1b(op259)* construct (Table 20). Worms from both strains did not look fully wildtype overall, however. I later detected a high copy number of the transgene by PCR in these lines.

	no IR		60 Gy	
	score	95% CI (n)	score	95% CI (n)
N2 wt	3.03	±0.16 (707)	8.17	±0.21 (875)
rpo-1b(op259)	1.43	±0.21 (152)	2.77	±0.31 (140)
rpo-1b(pS);op259;ed3	4.40	±0.83 (80)	10.44	±1.26 (87)
op259(pS);op259;ed3	2.56	±0.51 (100)	2.91	±0.43 (116)
rpo-1b(pS);ed3	1.43	±0.44 (40)	1.63	±0.42 (40)
op259(pS);ed3	1.75	±0.47 (40)	2.95	±0.50 (40)

Table 20 A transgenic construct with a relatively short promoter sequence can rescue cell death in *rpo-1b(op259)*. *rpo-1b(pS)* or *op259(pS)* stand for *[$P_{rpo\text{-}1b}$Short::rpo-1b(wt) or rpo-1b(op259)::rpo-1b 3'UTR; unc-119(+)]* wildtype or mutant transgenes with a short promoter sequence instead of the long sequence usually used as promoter $P_{rpo\text{-}1b}$ that reached into the upstream gene. Paradoxically, in *rpo-1b(wt)* background, IR response is suppressed with both transgenes. Average number of corpses per gonad, 95 % CI of the mean and number of worms scored per condition.

5.9.4.3 Considerations for the non-rescue

I considered several possible explanations for the non-rescue in most lines and tried to rule them out.

Possibility: F14B4.3 is not the relevant gene.

The apoptotic defect in the candidate from the EMS screen could be caused by another mutation than the one in *rpo-1b*. Despite extensive outcrossing of the candidate op259 from the mutagenised genetic background, a mutation closely linked to the one considered might confuse the role of *rpo-1b*. In fact, F14B4.3 is in the genomic context of a high density of DNA damage response factors on chromosome 1.

Preliminary rescue experiments with the cosmid F14B4 (containing the full-length F14B4.3 gene) that had been injected into young adult mutants had restored IR-induced germ cell death to almost wildtype levels. This corroborated the notion of the respective gene to be of relevance for apoptosis, as did RNAi knock down of F14B4.3, which could phenocopy the apoptotic defect (Figure 57).

Possibility: no or incorrect transgene is expressed.

The transgenic lines could be expressing *unc-119(+)* and rescue the Unc phenotype without also expressing the gene of interest.

Indeed, not all lines seemed to express transgenic RPO-1B. For the YFP constructs, I could detect expression by fluorescence only in a fraction of the lines. For both the YFP and the non-visible TAP constructs, I confirmed expression of a correct size protein by Western blot in some lines. Thus, full length YFP- or TAP-tagged RPO-1B was being expressed.

Possibility: the transgenes are non-functional.

As indicated, the N-terminal tags might interfere with protein function in a hardly predictable manner. RPO-1B is part of a large protein complex, and small changes to protein structure might disrupt normal complex assembly.

Several lines I got with the YFP::RPO-1B(wt) and YFP::RPO-1B(P70S) constructs were expressing fluorescent protein. Fluorescence was specifically localised to the large central nucleoli of *C. elegans* cells, with a darker halo representing the surrounding nucleoplasm. This expected localisation of the tagged transgenes did not suggest exclusion from the RNA pol I complex.

One non-tagged transgene *opEx1416[$P_{rpo\text{-}1b}$::rpo-1b(+); unc-119(+)]* could nicely rescue *rpo-1b(op259)* mutant worms from temperature sensitive sterility at 25°C and other germ line anomalies (Figure 48), indicating at least some functionality in the germ line. (The same transgenic lines however did not show a substantial apoptotic response to IR.)

Possibility: the transgenes have mis- or overexpression effects.

Germ line silencing

Silencing of repetitive sequences in germ cells is a frequent phenomenon, likely representing a defence mechanism against potentially hostile or adverse nucleic acids. This seems to be particularly relevant for high copy-number extrachromosomal transgenes. Often, germ line expression is absent even though there might be very strong expression in somatic cells and the transgene promoter should also be active in the germ line (Kelly 1997). Integrated transgenes are supposed to have a lower copy number and to be more successfully expressed in the germ line. In my transgenic lines, significant YFP-fluorescence was often limited to somatic nucleoli, whereas there was only a very weak signal from germ cell nucleoli. Only a few lines of YFP::RPO-1B(wt) and YFP::RPO-1B(P70S) nicely expressed fluorescent protein in the germ line. (Interestingly, in my case, this was not restricted to transgenes that had integrated; germ line expression also occurred from extrachromosomal arrays.) The large nucleoli in the germ line and the rapid uptake of 5-FU, a marker for rRNA synthesis, clearly indicate the presence of active RNA pol I in this tissue (Figure 27).

Transgenic worms with germ cell fluorescence generally looked healthier than the ones without, but I was still not able to demonstrate a rescue of the apoptotic defect of *rpo-1b(op259)*.

Overexpression

Stoichiometric expression of its polypeptide components might be particularly important for an abundant protein complex. Quantitative misexpression of only one member might disrupt proper assembly of the whole complex. This would certainly apply to RNA pol I of which *rpo-1b(op259)* forms one of the two core subunits. Overexpression might thus lead to phenotypes by itself, a likely explanation for the additional defects introduced to *rpo-1b(op259); unc-119(ed3)* worms with several of the transgenes.

I tested by qRT-PCR how strongly total RPO-1B mRNA would be expressed in the transgenic lines. Surprisingly, the levels were only slightly above the range for non-transgenic lines, indicating that there was not massive overexpression from the transgenes.

Misexpression

The promoter region and individual sequence elements around the translation initiation site are particularly important for the correct expression of genes. Kertesz et al. recently showed how base alterations might affect gene expression by changing the secondary structure of the mRNA (Kertesz 2010). When cloning with the Lazyboy system, the cloning sites are usually chosen at the transitions from elements like promoter and tag, or tag and gene of interest. In my constructs, I had introduced the YFP between the promoter of *rpo-1b* and its translation initiation site; at both ends it had to be linked with a minute linker sequence. The natural sequence immediately upstream of the translation initiation site of *rpo-1b* was thus disrupted. In retrospect, I realised that the predicted secondary structure for the mRNA in the region of the new translation initiation sites (N-terminus of YFP or TAP) was significantly different from the natural RPO-1B mRNA, theoretically disfavouring efficient translation. The transgenic constructs with no protein tag were cloned without this linker sequence between the $P_{rpo\text{-}1b}$ promoter and the genomic ORF of *rpo-1b*.

Possibility: Integration site-specific effects

Transgenes integrate randomly into the genome and might disrupt normal gene function around the integration site.

This seemed the least likely since I got similar effects in independent transgenic lines. It would have to be a more general effect of transgene uptake than specifically of local genomic disturbances.

5.9.4.4 Explanation for the non-rescue

In the following chapter *6 unc-119 and apoptosis: novel functions for an omnipresent bystander* I will present a genetic interference that was underlying all the above experiments with transgenic lines. The transgene selection marker *unc-119* is likely to have confounded the functionality of the *rpo-1b* transgenes in many cases. I have not examined the effects in detail, except for *opEx1416[*$P_{rpo\text{-}1b}$*::rpo-1b(+); unc-119(+)]* (present in strain number (1)-3-3 Ex in Table 21), which will be described in *6.2.1.3 Transgenes in an unc-119(ed3) background entail apoptotic defect*. This transgene eventually proofed to be proficient in rescuing the apoptotic defect of *rpo-1b(op259)*, once the *unc-119(ed3)* background was replaced by *unc-119(+)*. This supports that the mutation in F14B4.3 is the cause for the IR response defect in *rpo-1b(op259)*.

			no IR		*60 Gy*	
Group	**Transgene**	**Strain number**	**score**	**95% CI (n)**	**score**	**95% CI (n)**
N2	**N2**		3.03	±0.16 (707)	8.17	±0.21 (875)
rpo-1b(op259)	***rpo-1b(op259)***		1.43	±0.21 (152)	2.77	±0.31 (140)
TGrpo-1b(+);op259;ed3	***rpo-1b(pL);op259;ed3***	(1)-10-5	1.03	±0.44 (35)	1.76	±0.44 (33)
		(1)-10-6	1.20	±0.37 (20)	1.17	±0.73 (18)
		(1)-12-1 Ex	1.84	±0.72 (31)	4.27	±0.94 (26)
		(1)-3-3 Ex	1.65	±0.41 (54)	3.12	±0.75 (52)
	rpo-1b(pS);op259;ed3	(1)-3-5	4.40	±0.83 (80)	10.44	±1.26 (87)
		(1)-8-7	1.64	±0.80 (11)	2.45	±0.88 (20)
	yfp::rpo-1b;op259;ed3	(1)-16 Ex			3.14	±0.76 (14)
		(2)-14-6	2.90	±0.78 (30)	2.91	±0.48 (32)
		(3)-1-1-4			4.27	±0.75 (11)
		(3)-11			3.20	±1.12 (10)
	Phus-1::yfp::rpo-1b;op259;ed3	(1wt)-2-8_x_op259;ed3	2.06	±0.43 (31)	3.03	±0.52 (60)
		(1wt)-8-4_x_op259;ed3	1.65	±0.46 (20)	2.65	±0.81 (20)
	TAP::rpo-1b;op259;ed3	(1)-2-3	2.92	±1.26 (13)	5.00	±1.63 (17)
		(1)-6-2	3.14	±1.89 (21)	3.10	±0.99 (20)
	TAP::rpo-1b(trunc);op259;ed3	(1)-4-2	0.75	±0.49 (12)	0.71	±0.33 (17)
TGop259;op259;ed3	***op259(pS);op259;ed3***	(1)-12-3	2.56	±0.51 (100)	2.91	±0.43 (116)
	yfp::op259;op259;ed3	(1)-5-7	1.00	±0.38 (20)	2.10	±0.58 (20)
		(3)-4			1.50	±0.57 (4)
	Phus-1::yfp::op259;op259;ed3	(1wt)-8-2_x_op259;ed3	1.60	±0.54 (20)	1.65	±0.59 (20)
	gTAP::op259;op259;ed3	(1)-4-1	1.42	±0.78 (12)	0.92	±0.56 (12)
		(1)-6-4	1.14	±0.67 (7)	1.25	±0.55 (12)
TGrpo-1b(+);ed3	***rpo-1b(pS);ed3***	(1)-3-5_x_ed3	1.43	±0.44 (40)	1.63	±0.42 (40)
	yfp::rpo-1b;ed3	(2)14-6-1_x_ed3	1.96	±0.30 (80)	5.16	±0.51 (56)
	Phus-1::yfp::rpo-1b;ed3	(1wt)-2-8-8 Ex	4.28	±1.23 (18)	4.22	±0.75 (27)
		(1wt)-8-4	3.32	±0.54 (60)	3.75	±0.50 (60)
	TAP::rpo-1b;ed3	(1)-6-2-1_x_ed3	1.80	±0.44 (20)	2.20	±0.72 (20)
	TAP::rpo-1b(trunc);ed3	(1)-4-2-5_x_ed3	0.70	±0.32 (20)	1.45	±0.59 (20)
TGop259;ed3	***op259(pS);ed3***	(1)-12-3_x_ed3	1.75	±0.47 (40)	2.95	±0.50 (40)
	yfp::op259;ed3	(1wt)-17-2 Ex			3.00	±0.59 (16)
		(1)-5-7_x_ed3	2.92	±0.60 (60)	4.42	±0.72 (81)
	Phus-1::yfp::op259;ed3	(1wt)-8-2	2.48	±0.48 (60)	6.43	±0.84 (60)
	gTAP::op259;ed3	(1)-3-5-1_x_ed3	1.80	±0.75 (20)	7.76	±0.92 (34)

Table 21 Apoptotic response in *rpo-1b* transgenic lines. *TGrpo-1b(+)* transgenes with genomic *rpo-1b(wt)*, *TGop259* transgenes with genomic *rpo-1b(op259)*. Without further indication, the promoter sequence preceding the tag (TAP or yfp) is $P_{rpo\text{-}1b}$ (long sequence that reaches into the reversely oriented upstream gene); some constructs have the $P_{hus\text{-}1}$ promoter to favour germ line expression. *rpo-1b(pS)*, *op259(pS)* and *rpo-1b(pL)*, *op259(pL)* have $P_{rpo\text{-}1b}$Short (see Table 20) or $P_{rpo\text{-}1b}$Long (corresponding to $P_{rpo\text{-}1b}$) directly preceding the *rpo-1b* ORF without linker. Some transgenes were crossed into *rpo-1b(op259)* or *rpo-1b(wt)* background (indicated as _x_op259;ed3 or _x_ed3, respectively). Average number of corpses per gonad, 95 % CI of the mean and total number of worms scored per condition.

6 *unc-119* and apoptosis: novel functions for an omnipresent bystander

Analysis of the non-rescue from the apoptosis phenotype of *rpo-1b(op259)* by transgenic RPO-1B revealed an imminent involvement of the transgene selection marker *unc-119* in apoptosis regulation. I examined the effect of the widely used constellation of mutant *unc-119* with transgenic wildtype *unc-119* (termed here *unc-119(tg+)*) on irradiation-induced apoptosis and detected difficult to predict alterations of cell corpse levels. I found that *unc-119(lf)* animals have a significant deviation from wildtype apoptosis in the germline and differ in somatic cell death as well. Together with Sheng Zeng, we are performing additional experiments to characterise the role of *unc-119* in apoptosis.

We plan to submit our findings of the involvement of *unc-119* in apoptosis for publication soon. The observation how severely *unc-119(ed3)* can affect the results of studies with transgenes is of high relevance for the worm community. *unc-119* mutations are widely used in genetic research without suspicion, and often not considered in the interpretation of results. The potential influence of *unc-119* in transgenic lines can be very misleading if neglected. A combined analysis of the literature on mammalian UNC119 and of our experiments so far on *unc-119* in *C. elegans* suggest a role in engulfment of apoptotic cells. We plan to include this preliminary picture of how *unc-119* regulates death and removal of somatic and germ cells. The findings on UNC-119 are split here into two sections, addressing the implication for transgenic lines and the role of UNC-119 in cell death, respectively. The first section refers to findings in *rpo-1b(op259)*, which will be omitted in the manuscript to avoid confusion.

Chapter 6

6.1 Introduction to the use of *unc-119(ed3)*

6.1.1 Transgenes – an indispensable genetic tool

C. elegans offers itself as a versatile system to study the genetic basis of many aspects of life in a relatively simple, but nonetheless comprehensive unit. It is suitable for forward and reverse genetic approaches, that is, for finding novel genes underlying a phenotype of interest, or for studying the functions of a known gene and its consequences for biological processes, respectively. A wealth of genetic mutants have been isolated from forward genetic screens in various research fields (Jorgensen 2002) and have become available to the *C. elegans* community, together with mutants obtained in more targeted approaches by consortia like the Caenorhabditis Genetics Center at University of Minnesota (CGC) and the National BioResource Project (NBRP) in Japan (Mitani 2010). These mutants are in turn a helpful resource for reverse genetic studies; another powerful means is the reduction of specific gene expression by RNA interference. RNAi is comparatively simple in *C. elegans* and can be induced by feeding worms with bacteria that express dsRNA with the sequence of the gene of interest. All these tools are undoubtedly highly valuable to study gene function and genetic relations. In most cases, they lead to reduction or loss of the normal function of a gene product. Occasionally, a mutation enhances the function of a factor, e.g., by rendering it insensitive to some regulation and thus to a constitutively active player; or it indirectly activates a biological process by eliminating an inhibitor. More clarity, and more certainty, about the role of a factor in a particular process would be gained from its artificial introduction into the model system. Ideally, a phenotype seen in a mutant animal can be specifically overcome by expressing the wildtype copy of the suspect gene. Such a rescue experiment is key to causally linking an observed defect to the mutation in a certain gene. Tagging a gene product with visible markers helps to determine its expression pattern within the organism or within its cells. When refining the requirement for a gene with regards to a defined function, it can be helpful to express it with local or temporal constraints, i.e., in a specific cell or tissue, or at a specified developmental stage of the animal. It can also be useful to express altered versions of a protein – such as truncations or additions, deletions of certain protein domains or replacement of critical amino acid residues – to characterise its molecular functions. The use of molecular tags on a protein of interest facilitates isolation from the context of a biological system, when specific high-affinity antibodies are not available. The innovations based on transfer of a genetic construct into an organism are numerous and have become indispensable in biological research.

6.1.2 Transgenesis in *C. elegans*

C. elegans is amenable to genetic transformation. Genetic material can be introduced as dsDNA stretches or as plasmids and immediately be expressed in the transgenic animal. Originally, transformation was achieved by injection into the germ line rachis, a cylindrical structure to which all meiotic germ cells connect their cytoplasm. From this syncytium, genetic material is assumed to be taken up by the germ cells and thus to be propagated to some of the progeny (Stinchcomb 1985). Identification of successfully transformed progeny, if not by an obvious phenotype induced or suppressed by the transgene itself, is generally alleviated by the use of a co-injection marker (Giordano-

Santini 2011; Rieckher 2009). For example, such a marker highlights transformed animals by expression of a fluorescent protein from a tissue-specific promoter; or it confers a dominant trait like rolling movement (Mello 1991). In a somewhat more elaborate design, the worm strain to be injected is first crossed with a mutant that exhibits a strong phenotype or a conditional defect like temperature sensitive sterility (Granato 1994). Together with the transgene of interest, a rescue gene for this adverse mutation is then delivered to the worms. Successfully transformed progeny will thus become easy to select by loss of the adverse phenotype, i.e., regained wildtype appearance or fertility.

6.1.2.1 DNA injected into the germ line is expressed and replicated

Injection of individual animals is a laborious process that requires extensive training. Sometimes, worms are harmed by the procedure and die, or transgenes are transmitted very inefficiently. The injected DNA tends to form multicopy, tandem arrays that remain extrachromosomal and don't segregate in a Mendelian fashion (Stinchcomb 1985). Expression levels can vary considerably: the extrachromosomal arrays are usually very large (80-300 copies) (Mello 1991; MacMorris 1994) and can lead to massive overexpression of the transgene. The non-mendelian inheritance can lead to progeny carrying only a fraction or none of the transgene present in the parent. Or, within the developing offspring, not all cells inherit the construct, which leads to genetic mosaics. (This was already noticed by Stinchcomb et al. (Stinchcomb 1985), and has often been addressed in expression studies [e.g., (Erdélyi 2011)]; different systems were presented to visualise and to track the mosaic pattern of transgenic arrays by GFP (Gonzalez-Serricchio 2006; Yochem 1998).) When performing genetic crosses to transfer the transgene to another worm strain of interest, the mutation conferring a negative trait to non-transgenic animals might be lost on the way; all progeny will look like rescued animals even in the absence of a transgene. And transgenes will eventually be lost if not selected for. Furthermore, repetitive genetic elements are prone to becoming silenced in the germ line (Kelly 1997); this often precludes the reliable study of a gene with germ line expression by transgene injection. [Transgenic solutions for the germline, see recent WormBook chapter (Merritt 2010).] Most of these issues can be overcome by integrating the extrachromosomal DNA into the chromosomes [discussed in (Mello 1991)]. Several methods have been demonstrated to yield integrated arrays, although at variable, often low efficiency (Fire 1986; Mello 1991, 1995). For instance, chromosomal breaks are artificially induced by ionizing irradiation; the DNA repair system in the germ line would seal the breaks, but occasionally, it would erroneously amalgamate chromosomal DNA with transgenic DNA, and thus incorporate the transgenic construct into the genome. The transgene, which will be randomly integrated somewhere in the genome, will then be inherited to the descendant cells in a Mendelian way. It is to consider that the gamma treatment induces other damages, so that the newly integrated transgene has to be carefully outcrossed.

6.1.2.2 Gene bombardment allows to conveniently obtain integrated transgenes

For many genetic experiments, integrated transgenes are preferable. In 2001, Praitis et al. described a new method to directly create low-copy, integrated transgenes by ballistic transformation of *C. elegans* (Praitis 2001), which has become a standard for the generation of transgenic lines. Plasmid DNA is coupled to gold beads, which are, in a vacuum chamber, shot at high speed onto a lawn of young adult worms. The mechanism of transgene uptake and integration into the genome is not known. Upon gene bombardment, the transgenic constructs either form extrachromosomal arrays similar to the result of

plasmid injection, or in a reasonably high proportion of cases (10-30 %) integrate at non-predictable sites in the genome. The rate of successful transformations is orders of magnitude lower than with DNA injection; this is, however, compensated for by the extremely selective and convenient *unc-119* marker system used for ballistic transformation. *unc-119* is a highly conserved gene that was originally identified from a spontaneous mutation affecting locomotion (Maduro 1995), and named according to its mutant phenotype, a slow and uncoordinated (Unc) movement. *unc-119* mutants further exhibit feeding and metabolic phenotypes. When wildtype worms find no food, their pharyngeal pumping rate decreases; if young larvae starve for a longer period, they can enter an alternative developmental program, the "dauer" stage, in which they become more resilient and can survive without food up to several months. *unc-119* mutants are defective for both adaptations. The obvious movement phenotype and survival disadvantages made *unc-119* an optimal selection marker for the generation of transgenic strains and the transfer of transgenes in genetic crosses. It is extremely convenient. Biolistic transformation has become a routine tool; *unc-119* has been used in at least 900 studies [result of literature search for publications mentioning *C. elegans unc-119*, July 2011].

Integration site and copy number of the transgenic construct is variable and can present a challenge for functional analysis of the gene of interest. The random insertion of the transgene might disrupt phenotypically relevant gene functions. The unpredictably high copy number might lead to aberrant expression of the transgenic protein; overexpression might be an intended effect in some cases, more often however, a more physiological copy number or inducible overexpression systems would be preferred, since overexpression itself can significantly disturb cellular functions (Vavouri 2009). Also, the frequently observed germ line silencing of transgenes (not excepting integrated constructs) is supposedly the result of a cellular coping mechanism with repetitive sequences, and can lead as much as to co-suppression of the endogenous gene, which would then entail a loss-of-function effect [reviewed in (Merritt 2010)]. To circumvent all these issues, techniques have been developed to integrate transgenes at very specific sites in the genome in single copies (Frøkjaer-Jensen 2008). This *Mos1*-mediated single-copy insertion (MosSCI) approach, initially designed with transgene administration by germ line injection, also works in combination with *unc-119*-based selection. *unc-119* has also been used as a marker in other genome manipulation techniques. It was included in constructs for homologous gene targeting by bombardment (Berezikov 2004). In recently developed gene knockout techniques, an (mini) *unc-119* gene is used as temporary or permanent marker of transgene insertion and gene deletion [(Vázquez-Manrique 2010) or (Frøkjaer-Jensen 2010)]. Overall, *unc-119* is broadly used and many of the innumerable transgenic strains produced in the past 10 years contain combinations of loss-of-function alleles of endogenous *unc-119* with transgenic *unc-119(tg+)*.

6.2 Text elements for a manuscript

6.2.1 *unc-119* in transgenic lines

6.2.1.1 Mutant *unc-119* is a frequently used background for transgene selection

unc-119 has been widely used as a selection marker in transgenic strategies for one decade (Praitis 2001). Amenability to genetic transformation complements the power of *C. elegans* as a genetic model system, facilitating the study of genes and proteins in a cellular and tissue context. Transgenes have been introduced by injection of DNA into the germ line of *C. elegans*, or by microparticle bombardment. The latter technique has a principally low transformation rate; the convenient scalability of the worm number makes it an effective means nevertheless, provided a robust transgene selection system. Obvious morphological and locomotory defects and a conditional survival disadvantage have made *unc-119* mutants a popular genetic background for ballistic transformation. *unc-119* mutant animals are dumpy, they coil, and they remain in one position on a plate (Maduro 1995). When fed in liquid culture, they grow and reproduce well; however, *unc-119* mutants do not adapt normally to depletion of food: they do not reduce pharyngeal pumping and, importantly, starving young larvae do not enter the dauer stage and thus fail to prepare for long-term survival. Rescue of the *unc-119* mutant phenotypes by co-bombardment with a wildtype copy of the *unc-119* gene allows for easy selection of transgenic worms. These exhibit restored sinusoidal movement and endure starvation, and they become easy to identify, even if initially presenting a minute fraction (10^{-4}) of the whole worm population (Praitis 2001).

6.2.1.2 Apoptotic defect of a novel mutant persists in transgenic rescue lines

We repeatedly failed to rescue a defect in DNA damage-induced germ cell death in the mutant *op259* that we had isolated from a genetic screen; introducing a wildtype copy of the candidate gene by ballistic transformation could not restore normal apoptotic response to IR irradiation. A first line consideration was that, given transformation had worked effectively, the suspected gene was not responsible for the apoptotic phenotype. However, mutation mapping had confidently led us to this one single locus. Additionally, we had several reasons to expect rescue by at least some of the transgenic constructs we used. First, preliminary rescue experiments with a cosmid containing the full-length gene that had been injected into mutant animals had shown a return to almost wildtype levels of IR-induced germ cell death. This corroborated the notion of the respective gene to be of relevance for apoptosis, as did an RNAi knock down experiment in which the apoptotic defect could be phenocopied. Second, we could observe the expected protein expression and subcellular localisation pattern – that included germ line nucleoli – of an YFP tagged transgene in several independent lines; and we could confirm expression of correct size YFP- or TAP-tagged protein by Western blot. This excluded non-expression or germ line silencing as the likely causes for the failure to rescue. Third, a non-tagged transgene *opEx1416[*$P_{rpo\text{-}1b}$*::rpo-1b(+); unc-119(+)]* could nicely rescue *rpo-1b(op259)* mutant worms from temperature sensitive sterility that arose from other germ line phenotypes than apoptosis (Figure 48). The same transgenic lines nevertheless did not show a substantial apoptotic response to IR.

6.2.1.3 Transgenes in an *unc-119(ed3)* background entail apoptotic defect

We assumed that other aspects of transgene use were interfering with the apoptotic phenotype. The underlying point mutation might lead to a dominant negative effect that cannot be rescued by the transgenic wildtype copy, or overexpression of the transgene itself could disturb the normal function of the protein, which acts in a multimeric complex. We crossed some of the transgenes from the *rpo-1b(op259); unc-119(ed3)* double mutant background into *unc-119(ed3)* only, i.e., the wildtype background for the gene of interest. The transgenes all behaved similarly – wildtype and mutant versions alike – apparently rendering the germ cells resistant to IR-induced apoptosis (Table 22). As a control, we tested an independent, pre-existent transgenic line carrying *opIs204[$P_{eft\text{-}3}$::ph(ced-12)::yfp; unc-119(+)]* that had been used not in direct connection with apoptosis. Surprisingly, it also had reduced levels of IR-induced apoptosis in comparison to wildtype, down to the effect that our transgenes of interest had evoked (Figure 112 and Table 23). The common traits of all these worm strains were the transgene vector backbone and the *unc-119* mutant background. So far, the wildtype copy of *unc-119* on the vector had been thought to rescue the supposed null allele *ed3* of *unc-119*, a combination on which this selection system evidently bases. However, with regards to apoptosis, the *ed3* allele and the transgenic wildtype *unc-119* copy seem not a pair equal to endogenous wildtype *unc-119*.

	no IR			60 Gy		
	score	SEM (n)	n.tot	score	SEM (n)	n.tot
N2	3.03		707	8.17		875
rpo-1b(op259)	1.43		152	2.77		140
TGrpo-1b(+);op259;ed3	2.22	±0.30 (11)	346	3.61	±0.59 (14)	420
TG(op259);op259;ed3	1.54	±0.27 (5)	159	1.72	±0.29 (6)	184
TGrpo-1b(+);ed3	2.53	±0.44 (6)	218	3.43	±0.53 (6)	203
TG(op259);ed3	2.01	±0.31 (6)	180	4.34	±0.89 (7)	231

Table 22 Transgenic *rpo-1b(wt)* does not restore irradiation-induced apoptosis. Average of the means of different transgenic lines with a wildtype *rpo-1b* (*TGrpo-1b(+)*) or a mutant (*TG(op259)*) gene copy on the construct, in an *rpo-1b(op259); unc-119(ed3)* or in an *rpo-1b(+); unc-119(ed3)* background. Apoptotic corpses per gonad at 24 hours post irradiation; SEM (n), standard error of the means and number of lines included in the group; n.tot, total number of animals scored across all lines. (For individual lines, see Table 21)

6.2.1.4 *unc-119* mutants have reduced apoptotic response to irradiation

We tested the *unc-119(ed3)* bombardment strain for IR response. Indeed, it had low baseline levels of apoptotic germ cell corpses and failed to significantly increase cell death upon DNA-damage (Figure 111). To exclude that a possible additional mutation in this strain with close linkage to *unc-119* caused the apoptotic phenotype, which would thus not be rescued by *unc-119(tg+)*, we tested an independent allele of *unc-119*. The *e2498::Tc1* allele had been isolated from 'natural mutagenesis' by a cross of two different wildtype strains, which typically increases mobility of the transposable element Tc1, and which had led to Tc1 insertion into the *unc-119* locus. The *unc-119(e2498::Tc1)* mutant was almost equally defective in rising germ cell corpse number upon IR (Figure 112). Like *ed3*, the *unc-119(e2498::Tc1)* mutation leads to a premature stop in the penultimate exon of *unc-119* (Figure 113) (in the strain that we analysed, not the Tc1 element itself but only a scar of 4 nt was inserted in the *unc-119* gene sequence). Using again the same integrated transgene *opIs204*, we detected only little rescue of the *unc-119(e2498::Tc1)* apoptotic defect in crawling, i.e. transgenic, animals (Figure 112).

We assessed whether this non-rescue of the apoptotic defect of *unc-119* had been responsible for the non-rescue of the apoptotic phenotype of *rpo-1b(op259); unc-119(ed3)* by *opEx1416*. Indeed, when *unc-119(ed3)* was crossed away, *opEx1416* was capable of rescuing *rpo-1b(op259)* (Figure 112).

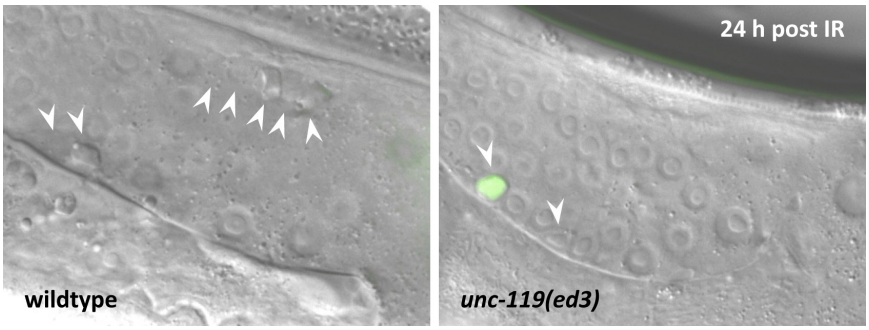

Figure 111 *unc-119* mutants have less apoptotic corpses (arrowheads) in late meiotic pachytene region following ionising radiation with 60 Gy. (Worms were incubated in Acridine Orange (green) for 1 hour and recovered for 1 hour before analysis with fluorescence and DIC microscopy. Acridine Orange (AO) accumulates in acidic compartments and fluoresces in the presence of nucleic acids – conditions that are fulfilled for apoptotic corpses within the late phagosomes of engulfing cells. It will have to be tested whether AO staining significantly differs between the strains.)

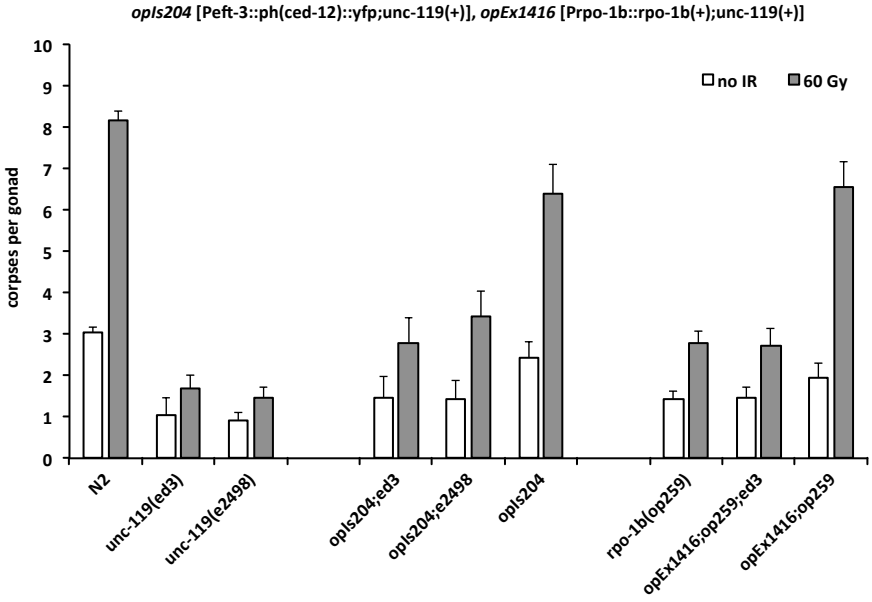

Figure 112 Transgenic *unc-119(+)* does not fully rescue the apoptotic defect of mutant *unc-119*. *opIs204* encodes an YFP-tagged protein domain only besides transgenic *unc-119(+)*. Non-rescue of the *unc-119(ed3)* apoptotic defect prevents restoration of normal apoptosis in *rpo-1b(op259)* by transgenic wildtype *rpo-1b*. Only in the absence of *unc-119(ed3)* the transgene *opEx1416[$P_{rpo\text{-}1b}$::rpo-1b(+); unc-119(+)]* evidently rescues *rpo-1b(op259)*. Apoptotic corpses at 24 hours post irradiation; error bars represent 95 % CI of the mean.

6.2.1.5 UNC-119 is a highly conserved protein with various isoforms in human

UNC-119 is an evolutionarily conserved protein with a high degree of identity of amino acid residues between the *C. elegans* and human homologs. The conservation is particularly high in a presumptive protein domain in the C-terminal region, resembling the phosphodiesterase delta subunit PDEδ (Kobayashi 2003). The gene structures of human UNC119 and *C. elegans unc-119* are also similar, with intron-exon boundaries at conserved sites (Figure 113). For the human UNC-119, two homologs have

been annotated, homolog A and homolog B. They differ mostly in their N-terminal region, outside the PDEδ domain. Further, two isoforms have been described for the homolog A, with the isoform b deviating in the C-terminal 37 residues of isoform a. Functional conservation of human, *Drosophila*, and *C. elegans* UNC-119 was demonstrated by heterologous expression and rescue of the *unc-119* loss-of-function phenotypes in *C. elegans* (Maduro 2000). These analyses also showed that the C-terminal, but not the N-terminal regions of the proteins were critical for protein function. Three different proteins have been hypothesised for *C. elegans* UNC-119, coded for by the same locus M142.1, and representing translations from alternative initiation sites (Figure 113). When the *unc-119* gene was being cloned (Maduro 1995), the M142 cosmid was sufficient to rescue the locomotion defects of UNC-119 mutants. The *unc-119* coding region could be localised at one end of the specific insert sequence of the cosmid (Figure 115), and the gene with its exon-intron boundaries could be defined. Again, a subclone of M142 in the construct pDP#M0016 with the sequence confined to the presumptive *unc-119* gene, could rescue the *unc-119* mutant phenotype. Consequently, this sequence was used in the bombardment vectors for ballistic transformation of *unc-119* mutant animals. Most bombardment vectors used in the *C. elegans* community inherited this initial *unc-119* cloning sequence as elementary part of the vector 'backbone'.

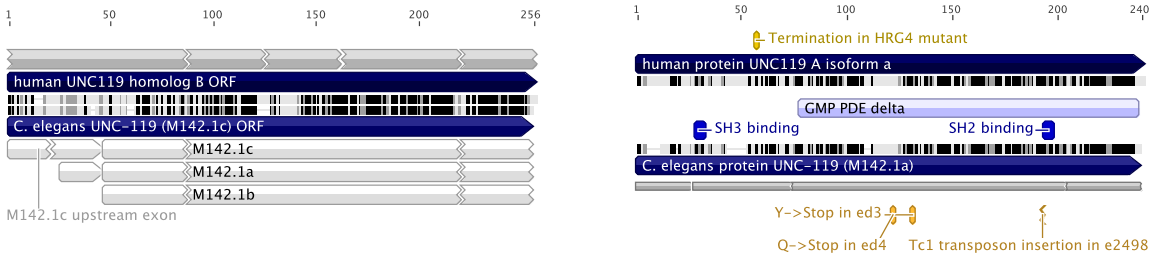

Figure 113 Left: *unc-119* ORF aligned with hUNC119 ORF (translation alignment). Best matching homolog of the full-length *C. elegans* UNC-119 (M142.1c) is human UNC119 homolog B. Amino acid identity is shown in black, similarity in grey. For *C. elegans*, the three alternative ORFs are shown as M142.1a, b and c. Exon-intron boundaries (breaks in grey bars) are partly conserved between human and *C. elegans*. Note the sequence identity at the N-terminus of M142.1c, which is encoded by the distant first exon of *unc-119* (shown in Figure 115). Right: Alignment of M142.1a, the 'consensus' *unc-119*, with its best matching human homolog UNC119 A isoform a. The SH3 binding domain is conserved in the A but not the B homolog. Conservation is very high in the C-terminal GMP PDEδ domain. All mutations lead to early stops between the SH3 and SH2 domain. The HRG4 mutant allele was shown not to behave like a genetic *null*.

6.2.1.6 *unc-119* alleles are likely recessive

We used the default bombardment vector without inserting an additional gene of interest to produce lines that only express UNC-119*(tg+)* from the construct (pSG12). In integrated (*opIs462*) and extrachromosomal (*opEx1475*) transgenic lines alike, germ cell apoptosis was clearly reduced (Figure 114), again supporting that transgenic *unc-119(tg+)* does not necessarily restore normal apoptosis in *unc-119(ed3)* mutants despite rescue of the Unc phenotype, and that this is independent of other gene sequences in the vector.

The *unc-119* alleles *ed3* and *e2498::Tc1* both have a premature stop codon in the second last exon, which would theoretically both lead to a truncated UNC-119 that preserves N-terminal sequence elements like a SH3 binding domain, but that has an interrupted PDEδ domain and lacks a SH2 binding site (Figure 113). To test the possibility of a dominant effect of the *unc-119* mutant alleles over the

wildtype copy, we irradiated the F1 cross progeny of N2 males and *unc-119* mutant hermaphrodites. *unc-119(ed3)/+* and *unc-119(e2498::Tc1)/+* heterozygous worms had significantly higher levels of germ cell death than the homozygous mutants (Figure 114). This applied also to the heterozygous cross progeny of N2 and transgenic lines with an *ed3* background. On average, animals heterozygous for *unc-119(+)* do not have fully wildtype apoptosis; their levels for IR-induced germ cell death are slightly below those of N2 × N2 cross progeny. This indicates a possible insufficiency of one single wildtype copy, but does not completely exclude a dominant effect of some sparse, truncated UNC-119 expressed from the mutant alleles.

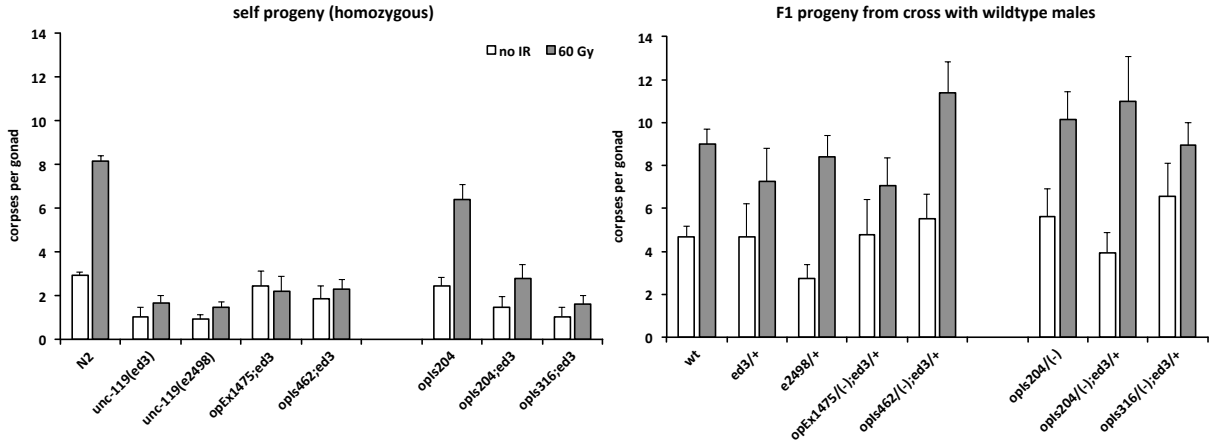

Figure 114 *unc-119(lf)* heterozygous animals have nearly wildtype levels of germ cell corpses. Strains were cross-fertilised with N2 wildtype males, and heterozygous F1 hermaphrodites were irradiated 12 hours post L4 or left untreated. Germ cell apoptosis was scored 24 hours later. Note that for wildtype, in the cross progeny, apoptosis levels are slightly higher than in the self-progeny for wildtype. *opIs462* and *opEx1475* are *[$P_{unc\text{-}119}$short::unc-119(+)]* from pSG12; integrated transgenes also become heterozygous by the cross (indicated by transgene/(-)). Error bars represent 95 % CI of the mean.

6.2.1.7 Transgenic *unc-119(tg+)* does not include the full-length gene

We realised that a more recent gene model in Wormbase replaces the 5'-most exon of the original *unc-119* annotation with a significantly more upstream exon (Figure 115). This short exon sequence possibly falls off the limits of the M142 cosmid and might therefore have been missed initially. It is likely present at one extreme of the adjoining C44B9 cosmid. The C44B9 and the M142 contigs overlap in a region that would correspond to the first, 3747 nt long intron of the newly annotated *unc-119* gene. The spliced transcript from the M142.1 gene conserving all five exons would harbour three open reading frames, defined at their 5' end by the three already mentioned alternative translation initiation sites. There is evidence for such a long transcript from ESTs [Wormbase WS220 entries MM454_FPK17YK01CI46C, MM454_contig07509, and yk258a1.5].

We wanted to confirm such an mRNA product reaching from the 5' exon into a downstream exon by RT-PCR. Using a forward primer annealing to the 5'-most exon and a reverse primer to the second or more downstream exons, we were able to amplify sequences of the expected size from a whole worm cDNA preparation. Sanger sequencing confirmed products with direct reads from the newly annotated 5'-most exon into exon 2. We could not amplify such a sequence from the RNA extract (no reverse transcriptase), indicating that the template is indeed cDNA and not a contaminating genomic DNA.

There was no additional product from the cDNA that would reveal an alternative splice variant for M142.1c, e.g., one that skips exon 1 (which has a length of a multiple of 3 nt). We have herewith demonstrated that the *unc-119* gene differs from the original annotation and that a transcript is produced that includes the formerly missed distant 5' exon. At this point, we cannot conclude what ratio of total M142.1 mRNA the transcript including the most 5' exon represents. It might be present at comparatively low levels or constitute the main fraction. We will have to evaluate how relevant this transcript is for the full functioning of *unc-119*. The *unc-119* mutants might or might not have such a transcript; in any case, no full-length wildtype UNC-119 protein would be expressed in *unc-119(ed3)*, *unc-119(ed4)* or *unc-119(e2498::Tc1)*. Introduction into *unc-119* mutants of the *unc-119* sequence represented in pDP#M0016 and thus in most bombardment vectors can mostly rescue the locomotion defects. However, transgenic worm lines often are not fully wildtype in several respects. Our analysis suggests that a full-length wildtype UNC-119 might be missing in the transgenic lines. How relevant this product actually is in different settings remains to be determined.

We have generated transgenic lines with a vector pZS004 that contains the new genomic *unc-119* ORF including an 820 bp upstream sequence (*unc-119*** in Figure 115). To our discontent, the new transgene did not restore wildtype apoptosis levels in *unc-119* mutants either.

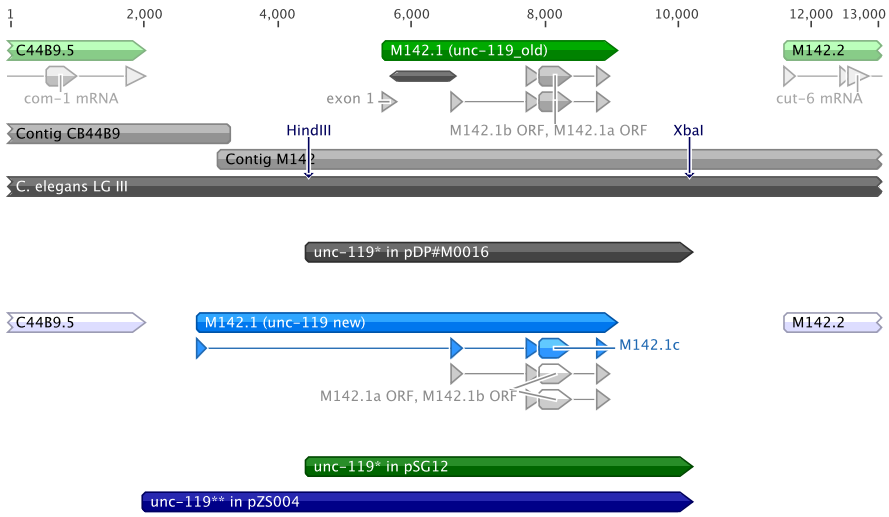

Figure 115 The original *unc-119* gene annotation (green) has been extended by one exon (blue), which offers an alternative translation start site. Two overlapping contigs cover the chromosomal region of *unc-119* on chromosome 3 (LG III). The restriction sites HindIII and XbaI had been used to clone the presumptive *unc-119* into pDP#M0016 and for downstream applications. The originally annotated exon 1 did not contain a start codon; the first intron (dark bar) was shown to be relevant for efficient gene expression. Recent transcript evidence revealed another short exon 3.75 kb upstream of M142.1a, including a translation initiation site. The sequence so far considered as *unc-119* promoter therefore constitutes part of the novel first intron. Obviously, this sequence does have promoting activity, leading to significant expression in various cells, particularly neurons. *unc-119(+)*** in pZS004 includes 820 bp upstream of the first exon.

6.2.1.8 Expression patterns of *unc-119* in transgenic lines are not reliably predictable

We tested different transgenic lines for IR-induced apoptosis. In many cases, transgenes with their *unc-119(tg+)* were not proficient to completely rescue the apoptotic phenotype of *unc-119* mutants, and in some instances, they could even induce an apoptotic phenotype by themselves. For some of the

transgenes, when the *unc-119(ed3)* in the background was replaced with *unc-119(+)*, apoptosis was still affected, indicating a possible dominant effect of transgenic *unc-119(tg+)* (Table 23). Generally, the expression pattern of transgenes can differ significantly from one line to another. This has long been known for, and can be particularly pronounced with, extrachromosomal arrays, where the expression from the multicopy plasmid varies not only between different transgenic lines, but can scatter widely between individual animals of the same line due to somatic mosaïcism. (The non-mendelian segregation of arrays has been enhanced and exploited to study tissue- or lineage-specific requirements of gene expression, e.g., for factors of the MAPK pathway (Lackner 1994). Different systems were presented to visualise the mosaic pattern of transgenic arrays by GFP (Gonzalez-Serricchio 2006; Yochem 1998). Mosaic patterns were also described for a transcriptional *unc-119* reporter (Maduro 1995).) Integrated transgenes of the same construct do not necessarily replicate the expression pattern of each other, either, as can often be observed with fluorescently tagged reporters. This might have to do with copy number or the genomic environment in which the transgene has integrated. Germ line silencing, even though somewhat less pronounced for integrated transgenes than for extrachromosomal arrays, is a recurrent phenomenon [discussed in (Merritt 2010)]. Transgenic *unc-119(tg+)* cannot be expected to behave differently in this regard. In many constructs, the $P_{unc-119}$short promoter and the promoter for the transgene of interest are cloned back to back and possibly interfere with each other. Altogether, it is therefore uncertain where the transgenic *unc-119(tg+)* is actually expressed in each line, the more as this gene product is hardly ever tagged itself. Initial characterisation with a lacZ expression vector and X-gal staining (Maduro 1995) and subsequent studies with fluorescent reporters from extrachromosomal arrays (Knobel 2001) suggested pan-neuronal expression of *unc-119*. It is based on this notion that the *unc-119* promoter has often been used to drive neuron-specific expression. A later study (Materi 2005) revealed the importance of the first intron in *unc-119(tg+)* for better rescue activity; cDNA instead of the genomic DNA led to a more restricted expression pattern and could not restore normal movement so efficiently. It further demonstrated that expression of *unc-119(tg+)* with a muscle-specific promoter could largely rescue the Unc phenotype as well as the Dauer defect; this was again dependent on the presence of the intron. Overall, these observations indicate that expression in different tissues might be necessary for different functions of *unc-119*, and that the first intron could be relevant for proper regulation of the expression pattern. It is difficult to judge whether the full-length intron according to the recent gene model instead of the short one from the original model (Figure 115) would have given the same results. We have not yet identified the tissue in which *unc-119* expression is required for regulation of germ cell apoptosis. Likely, expression of the three possible isoforms in different tissues is not identical between transgenic lines, be it in an *unc-119(ed3)*, an *unc-119* heterozygous, and even in an *unc-119(+)* background, and deviation from the wildtype pattern could lead to alterations in apoptosis regulation. Consistent with a delicate spatiotemporal regulation of UNC119 expression, markedly different retinal degeneration phenotypes were induced in mice expressing a dominant negative Mrg4 (mUnc119) transgene than in a knock-out model (Ishiba 2007).

		no IR		60 Gy	
		score	95% CI (n)	score	95% CI (n)
wildtype		3.03	±0.15 (745)	8.14	±0.21 (915)
unc-119(ed3)		0.96	±0.29 (47)	1.59	±0.31 (91)
unc-119(e2438)		0.93	±0.18 (112)	1.47	±0.24 (108)
opIs462;ed3	[$P_{unc-119}$short::unc-119(+)*]	1.68	±0.42 (40)	2.73	±0.52 (40)
opIs462		2.70	±0.89 (20)	4.80	±1.44 (20)
opEx1475;ed3	[$P_{unc-119}$short::unc-119(+)*]	2.43	±0.70 (37)	2.20	±0.66 (35)
opIs447;ed3	[$P_{unc-119}$long::unc-119(+)**]	2.75	±0.64 (36)	5.80	±0.94 (44)
opIs204;ed3	[P_{eft-3}::ph(ced-12)::yfp;unc-119(+)]	1.45	±0.53 (60)	2.80	±0.60 (60)
opIs204;e2498		1.44	±0.46 (48)	3.44	±0.60 (48)
opIs204		2.43	±0.38 (60)	6.41	±0.69 (69)
opIs110;ed3	[P_{lim-7}::act-5::yfp;unc-119(+)]	2.56	±0.30 (132)	6.86	±0.47 (132)
opIs110		1.78	±0.36 (36)	6.88	±1.22 (16)
opIs423;ed3	[P_{brd-1}::yfp::brd-1;unc-119(+)]	3.30	±0.91 (20)	4.75	±1.50 (20)
opIs423		2.85	±1.18 (20)	6.35	±1.24 (20)
opIs257;ed3	[P_{rad-54}::yfp::rad-54;unc-119(+)]			4.80	±1.20 (20)
opIs257				7.80	±1.07 (20)
opIs198;ed3	[P_{cep-1}::cep-1::gfp;unc-119(+)]			2.31	±0.70 (32)
opIs29;ed3	[P_{hus-1}::gfp::h2b;unc-119(+)]			8.29	±2.41 (14)
ruIs32;ed3	[P_{pie-1}::gfp;unc-119(+)]			8.30	±2.26 (20)
ygIs;unc-119(ed4)	[P_{baf-1}::gfp::baf-1;unc-119(+)]	0.85	±0.38 (20)	2.30	±0.65 (20)

Table 23 Irradiation-induced apoptosis is variable between different transgenic lines. *opIs462* and *opEx1475*, both *[$P_{unc-119}$short::unc-119(+)]* (* in Figure 115) are from pSG12, *opIs447[$P_{unc-119}$long::unc-119(+)]* (** in Figure 115) is from pSZ004; these transgenes only code for *unc-119(+)*. All other transgenes have *$P_{unc-119}$short::unc-119(+)* back-to-back with the gene of interest. Average number of corpses per gonad, 95 % CI of the mean, and number of worms scored per condition.

6.2.1.9 *unc-119* can confound experiments of germ cell death at the level of the core apoptotic machinery

Collectively, it is mandatory to know the allelic composition of the *unc-119* locus in any worm strain derived from a transgenic line. It seems recommendable to replace *unc-119(ed3)*, that has been commonly used for selection of transgenic lines, with the wildtype *unc-119(+)* allele. Interpretations and conclusions derived from results with transgenic worm strains that carry a mutant *unc-119* allele should be considered critically. Particular care should be taken if a transgene of interest seems not to rescue or to suppress apoptosis, an observation that could be confounded by the effects of non-wildtype *unc-119*. For instance, we assessed germ cell death in a CED-4::GFP *opIs219[P_{ced-4}::ced-4::gfp; unc-119(+)]* reporter line (Zermati 2007), either in an *unc-119(ed3)* mutant or *unc-119(+)* background. Indeed, whereas the strain *opIs219* showed wildtype apoptotic response to IR, the strain *opIs219; unc-119(ed3)* had low levels of apoptotic corpses; by itself, this strain could lead to the interpretation that overexpressing CED-4 suppresses germ cell death (Figure 116). When performing a genetic cross to shuttle the transgene from *opIs219; unc-119(ed3)* into a mutant of interest (in an *unc-119* wildtype background), the status of the *unc-119* locus might change in the F2 progeny to *unc-119(ed3/+)* or *unc-119(+/+)*, and apoptosis might increase accordingly, mimicking a significant effect of the gene of interest on apoptosis. If not carefully followed, loss of *unc-119(ed3)* would go unnoticed, since it has anyway not caused an Unc phenotype in the presence of the transgene.

In this experiment, we also tested whether transgenic CED-4 would improve the apoptotic defect of *rpo-1b(op259)*. Here, *unc-119(ed3)* in the background prohibited detection of the pro-apoptotic effect that CED-4 could actually exert in *rpo-1b(op259)*. (Eventually, even in the *unc-119(+)* background we

cannot be certain how much the deviation of baseline apoptosis levels from wildtype is a result of CED-4 overexpression and how much could be due to transgenic *unc-119(tg+)* in *opIs219*.)

Importantly, CED-4::GFP expression pattern and signal intensity did not grossly differ between the *unc-119(ed3)* and the *unc-119(+)* backgrounds (Figure 85).

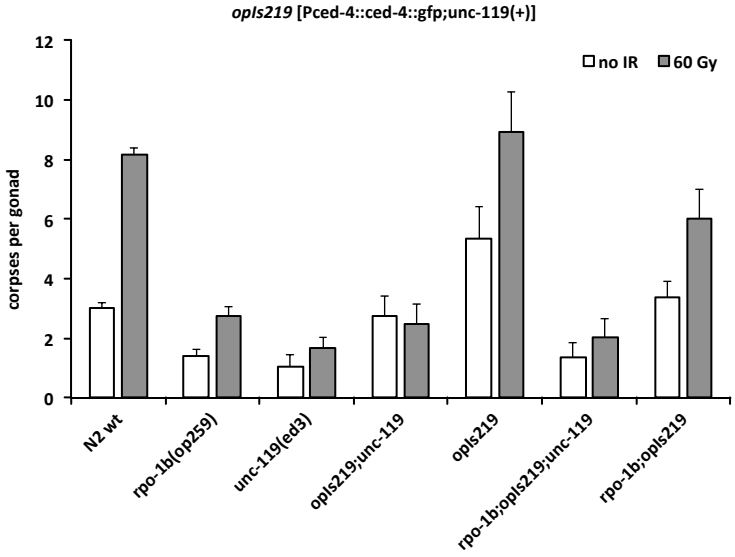

Figure 116 *unc-119(ed3)* confounds the interpretation of transgenic experiments. *unc-119(ed3)* prevents IR-induced apoptosis in the *opIs219* transgenic line that, disregarding *unc-119,* would indicate that transgenic CED-4 inhibits death. In *rpo-1b(op259)*, *unc-119(ed3)* hides a pro-apoptotic effect of *opIs219*. Apoptotic corpses at 24 hours post irradiation; error bars indicate 95 % CI of the mean.

6.2.1.10 Antibiotic resistance is an emerging alternative for transgene selection

Transgene selection in *C. elegans* has largely relied on markers that were derived from endogenous genes. Recently, strategies that allow to circumvent the use of 'mutant genetic background'/'rescue construct' combinations have been developed. Two groups have presented selection systems that are based on antibiotic resistance conferred to the worms with the transgene of interest. In one case, the bacterial gene NeoR (neomycin resistance, conferred by aminoglycoside phosphotransferase activity) is included in the transformation vector under the control of a ubiquitous promoter, which renders transgenic worms resistant to the translation inhibitor G-418 (Giordano-Santini 2011). The second system uses the toxic effect of another translational inhibitor, puromycin, in combination with the detergent Triton X-100 to kill non-transformed animals, and to enrich for transgenic animals carrying a puromycin resistance gene (Semple 2010). These methods have several advantages over current techniques. They do not rely on a mutant background; transgenes can directly be introduced into wildtype or mutant strains of interest without previously crossing those into the mutant background for selection (often, *unc-119(lf)*); transgene maintenance of non-integrated arrays is facilitated by continuous toxic selection against non-transgenic animals (formerly, manual selection by phenotype); for integrated transgenes, which should also be achievable, e.g., by the MosSCI technique (Giordano-Santini 2011), the antibiotics can be tapered. The worms will carry the transgene (including the resistance cassette), but not the combination of a background mutation with an exogenous rescue construct of a selection gene. In this case, exposure to the selective agents is transient and can be stopped before experiments, and is

therefore less likely to interfere with any phenotypes of interest. What remains is the resistance gene, a kinase in the case of NeoR. The methods will have to be cautiously evaluated for non-genetic long-term effects (that is, vertical transmission) of drug exposure, such as epigenetic modifications. It should be considered that both drugs are inhibitors of eukaryotic translation and thus potentially hazardous.

6.2.2 The function of *unc-119(ed3)* in apoptosis

6.2.2.1 Mammalian UNC119 regulates SRC-type kinases and influences internalisation

The high degree of sequence conservation between mammalian UNC119 and *C. elegans unc-119* is likely reflected in the structure and function of the protein.

The human homolog of UNC-119 is HRG4 or UNC119. It was identified in a screen for genes with high expression in the retina (Swanson 1998) and shown to localise to synapses (Higashide 1998; Alpadi 2008). A mutation leading to truncated HRG4 protein was found in a patient with cone-rod dystrophy, and expression of a homologous mutant protein in mice could reproduce late-onset retinal degeneration (Kobayashi 2000). Mori et al. suggested a mechanism involving mitochondrial ANT1-mediated apoptosis of photoreceptors (Mori 2006). In the context of the immune system, UNC119 was identified as a receptor-associated activator of SRC-type tyrosine kinases (Cen 2003). Stimulation of the IL-5Rα receptor increased association of hUNC119 with Lyn in eosinophils, which induced the catalytic activity of this Src family kinase. Overexpression of hUNC119 prolonged, and inhibition shortened, survival of eosinophils in culture. hUNC119 is also required for activation of T-cells (Gorska 2004), where it binds and activates Lck/Fyn. Lymphocyte-specific protein tyrosine kinase (Lck) by its enzymatic activity is required for initiating signalling from the TCR and subsequent cytokine production and T-cell clonal expansion. In a recent study, mUnc119 was shown to modulate the Th1 to Th2 balance of T-cells, involving Src type kinases, the tyrosine kinase Abl, and downstream, the MAP kinases ERK and JNK; in a mouse model, knockdown of mUnc119 inhibited pathogenetic features of hyperreactive airways; additionally, the expression of UNC119 protein was shown to be enhanced in CD4 T-cells from patients with asthma (Gorska 2010).

Unc119 was found to have significant binding affinity to Abl in an *in vitro* screen testing for interactions of Unc119 with SH3 domains of different cellular proteins (Vepachedu 2009). Unc119 could modulate the kinase activity of the tyrosine kinase Abl on Crk. The study suggested a direct inhibitory effect of Unc119 on Abl, involving the SH3-domain binding motif in Unc119. In a 3T3 cell culture system, this interaction was relevant for Shigella infection: knockdown of Unc119 increased, and overexpression reduced infectivity – effects that were dependent on Abl/Arg and that were mediated by Crk phosphorylation. In agreement with the positive regulatory effect of Abl on cytoskeletal rearrangement, overexpression of Unc119 inhibited actin polymerisation in this system. Following this study, the same group demonstrated an inhibitory effect of UNC119 on dynamin-dependent endocytic processes (Karim 2010). Yet a further study specified the role for Unc119 in immunological synapse formation in T-cells: Unc119 regulates the shuttling of the TCR associated tyrosine kinase Lck to the plasma membrane via activation of Rab11, recruitment of the actin-based motor protein myosin 5B, and organisation of multiprotein complexes on endosomes (Gorska 2009).

In agreement with a regulatory role in protein localisation, UNC119 was recently shown to stabilise the GTP-bound form of Gα of human transducin, and thereby to modulate its trafficking in photoreceptor cells. Similarly, *unc-119* was required for proper localisation of G-proteins in sensory neurons of *C. elegans* (Zhang 2011). Another study suggested the same function for UNC119 with an alternative mechanism how it regulates the GTPase transducin (Gopalakrishna 2011). Collectively, these studies demonstrated various regulatory effects of UNC119 on receptor activity and on cellular transport mechanisms. Quantitative changes in UNC119 had implications for cell death or for cellular uptake processes. We had detected a novel role for *C. elegans unc-119* in regulating the level of germ cell apoptosis. We aimed to learn whether this was an effect of altered cell death induction, or of changes in the ingestion of apoptotic cell corpses, or both.

6.2.2.2 IR-induced germ cell death is reduced by *unc-119(ed3)* also in engulfment mutant background

We have investigated possible mechanism for the reduced number of apoptotic germ cells in *unc-119* mutants. Grossly, either less cells die and/or the kinetics of cell death and removal are accelerated. [For an introduction to engulfment in *C. elegans*, see *2.1.8 Engulfment of apoptotic cells.*]

A reduced number of dying cells could result from impaired initiation or execution of the apoptotic program, so more cells survive and less cells can be found dead. Alternatively, at a constant relative death rate, a significant reduction in the total number of differentiating germ cells would also reduce the number of dying cells. We measured the egg-laying rate as a surrogate for oocyte production rate. Despite the seemingly unfavourable body morphology, *unc-119(ed3)* mutants laid 3.84 (SD ±0.41) eggs per animal per hour, in comparison to 5.20 (±0.38) in wildtype, which would not explain the gap in the number of apoptotic cells between the two.

In wildtype animals, dying cells are efficiently removed by neighbouring cells in the process of engulfment. Apoptotic germ cells are taken up by the gonad sheath and degraded in specialised cellular compartments, the phagosomes. Defects or delays in the engulfment or degradation processes lead to increased numbers of apoptotic corpses in the germ line. If these defects are strong enough and virtually prevent corpse removal completely, dead cells start accumulating at a rate that reflects the absolute death rate. To assess this rate for *unc-119(ed3)*, we tested it on the *ced-6(n1813)* engulfment mutant background. Slightly less corpses accumulated in non-irradiated *ced-6(n1813) unc-119(ed3)* than in *ced-6(n1813)* animals (Figure 117); upon IR treatment, the gap became much more pronounced: For *ced-6(n1813) unc-119(ed3)*, irradiated worms had only slightly higher numbers than non-irradiated controls, at a time point when the number in *ced-6(n1813)* was rocketing to non-countable levels above 100 corpses per gonad. These findings indicate a relatively well conserved rate of constitutive germ cell death in *unc-119(ed3)* but only a weak apoptotic response to IR irradiation.

We are testing other engulfment mutants for germ cell apoptosis with or without irradiation. In a preliminary experiment with the *ced-2(n1994)* background, we could no longer detect a suppressive effect on the corpse number by *unc-119(ed3)*; rather, the levels were slightly higher in the *unc-119* mutant (Figure 117). It is to note that the increase in the germ cell corpse number by *ced-2(n1994)* was only very moderate, speaking either for a weak engulfment defect in the gonad, or an additional role for

ced-2 in germ cell death itself. Whether *ced-2*, the *C. elegans* Crk homolog, is critical for the effect of *unc-119* remains to be further evaluated.

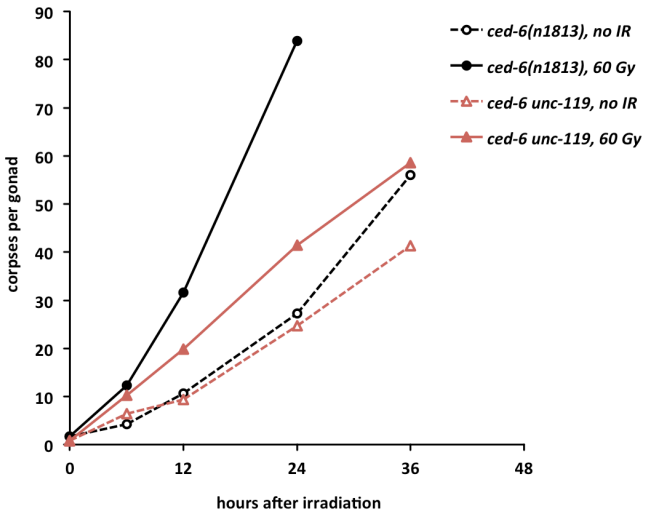

		ced-6(n1813)		ced-6 unc-119(ed3)	
		score	95% CI (n)	score	95% CI (n)
no IR	0 h	1.67	±0.37 (60)	0.76	±0.33 (21)
	6 h	4.29	±0.82 (86)	6.45	±1.23 (20)
	12 h	10.62	±0.98 (112)	9.32	±1.51 (94)
	24 h	27.27	±2.19 (92)	24.68	±2.59 (57)
	36 h	56.00	±3.55 (20)	41.29	±2.96 (63)
60 Gy	0 h				
	6 h	12.32	±1.40 (56)	10.27	±1.64 (12)
	12 h	31.61	±1.63 (76)	19.89	±2.10 (71)
	24 h	83.92	±6.59 (20)	41.39	±2.72 (81)
	36 h			58.62	±4.49 (47)

		ced-2(n1994)		unc-119;ced-2(n1994)	
		score	95% CI (n)	score	95% CI (n)
no IR	0 h	0.44	±0.24 (18)		
	12 h	3.35	±0.82 (20)	5.10	±1.52 (20)
	24 h	3.85	±1.17 (20)	7.25	±1.48 (20)
60 Gy	0 h				
	12 h	6.95	±1.22 (20)	6.40	±1.07 (20)
	24 h	10.15	±1.16 (20)	9.95	±1.70 (20)

Figure 117 Corpse accumulation upon irradiation in engulfment mutant background is reduced by *unc-119(ed3)*. Time course of apoptotic germ cells; irradiation was at a reference time point that was adjusted to the developmental delay in *unc-119;ced-6* mutants (24 hours versus 12 hours post L4 in *ced-6*). Tables indicate average number of corpses per gonad, 95 % CI of the mean, and total number of animals scored per condition.

6.2.2.3 Number of apoptotic corpses in L1 heads is reduced by *unc-119(ed3)*

The reduced corpse number observed in germ lines could represent a general defect in the apoptotic program and might apply to other programmed cell death events in *C. elegans* as well. We examined *unc-119* mutants for differences in corpse accumulation in the context of developmental apoptosis. In engulfment mutant backgrounds, apoptotic cells of the later embryonic development persist into larval stages and can be counted collectively in the heads of freshly hatched L1 larvae. We first tested *unc-119(ed3)* in the *ced-6(n1813)* background. *ced-6(n1813) unc-119(ed3)* had slightly but consistently lower numbers of L1 head corpses than *ced-6(n1813)* (Figure 118). To investigate whether suppression of the high corpse number in *ced-6(n1813)* by *unc-119(ed3)* was rather an effect of reduced cell death or the result of partially restored cell removal, we examined further engulfment mutants. In *C. elegans*, engulfment is carried by two main pathways converging on the small GTPase CED-10; they have partly complementary, partly redundant activity (Kinchen 2005). Phenotypes from the reduction of function of one pathway are enhanced by defects in the other; conversely, relieving negative regulation from one pathway can partly compensate for defects in the other [reviewed in (Reddien 2004)]. If *unc-119* were genetically acting on one of the two pathways – possibly as a negative regulator – loss of *unc-119* function would only improve engulfment defects of the parallel branch. We tested *unc-119(ed3)* on the mutant backgrounds *ced-1(e1735)*, *ced-7(n1892)*; on *ced-2(1752)*, *ced-2(n1994)*, *ced-5(n1812)*, *ced-12(oz167)*, and on *ced-10(n1993)*. *unc-119(ed3)* reduced the number of L1 head corpses in all of these mutants. Thus, *unc-119(ed3)* either has reduced cell death and/or it enhances engulfment by a pathway that is genetically parallel to, or downstream of, CED-1/CED-6/CED-7 and CED-2/CED-5/CED-12 signalling.

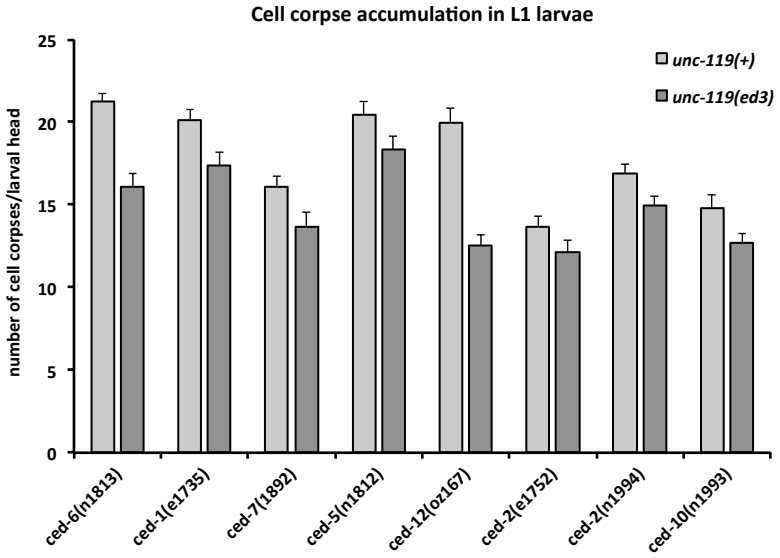

Figure 118 *unc-119(ed3)* reduces the number of cell corpses accumulating in the heads of freshly hatched L1 larvae of engulfment mutants. Mutants of both signalling branches *ced-1*/*ced-6*/*ced-7* and *ced-2*/*ced-5*/*ced-12* were scored in an *unc-119(ed3)* or *unc-119(+)* background within one hour from hatching. Error bars indicate 95 % CI of the mean.

6.2.2.4 Non-survival of Pn.aap cells suggest that loss of *unc-119* enhances engulfment

To better distinguish between the two possibilities, we used another well-established model for developmental cell death. In wildtype worms, only six distinct out of the 13 ventral cord Pn.aap neurons generated during development survive, the other seven are removed by programmed death. All surviving cells can be highlighted by the *nIs96[P_{lin-11}::gfp; lin-15(+)]* GFP reporter expressed under the P_{lin-11} promoter starting at the L3/L4 stage (one cell has only a weak signal and is not usually considered in this assay). In reduction-of-function mutants of *ced-3*, some of the cells normally destined to die will survive; additional loss of pro-apoptotic cues further increases the number of extra cells, whereas loss of anti-apoptotic activity reduces the number in this sensitised background. Interestingly, increased engulfment activity can promote execution of cell death and thus the reduction of aberrant cells in this setting (Reddien 2001). We tested *unc-119* loss-of-function in this system; here, it did not prevent cell death but rather reduced the number of extra surviving cells in the *ced-3(n2438)* background (Figure 119). To exclude that the reduced number of extra cells was a result of developmental defects in the generation of these neurons, we tested the extra cell number in the strong *ced-3(n717)* loss-of-function background. *unc-119(e2498::Tc1); ced-3(n717); nIs96* animals had 12 glowing neurons, confirming that loss of *unc-119* function reduces the survival of these cells and not their formation.

To confirm that *unc-119* mutants do not have a strong defect in the dying mechanisms during development, Sheng Zeng and Michael Hengartner looked for extra surviving nuclei in the pharynx of L3 stage larvae. No cells in addition to the cells normally surviving in wildtype were found in this system, supporting accelerated removal rather than reduced death.

Based on the combined results from L1 heads, L3 pharynxes, and Pn.aap cells we conclude that *unc-119* mutants have enhanced engulfment. The observations suggest that UNC-119 acts as a negative regulator of cell corpse removal in a molecular mechanism that is distinct from the two main engulfment pathways *ced-1*/*ced-6*/*ced-7* and *ced-2*/*ced-5*/*ced-12*. The reduction of apoptotic cells in L1 heads of

engulfment mutants and the reduction of extra surviving Pn.aap cells in *unc-119* mutants is likely the result of promoted cellular uptake.

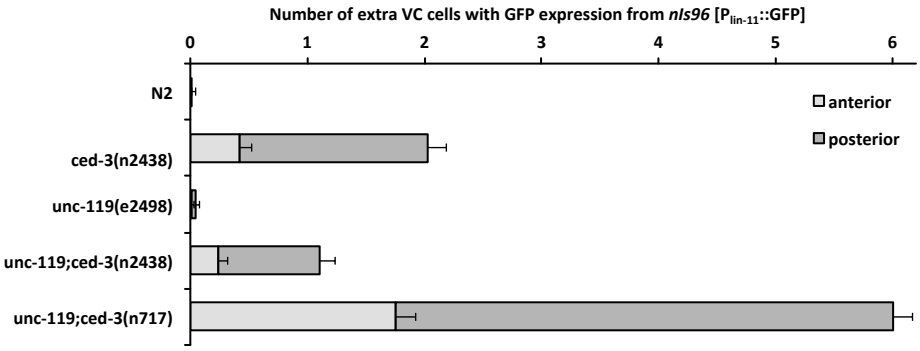

Figure 119 *unc-119(lf)* reduces the number of extra cells in the ventral nerve cord. Extra cells anterior (max. 2) and posterior (max. 4) to the vulva were assessed separately at L4 stage. *ced-3(n2438)* is a weak reduction-of-function allele, whereas *ced-3(n717)* is a strong loss-of-function allele. Error bars indicate 95 % CI of the mean for each group.

6.2.2.5 *unc-119(ed3)* and *abl-1(ok171)* have no synergistic effect on engulfment in L1 heads

Similarly to our observations with *unc-119*, *abl-1(lf)* mutants were shown to have enhanced removal of apoptotic cells in embryonic development, likely due to disinhibition of *abi-1*, a positive regulator of engulfment (Hurwitz 2009). ABL-1 was proposed to counteract engulfment of apoptotic cells via a pathway that is different from the two known engulfment pathways, and thus independently of the Crk homolog CED-2. Such an additional pathway could explain the opposing evidences for mammalian Abl as a positive regulator of cytoskeletal rearrangement and cellular uptake – involving CrkII – on the one hand (Vepachedu 2009), and the inhibitory role of *C. elegans abl-1* in engulfment on the other hand.

unc-119(ed3) reduces the number of apoptotic corpses in the L1 heads of mutants of both engulfment pathways, suggesting a function genetically downstream of the two or in yet another branch of the engulfment mechanism, similar to *abl-1*. We tested whether *unc-119(ed3)* and the *abl-1(ok171)* loss-of-function mutation had synthetic effects on engulfment in *ced-6* mutants. The number of apoptotic cells was equally high in L1 heads of *unc-119 ced-6; abl-1(ok171)* as in *unc-119(ed3) ced-6(n1813)*, suggesting no additive effect of *unc-119(ed3)* and *abl-1(ok171)* on this phenotype. Therefore, *unc-119* might be acting in a pathway with *abl-1* to regulate engulfment at this stage of development.

6.2.2.6 *unc-119* has distinct functions in germ cell death and removal

Regarding the germ line, enhanced engulfment in *unc-119* mutants could also be the reason for the low corpse number at a steady state of death and removal. It would also explain the slight reduction of total corpses accumulating in the *ced-6(n1813)* mutant background, given that severe engulfment defects can be alleviated by disinhibition of parallel pathways, as is the case in L1 heads.

While this model of enhanced engulfment is in good agreement with the observations for developmental cell death and physiological germ cell apoptosis, it falls short of explaining the weak response of *unc-119(ed3)* and *unc-119(ed3) ced-6(n1813)* mutants to irradiation. Death programs of somatic cells and of germ cells share the core components of apoptosis execution but have different routes to

apoptosis induction; DNA damage-induced apoptosis happens specifically in meiotic germ cells. Most somatic cells have been described to be insensitive to DNA damage-induced death (Weidhaas 2006a).

Also, the settings for corpse removal vary considerably: whereas during embryogenesis usually one dying cell is incorporated by one neighbouring cell, in the gonad only very few large sheath cells act as specialised phagocytes and take up a wealth of germ cell corpses.

Thus, genetic models in one system cannot be readily generalised and transferred to the other. For instance, ABL-1 reportedly has an inhibitory function on engulfment (Hurwitz 2009); loss-of-function mutations lead to accelerated uptake of corpses in the L1 heads of engulfment mutants. However, *abl-1(lf)* mutants do not show reduced numbers of germ cell corpses as would be expected. Rather, ABL-1 is also required to maintain levels of pro-apoptotic factors in germ cells low; consequently, the mutant has excessive apoptosis in the germ line, which dominates and conceals possible reductions caused in parallel by enhanced engulfment.

As the IR response defect of *unc-119* mutants suggests, UNC-119 has different or additional functions in germ cell death. Possibly, UNC-119 is involved in apoptosis induction in response to DNA damage. It is difficult to imagine that the much weaker increase of apoptotic corpses in irradiated *unc-119(ed3) ced-6(n1813)* than in irradiated *ced-6(n1813)* arises solely from changes in engulfment kinetics. When comparing *unc-119(ed3) ced-6(n1813)* to *ced-6(n1813)*, the reduction is strongly overproportionate for IR-induced corpses. If induction of IR-induced apoptosis were not affected itself, this would imply that engulfment is enhanced much more efficiently by *unc-119(ed3)* when more corpses occur. However, one would then wonder why there should be a minimal threshold for such a boost to kick in that is as high as the number of corpses accumulating already in non-irradiated *ced-6(n1813)* gonads. Consequently, we see mainly two attractive explanations. First, loss of *unc-119* function reduces DNA damage-induced cell death. Second, irradiation does not only activate pro-apoptotic cascades in germ cells, but it also stimulates cell removal; this effect is enhanced by *unc-119(lf)*; and the underlying molecular mechanism is still effective in the engulfment mutant background *ced-6(n1813)*.

6.2.2.7 Actin cytoskeleton in engulfing sheath cells is influenced by *unc-119*

Restructuring of the actin cytoskeleton is a key mechanical process for the formation of the phagocytic cup and for ingestion of large particles into a phagocytic cell. The CED-2/CED-5/CED-12 branch of the engulfment-signalling cascade acts towards activation of the small GTPase CED-10, and CED-10 in turn towards actin dynamics. The tyrosine kinase Abl with important regulatory activity on the cytoskeleton plays a role in cellular uptake, and in *C. elegans* specifically in engulfment. We wanted to study the influence of *unc-119* on the actin cytoskeleton in engulfing cells and used the *opIs110[P_{lim-7}::act-5::yfp; unc-119(+)]* reporter transgene to express Actin::YFP under the sheath cell specific promoter P_{lim-7}. With fluorescent microscopy, the thin planar cytoplasm of gonadal sheath cells is visible only where looked on orthotopically, that is, as a thin line at the borders of the gonads in longitudinal focal planes. Also, tagged Actin usually becomes visible in tangential planes as a fine grid corresponding to the marginal invaginations of the wrapping sheath cells between adjacent germ cells. Most prominently, Actin::YFP highlights apoptotic corpses in the process of being engulfed, with an intense halo representing the surrounding of the corpses by sheath cell protrusions. The halos are

supposed to wrap apoptotic cells early during the engulfment process, before fusion of the phagosome into phagolysosomes (Kinchen 2005).

Before, we have shown that transgenic *unc-119(tg+)*, even though potent to rescue some of the defects of *unc-119* mutations, does not necessarily restore *unc-119* wildtype function, and that a mutant *unc-119* in the background of a transgenic strain can matter as to the phenotype. We wondered whether background *unc-119(ed3)* would influence the corpse number and the relative number of Actin-halos in the *opIs110* strain. Unlike in many other comparisons of *transgene; unc-119(ed3)* versus *transgene; unc-119(+)*, *opIs110; unc-119(ed3)* did not have less apoptotic corpses by DIC than *opIs110*. Baseline levels were even a bit higher and the response to irradiation was similarly strong (Figure 120). This indicated once more that *unc-119(ed3)*/*unc-119(tg+)* transgene combinations were not always equally effective on germ cell death (yet, one cannot exclude that expression of transgenic actin drives the appearance of corpses epistatically to *unc-119*). We next counted the average number of Actin halos: here, *opIs110; unc-119(ed3)* had clearly higher numbers than *opIs110*. The ratio of Actin halos to DIC corpses was thus shifted to much higher values when *unc-119(ed3)* was in the background. There are two interpretations. First, altered *unc-119* influences actin halo formation around apoptotic corpses. Second, the use of transgenes that are based on the *unc-119* selection system for studying apoptosis and engulfment of germ cells has to be rethought. It is at the moment very difficult to sort out how the different components interact to give the readout of the system: non-rescued *unc-119(ed3)* functions, effects of overexpressed or incomplete transgenic *unc-119*, or possible effects of the reporter gene itself. Eventually, effects observed in mutant lines of interest on the number of reporter halos can not be clearly attributed to the mutant gene of interest.

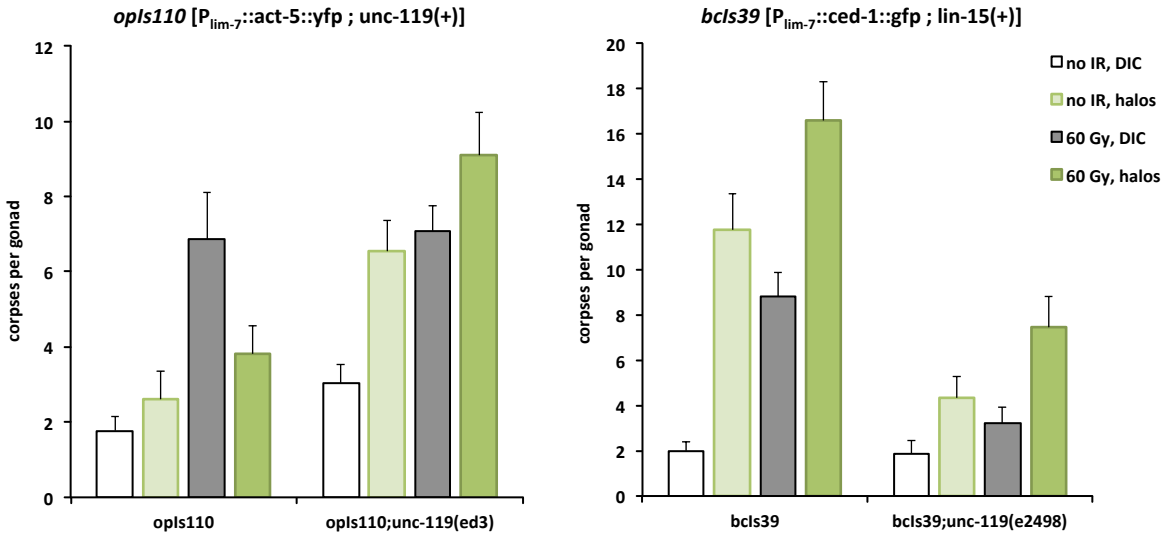

Figure 120 *unc-119* interferes with the number of halos around apoptotic corpses, downstream of CED-1 localisation to the engulfing sheath. The numbers of corpses assessed at 24 hours post irradiation by DIC and by CED-1::GFP halos are both reduced in the *unc-119(lf)* mutant. For Actin::YFP (which is encoded in a transgene with *unc-119(+)*) ratios vary considerably between *unc-119(ed3)* and *unc-119(wt)* background. Error bars indicate 95 % CI of the mean.

6.2.2.8 CED-1::GFP halos around apoptotic cells are not more frequent in *unc-119(ed3)*

We visualised the engulfment of apoptotic cells with another fluorescent reporter: transgenic CED-1::GFP, also expressed under the sheath cell specific *lim-7* promoter. Other than *opIs110[P_{lim-7}::act-5::yfp; unc-119(+)]*, the CED-1::GFP encoding transgene *bcIs39* (Schumacher 2005b) is not based on *unc-119* selection. It was created by integration of the construct *[P_{lim-7}::ced-1::gfp; lin-15(+)]*, and it could therefore be tested in an actual *unc-119* loss-of-function condition. CED-1::GFP clusters at membranes that contact apoptotic cells early during corpse recognition. By DIC, *bcIs39; unc-119(ed3)* had similarly low levels of corpses as *unc-119(ed3)* and little response to irradiation; the *bcIs39* strain was similar to N2 (Figure 120). The number of halos was also reduced in *bcIs39; unc-119(ed3)*, such that the ratio of halos to DIC corpses was similar to the one in *bcIs39*. Assuming that transgenic CED-1 or LIN-15 can be neglected for the phenotype (which, considering the effect we saw loss of *lin-15* function had on germ cell apoptosis (Figure 96), is daring), one can judge that a potential change in engulfment kinetics likely happens downstream of corpse recognition by the CED-1/CED-6/CED-7 pathway.

Acridine Orange (AO) live staining, which highlights phagocytosed corpses, should allow to further assess engulfment and degradation efficiency downstream of corpse recognition (Figure 111). We are applying AO staining to *unc-119(lf)* and to double mutants of *unc-119(lf)* with engulfment mutants. First results show an increase in the fraction of AO positive corpses.

6.2.2.9 CEP-1 is activated in *unc-119* mutants after irradiation

DNA damage-induced apoptosis of germ cells genetically depends on *cep-1*, the *C. elegans* homolog of p53. CEP-1 is activated during DNA damage response and increases transcription of the BH3-only factors EGL-1 and CED-13, which in turn activate the core apoptotic machinery. One possible explanation for the weak apoptotic response to irradiation in *unc-119* mutants could be insufficient activation of this transcriptional response, as is typical for DNA repair signalling mutants. Quantitative RT-PCR analysis of EGL-1 and CED-13 transcripts in whole animals however revealed normal increase upon IR, indicating that CEP-1 is activated sufficiently to enhance transcription. *unc-119* thus likely acts downstream of CEP-1 activation in DNA damage response.

6.2.2.10 Loss of *unc-119* can suppress IR hypersensitivity of *abl-1(lf)* mutants

abl-1(lf) mutants have an increased baseline level of germ cell apoptosis and are hypersensitive to DNA damage (Deng 2004). This increase in cell death is dependent on *cep-1*. We addressed epistasis of *unc-119* and *abl-1* in germ cell apoptosis. Consistent with the notion that *unc-119* likely acts downstream of *cep-1*, increased constitutive germ cell death in *abl-1(ok171)* was suppressed by *unc-119(ed3)*. Also, *unc-119(ed3); abl-1(ok171)* double mutants had very weak IR response. Thus, *unc-119* is epistatic to *abl-1* in germ cell apoptosis and in IR sensitivity.

6.2.2.11 *unc-119(ed3)* suppresses excessive apoptosis and sterility in *ced-9(n1653)* mutants

Mutations in the core cell death inhibitor CED-9 can lead to excessive germ cell apoptosis in the absence of exogenous apoptosis induction, supposedly due to aberrant release of the caspase activator CED-4 from inhibition by CED-9. Classically, *ced-9* mutations, e.g., *ced-9(n1653)* have been used to

resolve whether the core apoptotic machinery is basically intact in mutants with reduced apoptotic response [see *5.6.1 CED-9 – the core inhibitor of apoptosis*].

We had found that excessive death evoked by *ced-9(n1653)* could also be reduced by loss of the function of genes that likely act upstream of the core apoptotic factors *ced-4* and *ced-3* [*5.6.3.4 Loss of cep-1 or egl-1 function suppresses excessive death and sterility of rpo-1b(op259); ced-9(n1653)*]; therefore, a reduced number of corpses in *ced-9(n1653)* did not necessarily mean modulation of the core apoptotic components. We saw that suppression of excessive apoptosis in *ced-9(n1653)* went along with suppression of sterility at 25°C. In a genetic screen for suppressors of *ced-9(n1653)*-induced sterility [see *5.7 Genetic screens to find suppressors of apoptosis*] we had isolated a candidate with an Unc phenotype that was very similar to the Unc of *unc-119* mutants; this trait cosegregated with sterility suppression in multiple outcrossing steps. We did not know the identity of the affected gene nor whether the Unc phenotype was caused by the same mutation as suppression of apoptosis. Nevertheless, this stimulated us to not only ask whether *ced-9(n1653)* could increase germ cell death in *unc-119(ed3)*; but to look from a different perspective and test whether *unc-119(ed3)* is capable to suppress *ced-9(n1653)*-induced apoptosis.

Indeed, *unc-119(ed3)* significantly reduced the number of corpses in *ced-9(n1653)* at 20°C and it suppressed sterility at 25°C (Figure 121). It could also reduce excessive death in the enhanced *rpo-1b(op259); ced-9(n1653)* double mutant; apoptosis at 20°C was nearly abolished and fertility restored to a high level.

Unless there is an even more complex interplay between engulfment and *ced-9*, suppression of apoptosis and sterility by *unc-119(ed3)* suggests that more germ cells can survive when *unc-119* function is lost. This would argue for an effect of *unc-119(ed3)* on death in the germ line and not only on corpse removal.

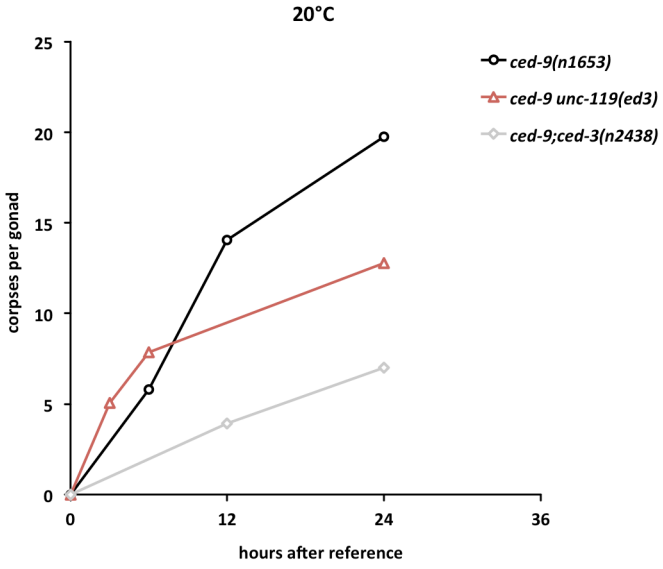

	15°C -> 25°C at L4	
	total eggs	95% CI (n)
N2 wt	106	±10.91 (8)
ced-9(n1653)	3	±1.29 (72)
ced-9 unc-119	21	±2.35 (15)
ced-9;nls96	5	±3.73 (24)
ced-9;ced-3(n2438);nls96	29	±4.05 (16)

	15°C -> 21°C at L4	
	total eggs	95% CI (n)
rpo-1b;ced-9	2	±1.65 (64)
rpo-1b;ced-9 unc-119	67	±4.50 (40)

Figure 121 *unc-119(ed3)* can suppress apoptosis and sterility of *ced-9(n1653)*. Time course of cell corpse numbers at 20°C; for comparison, the effect of a weak *ced-3(rf)* allele is included. For fertility, worms were transferred in small groups to individual plates at the L4 stage and shifted to the indicated temperature, and the total number of progeny was counted 3 days (at 25°C) or 4 days (at 21°C) after the temperature shift. *ced-3(n2438)* is a weak reduction-of-function allele. Average number of eggs laid per worm, 95 % CI of the mean, and total number of worms assessed per condition.

6.2.2.12 *ced-9(RNAi)* has different effect from *ced-9(n1653)* in *unc-119(ed3)*

We tested *unc-119* mutants also for *ced-9(RNAi)*-induced apoptosis. *ced-9(RNAi)* increased the number of corpses in *unc-119(ed3)* clearly more than *ced-9(n1653)* did; or – perspective turned over – loss of *unc-119* function did not strongly suppress the increase caused by *ced-9(RNAi)* whereas it did suppress the one caused by *ced-9(n1653)*. We had already observed a discrepancy between the *ced-9* mutant and RNAi knockdown in *rpo-1b(op259)*, in the opposite direction [*5.6.9 RNAi knockdown of ced-9*].

The difference between *ced-9(n1653)* and *ced-9(RNAi)* possibly reflects a specific alteration in mutant CED-9 that is critical for apoptosis regulation by UNC-119. Interestingly, the *n1653* allele is a point mutation that leads to an amino acid substitution Y149N at precisely a predicted Lck/Fyn target site. It is very likely that the *ced-9(n1653)* mutation disrupts some specific aspects of CED-9 regulation, which could be regulated by these SRC type kinases that in turn are potentially influenced by UNC-119. This might provide a link from *unc-119* function to the core apoptotic machinery.

Alternatively, the difference might arise from changed physiology in RNAi conditions; in fact, *unc-119* mutants – like *rpo-1b(op259)* – are very sensitive to food type (OP50 vs. HT115 in RNAi experiments) (Figure 128).

6.2.2.13 Hypothetical mechanisms of UNC-119 action

The studies on mammalian Unc119 have placed it in a molecular network that in *C. elegans* has diverse links to cell death and engulfment. Best matching homolog of the Fyn Src-type kinase in *C. elegans* is *src-1*. SRC-1 has recently been shown to relay signals from apoptotic cells to the molecular engulfment machinery, possibly by interactions with CED-2 (Hsu 2010). It is associated with the integrin α homolog INA-1, that receives SCRM-1 scramblase-dependent 'eat me' signals. INA-1 and SRC-1 are required in the engulfing cell for efficient removal of somatic cells that die during development. INA-1 associates on the plasma membrane with the integrin β PAT-3, that seems to also be required for engulfment. The same group has found that PAT-2, an alternative integrin α subunit that probably also associates with PAT-3, possibly defines a novel pathway in the removal of cell corpses [meeting abstract, (Hsieh 2010)]. Given the interactions of Unc119 with Fyn, it is not unlikely that SRC-1 and maybe the integrins provide the link of *unc-119* to engulfment. Loss of function of *src-1* or the integrins and loss of *unc-119* function have opposing effects on engulfment efficiency, which would be in agreement with negative regulation of *src-1* by *unc-119* for instance.

As to retinal degeneration in HRG4 mutant conditions, Mori et al. suggested a mechanism involving mitochondrial ANT1-mediated apoptosis of photoreceptors (Mori 2006). Formerly, HRG4 had been shown by the same group to interact with ARL2 (Kobayashi 2003), an ADP-ribosylation factor (ARF)-like protein. ARFs and ARLs form a large group of highly conserved GTPases (Li 2004b; Kahn 2006) with multiple functions, among others membrane and microtubule dynamics. An independent screen for binding partners of ARL2, in its GTP-bound state and in complex with BART (Binder of ARL2), had yielded ANT1, a mitochondrial adenine nucleotide transporter (Sharer 2002). Mori et al. speculated that an evidently altered affinity of mutant HRG4 to ARL2 could lead to the alterations in ANT1 levels they observed in the mouse model, and that this in turn might underlay apoptotic death of retinal neurons. In *C. elegans*, the ANT1 homolog *ant-1.1* (Farina 2008) (or *wan-1* in (Shen 2009)) has recently been shown to regulate somatic and germline apoptosis in conjunction with the core cell death machinery (Shen 2009;

Zhivotovsky 2009). ANT-1.1 binds to CED-4; it can also bind to CED-9, an interaction that is disrupted by the pro-apoptotic BH3-only protein EGL-1. An ARF GTPase activating protein, *cnt-2*, and *arf-1* itself are involved in ascertaining the apoptotic fate of neuroblasts during development (Singhvi 2011). A very recent publication demonstrated cooperative effects of Arf and Rac1 on the WAVE regulatory complex in the control of actin polymerisation *in vitro* (Koronakis 2011). The *C. elegans* homolog of Rac1 is CED-10, which provides an attractive possible link from UNC-119 to engulfment signalling.

A comprehensive analysis of human protein-protein interactions by Y2H has identified about 70 binding partners of UNC119 [(Stelzl 2005), and with search term "UNC119" at (Human protein-protein interaction network database search)]. One of the interactors is TP53BP2, or ASPP2, a pro-apoptotic regulator on p53. *C. elegans* has only one homolog of the ASPP group of proteins, *ape-1* (Bergamaschi 2003); it seems to unite pro- and anti-apoptotic functions of ASPPs and iASPP. Erica Bogan in our lab has shown that *ape-1* deletion mutants are defective in irradiation-induced germ cell death, but have increased baseline apoptosis [PhD thesis]. Many of the interactions of UNC-119 homologs are through SH2 and SH3 domain binding motifs; Arf family proteins, Abl or Crk have according domains. Very speculatively, Unc119 might be interacting with the TP53BP2 SH3 domain, which is also required for the interaction of the latter with p53 (Bergamaschi 2003).

7 Food type influences apoptosis levels and vulval development

When repeatedly scoring irradiation-induced apoptosis in the germ line, I noticed a significant difference of wildtype control levels between experiments performed in ordinary growth conditions and RNAi experiments. I quantified the difference and evaluated the type of bacteria that *C. elegans* fed on as the source of the strikingly different cell corpse levels. HT115 RNAi bacteria as the food supply were associated with clearly higher levels of germ cell apoptosis than OP50, with or without irradiation. It was intriguing that an external, not obviously noxious factor did so significantly influence not only the level of constitutive – and supposedly tissue homeostatic – cell death, but very strongly also the apoptotic response to exogenous damage. I assessed several genetic conditions to find potentially relevant signalling pathways in *C. elegans* that would determine this differential response to food type, and encircled Ras/MAPK as a potentially important mediator. Various recent reports demonstrated food type influences on phenotypes like body size or lifespan. Itay Nakdimon was, concurrently with my studies, investigating the effect of the bacteria type on vulval induction in *C. elegans*, the prototypic system for the study of Ras/MAPK signaling in developmental programs. He had found that certain types of bacteria could enhance the effect of constitutively increased Ras signaling in that system. We collaborated to establish a possible link between the observations in our two systems.

Here, I describe my findings of apoptosis modulation by the bacteria type. With Itay Nakdimon, we will try to strengthen the correlation between bacterial strains and cellular output in the models of vulval development and of programmed cell death, and to find common determinants for the response in the two systems. We plan to aggregate our data and write a joint manuscript, for which the following elements will serve as a basis.

Chapter 7

7.1 Introduction

Energy supply is the motor of all living. At the level of organisms, one could reduce the basic functions to reproduction and acquisition of nutrients, that is, structural components and energy sources. Even though nature seems to demand perpetuous struggle for food, it has become evident that more is not necessarily better. It is compelling that caloric restriction is correlated with increased lifespan in nematodes and mammals (Kenyon 2010; Fontana 2010). Possibly, 'reduced food uptake' in experimental conditions is not in fact a restriction when comparing to the situation in natural settings; rather 'normal' laboratory conditions are a surplus of energy supply and challenge the systems with harmful consequences of metabolic processes. Food and nutrition are important determinants of human health. Undernourishment and overfeeding, and maybe at least as importantly, malnutrition can overwhelm an organism's capacity to adjust and compensate. Quantity, composition and quality of food seem to have beneficial or adverse effects on health and lifespan. Globally, and even more pointedly in countries with a modern Western life style, diet and nutrition form a major risk factor for cancer [see also *1.3 Human cancer*]. It is currently thought that about 30 % of cancers in developed countries are accounted for by dietary factors [reviewed in (Key 2004, 2002)]. The precise role of food in cancer remains very challenging to assess, however. [The European Prospective Investigation into Cancer and Nutrition (EPIC) is a multicentre program surveying half a million subjects for a better understanding of the relationship between specific cancers and nutritional aspects (Gonzalez 2010, 2006).] It is to assume that nutrition and metabolic processes become particularly relevant in pathological conditions where basic regulation of homeostasis is altered. For the assessment of principle connections between food and cellular programs, adequate model organisms might be a more revealing system than epidemiological studies in human; environmental conditions can be standardised to a large extent and more drastic interventions are feasible.

C. elegans mainly feeds on bacteria; the worms show preferences for food types if given a choice; they seek high quality food and leave hard-to-eat bacteria, a behavior that is reinforced by experience and learning (Shtonda 2006). The choice of bacteria is not a matter solely of gustatory preference, but it has significant implications on phenotypic and metabolic characteristics of the predatory worms. Several recent publications have demonstrated that the type of bacteria that worms are feeding on determines various features to the same extent as mutations in worm genes do. Usually, the standard laboratory *E. coli* strain OP50 was compared in this studies with other *E. coli* derivatives. Impressively, the body size of adult animals was more than 50 % larger when worms were fed on HB101 instead of OP50 (So 2011a). Also, lifespan is influenced by the type of bacteria. Several mutant conditions have been identified that enhance or reduce the effect of food type differences on lifespan: mutants with altered feeding behaviour or of innate immunity (So 2011b), or of neuronal receptor molecules and the sensory system (Maier 2010). The differences arising from different bacterial food sources are reflected on a molecular level. Fat storage levels were clearly variable between worms fed on different bacterial strains (Brooks 2009). Metabolic profiling revealed very different patterns of analyte abundances between worms fed on OP50 or on the RNAi bacterial strain HT115 (Reinke 2010). Modulation of food-type dependent effects by mutations in *C. elegans* have indicated molecular pathways that are likely to be involved in the food type response, such as insulin signalling (So 2011b), intestinal peptide transport (Brooks 2009),

mitochondrial respiratory chain (Reinke 2010), or neuroreceptor molecules (Maier 2010). On the bacteria, the LPS structure has been suggested to present a major determinant of the lifespan effect in the worms (Maier 2010).

Collectively, these studies demonstrate the importance of food quality on major life parameters. The multiple correlations of certain bacteria (mostly OP50 and other *E. coli* strains) and various worm phenotypes indicate that these phenotypes have a shared link to the food source. If they are not directly dependent on one another – e.g., lifespan on body size and body size and lipid composition – there ought to be a master switch that regulates the various phenotypes in response to food type. Whether this is a distinct bacterial factor, some specific behaviour of the worm, a receptor molecule or an organ, a host-defence mechanism, or a central molecular pathway remains an open question. Together with Itay Nakdimon, we have identified two further phenotypes that are significantly modulated by the bacteria type and that might share such a link. An enhancing effect of some bacteria on vulval induction, typically a readout for EGF/Ras/MAPK activity, and on germ line apoptosis, which is also subject to MAPK signalling, suggests a possible role for this pathway in the multiple food-type effects.

The nutritional situation of *C. elegans* is remarkable: bacteria are the nematode's energy source, but as potentially pathogenic microbes also pose a constant threat (Zhang 2005). Feeding is necessary, sometimes satisfying, sometimes satisfactory, and sometimes dangerous – for worms and men.

7.2 Text elements for a manuscript

7.2.1 Food type modulates apoptosis levels

7.2.1.1 Different food types are used for standard worm culturing or for RNAi experiments

The most commonly used bacterial strain for feeding *C. elegans* in laboratory conditions is OP50. This *E. coli B* derivative has a relatively slow growth rate due to a metabolic defect (uracil auxotrophy), which is optimal for culturing *C. elegans* without the worms being overgrown by rapidly replicating bacteria (Brenner 1974). OP50 form a lawn of about 1 mm thickness when seeded on NGM agar plates. OP50 are considered to be of the less pathogenic (Mallo 2002), but also less nutritious food sources for *C. elegans*, and they are often not the preferred bacteria if the worms are given a choice [(Shtonda 2006); for food type preference in conditions that better mimic the natural environment see (Freyth 2010) and (Abada 2009)].

Alternatively, for RNA interference experiments, worms can be transferred to bacteria that specifically express dsRNA of the target sequence, and they often show a knock down phenotype in the same generation. For this convenient approach, the HT115 *E. coli* strain is commonly transformed with the plasmid vector pL4440 (including an ampicillin resistance cassette), and dsRNA expression from the target sequence is induced by IPTG mediated activation of T7 polymerase, that transcribe from the two flanking T7 promoters; selectable RNase III-deficiency (Tetracycline resistance) of the HT115 strain prevents degradation of dsRNA. These RNAi bacteria are usually grown on NGM agarose plates supplemented with ampicillin and IPTG (Kamath 2001).

RNAi has been an important tool in elucidating the role of many apoptosis genes and it can often be applied for the efficient study germ cell apoptosis. For instance, knock-down of pro-apoptotic *ced-3*, the effector caspase in *C. elegans*, blocks almost all germ cell apoptosis already in the generation of worms treated with RNAi. The worms are also sensitive to knock-down of the anti-apoptotic *ced-9*, which evokes the opposite phenotype, i.e. increased germ cell death. Further, targeting of engulfment genes can rapidly lead to a marked effect in the adult gonad; *ced-6(RNAi)* treated worms accumulate a vast number of non-removed germ cell corpse. Special aspects of germ cell death, such as DNA damage-induced apoptosis, have been successfully studied by RNAi as well; often, RNAi treatment reproduces the effects of a reduction- or loss-of-function mutation in the respective genes.

7.2.1.2 Germ cell apoptosis levels depend on food type

When studying irradiation-induced apoptosis, we realized that there were reproducibly higher numbers of germ cell corpses in worms treated with control vector RNAi than in worms classically fed on OP50. For N2 wildtype worms, such a difference could already be noted at the levels of 'physiological' germ cell death (that is, baseline apoptosis without exogenous DNA damage), and it became particularly evident after irradiation with IR or UV-C [for UV-C response, see Figure 130].

We excluded that factors as simple as the plate medium or the presence of antibiotics could be responsible for the difference. (OP50 had been shown to cause significant killing of worms when cultured on a particularly rich medium BHI (Garsin 2001).) OP50 grown on agarose instead of NGM

classic plates did not increase germ cell apoptosis; growing RNAi bacteria without ampicillin did not reduce the high number of corpses, either. We further tested the attractive hypothesis that HT115 RNAi bacteria mainly provoke higher corpse numbers by activating RNAi mechanism in the predator. The empty vector (pL4440) containing control strain presumably expresses double stranded RNA of about 200 nucleotides from the two opposing T7 promoters flanking the cloning site. Even though this dsRNA has no obvious target in *C. elegans*, the RNAi machinery is likely getting involved, and this process itself could have consequences for apoptosis. To minimize dsRNA synthesis, empty vector RNAi bacteria were grown on NGM classic without IPTG; they still caused higher cell corpse numbers than OP50. A control experiment with the RNAi clone targeting *unc-22* however showed that – at low penetrance – worms still exhibited specific knockdown phenotypes, pointing at residual RNAi effects at this condition. Therefore, we fed worms on the non-transformed (i.e., no pL4440 plasmid) HT115 host strain; this also resulted in increased apoptosis compared to OP50. Thus, the generally higher levels of germ cell apoptosis observed in RNAi experiments are most likely a result of the bacterial strain rather than an effect of RNAi treatment.

We evaluated additional *E. coli* strains for their effect on germ cell apoptosis: DR3.1 and BL21 which is, similar to OP50, an *E. coli* B derivative. Worms fed on DR3.1 had high levels of corpses if untreated and a strong increase after irradiation, and those fed on BL21 had low levels at baseline and a moderate response to IR (Figure 122). Regarding apoptosis in the predator, these bacterial strains were thus similar to HT115 and OP50, respectively.

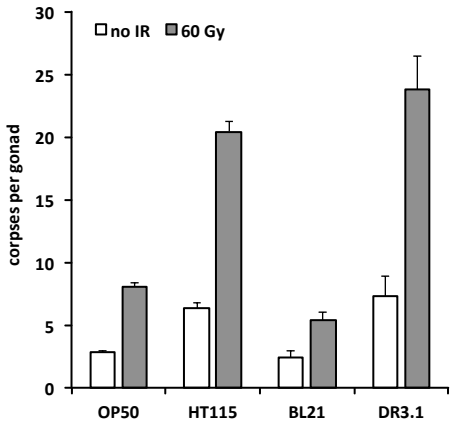

Figure 122 Different bacterial strains evoke highly different apoptosis levels. Average number of corpses at 24 hours post irradiation in worms fed on the indicated bacterial strains, starting at L1 stage. Error bars indicate 95 % CI of the mean.

7.2.1.3 HT115 bacteria dominantly increase cell corpse levels

Based on these observations, there seems to be a categorical response to bacteria. Possibly, HT115 bacteria (and others) present a feature that OP50 (and others) do not have and that eventually sensitizes *C. elegans* for germ cell apoptosis, leading to high levels of germ cell death. Alternatively, OP50 could have some properties that desensitize the worms, leading to low levels. To test which of the two mechanisms likely prevailed, we cultured worms on graded mixtures of the two bacterial strains. In the first case, if apoptosis was stimulated by some feature present in HT115, apoptosis would probably be increased even if only a fraction of the bacteria in a mixture carried it; in the alternative case of a

suppressive effect coming from OP50 – with the high levels on HT115 being the normal state – this would probably dominate in the mixture and apoptosis would be low. We grew OP50 and HT115 separately in liquid medium to the same optical density and seeded NGM plates either with OP50; a mixture of OP50:HT115 at 9:1, 1:1 or 1:9; or with HT115, before we transferred L1 larvae from bleached worm cultures (formerly on OP50) and grew them to adulthood on the mixed bacteria; all plates had a bacterial lawn with similar appearance after seeding and maintained the same aspect when worms grew adult. Surprisingly, with or without irradiation, worms grown on a mixture of the two bacteria had at least as high corpse numbers as the ones on pure HT115, irrespective of the OP50:HT115 ratio (Figure 123). Thus, the presence of only 10 % HT115 could significantly increase the corpse number observed on OP50 alone. (We have not further exhausted this ratio to find the maximal active dilution of HT115 in OP50.) We conclude that HT115 exhibits some properties that favor the appearance of germ cell corpses in its predator *C. elegans*. The corpse numbers on mixtures of HT115 and OP50 at all dilutions tested were even slightly higher than on HT115 alone; this could signify an additive effect of two distinct pro-apoptotic cues on the two bacteria types.

We tested another wildtype strain of *C. elegans*, the Hawaii isolate CB4856 for differential apoptosis levels between the two food types. Hawaii worms had lower baseline levels of germ cell apoptosis than N2. On OP50, IR treatment increased the corpse number of Hawaii wildtype only moderately; worms grown on HT115, however, showed a significantly more pronounced response to IR (Figure 123). Like for N2, on mixtures of HT115 and OP50, the HT115 phenotype dominated at all dilutions tested.

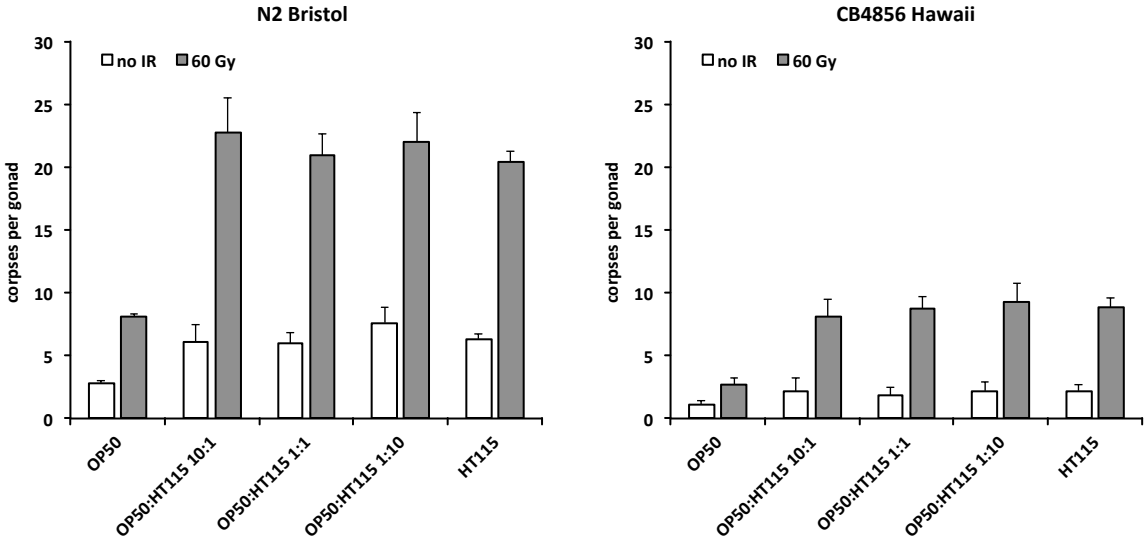

Figure 123 HT115 dominantly increases the corpse number. Wildtype worms were grown on a mixture of OP50 and HT115 bacteria, starting at stage L1. Irradiation was at 12 hours post L4 and scoring of corpses 24 hours later. N2 Bristol and CB4856 Hawaii are descendants from different wildtype isolates. Error bars indicate 95 % CI of the mean.

7.2.1.4 Increased apoptosis is partially independent of *cep-1* and *egl-1*

The bacteria type had an influence on IR-induced death as well as on baseline levels of corpses; both modes of germ cell apoptosis were shifted towards higher levels on HT115. Molecularly, this suggests some modulation of apoptosis at a level where different pathways to cell death induction have already

converged. Another explanation would be the activation of the same signaling cascades by HT115 that are otherwise involved in DNA damage responses.

A key molecule for stress responses in *C. elegans* is the p53 homolog CEP-1 [see *2.1.6 DNA damage-induced germ cell apoptosis*]. Induction of germ cell death upon DNA damage requires CEP-1; loss of CEP-1 abolishes this response completely (Schumacher 2001). CEP-1 activation is transmitted to the core apoptotic machinery via transcriptional upregulation of the pro-apoptotic BH3-only factors EGL-1 and CED-13. To determine whether over-activation of CEP-1 could be underlying the increased apoptotic response on HT115, we measured the mRNA levels of EGL-1 and CED-13 by qRT-PCR. The transcript levels of irradiated wildtype were similar between worms fed on HT115 or fed on OP50. (Interestingly, in the mutant condition *rpo-1b(op259)*, CEP-1 activity as measured by these transcripts was significantly enhanced by HT115). We confirmed that the high number of IR-induced corpses on HT115 was CEP-1-dependent: loss of CEP-1 in the deletion mutant *cep-1(gk138)* prevented all incremental apoptosis upon irradiation on HT115 (Table 24). While the loss-of-function mutant allowed to show that CEP-1 is required for the higher apoptotic response to IR, it could not answer whether CEP-1 is sufficient for this increase.

In contrast to DNA damage-induced apoptosis, constitutive germ cell death has been shown not to depend on *cep-1* (Schumacher 2001). We considered that the enhancement of baseline apoptosis on HT115 could be stress-induced and that *cep-1* might be involved in this increase. However, EGL-1 and CED-13 transcript levels were not significantly different between wildtype worms fed on OP50 or on HT115 without irradiation. Regarding apoptosis levels, *cep-1* seemed not critical; *cep-1(gk138)* mutants showed an enhancement of baseline apoptosis on HT115 (yet to slightly lower levels than wildtype). Thus, increased germ cell apoptosis on HT115 relative to OP50 was not mainly mediated by CEP-1 signaling.

The pro-apoptotic *egl-1* closely resembles *cep-1* regarding the differential requirement for DNA damage-induced versus physiological germ cell death (Gartner 2000). Besides DNA damage signaling towards germ apoptosis, EGL-1 was shown to be required for pathogen driven germ cell death caused by Salmonella strains (Aballay 2003), in a pathway that involved the p38 kinase PMK-1. CEP-1 has not been evaluated in this context; however, it has recently been discovered to regulate innate immunity, in a pathway that includes nucleolar proteins (Fuhrman 2009).

We hypothesized that EGL-1 might be mediating the increase in baseline apoptosis on HT115 in the context of pathogen signaling, independently of transcriptional upregulation by *cep-1*. To assess this possibility, we tested a double mutant of *cep-1(gk138)* and *egl-1(n3082)*. Apoptosis levels with or without irradiation on OP50 or on HT115 were unchanged in *cep-1(gk138); egl-1(n3082)* in comparison to *cep-1(gk138)* at the same conditions (Table 24). Thus, it is unlikely that *egl-1(n3082)* plays a role in addition to *cep-1* that would be crucial in this process.

CED-9, the Bcl2 homolog in *C. elegans*, regulates apoptosis as part of the core apoptotic machinery, mainly by antagonizing pro-apoptotic CED-4. The hypomorphic allele *ced-9(n1653)* leads to high levels of germ cell apoptosis at increasing temperature, supposedly due to inappropriate release of CED-4 [(Yan 2004) and introduction in *5.6.1 CED-9 – the core inhibitor of apoptosis*]. We tested this mutant for sensitivity towards HT115 at 20°C and found in a preliminary experiment that it exhibited higher numbers of germ

cell corpses than when grown on OP50 (49 ±9 vs. 29 ±8 [average ±SD] at 24 hours post reference, n=20). There seems to be a potentiating effect of HT115 on apoptosis induced by loss of normal CED-9 function.

7.2.1.5 Ras/MAPK activation renders germ cells hypersensitive to irradiation

Itay Nakdimon had been investigating the role of the food type for vulval induction, the prototypic system for the study of Ras/MAPK signaling in development. He had found that certain types of bacteria could enhance the effect of constitutively increased Ras signaling in that system. Animals with a gain-of-function allele of the *C. elegans* Ras homolog *let-60* have excessive vulval induction due to overactivation of MPK-1. This effect was further promoted by feeding the worms on DA1877 rather than on OP50. We collaborated to establish a possible link between the observations in our two systems.

For the bacterial strains tested so far, we saw good correlation between the potency to increase vulval induction of *let-60(n1046gf)* and to enhance germ cell apoptosis levels. Possibly, the two phenomena share a common underlying mechanism. An increased vulval induction index of the *let-60(n1046gf)* mutant clearly points to some process that eventually enhances Ras/MAPK signaling or its effects on vulval development. If the effects of the food type on vulval induction and on apoptosis are linked, the mechanism that hyperactivates Ras/MAPK signaling also influences some core process of apoptosis; or Ras/MAPK pathway activity itself has some role in setting the sensitivity of germ cells to additional pro-apoptotic cues. We evaluated this latter hypothesis, also in the context of *5.5 rpo-1b(op259) and the Ras/MAPK pathway*. The Ras/MAPK pathway had been found to be a key regulator of germ cell progression in *C. elegans*. MPK-1 activation is required for exit from late meiotic pachytene (Church 1995); physiologically occurring cell death is linked to this process and is defective when MAP kinase activity is too low (Gumienny 1999). To test what would happen to cell death with increased MPK-1 activation, we counted apoptotic germ cells in the *let-60(n1046gf)* gain-of-function mutant that we were also using as the genetic background for vulval induction experiments. The corpse number was similar to wildtype in non-treated *let-60(n1046gf)* animals grown on OP50; upon irradiation, the increase in germ cell corpses was significantly higher in *let-60(n1046gf)* than in wildtype (Table 12). Thus, mutants with overactive Ras/MAPK appear hypersensitive to IR-induced apoptosis. To endorse a possible novel role for the Ras/MAPK pathway in regulating DNA damage-induced germ cell apoptosis, we tested the loss-of-function mutant *lip-1(zh15)*. LIP-1 is a dual specificity phosphatase that negatively regulates MPK-1 during vulval development (Berset 2001) as well as in germ cell proliferation and maturation (Lee 2006; Hajnal 2002). *lip-1(zh15)* animals had increased apoptosis already at baseline and showed a massive increase after irradiation. Together, these observations suggest that high activity of MPK-1 in the germ line facilitates cell death.

7.2.1.6 Food type can compensate for reduction of Ras/MAPK function

The high apoptotic response in *let-60(n1046gf)* mutants to irradiation was further increased when the worms were fed on HT115 rather than on OP50 (Table 24). Thus, Ras/MAPK overactivation by *let-60(n1046gf)* and the effect of the bacterial strain here too act additively.

The hypomorphic allele *mpk-1(ga111)* causes temperature sensitive defects in the germ line, leading to sterility at 25°C in a majority of animals due to arrest of the germ cells in late pachytene of the first

meiotic division (Lackner 1998). At 20°C, this Ras/MAPK loss-of-function effect is less pronounced. Germ lines show only weak abnormalities in the gonad bend region and at least some germ cells progress into maturing oocytes. Worms grow to adulthood and develop normal vulvae, speaking for residual MPK-1 activity. We tested the *mpk-1(ga111)* mutant at this more permissive temperature for germ cell apoptosis. When worms were grown on OP50 and left untreated, the levels of apoptotic corpses were reduced in comparison to non-irradiated wildtype, in agreement with previous observations for MPK-1 reduction; upon irradiation, this number increased only moderately (Table 12). Reduction of MPK-1 function thus reduces apoptotic response of germ cells to DNA damage. Interestingly, the mutant remained sensitive to an increase of the corpse number on HT115 bacteria; non-irradiated and irradiated *mpk-1(ga111)* mutants on HT115 approximately reached the levels of non-irradiated and irradiated N2 wildtype on OP50.

7.2.1.7 Loss of *lin-15* abolishes germ cell apoptosis and response to food type

To further investigate which pathways might lead to activation of Ras/MAPK and to enhanced vulval induction in response to certain bacteria, we are testing mutants of factors known to influence MAP kinase activation: *lin-15*, *lip-1*, and insulin signaling factors. *lin-15* is a negative regulator of MAPK activation; loss of the two isoforms *lin-15a* and *lin-15b* in the *lin-15(n309)* mutant leads to an highly penetrant Muv phenotype (Clark 1994; Huang 1994). LIP-1 negatively regulates MPK-1 phosphorylation; it is activated in the developing vulva by lateral signaling via the Notch pathway (Berset 2001). Insulin signaling is involved in most aspects of metabolism and seems to also influence the activation state of MPK-1 [PhD thesis of Itay Nakdimon].

lin-15(n309) mutants have strong ERK/Ras/MAPK gain-of-function effects on vulval induction. The mechanism of *lin-15a/b* function is not known in detail; transgenic mosaic studies suggested synthesis of the proteins from hypodermal cells (Herman 1990), and further experiments demonstrated an anchor cell (source of the EGF homolog LIN-3) independent effect on vulval induction, that was genetically upstream of EGFR/LIN-23 (Clark 1994). We tested whether this would be reflected in germ line apoptosis. The gonads however did not resemble those of *let-60(n1046gf)* or *lip-1(zh15)*; they were thinner and contained less germ cells overall. Surprisingly, the levels of apoptotic corpses were low in non-irradiated animals and increased only very slightly in response to irradiation. To our knowledge, it has not been studied in detail what the roles of the *lin-15a* and *lin-15b* isoforms in tissues other than the developing vulva could be and how it changes MPK-1 activity levels; thus the observation does not necessarily contradict a potentiating effect of high MAP kinase activity on germ cell death. We tested whether we could increase the (defective) apoptotic response on HT115 bacteria. However, unlike wildtype or *let-60(n1046gf)* or *mpk-1(ga111)* mutants, *lin-15(n309)* animals did not exhibit higher levels of germ cell corpses on HT115 than on OP50; rather, any apoptotic response to IR appeared to be abolished. These observations certainly need some refinement; germ line morphology and apoptosis levels of *lin-15(n309)* mutants don't agree with other mutants of Ras/MAPK pathway overactivation. Hypothetically, the effect of *lin-15(lf)* on germ line MPK-1 activation is very different from *let-60(n1046gf)*. The corpse number in *lin-15(lf)* mutants is very low so that the clear distinction of different levels on different bacteria strains becomes difficult.

7.2.1.8 Food type sensitivity does not depend on classical infection signaling

PMK-1 is one of the *C. elegans* homologs of the mammalian MAP kinase p38 family. It was shown to be involved in the response to danger signals, such as from infectious agents or excess transition metals (Kim 2002; Berman 2001; Shivers 2009; Wang 2009); lack of functional PMK-1 sensitizes *C. elegans* to toxic effects of pathogens (Bolz 2010; Aballay 2003). Salmonella infection was shown to have a more dramatic effect on lethality in *pmk-1* mutants than in N2; concomitantly, as mentioned above, the mutant did not increase germ cell apoptosis in response to this infection (Aballay 2003). We tested the hypothesis that PMK-1 might also be mediating the increase in apoptosis evoked by HT115 bacteria and that hypersensitivity to irradiation would depend on an infection-induced pathway involving *pmk-1*. Interestingly, the loss-of-function mutant *pmk-1(km25)* had very little apoptosis on OP50 at baseline and only few additional corpses upon irradiation (Table 24). This attributes a role to the MAP kinase *pmk-1* in setting apoptosis levels more broadly, similar to the ERK homolog *mpk-1*. On HT115, IR response was clearly higher than on OP50. PMK-1 is thus not essential for the increase in IR-induced germ cell apoptosis observed on HT115.

	no IR				60 Gy			
	OP50		HT115		OP50		HT115	
	score	95% CI (n)	score	95% CI (n)	score	95% CI (n)	score	95% CI (n)
wt	2.84	±0.16 (647)	4.79	±0.24 (746)	8.10	±0.22 (831)	17.50	±0.48 (853)
cep-1(gk138)	1.89	±0.30 (96)	2.56	±0.44 (108)	1.90	±0.26 (136)	2.98	±0.51 (96)
cep-1;egl-1(n3082)	1.90	±0.55 (20)	3.40	±0.76 (20)	1.80	±0.54 (20)	3.20	±0.69 (20)
dpl-1(n3643)	0.94	±0.49 (16)	1.76	±0.90 (34)	2.00	±0.62 (16)	6.07	±1.56 (58)
let-60(n1046gf)	1.98	±0.40 (56)			19.53	±1.96 (60)	31.20	±2.22 (20)
mpk-1(ga111)	0.94	±0.39 (17)	4.10	±1.21 (20)	2.25	±1.07 (20)	8.50	±2.13 (20)
lin-15(n309)	0.50	±0.39 (20)			1.25	±0.60 (20)	0.10	±0.13 (20)
pmk-1(km25)	0.72	±0.32 (36)	1.00	±0.40 (20)	3.36	±0.74 (59)	7.90	±1.80 (20)
rrf-1(pk1417)			2.04	±0.35 (72)	3.13	±0.98 (16)	13.25	±1.07 (88)
rrf-3(pk1426)	1.56	±0.62 (16)	3.06	±0.77 (32)	7.88	±1.69 (16)	13.72	±2.23 (32)
mut-7(pk204)			8.81	±1.75 (48)	9.35	±2.28 (20)	13.88	±2.06 (52)
unc-119(ed3)	1.04	±0.41 (27)	1.40	±0.39 (20)	1.68	±0.34 (71)	2.30	±0.59 (20)
opIs204	2.43	±0.38 (60)	7.00	±1.33 (20)	6.41	±0.69 (69)	24.90	±2.27 (20)
opIs204;unc-119(ed3)	1.45	±0.53 (60)	3.05	±0.77 (20)	2.80	±0.60 (60)	6.10	±1.44 (20)
ygIs;unc-119(ed4)	0.85	±0.38 (20)	2.05	±0.59 (20)	2.30	±0.65 (20)	6.08	±1.06 (24)
nmur-1(ok1387)	2.25	±1.01 (20)	3.90	±1.14 (20)	5.90	±1.56 (20)	7.85	±2.06 (20)
hcf-1(ok559)	4.65	±1.43 (20)	2.85	±0.66 (20)	11.78	±1.52 (45)	10.20	±1.35 (20)
hcf-1(pk924)	3.18	±0.47 (45)	4.10	±0.92 (20)	4.38	±0.93 (40)	5.05	±1.28 (20)
rpo-1b(op259)	1.43	±0.21 (152)	0.80	±0.17 (164)	2.77	±0.31 (140)	1.66	±0.28 (200)
cep-1 rpo-1b	0.25	±0.15 (40)	0.18	±0.12 (60)	0.08	±0.08 (40)	0.40	±0.19 (60)
rpo-1b (12 h)	1.19	±0.22 (67)	1.59	±0.64 (27)	1.75	±0.35 (60)	0.50	±0.40 (16)
gld-1(op236) (12 h)	3.98	±0.64 (40)	8.73	±1.35 (40)	13.70	±1.31 (20)	25.05	±2.55 (40)
gld-1 rpo-1b (12 h)	5.82	±0.89 (40)	14.60	±3.93 (20)	13.28	±1.50 (40)	36.85	±3.79 (20)

Table 24 Apoptosis levels in various mutants grown on OP50 or HT115 bacteria, starting at the L1 stage. Average number of corpses per gonad in non-irradiated and irradiated animals at 24 hours post treatment, 95 % CI of the mean, and total number of animals assessed per condition.

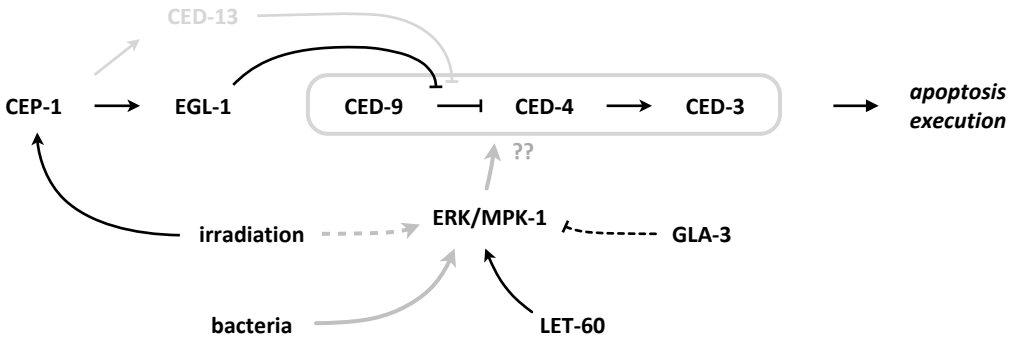

Figure 124 Model for the food type influence on irradiation induced germ cell apoptosis. In *5.5 rpo-1b(op259) and the Ras/MAPK pathway*, we have found that the Ras/MAPK pathway determines the sensitivity of germ cells for apoptosis, likely by a permissive effect on apoptosis at the level of the core apoptotic machinery (the precise level needs to be defined, indicated by ??). Possibly, the modulatory effect of the bacteria type on apoptosis is via the Ras/MAPK pathway. *let-60(gf)*, a well-established activator of MPK-1, and *gla-3(rf)* that was also shown to increase MPK-1 activation sensitise germ cells to constitutive apoptosis as well as to CEP-1-induced death. Some bacteria have an additional potentiating effect. Black lines indicate established links, grey arrows are hypothetical activation paths. Dashed lines have limited evidence.

7.2.1.9 Food type influences developmental cell death

In *C. elegans*, apoptosis can be observed in different contexts. Whereas germ cells die in an apparently stochastic manner, somatic cells in wildtype worms undergo apoptosis in a highly predictive pattern, as part of the fixed cell lineages. Genetically, germ cell apoptosis and developmental cell death share their dependency on factors of the core apoptotic machinery and on many of the cell engulfment factors for proper removal of dying cells; upstream of the core apoptotic machinery, the two processes have distinct requirements [see *2.1 Cell death in the soma and in the germ line*]. The pro-apoptotic BH3-only factor EGL-1 is necessary to initiate cell death in most of the somatic cells that are destined to die during development; it is activated by different cues depending on the cell type. In contrast, germ cell death is possible at a baseline level without functional EGL-1. For IR-induced germ cell apoptosis however, EGL-1 is mandatory; its transcription is mainly activated by CEP-1 in this setting. *cep-1* is assumed to be dispensable for EGL-1-induced developmental cell death; and no additional apoptosis is executed in somatic cells upon stress such as DNA damage or infection (Gartner 2008). To test whether food type can affect the course of apoptosis more generally, we assessed developmental cell death in the heads of freshly hatched L1 larvae. In engulfment mutants, apoptotic cells of the later embryonic development persist into larval stages and can be counted collectively. We found that *ced-6(n1813)* mutants had a higher number of corpses in L1 heads when grown on HT115 than on OP50. Thus, food type also affects developmental apoptosis.

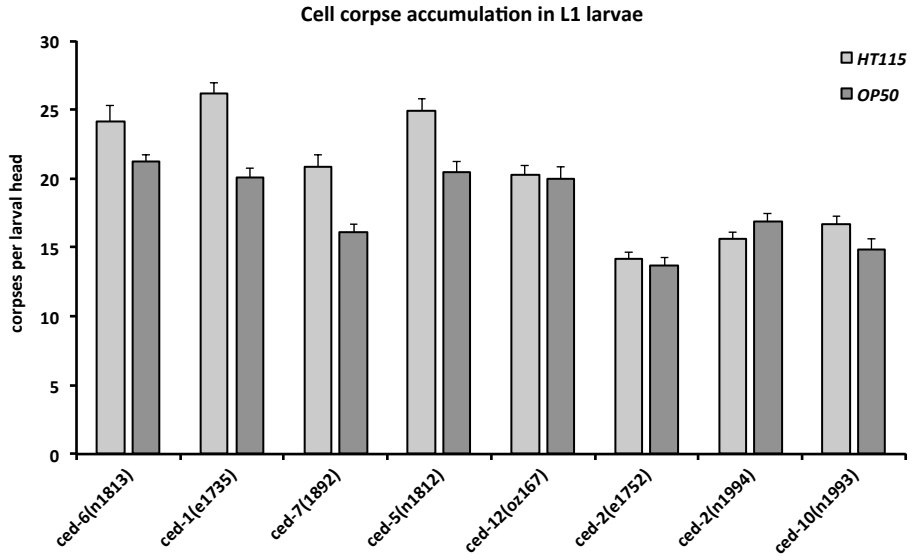

Figure 125 HT115 bacteria increase the number of accumulated corpses in the heads of freshly hatched larvae of engulfment mutants. Error bars indicate 95 % CI of the mean.

7.2.1.10 Food type difference involves a branch of engulfment signaling

We considered that a higher cell corpse number in the larval heads, and possibly in the germ line as well, has not to be a mere result of increased cell death, but could also reflect less efficient corpse removal. Engulfment genes in *C. elegans* are categorized into partly redundant pathways that converge on the small GTPase *ced-10* (Reddien 2004): *ced-1*, *ced-6* and *ced-7* together act in corpse recognition; and *ced-2*/CrkII, *ced-5*/DOCK180 and *ced-12*/ELMO are grouped in another branch of signal transduction toward activation of *ced-10* in the engulfing cells of the developing animal. An engulfment defect resulting from loss of any one of these factors can be further enhanced by simultaneous loss of a member of the parallel pathway. If the higher corpse number observed in worms fed on HT115 was the result of increased apoptosis, one would expect additional cells on this food type in all of the engulfment mutants. If, however, the higher corpse number arose from altered engulfment activity, potentially not all of the mentioned engulfment mutants would exhibit additional corpses: in case food type impacts on engulfment dependently on one of the known signaling pathways, corpse numbers would not differ in the corresponding loss-of-function mutants.

All, *ced-1(e1735)*, *ced-6(n1813)* and *ced-7(n1892)* L1 larvae had higher numbers of corpses on HT115 than on OP50. *ced-2(n1994)*, *ced-2(n1752), ced-12(oz167)* and *ced-10(n1993)* mutants on the other hand did not show more corpses on HT115. Thus, the food type response in young larvae does require these factors; the difference in the number of apoptotic corpses likely involves regulation of cell engulfment. A plausible explanation so far is that some types of bacteria provoke inhibition of the CED-2-CED-10 axis and in turn of engulfment. It has not been excluded, however, that some of these factors could also be involved in apoptotic mechanisms of the dying cell.

We determined the effect of the food type on apoptosis in the germ line of engulfment mutants. If corpse removal is strongly inhibited, dying cells accumulate in high numbers. We first tested *ced-6(n1813)*. The corpse number increased rapidly on OP50, according to previous observations. On HT115, the corpse number rose more rapidly (Figure 126), in agreement with the observation in wildtype gonads and in L1

heads of *ced-6(n1813)*. In contrast, *ced-2(n1994)* animals (but not mutants of the weaker *ced-2(n1752)* allele) had very few germ cell corpses (in the range of wildtype on OP50). Either, the engulfment defect is somehow compensated in the germ line, or *ced-2* plays an additional role in death mechanisms. Cell corpse levels were not higher on HT115 than on OP50, supporting a role for *ced-2* in the food type response in the germ line. The number of corpses in irradiated *ced-2(n1994)* engulfment mutants remained therewith below the level of wildtype animals on HT115.

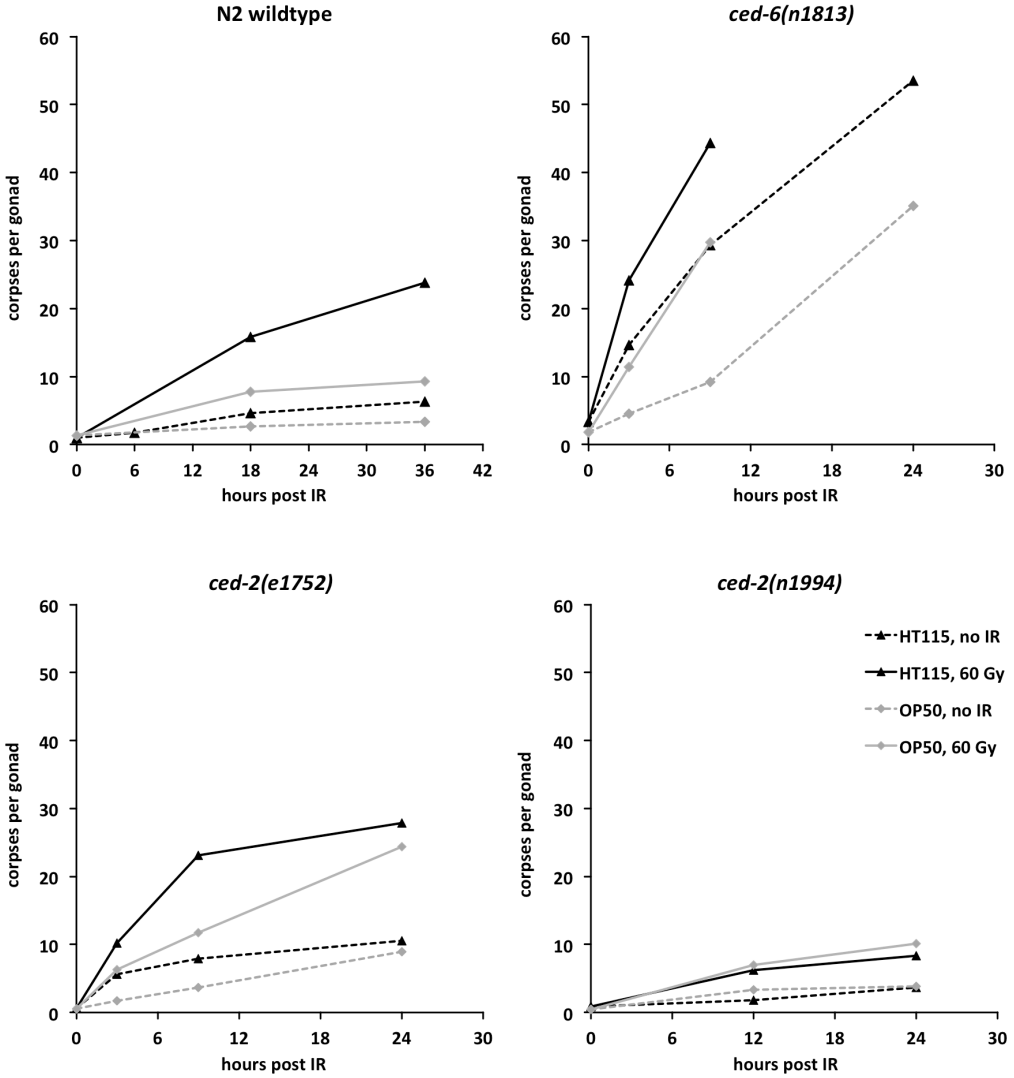

Figure 126 Accumulation of apoptotic germ cell corpses in engulfment mutants. Worms were grown either on OP50 or on HT115 starting at L1 and irradiated 12 hours post L4 stage. *e1752* is a supposedly weaker allele of the Crk homolog *ced-2* than *n1994*. Single experiment with n=20 worms per condition.

7.2.1.11 Somatic cell death is enhanced by *let-60(n1046gf)*

We used the ventral cord Pn.aap neurons as a third system to test the effect of food type on apoptosis. In wildtype worms, only six out of the 13 Pn.aap cells generated during development survive, the other seven are removed by programmed death. All surviving cells can be highlighted by GFP expressed under the P_{lin-11} promoter starting at the L3/L4 stage. In a reduction-of-function mutant of *ced-3*, some of the cells normally destined to die survive; additional loss of pro-apoptotic cues further increases the number of extra cells, whereas loss of anti-apoptotic activity reduces the number in this sensitized

background (Reddien 2001). *ced-3(n2438)* worms grown on HT115 on average had slightly less extra cells than those grown on OP50, supporting a pro-apoptotic effect of HT115 in this system. To test whether Ras/MAPK overactivation could reproduce this reduction of extra cell survival, we scored a *let-60(n1046gf) ced-3(n2438)* double mutant. The precise number of Pn.aap cells was often difficult to assess in this mutant due to overlapping GFP signal from ectopically induced vulvae; with this uncertainty, we found that on average *let-60(n1046gf)* reduced the number of extra surviving cells almost by half. We will have to test *let-60(n1046gf) ced-3(n2438)* on HT115 to see whether there are additive effects of MAPK overactivity and certain bacteria, as we observed for vulval induction and germ cell apoptosis. Also, it will be interesting to test the effect of *let-60(n1046gf)* on corpse accumulation in L1 heads.

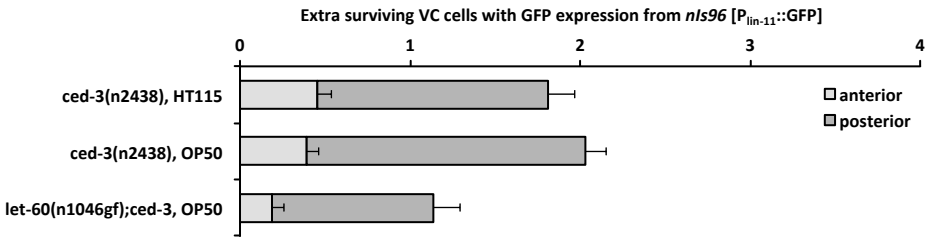

Figure 127 Gain of *let-60* function and HT115 bacteria enhance cell death in the ventral nerve cord of weak *ced-3(n2438)* reduction-of-function mutants. Extra surviving cells anterior (max. 2) and posterior (max. 4) to the orthotopic vulva were assessed separately at L4 stage. Error bars indicate 95 % CI of the mean for each group.

7.2.2 Further findings on food type-induced differences

7.2.2.1 *unc-119* mutants are very sensitive to food type

We have realised that *unc-119* mutants, which have a growth delay on OP50, grow much faster on HT115 (Figure 128) and thus almost catch up with the developmental speed of wildtype worms. The egg laying rate of 48 hours-old adults was also increased from 3.8 ±0.4 to 4.9 ±0.4 eggs per animal per hour. The low level of germ cell apoptosis did however not rise significantly on HT115.

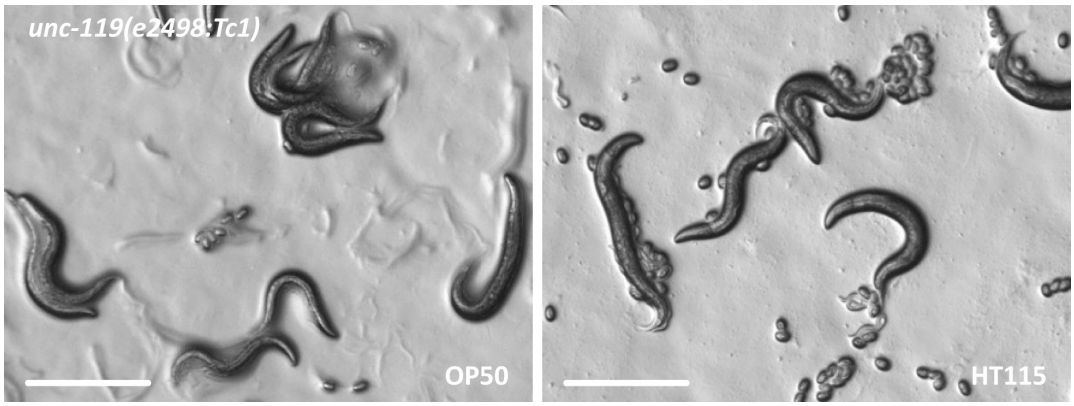

Figure 128 *unc-119(lf)* mutants grow faster into adulthood on HT115. Worms were synchronised as L1 larvae and grown on OP50 or HT115 at 20°C. Pictures were taken 72 hours later.

7.2.2.2 Apoptosis is more strongly affected in posterior gonad

The reproductive system of *C. elegans* is a symmetric organ with two gonads extending from the vulva and describing a U-shaped turn: one anteriorly and one posteriorly [see *2.2 The germ line of C. elegans and germ line modelling*]. The zones of late meiotic prophase cells, to which germ cell apoptosis is restricted, localise to the two gonad loop regions that are maximally distant. The anterior loop is just behind the pharyngeal bulb; the posterior loop reaches close to the tail. So far, the two gonads had been assumed to be functionally identical, also with regard to cell death. I realized that often, within individual animals grown on HT115, germ cell apoptosis levels were markedly higher in the posterior gonad. I inspected data points from many independent experiments where wildtype worms had been feeding either on HT115 or on OP50. In irradiated worms, there was a moderate but statistically significant difference between the average number of corpses in the anterior and the posterior gonads on HT115, whereas on OP50 the scores were identical (Figure 129). This suggests that the effect on apoptosis by the bacterial strain follows a mechanism involving local environments or a gradient within the animal. (Interestingly, I had seen the inverse of these effects of HT115 in a particular mutant fed on OP50: generally higher corpse numbers in the anterior gonad, and completely abolished apoptotic response to irradiation in both gonads [see Figure 36 in *4.6.1.4 A new allele of rpo-1b, F14B4.3(ok1970), leads to apoptotic defect*])

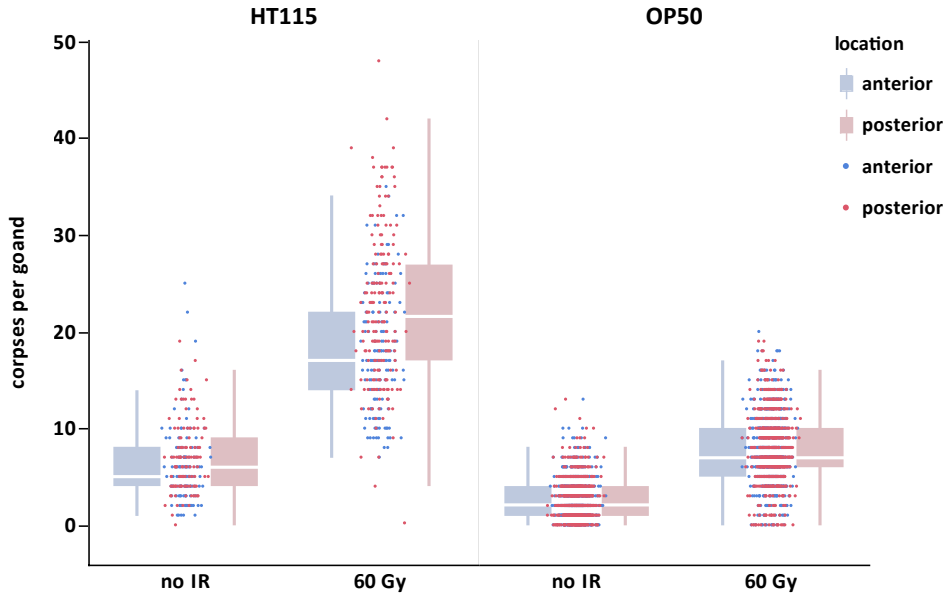

Figure 129 Position-dependent effect for the number of apoptotic corpses in worms fed on HT115. Pool of data from multiple independent experiments where wildtype N2 worms were grown on either HT115 or OP50 starting at L1 stage. Irradiation was 12 hours post L4 and corpses were counted 24 hours later randomly in the anterior or posterior gonad. Each point indicates one gonad; Outlier Box Plots separately for anterior (blue, left) and posterior (red, right) gonads indicating the 25th and 75th percentiles and the median (white horizontal line), which was very close to the mean for all groups. Analysis and graphing was performed with JMP 9.0 Software.

7.2.3 Conclusion for the effect of food type in apoptosis regulation

Some properties of bacteria largely influence the number of germ cell corpses in the predatory worms. Constitutive as well as irradiation-induced corpse levels are dominantly increased when worms are fed on HT115 bacteria instead of OP50. This is to consider when findings in mutants are compared with

RNAi experiments. The effect from the bacteria can be very pronounced and easily double the number of corpses found per gonad.

The food type was shown to influence other physiological parameters such as body size or lifespan. We have found that some bacteria also enhance aberrant vulval induction of *let-60(gf)*. Since there is a consistent pattern of bacteria type and phenotypes, they are likely to result from a common stimulus. We suggest that the Ras/MAPK pathway could be the central mediator. The enhancement of vulval induction by some bacteria is a strong indicator that the Ras/MAPK pathway is activated. That an effect on Ras/MAPK could be underlying the apoptotic phenotype is in agreement with our observation that Ras/MAPK activity is decisive for the levels of germ cell corpses, particularly in response to irradiation.

Could the effect on apoptosis be relevant for animal health in the pool of potentially noxious food? It is conceivable that increased germ cell apoptosis protects from pathogenic influences. Defects in apoptosis due to loss of *ced-3* or *ced-4* function were shown to sensitize worms towards Salmonella infection (Aballay 2001). However, the increase is unlikely to be a response to infection signalling, as mutants of the main infection-associated MAP kinase *pmk-1* also show the difference between bacteria types.

Besides increased death, the higher corpse number could be a result of reduced cellular uptake by the gonadal sheath cells (or the neighbouring cells in the soma). We have not been able to clearly distinguish which effect prevails. The observation of slightly less extra surviving Pn.aap cells would speak more for a pro-apoptotic effect than for reduced engulfment. However, the food-type induced difference of corpse numbers in L1 heads and in the germ line seems to depend on certain engulfment signalling factors. Simultaneously, the experiments revealed that at least *ced-2* might play a role in cell death as well. Further experiments are needed to determine the role of engulfment signalling in germ cell death and in the food type response.

We have found that a further germ line phenotype, distal oogenesis and associated ectopic apoptosis (termed Gogo) that occurs in in *rpo-1b(op259)* mutants was strongly enhanced by RNAi bacteria. This is an indication that the food type might become highly relevant in multiple conditions where basic biological processes are perturbed. The simplicity in the combination of a genetic model organism with mainly one food source makes *C. elegans* an ideal system to study the influence of food type on organism physiology. It should help to search for factors in the food, in the perception of these factors, or in the downstream signalling, and thus to ample our knowledge on the interactions of environmental influences with healthy or pathologic tissues.

8 Additional findings, Assays, Alleles, Resources

Chapter 8

8.1 Additional findings on germ cell apoptosis

8.1.1 *cct-2(RNAi)* reduces IR-induced apoptosis

I accidentally included an RNAi clone targeting T21B10.7 in my experiments of IR-induced apoptosis. Knockdown of this gene starting at L1 stage in N2 wildtype worms blocked the apoptotic response to ionizing irradiation (*empty(RNAi)*: 13.8 ±4.3 corpses (n=36), T21B10.7*(RNAi)*: 4.6 ±3.9 corpses (n=16)). T21B10.7 encodes the subunit *cct-2* of the eukaryotic cytosolic chaperonin (TCP1 complex). I have not followed this observation any further.

8.1.2 *hcf-1* regulates irradiation response

The group of Winship Herr in Lausanne contacted us to test the role of *hcf-1* in DNA damage responses in the worm. *hcf-1* is the homolog of human herpes simplex virus (HSV) host cell factor, a transcriptional coregulator with histone deacetylase activity. They had described the function of this gene in epigenetic regulation of histone H3 serine 10 phosphorylation status and in embryonic mitosis and cytokinesis (Lee 2007d). Also, they had found that in mammalian cells, HCF-1 binds E2F1 and modulates its effects on DNA damage-induced apoptosis (Tyagi 2009). With Christina Dittrich, we tested the effect of UV-C and IR irradiation on embryonic survival and on germ cell apoptosis in the two mutants *hcf-1(ok559)* and *hcf-1(pk924)* that they had characterised. Both alleles led to increased embryonic lethality following UV-C irradiation. The *hcf-1(ok559)* mutant was also hypersensitive to IR (15 Gy). The two alleles also diverged in their effect on irradiation-induced apoptosis. Both mutant strains had reduced apoptotic response to UV-C. *hcf-1(pk924)* mutants did not show any increase of apoptotic corpses following irradiation, whereas the number of corpses increased in *hcf-1(ok559)* worms (Figure 130). Interestingly, other than in most genetic conditions that we tested in *7 Food type influences apoptosis levels and vulval development, hcf-1(ok559)* mutants did not have higher numbers of germ cell corpses on HT115 bacteria than on OP50, which might indicate a role for *hcf-1* in the food type effect on germ cell corpse levels [see Table 24].

Further anomalies: some *hcf-1(ok559)* worms had multinucleated cells in the germ line. In *hcf-1(pk924)*, we occasionally observed irregular nucleoli with large indentations.

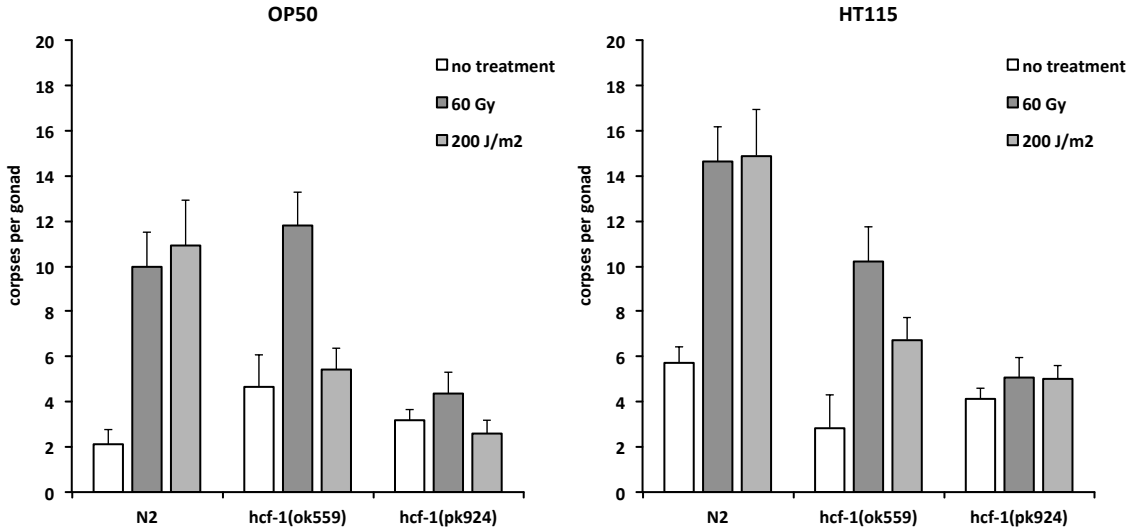

Figure 130 *hcf-1* mutants have a defective apoptotic response to UV-C irradiation. *hcf-1(pk924)* is also defective for IR-induced death. *hcf-1(ok559)* does not show the increase of corpse levels typically seen in wildtype when grown on HT115 instead of OP50. Error bars represent 95 % CI of the mean of at least 20 animals.

8.1.3 Growing up with adult males increases germ cell corpse number

In populations of wildtype *C. elegans* growing in laboratory conditions, only few males can be found (usually much less than 1 %). The percentage of males increases in situations of stress (e.g., heat shock treatment) or in mutant strains (e.g., mutations of chromosome segregation factors leading to non-disjunction). In experimental genetic crosses, an excess of males is used for efficient cross-fertilisation of the hermaphrodites. If a young adult hermaphrodite is mated with a male, the herewith-transferred sperm dominates the hermaphrodite's own sperm and fertilises the oocytes, leading to cross-progeny. In the experiments described in *6.2.1.6 unc-119 alleles are likely recessive*, I wanted to analyse animals that were heterozygous for various mutations and transgenes regarding irradiation-induced germ cell apoptosis. I therefore analysed the F1 cross-progeny from a cross of N2 wildtype males with the homozygous mutants of interest. In the control experiment (N2 males crossed with N2 hermaphrodites), I detected higher numbers of germ cell corpses than in the progeny of self-fertilising N2 hermaphrodites (Figure 114). I had grown the F1 cross-progeny on the mating plate, where the parental generation was still present and where up to 50 % of the growing larvae were males, and had separated the hermaphrodites as L4 larvae for the experiment. I considered possible explanations for the higher levels in cross-progeny animals: 1) Animals deriving from a father's sperm have different physiology from those conceived with a hermaphrodite's sperm. 2) The contact with males or their presence in the population produces a signal that leads to higher corpse numbers in the hermaphrodite's germ line. The possibility that the increased levels are from insemination with males' sperm of the F1 adult hermaphrodites themselves was already excluded, as they had been separated from males before young adulthood. To distinguish between the two possibilities, I grew self or cross-progeny animals in the presence or absence of extra-added males. On mating plates, 5 L4 stage hermaphrodites were joined with 20 young males or left alone. The resulting progeny was transferred to new plates as eggs. In the progeny from the cross, approximately 50 % of the animals would turn out to be males at later stages. To approximately 60 (cross-progeny) or 40 (self-progeny) eggs, 20 young adult wildtype males were

added or not. The F1 hermaphrodites were separated from the mating plates as L4 stage larvae and IR irradiated 12 hours later. I found an increase in the number of germ cell corpses in hermaphrodites grown in the presence of extra-added males (Figure 131). Thus, the contact during larval stages with adult males increases the number of cell corpses observed in grown-up animals without further contact. I cannot conclude whether the moderate increases when comparing self-progeny with cross-progeny are due to cross-fertilisation or due to the F1 cross-progeny males that grow up together with the hermaphrodites.

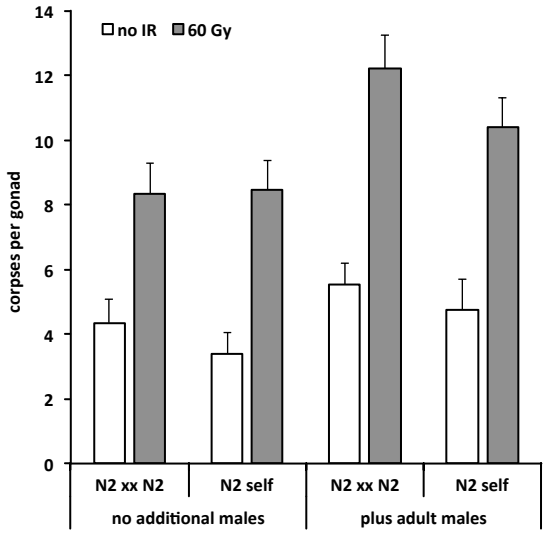

Figure 131 The presence of adult males increases the number of germ cell corpses. L4 stage hermaphrodites were separated from the crossing plate and irradiated 12 hours thereafter. Germ cell corpses were counted 24 hours later. Average number of corpses per gonad; the experiment was run in duplicate; error bars represent 95 % CI of the mean of all animals (total n=40 per condition).

8.2 Frequently used assays

8.2.1 Timing of experiments

The delay of developmental progression and temperature sensitivity of *rpo-1b(op259)* had implications on most experiments and had to be considered in all experiment planning [*5.1 Phenotypic Characterisation of the rpo-1b(op259) mutant*]. Developmental delay of embryos and larvae, and slowed maturation of the germ line in young adults required adjustment of the reference time points. I usually performed germ cell apoptosis experiments with a deferral of 24 hours in *rpo-1b(op259)* to compensate for the delay in larval growth and oocyte maturation. Since different mutant and double mutant constellations led to varying delay, I commonly set that moment as the reference when the first eggs had been laid by a synchronous worm population, and I irradiated worms at that time point. Some experiments included treatment of gravid adults; *rpo-1b(op259)* mutants needed at least 24 hours longer to be in a steady state of germ cell turn-over, that is, balance of germ cell proliferation and progression into oocytes/embryos. Accordingly, I timed the treatment and collection of samples to the age when the majority of the adult worm population had started laying eggs; I chose the timeframe when the eggs on the bacterial lawn would already clearly outnumber the parents but when no progeny had hatched yet. This orienting to the germ line age seemed appropriate when I measured transcription or translation mostly with focus on the gonad. This was the case with qRT-PCR and northern blot experiments, or with immunofluorescence staining, for instance. Also, I had to be very careful with temperature settings. *rpo-1b(op259)* mutants were highly sensitive to variations in temperature. All worms were strictly kept at 20°C (or at another, well fixed temperature) when grown for an experiment.

8.2.2 Apoptosis

Different methods have been established in different systems to define, detect and count apoptotic cells at various stages of the apoptotic process (Galluzzi 2009). Apoptotic assays for *C. elegans* have been reviewed in (Schwartz 2007) and with a special focus on cell clearance in (Lu 2009).

8.2.2.1 Scoring of apoptotic germ cell corpses by DIC

The number of germ cell corpses was the major read-out in my experiments. Nomarski optics allows to observe any cell in the transparent worm by phase contrast, including the germ cells that impose as a mostly regular arrangement of nuclei with large nucleoli [*2.2 The germ line of C. elegans and germ line modelling*]. In wildtype germ lines, apoptotic cells become visible as highly refractile discs and are easily identified at a progressed state of cell death execution. Early corpses are apparent as nucleated cells with a distinct, round cellular border but are more likely to be missed. In some of the mutant conditions studied here, apoptotic cells – defined by suppressibility with *ced-3(lf)* – had deviant morphology like increased cell size, granularity, or persistence of nuclei/nucleoli.

I counted the cumulative number of apoptotic cells in all optical planes of the gonad bend region. For each score, I added the information whether it was from an anterior or a posterior gonad; I considered anterior and posterior gonads of an individual worm as independent. I randomly selected worms on an agar slide, focused on one gonad bend region and assessed whether it was optically clear for complete scoring. In one experimental replicate, I usually scored 20 gonads per condition. Retrospectively,

anterior and posterior gonads were represented in a balanced fashion. As the steady state corpse number increases in aging adults, I assessed cell death at defined intervals after a reference time point. Normally, the L4 stage is a well defined reference; since many of the mutants I worked with exhibited delayed maturation of the reproductive system post L4, I chose the time point as the reference when most worms had developing embryos inside their uterus and when the first few eggs could be found on the plate.

8.2.2.2 Scoring of apoptotic germ cell corpses with fluorescent markers

Different transgenes are available that express fluorescently tagged proteins specifically in the engulfing cells. If enriched in the protrusion of the engulfing cell around an apoptotic cell, the markers form a halo highlighting the apoptotic corpse. Depending on the role of the tagged protein in engulfment, it is recruited around the corpse at certain stages of the engulfment process. Different markers therefore might highlight different sets of corpses and vary in the detected number of apoptotic cells; this number usually also differs from the number of corpses counted by DIC. In this work used the two transgenes *bcIs39[P_{lim-7}::ced-1::gfp; lin-15(+)]* and *opIs110[P_{lim-7}::yfp::act-5; unc-119(+)]*.

8.2.2.3 Irradiation of young adult hermaphrodites

Most of the irradiation treatments were performed at the reference time point described above. I irradiated well-fed worms on agar plates with a short pulse of UV-C in a Stratalinker, or with X-rays in an Isovolt irradiation device that applied 60 Gy in 18.5 min. All samples were placed within an irradiation area that received at least 95 % of the maximal dose. For some experiments, I followed the time course of apoptotic corpse numbers following irradiation; in many cases, I selectively scored at 24 hours, when the irradiation-induced corpse number was tending towards a plateau and when the germ lines were still mostly intact.

8.2.2.4 Corpse accumulation in the L1 head of engulfment mutants

Many of the programmed cell deaths occur during embryogenesis. Whereas in wildtype worms, the apoptotic corpses are swiftly removed by neighboring cells, in engulfment mutants, they persist into larval stages. The head region offers a circumscript area with a high number of cell death events, yielding approximately 20 residual non-engulfed cells in L1 larval heads of engulfment defective mutants. To get well-synchronized animals for scoring, I washed off all crawling worms from bacterial plates so only the sticky eggs would remain and I picked freshly hatched larvae one hour after washing; the animals were thus well staged within an hour from hatching.

8.2.2.5 Extra cell survival in Pn.aap ventral nerve cord cells

In wildtype larvae, only six out of the 13 ventral cord Pn.aap neurons that are generated during development survive; the other seven are removed by programmed death. In a *ced-3(lf)* situation, none of the cells can undergo apoptosis and 13 cells remain (one has weak fluorescence and is usually not considered). With the transgene *nIs96*, all surviving Pn.aap cells are highlighted by a GFP reporter expressed under the P_{lin-11} promoter, starting at the L3/L4 stage (Reddien 2001). This system can reveal both pro-apoptotic and anti-apoptotic conditions if set to a sensitized state: reduction of *ced-3* function causes some of the cells normally destined to die to survive instead. Loss of pro-apoptotic cues further increases, and loss of anti-apoptotic cues reduces the number of extra surviving cells.

8.2.3 Germ line proliferation and embryonic health

8.2.3.1 Egg laying rate

To assess fertilization rate, I transferred a small number of well-fed animals of a defined age (usually 24 hours after the young adult reference time point [see above]) to fresh plates and let them lay eggs for some hours (usually six). The total number of eggs on the plate allowed to derive the average number of eggs laid per animal per hour. Several replicates were run in parallel.

8.2.3.2 Embryonic survival

Embryonic survival expresses the fraction of laid eggs that produce viable larvae. I transferred a small number of adult worms to fresh plates – usually 24 hours after DNA damaging (or control) treatment – let them lay eggs for a short duration (usually 4 hours) and then removed all adults from the plates again; at this point, I counted the total number of eggs on each plate. Most larvae should have hatched within 12 hours after the eggs had been laid; however, I realized that for some mutants and individuals, hatching would happen later. I therefore counted the number of non-hatched eggs – in contrast to earlier methods – 24 hours after egg laying. Possibly, earlier scores of embryonic lethality yielded aberrantly high ratios due to late hatching larvae.

8.2.4 Vulval induction

The six pairs of vulval precursor cells are instructed to adopt a certain fate mainly by signalling from the anchor cell (EGFR/Ras) and by lateral crosstalk (Notch). Some mutants of the EGFR/Ras/MAPK signalling pathway lead to apparent vulval defects whereas other mutations lead to obvious alterations only in synthetic combination. Aberrant vulval inductions can be observed either as extra vulvae (Muv) or a missing vulva (Vul) in adult animals, and more accurately with DIC microscopy of L4 larvae at the vulval Christmas tree stage (Sternberg 1986). Itay Nakdimon kindly instructed me how to score abnormal vulval induction events by the latter method. The vulval induction index represented the average number per animal of VPCs that had adopted a 1° or 2° vulval fate (in wildtype, VI index is 3.0).

8.2.5 RNAi experiments

Gene expression knockdown is most conveniently performed in *C. elegans* with RNAi by feeding. Comprehensive bacterial libraries with clones expressing double stranded RNA to target most genes have facilitated this approach (Kamath 2003; Rual 2004a). In my experiments, I grew the bacteria on tetracycline/ampicillin plates and amplified them in liquid medium before seeding fresh NGM agarose plates supplemented with ampicillin and 3 mM IPTG for efficient induction of dsRNA transcription. The worm populations were synchronised by bleaching of gravid hermaphrodites; depending on the stage when RNAi had to be initiated, freshly hatched L1 larvae were either transferred to the RNAi plates directly, or they were grown on OP50 seeded plates until reaching the appropriate stage and were then washed and transferred to RNAi plates. As controls, an empty vector RNAi clone and a clone targeting *unc-22*, leading to a twitching Unc phenotype already in the first treated generation if the RNAi effect was sufficient, were always included.

8.2.6 RNA or protein extraction

For extraction of DNA, RNA, or proteins from synchronised adult worms, I bleached the parental population, let the isolated eggs hatch in the absence of food, and transferred the L1 larvae to seeded plates, where the worms were feeding until reaching the right stage for collection. Because a worm population is not perfectly synchronised and the young adults start producing and laying eggs at slightly different time points, and even more because different mutant strains did not enter adulthood at the same time after bleaching or the L4 reference stage, I waited for the vast majority of worms in a population to be laying eggs (approximately 24 hours post L4 for N2 wildtype). This way, most adult hermaphrodites were in a steady state of oocyte production and egg laying and carried a similar number of embryos [see above]. In irradiation experiments, this was chosen as time point of treatment. For collection, I carefully washed the worms off the plates, which would leave the already laid eggs behind on the plate. To separate gravid adults from occasional larvae that had hatched already, and to clean the worms from bacteria, I repeatedly let the adult worms settle by gravitation for 5 minutes and replaced the supernatant with fresh buffer. The purified worms were shock-frozen in liquid nitrogen before storage at -80°C and further processing.

8.2.7 Dot-Blot protocol for CPD lesions

[See *3.2.2.1* Repair kinetics of CPD lesions]. I first tested a fast procedure with worm lysis by the common worm lysis protocol (worm lysis buffer containing proteinase K (The Nematode Caenorhabditis elegans 1988)) or even more crudely by quick boiling in NaOH/EDTA, which would allow parallel processing of many samples. With this crude and rapid protocol, I was able to produce a signal that correlated with the number of worms in a sample. The signal was stronger with the NaOH/EDTA than with the worm lysis buffer method. There was, however, no clear trend of the signal intensity between samples collected at different time points after UV-treatment; most of the signal was from non-specific binding of the antibodies to the crude worm samples, since non-irradiated worms gave only mildly lower signals than irradiated worms. I therefore had to adjust the protocol and implement a proper DNA extraction step; also, instead of incubating the worms in liquid buffer without food after irradiation, I transferred them back to bacteria (except for the very early time points):

- Collection of adult worms from bacterial plates, repeated washing to remove most bacteria, and transfer with physiological buffer into an open dish for UV-C treatment
- Irradiation and aliquoting of the worm sample onto OP50 seeded plates
- At all time points of interest, collection of worms 15 min before freezing, repeated washing in buffer, shock freezing in liquid nitrogen
- DNA extraction using the tissue lysis protocol of the Qiagen “DNeasy Blood and Tissue kit” with lysis at 55°C for >4 hours
- Optionally, digestion of the DNA into smaller fragments by restriction with EcoRI
- Optionally, digestion of residual RNA with RNase H
- Quantification of DNA concentration and preparation of equal amounts of DNA denaturation and transfer to Dot-Blot wells, flow-through of the samples by suction, and heat fixation of DNA on the membrane
- Detection of CPDs by immunochemistry.

With this method, the signal intensity of irradiated worms was significantly higher than of non-irradiated controls. As a further control, I extracted DNA from non-irradiated worms and UV-C-irradiated the DNA in solution with different doses of UV-C. The signal intensity correlated with the dose applied.

8.2.7.1 Normalization to rDNA

I thought of a way to normalize for the amount of DNA fixed onto the membrane. There are antibodies available that recognize eukaryotic DNA (which we successfully used for immunofluorescence). Instead, I decided for a hybridization protocol with DIG-labeled DNA-probes. The rDNA of *C. elegans* is organized as a tandem repeat of approximately 55 nearly identical sequence units [see *4.1.8 Ribosome synthesis in C. elegans*] and therefore lent itself as an abundant target that should be proportional to the number of genomes and thus the amount of DNA on one dot. I designed a probe complementary to the 26S rDNA (rDNA-26S); to control for potential interference with residual ribosomal RNA in the samples, I made an additional probe that would anneal to intergenic sequences of the rDNA (rDNAext) and thus not find relevant rRNA in the samples to bind to.

To determine whether the approach would yield linear dose-signal relations, I loaded a two-dimensional array of serial dilutions of worm DNA that had been irradiated after extraction with different doses of UV-C. CPD signals correlated well with DNA amount and UV-dose (Figure 132). Also, the rDNA-26S and rDNAext probes both gave a linear relationship of signal intensity and DNA amount loaded (the ratio of rDNA-26S to rDNAext was thus quite stable). Unfortunately, the great dose-signal relationship for the CPD signal and for the amount of DNA was deteriorated when the immunochemical and hybridization protocol were applied successively to the same membrane. Relatively less rDNA signal appeared from the spots that had had a high CPD signal, probably due to some hindrance to probe hybridization by remaining antibody; thus, given equal DNA loading, samples with high CPD density would have a lower DNA signal. At least, when normalizing CPDs to the loading amount of DNA, this would exaggerate and not annihilate CPD differences between samples.

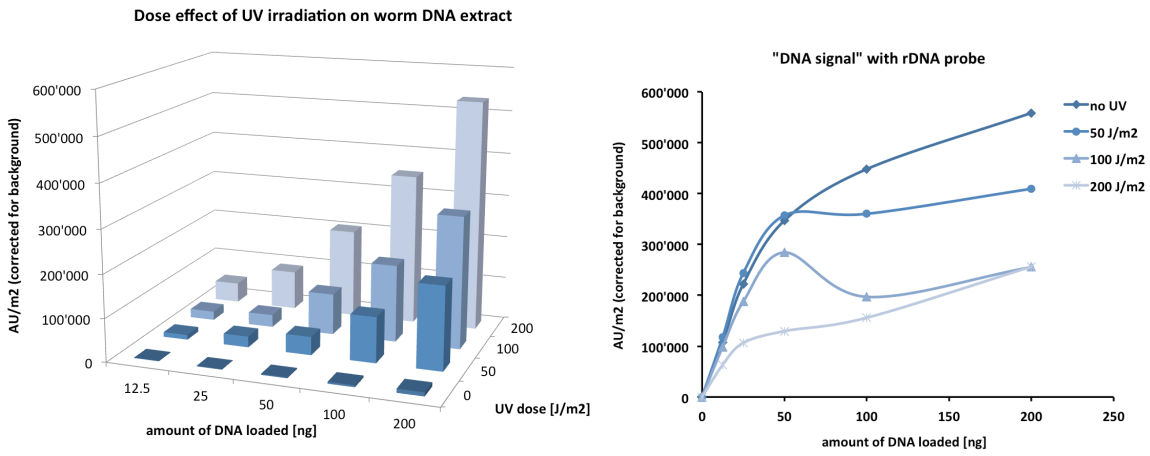

Figure 132 Evaluation of the Dot-Blot blot method to quantify CPD lesions in worm DNA. Left: CPD signal intensity on Dot-Blot membrane with DNA that had been irradiated after extraction from adults worms. Right: The signal of the DIG-labelled DNA probe (rDNA-26S) was influenced by the amount of antibody having bound CPD lesions on the same membrane spot previously.

8.3 Frequently used alleles in this study

rpo-1b(op259)

RNA polymerase I beta subunit. Typical EMS-induced C→T transition in the second exon of F14B4.3, at position 263 of the genomic ORF. Leads to P70S substitution in the F14B4.3 gene product, which we provisionally named RPO-1B. See Figure 35 and *4.3 Characterisation of the rpo-1b(op259) allele*. I used the multiply backcrossed strain WS2721 (source: Jen Hofmann) for all experiments.

cep-1(gk138)

C. elegans p53 homolog. Deletion in ORF likely leading to full loss of *cep-1* function. The effect of this mutation was found to differ from another frequently used allele, *cep-1(lg12501)*. Probably, the product of *cep-1(lg12501)* retains some function (Waters 2010).

egl-1(n1084 n3082)

BH3-only protein. *n3082* is an intragenic suppressor mutation of the *egl-1* gain-of-function allele *n1084* (itself a sequence alteration in a critical promoter element). Deletion of 5 nucleotides in *n3082*, leading to a frameshift upstream of the BH3-like region, that is elemental for EGL-1 function (Conradt 1998).

ced-9(n1653)

C. elegans Bcl2 homolog. T→A transversion in the second exon of T07C4.8, at position 493 of the genomic ORF. Leads to Y149N in CED-9, a substitution at a predicted phosphorylation site for Src type kinases. See *5.6.1.3 The temperature sensitive ced-9(n1653) mutant is a viable approach to ced-9 function*.

let-60(n1046gf)

C. elegans Ras homolog. Dominant gain-of-function mutation in codon 13, leading to Gly→Glu. An identical mutation was found in five independent dominant Muv (Multivulva) mutants. Substitution leads to constitutive activation of Ras (Beitel 1990).

unc-119(ed3)

C → T non-sense mutation in penultimate exon (Maduro 1995). Similar to *unc-119(ed4)* and *unc-119(e2438)*, it truncates the protein upstream of an SH2 domain binding region (Figure 113).

8.4 Cancer epidemiology resources

The epidemiological numbers on cancer as mentioned in the introductory chapter *1.3 Human cancer* are estimates based on highly complex survey data. Incidence and mortality rates are of variable accuracy in different countries and geographical regions; only a fraction of the cases is usually reported. Moreover, the available statistical numbers do not cover identical time periods. Whenever trends and projections are calculated, differences in the age structure of populations have to be accounted for. Thus, except for (absolute) incidence numbers, epidemiological values are derived from theoretical considerations and intricate calculations. Several national and international programs are dedicated to studying and reporting the epidemiology of cancer. The World Health Organisation (WHO) regularly issues World Health Statistics reports (WHO); the International Agency for Research on Cancer (IARC), part of the WHO, has published regular estimates of the incidence of, and mortality rates from cancer worldwide for the past thirty years (IARC). The GLOBOCAN project, within the IARC, aims to provide contemporary estimates on the major types of cancer, at national level, for all countries of the world (GLOBOCAN). The European Network of Cancer Registries (ENCR) regularly disseminates information on incidence and mortality from cancer in the European Union and Europe (European Network of Cancer Registries (ENCR)); the American Cancer Society (ACS) provides analyses and summaries of national and international data (American Cancer Society).

The numbers above are extracted from interrelated data and reports of these institutions. A comprehensible overview of the global epidemiology of cancer was recently published in a second edition by the ACS (American Cancer Society 2011). The GLOBOCAM webpage allows access to detailed data on selectable countries or regions. Two publications address in detail the data collecting and analysis methods for the burden of cancer worldwide and in Europe in 2008 (Ferlay 2010b, 2010a). The IACR publication (Curado 2007) discusses in great detail the challenges of data collection and analysis, and lists the data sources for all geographical units included. Finally, the WHO statistics on Health put cancer into relation to other diseases by country and region [latest issue (World Health Organization 2011)].

References

Aas, P. A., Otterlei, M., Falnes, P. O., Vågbø, C. B., Skorpen, F., Akbari, M., Sundheim, O., Bjørås, M., Slupphaug, G., Seeberg, E., et al. (2003). Human and bacterial oxidative demethylases repair alkylation damage in both RNA and DNA. Nature *421*, 859-863.

Abada, E. A.-elmoniem, Sung, H., Dwivedi, M., Park, B.-J., Lee, S.-K., and Ahnn, J. (2009). C. elegans behavior of preference choice on bacterial food. Mol. Cells *28*, 209-213.

Aballay, A., Drenkard, E., Hilbun, L. R., and Ausubel, F. M. (2003). Caenorhabditis elegans innate immune response triggered by Salmonella enterica requires intact LPS and is mediated by a MAPK signaling pathway. Curr. Biol *13*, 47-52.

Aballay, A., and Ausubel, F. M. (2001). Programmed cell death mediated by ced-3 and ced-4 protects Caenorhabditis elegans from Salmonella typhimurium-mediated killing. Proc. Natl. Acad. Sci. U.S.A *98*, 2735-2739.

Abramoff, M., Magalhaes, P., and Ram, S. (2004). Image Processing with ImageJ. In Biophotonics International (Laurin Publishing Co. Inc.), pp. 36-42.

Ahmed, S., Alpi, A., Hengartner, M., and Gartner, A. (2001). C. elegans RAD-5/CLK-2 defines a new DNA damage checkpoint protein. Curr Biol *11*, 1934-44.

Ahmed, S., and Hodgkin, J. (2000). MRT-2 checkpoint protein is required for germline immortality and telomere replication in C. elegans. Nature *403*, 159-64.

Albertson, D. G. (1984). Localization of the ribosomal genes in Caenorhabditis elegans chromosomes by in situ hybridization using biotin-labeled probes. EMBO J *3*, 1227-34.

Allmang, C., Mitchell, P., Petfalski, E., and Tollervey, D. (2000). Degradation of ribosomal RNA precursors by the exosome. Nucleic Acids Research *28*, 1684-1691.

Alpadi, K., Magupalli, V. G., Käppel, S., Köblitz, L., Schwarz, K., Seigel, G. M., Sung, C.-H., and Schmitz, F. (2008). RIBEYE recruits Munc119, a mammalian ortholog of the Caenorhabditis elegans protein unc119, to synaptic ribbons of photoreceptor synapses. J. Biol. Chem *283*, 26461-26467.

American Cancer Society (2011). Global Cancer Facts & Figures 2nd Edition. Available at: http://www.cancer.org/Research/CancerFactsFigures/GlobalCancerFactsFigures/global-facts-figures-2nd-ed [Accessed July 13, 2011].

American Cancer Society Information and Resources for Cancer: Breast, Colon, Prostate, Lung and Other Forms. Available at: http://www.cancer.org/index [Accessed July 13, 2011].

Amsterdam, A., Sadler, K. C., Lai, K., Farrington, S., Bronson, R. T., Lees, J. A., and Hopkins, N. (2004). Many ribosomal protein genes are cancer genes in zebrafish. PLoS Biol *2*, E139.

Andersen, J. S., Lam, Y. W., Leung, A. K. L., Ong, S.-E., Lyon, C. E., Lamond, A. I., and Mann, M. (2005). Nucleolar proteome dynamics. Nature *433*, 77-83.

Andux, S., and Ellis, R. E. (2008). Apoptosis maintains oocyte quality in aging Caenorhabditis elegans females. PLoS Genet *4*, e1000295.

Aravind, L., and Koonin, E. (2001). The DNA-repair protein AlkB, EGL-9, and leprecan define new families of 2-oxoglutarate- and iron-dependent dioxygenases. Genome Biol *2*, RESEARCH0007.

Armache, J.-P., Jarasch, A., Anger, A. M., Villa, E., Becker, T., Bhushan, S., Jossinet, F., Habeck, M., Dindar, G., Franckenberg, S., et al. (2010a). Cryo-EM structure and rRNA model of a translating eukaryotic 80S ribosome at 5.5-A resolution. Proc. Natl. Acad. Sci. U.S.A *107*, 19748-19753.

Armache, J.-P., Jarasch, A., Anger, A. M., Villa, E., Becker, T., Bhushan, S., Jossinet, F., Habeck, M., Dindar, G., Franckenberg, S., et al. (2010b). Localization of eukaryote-specific ribosomal proteins in a 5.5-Å cryo-EM map of the 80S eukaryotic ribosome. Proc. Natl. Acad. Sci. U.S.A *107*, 19754-19759.

Artal-Sanz, M., de Jong, L., and Tavernarakis, N. (2006). Caenorhabditis elegans: a versatile platform for drug discovery. Biotechnol J *1*, 1405-1418.

Banerjee, S., An, S., Zhou, A., Silverman, R., and Makino, S. (2000). RNase L-independent specific 28S rRNA cleavage in murine coronavirus-infected cells. J Virol *74*, 8793-802.

Bartek, J., Bartkova, J., and Lukas, J. (2007). DNA damage signalling guards against activated oncogenes and tumour progression. Oncogene *26*, 7773-7779.

Beitel, G. J., Clark, S. G., and Horvitz, H. R. (1990). Caenorhabditis elegans ras gene let-60 acts as a switch in the pathway of vulval induction. Nature *348*, 503-509.

Bekker-Jensen, S., Lukas, C., Kitagawa, R., Melander, F., Kastan, M. B., Bartek, J., and Lukas, J. (2006). Spatial organization of the mammalian genome surveillance machinery in response to DNA strand breaks. J. Cell Biol *173*, 195-206.

Ben-Shem, A., Jenner, L., Yusupova, G., and Yusupov, M. (2010). Crystal structure of the eukaryotic ribosome. Science *330*, 1203-1209.

Berezikov, E., Bargmann, C. I., and Plasterk, R. H. A. (2004). Homologous gene targeting in Caenorhabditis elegans by biolistic transformation. Nucleic Acids Res *32*, e40.

Bergamaschi, D., Samuels, Y., O'Neil, N., Trigiante, G., Crook, T., Hsieh, J., O'Connor, D., Zhong, S., Campargue, I., Tomlinson, M., et al. (2003). iASPP oncoprotein is a key inhibitor of p53 conserved from worm to human. Nat Genet *33*, 162-7.

Berman, K., McKay, J., Avery, L., and Cobb, M. (2001). Isolation and characterization of pmk-(1-3): three p38 homologs in Caenorhabditis elegans. Mol. Cell Biol. Res. Commun *4*, 337-344.

Berset, T., Hoier, E. F., Battu, G., Canevascini, S., and Hajnal, A. (2001). Notch inhibition of RAS signaling through MAP kinase phosphatase LIP-1 during C. elegans vulval development. Science *291*, 1055-1058.

Bessler, J., Reddy, K., Hayashi, M., Hodgkin, J., and Villeneuve, A. (2007). A Role for Caenorhabditis elegans Chromatin-Associated Protein HIM-17 in the Proliferation vs. Meiotic Entry Decision. Genetics *175*, 2029-2037.

Biggiogera, M., Malatesta, M., Abolhassani-Dadras, S., Amalric, F., Rothblum, L. I., and Fakan, S. (2001). Revealing the unseen: the organizer region of the nucleolus. J. Cell. Sci *114*, 3199-3205.

Bloss, T. A., Witze, E. S., and Rothman, J. H. (2003). Suppression of CED-3-independent apoptosis by mitochondrial betaNAC in Caenorhabditis elegans. Nature *424*, 1066-71.

Boag, P. (2005). A conserved RNA-protein complex component involved in physiological germline apoptosis regulation in C. elegans. Development *132*, 4975-4986.

Boag, P. R., Nakamura, A., and Blackwell, T. K. (2005). A conserved RNA-protein complex component involved in physiological germline apoptosis regulation in C. elegans. Development *132*, 4975-86.

Boffetta, P., McLaughlin, J. K., La Vecchia, C., Tarone, R. E., Lipworth, L., and Blot, W. J. (2008). False-positive results in cancer epidemiology: a plea for epistemological modesty. J. Natl. Cancer Inst *100*, 988-995.

Boisvert, F.-M., van Koningsbruggen, S., Navascués, J., and Lamond, A. I. (2007). The multifunctional nucleolus. Nat. Rev. Mol. Cell Biol *8*, 574-585.

Boisvert, F.-M., Lam, Y. W., Lamont, D., and Lamond, A. I. (2010a). A quantitative proteomics analysis of subcellular proteome localization and changes induced by DNA damage. Mol. Cell Proteomics *9*, 457-470.

Boisvert, F.-M., and Lamond, A. I. (2010b). p53-Dependent subcellular proteome localization following DNA damage. Proteomics. Available at: http://www.ncbi.nlm.nih.gov/pubmed/21046615 [Accessed August 17, 2011].

Bolz, D. D., Tenor, J. L., and Aballay, A. (2010). A conserved PMK-1/p38 MAPK is required in Caenorhabditis elegans tissue-specific immune response to Yersinia pestis infection. J. Biol. Chem *285*, 10832-10840.

van den Born, E., Omelchenko, M. V., Bekkelund, A., Leihne, V., Koonin, E. V., Dolja, V. V., and Falnes, P. Ø. (2008). Viral AlkB proteins repair RNA damage by oxidative demethylation. Nucleic Acids Res *36*, 5451-5461.

Boulin, T., and Bessereau, J. (2007). Mos1-mediated insertional mutagenesis in Caenorhabditis elegans. Nat Protoc *2*, 1276-87.

Boulon, S., Westman, B. J., Hutten, S., Boisvert, F.-M., and Lamond, A. I. (2010). The nucleolus under stress. Mol. Cell *40*, 216-227.

Boulton, S. J., Martin, J. S., Polanowska, J., Hill, D. E., Gartner, A., and Vidal, M. (2004a). BRCA1/BARD1 orthologs required for DNA repair in Caenorhabditis elegans. Curr Biol *14*, 33-9.

Boulton, S., Martin, J., Polanowska, J., Hill, D., Gartner, A., and Vidal, M. (2004b). BRCA1/BARD1 orthologs required for DNA repair in Caenorhabditis elegans. Curr Biol *14*, 33-9.

Boyd, W., Crocker, T., Rodriguez, A., Leung, M., Lehmann, D., Freedman, J., Van Houten, B., and Meyer, J. (2010). Nucleotide excision repair genes are expressed at low levels and are not detectably inducible in Caenorhabditis elegans somatic tissues, but their function is required for normal adult life after UVC exposure. Mutat Res *683*, 57-67.

Brenner, S. (1974). The genetics of Caenorhabditis elegans. Genetics *77*, 71-94.

Brooks, K. K., Liang, B., and Watts, J. L. (2009). The influence of bacterial diet on fat storage in C. elegans. PLoS ONE *4*, e7545.

Brueckner, F., Ortiz, J., and Cramer, P. (2009). A movie of the RNA polymerase nucleotide addition cycle. Curr. Opin. Struct. Biol *19*, 294-299.

Brunet, A. (2007). Aging and cancer: killing two birds with one worm. Nat Genet *39*, 1306-7.

Brégeon, D., and Sarasin, A. (2005). Hypothetical role of RNA damage avoidance in preventing human disease. Mutat Res *577*, 293-302.

Bushnell, D., and Kornberg, R. (2003). Complete, 12-subunit RNA polymerase II at 4.1-A resolution: implications for the initiation of transcription. P Natl Acad Sci Usa *100*, 6969-73.

Bustin, S. (2002). Quantification of mRNA using real-time reverse transcription PCR (RT-PCR): trends and problems. J Mol Endocrinol *29*, 23-39.

Butschi, A., Titz, A., Wälti, M. A., Olieric, V., Paschinger, K., Nöbauer, K., Guo, X., Seeberger, P. H., Wilson, I. B. H., Aebi, M., et al. (2010). Caenorhabditis elegans N-glycan core beta-galactoside confers sensitivity towards nematotoxic fungal galectin CGL2. PLoS Pathog *6*, e1000717.

CGC Caenorhabditis Genetics Center University of Minnesota. Available at: http://www.cbs.umn.edu/CGC/ [Accessed July 7, 2011].

Carmona-Gutierrez, D., Eisenberg, T., Büttner, S., Meisinger, C., Kroemer, G., and Madeo, F. (2010). Apoptosis in yeast: triggers, pathways, subroutines. Cell Death Differ *17*, 763-773.

Cavanaugh, A. (2002). Rrn3 Phosphorylation Is a Regulatory Checkpoint for Ribosome Biogenesis. Journal of Biological Chemistry *277*, 27423-27432.

Cavanaugh, A. H., Hempel, W. M., Taylor, L. J., Rogalsky, V., Todorov, G., and Rothblum, L. I. (1995). Activity of RNA polymerase I transcription factor UBF blocked by Rb gene product. Nature *374*, 177-180.

Cen, O., Gorska, M. M., Stafford, S. J., Sur, S., and Alam, R. (2003). Identification of UNC119 as a novel activator of SRC-type tyrosine kinases. J. Biol. Chem *278*, 8837-8845.

Ceol, C. J., and Horvitz, H. R. (2001). dpl-1 DP and efl-1 E2F act with lin-35 Rb to antagonize Ras signaling in C. elegans vulval development. Mol. Cell *7*, 461-473.

Chen, F., Hersh, B., Conradt, B., Zhou, Z., Riemer, D., Gruenbaum, Y., and Horvitz, H. (2000). Translocation of C. elegans CED-4 to nuclear membranes during programmed cell death. Science *287*, 1485-9.

Chen, L., McCloskey, T., Joshi, P., and Rothman, J. (2008). ced-4 and Proto-Oncogene tfg-1 Antagonistically Regulate Cell Size and Apoptosis in C. elegans. Curr Biol *18*, 1025-33.

Chi, W., and Reinke, V. (2009). DPL-1 (DP) acts in the germ line to coordinate ovulation and fertilization in C. elegans. Mech. Dev *126*, 406-416.

Chi, W., and Reinke, V. (2006). Promotion of oogenesis and embryogenesis in the C. elegans gonad by EFL-1/DPL-1 (E2F) does not require LIN-35 (pRB). Development *133*, 3147-3157.

Chong, R., Ke-zhou, C., and Zeng-liang, Y. (2009). Induction of germline apoptosis by cobalt and relevant signal transduction pathways in Caenorhabditis elegans. Toxicol. Mech. Methods *19*, 541-546.

Chonghaile, T. N., and Letai, A. (2008). Mimicking the BH3 domain to kill cancer cells. Oncogene *27 Suppl 1*, S149-157.

Church, D. L., Guan, K. L., and Lambie, E. J. (1995). Three genes of the MAP kinase cascade, mek-2, mpk-1/sur-1 and let-60 ras, are required for meiotic cell cycle progression in Caenorhabditis elegans. Development *121*, 2525-2535.

Chédin, S., Laferté, A., Hoang, T., Lafontaine, D. L. J., Riva, M., and Carles, C. (2007). Is ribosome synthesis controlled by pol I transcription? Cell Cycle *6*, 11-15.

Ciarmatori, S., Scott, P. H., Sutcliffe, J. E., McLees, A., Alzuherri, H. M., Dannenberg, J. H., te Riele, H., Grummt, I., Voit, R., and White, R. J. (2001). Overlapping functions of the pRb family in the regulation of rRNA synthesis. Mol. Cell. Biol *21*, 5806-5814.

Ciccia, A., and Elledge, S. (2010). The DNA damage response: making it safe to play with knives. Molecular Cell *40*, 179-204.

Clapp, R. W., and Kriebel, D. (2009). Re: False-positive results in cancer epidemiology: a plea for epistemological modesty. J. Natl. Cancer Inst *101*, 211-212; author reply 213-214.

Clark, S. G., Lu, X., and Horvitz, H. R. (1994). The Caenorhabditis elegans locus lin-15, a negative regulator of a tyrosine kinase signaling pathway, encodes two different proteins. Genetics *137*, 987-997.

Cleaver, J. (2005). Cancer in xeroderma pigmentosum and related disorders of DNA repair. Nat Rev Cancer *5*, 564-73.

Cogliano, V., and Straif, K. (2010). Re: False-positive results in cancer epidemiology: a plea for epistemological modesty. J. Natl. Cancer Inst *102*, 134; author reply 134-135.

Collis, S., Barber, L., Clark, A., Martin, J., Ward, J., and Boulton, S. (2007). HCLK2 is essential for the mammalian S-phase checkpoint and impacts on Chk1 stability. Nat Cell Biol *9*, 391-401.

Collis, S., Barber, L., Ward, J., Martin, J., and Boulton, S. (2006). C. elegans FANCD2 responds to replication stress and functions in interstrand cross-link repair. DNA Repair *5*, 1398-1406.

Conradt, B., and Horvitz, H. R. (1998). The C. elegans protein EGL-1 is required for programmed cell death and interacts with the Bcl-2-like protein CED-9. Cell *93*, 519-529.

Contreras, V., Richardson, M. A., Hao, E., and Keiper, B. D. (2008). Depletion of the cap-associated isoform of translation factor eIF4G induces germline apoptosis in C. elegans. Cell Death Differ *15*, 1232-1242.

Cragg, M. S., Harris, C., Strasser, A., and Scott, C. L. (2009). Unleashing the power of inhibitors of oncogenic kinases through BH3 mimetics. Nat. Rev. Cancer *9*, 321-326.

Cramer, P. (2000). Architecture of RNA Polymerase II and Implications for the Transcription Mechanism. Science *288*, 640-649.

Cramer, P. (2002). Multisubunit RNA polymerases. Current Opinion in Structural Biology *12*, 89-97.

Cramer, P. (2001). Structural Basis of Transcription: RNA Polymerase II at 2.8 Angstrom Resolution. Science *292*, 1863-1876.

Crittenden, S., Leonhard, K., Byrd, D., and Kimble, J. (2006). Cellular analyses of the mitotic region in the Caenorhabditis elegans adult germ line. Molecular Biology of the Cell *17*, 3051-61.

Crosignani, P. (2009). Re: False-positive results in cancer epidemiology: a plea for epistemological modesty. J. Natl. Cancer Inst *101*, 212-213; author reply 213-214.

Curado, M., and International Agency for Research on Cancer.;World Health Organization. (2007). Cancer incidence in five continents. (Lyon: I.A.R.C.).

Defossez, P. A., Park, P. U., and Guarente, L. (1998). Vicious circles: a mechanism for yeast aging. Curr Opin Microbiol *1*, 707-11.

Degen, W., Pruijn, G., Raats, J., and van Venrooij, W. (2000). Caspase-dependent cleavage of nucleic acids. Cell Death Differ *7*, 616-27.

Deisenroth, C., and Zhang, Y. (2010). Ribosome biogenesis surveillance: probing the ribosomal protein-Mdm2-p53 pathway. Oncogene *29*, 4253-4260.

van Delft, M. F., Wei, A. H., Mason, K. D., Vandenberg, C. J., Chen, L., Czabotar, P. E., Willis, S. N., Scott, C. L., Day, C. L., Cory, S., et al. (2006). The BH3 mimetic ABT-737 targets selective Bcl-2 proteins and efficiently induces apoptosis via Bak/Bax if Mcl-1 is neutralized. Cancer Cell *10*, 389-399.

Deng, X., Hofmann, E. R., Villanueva, A., Hobert, O., Capodieci, P., Veach, D. R., Yin, X., Campodonico, L., Glekas, A., Cordon-Cardo, C., et al. (2004). Caenorhabditis elegans ABL-1 antagonizes p53-mediated germline apoptosis after ionizing irradiation. Nat Genet *36*, 906-12.

Deng, X., Yin, X., Allan, R., Lu, D. D., Maurer, C. W., Haimovitz-Friedman, A., Fuks, Z., Shaham, S., and Kolesnick, R. (2008). Ceramide biogenesis is required for radiation-induced apoptosis in the germ line of C. elegans. Science *322*, 110-115.

Derenzini, M. (2000). The AgNORs. Micron *31*, 117-120.

Derry, W. B., Putzke, A. P., and Rothman, J. H. (2001). Caenorhabditis elegans p53: role in apoptosis, meiosis, and stress resistance. Science *294*, 591-5.

Desai, C., Garriga, G., McIntire, S. L., and Horvitz, H. R. (1988). A genetic pathway for the development of the Caenorhabditis elegans HSN motor neurons. Nature *336*, 638-646.

Desai, C., and Horvitz, H. R. (1989). Caenorhabditis elegans mutants defective in the functioning of the motor neurons responsible for egg laying. Genetics *121*, 703-721.

Diderich, K., Alanazi, M., and Hoeijmakers, J. H. J. (2011). Premature aging and cancer in nucleotide excision repair-disorders. DNA Repair (Amst.) *10*, 772-780.

Dimitriadi, M., and Hart, A. C. (2010). Neurodegenerative disorders: insights from the nematode Caenorhabditis elegans. Neurobiol. Dis *40*, 4-11.

Dinkova, T., Keiper, B., Korneeva, N., Aamodt, E., and Rhoads, R. (2005). Translation of a small subset of Caenorhabditis elegans mRNAs is dependent on a specific eukaryotic translation initiation factor 4E isoform. Molecular and Cellular Biology *25*, 100-13.

Drabløs, F., Feyzi, E., Aas, P. A., Vaagbø, C. B., Kavli, B., Bratlie, M. S., Peña-Diaz, J., Otterlei, M., Slupphaug, G., and Krokan, H. E. (2004). Alkylation damage in DNA and RNA--repair mechanisms and medical significance. DNA Repair (Amst) *3*, 1389-407.

Drygin, D., Lin, A., Bliesath, J., Ho, C. B., O'Brien, S. E., Proffitt, C., Omori, M., Haddach, M., Schwaebe, M. K., Siddiqui-Jain, A., et al. (2011). Targeting RNA polymerase I with an oral small molecule CX-5461 inhibits ribosomal RNA synthesis and solid tumor growth. Cancer Res *71*, 1418-1430.

Drygin, D., Rice, W. G., and Grummt, I. (2010). The RNA polymerase I transcription machinery: an emerging target for the treatment of cancer. Annu. Rev. Pharmacol. Toxicol *50*, 131-156.

Drygin, D., Siddiqui-Jain, A., O'Brien, S., Schwaebe, M., Lin, A., Bliesath, J., Ho, C. B., Proffitt, C., Trent, K., Whitten, J. P., et al. (2009). Anticancer activity of CX-3543: a direct inhibitor of rRNA biogenesis. Cancer Res *69*, 7653-7661.

Dundr, M., Hoffmann-Rohrer, U., Hu, Q., Grummt, I., Rothblum, L. I., Phair, R. D., and Misteli, T. (2002). A kinetic framework for a mammalian RNA polymerase in vivo. Science *298*, 1623-1626.

Duverger, Y., Belougne, J., Scaglione, S., Brandli, D., Beclin, C., and Ewbank, J. J. (2007). A semi-automated high-throughput approach to the generation of transposon insertion mutants in the nematode Caenorhabditis elegans. Nucleic Acids Res *35*, e11.

Eickbush, T. H., and Eickbush, D. G. (2007). Finely Orchestrated Movements: Evolution of the Ribosomal RNA Genes. Genetics *175*, 477–485.

Ellis, H. M., and Horvitz, H. R. (1986a). Genetic control of programmed cell death in the nematode C. elegans. Cell *44*, 817-829.

Ellis, R., Sulston, J., and Coulson, A. (1986b). The rDNA of C. elegans: sequence and structure. Nucleic Acids Research *14*, 2345-64.

Elmore, S. (2007). Apoptosis: a review of programmed cell death. Toxicol Pathol *35*, 495-516.

Erdélyi, P., Borsos, E., Takács-Vellai, K., Kovács, T., Kovács, A., Sigmond, T., Hargitai, B., Pásztor, L., Sengupta, T., Dengg, M., et al. (2011). Shared developmental roles and transcriptional control of autophagy and apoptosis in Caenorhabditis elegans. Journal of Cell Science *124*, 1510-8.

Essers, J., Vermeulen, W., and Houtsmuller, A. B. (2006). DNA damage repair: anytime, anywhere? Curr. Opin. Cell Biol *18*, 240-246.

European Network of Cancer Registries (ENCR) Available at: http://www.encr.com.fr/ [Accessed July 13, 2011].

Fadeel, B., and Orrenius, S. (2005). Apoptosis: a basic biological phenomenon with wide-ranging implications in human disease. J. Intern. Med *258*, 479-517.

Fairlie, W. D., Perugini, M. A., Kvansakul, M., Chen, L., Huang, D. C. S., and Colman, P. M. (2006). CED-4 forms a 2□: 2 heterotetrameric complex with CED-9 until specifically displaced by EGL-1 or CED-13. Cell Death Differ *13*, 426-434.

Falnes, P. Ø., Bjørås, M., Aas, P. A., Sundheim, O., and Seeberg, E. (2004). Substrate specificities of bacterial and human AlkB proteins. Nucleic Acids Res *32*, 3456-3461.

Falnes, P. Ø., Johansen, R. F., and Seeberg, E. (2002). AlkB-mediated oxidative demethylation reverses DNA damage in Escherichia coli. Nature *419*, 178-182.

Falnes, P. Ø., Klungland, A., and Alseth, I. (2007). Repair of methyl lesions in DNA and RNA by oxidative demethylation. Neuroscience *145*, 1222-1232.

Farina, F., Alberti, A., Breuil, N., Bolotin-Fukuhara, M., Pinto, M., and Culetto, E. (2008). Differential expression pattern of the four mitochondrial adenine nucleotide transporter ant genes and their roles during the development of Caenorhabditis elegans. Dev. Dyn *237*, 1668-1681.

Fatica, A., and Tollervey, D. (2002). Making ribosomes. Curr Opin Cell Biol *14*, 313-8.

Ferlay, J., Parkin, D. M., and Steliarova-Foucher, E. (2010a). Estimates of cancer incidence and mortality in Europe in 2008. Eur. J. Cancer *46*, 765-781.

Ferlay, J., Shin, H.-R., Bray, F., Forman, D., Mathers, C., and Parkin, D. M. (2010b). Estimates of worldwide burden of cancer in 2008: GLOBOCAN 2008. Int. J. Cancer *127*, 2893-2917.

Files, J., and Hirsh, D. (1981). Ribosomal DNA of Caenorhabditis elegans. Journal of Molecular Biology *149*, 223-40.

Fimognari, C., Sestili, P., Lenzi, M., Bucchini, A., Cantelli-Forti, G., and Hrelia, P. (2008). RNA as a new target for toxic and protective agents. Mutat. Res *648*, 15-22.

Finishing the euchromatic sequence of the human genome (2004). Nature *431*, 931-945.

Fire, A. (1986). Integrative transformation of Caenorhabditis elegans. EMBO J *5*, 2673-2680.

Fischer, P. M. (2009). Cap in hand: targeting eIF4E. Cell Cycle *8*, 2535-2541.

Fontana, L., Partridge, L., and Longo, V. D. (2010). Extending healthy life span--from yeast to humans. Science *328*, 321-326.

Fontoura, B. M., Atienza, C. A., Sorokina, E. A., Morimoto, T., and Carroll, R. B. (1997). Cytoplasmic p53 polypeptide is associated with ribosomes. Mol Cell Biol *17*, 3146-54.

Fontoura, B. M., Sorokina, E. A., David, E., and Carroll, R. B. (1992). p53 is covalently linked to 5.8S rRNA. Mol Cell Biol *12*, 5145-51.

Ford, E., Voit, R., Liszt, G., Magin, C., Grummt, I., and Guarente, L. (2006). Mammalian Sir2 homolog SIRT7 is an activator of RNA polymerase I transcription. Genes Dev. *20*, 1075-1080.

Frank, D., and Roth, M. (1998). ncl-1 is required for the regulation of cell size and ribosomal RNA synthesis in Caenorhabditis elegans. The Journal of Cell Biology *140*, 1321-9.

Fraser, A. G., Kamath, R. S., Zipperlen, P., Martinez-Campos, M., Sohrmann, M., and Ahringer, J. (2000). Functional genomic analysis of C. elegans chromosome I by systematic RNA interference. Nature *408*, 325-330.

French, S. L., Osheim, Y. N., Cioci, F., Nomura, M., and Beyer, A. L. (2003). In exponentially growing Saccharomyces cerevisiae cells, rRNA synthesis is determined by the summed RNA polymerase I loading rate rather than by the number of active genes. Mol. Cell. Biol *23*, 1558-1568.

Freyth, K., Janowitz, T., Nunes, F., Voss, M., Heinick, A., Bertaux, J., Scheu, S., and Paul, R. J. (2010). Reproductive fitness and dietary choice behavior of the genetic model organism Caenorhabditis elegans under semi-natural conditions. Mol. Cells *30*, 347-353.

Fromont-Racine, M., Senger, B., Saveanu, C., and Fasiolo, F. (2003). Ribosome assembly in eukaryotes. Gene *313*, 17-42.

Frøkjaer-Jensen, C., Davis, M. W., Hollopeter, G., Taylor, J., Harris, T. W., Nix, P., Lofgren, R., Prestgard-Duke, M., Bastiani, M., Moerman, D. G., et al. (2010). Targeted gene deletions in C. elegans using transposon excision. Nat. Methods *7*, 451-453.

Frøkjaer-Jensen, C., Davis, M. W., Hopkins, C. E., Newman, B. J., Thummel, J. M., Olesen, S.-P., Grunnet, M., and Jorgensen, E. M. (2008). Single-copy insertion of transgenes in Caenorhabditis elegans. Nat. Genet *40*, 1375-1383.

Fuhrman, L. E., Goel, A. K., Smith, J., Shianna, K. V., and Aballay, A. (2009). Nucleolar proteins suppress Caenorhabditis elegans innate immunity by inhibiting p53/CEP-1. PLoS Genet *5*, e1000657.

Fullard, J. F., Kale, A., and Baker, N. E. (2009). Clearance of apoptotic corpses. Apoptosis *14*, 1029-1037.

Furukawa, K., Estus, S., Fu, W., Mark, R. J., and Mattson, M. P. (1997). Neuroprotective action of cycloheximide involves induction of bcl-2 and antioxidant pathways. J Cell Biol *136*, 1137-49.

GLOBOCAN Cancer Incidence and Mortality Worldwide in 2008. Available at: http://globocan.iarc.fr/ [Accessed July 13, 2011].

Gallagher, J., Dunbar, D., Granneman, S., Mitchell, B., Osheim, Y., Beyer, A., and Baserga, S. (2004). RNA polymerase I transcription and pre-rRNA processing are linked by specific SSU processome components. Genes & Development *18*, 2506-17.

Galluzzi, L., Aaronson, S. A., Abrams, J., Alnemri, E. S., Andrews, D. W., Baehrecke, E. H., Bazan, N. G., Blagosklonny, M. V., Blomgren, K., Borner, C., et al. (2009). Guidelines for the use and interpretation of assays for monitoring cell death in higher eukaryotes. Cell Death Differ *16*, 1093-1107.

Galluzzi, L., Joza, N., Tasdemir, E., Maiuri, M. C., Hengartner, M., Abrams, J. M., Tavernarakis, N., Penninger, J., Madeo, F., and Kroemer, G. (2008). No death without life: vital functions of apoptotic effectors. Cell Death Differ *15*, 1113-1123.

Gao, M., Liao, E., Yu, B., Wang, Y., Zhen, M., and Borsello, T. (2008). The SCFFSN-1 ubiquitin ligase controls germline apoptosis through CEP-1/p53 in C. elegans. Cell Death Differ *15*, 1054-1062.

Gao, W., Li, L., Xu, P., Fang, J., Xiao, S., and Chen, S. (2011). Frequent down-regulation of hABH2 in gastric cancer and its involvement in growth of cancer cells. J. Gastroenterol. Hepatol *26*, 577-584.

Garcia-Muse, T., and Boulton, S. (2005). Distinct modes of ATR activation after replication stress and DNA double-strand breaks in Caenorhabditis elegans. EMBO J *24*, 4345-4355.

Garsin, D. A., Sifri, C. D., Mylonakis, E., Qin, X., Singh, K. V., Murray, B. E., Calderwood, S. B., and Ausubel, F. M. (2001). A simple model host for identifying Gram-positive virulence factors. Proc. Natl. Acad. Sci. U.S.A *98*, 10892-10897.

Gartner, A., Boag, P. R., and Blackwell, T. K. (2008). Germline survival and apoptosis. Available at: http://www.wormbook.org.

Gartner, A., Milstein, S., Ahmed, S., Hodgkin, J., and Hengartner, M. O. (2000). A conserved checkpoint pathway mediates DNA damage--induced apoptosis and cell cycle arrest in C. elegans. Mol Cell *5*, 435-43.

Geiger, S., Lorenzen, K., Schreieck, A., Hanecker, P., Kostrewa, D., Heck, A., and Cramer, P. (2010). RNA polymerase I contains a TFIIF-related DNA-binding subcomplex. Molecular Cell *39*, 583-94.

Gene Summary for smo-1 Available at: http://www.wormbase.org/db/gene/gene?name=WBGene00004888;class=Gene [Accessed July 21, 2011].

Genovac Peptide Immunization. Available at: http://www.aldevron.com/antibody/immunization/peptideimmunization/ [Accessed July 8, 2011].

Gewandter, J. S., Bambara, R. A., and O'Reilly, M. A. (2011). The RNA surveillance protein SMG1 activates p53 in response to DNA double-strand breaks but not exogenously oxidized mRNA. Cell Cycle *10*. Available at: http://www.ncbi.nlm.nih.gov/pubmed/21701263 [Accessed August 17, 2011].

Ghoshal, K., and Jacob, S. (1997). An alternative molecular mechanism of action of 5-fluorouracil, a potent anticancer drug. Biochemical Pharmacology *53*, 1569-75.

Giam, M., Huang, D. C. S., and Bouillet, P. (2008). BH3-only proteins and their roles in programmed cell death. Oncogene *27 Suppl 1*, S128-136.

Giordano-Santini, R., and Dupuy, D. (2011). Selectable genetic markers for nematode transgenesis. Cell Mol Life Sci. Available at: http://www.ncbi.nlm.nih.gov/pubmed/21431833 [Accessed April 2, 2011].

Goh, A. M., Coffill, C. R., and Lane, D. P. (2011). The role of mutant p53 in human cancer. J. Pathol *223*, 116-126.

Goidin, D. (2001). Ribosomal 18S RNA Prevails over Glyceraldehyde-3-Phosphate Dehydrogenase and β-Actin Genes as Internal Standard for Quantitative Comparison of mRNA Levels in Invasive and Noninvasive Human Melanoma Cell Subpopulations. Analytical Biochemistry *295*, 17-21.

Gokal, P., Cavanaugh, A., and Thompson, E. (1986). The effects of cycloheximide upon transcription of rRNA, 5 S RNA, and tRNA genes. J Biol Chem *261*, 2536-41.

Gonzalez, C. A. (2006). The European Prospective Investigation into Cancer and Nutrition (EPIC). Public Health Nutr *9*, 124-126.

Gonzalez, C. A., and Riboli, E. (2010). Diet and cancer prevention: Contributions from the European Prospective Investigation into Cancer and Nutrition (EPIC) study. Eur. J. Cancer *46*, 2555-2562.

Gonzalez-Serricchio, A. S., and Sternberg, P. W. (2006). Visualization of C. elegans transgenic arrays by GFP. BMC Genet *7*, 36.

Gopalakrishna, K. N., Doddapuneni, K., Boyd, K. K., Masuho, I., Martemyanov, K. A., and Artemyev, N. O. (2011). Interaction of transducin with uncoordinated 119 protein (UNC119): implications for the model of transducin trafficking in rod photoreceptors. J. Biol. Chem. *286*, 28954-28962.

Gorska, M. M., Goplen, N., Liang, Q., and Alam, R. (2010). Uncoordinated 119 preferentially induces Th2 differentiation and promotes the development of asthma. J. Immunol *184*, 4488-4496.

Gorska, M. M., Liang, Q., Karim, Z., and Alam, R. (2009). Uncoordinated 119 protein controls trafficking of Lck via the Rab11 endosome and is critical for immunological synapse formation. J. Immunol *183*, 1675-1684.

Gorska, M. M., Stafford, S. J., Cen, O., Sur, S., and Alam, R. (2004). Unc119, a novel activator of Lck/Fyn, is essential for T cell activation. J. Exp. Med *199*, 369-379.

Granato, M., Schnabel, H., and Schnabel, R. (1994). pha-1, a selectable marker for gene transfer in C. elegans. Nucleic Acids Res *22*, 1762-1763.

Granneman, S., and Baserga, S. (2005). Crosstalk in gene expression: coupling and co-regulation of rDNA transcription, pre-ribosome assembly and pre-rRNA processing. Current Opinion in Cell Biology *17*, 281-286.

Greco, A. (2009). Involvement of the nucleolus in replication of human viruses. Rev. Med. Virol *19*, 201-214.

Greiss, S., Hall, J., Ahmed, S., and Gartner, A. (2008). C. elegans SIR-2.1 translocation is linked to a proapoptotic pathway parallel to cep-1/p53 during DNA damage-induced apoptosis. Genes Dev *22*, 2831-42.

Grob, A., Roussel, P., Wright, J. E., McStay, B., Hernandez-Verdun, D., and Sirri, V. (2009). Involvement of SIRT7 in resumption of rDNA transcription at the exit from mitosis. J. Cell. Sci *122*, 489-498.

Grummt, I. (2003). Life on a planet of its own: regulation of RNA polymerase I transcription in the nucleolus. Genes Dev *17*, 1691-1702.

Grummt, I., and Voit, R. (2010). Linking rDNA transcription to the cellular energy supply. Cell Cycle *9*, 225-226.

Gumienny, T. L., Lambie, E., Hartwieg, E., Horvitz, H. R., and Hengartner, M. O. (1999). Genetic control of programmed cell death in the Caenorhabditis elegans hermaphrodite germline. Development *126*, 1011-22.

Haag, J., and Pikaard, C. (2007). RNA polymerase I: a multifunctional molecular machine. Cell *131*, 1224-5.

Hajnal, A., Whitfield, C. W., and Kim, S. K. (1997). Inhibition of Caenorhabditis elegans vulval induction by gap-1 and by let-23 receptor tyrosine kinase. Genes Dev *11*, 2715-2728.

Hajnal, A., and Berset, T. (2002). The C.elegans MAPK phosphatase LIP-1 is required for the G(2)/M meiotic arrest of developing oocytes. EMBO J *21*, 4317-4326.

Hanahan, D., and Weinberg, R. A. (2011). Hallmarks of cancer: the next generation. Cell *144*, 646-674.

Hanahan, D., and Weinberg, R. A. (2000). The hallmarks of cancer. Cell *100*, 57-70.

Hanawalt, P. C. (2002). Subpathways of nucleotide excision repair and their regulation. Oncogene *21*, 8949-56.

Hanawalt, P., and Spivak, G. (2008). Transcription-coupled DNA repair: two decades of progress and surprises. Nat Rev Mol Cell Biol *9*, 958-70.

Hannan, K. M., Kennedy, B. K., Cavanaugh, A. H., Hannan, R. D., Hirschler-Laszkiewicz, I., Jefferson, L. S., and Rothblum, L. I. (2000). RNA polymerase I transcription in confluent cells: Rb downregulates rDNA transcription during confluence-induced cell cycle arrest. Oncogene *19*, 3487-3497.

Hannan, K., Hannan, R., and Rothblum, L. (1998a). Transcription by RNA polymerase I. Front. Biosci *3*, d376-d398.

Hannan, R. D., Hempel, W. M., Cavanaugh, A., Arino, T., Dimitrov, S. I., Moss, T., and Rothblum, L. (1998b). Affinity purification of mammalian RNA polymerase I. Identification of an associated kinase. J. Biol. Chem *273*, 1257-1267.

Hansen, M., Taubert, S., Crawford, D., Libina, N., Lee, S., and Kenyon, C. (2007). Lifespan extension by conditions that inhibit translation in Caenorhabditis elegans. Aging Cell *6*, 95-110.

Harris, J., Lowden, M., Clejan, I., Tzoneva, M., Thomas, J., Hodgkin, J., and Ahmed, S. (2006). Mutator Phenotype of Caenorhabditis elegans DNA Damage Checkpoint Mutants. Genetics *174*, 601-616.

Harrison, M. M., Ceol, C. J., Lu, X., and Horvitz, H. R. (2006). Some C. elegans class B synthetic multivulva proteins encode a conserved LIN-35 Rb-containing complex distinct from a NuRD-like complex. Proc. Natl. Acad. Sci. U.S.A *103*, 16782-16787.

Hartman, P. S., and Herman, R. K. (1982). Radiation-sensitive mutants of Caenorhabditis elegans. Genetics *102*, 159-178.

Hartman, P., Hevelone, J., Dwarakanath, V., and Mitchell, D. (1989). Excision repair of UV radiation-induced DNA damage in Caenorhabditis elegans. Genetics *122*, 379-85.

Hasegawa, E., Karashima, T., Sumiyoshi, E., and Yamamoto, M. (2006). C. elegans CPB-3 interacts with DAZ-1 and functions in multiple steps of germline development. Dev. Biol *295*, 689-699.

Hedgecock, E. M., Sulston, J. E., and Thomson, J. N. (1983). Mutations affecting programmed cell deaths in the nematode Caenorhabditis elegans. Science *220*, 1277-1279.

Hedgecock, E., and Herman, R. (1995). The ncl-1 gene and genetic mosaics of Caenorhabditis elegans. Genetics *141*, 989-1006.

Henderson, M., Cronland, E., Dunkelbarger, S., Contreras, V., Strome, S., and Keiper, B. (2009). A germline-specific isoform of eIF4E (IFE-1) is required for efficient translation of stored mRNAs and maturation of both oocytes and sperm. Journal of Cell Science *122*, 1529-39.

Hengartner, M. (2000). The biochemistry of apoptosis. Nature *407*, 770-6.

Hengartner, M. O., Ellis, R. E., and Horvitz, H. R. (1992). Caenorhabditis elegans gene ced-9 protects cells from programmed cell death. Nature *356*, 494-499.

Hengartner, M. O., and Horvitz, H. R. (1994a). Activation of C. elegans cell death protein CED-9 by an amino-acid substitution in a domain conserved in Bcl-2. Nature *369*, 318-320.

Hengartner, M. O., and Horvitz, H. R. (1994b). C. elegans cell survival gene ced-9 encodes a functional homolog of the mammalian proto-oncogene bcl-2. Cell *76*, 665-676.

Herman, R. K., and Hedgecock, E. M. (1990). Limitation of the size of the vulval primordium of Caenorhabditis elegans by lin-15 expression in surrounding hypodermis. Nature *348*, 169-171.

Hernandez-Verdun, D. (2006). The nucleolus: a model for the organization of nuclear functions. Histochem. Cell Biol *126*, 135-148.

Hetz, C., and Glimcher, L. (2008). The daily job of night killers: alternative roles of the BCL-2 family in organelle physiology. Trends Cell Biol *18*, 38-44.

Heyer, W.-D., Ehmsen, K. T., and Liu, J. (2010). Regulation of homologous recombination in eukaryotes. Annu. Rev. Genet *44*, 113-139.

Higashide, T., McLaren, M., and Inana, G. (1998). Localization of HRG4, a photoreceptor protein homologous to Unc-119, in ribbon synapse. Invest Ophthalmol Vis Sci *39*, 690-8.

Hiscox, J. A. (2002). The nucleolus--a gateway to viral infection? Arch. Virol *147*, 1077-1089.

Hoeijmakers, J. H. J. (2009). DNA damage, aging, and cancer. N. Engl. J. Med *361*, 1475-1485.

Hoeppner, D., Spector, M., Ratliff, T., Kinchen, J., Granat, S., Lin, S., Bhusri, S., Conradt, B., Herman, M., and Hengartner, M. (2004). eor-1 and eor-2 are required for cell-specific apoptotic death in C-elegans. Developmental Biology *274*, 125-138.

Hofmann, E. R., Milstein, S., Boulton, S. J., Ye, M., Hofmann, J. J., Stergiou, L., Gartner, A., Vidal, M., and Hengartner, M. O. (2002). Caenorhabditis elegans HUS-1 Is a DNA Damage Checkpoint Protein Required for Genome Stability and EGL-1-Mediated Apoptosis. Current Biology *12*, 1908–1918.

Hokii, Y., Sasano, Y., Sato, M., Sakamoto, H., Sakata, K., Shingai, R., Taneda, A., Oka, S., Himeno, H., Muto, A., et al. (2010). A small nucleolar RNA functions in rRNA processing in Caenorhabditis elegans. Nucleic Acids Res *38*, 5909-5918.

Hoogewijs, D., Houthoofd, K., Matthijssens, F., Vandesompele, J., and Vanfleteren, J. (2008). Selection and validation of a set of reliable reference genes for quantitative sod gene expression analysis in C. elegans. BMC Mol Biol *9*, 9.

Hosono, R., Nishimoto, S., and Kuno, S. (1989). Alterations of life span in the nematode Caenorhabditis elegans under monoxenic culture conditions. Exp. Gerontol *24*, 251-264.

Houge, G., Døskeland, S., Bøe, R., and Lanotte, M. (1993). Selective cleavage of 28S rRNA variable regions V3 and V13 in myeloid leukemia cell apoptosis. FEBS Letters *315*, 16-20.

Houge, G., Robaye, B., Eikhom, T., Golstein, J., Mellgren, G., Gjertsen, B., Lanotte, M., and Døskeland, S. (1995). Fine mapping of 28S rRNA sites specifically cleaved in cells undergoing apoptosis. Molecular and Cellular Biology *15*, 2051-62.

Houseley, J., and Tollervey, D. (2009). The many pathways of RNA degradation. Cell *136*, 763-76.

Howard, R. M., and Sundaram, M. V. (2002). C. elegans EOR-1/PLZF and EOR-2 positively regulate Ras and Wnt signaling and function redundantly with LIN-25 and the SUR-2 Mediator component. Genes Dev *16*, 1815-1827.

Hsieh, H.-H., Hsu, T.-Y., and Wu, Y.-C. (2010). Integrin alpha PAT 2 is important for the engulfment of cell corpses. In Available at: http://www.wormbase.org/db/misc/paper?name=WBPaper00036496;class=Paper [Accessed August 9, 2011].

Hsu, T., and Wu, Y. (2010). Engulfment of apoptotic cells in C. elegans is mediated by integrin alpha/SRC signaling. Curr Biol *20*, 477-86.

Hu, H., and Li, X. (2007). Transcriptional regulation in eukaryotic ribosomal protein genes. Genomics *90*, 421-423.

Hu, L., Wang, J., Liu, Y., Zhang, Y., Zhang, L., Kong, R., Zheng, Z., Du, X., and Ke, Y. (2011). A small ribosomal subunit (SSU) processome component, the human U3 protein 14A (hUTP14A) binds p53 and promotes p53 degradation. J. Biol. Chem *286*, 3119-3128.

Huang, L. S., Tzou, P., and Sternberg, P. W. (1994). The lin-15 locus encodes two negative regulators of Caenorhabditis elegans vulval development. Mol. Biol. Cell *5*, 395-411.

Huang, S. (2002). Building an efficient factory: where is pre-rRNA synthesized in the nucleolus? J. Cell Biol *157*, 739-741.

Hubbard, E. J., and Greenstein, D. (2000). The Caenorhabditis elegans gonad: a test tube for cell and developmental biology. Dev. Dyn *218*, 2-22.

Human protein-protein interaction network database search Available at: http://141.80.164.19/y2h_network/ppi_search.php [Accessed August 9, 2011].

Hurwitz, M. E., Vanderzalm, P. J., Bloom, L., Goldman, J., Garriga, G., and Horvitz, H. R. (2009). Abl kinase inhibits the engulfment of apoptotic cells in Caenorhabditis elegans. PLoS Biol *7*, e99.

Hölzel, M., Orban, M., Hochstatter, J., Rohrmoser, M., Harasim, T., Malamoussi, A., Kremmer, E., Längst, G., and Eick, D. (2010). Defects in 18 S or 28 S rRNA processing activate the p53 pathway. J. Biol. Chem *285*, 6364-6370.

IARC International Agency for Research on Cancer. Available at: http://www.iarc.fr/ [Accessed July 13, 2011].

Iordanov, M. S., Ryabinina, O. P., Wong, J., Dinh, T. H., Newton, D. L., Rybak, S. M., and Magun, B. E. (2000). Molecular determinants of apoptosis induced by the cytotoxic ribonuclease onconase: evidence for cytotoxic mechanisms different from inhibition of protein synthesis. Cancer Res *60*, 1983-1994.

Ishiba, Y., Higashide, T., Mori, N., Kobayashi, A., Kubota, S., McLaren, M. J., Satoh, H., Wong, F., and Inana, G. (2007). Targeted inactivation of synaptic HRG4 (UNC119) causes dysfunction in the distal photoreceptor and slow retinal degeneration, revealing a new function. Exp. Eye Res *84*, 473-485.

Ito, S., Greiss, S., Gartner, A., and Derry, W. B. (2010). Cell-nonautonomous regulation of C. elegans germ cell death by kri-1. Curr. Biol *20*, 333-338.

Jackson, S. P., and Bartek, J. (2009). The DNA-damage response in human biology and disease. Nature *461*, 1071-1078.

Jacobs, D., Beitel, G. J., Clark, S. G., Horvitz, H. R., and Kornfeld, K. (1998). Gain-of-function mutations in the Caenorhabditis elegans lin-1 ETS gene identify a C-terminal regulatory domain phosphorylated by ERK MAP kinase. Genetics *149*, 1809-1822.

Jagasia, R., Grote, P., Westermann, B., and Conradt, B. (2005). DRP-1-mediated mitochondrial fragmentation during EGL-1-induced cell death in C. elegans. Nature *433*, 754-760.

Jang, C., Lee, J., and Kim, J. (2004). RpS3, a DNA repair endonuclease and ribosomal protein, is involved in apoptosis. FEBS Letters *560*, 81-5.

Jiricny, J. (2002). DNA Repair: Bioinformatics Helps Reverse Methylation Damage. Current Biology *12*, R846-R848.

Jiricny, J. (2006). The multifaceted mismatch-repair system. Nat. Rev. Mol. Cell Biol *7*, 335-346.

Johnson, T. E. (2008). Caenorhabditis elegans 2007: the premier model for the study of aging. Exp. Gerontol *43*, 1-4.

Jones, A. M. (2001). Programmed cell death in development and defense. Plant Physiol *125*, 94-97.

Jones, K. T., and Ashrafi, K. (2009). Caenorhabditis elegans as an emerging model for studying the basic biology of obesity. Dis Model Mech *2*, 224-229.

Jorgensen, E. M., and Mango, S. E. (2002). The art and design of genetic screens: caenorhabditis elegans. Nat Rev Genet *3*, 356–69.

Joshi, P. M., Riddle, M. R., Djabrayan, N. J. V., and Rothman, J. H. (2010a). Caenorhabditis elegans as a model for stem cell biology. Dev. Dyn *239*, 1539-1554.

Joshi, P., Riddle, M., Djabrayan, N., and Rothman, J. (2010b). Caenorhabditis elegans as a model for stem cell biology. Dev Dyn *239*, 1539-54.

Kahn, R. A., Cherfils, J., Elias, M., Lovering, R. C., Munro, S., and Schurmann, A. (2006). Nomenclature for the human Arf family of GTP-binding proteins: ARF, ARL, and SAR proteins. J. Cell Biol *172*, 645-650.

Kaletta, T., and Hengartner, M. O. (2006). Finding function in novel targets: C. elegans as a model organism. Nat Rev Drug Discov *5*, 387-398.

Kalita, K., Makonchuk, D., Gomes, C., Zheng, J.-J., and Hetman, M. (2008). Inhibition of nucleolar transcription as a trigger for neuronal apoptosis. J. Neurochem *105*, 2286-2299.

Kamath, R. S., Martinez-Campos, M., Zipperlen, P., Fraser, A. G., and Ahringer, J. (2001). Effectiveness of specific RNA-mediated interference through ingested double-stranded RNA in Caenorhabditis elegans. Genome Biol *2*, RESEARCH0002.

Kamath, R., and Ahringer, J. (2003). Genome-wide RNAi screening in Caenorhabditis elegans. Methods (San Diego, Calif) *30*, 313-21.

Karim, Z., Vepachedu, R., Gorska, M., and Alam, R. (2010). UNC119 inhibits dynamin and dynamin-dependent endocytic processes. Cell. Signal *22*, 128-137.

Karni-Schmidt, O., Zupnick, A., Castillo, M., Ahmed, A., Matos, T., Bouvet, P., Cordon-Cardo, C., and Prives, C. (2008). p53 is localized to a sub-nucleolar compartment after proteasomal inhibition in an energy-dependent manner. J. Cell. Sci *121*, 4098-4105.

Kato, M., Paranjape, T., Müller, R. U., Ullrich, R., Nallur, S., Gillespie, E., Keane, K., Esquela-Kerscher, A., Weidhaas, J. B., and Slack, F. J. (2009). The mir-34 microRNA is required for the DNA damage response in vivo in C. elegans and in vitro in human breast cancer cells. Oncogene *28*, 2419-2424.

Kaufmann, S. H., and Gores, G. J. (2000). Apoptosis in cancer: cause and cure. Bioessays *22*, 1007-1017.

Keiper, B., Lamphear, B., Deshpande, A., Jankowska-Anyszka, M., Aamodt, E., Blumenthal, T., and Rhoads, R. (2000). Functional Characterization of Five eIF4E Isoforms in Caenorhabditis elegans. Journal of Biological Chemistry *275*, 10590-10596.

Kelly, W. G., Xu, S., Montgomery, M. K., and Fire, A. (1997). Distinct requirements for somatic and germline expression of a generally expressed Caernorhabditis elegans gene. Genetics *146*, 227-238.

Kenyon, C. J. (2010). The genetics of ageing. Nature *464*, 504-512.

Kerr, J. F., Wyllie, A. H., and Currie, A. R. (1972). Apoptosis: a basic biological phenomenon with wide-ranging implications in tissue kinetics. Br. J. Cancer *26*, 239-257.

Kertesz, M., Wan, Y., Mazor, E., Rinn, J., Nutter, R., Chang, H., and Segal, E. (2010). Genome-wide measurement of RNA secondary structure in yeast. Nature *467*, 103-7.

Ketting, R. F., Haverkamp, T. H., van Luenen, H. G., and Plasterk, R. H. (1999). Mut-7 of C. elegans, required for transposon silencing and RNA interference, is a homolog of Werner syndrome helicase and RNaseD. Cell *99*, 133-141.

Key, T. J., Allen, N. E., Spencer, E. A., and Travis, R. C. (2002). The effect of diet on risk of cancer. Lancet *360*, 861-868.

Key, T. J., Schatzkin, A., Willett, W. C., Allen, N. E., Spencer, E. A., and Travis, R. C. (2004). Diet, nutrition and the prevention of cancer. Public Health Nutr *7*, 187-200.

Killian, D., and Hubbard, E. (2004). C-elegans pro-1 activity is required for soma/germline interactions that influence proliferation and differentiation in the germ line. Development *131*, 1267-1278.

Kim, D. H., Feinbaum, R., Alloing, G., Emerson, F. E., Garsin, D. A., Inoue, H., Tanaka-Hino, M., Hisamoto, N., Matsumoto, K., Tan, M.-W., et al. (2002). A conserved p38 MAP kinase pathway in Caenorhabditis elegans innate immunity. Science *297*, 623-626.

Kinchen, J. M., Cabello, J., Klingele, D., Wong, K., Feichtinger, R., Schnabel, H., Schnabel, R., and Hengartner, M. O. (2005). Two pathways converge at CED-10 to mediate actin rearrangement and corpse removal in C. elegans. Nature *434*, 93-99.

Kirienko, N. V., and Fay, D. S. (2007). Transcriptome profiling of the C. elegans Rb ortholog reveals diverse developmental roles. Dev. Biol *305*, 674-684.

Klass, M. R. (1977). Aging in the nematode Caenorhabditis elegans: major biological and environmental factors influencing life span. Mech. Ageing Dev *6*, 413-429.

Klinger, C., Huet, J., Song, D., Petersen, G., Riva, M., Bautz, E. K., Sentenac, A., Oudet, P., and Schultz, P. (1996). Localization of yeast RNA polymerase I core subunits by immunoelectron microscopy. EMBO J *15*, 4643.

Knobel, K. M., Davis, W. S., Jorgensen, E. M., and Bastiani, M. J. (2001). UNC-119 suppresses axon branching in C. elegans. Development *128*, 4079–92.

Kobayashi, A., Higashide, T., Hamasaki, D., Kubota, S., Sakuma, H., An, W., Fujimaki, T., McLaren, M., Weleber, R., and Inana, G. (2000). HRG4 (UNC119) mutation found in cone-rod dystrophy causes retinal degeneration in a transgenic model. Invest Ophthalmol Vis Sci *41*, 3268-77.

Kobayashi, A., Kubota, S., Mori, N., McLaren, M., and Inana, G. (2003). Photoreceptor synaptic protein HRG4 (UNC119) interacts with ARL2 via a putative conserved domain. FEBS Letters *534*, 26-32.

Koberna, K., Malínský, J., Pliss, A., Masata, M., Vecerova, J., Fialová, M., Bednár, J., and Raska, I. (2002). Ribosomal genes in focus: new transcripts label the dense fibrillar components and form clusters indicative of “Christmas trees” in situ. J. Cell Biol *157*, 743-748.

Komatsu, Y., Tsujino, T., Suzuki, T., Nikaido, O., and Ohtsuka, E. (1997). Antigen structural requirements for recognition by a cyclobutane thymine dimer-specific monoclonal antibody. Nucleic Acids Research *25*, 3889-94.

Kondo, N., Takahashi, A., Ono, K., and Ohnishi, T. (2010). DNA damage induced by alkylating agents and repair pathways. J Nucleic Acids *2010*, 543531.

Koronakis, V., Hume, P. J., Humphreys, D., Liu, T., Hørning, O., Jensen, O. N., and McGhie, E. J. (2011). WAVE regulatory complex activation by cooperating GTPases Arf and Rac1. Proc. Natl. Acad. Sci. U.S.A. *108*, 14449-14454.

Kos, M., and Tollervey, D. (2010). Yeast pre-rRNA processing and modification occur cotranscriptionally. Mol. Cell *37*, 809-820.

Kourtis, N., and Tavernarakis, N. (2009). Cell-specific monitoring of protein synthesis in vivo. PLoS ONE *4*, e4547.

Kraemer, K. H., Patronas, N. J., Schiffmann, R., Brooks, B. P., Tamura, D., and DiGiovanna, J. J. (2007). Xeroderma pigmentosum, trichothiodystrophy and Cockayne syndrome: a complex genotype-phenotype relationship. Neuroscience *145*, 1388-1396.

Krantic, S., Mechawar, N., Reix, S., and Quirion, R. (2005). Molecular basis of programmed cell death involved in neurodegeneration. Trends Neurosci *28*, 670-6.

Kratz, K., Schöpf, B., Kaden, S., Sendoel, A., Eberhard, R., Lademann, C., Cannavó, E., Sartori, A. A., Hengartner, M. O., and Jiricny, J. (2010). Deficiency of FANCD2-associated nuclease KIAA1018/FAN1 sensitizes cells to interstrand crosslinking agents. Cell *142*, 77-88.

Kressler, D., Hurt, E., and Bassler, J. (2010). Driving ribosome assembly. Biochim. Biophys. Acta *1803*, 673-683.

Kritikou, E. A., Milstein, S., Vidalain, P.-O., Lettre, G., Bogan, E., Doukoumetzidis, K., Gray, P., Chappell, T. G., Vidal, M., and Hengartner, M. O. (2006). C. elegans GLA-3 is a novel component of the MAP kinase MPK-1 signaling pathway required for germ cell survival. Genes Dev *20*, 2279-92.

Krokan, H., Kavli, B., and Slupphaug, G. (2004). Novel aspects of macromolecular repair and relationship to human disease. Journal of Molecular Medicine *82*, 280-297.

Kruhlak, M., Crouch, E., Orlov, M., Montaño, C., Gorski, S., Nussenzweig, A., Misteli, T., Phair, R., and Casellas, R. (2007). The ATM repair pathway inhibits RNA polymerase□I transcription in response to chromosome breaks. Nature *447*, 730-734.

Kruse, J.-P., and Gu, W. (2009). Modes of p53 regulation. Cell *137*, 609-622.

Krüger, T., and Scheer, U. (2010). p53 localizes to intranucleolar regions distinct from the ribosome production compartments. J. Cell. Sci *123*, 1203-1208.

Kuai, L., Fang, F., Butler, J., and Sherman, F. (2004). Polyadenylation of rRNA in Saccharomyces cerevisiae. P Natl Acad Sci Usa *101*, 8581-6.

Kudron, M. M., and Reinke, V. (2008). C. elegans nucleostemin is required for larval growth and germline stem cell division. PLoS Genet *4*, e1000181.

Kuhn, C., Geiger, S., Baumli, S., Gartmann, M., Gerber, J., Jennebach, S., Mielke, T., Tschochner, H., Beckmann, R., and Cramer, P. (2007a). Functional architecture of RNA polymerase I. Cell *131*, 1260-72.

Kuhn, C.-D., Geiger, S. R., Baumli, S., Gartmann, M., Gerber, J., Jennebach, S., Mielke, T., Tschochner, H., Beckmann, R., and Cramer, P. (2007b). Functional architecture of RNA polymerase I. Cell *131*, 1260-1272.

Kumazawa, T., Nishimura, K., Kuroda, T., Ono, W., Yamaguchi, C., Katagiri, N., Tsuchiya, M., Masumoto, H., Nakajima, Y., Murayama, A., et al. (2011). Novel Nucleolar Pathway Connecting Intracellular Energy Status with p53 Activation. J. Biol. Chem *286*, 20861-20869.

Lackner, M. R., Kornfeld, K., Miller, L. M., Horvitz, H. R., and Kim, S. K. (1994). A MAP kinase homolog, mpk-1, is involved in ras-mediated induction of vulval cell fates in Caenorhabditis elegans. Genes Dev *8*, 160-173.

Lackner, M. R., and Kim, S. K. (1998). Genetic analysis of the Caenorhabditis elegans MAP kinase gene mpk-1. Genetics *150*, 103-117.

Laferté, A., Favry, E., Sentenac, A., Riva, M., Carles, C., and Chédin, S. (2006a). The transcriptional activity of RNA polymerase I is a key determinant for the level of all ribosome components. Genes Dev *20*, 2030-2040.

Laferté, A., Favry, E., Sentenac, A., Riva, M., Carles, C., and Chédin, S. (2006b). The transcriptional activity of RNA polymerase I is a key determinant for the level of all ribosome components. Genes Dev *20*, 2030-2040.

Lafontaine, D. L., and Tollervey, D. (2001). Ribosomal RNA. Available at: http://onlinelibrary.wiley.com/doi/10.1038/npg.els.0000877/abstract [Accessed July 29, 2011].

Lakowski, B., and Hekimi, S. (1998). The genetics of caloric restriction in Caenorhabditis elegans. Proc Natl Acad Sci US A *95*, 13091-13096.

Lam, Y., Trinkle-Mulcahy, L., and Lamond, A. (2005). The nucleolus. Journal of Cell Science *118*, 1335-7.

Lane, D. P., Cheok, C. F., Brown, C., Madhumalar, A., Ghadessy, F. J., and Verma, C. (2010). Mdm2 and p53 are highly conserved from placozoans to man. Cell Cycle *9*, 540-547.

Lans, H., Marteijn, J. A., Schumacher, B., Hoeijmakers, J. H. J., Jansen, G., and Vermeulen, W. (2010). Involvement of global genome repair, transcription coupled repair, and chromatin remodeling in UV DNA damage response changes during development. PLoS Genet *6*, e1000941.

Latonen, L., Moore, H. M., Bai, B., Jäämaa, S., and Laiho, M. (2011). Proteasome inhibitors induce nucleolar aggregation of proteasome target proteins and polyadenylated RNA by altering ubiquitin availability. Oncogene *30*, 790-805.

Lee, D. (2005). Repair of Methylation Damage in DNA and RNA by Mammalian AlkB Homologues. Journal of Biological Chemistry *280*, 39448-39459.

Lee, J. T., and Gu, W. (2010a). The multiple levels of regulation by p53 ubiquitination. Cell Death Differ *17*, 86-92.

Lee, J., Nam, S., Hwang, S. B., Hong, M., Kwon, J. Y., Joeng, K. S., Im, S. H., Shim, J., and Park, M. C. (2004). Functional genomic approaches using the nematode Caenorhabditis elegans as a model system. J. Biochem. Mol. Biol *37*, 107-113.

Lee, K. Y., Yang, I., Park, J.-E., Baek, O.-R., Chung, K. Y., and Koo, H.-S. (2007a). Developmental stage- and DNA damage-specific functions of C. elegans FANCD2. Biochemical and Biophysical Research Communications *352*, 479-485.

Lee, M.-H., Hook, B., Lamont, L. B., Wickens, M., and Kimble, J. (2006). LIP-1 phosphatase controls the extent of germline proliferation in Caenorhabditis elegans. EMBO J *25*, 88-96.

Lee, M.-H., Hook, B., Pan, G., Kershner, A. M., Merritt, C., Seydoux, G., Thomson, J. A., Wickens, M., and Kimble, J. (2007b). Conserved regulation of MAP kinase expression by PUF RNA-binding proteins. PLoS Genet *3*, e233.

Lee, M.-H., Ohmachi, M., Arur, S., Nayak, S., Francis, R., Church, D., Lambie, E., and Schedl, T. (2007c). Multiple functions and dynamic activation of MPK-1 extracellular signal-regulated kinase signaling in Caenorhabditis elegans germline development. Genetics *177*, 2039-2062.

Lee, S. B., Kwon, I.-S., Park, J., Lee, K.-H., Ahn, Y., Lee, C., Kim, J., Choi, S. Y., Cho, S.-W., and Ahn, J.-Y. (2010b). Ribosomal protein S3, a new substrate of Akt, serves as a signal mediator between neuronal apoptosis and DNA repair. J. Biol. Chem *285*, 29457-29468.

Lee, S., Horn, V., Julien, E., Liu, Y., Wysocka, J., Bowerman, B., Hengartner, M., Herr, W., and Van Lohuizen, M. (2007d). Epigenetic Regulation of Histone H3 Serine 10 Phosphorylation Status by HCF-1 Proteins in C. elegans and Mammalian Cells. PLoS ONE *2*, e1213.

Lehmann, A. R. (2003). DNA repair-deficient diseases, xeroderma pigmentosum, Cockayne syndrome and trichothiodystrophy. Biochimie *85*, 1101-1111.

Lehner, B., Calixto, A., Crombie, C., Tischler, J., Fortunato, A., Chalfie, M., and Fraser, A. (2006). Loss of LIN-35, the Caenorhabditis elegans ortholog of the tumor suppressor p105Rb, results in enhanced RNA interference. Genome Biol *7*, R4.

Lemmens, B. B. L. G., and Tijsterman, M. (2011). DNA double-strand break repair in Caenorhabditis elegans. Chromosoma *120*, 1-21.

Lessard, F., Morin, F., Ivanchuk, S., Langlois, F., Stefanovsky, V., Rutka, J., and Moss, T. (2010). The ARF tumor suppressor controls ribosome biogenesis by regulating the RNA polymerase I transcription factor TTF-I. Molecular Cell *38*, 539-50.

Lettre, G., Kritikou, E., Jaeggi, M., Calixto, A., Fraser, A., Kamath, R., Ahringer, J., and Hengartner, M. (2004). Genome-wide RNAi identifies p53-dependent and -independent regulators of germ cell apoptosis in C. elegans. Cell Death Differ *11*, 1198-1203.

Li, S., Armstrong, C. M., Bertin, N., Ge, H., Milstein, S., Boxem, M., Vidalain, P.-O., Han, J.-D. J., Chesneau, A., Hao, T., et al. (2004a). A map of the interactome network of the metazoan C. elegans. Science *303*, 540-543.

Li, Y., Kelly, W. G., Logsdon, J. M., Jr, Schurko, A. M., Harfe, B. D., Hill-Harfe, K. L., and Kahn, R. A. (2004b). Functional genomic analysis of the ADP-ribosylation factor family of GTPases: phylogeny among diverse eukaryotes and function in C. elegans. FASEB J *18*, 1834-1850.

Li, Z., Wu, J., and Deleo, C. J. (2006). RNA damage and surveillance under oxidative stress. IUBMB Life *58*, 581-588.

Lin, B., and Reinke, V. (2008). The candidate MAP kinase phosphorylation substrate DPL-1 (DP) promotes expression of the MAP kinase phosphatase LIP-1 in C. elegans germ cells. Dev. Biol *316*, 50-61.

Lindahl, T. (1993). Instability and decay of the primary structure of DNA. Nature *362*, 709-715.

Lindström, M. (2009). Emerging functions of ribosomal proteins in gene-specific transcription and translation. Biochemical and Biophysical Research Communications *379*, 167-70.

Lindström, M. S. (2011). NPM1/B23: A Multifunctional Chaperone in Ribosome Biogenesis and Chromatin Remodeling. Biochem Res Int *2011*, 195209.

Liu, T., Ghosal, G., Yuan, J., Chen, J., and Huang, J. (2010). FAN1 acts with FANCI-FANCD2 to promote DNA interstrand cross-link repair. Science *329*, 693-696.

Lo, S., Lee, C., and Lai, H. (2006). The nucleolus: reviewing oldies to have new understandings. Cell Res *16*, 530-8.

Lobner, D., and Choi, D. W. (1996). Preincubation with protein synthesis inhibitors protects cortical neurons against oxygen-glucose deprivation-induced death. Neuroscience *72*, 335-341.

Lockshin, R. A., and Zakeri, Z. (2001). Programmed cell death and apoptosis: origins of the theory. Nat. Rev. Mol. Cell Biol *2*, 545-550.

Lolle, S. J., Victor, J. L., Young, J. M., and Pruitt, R. E. (2005). Genome-wide non-mendelian inheritance of extra-genomic information in Arabidopsis. Nature *434*, 505-509.

Lomonosova, E., and Chinnadurai, G. (2008). BH3-only proteins in apoptosis and beyond: an overview. Oncogene *27 Suppl 1*, S2-19.

Lowe, S. W., and Lin, A. W. (2000). Apoptosis in cancer. Carcinogenesis *21*, 485-495.

Lu, N., Yu, X., He, X., and Zhou, Z. (2009). Detecting Apoptotic Cells and Monitoring Their Clearance in the Nematode Caenorhabditis elegans. Methods Mol. Biol *559*, 357-370.

Lu, X., and Horvitz, H. R. (1998). lin-35 and lin-53, two genes that antagonize a C. elegans Ras pathway, encode proteins similar to Rb and its binding protein RbAp48. Cell *95*, 981-991.

Luo, J., Shah, S., Riabowol, K., and Mains, P. E. (2009). The Caenorhabditis elegans ing-3 Gene Regulates Ionizing Radiation-Induced Germ-Cell Apoptosis in a p53-Associated Pathway. Genetics *181*, 473-82.

MacKay, C., Déclais, A.-C., Lundin, C., Agostinho, A., Deans, A. J., MacArtney, T. J., Hofmann, K., Gartner, A., West, S. C., Helleday, T., et al. (2010). Identification of KIAA1018/FAN1, a DNA repair nuclease recruited to DNA damage by monoubiquitinated FANCD2. Cell *142*, 65-76.

MacMorris, M., Spieth, J., Madej, C., Lea, K., and Blumenthal, T. (1994). Analysis of the VPE sequences in the Caenorhabditis elegans vit-2 promoter with extrachromosomal tandem array-containing transgenic strains. Mol. Cell. Biol *14*, 484-491.

Maciejowski, J., Ugel, N., Mishra, B., Isopi, M., and Hubbard, E. (2006). Quantitative analysis of germline mitosis in adult C. elegans. Developmental Biology *292*, 142-51.

Maduro, M. F., Gordon, M., Jacobs, R., and Pilgrim, D. B. (2000). The UNC-119 family of neural proteins is functionally conserved between humans, Drosophila and C. elegans. J. Neurogenet *13*, 191-212.

Maduro, M., and Pilgrim, D. (1995). Identification and cloning of unc-119, a gene expressed in the Caenorhabditis elegans nervous system. Genetics *141*, 977-988.

Mager, W. H., Planta, R. J., Ballesta, J. G., Lee, J. C., Mizuta, K., Suzuki, K., Warner, J. R., and Woolford, J. (1997). A new nomenclature for the cytoplasmic ribosomal proteins of Saccharomyces cerevisiae. Nucleic Acids Res *25*, 4872-4875.

Maier, W., Adilov, B., Regenass, M., and Alcedo, J. (2010). A neuromedin U receptor acts with the sensory system to modulate food type-dependent effects on C. elegans lifespan. PLoS Biol *8*, e1000376.

Mallo, G. V., Kurz, C. L., Couillault, C., Pujol, N., Granjeaud, S., Kohara, Y., and Ewbank, J. J. (2002). Inducible antibacterial defense system in C. elegans. Curr. Biol *12*, 1209-1214.

de Martel, C., and Franceschi, S. (2009). Infections and cancer: established associations and new hypotheses. Crit. Rev. Oncol. Hematol *70*, 183-194.

Martins, A., and Shuman, S. (2004). An RNA Ligase from Deinococcus radiodurans. J. Biol. Chem. *279*, 50654-50661.

Materi, W., and Pilgrim, D. (2005). Novel Caenorhabditis elegans unc-119 axon outgrowth defects correlate with behavioral phenotypes that are partially rescued by nonneural unc-119. Genesis *42*, 104-116.

Mathers, C. D., and Loncar, D. (2006). Projections of global mortality and burden of disease from 2002 to 2030. PLoS Med *3*, e442.

Matsui, H., Yazawa, H., Suzuki, N., and Hosoya, T. (1986). Effects of glucocorticoid and cycloheximide on the activity and amount of RNA polymerase I in nuclei of rat liver. Biochem. J *235*, 699–705.

Matsuoka, S., Ballif, B. A., Smogorzewska, A., McDonald, E. R., 3rd, Hurov, K. E., Luo, J., Bakalarski, C. E., Zhao, Z., Solimini, N., Lerenthal, Y., et al. (2007). ATM and ATR substrate analysis reveals extensive protein networks responsive to DNA damage. Science *316*, 1160-1166.

Maurer, C. W., Chiorazzi, M., and Shaham, S. (2007). Timing of the onset of a developmental cell death is controlled by transcriptional induction of the C. elegans ced-3 caspase-encoding gene. Development *134*, 1357-1368.

Mayer, C., and Grummt, I. (2005). Cellular stress and nucleolar function. Cell Cycle *4*, 1036-8.

Mayer, C., and Grummt, I. (2006). Ribosome biogenesis and cell growth: mTOR coordinates transcription by all three classes of nuclear RNA polymerases. Oncogene *25*, 6384-6391.

McGovern, M., Voutev, R., Maciejowski, J., Corsi, A., and Hubbard, E. (2009). A “latent niche” mechanism for tumor initiation. P Natl Acad Sci Usa *106*, 11617-22.

McStay, B., and Grummt, I. (2008). The epigenetics of rRNA genes: from molecular to chromosome biology. Annu Rev Cell Dev Biol *24*, 131-57.

Mekhail, K., Khacho, M., Carrigan, A., Hache, R. R. J., Gunaratnam, L., and Lee, S. (2005). Regulation of ubiquitin ligase dynamics by the nucleolus. J. Cell Biol *170*, 733-744.

Mekhail, K., Rivero-Lopez, L., Khacho, M., and Lee, S. (2006). Restriction of rRNA synthesis by VHL maintains energy equilibrium under hypoxia. Cell cycle (Georgetown, Tex) *5*, 2401-13.

Mello, C. C., Kramer, J. M., Stinchcomb, D., and Ambros, V. (1991). Efficient gene transfer in C.elegans: extrachromosomal maintenance and integration of transforming sequences. EMBO J *10*, 3959-3970.

Mello, C., and Fire, A. (1995). DNA transformation. Methods Cell Biol *48*, 451-482.

Meléndez, A., Hall, D. H., and Hansen, M. (2008). Monitoring the role of autophagy in C. elegans aging. Meth. Enzymol *451*, 493-520.

Meléndez, A., Tallóczy, Z., Seaman, M., Eskelinen, E.-L., Hall, D. H., and Levine, B. (2003). Autophagy genes are essential for dauer development and life-span extension in C. elegans. Science *301*, 1387-1391.

Merritt, C., Gallo, C. M., Rasoloson, D., and Seydoux, G. (2010). Transgenic solutions for the germline. Available at: http://www.wormbook.org.

Meyer, J., Boyd, W., Azzam, G., Haugen, A., Freedman, J., and Van Houten, B. (2007). Decline of nucleotide excision repair capacity in aging Caenorhabditis elegans. Genome Biol *8*, R70.

Meyskens, F. L., Jr, and Szabo, E. (2005). Diet and cancer: the disconnect between epidemiology and randomized clinical trials. Cancer Epidemiol. Biomarkers Prev *14*, 1366-1369.

Meyuhas, O. (2000). Synthesis of the translational apparatus is regulated at the translational level. Eur. J. Biochem *267*, 6321-6330.

Michaelidis, T. M., and Grummt, I. (2002). Mechanism of inhibition of RNA polymerase I transcription by DNA-dependent protein kinase. Biol. Chem *383*, 1683-1690.

Michels, A. A., and Hernandez, N. (2006). Does Pol I talk to Pol II? Coordination of RNA polymerases in ribosome biogenesis. Genes Dev *20*, 1982-5.

Miley, G. R., Fantz, D., Glossip, D., Lu, X., Saito, R. M., Palmer, R. E., Inoue, T., Van Den Heuvel, S., Sternberg, P. W., and Kornfeld, K. (2004). Identification of residues of the Caenorhabditis elegans LIN-1 ETS domain that are necessary for DNA binding and regulation of vulval cell fates. Genetics *167*, 1697-1709.

Milkereit, P., Gadal, O., Podtelejnikov, A., Trumtel, S., Gas, N., Petfalski, E., Tollervey, D., Mann, M., Hurt, E., and Tschochner, H. (2001). Maturation and intranuclear transport of pre-ribosomes requires Noc proteins. Cell *105*, 499-509.

Miller, A. B., and Linseisen, J. (2010). Achievements and future of nutritional cancer epidemiology. Int. J. Cancer *126*, 1531-1537.

Miller, M., Nguyen, V., Lee, M., Kosinski, M., Schedl, T., Caprioli, R., and Greenstein, D. (2001). A sperm cytoskeletal protein that signals oocyte meiotic maturation and ovulation. Science *291*, 2144-7.

Mitani, S., Iino, Y., Ishihara, T., Katsura, I., Mori, I., Nomura, K., Sawa, H., Sugimoto, A., and Takagi, S. (2010). National BioResource Project (NBRP): C.elegans, Tokyo Women's Medical University School of Medicine. Available at: http://www.shigen.nig.ac.jp/c.elegans/index.jsp [Accessed July 4, 2011].

Mitchell, J. R., Hoeijmakers, J. H. J., and Niedernhofer, L. J. (2003). Divide and conquer: nucleotide excision repair battles cancer and ageing. Curr. Opin. Cell Biol *15*, 232-240.

Moldovan, G.-L., and D'Andrea, A. D. (2009). How the fanconi anemia pathway guards the genome. Annu. Rev. Genet *43*, 223-249.

Montanaro, L., Treré, D., and Derenzini, M. (2008). Nucleolus, ribosomes, and cancer. Am. J. Pathol *173*, 301-310.

Mori, N., Ishiba, Y., Kubota, S., Kobayashi, A., Higashide, T., McLaren, M. J., and Inana, G. (2006). Truncation mutation in HRG4 (UNC119) leads to mitochondrial ANT-1-mediated photoreceptor synaptic and retinal degeneration by apoptosis. Invest. Ophthalmol. Vis. Sci *47*, 1281-1292.

Moss, T. (2004). At the crossroads of growth control; making ribosomal RNA. Current Opinion in Genetics & Development *14*, 210-217.

Mukhopadhyay, A., and Tissenbaum, H. (2007). Reproduction and longevity: secrets revealed by C. elegans. Trends in Cell Biology *17*, 65-71.

Mörck, C., and Pilon, M. (2006). C. elegans feeding defective mutants have shorter body lengths and increased autophagy. BMC Dev. Biol *6*, 39.

Müller (2006). Re-creating an RNA world. Cellular and Molecular Life Sciences (CMLS) *63*, 1278-1293.

Nadano, D., and Sato, T. (2000). Caspase-3-dependent and -independent degradation of 28 S ribosomal RNA may be involved in the inhibition of protein synthesis during apoptosis initiated by death receptor engagement. Journal of Biological Chemistry *275*, 13967-13973.

Nandakumar, J., Schwer, B., Schaffrath, R., and Shuman, S. (2008). RNA repair: an antidote to cytotoxic eukaryal RNA damage. Molecular Cell *31*, 278-86.

Narayanan, S., Surendranath, K., Bora, N., Surolia, A., and Karande, A. A. (2005). Ribosome inactivating proteins and apoptosis. FEBS Lett *579*, 1324-1331.

Nehme, R., Grote, P., Tomasi, T., Löser, S., Holzkamp, H., Schnabel, R., and Conradt, B. (2010). Transcriptional upregulation of both egl-1 BH3-only and ced-3 caspase is required for the death of the male-specific CEM neurons. Cell Death Differ *17*, 1266-1276.

Nehme, R., and Conradt, B. (2008). egl-1: a key activator of apoptotic cell death in C. elegans. Oncogene *27 Suppl 1*, S30-40.

Nelson, D. W., and Honda, B. M. (1985). Genes coding for 5S ribosomal RNA of the nematode Caenorhabditis elegans. Gene *38*, 245-251.

Nelson, D. W., and Honda, B. M. (1986). Genetic mapping of the 5S rRNA gene cluster of the nematode Caenorhabditis elegans. Can. J. Genet. Cytol *28*, 545-553.

Neukomm, L. J., Frei, A. P., Cabello, J., Kinchen, J. M., Zaidel-Bar, R., Ma, Z., Haney, L. B., Hardin, J., Ravichandran, K. S., Moreno, S., et al. (2011). Loss of the RhoGAP SRGP-1 promotes the clearance of dead and injured cells in Caenorhabditis elegans. Nat. Cell Biol *13*, 79-86.

Nunomura, A., Hofer, T., Moreira, P. I., Castellani, R. J., Smith, M. A., and Perry, G. (2009). RNA oxidation in Alzheimer disease and related neurodegenerative disorders. Acta Neuropathol *118*, 151-166.

Nunomura, A., Moreira, P. I., Takeda, A., Smith, M. A., and Perry, G. (2007). Oxidative RNA damage and neurodegeneration. Curr Med Chem *14*, 2968-75.

Obenauer, J. C., Cantley, L. C., and Yaffe, M. B. (2003). Scansite 2.0: Proteome-wide prediction of cell signaling interactions using short sequence motifs. Nucleic Acids Res *31*, 3635-3641.

Olson, M. (2009). Induction of apoptosis by viruses: what role does the nucleolus play? Cell Cycle *8*, 3452-3.

Olson, M. (2004). Sensing Cellular Stress: Another New Function for the Nucleolus? Science's STKE *2004*, pe10.

Olson, M. O., Dundr, M., and Szebeni, A. (2000). The nucleolus: an old factory with unexpected capabilities. Trends Cell Biol *10*, 189-196.

Oskarsson, T., and Trumpp, A. (2005). The Myc trilogy: lord of RNA polymerases. Nat Cell Biol *7*, 215-7.

Ouellet, J., and Roy, R. (2007). The lin-35/Rb and RNAi pathways cooperate to regulate a key cell cycle transition in C. elegans. BMC Dev. Biol *7*, 38.

O'Driscoll, M., and Jeggo, P. (2006). The role of double-strand break repair — insights from human genetics. Nat Rev Genet *7*, 45-54.

Page, B. D., Guedes, S., Waring, D., and Priess, J. R. (2001). The C. elegans E2F- and DP-related proteins are required for embryonic asymmetry and negatively regulate Ras/MAPK signaling. Mol. Cell *7*, 451-460.

Paik, J. C., Wang, B., Liu, K., Lue, J. K., and Lin, W.-C. (2010). Regulation of E2F1-induced apoptosis by the nucleolar protein RRP1B. J. Biol. Chem *285*, 6348-6363.

Pan, K. Z., Palter, J. E., Rogers, A. N., Olsen, A., Chen, D., Lithgow, G. J., and Kapahi, P. (2007). Inhibition of mRNA translation extends lifespan in Caenorhabditis elegans. Aging Cell *6*, 111-119.

Pardo, B., Gómez-González, B., and Aguilera, A. (2009). DNA repair in mammalian cells: DNA double-strand break repair: how to fix a broken relationship. Cell. Mol. Life Sci *66*, 1039-1056.

Park, D., Jia, H., Rajakumar, V., and Chamberlin, H. M. (2006). Pax2/5/8 proteins promote cell survival in C. elegans. Development *133*, 4193-4202.

Parkin, D. M. (2006). The global health burden of infection-associated cancers in the year 2002. Int. J. Cancer *118*, 3030-3044.

Parlato, R., Kreiner, G., Erdmann, G., Rieker, C., Stotz, S., Savenkova, E., Berger, S., Grummt, I., and Schütz, G. (2008). Activation of an Endogenous Suicide Response after Perturbation of rRNA Synthesis Leads to Neurodegeneration in Mice. J Neurosci *28*, 12759-64.

Parrish, J., Metters, H., Chen, L., and Xue, D. (2000). Demonstration of the in vivo interaction of key cell death regulators by structure-based design of second-site suppressors. Proc. Natl. Acad. Sci. U.S.A *97*, 11916-11921.

Parrish, J., and Xue, D. (2003). Functional genomic analysis of apoptotic DNA degradation in C. elegans. Molecular Cell *11*, 987-96.

Patterson, G. I., and Padgett, R. W. (2000). TGF beta-related pathways. Roles in Caenorhabditis elegans development. Trends Genet *16*, 27-33.

Paule, M. R., and White, R. J. (2000). Survey and summary: transcription by RNA polymerases I and III. Nucleic Acids Res *28*, 1283-98.

Peden, E., Killian, D. J., and Xue, D. (2008). Cell death specification in C. elegans. Cell Cycle *7*, 2479-2484.

Pederson, T., and Tsai, R. Y. L. (2009). In search of nonribosomal nucleolar protein function and regulation. J. Cell Biol *184*, 771-776.

Pei, B., Wang, S., Guo, X., Wang, J., Yang, G., Hang, H., and Wu, L. (2008). Arsenite-induced germline apoptosis through a MAPK-dependent, p53-independent pathway in Caenorhabditis elegans. Chem Res Toxicol *21*, 1530-5.

Pepper, A. (2003). The establishment of Caenorhabditis elegans germline pattern is controlled by overlapping proximal and distal somatic gonad signals. Developmental Biology *259*, 336-350.

Perry, R. P. (2007). Balanced production of ribosomal proteins. Gene *401*, 1-3.

del Peso, L., Gonzalez, V. M., Inohara, N., Ellis, R. E., and Núñez, G. (2000). Disruption of the CED-9.CED-4 complex by EGL-1 is a critical step for programmed cell death in Caenorhabditis elegans. J. Biol. Chem *275*, 27205-27211.

Pettersen, E. F., Goddard, T. D., Huang, C. C., Couch, G. S., Greenblatt, D. M., Meng, E. C., and Ferrin, T. E. (2004). UCSF Chimera--a visualization system for exploratory research and analysis. J Comput Chem *25*, 1605-1612.

Pich, A., Chiusa, L., and Margaria, E. (2000). Prognostic relevance of AgNORs in tumor pathology. Micron *31*, 133-141.

Polunovsky, V. A., Rosenwald, I. B., Tan, A. T., White, J., Chiang, L., Sonenberg, N., and Bitterman, P. B. (1996). Translational control of programmed cell death: eukaryotic translation initiation factor 4E blocks apoptosis in growth-factor-restricted fibroblasts with physiologically expressed or deregulated Myc. Mol Cell Biol *16*, 6573-81.

Ponti, D., Troiano, M., Bellenchi, G. C., Battaglia, P., and Gigliani, F. (2008). The HIV Tat protein affects processing of ribosomal RNA precursor. BMC Cell Biol *9*, 32.

Poole, A. M., and Logan, D. T. (2005). Modern mRNA proofreading and repair: clues that the last universal common ancestor possessed an RNA genome? Mol. Biol. Evol *22*, 1444-1455.

Potts, M. B., and Cameron, S. (2011). Cell lineage and cell death: Caenorhabditis elegans and cancer research. Nat. Rev. Cancer *11*, 50-58.

Pourkarimi, E., Greiss, S., and Gartner, A. (2011). Evidence that CED-9/Bcl2 and CED-4/Apaf-1 localization is not consistent with the current model for C. elegans apoptosis induction. Cell Death and Differentiation. Available at: http://www.ncbi.nlm.nih.gov/pubmed/21886181 [Accessed November 6, 2011].

Praitis, V., Casey, E., Collar, D., and Austin, J. (2001). Creation of low-copy integrated transgenic lines in Caenorhabditis elegans. Genetics *157*, 1217-1226.

Prieto, J.-L., and McStay, B. (2005). Nucleolar biogenesis: the first small steps. Biochem. Soc. Trans *33*, 1441-1443.

Qi, S., Pang, Y., Hu, Q., Liu, Q., Li, H., Zhou, Y., He, T., Liang, Q., Liu, Y., Yuan, X., et al. (2010). Crystal structure of the Caenorhabditis elegans apoptosome reveals an octameric assembly of CED-4. Cell *141*, 446-457.

Quevedo, C., Kaplan, D. R., and Derry, W. B. (2007). AKT-1 regulates DNA-damage-induced germline apoptosis in C. elegans. Curr Biol *17*, 286-92.

Ranish, J. A., Yi, E. C., Leslie, D. M., Purvine, S. O., Goodlett, D. R., Eng, J., and Aebersold, R. (2003a). The study of macromolecular complexes by quantitative proteomics. Nat Genet *33*, 349-55.

Ranish, J., Yi, E., Leslie, D., Purvine, S., Goodlett, D., Eng, J., and Aebersold, R. (2003b). The study of macromolecular complexes by quantitative proteomics. Nat Genet *33*, 349-55.

Raska, I., Shaw, P. J., and Cmarko, D. (2006). Structure and function of the nucleolus in the spotlight. Curr. Opin. Cell Biol *18*, 325-334.

Reddien, P. W., Andersen, E. C., Huang, M. C., and Horvitz, H. R. (2007). DPL-1 DP, LIN-35 Rb and EFL-1 E2F act with the MCD-1 zinc-finger protein to promote programmed cell death in Caenorhabditis elegans. Genetics *175*, 1719-1733.

Reddien, P. W., and Horvitz, H. R. (2004). The engulfment process of programmed cell death in caenorhabditis elegans. Annu. Rev. Cell Dev. Biol *20*, 193-221.

Reddien, P., Cameron, S., and Horvitz, H. (2001). Phagocytosis promotes programmed cell death in C. elegans. Nature *412*, 198-202.

Reinke, S. N., Hu, X., Sykes, B. D., and Lemire, B. D. (2010). Caenorhabditis elegans diet significantly affects metabolic profile, mitochondrial DNA levels, lifespan and brood size. Mol. Genet. Metab *100*, 274-282.

Richardson, A., and Kaye, S. B. (2008). Pharmacological Inhibition of the Bcl-2 Family of Apoptosis Regulators as Cancer Therapy. Curr Mol Pharmacol *1*, 244-254.

Rieckher, M., Kourtis, N., Pasparaki, A., and Tavernarakis, N. (2009). Transgenesis in Caenorhabditis elegans. Methods Mol. Biol *561*, 21-39.

Roche Applied Science Labeling and Detection - DIG System - DIG System Basics. Available at: http://www.roche-applied-science.com/sis/lad/index.jsp?id=lad_040100 [Accessed July 2, 2011].

Rocheleau, C. E., Howard, R. M., Goldman, A. P., Volk, M. L., Girard, L. J., and Sundaram, M. V. (2002). A lin-45 raf enhancer screen identifies eor-1, eor-2 and unusual alleles of Ras pathway genes in Caenorhabditis elegans. Genetics *161*, 121-131.

Rogers, A. N., Chen, D., McColl, G., Czerwieniec, G., Felkey, K., Gibson, B. W., Hubbard, A., Melov, S., Lithgow, G. J., and Kapahi, P. (2011). Life Span Extension via eIF4G Inhibition Is Mediated by Posttranscriptional Remodeling of Stress Response Gene Expression in C. elegans. Cell Metab *14*, 55-66.

Ross, A. J., Li, M., Yu, B., Gao, M. X., and Derry, W. B. (2011). The EEL-1 ubiquitin ligase promotes DNA damage-induced germ cell apoptosis in C. elegans. Cell Death Differ *18*, 1140-1149.

Rual, J.-F., Ceron, J., Koreth, J., Hao, T., Nicot, A.-S., Hirozane-Kishikawa, T., Vandenhaute, J., Orkin, S. H., Hill, D. E., van den Heuvel, S., et al. (2004a). Toward improving Caenorhabditis elegans phenome mapping with an ORFeome-based RNAi library. Genome Res *14*, 2162-2168.

Rual, J.-F., Ceron, J., Koreth, J., Hao, T., Nicot, A.-S., Hirozane-Kishikawa, T., Vandenhaute, J., Orkin, S. H., Hill, D. E., van den Heuvel, S., et al. (2004b). Toward improving Caenorhabditis elegans phenome mapping with an ORFeome-based RNAi library. Genome Res *14*, 2162-2168.

Rubbi, C. P., and Milner, J. (2003a). Disruption of the nucleolus mediates stabilization of p53 in response to DNA damage and other stresses. EMBO J *22*, 6068-77.

Rubbi, C., and Milner, J. (2003b). Disruption of the nucleolus mediates stabilization of p53 in response to DNA damage and other stresses. EMBO J *22*, 6068-6077.

Rudra, D., and Warner, J. R. (2004). What better measure than ribosome synthesis? Genes Dev *18*, 2431-2436.

Ruggero, D., and Pandolfi, P. P. (2003). Does the ribosome translate cancer? Nat. Rev. Cancer *3*, 179-192.

Russell, J., and Zomerdijk, J. (2005). RNA-polymerase-I-directed rDNA transcription, life and works. Trends in Biochemical Sciences *30*, 87-96.

Ruszczyńska-Bartnik, K., Maciejczyk, M., and Stolarski, R. (2011). Dynamical insight into Caenorhabditis elegans eIF4E recognition specificity for mono-and trimethylated structures of mRNA 5' cap. J Mol Model *17*, 727-737.

Rutkowski, R., Dickinson, R., Stewart, G., Craig, A., Schimpl, M., Keyse, S. M., and Gartner, A. (2011). Regulation of Caenorhabditis elegans p53/CEP-1-dependent germ cell apoptosis by Ras/MAPK signaling. PLoS Genet. *7*, e1002238.

Saijou, E., Fujiwara, T., Suzaki, T., Inoue, K., and Sakamoto, H. (2004). RBD-1, a nucleolar RNA-binding protein, is essential for Caenorhabditis elegans early development through 18S ribosomal RNA processing. Nucleic Acids Res *32*, 1028-36.

Sakashita, T., Takanami, T., Yanase, S., Hamada, N., Suzuki, M., Kimura, T., Kobayashi, Y., Ishii, N., and Higashitani, A. (2010). Radiation biology of Caenorhabditis elegans: germ cell response, aging and behavior. J. Radiat. Res *51*, 107-121.

Salinas, L. S., Maldonado, E., and Navarro, R. E. (2006). Stress-induced germ cell apoptosis by a p53 independent pathway in Caenorhabditis elegans. Cell Death Differ *13*, 2129-2139.

Samali, A., Gilje, B., Doskeland, S., Cotter, T., and Houge, G. (1997). The ability to cleave 28S ribosomal RNA during apoptosis is a cell-type dependent trait unrelated to DNA fragmentation. Cell Death Differ *4*, 289-293.

Sancar, A. (1996). DNA excision repair. Annu. Rev. Biochem *65*, 43-81.

Sancar, A., Lindsey-Boltz, L. A., Unsal-Kaçmaz, K., and Linn, S. (2004). Molecular mechanisms of mammalian DNA repair and the DNA damage checkpoints. Annu Rev Biochem *73*, 39-85.

Saunders, J. W., Jr (1966). Death in embryonic systems. Science *154*, 604-612.

Schertel, C., and Conradt, B. (2007). C. elegans orthologs of components of the RB tumor suppressor complex have distinct pro-apoptotic functions. Development *134*, 3691-3701.

Schneider, D. A., Michel, A., Sikes, M. L., Vu, L., Dodd, J. A., Salgia, S., Osheim, Y. N., Beyer, A. L., and Nomura, M. (2007). Transcription elongation by RNA polymerase I is linked to efficient rRNA processing and ribosome assembly. Mol. Cell *26*, 217-229.

Schouest, K. R., Kurasawa, Y., Furuta, T., Hisamoto, N., Matsumoto, K., and Schumacher, J. M. (2009). The germinal center kinase GCK-1 is a negative regulator of MAP kinase activation and apoptosis in the C. elegans germline. PLoS ONE *4*, e7450.

Schuler, M., and Green, D. R. (2005). Transcription, apoptosis and p53: catch-22. Trends Genet *21*, 182-187.

Schumacher, B., Hanazawa, M., Lee, M.-H., Nayak, S., Volkmann, K., Hofmann, E. R., Hofmann, R., Hengartner, M., Schedl, T., and Gartner, A. (2005a). Translational repression of C. elegans p53 by GLD-1 regulates DNA damage-induced apoptosis. Cell *120*, 357-368.

Schumacher, B., Hofmann, K., Boulton, S., and Gartner, A. (2001). The C. elegans homolog of the p53 tumor suppressor is required for DNA damage-induced apoptosis. Curr Biol *11*, 1722-7.

Schumacher, B., Schertel, C., Wittenburg, N., Tuck, S., Mitani, S., Gartner, A., Conradt, B., and Shaham, S. (2005b). C. elegans ced-13 can promote apoptosis and is induced in response to DNA damage. Cell Death Differ *12*, 153–61.

Schwartz, H. T. (2007). A protocol describing pharynx counts and a review of other assays of apoptotic cell death in the nematode worm Caenorhabditis elegans. Nat Protoc *2*, 705-714.

Searle, B. C. (2010). Scaffold: a bioinformatic tool for validating MS/MS-based proteomic studies. Proteomics *10*, 1265-1269.

Semple, J. I., Garcia-Verdugo, R., and Lehner, B. (2010). Rapid selection of transgenic C. elegans using antibiotic resistance. Nat. Methods *7*, 725-727.

Sendoel, A., Kohler, I., Fellmann, C., Lowe, S. W., and Hengartner, M. O. (2010). HIF-1 antagonizes p53-mediated apoptosis through a secreted neuronal tyrosinase. Nature *465*, 577-583.

Shaham, S., and Horvitz, H. R. (1996a). An alternatively spliced C. elegans ced-4 RNA encodes a novel cell death inhibitor. Cell *86*, 201-208.

Shaham, S., and Horvitz, H. R. (1996b). Developing Caenorhabditis elegans neurons may contain both cell-death protective and killer activities. Genes Dev *10*, 578-591.

Sharer, J., Shern, J., Van Valkenburgh, H., Wallace, D., and Kahn, R. (2002). ARL2 and BART enter mitochondria and bind the adenine nucleotide transporter. Molecular Biology of the Cell *13*, 71-83.

Shaw, P., and Doonan, J. (2005). The nucleolus. Playing by different rules? Cell Cycle *4*, 102-105.

Shcherbik, N., Wang, M., Lapik, Y. R., Srivastava, L., and Pestov, D. G. (2010). Polyadenylation and degradation of incomplete RNA polymerase I transcripts in mammalian cells. EMBO Rep *11*, 106-111.

Shen, Q., Qin, F., Gao, Z., Cui, J., Xiao, H., Xu, Z., and Yang, C. (2009). Adenine nucleotide translocator cooperates with core cell death machinery to promote apoptosis in Caenorhabditis elegans. Mol. Cell. Biol *29*, 3881-3893.

Shimada, K., Nakamura, M., Anai, S., De Velasco, M., Tanaka, M., Tsujikawa, K., Ouji, Y., and Konishi, N. (2009). A novel human AlkB homologue, ALKBH8, contributes to human bladder cancer progression. Cancer Res *69*, 3157-3164.

Shivers, R. P., Kooistra, T., Chu, S. W., Pagano, D. J., and Kim, D. H. (2009). Tissue-specific activities of an immune signaling module regulate physiological responses to pathogenic and nutritional bacteria in C. elegans. Cell Host Microbe *6*, 321-330.

Shtonda, B. B., and Avery, L. (2006). Dietary choice behavior in Caenorhabditis elegans. J. Exp. Biol *209*, 89-102.

Sigmond, T., Barna, J., Tóth, M. L., Takács-Vellai, K., Pásti, G., Kovács, A. L., and Vellai, T. (2008). Autophagy in Caenorhabditis elegans. Methods Enzymol *451*, 521-40.

Sijen, T., Fleenor, J., Simmer, F., Thijssen, K., Parrish, S., Timmons, L., Plasterk, R., and Fire, A. (2001). On the role of RNA amplification in dsRNA-triggered gene silencing. Cell *107*, 465-76.

Sikriwal, D., Ghosh, P., and Batra, J. K. (2008). Ribosome inactivating protein saporin induces apoptosis through mitochondrial cascade, independent of translation inhibition. Int. J. Biochem. Cell Biol.

Silverman, G. A., Luke, C. J., Bhatia, S. R., Long, O. S., Vetica, A. C., Perlmutter, D. H., and Pak, S. C. (2009). Modeling molecular and cellular aspects of human disease using the nematode Caenorhabditis elegans. Pediatr. Res *65*, 10-18.

Simmer, F., Moorman, C., van der Linden, A., Kuijk, E., van den Berghe, P., Kamath, R., Fraser, A., Ahringer, J., and Plasterk, R. (2003). Genome-wide RNAi of C. elegans using the hypersensitive rrf-3 strain reveals novel gene functions. Plos Biol *1*, E12.

Sinclair, D. A., and Guarente, L. (1997). Extrachromosomal rDNA circles--a cause of aging in yeast. Cell *91*, 1033-42.

Singhvi, A., Teuliere, J., Talavera, K., Cordes, S., Ou, G., Vale, R. D., Prasad, B. C., Clark, S. G., and Garriga, G. (2011). The Arf GAP CNT-2 regulates the apoptotic fate in C. elegans asymmetric neuroblast divisions. Curr. Biol *21*, 948-954.

Sirri, V., Urcuqui-Inchima, S., Roussel, P., and Hernandez-Verdun, D. (2008). Nucleolus: the fascinating nuclear body. Histochem. Cell Biol *129*, 13-31.

Skjeldam, H. K., Kassahun, H., Fensgård, O., SenGupta, T., Babaie, E., Lindvall, J. M., Arczewska, K., and Nilsen, H. (2010). Loss of Caenorhabditis elegans UNG-1 uracil-DNA glycosylase affects apoptosis in response to DNA damaging agents. DNA Repair (Amst.) *9*, 861-870.

Smogorzewska, A., Desetty, R., Saito, T. T., Schlabach, M., Lach, F. P., Sowa, M. E., Clark, A. B., Kunkel, T. A., Harper, J. W., Colaiácovo, M. P., et al. (2010). A genetic screen identifies FAN1, a Fanconi anemia-associated nuclease necessary for DNA interstrand crosslink repair. Mol. Cell *39*, 36-47.

So, S., Miyahara, K., and Ohshima, Y. (2011a). Control of body size in C. elegans dependent on food and insulin/IGF-1 signal. Genes Cells *16*, 639-651.

So, S., Tokumaru, T., Miyahara, K., and Ohshima, Y. (2011b). Control of lifespan by food bacteria, nutrient limitation and pathogenicity of food in C. elegans. Mech. Ageing Dev *132*, 210-212.

Sonenberg, N., and Hinnebusch, A. (2009). Regulation of translation initiation in eukaryotes: mechanisms and biological targets. Cell *136*, 731-45.

Song, A., Labella, S., Korneeva, N., Keiper, B., Aamodt, E., Zetka, M., and Rhoads, R. (2010). A C. elegans eIF4E-family member upregulates translation at elevated temperatures of mRNAs encoding MSH-5 and other meiotic crossover proteins. Journal of Cell Science *123*, 2228-37.

Spriggs, K., Bushell, M., and Willis, A. (2010). Translational regulation of gene expression during conditions of cell stress. Molecular Cell *40*, 228-37.

Stage, D. E., and Eickbush, T. H. (2007). Sequence variation within the rRNA gene loci of 12 Drosophila species. Genome Res.

Stallings, C. L., Stephanou, N. C., Chu, L., Hochschild, A., Nickels, B. E., and Glickman, M. S. (2009). CarD is an essential regulator of rRNA transcription required for Mycobacterium tuberculosis persistence. Cell *138*, 146-159.

Stefanovsky, V. Y., Pelletier, G., Hannan, R., Gagnon-Kugler, T., Rothblum, L. I., and Moss, T. (2001). An immediate response of ribosomal transcription to growth factor stimulation in mammals is mediated by ERK phosphorylation of UBF. Mol. Cell *8*, 1063-1073.

Stelzl, U., Worm, U., Lalowski, M., Haenig, C., Brembeck, F., Goehler, H., Stroedicke, M., Zenkner, M., Schoenherr, A., Koeppen, S., et al. (2005). A human protein-protein interaction network: a resource for annotating the proteome. Cell *122*, 957-68.

Stergiou, L. (2006). Deciphering the DNA damage signaling networks in Caenorhabditis elegans. Available at: http://www.dissertationen.unizh.ch/2006/stergiou/abstract.html [Accessed February 18, 2008].

Stergiou, L., Doukoumetzidis, K., Sendoel, A., and Hengartner, M. O. (2007). The nucleotide excision repair pathway is required for UV-C-induced apoptosis in Caenorhabditis elegans. Cell Death Differ *14*, 1129-38.

Stergiou, L., Eberhard, R., Doukoumetzidis, K., and Hengartner, M. O. (2011). NER and HR pathways act sequentially to promote UV-C-induced germ cell apoptosis in Caenorhabditis elegans. Cell Death Differ *18*, 897-906.

Stergiou, L., and Hengartner, M. O. (2004). Death and more: DNA damage response pathways in the nematode C. elegans. Cell Death Differ *11*, 21-8.

Sternberg, P. W. (2005). Vulval development. Available at: http://www.wormbook.org.

Sternberg, P. W., and Horvitz, H. R. (1986). Pattern formation during vulval development in C. elegans. Cell *44*, 761-772.

Stinchcomb, D. T., Shaw, J. E., Carr, S. H., and Hirsh, D. (1985). Extrachromosomal DNA transformation of Caenorhabditis elegans. Mol. Cell. Biol *5*, 3484-3496.

Stirpe, F., and Battelli, M. G. (2006). Ribosome-inactivating proteins: progress and problems. Cell. Mol. Life Sci *63*, 1850-1866.

Stokes, M. P., Rush, J., Macneill, J., Ren, J. M., Sprott, K., Nardone, J., Yang, V., Beausoleil, S. A., Gygi, S. P., Livingstone, M., et al. (2007). Profiling of UV-induced ATM/ATR signaling pathways. Proc. Natl. Acad. Sci. U.S.A *104*, 19855-19860.

Storici, F., Bebenek, K., Kunkel, T., Gordenin, D., and Resnick, M. (2007). RNA-templated DNA repair. Nature *447*, 338-341.

Strome, S. (2005). Specification of the germ line. Available at: http://www.wormbook.org.

Sugimoto, M., Kuo, M.-L., Roussel, M. F., and Sherr, C. J. (2003). Nucleolar Arf tumor suppressor inhibits ribosomal RNA processing. Mol. Cell *11*, 415-24.

Sulston, J. E., and Brenner, S. (1974). The DNA of Caenorhabditis elegans. Genetics *77*, 95-104.

Sulston, J. E., and Horvitz, H. R. (1977). Post-embryonic cell lineages of the nematode, Caenorhabditis elegans. Dev. Biol *56*, 110-156.

Sun, X.-X., Dai, M.-S., and Lu, H. (2007). 5-fluorouracil activation of p53 involves an MDM2-ribosomal protein interaction. J. Biol. Chem *282*, 8052-8059.

Sun, X.-X., Dai, M.-S., and Lu, H. (2008). Mycophenolic acid activation of p53 requires ribosomal proteins L5 and L11. J Biol Chem *283*, 12387-92.

Sundaram, M. V. (2006). RTK/Ras/MAPK signaling. Available at: http://www.wormbook.org.

Suthers, P., Gourse, R., and Yin, J. (2007). Rapid responses of ribosomal RNA synthesis to nutrient shifts. Biotechnol. Bioeng. *97*, 1230-1245.

Swanson, D., Chang, J., Campochiaro, P., Zack, D., and Valle, D. (1998). Mammalian orthologs of C. elegans unc-119 highly expressed in photoreceptors. Invest Ophthalmol Vis Sci *39*, 2085-94.

Syntichaki, P., Troulinaki, K., and Tavernarakis, N. (2007a). Protein Synthesis Is a Novel Determinant of Aging in Caenorhabditis elegans. Ann N Y Acad Sci *1119*, 289-95.

Syntichaki, P., Troulinaki, K., and Tavernarakis, N. (2007b). eIF4E function in somatic cells modulates ageing in Caenorhabditis elegans. Nature *445*, 922-926.

Sönnichsen, B., Koski, L., Walsh, A., Marschall, P., Neumann, B., Brehm, M., Alleaume, A., Artelt, J., Bettencourt, P., Cassin, E., et al. (2005). Full-genome RNAi profiling of early embryogenesis in Caenorhabditis elegans. Nature *434*, 462-9.

Tabuse, Y., Nabetani, T., and Tsugita, A. (2005). Proteomic analysis of protein expression profiles during Caenorhabditis elegans development using two-dimensional difference gel electrophoresis. Proteomics *5*, 2876-2891.

Takagi, M., Absalon, M. J., McLure, K. G., and Kastan, M. B. (2005). Regulation of p53 translation and induction after DNA damage by ribosomal protein L26 and nucleolin. Cell *123*, 49-63.

Tan, F. J., Zuckerman, J. E., Wells, R. C., and Hill, R. B. (2011). The C. elegans B-cell lymphoma 2 (Bcl-2) homolog cell death abnormal 9 (CED-9) associates with and remodels LIPID membranes. Protein Sci *20*, 62-74.

Tan, F., Fire, A., and Hill, R. (2007). Regulation of apoptosis by C. elegans CED-9 in the absence of the C-terminal transmembrane domain. Cell Death Differ *14*, 1925-35.

Tasaki, M., Shimada, K., Kimura, H., Tsujikawa, K., and Konishi, N. (2011). ALKBH3, a human AlkB homologue, contributes to cell survival in human non-small-cell lung cancer. Br. J. Cancer *104*, 700-706.

Tavernarakis, N. (2007). Protein synthesis and aging: eIF4E and the soma vs. germline distinction. Cell cycle (Georgetown, Tex) *6*, 1168-71.

Taylor, D. J., Devkota, B., Huang, A. D., Topf, M., Narayanan, E., Sali, A., Harvey, S. C., and Frank, J. (2009a). Comprehensive molecular structure of the eukaryotic ribosome. Structure *17*, 1591-1604.

Taylor, D., Devkota, B., Huang, A., Topf, M., Narayanan, E., Sali, A., Harvey, S., and Frank, J. (2009b). Comprehensive molecular structure of the eukaryotic ribosome. Structure *17*, 1591-604.

The Nematode Caenorhabditis elegans (1988). (New York: Cold Spring Harbor Laboratory Press).

Timmer, J., and Salvesen, G. (2007). Caspase substrates. Cell Death Differ *14*, 66-72.

Torizawa, T., Yamamoto, N., Suzuki, T., Nobuoka, K., Komatsu, Y., Morioka, H., Nikaido, O., Ohtsuka, E., Kato, K., and Shimada, I. (2000). DNA binding mode of the Fab fragment of a monoclonal antibody specific for cyclobutane pyrimidine dimer. Nucleic Acids Research *28*, 944-51.

Trewick, S. C., Henshaw, T. F., Hausinger, R. P., Lindahl, T., and Sedgwick, B. (2002). Oxidative demethylation by Escherichia coli AlkB directly reverts DNA base damage. Nature *419*, 174-178.

Tsai, R. Y. L., and Meng, L. (2009). Nucleostemin: a latecomer with new tricks. Int. J. Biochem. Cell Biol *41*, 2122-2124.

Tyagi, S., and Herr, W. (2009). E2F1 mediates DNA damage and apoptosis through HCF-1 and the MLL family of histone methyltransferases. EMBO J *28*, 3185-95.

Vanfleteren, J., and Braeckman, B. (1999). Mechanisms of life span determination in Caenorhabditis elegans. Neurobiol Aging *20*, 487-502.

Vavouri, T., Semple, J. I., Garcia-Verdugo, R., and Lehner, B. (2009). Intrinsic protein disorder and interaction promiscuity are widely associated with dosage sensitivity. Cell *138*, 198-208.

Vepachedu, R., Karim, Z., Patel, O., Goplen, N., and Alam, R. (2009). Unc119 protects from Shigella infection by inhibiting the Abl family kinases. PLoS ONE *4*, e5211.

Voutev, R., Killian, D. J., Ahn, J. H., and Hubbard, E. J. A. (2006). Alterations in ribosome biogenesis cause specific defects in C. elegans hermaphrodite gonadogenesis. Dev Biol *298*, 45-58.

Vázquez-Manrique, R. P., Legg, J. C., Olofsson, B., Ly, S., and Baylis, H. A. (2010). Improved gene targeting in C. elegans using counter-selection and Flp-mediated marker excision. Genomics *95*, 37-46.

WHO World Health Organization. Available at: http://www.who.int/en/ [Accessed July 13, 2011].

Wang, S., Wu, L., Wang, Y., Luo, X., and Lu, Y. (2009). Copper-induced germline apoptosis in Caenorhabditis elegans: the independent roles of DNA damage response signaling and the dependent roles of MAPK cascades. Chem. Biol. Interact *180*, 151-157.

Warner, J. R. (1999). The economics of ribosome biosynthesis in yeast. Trends Biochem. Sci *24*, 437-440.

Warner, J. R., and McIntosh, K. B. (2009). How common are extraribosomal functions of ribosomal proteins? Mol. Cell *34*, 3-11.

Waters, K., Yang, A., and Reinke, V. (2010). Genome-wide analysis of germ cell proliferation in C.elegans identifies VRK-1 as a key regulator of CEP-1/p53. Developmental Biology *344*, 1011-25.

Weidhaas, J. B., Eisenmann, D. M., Holub, J. M., and Nallur, S. V. (2006a). A Caenorhabditis elegans tissue model of radiation-induced reproductive cell death. Proc. Natl. Acad. Sci. U.S.A *103*, 9946-9951.

Weidhaas, J. B., Eisenmann, D. M., Holub, J. M., and Nallur, S. V. (2006b). A conserved RAS/mitogen-activated protein kinase pathway regulates DNA damage-induced cell death postirradiation in Radelegans. Cancer Res *66*, 10434-10438.

Werner, M., Thuriaux, P., and Soutourina, J. (2009). Structure-function analysis of RNA polymerases I and III. Curr. Opin. Struct. Biol *19*, 740-745.

Wertz, I. E., Kusam, S., Lam, C., Okamoto, T., Sandoval, W., Anderson, D. J., Helgason, E., Ernst, J. A., Eby, M., Liu, J., et al. (2011). Sensitivity to antitubulin chemotherapeutics is regulated by MCL1 and FBW7. Nature *471*, 110-114.

West, S., Gromak, N., Norbury, C., and Proudfoot, N. (2006). Adenylation and exosome-mediated degradation of cotranscriptionally cleaved pre-messenger RNA in human cells. Molecular Cell *21*, 437-43.

Williams, D., Boulin, T., Ruaud, A., Jorgensen, E., and Bessereau, J. (2005). Characterization of Mos1-mediated mutagenesis in Caenorhabditis elegans: a method for the rapid identification of mutated genes. Genetics *169*, 1779-85.

Woo, J.-S., Jung, J.-S., Ha, N.-C., Shin, J., Kim, K.-H., Lee, W., and Oh, B.-H. (2003). Unique structural features of a BCL-2 family protein CED-9 and biophysical characterization of CED-9/EGL-1 interactions. Cell Death Differ *10*, 1310-1319.

Wood, W. B., Hecht, R., Carr, S., Vanderslice, R., Wolf, N., and Hirsh, D. (1980). Parental effects and phenotypic characterization of mutations that affect early development in Caenorhabditis elegans. Dev. Biol *74*, 446-469.

World Health Organization (2007). Ten statistical highlights in global public health. World health statistics 2007 (Geneva Switzerland: ISBN: 9789241563406).

World Health Organization (2011). World health statistics 2011 (Geneva Switzerland: ISBN: 9789241564199).

Wright, J. E., Gaidatzis, D., Senften, M., Farley, B. M., Westhof, E., Ryder, S. P., and Ciosk, R. (2010). A quantitative RNA code for mRNA target selection by the germline fate determinant GLD-1. EMBO J. Available at: http://www.ncbi.nlm.nih.gov/pubmed/21169991 [Accessed December 22, 2010].

Wurtmann, E., and Wolin, S. (2008). RNA Under Attack: Cellular Handling of RNA Damage. Crit Rev Biochem Mol Biol, 1.

Xu, P.-Z., Yuan, S., Li, Y., Zhang, H.-Y., Wang, X.-D., Lin, H.-H., and Wu, X.-J. (2007). Genome-wide high-frequency non-Mendelian loss of heterozygosity in rice. Genome *50*, 297-302.

Yadavilli, S., Hegde, V., and Deutsch, W. (2007). Translocation of human ribosomal protein S3 to sites of DNA damage is dependant on ERK-mediated phosphorylation following genotoxic stress. DNA Repair *6*, 1453-1462.

Yan, N., Chai, J., Lee, E. S., Gu, L., Liu, Q., He, J., Wu, J.-W., Kokel, D., Li, H., Hao, Q., et al. (2005). Structure of the CED-4-CED-9 complex provides insights into programmed cell death in Caenorhabditis elegans. Nature *437*, 831-837.

Yan, N., Gu, L., Kokel, D., Chai, J., Li, W., Han, A., Chen, L., Xue, D., and Shi, Y. (2004). Structural, biochemical, and functional analyses of CED-9 recognition by the proapoptotic proteins EGL-1 and CED-4. Mol. Cell *15*, 999-1006.

Yan, N., Xu, Y., and Shi, Y. (2006). 2:1 Stoichiometry of the CED-4-CED-9 complex and the tetrameric CED-4: insights into the regulation of CED-3 activation. Cell Cycle *5*, 31-34.

Yang, M., Sun, J., Sun, X., Shen, Q., Gao, Z., and Yang, C. (2009). Caenorhabditis elegans protein arginine methyltransferase PRMT-5 negatively regulates DNA damage-induced apoptosis. PLoS Genet *5*, e1000514.

Yochem, J., Gu, T., and Han, M. (1998). A new marker for mosaic analysis in Caenorhabditis elegans indicates a fusion between hyp6 and hyp7, two major components of the hypodermis. Genetics *149*, 1323-1334.

Yokoyama, H., Mizutani, R., Satow, Y., Komatsu, Y., Ohtsuka, E., and Nikaido, O. (2000). Crystal structure of the 64M-2 antibody Fab fragment in complex with a DNA dT(6-4)T photoproduct formed by ultraviolet radiation. J. Mol. Biol *299*, 711-723.

Yook, K., and Hodgkin, J. (2007). Mos1 mutagenesis reveals a diversity of mechanisms affecting response of Caenorhabditis elegans to the bacterial pathogen Microbacterium nematophilum. Genetics *175*, 681-697.

Yoshikiyo, K., Kratz, K., Hirota, K., Nishihara, K., Takata, M., Kurumizaka, H., Horimoto, S., Takeda, S., and Jiricny, J. (2010). KIAA1018/FAN1 nuclease protects cells against genomic instability induced by interstrand cross-linking agents. Proc. Natl. Acad. Sci. U.S.A *107*, 21553-21557.

Youds, J. L., Barber, L. J., Ward, J. D., Collis, S. J., O'Neil, N. J., Boulton, S. J., and Rose, A. M. (2007). DOG-1 is the Caenorhabditis elegans BRIP1/FANCJ homologue and functions in interstrand cross-link repair. Mol Cell Biol.

Youds, J. L., Barber, L. J., and Boulton, S. J. (2009). C. elegans: a model of Fanconi anemia and ICL repair. Mutat. Res *668*, 103-116.

Youle, R. J., and Strasser, A. (2008). The BCL-2 protein family: opposing activities that mediate cell death. Nat. Rev. Mol. Cell Biol *9*, 47-59.

Yuan, J., Shaham, S., Ledoux, S., Ellis, H. M., and Horvitz, H. R. (1993). The C. elegans cell death gene ced-3 encodes a protein similar to mammalian interleukin-1 beta-converting enzyme. Cell *75*, 641-652.

Yuan, X., Zhou, Y., Casanova, E., Chai, M., Kiss, E., Grone, H., Schutz, G., and Grummt, I. (2005). Genetic Inactivation of the Transcription Factor TIF-IA Leads to Nucleolar Disruption, Cell Cycle Arrest, and p53-Mediated Apoptosis. Molecular Cell *19*, 77-87.

Yung, Y., Dolginov, Y., Yao, Z., Rubinfeld, H., Michael, D., Hanoch, T., Roubini, E., Lando, Z., Zharhary, D., and Seger, R. (1997). Detection of ERK activation by a novel monoclonal antibody. FEBS Lett *408*, 292-296.

Zemp, I., and Kutay, U. (2007). Nuclear export and cytoplasmic maturation of ribosomal subunits. FEBS Lett *581*, 2783-2793.

Zermati, Y., Mouhamad, S., Stergiou, L., Besse, B., Galluzzi, L., Boehrer, S., Pauleau, A.-L., Rosselli, F., D'Amelio, M., Amendola, R., et al. (2007). Nonapoptotic role for Apaf-1 in the DNA damage checkpoint. Mol. Cell *28*, 624-637.

Zglinicki, T., Saretzki, G., Ladhoff, J., Fagagna, F., and Jackson, S. (2005). Human cell senescence as a DNA damage response. Mechanisms of Ageing and Development *126*, 111-117.

Zhai, W., and Comai, L. (2000). Repression of RNA polymerase I transcription by the tumor suppressor p53. Mol Cell Biol *20*, 5930-8.

Zhang, H., Constantine, R., Vorobiev, S., Chen, Y., Seetharaman, J., Huang, Y. J., Xiao, R., Montelione, G. T., Gerstner, C. D., Davis, M. W., et al. (2011). UNC119 is required for G protein trafficking in sensory neurons. Nat. Neurosci *14*, 874-880.

Zhang, Y., Lu, H., and Bargmann, C. I. (2005). Pathogenic bacteria induce aversive olfactory learning in Caenorhabditis elegans. Nature *438*, 179-184.

Zhang, Y., and Lu, H. (2009). Signaling to p53: ribosomal proteins find their way. Cancer Cell *16*, 369-377.

Zhao, J., Yuan, X., Frodin, M., and Grummt, I. (2003a). ERK-dependent phosphorylation of the transcription initiation factor TIF-IA is required for RNA polymerase I transcription and cell growth. Molecular Cell *11*, 405-413.

Zhao, J., Yuan, X., Frödin, M., and Grummt, I. (2003b). ERK-dependent phosphorylation of the transcription initiation factor TIF-IA is required for RNA polymerase I transcription and cell growth. Molecular Cell *11*, 405-13.

Zhivotovsky, B., Galluzzi, L., Kepp, O., and Kroemer, G. (2009). Adenine nucleotide translocase: a component of the phylogenetically conserved cell death machinery. Cell Death Differ *16*, 1419-1425.

Zhou, B., and Elledge, S. (2000). The DNA damage response: putting checkpoints in perspective. Nature *408*, 433-439.

Zilfou, J. T., and Lowe, S. W. (2009). Tumor suppressive functions of p53. Cold Spring Harb Perspect Biol *1*, a001883.

Zou, H., Henzel, W. J., Liu, X., Lutschg, A., and Wang, X. (1997). Apaf-1, a human protein homologous to C. elegans CED-4, participates in cytochrome c-dependent activation of caspase-3. Cell *90*, 405-413.

Zuryn, S., Le Gras, S., Jamet, K., and Jarriault, S. (2010). A strategy for direct mapping and identification of mutations by whole-genome sequencing. Genetics *186*, 427-430.

Published Papers

A-1

A Dynamic Physical Model of Cell Migration, Differentiation and Apoptosis in *Caenorhabditis elegans*

Antje Beyer, Ralf Eberhard, Nir Piterman, Michael O. Hengartner, Alex Hajnal, and Jasmin Fisher

Proceedings of the 11th ICSB, in the Springer series
Advances in Experimental Medicine and Biology, 2012; 736:211-33

A-2

NER and HR pathways act sequentially to promote UV-C-induced germ cell apoptosis in *Caenorhabditis elegans*

Lilli Stergiou, Ralf Eberhard, Kimon Doukoumetzidis, and Michael O. Hengartner

Cell Death and Differentiation, 2011; 18:897-906

A-3

Deficiency of FANCD2-Associated Nuclease KIAA1018/FAN1 Sensitizes Cells to Interstrand Crosslinking Agents

Katja Kratz, Barbara Schöpf, Svenja Kaden, Ataman Sendoel, Ralf Eberhard, Claudio Lademann, Elda Cannavó, Alessandro A. Sartori, Michael O. Hengartner, and Josef Jiricny

Cell, 2010; 142:77–88

Chapter 12
A Dynamic Physical Model of Cell Migration, Differentiation and Apoptosis in *Caenorhabditis elegans*

Antje Beyer, Ralf Eberhard, Nir Piterman, Michael O. Hengartner, Alex Hajnal, and Jasmin Fisher

Abstract The germ line of the nematode *C. elegans* provides a paradigm to study essential developmental concepts like stem cell differentiation and apoptosis. Here, we have created a computational model encompassing these developmental landmarks and the resulting movement of germ cells along the gonadal tube. We have used a technique based on molecular dynamics (MD) to model the physical movement of cells solely based on the force that arises from dividing cells. This novel way of using MD to drive the model enables calibration of simulation and experimental time. Based on this calibration, the analysis of our model shows that it is in accordance with experimental observations. In addition, the model provides insights into kinetics of molecular pathways within individual cells as well as into physical aspects like the cell density along the germ line and in local neighbourhoods of individual germ cells. In the future, the presented model can be used to test hypotheses

A. Beyer
Department of Genetics, University of Cambridge, Cambridge, UK
e-mail: ab704@cam.ac.uk

R. Eberhard
Institute of Molecular Life Sciences, University of Zurich, Zurich, Switzerland

PhD Program in Molecular Life Sciences, Life Science Zurich Graduate School and MD/PhD Program, University of Zurich, Zurich, Switzerland
e-mail: ralf.eberhard@imls.uzh.ch

N. Piterman
Department of Computer Science, University of Leicester, Leicester, UK
e-mail: nir.piterman@leicester.ac.uk

M.O. Hengartner • A. Hajnal
Institute of Molecular Life Sciences, University of Zurich, Zurich, Switzerland
e-mail: michael.hengartner@mnf.uzh.ch; alex.hajnal@imls.uzh.ch

J. Fisher (✉)
Microsoft Research, Cambridge, UK
e-mail: Jasmin.Fisher@microsoft.com

I.I. Goryanin and A.B. Goryachev (eds.), *Advances in Systems Biology*,
Advances in Experimental Medicine and Biology 736,
DOI 10.1007/978-1-4419-7210-1_12, © Springer Science+Business Media, LLC 2012

about diverse aspects of development like stem cell division or programmed cell death. An iterative process of evolving this model and experimental testing in the model system *C. elegans* will provide new insights into key developmental aspects.

1 Introduction

Since the early 1970s [1], the nematode *C. elegans* has been a widely studied model in biomedical research (reviewed in e.g. [2–5]). Through the worm's transparent body it is possible to trace any cell by light microscopy or to study gene expression and cellular development *in situ* [6]. The fixed number of cells of the somatic cell lineages have been meticulously described (cf. [7]) and are invaluable for the genetic analysis of regulatory pathways in development (cf. [8]) or in neurobiology. The germ line of *C. elegans* allows for the observation of several essential developmental processes like stem cell proliferation, gametogenesis and programmed cell death, also termed apoptosis. Importantly, these biological processes are spatially well-resolved in this system, where germ cells mature in sequential steps along a tube-shaped gonad. It has, therefore, been extensively used in basic research (reviewed in [9–12]). Other than the highly predictable development of somatic tissues, cellular events in the germ line seem to be very stochastic; consequently the underlying general mechanisms are little understood for some of these processes. This is particularly true for physiological germ cell apoptosis. Programmed cell death is a crucial developmental process that is found in many different species; aberrations in this program have important implications in complex diseases like human cancers [13] or neurodegenerative disorders [14]. It is, therefore, key to gain fundamental understanding of its mechanisms. In this work, we propose a computational model of the germ line that is mainly based on physical properties and which aims to provide more insights into the previously mentioned developmental processes. With our model, we are able to test hypotheses about the causes and mechanisms of programmed cell death, among other developmental processes, and to highlight promising theories to be validated experimentally.

1.1 The C. elegans Germ Line

The reproductive system of *C. elegans* has a symmetric structure with two U-shaped gonads extending from a single vulva, one anteriorly and one posteriorly. Our model considers the development from stem cells to mature oocytes within one gonad (see Fig. 12.1). Although the nuclei and their cytoplasm within the germ line are not completely encapsulated cells and thus are part of a syncytium, they are usually referred to as germ "cells". As the differential interference contrast (DIC) picture and the electron microscopy imaging in Fig. 12.1 indicate, the cytoplasmic membranes are not fully delimiting, leaving a connection of all cells to a common shared cytoplasm in the centre of the gonad tube, called rachis.

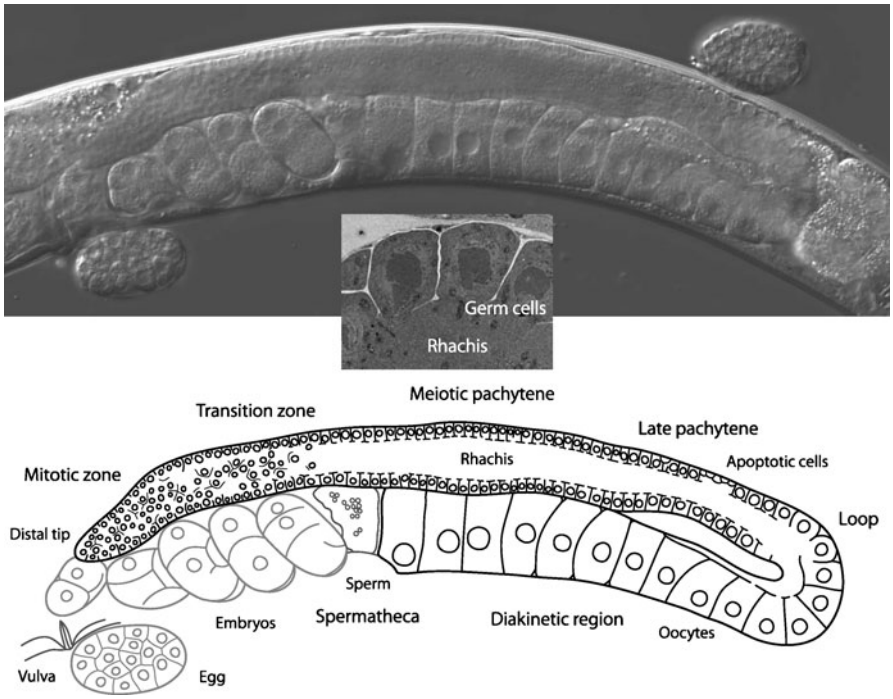

Fig. 12.1 The germ line of *Caenorhabditis elegans* by DIC (*top*), as a schematic (*bottom*), and in a cross-section (transmission electron microscopy, *middle*). The head of the worm is to the *right*, the posterior gonad to the *left* of the picture. Differential interference contrast (DIC) microscopy allows us to observe live animals in any focal plane; here, an adult hermaphrodite is virtually dissected along a plane through the centre of the gonad tube. The germ cells in the meiotic pachytene region form a monolayer around a concentric inner tube, seen as a nuclei-free area in the longitudinal and cross-sections (rachis). The limits of the transition zone and of the late pachytene stage within the meiotic pachytene region are not strictly defined by DIC. The oocytes in the loop have exited pachytene and begin the diakinetic stage of meiosis

The mature hermaphroditic germ line can be divided into functionally different zones with specific developmental properties [15–18]. At the distal most end of the gonadal tube, the mitotic zone is located ("distal" here meaning farthest from the uterus), containing dividing stem cells and representing a stem cell niche. The potential of the mitotic cell pool to divide is maintained by molecular signals – directly via activation of proliferation or, more likely, indirectly via inhibition of differentiation. Delta ligand from extrinsic sources (the distal tip cell) activates the Notch pathway, promoting a high Notch within the germ cells of this region. In the transition zone, where no external Delta ligand is presented, the Notch level gradually decays. When the germ cells are left without Notch, they complete the mitotic cell cycle, enter meiosis and start their differentiation into oocytes [16]. A small transition zone in which mitotic and first meiotic cells are interspersed links to a seemingly well-orchestrated meiotic pachytene region, where chromosomes

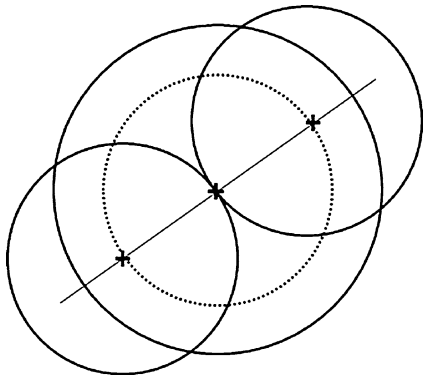

Fig. 12.2 Schematic representation of a dividing cell. The *big circle* represents the parent cell, the two *diametrically positioned circles* are the daughter cells, the *centres* of the three cells are represented by the + signs. The *straight line* signifies the division axis and the *dotted circle* is the imaginary circle with one basic radius around the centre of the parent cell on which the centres of the daughter cells are placed

undergo homologous recombination. At some point within the meiotic zone, the germ cells start growing at a low rate so that they have visibly increased their size by the time they reach the bend of the gonad and exit the pachytene stage of meiosis. In this loop region, the rachis is thinned to an eccentric tube, but still connecting the growing oocytes before they become proper cells with a fully closed membrane. Distal to the loop with the young oocytes, programmed cell death can be observed as part of normal oogenesis [19]. Physiological apoptosis, the fate of about half of all germ cells, is considered to be restricted to this area of the gonad [11]. Ras/MAPK activity is required for pachytene exit [20] and oocyte maturation; its absence also disables apoptosis [19]. For our model, we premise that germ cells start accumulating Ras activity towards the end of the meiotic pachytene region, induced by an external Ras signal. If the Ras level surpasses a certain threshold in a germ cell, it starts to grow to become a fully grown oocyte filling the complete diameter of the tube when it reaches the proximal end of the gonad. We also assume here that the Ras level is decisive for germ cell death: it renders a cell capable for or insensitive to physiological apoptosis.

1.2 Molecular Dynamics Model

Dividing cells in the mitotic zone apply pressure on the surrounding cells as the two daughter cells need more space than the parent cell (cf. Fig. 12.2). This leads to physical movement of the cells away from the pressure centre. We have constructed our model using an algorithm based on the molecular dynamics (MD) modelling framework [21] to capture this movement according to the physical properties of

each individual cell. This makes the movement of cells in our model very realistic so that we get a "virtual germ line". Apart from realistic movement, the MD framework allows for good visualisation and tracing of parameters for single or multiple cells. Originating from theoretical physics and chemistry to investigate the behaviour and properties of various particles like planets or molecules, physical algorithms similar to MD have also been used in a few biological settings [22–27]. In contrast to our specific modelling system, these MD models were applied to simulate the collective behaviour of tissues and aggregations of cells moving along a chemical or nutritional gradient. In these cases, the physical movement through MD is just a side effect of the main movement along the gradient, while in our case the MD-movement is the main component of movement. In fact, it is the only driving source of movement; without the forces derived within the MD approach, the cells in our model would not move at all.

In addition to movement, we have built our MD-model to include developmental processes such as cell growth and division, as well as apoptosis, to make it sufficiently realistic. These processes depend on signals received by the cells according to their location in the tube. We show that our model reproduces cellular behaviour observed in experimental settings [15, 28, 29] very closely. This suggests that our model is a useful tool to gain novel insights into the core developmental processes observed in the *C. elegans* germ line.

2 Model

The main part of our model is the movement algorithm from molecular dynamics. We have used the *velocity Verlet* algorithm [30], which is based on the following basic formula of Newtonian motion:

$$F = ma. \tag{12.1}$$

A Taylor series development of formula (12.1) and some further transformations imply the following steps of the algorithm for each cell. We will elaborate them a little more in the subsequent two paragraphs.

Step 1: $\vec{v}\left(t + \frac{1}{2}\Delta t\right) = \vec{v}(t) + \frac{1}{2}\vec{a}(t)\Delta t$.
Step 2: $\vec{x}\,(t + \Delta t) = \vec{x}(t) + \vec{v}\left(t + \frac{1}{2}\Delta t\right)\Delta t$.
Step 3: Derive $\vec{a}(t + \Delta t)$ from the interaction potential using $\vec{x}(t + \Delta t)$.
Step 4: $\vec{v}(t + \Delta t) = \vec{v}\left(t + \frac{1}{2}\Delta t\right) + \frac{1}{2}\vec{a}(t + \Delta t)\Delta t$.

Here, t represents the time and Δt signifies the timestep of the execution which is usually very small. The variable $\vec{x}(t)$ represents the location at the current time, $\vec{v}(t)$ stands for the velocity at the current time and $\vec{a}(t)$ for the acceleration at the current time. In our model, we replace acceleration with the force and the mass based on formula (12.1), i.e. $a = F/m$. For now, we simplify this further by assuming the mass to be one, which leads to $a = F$.

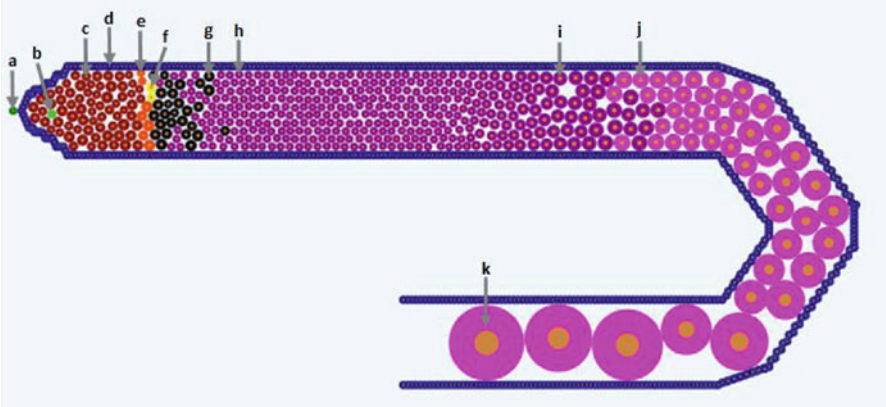

Fig. 12.3 Snapshot of an execution of the germ line model: (*a*) distal tip cell (*dark green*), (*b*) marked cell (*light green*), (*c*) mitotic cell with highest Notch level (*dark red*), (*d*) cells defining the border of the tube (*blue*), (*e*) mitotic cell with Notch level between highest and 0.5 times the highest level (*orange*), (*f*) mitotic cell with Notch level between 0.5 times the highest level and 0 (*yellow*), (*g*) mitotic cell with Notch level equal to 0 (*black*), (*h*) meiotic cell (*purple*), (*i*) meiotic cell that has grown to about twice its original size (*purple*), (*j*) oocyte with Ras level above threshold (pink) and (*k*) fully grown oocyte (*pink*)

The first step of the algorithm computes the velocity at the intermediate time $t + 1/2\Delta t$, which is used in the next step to evaluate the location of the cell at the next time, $t + \Delta t$. Using this new location of the cell, the force working on it at time $t + \Delta t$ is derived from the so-called interaction potential in the third step. The interaction potential is a function describing how a particle, here a cell, interacts with its environment. In our case, the potential acts in such a way that the cell is pushed away from cells that overlap it and there is no force working on the cell if other cells do not overlap it. The force on the cell is stronger the more overlap there is. If more than one cell overlaps the cell, the forces are accumulated. In the last step of the algorithm, this new force is used to calculate the velocity at the next time $t + \Delta t$. This algorithm is computed for each cell and each timestep Δt of the execution for a certain number of timesteps.

Since the algorithm works on a per cell basis, we have constructed the cells in our model as objects. To unite the functional style of the algorithm and the object oriented style of the cells, we have used the F# programming language [31], which incorporates both of these environments in a natural way. Additionally, the language also provides us with a very straightforward visual front end. For simplification, our current model is a two-dimensional representation of the germ line as shown in Fig. 12.3. A movie of an execution of the model can be viewed at [32]. The different colours are used to represent different states or component levels of the cells. To define the general structure of the germ line in our model, we estimated germ cell numbers along the gonadal tube from microscopic pictures of the germ line. This

provided us with estimates of cells across the tube diameter (cells per column in our model) and per developmental zone along the tube. The sizes of the different zones of the germ line were translated into the range of pathway activation in our model.

2.1 Internal Properties of Cells

As previously mentioned, the cells in our model are represented as objects. All cells are described by the same object class; they all have the same general internal properties. The different values of these properties describe the cells' current status within the model. Differences in cell behaviour between cells arise from differences in the specific momentary environment and slight randomisations of certain internal properties. In this section, we will describe the most important of these internal properties and how their values are derived.

2.1.1 Location

Every cell has a specific two-dimensional location assigned to it. The location is updated at each timestep of the execution depending on the velocity Verlet algorithm. The location is in continuous space as opposed to models which work with a grid of possible locations.

2.1.2 Velocity and Force

As previously mentioned, the velocity Verlet algorithm computes the new cell locations based on the velocity and force that are acting on the cell. For this purpose, we have equipped each cell with two-dimensional velocity and force vectors which are changed by the algorithm. The values of these two properties define the degree of change in the location through the velocity Verlet algorithm.

2.1.3 Cell State

Another important property of the cells in our model is the state of a cell. We have defined the states "Mitotic" (c, e, f and g in Fig. 12.3) and "Meiotic" (h, i, j and k in Fig. 12.3) which depend on the location and the cell cycle state of the cells. We also mark dead and fertilised cells in this way to make them countable and to be able to remove them from the model. Furthermore, we defined a state "Stopped" (a and d in Fig. 12.3) that marks all boundary cells of the tube not to move and to form the walls of the germ line. This definition of the germ line walls does not exactly conform to nature, but it is a simplification for computation purposes that is sufficiently realistic.

2.1.4 Ras and Notch Level

The cells also contain variables defining their Ras and Notch levels. These are changed according to the environment at a cell's location along the tube as this informs about the presence of external ligand molecules for the two signalling pathways. Along the x-axis of the coordinate system of our model, the Delta ligand is active in the region from 3.8 (which is the beginning of the tube) to 22. From coordinate 22, the Delta ligand is turned off; this is where the transition zone starts. The external Ras is present from 75 up to the beginning of the bend at 117 when it is turned off. When Delta ligand is present, the Notch level within the cells will jump to its highest value (c in Fig. 12.3). The level decays linearly over time in the absence of ligand (from c to e to f to g, representing no Notch, in Fig. 12.3). The Ras level is accumulated linearly over time as long as the ligand is present.

2.1.5 Size and Growth

The cells are also assigned a size that is updated at each step of the execution. For simplicity, we consider our cells to be round. Hence, the size of a cell is its radius. The size of a cell changes as it progresses along the gonadal tube depending on the cell's status and location. All cells have the same basic size to which they go back after a division. The change of size is defined by growth functions common to all cells. An exception to this is the function defining the growth rate of mitotic cells that is randomised for each cell. This assures that cells which are born at the same time do not necessarily divide synchronously, but at slightly different times. This results in a more realistic timing of the cell divisions.

2.1.6 Analysis Parameters

The previously mentioned cell properties are all included to achieve a behaviour and movement of the cells that is as realistic as possible. We have also included a few parameters for purely analytical purposes.

GFP

All cells contain a variable GFP – named after the visual marker green fluorescent protein in biological experiments – that can be turned on to visually follow this cell and its offspring in the simulation (b in Fig. 12.3). In addition, the data for these cells, i.e. the values of the previously mentioned parameters and the analytical parameters described below, can be read out to be analysed. If desired, this could be adjusted to track only one cell.

Density Factor

The cells also have a density factor associated with them. This density factor f of cell c is computed at each timestep using the following equation:

$$f(c) = \sum_{c_i \in N(c)} \frac{r_i}{6\,(d\,(c_i, c) - r_i)},$$

where $N(c)$ is the set of all cells touching cell c, r_i is the radius of cell c_i and $d(c_i, c)$ is the distance between the cells c_i and c. This factor is set to zero if no cell is touching c and to one if the neighbouring cells are ideally packed, i.e. c is surrounded by six cells of the same radius as c. The density is above one if other cells are overlapping c. This density factor could later be used to test hypotheses about the apoptotic mechanism.

Movement and Division Rates

To compare the movement rate of the cells with experimental findings, we have also introduced a list to represent this rate. A function writes each timestep to this list in which the cell has moved at least one diameter along the x-axis compared to the location at the previously stored timestep. Similarly to the movement rate, we have also defined a list representing the division rate. This list is appended by the current timestep when the cell divides so that each cell carries a history of all previous divisions for its ancestors. This list is passed to both daughter cells upon a division.

2.2 Other Properties of the Model

The cells in our model are not stand alone objects, but they interact with each other and their environment, i.e. the gonadal tube. The interplay between the internal configuration of the cells and their surroundings results in the behaviour that can be observed in the model. For the specification of these interactions, we have defined some general properties of the model which are described in this section.

2.2.1 Cell Growth and Division

Before they divide to form two daughter cells, cells marked as mitotic grow to a size of $\sqrt{2}$ times their basic radius, which corresponds to twice their area. The two daughter cells both have the same basic radius and are placed so that the distance of their centres is two basic radii (cf. Fig. 12.2). In the *C. elegans* germ cells, the orientation of the division axis appears to be random. In our model, the daughter cells are placed symmetrically with regards to a random central division axis in

their parental cell (straight line in Fig. 12.2). Their centres will thus be positioned diametrically on an imaginary circle around the centre of the parent cell with the basic radius (dotted circle in Fig. 12.2). The daughter cells inherit the Notch level and GFP status from their parent. At the same time, the division rate list in the daughter cells is updated and a cell is added to a counter of the total number of cells.

2.2.2 Growth of Early Meiotic Cells and Oocytes

Meiotic cells stay at the basic radius until they reach a certain point in the tube from which they start growing slowly, i.e. their radius is increased, until they have reached about double their area right before the loop. When the Ras level within these cells has reached a certain threshold, they exit the pachytene stage of meiosis and proceed into diakinesis to become mature oocytes (j and k in Fig. 12.3). Initially, the radii of the oocytes grow about ten times faster than the ones of late pachytene cells and, as they reach the end of the loop, this growth rate is increased by another 10-fold. The oocytes stop growing when their diameter is the width of the tube (k in Fig. 12.3). All cell growth in our model is defined by an increase in radius and happens at linear rates.

2.2.3 Death

In vivo, programmed cell death is normally confined to the late meiotic pachytene region before the loop where some cells become apoptotic. Accordingly, we defined a death zone in our model. In the worm, the death zone seems to be dependent on the location of the oocytes. Hence, we have defined a death zone of fixed size which ends at the x-axis location of the eighth oocyte and begins at a fixed distance distal to it. At the moment, random cells within this death zone will be eliminated as soon as the amount of cells surpasses a certain number. As a constraint to random cell death, we defined an artificial Ras threshold, above which cells become insensitive to apoptosis; only cells below this level are selectable for cell death. This is a somewhat naïve approach to the induction of apoptosis; the present model is just preliminary in this respect. Once a cell has died, the timestep number of its death is recorded for analysis purposes and the cell disappears from the model.

2.2.4 Fertilisation

For simplicity, we currently define a cell as being fertilised when it reaches the end of the tube. As with the dead cells, the timestep numbers when fertilisations happen are recorded and the cells are removed from the model.

3 Results

3.1 Calibration

To calibrate the model, we extracted parameter values (shown in the first column of Table 12.1) from the literature and from our own videos of the germ line to compare with our model. Our observations have shown that, on average, it takes the cells 90 minutes to advance along the x-axis by the distance of their own diameter. Literature [28, 29] suggests that one mitotic cell cycle in the germ line is 16 to 24 hours. This calculates to an average time of 20 hours between divisions. For the death rate, our observations suggest that on average two cells die per hour per gonad arm, a value observed independently by many groups since the first characterisation of physiological germ cell apoptosis in *C. elegans* [19]. The literature and our own observations further suggest that the average egg laying rate is about four eggs per hour per animal [15]. We have to be careful to translate this for our model since we only consider one gonad, whereas the egg laying rate accounts collectively for both the anterior and posterior gonad. Consequently, we consider a fertilisation rate of two oocytes per hour per gonad arm as an approximation of the average over time.

As we will delineate in the following sections, our model produces values which are in correspondence with these expected experimental values.

3.1.1 Movement Rate

For the calculation of the movement rate, each cell is equipped with a list containing every timestep at which the cell has moved a distance forward equal to its current diameter. To evaluate the time that each of these steps has taken, we calculated the difference between every two succeeding timesteps. Figure 12.4 shows a histogram of these differences for all of the cells within the model. The distribution looks basically like a Gaussian. The average movement rate in our model is 5,250 steps for one diameter. Since we have observed the movement rate to be one diameter per 90 minutes *in vivo*, we can derive here that 90 minutes is equivalent to approximately 5,250 steps in our model. As a consequence, we can assume that one hour in real time is approximately 3,500 steps in our model.

Table 12.1 Table showing different properties extracted from experiments and literature (expected) and the according values derived from the present model (model) with the translation of these values into real time in the fourth column

Rate	Expected	Model	
Movement rate	1 row/90 min	1 row/5,250 steps	1 h = 3,500 steps
Time between divisions	20 h	$40k$ to $90k$ steps	19.19 h
Death rate	2 cells per h	1.57 cells/3,500 steps	2 cells per h
Fertilisation rate	2 cells per h	4.27 cells/3,500 steps	4 cells per h

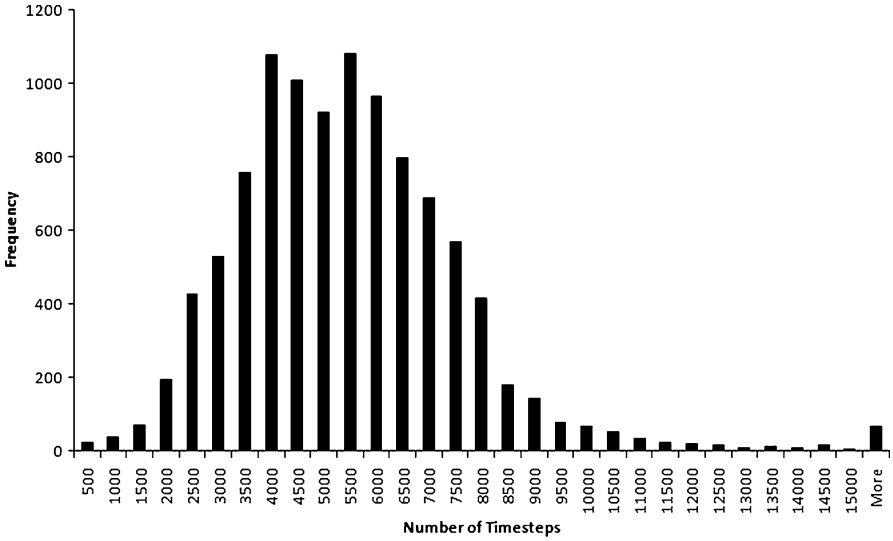

Fig. 12.4 Histogram showing a distribution of the number of timesteps needed for the advancement of each cell by one diameter

3.1.2 Time Between Divisions

Each cell carries a list containing all timesteps in which a division has occurred for this cell. By subtracting succeeding values, we have calculated the number of timesteps between two divisions. Figure 12.5 shows a histogram of these numbers for all of the cells in the model. The values for the time between divisions range from 40,000 to 90,000 timesteps. Using our estimation for real time from above, this is a range of 11 to 26 hours. The average of all times between divisions for all cells in our model is 67,158 timesteps which evaluates to about 19 hours.

3.1.3 Death Rate

For each dead cell, we have recorded the timestep number at which it died. To get an estimate of the death rate, we looked at bins of 3,500 timesteps, which is approximately one hour in real time (cf. Section 3.1.1). Figure 12.6 shows a histogram of the number of cell deaths occurring in these bins during an execution. Averaged over all bins, this computes to 1.57 deaths per bin or, in real time, 1.57 deaths per hour (continuous horizontal line). The figure shows that our reference indicated by the dashed horizontal line is only slightly higher than the average resulting in the model.

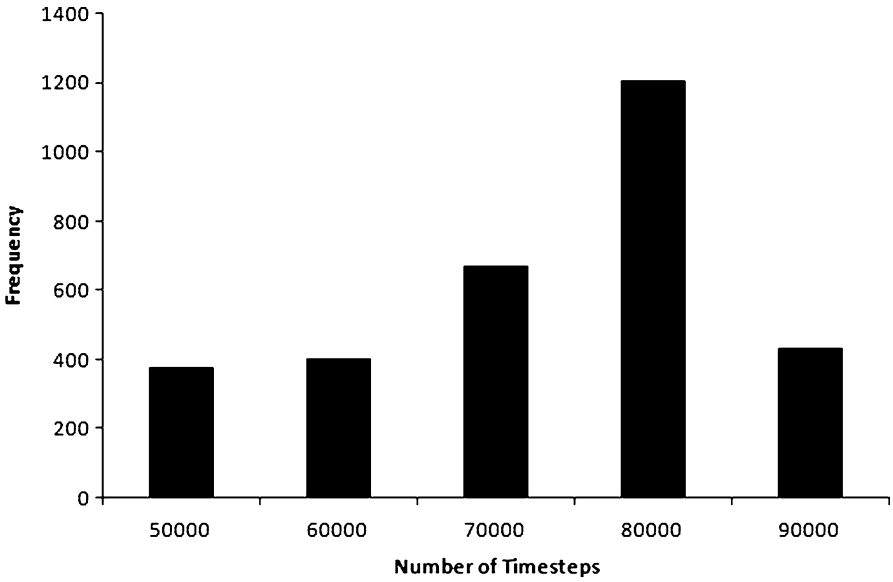

Fig. 12.5 Histogram showing the distribution of timesteps between divisions for all cells

3.1.4 Fertilisation Rate

We have also recorded the timestep at which fertilisation occurred for each fertilised cell. In a similar fashion to the death rate, we have sectioned this data in bins of 3,500 timesteps to get an estimate of the fertilisation rate. Figure 12.7 shows a histogram of the number of fertilisations per 3,500 timesteps. The figure also shows the average number of fertilisations per bin (or hour) which is 4.27 cells (continuous horizontal line). The literature reference, indicated by the dashed horizontal line in the figure, is lower than our model average.

3.1.5 Summary

Table 12.1 summarises the findings of our model calibration. Relative to the movement rate observed in our model, the time between divisions and the death rate in our model are very much in accordance with the values observed *in vivo*. Solely the fertilisation rate differs between our model and the experimental observations. These parameters are the major developmental components in our model. As a consequence, we can consider this model as, for our purposes, a very good approximation to the real organ since it reproduces the major developmental features very accurately.

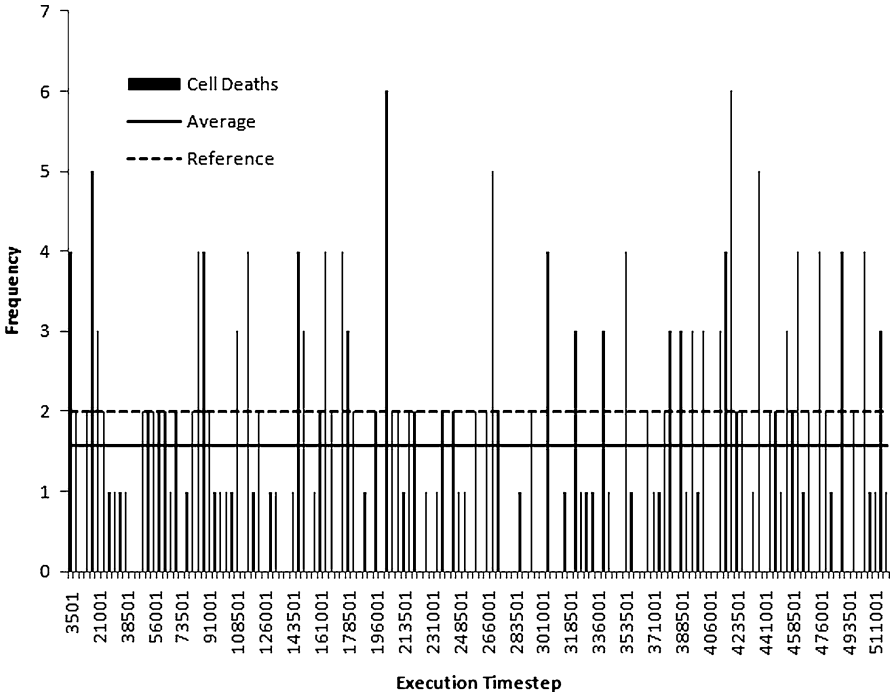

Fig. 12.6 Histogram of the number of cell deaths over bins of 3,500 execution timesteps. The *continuous horizontal line* indicates the average number of cell deaths per 3,500 timesteps, the *dashed line* shows the experimental reference

3.2 Further Results

3.2.1 Cell Numbers

Figure 12.8 shows the development of cell numbers in the different developmental stages and of the total number of cells over execution time. One can see that our model is in a steady state in terms of cell numbers and that none of these values significantly fluctuates. This is in accordance with *in vivo* observations of the germ line of an adult wild-type animal [15, 28].

3.2.2 Density

Figure 12.9 shows the average density in bins of about 1.5 basic cell radii from the distal end of the germ line up to the beginning of the loop. The average is taken of the density factors of all cells whose centre is within the respective bin. As defined earlier, a density factor of 1 represents an ideal packaging around an individual cell, while a factor of 0 indicates a cell that does not have neighbours that touch it.

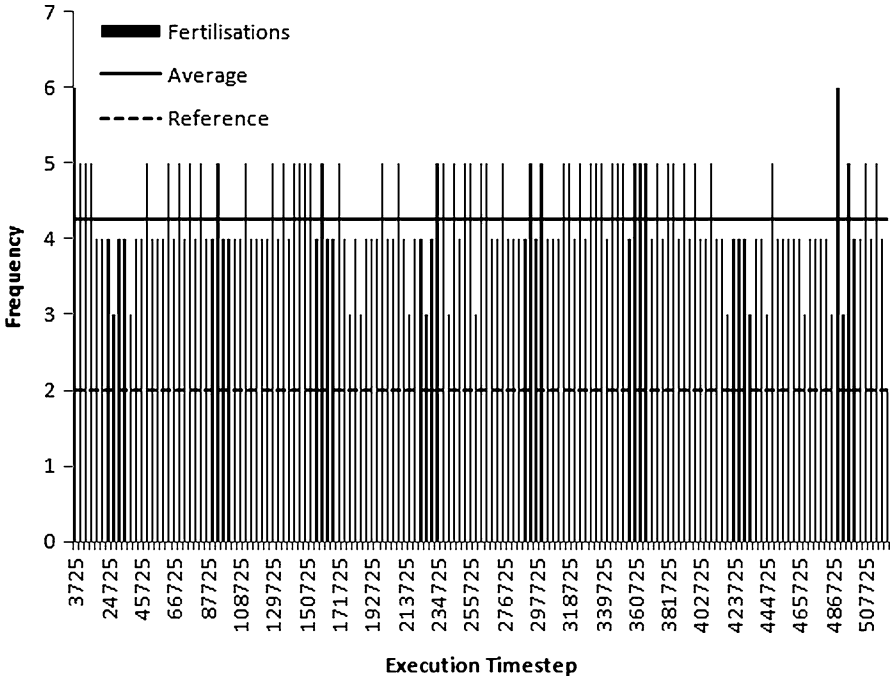

Fig. 12.7 Histogram of the number of fertilised cells over bins of 3,500 execution timesteps. The *continuous horizontal line* indicates the average number of fertilised cells per 3,500 timesteps, the *dashed line* shows the literature reference

A value above 1 hence indicates overcrowding through overlap of neighbouring cells. Figure 12.9 shows that the average density factor is relatively low. The figure also shows that the size changes of germ cells are especially important in terms of the density factor. In the region between 33 and 75, where there should be only few dividing cells – apart from a few outliers – and where the cells do not grow, the density is lowest and it does not fluctuate as much as in the other regions. The changes in density by growth are especially apparent in the region from 75 up to the end of the plot. Apart from a dip between 105 and 109, the density constantly increases, which is also true for the size of the cells in this region. The dip in this increase could be due to space that is freed up by dead cells since this is the region of the tube where the death zone is located.

3.2.3 Following Marked Cells

As mentioned in the Model section, we are able to label cells in our model and follow them on their course through the germ line. Here, we have followed one cell and its 12 offspring to get more information about what happens to individual cells in our model.

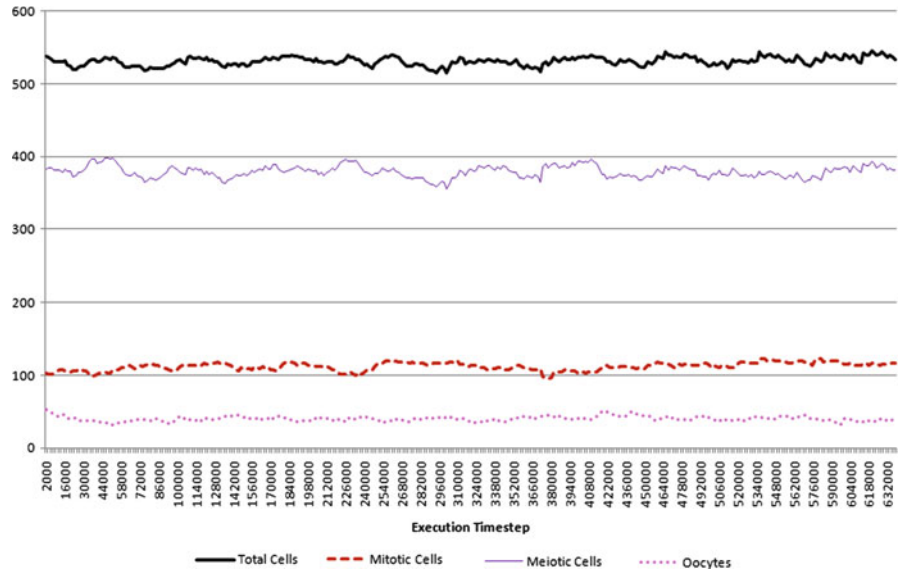

Fig. 12.8 Graph showing the development of cell numbers over execution time; the *thick continuous line* represents the total number of cells, the thin continuous line stands for the number of meiotic cells, the *dashed line* is for the mitotic cells and the *dotted line* for the oocytes

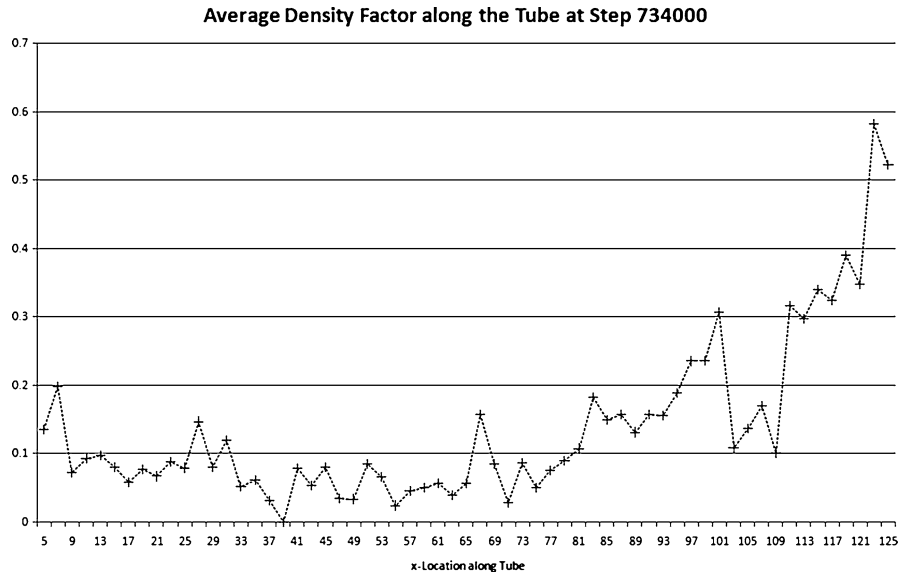

Fig. 12.9 Graph showing the average density along the germ line from the distal end up to the bend in bins of approximately 1.5 basic cell radii at execution step 734,000

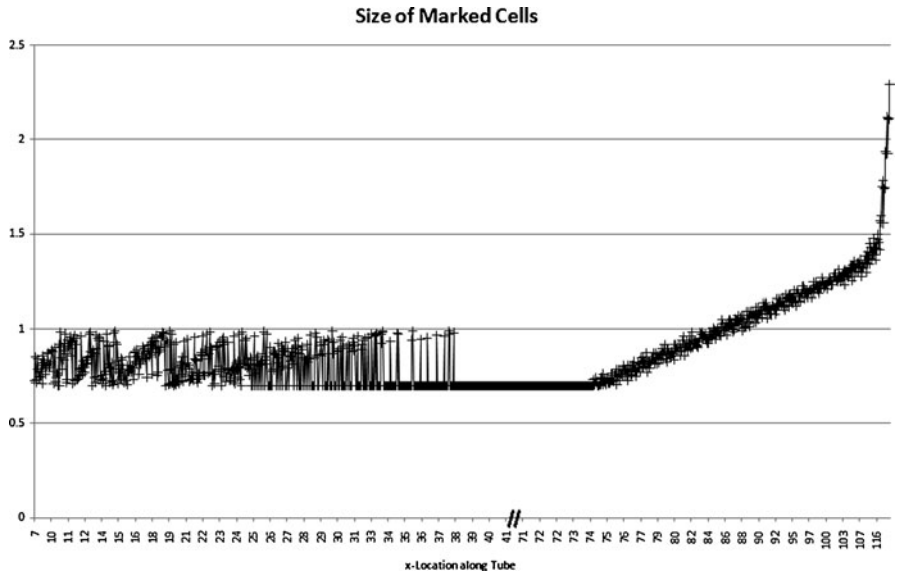

Fig. 12.10 Graph showing the sizes of the marked cells according to their location in the germ line from the distal end up to the bend during the whole execution

Figure 12.10 depicts the development of size of these individually marked cells from the distal end up to the beginning of the loop. For illustration, we have excluded values ranging between 42 and 70 on the x-axis since the values remain constant. The figure shows that the size of cells in the mitotic zone and the transition zone ranges between 0.7 and a value just below 1. This is due to the fact that the basic cell size is 0.7 and dividing cells grow from this size up to $\sqrt{2} \cdot 0.7$ which is just below 1. From about 30 up to 37 there does not seem to be a smooth change of size but rather an oscillation between maximal and basic size. This indicates that cells of big size are pushed from the mitotic zone into this area of the germ line to divide there. They do not grow anymore since they enter meiosis after the division. This area represents the transition zone. The figure also shows that between about 37 and 75 there is no growth before a constant linear growth of the cells sets in. This growth changes to a much steeper one at the end which corresponds to the region of the tube where the first cells reach Ras levels above the threshold causing them to grow faster. This figure also underlines our assumptions in the previous paragraph that growth and division of cells are very important in the development of the density factor.

Figure 12.11 shows the development of the density factor for the marked cells over the distance from the distal end of the gonad to the beginning of the loop. As in the averaged case, the density factor is generally fairly low. Since each mark in the graph stands for the density factor of one single cell, it is expected that the factor scatters more widely here. While some cells have a density factor of 0, others have

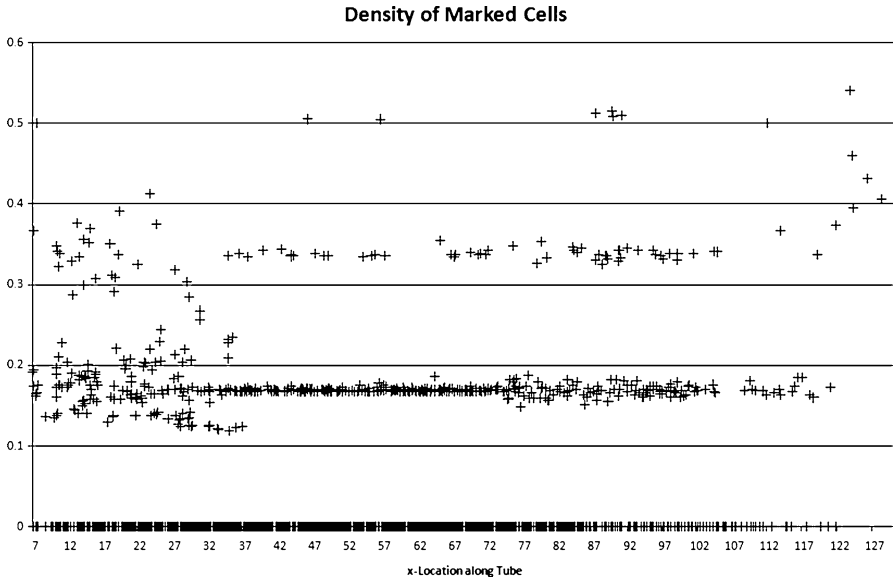

Fig. 12.11 Graph showing the density factors of the marked cells according to their location in the germ line from the distal end up to the bend during the whole execution

one of more than 0.5. While in Fig. 12.9, the average density is never above 0.2 up to about 95 on the x-axis, individual cells in Fig. 12.11 show several values above 0.2 and even some that are above 0.5 in the same region. Similar to Fig. 12.9, Fig. 12.11 also shows that in the region without cell growth and with only some division, i.e. between about 35 and 75 (cf. Fig. 12.10), the density stays relatively constant and there are more cells with very low density factors. In fact, Fig. 12.11 shows that from about 80, where growth is continuously strong, less and less of the marked cells retain a density factor of 0.

Figure 12.12 shows the dynamic behaviour of Notch and Ras within the marked cells according to their location between the distal end and the beginning of the loop in response to external signals. Similar to Fig. 12.10, we have excluded the range between 28 and 72 on the x-axis since the component levels do not change in this area. In the most distal part of the tube, the external Delta ligand of Notch signalling is present. Figure 12.12 shows that, in response to this, all cells reach the maximal Notch level, which again decays in the absence of Delta. The figure further shows that some cells reach the lowest Notch level farther down the tube than others. Since, in each cell, the Notch level linearly decays over time at the same rate, this indicates a difference in speed of the marked cells. Figure 12.12 also shows that in the presence of external Ras inducing signal, generally the Ras level within the cells constantly increases as they progress along the tube. There are a few cells before the area where the external Ras signal is present which nonetheless have an internal Ras level above 0. These are probably cells that were pushed back out of the Ras zone

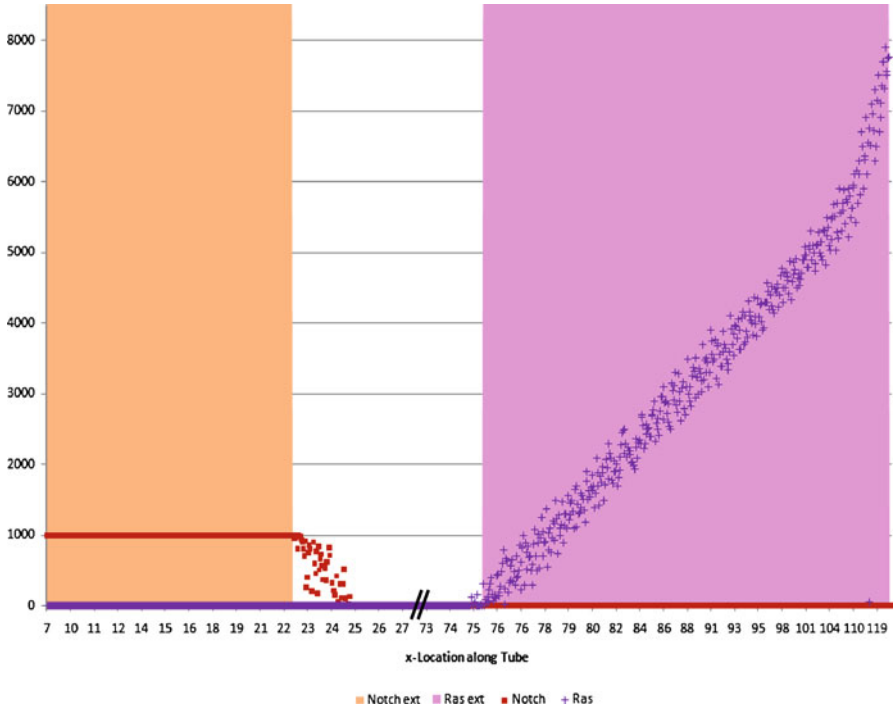

Fig. 12.12 Graph showing the Notch and Ras levels within the marked cells along with the status of external Delta and external Ras according to location in the germ line from the distal end up to the bend during the whole execution. The *shaded area* on the left indicates the region of the germ line where the Delta ligand is present (corresponding to the mitotic region), the *shaded area* on the right signifies the same for the external Ras (corresponding to the region before the gonad bend). The *squares* represent the cell internal Notch levels, the *crosses* represent the internal Ras levels

after having been in it for a short while. Similar to the speed of the cells relating to the Notch decay, Fig. 12.12 shows that there seems to be one cell at location 114 which still has a very low Ras level. Presumably, this cell was pushed much faster to this location than the other ones and has hence not had enough time to accumulate as much Ras. Apart from this single case, the Ras level does not seem to fluctuate significantly, which indicates a mainly constant forward speed of the cells.

4 Discussion

In the present work, we have developed and calibrated a physical computational model of the *C. elegans* germ line. The model highlights a novel way of using MD as a central engine of computational models simulating physical cell movement. The usage of the accurate physical features allows our model to be calibrated in a way that matches simulation and experimental time. The stress on physical features allows us to combine important developmental aspects such as cell division and

growth in a realistic way. In addition, key molecular pathways, differentiation and apoptosis are added, leading to a realistic model that can be used to an extensive analysis of our concept of the underlying system.

The usefulness of physical and molecular dynamics-like approaches to cell movement has been demonstrated in different settings [22, 24, 25, 27], mostly involving cell populations of tissues. In these models, especially the ones modelling more or less constant tissue-cell populations without cell divisions [24, 25], the physical movement caused by overlap of cells is only a by-product of an active movement along a chemical or nutritional gradient. In models including cell division [22, 27], this aspect of movement is more prominent but still limited due to nutrient dependence or contact inhibition. In our model, however, cells move purely due to physical compression by other cells arising from cell divisions and growth of cells. Our model visually represents this compression by overlap of the circles. To our knowledge, the present model is the first to simulate cell movement purely based on these physical aspects without any active migration. The lack of active movement in our model is in accordance with the experimental observations in the biological system [28, 29].

While still a simplified representation of the germ line, our model produces cell movement that looks very natural, and we were able to calibrate the model in accordance to different experimental observations found in the literature [15, 19, 28] as well as from our own experiments. We have used the cell movement rate derived from our own observations and [28, 29] to incorporate a measure of real time in our model. The comparison allowed us to identify the approximate number of timesteps in our model that represents an hour in real time. Based on this value, the division rate from our model is very much in accordance with the one observed in the literature [28]. The same is true for the death rates that we observed in the model and experimentally. Only the fertilisation rate differed slightly from the value in the literature [15]. Furthermore, the value might change after including the rachis in a revised version of our model, which will change the cell movement close to the end of the germ line. In addition to calibrating, our model allows us to observe properties of single marked cells like density factor, size and kinetics at any timepoint. These aspects can be used in the future to test or evolve new hypotheses like density dependent apoptosis or time-dependent developmental progression of individual cells. Furthermore, these parameters allow feeding the model by results from wet lab experimentation and vice versa. Conclusively, our physical MD modelling approach can be very useful in this setting and extensions to the present model promise to advance our understanding of fundamental biological processes.

5 Future Prospects

We will try to overcome certain limitations of our current simplified model. Including the rachis into our model is very important as this might improve the values of the death and fertilisation rates and will render the model as a whole

visually more realistic. Further, extending the abstract "Notch" and "Ras" signalling pathways by their individual regulatory components could help us to gain a more detailed understanding of the biological system.

The successful calibration of our model renders it amenable to testing hypotheses about the germ line system and about specific aspects of development. Our major goal will be to test different possible mechanisms of apoptosis. It is known that about 50% of all potential oocytes die; one likely explanation is the need for nurse cells that synthesise enough cytoplasm for the rapidly growing oocytes [15, 19]. So far it is unclear how the decision is taken when and which of the cells should die. A probable explanation is that there is a balance between the cytoplasm being produced and the number of cells allowed to progress [19]. Still, apoptosis could be random or clearly determined by aspects like Ras activity level, developmental timing or cell size. Another very interesting aspect of the germ line is the question of symmetric versus asymmetric division of stem cells. It has not been fully resolved whether the post-larval germinal stem cells divide symmetrically or asymmetrically, i.e. if both daughter cells retain stem cell properties and can divide further or if only one of the daughter cells remains in the mitotic zone whereas the sister progresses toward maturation into a gamete, respectively. The prevailing model assumes that the division happens symmetrically [33]. Still, some of the cells might remain in the mitotic zone if they are not pushed by other dividing cells [28]. We will focus our future modelling work on these two and other sparsely understood aspects of the *C. elegans* germ line to gain further understanding and generate input for wet lab experiments that can validate the model's predictions.

Acknowledgements We are grateful to James Margetson for contributing an initial environment program in F# on which this model is based and for his support on the usage of F#. Antje Beyer is grateful to Adrian Hemmen for introducing her to the MD framework and for critical and helpful discussions of the model. This work was supported in part by the European Union grant FP7 PANACEA 222936 (Jasmin Fisher, Michael O. Hengartner and Alex Hajnal) and the Swiss National Science Foundation (Michael O. Hengartner). Antje Beyer is funded by Microsoft Research through its PhD Scholarship Programme.

References

1. Brenner S (1974) The genetics of *Caenorhabditis elegans*. Genetics 77(1):71–94
2. Hillier LW, Coulson A, Murray JI, Bao Z, Sulston JE, Waterston RH (2005) Genomics in *C. elegans*: so many genes, such a little worm. Genome Res 15(12):1651–1660
3. Potts MB, Cameron S (2010) Cell lineage and cell death: *Caenorhabditis elegans* and cancer research. Nat Rev Cancer 11:50–58
4. Joshi PM, Riddle MR, Djabrayan NJV, Rothman JH (2010) *Caenorhabditis elegans* as a model for stem cell biology. Dev Dynam 239(5):1539–1554
5. Riddle DL, Blumenthal T, Meyer BJ, Priess JR (1997) *C. elegans* II. CSHL, Cold Spring Harbor, New York
6. Corsi AK (2006) A biochemist's guide to *Caenorhabditis elegans*. Anal Biochem 359(1):1–17
7. Sulston J (1977) Post-embryonic cell lineages of the nematode, *Caenorhabditis elegans*. Dev Biol 56(1):110–156

8. Kipreos ET (2005) *C. elegans* cell cycles: invariance and stem cell divisions. Nature reviews. Mol Cell Biol 6(10):766–776
9. Hubbard EJA, Greenstein D (2005) Introduction to the germ line. WormBook: the online review of *C. elegans* biology, ed. The C. elegans Research Community, WormBook, doi/10.1895/wormbook.1.18.1, http://www.wormbook.org
10. Kimble J, Crittenden SL (2005) Germline proliferation and its control. WormBook: the online review of *C. elegans* biology, ed. The C. elegans Research Community, WormBook, doi/10.1895/wormbook.1.13.1, http://www.wormbook.org
11. Gartner A, Boag PR, Blackwell TK (2008) Germline survival and apoptosis. WormBook: the online review of *C. elegans* biology, ed. The C. elegans Research Community, WormBook, doi/10.1895/wormbook.1.145.1, http://www.wormbook.org
12. Korta DZ, Hubbard EJA (2010) Soma-germline interactions that influence germline proliferation in *Caenorhabditis elegans*. Dev Dynam 239(5):1449–1459
13. Hanahan D, Weinberg RA (2011) Hallmarks of cancer: the next generation. Cell144(5):646–674
14. Krantic S, Mechawar N, Reix S, Quirion R (2005) Molecular basis of programmed cell death involved in neurodegeneration. Trends Neurosci 28(12):670–676
15. Hirsh D, Oppenheim D, Klass M (1976) Development of the reproductive system of *Caenorhabditis elegans*. Dev Biol 49(1):200–219
16. Hansen D, Hubbard EJA, Schedl T (2004) Multi-pathway control of the proliferation versus meiotic development decision in the *Caenorhabditis elegans* germline. Dev Biol 268(2):342–357
17. Kimble J, White J (1981) On the control of germ cell development in *Caenorhabditis elegans* 1. Dev Biol 81(2):208–219
18. Waters KA, Reinke V (2011) Extrinsic and intrinsic control of germ cell proliferation in *Caenorhabditis elegans*. Mol Rep Dev 78(3):151–160
19. Gumienny TL, Lambie E, Hartwieg E, Horvitz HR, Hengartner MO (1999) Genetic control of programmed cell death in the *Caenorhabditis elegans* hermaphrodite germline. Development 126(5):1011–1022
20. Church DL, Guan KL, Lambie EJ (1995) Three genes of the MAP kinase cascade, mek-2, mpk-1/sur-1 and let-60 ras, are required for meiotic cell cycle progression in *Caenorhabditis elegans*. Development 121(8):2525–2535
21. Alder BJ, Wainwright TE (1959) Studies in molecular dynamics. I. General method. J Chem Phys 31(2):459
22. Drasdo D, Kree R, McCaskill J (1995) Monte Carlo approach to tissue-cell populations. Phys Rev E 52(6):6635–6657
23. Beyer T, Meyer-Hermann M (2007) Modeling emergent tissue organization involving high-speed migrating cells in a flow equilibrium. Phys Rev E 76(2):27
24. Beyer T, Meyer-Hermann M (2009) Multiscale modeling of cell mechanics and tissue organization. IEEE Eng Med Biol Mag 28(2):38–45
25. Palsson E (2001) A three-dimensional model of cell movement in multicellular systems. Future Gener Comput Syst 17(7):835–852
26. Palsson E, Othmer HG (2000) A model for individual and collective cell movement in *Dictyostelium discoideum*. Proc Natl Acad Sci USA 97(19):10448–10453
27. Schaller G, Meyer-Hermann M (2005) Multicellular tumor spheroid in an off-lattice Voronoi–Delaunay cell model. Phys Rev E 71(5):1–16
28. Crittenden SL, Leonhard KA, Byrd DT, Kimble J (2006) Cellular analyses of the mitotic region in the *Caenorhabditis elegans* adult germ line. Mol Biol Cell 17(7):3051–3061
29. Maciejowski J, Ugel N, Mishra B, Isopi M, Hubbard EJA (2006) Quantitative analysis of germline mitosis in adult *C. elegans*. Dev Biol 292(1):142–151
30. Swope WCA (1982) Computer simulation method for the calculation of equilibrium constants for the formation of physical clusters of molecules: application to small water clusters. J Chem Phys 76(1):637

31. Syme D, Granicz A, Cisternino A (2007) Expert F#. Apress, Berkeley, California
32. Accompanying movie [Internet] (2011) [cited 2011 Mar 27]. http://www.cs.le.ac.uk/people/npiterman/publications/2011/BEPHHF/index.html
33. Cinquin O, Crittenden SL, Morgan DE, Kimble J (2010) Progression from a stem cell-like state to early differentiation in the *C. elegans* germ line. Proc Natl Acad Sci USA 107(5):2048–2053

Cell Death and Differentiation (2011) 18, 897–906

www.nature.com/cdd

NER and HR pathways act sequentially to promote UV-C-induced germ cell apoptosis in *Caenorhabditis elegans*

L Stergiou[1,3,4], R Eberhard[1,2,4], K Doukoumetzidis[1] and MO Hengartner*[,1]

Ultraviolet (UV) radiation-induced DNA damage evokes a complex network of molecular responses, which culminate in DNA repair, cell cycle arrest and apoptosis. Here, we provide an in-depth characterization of the molecular pathway that mediates UV-C-induced apoptosis of meiotic germ cells in the nematode *Caenorhabditis elegans*. We show that UV-C-induced DNA lesions are not directly pro-apoptotic. Rather, they must first be recognized and processed by the nucleotide excision repair (NER) pathway. Our data suggest that NER pathway activity transforms some of these lesions into other types of DNA damage, which in turn are recognized and acted upon by the homologous recombination (HR) pathway. HR pathway activity is in turn required for the recruitment of the *C. elegans* homolog of the yeast Rad9-Hus1-Rad1 (9-1-1) complex and activation of downstream checkpoint kinases. Blocking either the NER or HR pathway abrogates checkpoint pathway activation and UV-C-induced apoptosis. Our results show that, following UV-C, multiple DNA repair pathways can cooperate to signal to the apoptotic machinery to eliminate potentially hazardous cells.
Cell Death and Differentiation (2011) **18,** 897–906; doi:10.1038/cdd.2010.158; published online 10 December 2010

Eukaryotic cells possess several surveillance mechanisms that, upon sensing DNA damage, initiate signaling cascades that lead to response programs such as cell cycle arrest, DNA repair and apoptosis, to protect the organism against the introduction of new mutations. Disruption of such pathways results in increased genomic instability, a hallmark of most types of cancers.[1,2]

Genetic and biochemical studies have provided a thorough mechanistic understanding of the various repair processes initiated upon recognition of specific types of lesions. For example, the nucleotide excision repair (NER) pathway removes cyclobutane pyrimidine dimers (CPDs) and 6-4 photoproducts generated upon exposure to ultraviolet (UV-C) light, whereas the homologous recombination (HR) machinery repairs double-strand DNA breaks (DSBs) induced by treatments such as ionizing radiation (IR).[3]

Mutations in NER components underlie the syndromes xeroderma pigmentosum (XP), trichothiodystrophy or Cockayne syndrome. Patients are hypersensitive to sunlight and exhibit a variety of clinical features, including developmental defects, predisposition to skin cancer or internal tumors, neurological disorders and highly accelerated aging.[4] Studies in cell culture and mouse models,[5,6] as well as in yeast have led to the detailed molecular characterization of the NER factors.[3] Besides repair, many of these factors participate in the signaling network that ultimately balances cellular DNA damage responses between genome maintenance, senescence and death. Accordingly, loss of their function has consequences for DNA repair, cellular proliferation and survival.[6–8]

Simple model organisms are very useful to decipher complex DNA damage responses. In *Caenorhabditis elegans*, the effects of IR have been studied extensively.[9,10] We previously reported a genetic pathway that induces both apoptotic cell death of meiotic cells and cell cycle arrest of proliferating mitotic cells following UV-C treatment.[11] We identified several new genes required for these responses and genetically ordered them into a signaling pathway that overlaps with, but is distinct from the pathway(s) activated upon IR.

In this study, we investigate the molecular mechanism by which UV-C triggers apoptosis in the *C. elegans* adult hermaphrodite germ line. We show that lesions caused by UV-C are not pro-apoptotic *per se*; rather, they first require processing by the NER machinery before they can activate apoptosis. A fraction of UV-C lesions is likely transformed by NER into DNA intermediates that are substrates for the HR machinery. Activation of the latter, in turn, leads to recruitment of the *C. elegans* homolog of the yeast Rad9-Hus1-Rad1 (9-1-1) complex, activation of downstream checkpoint kinases

[1]Institute of Molecular Life Sciences, University of Zurich, Winterthurerstrasse 190, Zurich 8057, Switzerland and [2]PhD Program in Molecular Life Sciences, Life Science Zurich Graduate School and MD/PhD Program, University of Zurich, Zurich, Switzerland
*Corresponding author: MO Hengartner, Institute of Molecular Life Sciences, University of Zurich, Winterthurerstrasse 190, Zurich 8057, Switzerland. Tel: +41 44 635 3140; Fax: +41 44 635 6861; E-mail: michael.hengartner@imls.uzh.ch
[3]Current address: Pike Pharma, Schlieren-Zurich, Switzerland.
[4]These authors contributed equally to this work.
Keywords: apoptosis; *C. elegans*; HR; NER; UV-C
Abbreviations: UV-C, ultraviolet light C (254 nm); IR, ionizing radiation; CPDs, cyclobutane pyrimidine dimers; DSB, double-strand DNA break; NER, nucleotide excision repair; HR, homologous recombination; 9-1-1 complex, Rad9-Hus1-Rad1 complex (HPR-9/HUS-1/MRT-2 in *C. elegans*); XPA, XPB, XPD, XPF, XPG, xeroderma pigmentosum complementation group A, B, D, F, G; RPA-1, replication protein A large subunit homolog in *C. elegans*
Received 06.5.10; revised 07.9.10; accepted 20.9.10; Edited by E Baehrecke; published online 10.12.10

and initiation of p53-dependent apoptosis. Our results indicate that UV-C-induced apoptosis in *C. elegans* requires the sequential activation of at least two distinct DNA damage response pathways.

Results

Components of the HR pathway are required for UV-C-induced apoptosis. We previously showed that in *C. elegans* UV-C radiation induces cell cycle arrest in mitotic germ cells and apoptosis of meiotic cells at the pachytene stage.[11] We also reported that XPA-1 and XPC-1, two components of the NER pathway, are required for the activation of these responses, with XPA-1 acting upstream of the 9-1-1 complex protein HUS-1 and the p53 homolog CEP-1 in UV-induced apoptosis.[11]

How does XPA-1 function promote p53 activation following UV-C exposure? One possibility is that NER processes a fraction of UV-C-induced damage into other types of DNA structures, which might in turn activate apoptosis. Given our previous observation that many genes involved in response to DSBs are also activated following UV-C, we focused our initial attention on the HR pathway. *mre-11(ok179)* mutants, which lack the exonuclease responsible for the initial processing of DSBs during meiosis, showed a compromised apoptotic response to UV-C, suggesting a requirement for MRE-11 in the initiation of UV-C-induced apoptosis (Figure 1a). By contrast, IR-induced apoptosis was only slightly reduced (Figure 1a), in agreement with previous reports,[12] possibly owing to alternative processing pathways.

The homologs of RAD-54 and RAD-51 functionally interact during recombinational repair in yeasts and mammals.[13,14] We analyzed two previously uncharacterized, likely null *rad-54* mutants, *tm1268* and *ok615* (Supplementary Figure 1a). As homozygous *rad-54* progeny from heterozygous mothers show fully penetrant maternal-effect lethality, we analyzed first-generation homozygotes for germline apoptosis. Under normal growth conditions, both *rad-54(ok615)* and *rad-54(tm1268)* mutants exhibit a strong increase in germline apoptosis, an effect that could be phenocopied by RNAi (Figure 1b). This increase was dependent on the endonuclease SPO-11, which specifically generates the DSBs that initiate meiotic recombination (Figure 1c),[12] suggesting that the increased germ cell death is due to the accumulation of unresolved recombination intermediates. *rad-54(rf)*-induced apoptosis was abrogated in *atl-1(tm853)* or *cep-1(RNAi)* animals, and reduced in *atm-1(gk186)* mutants (Figures 1d and e). These results suggest that *rad-54(lf)* mutants accumulate DSBs, which activate apoptosis in an ATL-1/ATM-1- and CEP-1-dependent manner.

Interestingly, exogenous damage by X-rays or UV failed to further increase the levels of germ cell apoptosis in *rad-54(ok615)* mutants (Figure 1f), suggesting either that the DNA damage response pathway (or the apoptotic machinery to which it signals) is already 'saturated' by the strong signal generated by the unresolved meiotic intermediates in *rad-54* mutants or that the HR pathway is required for IR- and UV-induced apoptosis. To address this issue, we blocked SPO-11 endonuclease function. We found that *rad-54(RNAi);spo-11(ok79)* animals showed a greatly reduced response to IR and, surprisingly, also to UV (Figure 1g). Importantly, *spo-11(ok79)* mutants respond normally to both IR and UV, showing that the DNA damage response pathways are functional (Figure 1g). The HR pathway therefore plays an important role in promoting apoptosis in response to UV-C.

Finally, we tested animals lacking the recombinase RAD-51. In the human and yeast homologs, RAD-51 acts downstream of MRE-11 and RAD-54 to promote strand exchange during HR. *rad-51(RNAi)* animals also fail to complete meiotic recombination, resulting in increased basal levels of apoptosis (Figure 1h). However, unlike in *rad-54* mutants, this increase can be suppressed only by *atl-1(tm853)*, but not *atm-1(gk186)* (Supplementary Figure 2). In contrast to *mre-11* and *rad-54* mutants, *rad-51(lf)* animals did not show any defect in either UV- or IR-induced apoptosis (Figure 1h).[15] Moreover, UV-C treatment led to RAD-51 foci formation (Supplementary Figure 3a), independent of both *xpa-1* and *rad-54* (Supplementary Figures 3b and c). These observations suggest that UV-C-induced RAD-51 foci formation and apoptosis are independent events, and that RAD-51 is not essential for UV-C-induced apoptosis.

Taken together, our results support the idea that the proteins involved in early stages of HR also act to promote apoptosis in response to UV-C damage.

The HR pathway acts downstream of the NER pathway to promote UV-C-induced apoptosis

The data above suggest that both NER and HR pathways are required for UV-C-induced apoptosis. These two pathways might act in parallel and be simultaneously required for the induction of apoptosis. Alternatively, they might act in succession, with NER recognizing and processing the initial UV-C lesions and HR relaying the signal to the apoptotic machinery. To distinguish between these two possibilities, we determined the effect of mutations in the NER or HR pathways on the subcellular localization of selected DNA damage response proteins.

We started by examining the distribution of a functional RAD-54::YFP fusion protein (Supplementary Figure 1b). RAD-54::YFP formed foci following exposure to both IR or UV-C, consistent with our observation that the HR pathway participates in UV-C-induced responses (Figure 2a). In *xpa-1* and *xpc-1* mutants, foci accumulation following UV treatment, but not IR, was dramatically reduced (Figure 2b), suggesting that the NER component XPA-1 acts upstream of RAD-54 recruitment in the UV-C response pathway.

We previously showed that *xpa-1* or *xpc-1* mutants exhibit increased basal levels of apoptosis in the germ line,[11] probably because accumulation of unrepaired endogenous damage leads to apoptosis through the activation of (an)other DNA damage signaling pathway(s). Interestingly, the basal levels of RAD-54::YFP foci were also elevated in the absence of *xpa-1* (Figure 2b), suggesting that the HR pathway mediates the increased apoptosis observed in *xpa-1* mutants. Consistent with this hypothesis, mutations in genes that act downstream of DNA DSBs, such as *hus-1* and *atl-1* (Supplementary Table S1), as well as *atm-1* and *cep-1*[11] abrogated the apoptosis phenotype of *xpa-1* mutants.

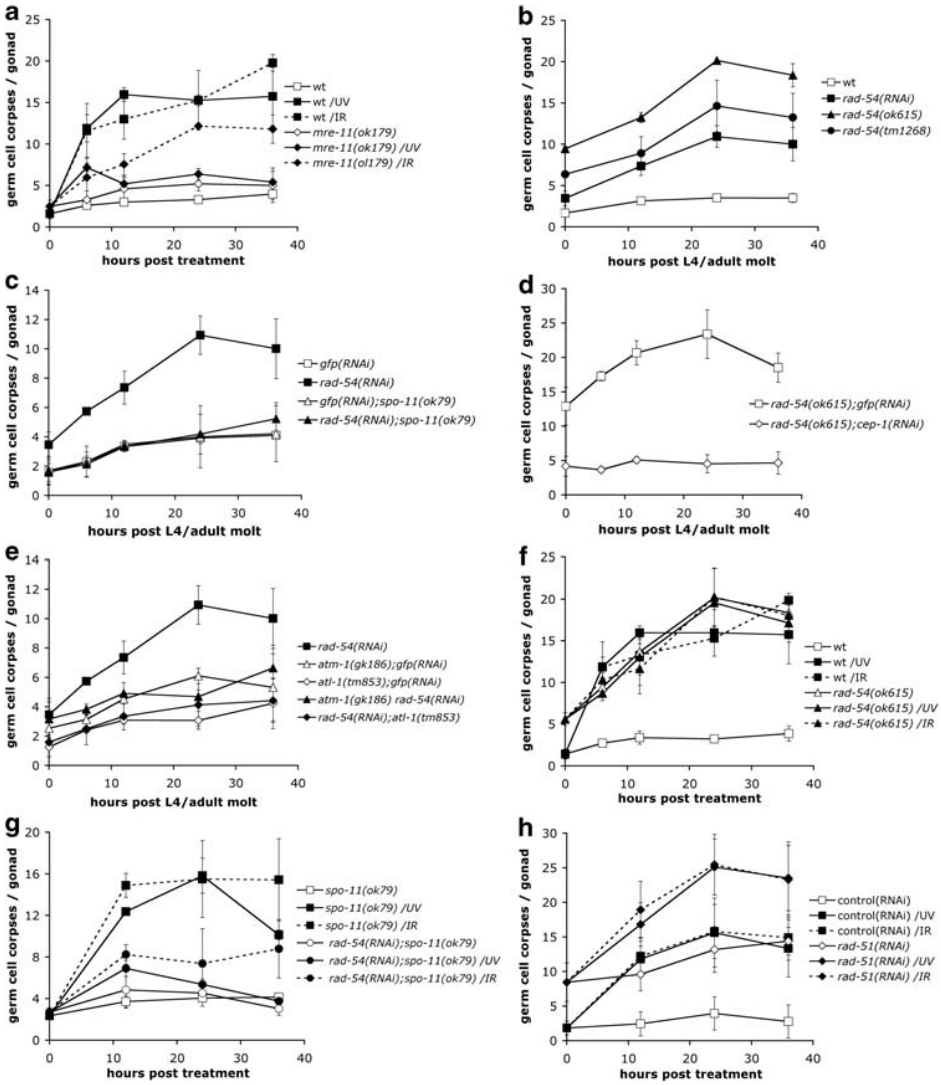

Figure 1 Several components of the HR repair pathway are required for UV-C-induced germ cell apoptosis. (**a**) *mre-11* mutants fail to induce apoptosis in response to UV-C. Staged young adult *mre-11(ok179)* animals were treated with either 100 J/m^2 UV-C or 120 Gy X-rays and germ cell corpses were scored at the indicated time points. (**b**–**e**) Genetic characterization of *rad-54* mutants. (**b**) *rad-54(lf)* results in increased levels of germ cell apoptosis. Germ cell corpses were scored every 12 h until 36 post the L4/adult molt in staged *rad-54(ok615)* or *rad-54(tm1268)* mutants, or *rad-54(RNAi)*-treated animals. (**c**–**e**) *rad-54(lf)*-induced germ cell death depends on *spo-11* (**c**), *cep-1* (**d**) and ATM/ATR function (**e**). (**f**) *rad-54* mutants fail to induce apoptosis in response to UV-C and IR. Staged young adult *rad-54(ok615)* animals were treated with either 100 J/m^2 UV-C or 120 Gy X-rays and germ cell corpses were scored at the indicated time points. (**g**) Loss of *spo-11* function does not restore UV-C- and IR-induced apoptosis in *rad-54(RNAi)* animals. Staged *spo-11(ok79)* L1 larvae were raised on bacteria expressing *rad-54* or gfp dsRNA, and were treated with either 100 J/m^2 UV-C or 120 Gy X-rays as young adults. Germ cell corpses were scored at the indicated time points. (**h**) *rad-51(lf)* animals normally induce apoptosis in response to UV-C. Staged wild-type L1 larvae were raised on bacteria expressing *rad-51* or control dsRNA, and were treated with either 100 J/m^2 UV-C or 120 Gy X-rays as young adults. Germ cell corpses were scored at the indicated time points. Data shown in all cases represent the average ± S.D. of two or three independent experiments ($n > 20$ animals for each experiment)

We also examined the localization of RAD-54::YFP in *atm-1*, *hus-1* and *mre-11* mutants. Foci formation was essentially wild type in *atm-1* mutants and only mildly affected in *hus-1* mutants, indicating that ATM-1 and HUS-1 are either not required for or act downstream of RAD-54 recruitment to sites of DNA damage. By contrast, UV-C-treated *mre-11* animals failed to show any focal accumulation of RAD-54::YFP in the mid–late pachytene cells (Figure 2b), whereas IR-treated animals exhibited wild-type foci numbers throughout the gonad (Figure 2b). Therefore, two (or more) distinct mechanisms for RAD-54 recruitment to sites of damage might exist, which differ in their requirement for MRE-11. Interestingly, Hayashi and co-workers[16] have shown a similar difference in the requirement of RAD-50 for RAD-51 loading onto sites of DSBs.

Next, we examined the distribution of the replication protein A subunit homolog in *C. elegans* (RPA-1). RPA is a heterotrimeric single-stranded DNA-binding protein highly conserved in eukaryotes that plays an important role in DNA replication and repair.[17–20] Transgenic animals expressing

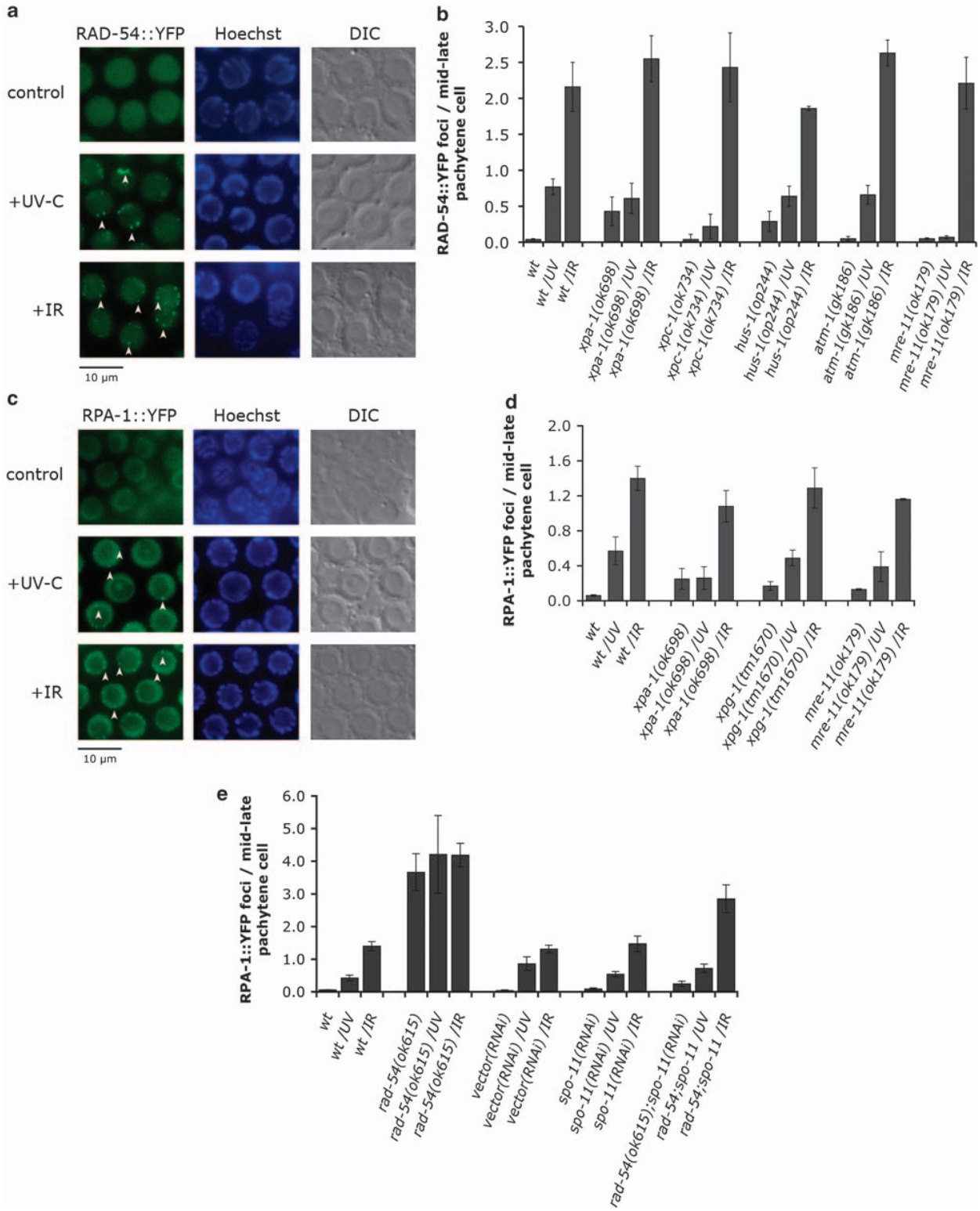

Figure 2 The HR pathway acts downstream of the NER pathway to induce UV-C-induced germ cell apoptosis. (**a** and **c**) Fluorescent microscopy of mid–late pachytene germ cells expressing RAD-54::YFP (**a**) or RPA-1::YFP (**c**). Germ cell nuclei from staged young adult wild-type animals were scored for the presence of YFP, 3 h after exposure to 100 J/m^2 of UV-C or 120 Gy of X-rays. RAD-54 or RPA-1 show a diffuse nuclear staining in control animals, but relocalize into distinct foci following treatment (arrowheads). (**b**) XPA-1, XPC-1 and MRE-11 are required for RAD-54 foci formation in response to UV-C, but not IR. (**d** and **e**) UV-C-induced RPA-1 foci require XPA-1 (**d**), but not MRE-11 (**d**) or RAD-54 (**e**). RAD-54::YFP and RPA-1::YFP foci were quantified as described in Materials and Methods. Data shown represent the average ± S.D. of at least two experiments ($n \geq 15$ worms for each experiment)

YFP-tagged RPA-1, the homolog of the largest human RPA subunit p70, showed foci as early as 30 min after UV-C or IR treatment, reaching a plateau 3.5 h later (Figures 2c and d; Supplementary Figures 4a and b). Loss of XPA-1 completely blocked the increase of RPA-1 foci following UV, but not IR, suggesting that the NER machinery is required for UV-C-, but not for IR-induced accumulation of RPA-1 (Figure 2d).

In *rad-54* mutants, RPA-1::YFP foci numbers were increased even in the absence of treatment (Figure 2e), likely marking sites of unresolved meiotic recombination intermediates.[21] Surprisingly, UV-C and IR treatment did not increase much further the number of RPA-1::YFP foci in *rad-54* mutants (Figure 2e). To distinguish between saturation in DNA damage signaling and a requirement for RAD-54 in damage-induced foci formation, we used a *spo-11*-deficient background. Both the excess in apoptosis and the high levels of RPA-1::YFP foci were abrogated in *rad-54(ok615);spo-11(RNAi)* animals (Figures 1g and 2e), and exposure to UV-C now led to a robust increase in foci number, suggesting that RPA-1 foci formation occurs upstream of, or in parallel to, RAD-54 in the UV response. RPA-1::YFP foci similarly increased following UV-C in *mre-11(ok179)* mutants (Figure 2d). Thus, most RPA-1::YFP foci following UV-C require the NER machinery and occur upstream of the HR components tested here.

In summary, our results so far show that components of the HR pathway act downstream of the NER DNA damage recognition step to trigger UV-C-induced apoptosis. NER pathway activity leads to focal recruitment of RPA-1 and RAD-54 and signaling to the apoptotic machinery.

The NER components XPG, XPB and XPD are required to promote UV-C-induced apoptosis by recruitment of HR proteins. During NER, initial recognition of the lesion, carried out by XPA and XPC, is followed by local unwinding of the DNA, performed by two DNA helicases with opposite polarities, XPB and XPD.[22] This enables the excision step carried out by two structure-specific endonucleases, XPF and XPG.[23]

To determine whether NER steps downstream of DNA lesion recognition also play a role in UV-C-induced apoptosis, we analyzed germ cell apoptosis in animals with compromised or abolished XPB, XPD or XPG function. As with *xpa-1* and *xpc-1*, RNAi knockdown of *xpb-1* (Y66D12A.15) and *xpd-1* (Y50D7A.2) gave rise to increased basal levels of apoptosis (Figures 3a and b). These findings strengthen the notion that in the absence of NER, unrepaired endogenous damage can activate (an)other DNA damage signaling pathway(s) that lead to apoptosis. *xpb-1(RNAi)*- and *xpd-1(RNAi)*-treated animals showed reduced apoptosis levels upon both UV-C and IR (Figures 3a and b), suggesting that these two helicases are also involved in promoting UV-C-induced apoptosis.

We also analyzed the effect on apoptosis of two likely null alleles of the endonuclease gene *xpg-1* (F576B10.6) (Supplementary Figure 1c). UV-C-induced apoptosis was abolished in *xpg-1* mutants (Figure 3c). The observed defect in *xpg-1* (and *xpa-1*) mutants is not due to a general defect in germline physiology, which could reduce the number of cells that can undergo apoptosis: loss of *xpg-1* (or *xpa-1*) did not reduce apoptosis in animals defective in the antiapoptotic Bcl-2 homolog CED-9, nor did it affect the egg laying rate (Supplementary Figures 5a and b). IR-induced apoptosis still occurred in *xpg-1* mutants, although with reduced levels (Figure 3d). As IR-induced apoptosis is normal in other NER mutants (e.g., *xpa-1*, *xpc-1*), XPG-1 likely participates in other repair pathways following IR. Indeed, human XPG has been suggested to also function in base excision repair, as a cofactor for hNth1 DNA-glycosylase-AP-lyase during oxidative DNA damage repair.[24] Remarkably, the increased apoptosis in *rad-54(RNAi)* animals (Figure 1b) was suppressed by the loss of *xpg-1* function (Figure 3g), suggesting that XPG-1 acts downstream of, or in parallel to, RAD-54 to promote apoptosis in response to unresolved recombination intermediates. This effect was specific to *rad-54*, as *xpg-1(tm1670)* did not suppress the increased apoptosis in *rad-51(RNAi)* animals (Supplementary Figure 3d).

We showed above that XPA-1 is required for UV-C-induced RAD-54::YFP foci formation. Similarly, foci formation was reduced by twofold or more in *xpb-1(RNAi)* or *xpd-1(RNAi)* animals (Figure 3e). By contrast, loss of XPG-1 function did not have any strong effect (Figure 3e). Notably, untreated animals had elevated foci numbers in all three cases, likely reflecting accumulation of unrepaired lesions. Similarly, loss of *xpg-1* did not inhibit recruitment of RPA-1::YFP (Figure 2d), which we showed to be recruited upstream of RAD-54 upon UV-C (Figure 2e).

Taken together, our findings suggest that recruitment of RAD-54 onto sites of UV-C damage does not require the whole complement of NER genes we analyzed: the DNA-binding protein XPA-1, and the XPB-1 and XPD-1 helicases appear sufficient for this step.

The HUS-1 complex functions downstream of the HR machinery to promote UV-C-induced apoptosis. We previously showed that recruitment of the HUS-1-containing 9-1-1 complex in response to UV-C requires XPA-1 function.[11] Similarly, elimination of *rad-54* blocked accumulation of HUS-1::GFP foci following UV treatment (Figure 3f). By contrast, we observed a modest increase in foci numbers following IR (Figure 3f). Proteins involved in early stages of HR, therefore, act upstream of and are important for 9-1-1 recruitment in UV response. By contrast, lack of *xpg-1* did not affect HUS-1::GFP foci formation following either UV-C or IR treatment (Figure 3f). Thus, XPG-1 must impinge on the apoptotic signaling pathway at a step downstream of, or in parallel to, 9-1-1 recruitment.

The HR repair factors are involved in a signaling process to the apoptotic machinery following UV-C. Our finding that HR components are involved in UV-C-induced apoptosis led us to speculate on their exact role: are these proteins merely involved in signaling to the apoptotic apparatus, or do they also participate in the repair of the initial UV-C lesions?

To address this, we assessed the DNA repair activity in mutants defective in either NER or HR. We performed *in vivo* immunofluorescence to measure the presence of CPDs – one of the two major types of lesions caused by UV exposure – at defined time intervals in wild-type animals. Pachytene germ cells showed a maximum CPD signal immediately following

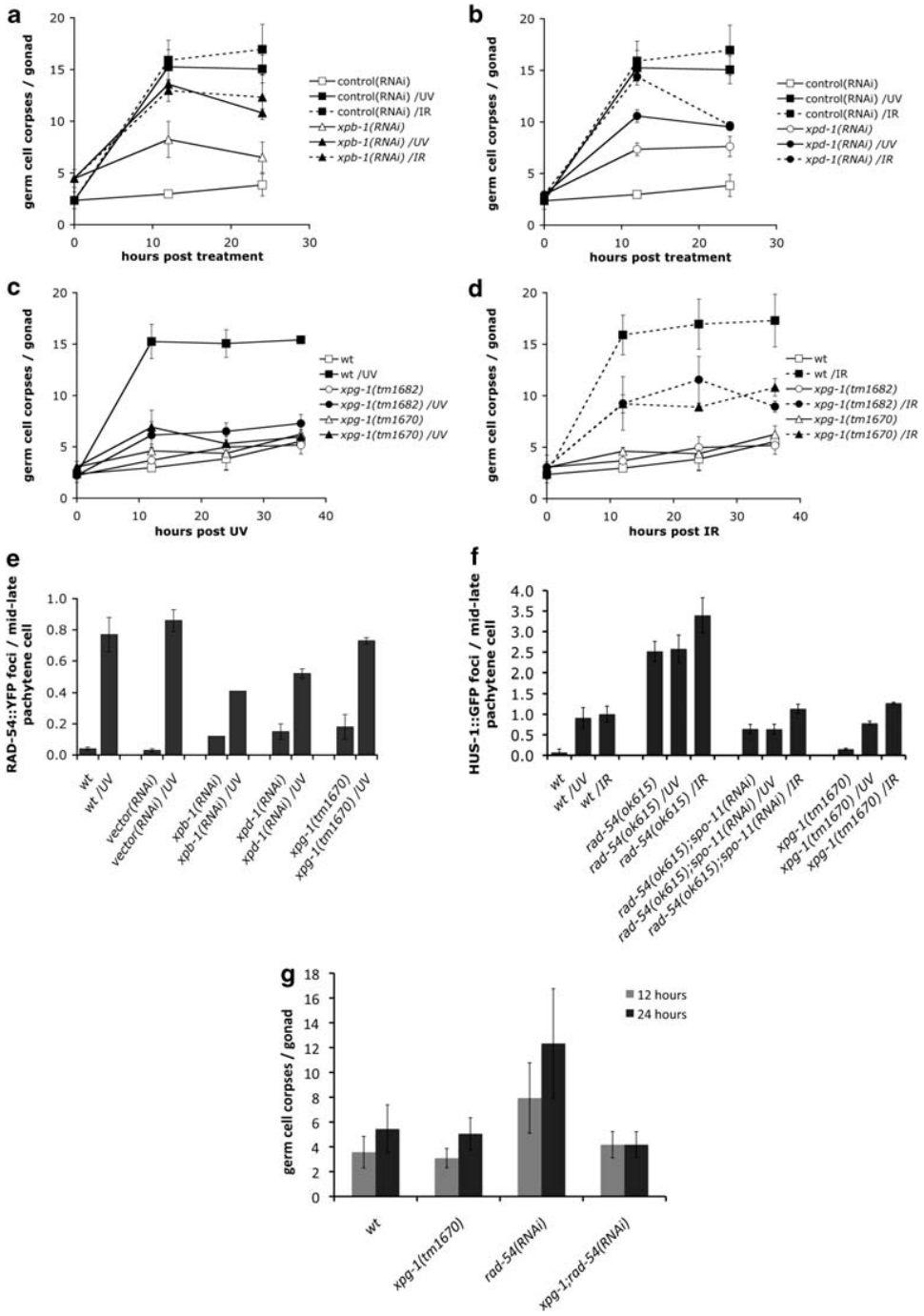

Figure 3 *C. elegans* NER component XPG-1 is required for UV-C-induced germ cell apoptosis, but not for recruitment of RAD-54. Staged wild-type L1 larvae were raised on bacteria expressing *xpb-1* (**a**), *xpd-1* (**b**) or control dsRNA, and were treated with either 100 J/m^2 UV-C or 120 Gy X-rays as young adults. Germ cell corpses were scored at the indicated time points. We could not score the 36-h time point in these animals, as the germ lines started to degenerate. This is possibly owing to the fact that both XPB-1 and XPD-1 are components of TFIIH, and thus might also affect mRNA transcription. (**c** and **d**) Apoptosis was scored in *xpg-1(tm1670)* or *xpg-1(tm1682)* mutant animals after treatment with 100 J/m^2 UV-C (**c**) or 120 Gy X-rays (d). (**e**) XPG-1 is not required for UV-C-induced RAD-54 foci formation. RAD-54::YFP foci were quantified 3 h after treatment with 100 J/m^2 UV-C as described in Materials and Methods. (**f**) RAD-54, but not XPG-1, is required for UV-C-induced HUS-1 foci formation. HUS-1::GFP foci were quantified in mid–late pachytene germ cell nuclei from staged young adult animals expressing HUS-1::GFP (*opls34*) 3 h after exposure to 100 J/m^2 of UV-C or 120 Gy of X-rays. Data shown in all cases represent the average ± S.D. of three independent experiments ($n > 15$ animals for each experiment). (**g**) Increased levels of apoptosis in *rad-54* mutants are suppressed by *xpg-1*. Germ cell apoptosis was scored 12 and 24 h post the L4/adult molt in staged wild-type (wt), *xpg-1(tm1670)*, *rad-54(RNAi)* and *xpg-1(tm1670);rad-54(RNAi)* animals. Data shown represent the average ± S.D. of two independent experiments ($n > 20$ animals for each experiment)

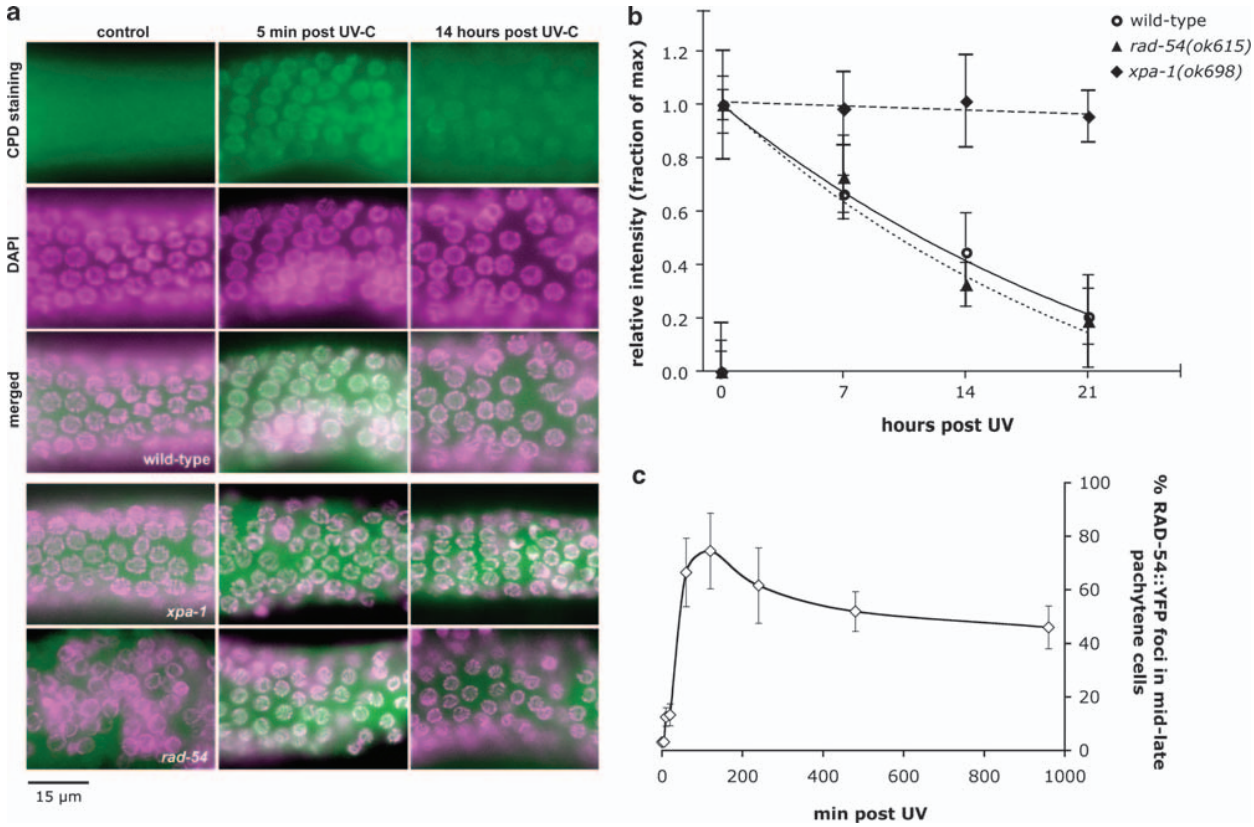

Figure 4 CPD repair kinetics in NER and HR pathway mutants. (**a**) Immunofluorescence images of germ cell nuclei from UV-C-irradiated wild-type, *rad-54(ok615)* and *xpa-1(ok698)* worms. Gonads were extruded and fixed immediately following UV-C radiation or after 14 h. Images in the upper panel represent the CPD staining (green), the nuclei DAPI staining (magenta) and an overlay of the CPD staining and DAPI in wild-type animals, resulting in a white ring where UV lesions are detected on germ cell chromatin. Although in the absence of NER in *xpa-1(ok698)* mutants nuclei remain white (lower panel), CPDs are removed in *rad-54(ok615)* mutants similar to wild type mutants (chromatin turns magenta). (**b**) CPD signal intensity after irradiation with 100 J/m^2 UV-C was determined by fluorescence image analysis of isolated gonads. Intensity before irradiation was defined as 0 and the value immediately after UV-C as 1 for each strain, and later time points were expressed as a fraction of the initial UV-C-induced intensity. At least 10 animals were scored per data point. Error bars represent the S.E.M. Repair kinetics for CPD lesions in transition cell nuclei of wild-type hermaphrodites ($t_{1/2}$ approx. 10 h) are in good agreement with repair kinetics reported for other systems. *xpa-1(ok698)* mutants lacking a functional NER show no significant repair, whereas *rad-54(ok615)* mutants exhibit a response similar to wild type mutants. (**c**) RAD-54::YFP foci develop slowly and persist for long in UV-C-irradiated wild-type animals. Mid–late pachytene germ cell nuclei from staged young adult wild-type animals were scored for the presence of RAD-54::YFP foci, at 5, 10, 20 min, 1, 2, 4, 8 and 16 h post 100 J/m^2 of UV-C treatment

UV-C (Figures 4a and b), which gradually disappeared with a half-life of approximately 10 h. These repair kinetics fall within the range reported for other systems.[25,26] Interestingly, CPDs were cleared at the same rate in *rad-54(ok615)* mutants as in wild type (Figure 4b), consistent with the notion that RAD-54 is not involved in CPD lesion repair. By contrast, *xpa-1* mutants showed a greatly reduced ability to remove CPDs (Figure 4b), confirming the role of *C. elegans xpa-1* in NER.

Unlike the relatively rapid appearance and repair of CPDs, RAD-54::YFP foci developed more slowly, peaking 2 h after treatment, and also persisted for much longer (Figure 4c). Their perdurance might explain the apparent conundrum that UV-C-induced apoptosis persists for much longer than the CPDs (over 36 *versus* 10–20 h): it is not the CPDs themselves, but rather some type of DNA intermediates, recognized or marked by RAD-54, which promote apoptosis.

How might these two types of damage be linked? We suggest the following model: UV lesions by themselves are not pro-apoptotic. However, their processing by NER can lead, in a fraction of cases, to the generation of other types of DNA damage (e.g., DSBs, or long stretches of ssDNA). These are in turn recognized and processed by HR, leading to repair and, if necessary, apoptosis of the damaged cell (Figure 5).

Discussion

In this paper, we took advantage of the powerful genetics in *C. elegans* to investigate in detail the signaling pathways that activate apoptosis in response to UV-C light. We show that apoptosis requires the coordinated action of two repair systems, the NER and HR pathways, and present a molecular model that explains this novel finding.

How does UV-C cause apoptosis in *C. elegans*? A simple explanation would be that UV-C directly causes double-strand breaks, which could activate the well-characterized ATM (/ATR)/CHK2/p53 pathway previously shown to respond to

a

	Loss-of-function	Apoptosis	Foci formation: RAD-54::YFP	RPA-1::YFP	HUS-1::GFP
NER genes	*xpa-1*	–	–	–	–
	xpc-1	–	–	nd	nd
	xpb-1	reduced	reduced	nd	nd
	xpd-1	reduced	reduced	nd	nd
	xpg-1	–	+	+	+
HR genes	*mre-11*	–	–	+	nd
	rad-54	–	na	+	–
	rad-51	+	nd	nd	nd

– absent
\+ present
nd not determined
na not applicable

b

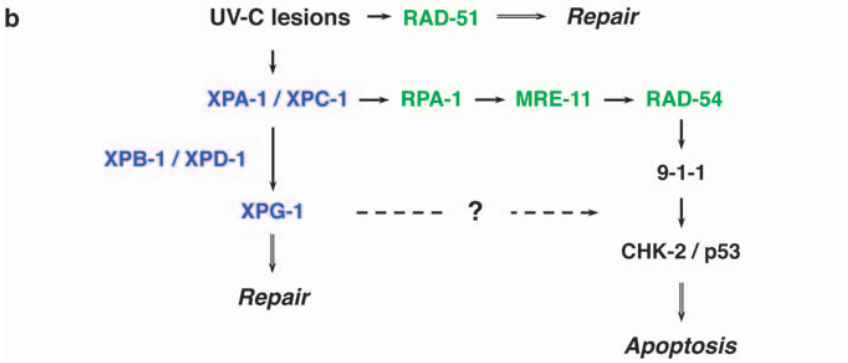

Figure 5 UV-C-induced apoptosis requires the action of both the NER and HR pathways. (**a**) Summary of the genetic requirements for the recruitment of NER and HR pathway components onto DNA lesions, as well as the induction of apoptosis following UV-C treatment. (**b**) Molecular model for UV-C-induced apoptosis in *C. elegans*. The NER machinery (blue) transforms a fraction of the UV-C lesions into other types of DNA damage (e.g., double-strand breaks). These, in turn, are then recognized by the HR machinery (green), leading to DNA repair and/or apoptosis of the damaged cell. Remarkably, XPG-1 defines a new branch that acts downstream of 9-1-1 to induce apoptosis

such lesions.[27,28] However, while mutagenic and cytotoxic, UV-C lesions are not pro-apoptotic *per se*: mutants in the DNA damage recognition components of the NER machinery, *xpa-1* and *xpc-1*, are defective in UV-C-induced apoptosis.[11] The requirement for these components suggests that their substrates, CPDs and 6-4PPs, are the relevant lesions, and not DSBs. Furthermore, induction of apoptosis requires both recognition and processing of these lesions by the NER machinery, as the DNA helicases XPB-1 and XPD-1 and the ssDNA endonuclease XPG-1 were also important for the activation of UV-C-induced apoptosis (Figure 3). A similar requirement for XPB and XPD has also been reported in human primary fibroblasts, as part of a p53-mediated apoptotic pathway.[29]

The requirement of a functional NER pathway for UV-C-induced apoptosis raises the question as to whether it is the repair process *per se*, or rather its output (the resulting DNA structures) that triggers apoptosis. Interestingly, the NER pathway is not the only repair pathway involved. We showed here that mutations in the HR pathway genes *mre-11* and *rad-54* also abrogate UV-C-induced cell death (Figures 1a and f). This lack of apoptosis in a post-mitotic cell population (mid–late pachytene germ cells), in which UV-C lesions cannot be converted into DSBs via replication, strongly suggests that the damage recognized by the HR repair system is a product of NER activity.

On the basis of these results, an attractive model for UV-C-induced apoptosis would be that the NER machinery transforms a fraction of the UV-C lesions – wittingly or unwittingly – into DSBs. These, in turn, are recognized by the HR pathway and lead to apoptosis via the pathway that we and others described previously (Figure 5).[11,30] Consistent with this model, the lesions or DNA structures positive for the presence of RAD-54 only appear progressively, over a few hours, in response to NER activity. How the latter can generate DSBs remains elusive. Might they happen accidentally when the NER machinery excises a stretch of the damaged strand? Assuming two CPDs per 10^4 bases at 100 J/m^2 (compare Boyd *et al*.[31]), one haploid worm genome (10^8 bp) would initially harbor 4×10^4 lesions. Theoretically, this leaves a risk of almost 500 occurrences per cell of two lesions on opposing DNA strands within 30 nt, which, when processed simultaneously, could result in a DSB. For comparison, Vilenchik *et al*.[32,33] estimated that in one mammalian cell cycle, 1% of single-strand lesions are converted into 50 endogenous DSBs.

Although attractive, this model cannot fully explain a number of intriguing observations. First, we previously

showed that UV-C and IR activate different sets of checkpoint kinases.[11] However, we propose here that both treatments activate apoptosis via DSBs. Perhaps, the nature of the DSBs or of the associated protein complexes is different in the two cases. Second, we showed that while XPG-1 is required for UV-C-induced apoptosis, it is not needed for the generation of RAD-54-positive foci; furthermore, loss of *xpg-1* function can suppress the increased apoptosis in non-irradiated worms defective for *rad-54*. At which level precisely XPG-1 functions to promote apoptosis is itself an intriguing topic.

Muzi-Falconi and co-workers[34,35] have suggested a functional link between NER and checkpoint activation in both yeast and mammalian cells, in which processing of UV lesions by the XPA-1 homolog enables 9-1-1 complex recruitment and activation of the ATR kinase.[34] Toussaint *et al*.[36] have characterized the co-participation of HR components in rendering G2-phase yeast cells more resistant to UV irradiation. Recent evidence might shift the concept of individual repair pathways toward that of a DNA damage response network, in which DNA repair factors interact to drive a coordinated response toward genome integrity and cell survival,[37] or towards cell death.

Our findings suggest the existence of a cross-talk between the NER and HR repair pathways, and assign a role to several DNA repair components in apoptotic signaling. As repair pathways are highly conserved through evolution, the interaction between the NER and the HR pathways that we describe here for *C. elegans* might also occur in vertebrates, including humans.

Materials and Methods

Genetics. All strains were grown at 20°C on NGM agar seeded with *Escherichia coli* OP50. The Bristol N2 strain was used as the wild-type strain. Mutant alleles used are listed below: LGI: *atm-1(gk186)*,[11] *hus-1(op244)*,[38] *xpg-1(tm1670)* (this study), *xpg-1(tm1682)* (this study), *xpa-1(ok698)*,[11] *rad-54(ok615)* (this study), *rad-54(tm1268)* (this study); LGIV: *xpc-1(ok734)*,[11] *spo-11(ok79)*;[39] and LGV: *atl-1(tm853)*,[30] *mre-11(ok179)*,[12] *chk-2(gk212)*.[11] Transgenes: *opIs257* (RAD-54::YFP) and *opIs263* (RPA-1::YFP) (this study). Essential mutations were maintained as balanced strains: *rad-54(ok615)/hT2[qIs51](IV;V)*, *rad-54(tm1268)/hT2[qIs51](IV;V)*, *spo-11(ok79)/nT1[n754 let](IV;V)*, *atl-1(tm853)/nT1[qIs51](IV;V)* and *mre-11(ok179)/nT1[n754 let](IV;V)*. Additional information on mutations cited here can be obtained at www.wormbase.org.

Germline apoptosis. Staged young adult worms (12 h post the L4/adult molt) were exposed to different doses of UV-C light (254 nm) (J/m^2) or X-rays (Gy). A Stratalinker UV crosslinker, model 1800 (Stratagene, Basel, Switzerland) and an Isovolt 160/225/320/450 HS X-ray machine (Rich. Seifert & Co., Ahrensburg, Germany) were used to deliver the appropriate doses. Corpses were scored in the meiotic region of one gonad arm at indicated time points using Nomarski optics. For the RNAi experiments, staged L1 larvae were transferred onto plates containing 2 mM IPTG seeded with *E. coli* strain HT115(DH3) expressing the respective RNAi clone, and scored as young adults for germline apoptosis.

Immunocytochemistry. For antibody staining of gonads, young adult hermaphrodites were dissected and fixed in 3% PFA/0.1 M K_2HPO_4 (pH 7.2) for 50 min at room temperature, followed by a 10-min incubation in 100% methanol on ice. Gonads were blocked in 5% BSA/PBS–Tween-20 0.1% for 1 h, followed by incubation with 1 : 50 anti-RAD-51 polyclonal[15] antibody overnight at 4°C. Alexa Fluor 594 goat anti-rabbit IgG (Invitrogen, Basel, Switzerland) was used as secondary antibody (1 : 500). The tissues were co-stained with DAPI before mounting. Fluorescent images were captured with a Leica DMRA2 microscope equipped with an ORCA-ER digital CCD camera and processed with an Openlab software.

CPD staining and quantification. A modified fixation protocol was applied to preserve/create denatured DNA structures for CPD staining, as this antibody specifically binds to CPDs in ssDNA.[40] Adult hermaphrodites were irradiated with 100 J/m^2 UVC and, at the indicated time points, were dissected in M9 (0.5 mM levamisole) to extrude the gonads and fixed in M9/3% PFA for 30 min. Fixed worms were transferred to poly-lysine-coated slides, freeze-cracked and permeabilized in PBS/Tween-20 0.1% for 3 × 10 min. For DNA denaturation, slides were incubated in PBS/0.07 N NaOH for 8 min and washed in PBS/Tween-20 0.1% for 3 × 10 min before blocking (1 h at RT) and incubation with 1 : 500 anti-CPD monoclonal antibody (MBL International, Woburn, MA, USA; product no. D194-1) for at least 6 h at 4°C. Samples were washed and incubated (1 h at RT) with Alexa Fluor 488 goat anti-rabbit (Invitrogen) as secondary antibody (1 : 500) and counterstained with DAPI (200 ng/ml) before mounting in Prolong Gold (Invitrogen). Blocking and antibody incubations were in antibody buffer/10% goat serum.

Fluorescent images were captured as described above with defined exposure settings. For quantification of CPD signal intensity, a macro was created and run in ImageJ (version 1.42q; http://rsb.info.nih.gov/nih-image/), allowing for automated measurements after definition of a region of interest (ROI) in the immunofluorescence pictures. Briefly, an ROI was drawn around approximately 100 germ cell nuclei of the transition/early meiotic region. A mask was defined from a binary threshold image of the DAPI staining to account for DNA containing areas and applied to the anti-CPD image. Average anti-CPD signal intensity over DAPI-positive areas was compared with average intensity of the background within the ROI, and expressed as difference.

Foci quantification. Staged young adult hermaphrodites were treated with either 100 J/m^2 of UV-C light or 120 Gy of X-rays, and gonads were dissected at indicated time points. RAD-54::YFP and RPA-1::YFP foci formation was quantified by counting the number of bright foci present in mid–late pachytene germ cells, in one focal plane within 100 μm from the first oocyte. Fluorescent images were captured with a Leica DMRA2 microscope equipped with an ORCA-ER digital CCD camera and were processed with an Openlab software.

RNAi constructs. Fragments corresponding to exonic sequences of *xpb-1* (Y66D12A.15) and *xpd-1* (Y50D7A.2) were amplified by PCR from a wild-type cDNA library using primers listed in Supplementary Table S2, and cloned into the L4440 RNAi vector. The constructs were used to transform HT115(DH3) bacteria, which were subsequently used to feed worms in the RNAi experiments. For the rest of the RNAi clones in this study, we used the Ahringer RNAi library. A standard gfp sequence cloned into L4440 vector or the empty vector was used as controls for the RNAi experiments.

Transgenic worms. Genomic fragments corresponding to *rpa-1* and *rad-54* promoter and ORF, as well as the 3′-UTR region were separately amplified by PCR from N2 genomic DNA using primers (Supplementary Table S2) that added the appropriate restriction sites. The amplified fragments were cloned into the pLN022 expression vector upstream of *yfp* to generate pLS69 (RPA-1::YFP) or pLS57 (RAD-54::YFP). Low-copy transgenic worms were then generated by ballistic transformation. Sequences of all used plasmids are available upon request.

Conflict of interest

The authors declare no conflict of interest.

Acknowledgements. We thank Professor H Naegeli and Dr A Gartner for critical comments on our manuscript, and members of the Hengartner lab for discussions. This work was supported by the Kanton of Zurich, the Swiss National Science Foundation, the Ernst Hadorn Foundation and the Josef Steiner Cancer Research Foundation. RE was supported by an MD-PhD fellowship from the Swiss National Science Foundation. We also thank Dr A Gartner for providing us with the RAD-51 antibody, and the *Caenorhabditis* Genetics Center, which is funded by the National Institute of Health (NIH), National Center for Research Resources (NCRR) as well as Shohei Mitani of the National Bioresource Project in Japan for strains.

1. Hanahan D, Weinberg RA. The hallmarks of cancer. *Cell* 2000; **100**: 57–70.
2. Bartek J, Lukas J. DNA damage checkpoints: from initiation to recovery or adaptation. *Curr Opin Cell Biol* 2007; **19**: 238–245.

3. Sancar A, Lindsey-Boltz LA, Unsal-Kacmaz K, Linn S. Molecular mechanisms of mammalian DNA repair and the DNA damage checkpoints. *Annu Rev Biochem* 2004; **73**: 39–85.
4. Cleaver JE. Cancer in xeroderma pigmentosum and related disorders of DNA repair. *Nat Rev Cancer* 2005; **5**: 564–573.
5. de Boer J, Hoeijmakers JH. Cancer from the outside, aging from the inside: mouse models to study the consequences of defective nucleotide excision repair. *Biochimie* 1999; **81**: 127–137.
6. Wijnhoven SW, Hoogervorst EM, de Waard H, van der Horst GT, van Steeg H. Tissue specific mutagenic and carcinogenic responses in NER defective mouse models. *Mutat Res* 2007; **614**: 77–94.
7. van der Wees C, Jansen J, Vrieling H, van der Laarse A, Van Zeeland A, Mullenders L. Nucleotide excision repair in differentiated cells. *Mutat Res* 2007; **614**: 16–23.
8. Carvalho H, Ortolan TG, dePaula T, Leite RA, Weinlich R, Amarante-Mendes GP *et al.* Sustained activation of p53 in confluent nucleotide excision repair-deficient cells resistant to ultraviolet-induced apoptosis. *DNA Repair* 2008; **7**: 922–931.
9. Stergiou L, Hengartner MO. Death and more: DNA damage response pathways in the nematode *C. elegans*. *Cell Death Differ* 2004; **11**: 21–28.
10. Gartner A, Boag PR, Blackwell TK. Germline survival and apoptosis. In: WormBook (ed). *The C. elegans Research Community*, vol. 145.1. 2008, pp 1–20. http://www.wormbook.org.
11. Stergiou L, Doukoumetzidis K, Sendoel A, Hengartner MO. The nucleotide excision repair pathway is required for UV-C-induced apoptosis in *Caenorhabditis elegans*. *Cell Death Differ* 2007; **14**: 1129–1138.
12. Chin GM, Villeneuve AM. *C. elegans mre-11* is required for meiotic recombination and DNA repair but is dispensable for the meiotic G DNA damage checkpoint. *Genes Dev* 2001; **15**: 522–534.
13. Petukhova G, Stratton S, Sung P. Catalysis of homologous DNA pairing by yeast Rad51 and Rad54 proteins. *Nature* 1998; **393**: 91–94.
14. Sigurdsson S, Van Komen S, Petukhova G, Sung P. Homologous DNA pairing by human recombination factors Rad51 and Rad54. *J Biol Chem* 2002; **277**: 42790–42794.
15. Alpi A, Pasierbeck P, Gartner A, Loidl J. Genetic and cytological characterization of the recombination protein RAD-51 in *Caenorhabditis elegans*. *Chromosoma* 2003; **112**: 6–16.
16. Hayashi M, Chin GM, Villeneuve AM. *C. elegans* germ cells switch between distinct modes of double-strand break repair during meiotic prophase progression. *PLoS Genet* 2007; **3**: e191.
17. Zou Y, Liu Y, Wu X, Shell SM. Functions of human replication protein A (RPA): from DNA replication to DNA damage and stress responses. *J Cell Physiol* 2006; **208**: 267–273.
18. Missura M, Buterin T, Hindges R, Hübscher U, Kaspárková J, Brabec V, Naegeli H. Double-check probing of DNA bending and unwinding by XPA–RPA: an architectural function in DNA repair. *EMBO J* 2001; **20**: 3554–3564.
19. Van Komen S, Petukhova G, Sigurdsson S, Sung P. Functional cross-talk among Rad51, Rad54, and replication protein A in heteroduplex DNA joint formation. *J Biol Chem* 2002; **277**: 43578–43587.
20. Stauffer ME, Chazin WJ. Physical interaction between replication protein A and Rad51 promotes exchange on single-stranded DNA. *J Biol Chem* 2004; **279**: 25638–25645.
21. Solinger JA, Heyer WD. Rad54 protein stimulates the postsynaptic phase of Rad51 protein-mediated DNA strand exchange. *Proc Natl Acad Sci USA* 2001; **98**: 8447–8453.
22. de Laat WL, Jaspers NG, Hoeijmakers JH. Molecular mechanism of nucleotide excision repair. *Genes Dev* 1999; **13**: 768–785.
23. Prakash S, Prakash L. Nucleotide excision repair in yeast. *Mutat Res* 2000; **451**: 13–24.
24. Klungland A, Hoss M, Gunz D, Constantinou A, Clarkson SG, Doetsch PW *et al.* Base excision repair of oxidative DNA damage activated by XPG protein. *Mol Cell* 1999; **3**: 33–42.
25. Tang JY, Hwang BJ, Ford JM, Hanawalt PC, Chu G. Xeroderma pigmentosum p48 gene enhances global genomic repair and suppresses UV-induced mutagenesis. *Mol Cell* 2000; **5**: 737–744.
26. Costa RM, Chigançcas V, Galhardo R, Carvalho H, Menck CF. The eukaryotic nucleotide excision repair pathway. *Biochimie* 2003; **85**: 1083–1099.
27. Cann KL, Hicks GG. Regulation of the cellular DNA double-strand break response. *Biochem Cell Biol* 2007; **85**: 663–674.
28. Lee JH, Paull TT. Activation and regulation of ATM kinase activity in response to DNA double-strand breaks. *Oncogene* 2007; **26**: 7741–7748.
29. Wang XW, Vermeulen W, Coursen JD, Gibson M, Lupold SE, Forrester K *et al.* The XPB and XPD DNA helicases are components of the p53-mediated apoptosis pathway. *Genes Dev* 1996; **10**: 1219–1232.
30. Garcia-Muse T, Boulton SJ. Distinct modes of ATR activation after replication stress and DNA double-strand breaks in *Caenorhabditis elegans*. *EMBO J* 2005; **24**: 4345–4355.
31. Boyd WA, Crocker TL, Rodriguez AM, Leung MC, Lehmann DW, Freedman JH *et al.* Nucleotide excision repair genes are expressed at low levels and are not detectably inducible in *Caenorhabditis elegans* somatic tissues, but their function is required for normal adult life after UVC exposure. *Mutat Res* 2010; **683**: 57–67.
32. Vilenchik MM, Knudson AG. Radiation dose-rate effects, endogenous DNA damage, and signaling resonance. *Proc Natl Acad Sci USA* 2006; **103**: 17874–17879.
33. Vilenchik MM, Knudson AG. Endogenous DNA double-strand breaks: production, fidelity of repair, and induction of cancer. *Proc Natl Acad Sci USA* 2003; **100**: 12871–12876.
34. Giannattasio M, Lazzaro F, Longhese MP, Plevani P, Muzi-Falconi M. Physical and functional interactions between nucleotide excision repair and DNA damage checkpoint. *EMBO J* 2004; **23**: 429–438.
35. Marini F, Nardo T, Giannattasio M, Minuzzo M, Stefanini M, Plevani P *et al.* DNA nucleotide excision repair-dependent signaling to checkpoint activation. *Proc Natl Acad Sci USA* 2006; **103**: 17325–17330.
36. Toussaint M, Wellinger RJ, Conconi A. Differential participation of homologous recombination and nucleotide excision repair in yeast survival to ultraviolet light radiation. *Mutat Res* 2010; **698**: 52–59.
37. Zhang Y, Rohde LH, Wu H. Involvement of nucleotide excision and mismatch repair mechanisms in double strand break repair. *Curr Genomics* 2009; **10**: 250–258.
38. Hofmann ER, Milstein S, Boulton SJ, Ye M, Hofmann JJ, Stergiou L *et al. Caenorhabditis elegans* HUS–1 is a DNA damage checkpoint protein required for genome stability and EGL-1-mediated apoptosis. *Curr Biol* 2002; **12**: 1908–1918.
39. Dernburg AF, McDonald K, Moulder G, Barstead R, Dresser M, Villeneuve AM. Meiotic recombination in *C. elegans* initiates by a conserved mechanism and is dispensable for homologous chromosome synapsis. *Cell* 1998; **94**: 387–398.
40. Komatsu Y, Tsujino T, Suzuki T, Nikaido O, Ohtsuka E. Antigen structural requirements for recognition by a cyclobutane thymine dimer-specific monoclonal antibody. *Nucleic Acids Res* 1997; **25**: 3889–3894.

Supplementary Information accompanies the paper on Cell Death and Differentiation website (http://www.nature.com/cdd)

Cell

Deficiency of FANCD2-Associated Nuclease KIAA1018/FAN1 Sensitizes Cells to Interstrand Crosslinking Agents

Katja Kratz,[1,4] Barbara Schöpf,[1,4] Svenja Kaden,[1,4] Ataman Sendoel,[2] Ralf Eberhard,[2] Claudio Lademann,[1] Elda Cannavó,[1,5] Alessandro A. Sartori,[1] Michael O. Hengartner,[2] and Josef Jiricny[1,3,*]
[1]Institute of Molecular Cancer Research, University of Zurich
[2]Institute of Molecular Life Sciences, University of Zurich
[3]Department of Biology
ETH Zurich, Winterthurerstrasse 190, 8057 Zurich, Switzerland
[4]These authors contributed equally to this work
[5]Present address: Department of Microbiology, University of California, Davis, CA 95616-8665, USA
*Correspondence: jiricny@imcr.uzh.ch
DOI 10.1016/j.cell.2010.06.022

SUMMARY

Cytotoxicity of cisplatin and mitomycin C (MMC) is ascribed largely to their ability to generate interstrand crosslinks (ICLs) in DNA, which block the progression of replication forks. The processing of ICLs requires the *Fanconi anemia* (FA) pathway, excision repair, and translesion DNA synthesis (TLS). It also requires homologous recombination (HR), which repairs double-strand breaks (DSBs) generated by cleavage of the blocked replication forks. Here we describe KIAA1018, an evolutionarily conserved protein that has an N-terminal ubiquitin-binding zinc finger (UBZ) and a C-terminal nuclease domain. KIAA1018 is a 5′→3′ exonuclease and a structure-specific endonuclease that preferentially incises 5′ flaps. Like cells from FA patients, human cells depleted of KIAA1018 are sensitized to ICL-inducing agents and display chromosomal instability. The link of KIAA1018 to the FA pathway is further strengthened by its recruitment to DNA damage through interaction of its UBZ domain with monoubiquitylated FANCD2. We therefore propose to name KIAA1018 FANCD2-associated nuclease, FAN1.

INTRODUCTION

The *Fanconi anemia* (FA) pathway (Figure 1A) plays a key role in interstrand crosslink (ICL) metabolism in higher eukaryotes by coordinating S phase arrest and DNA repair (Moldovan and D'Andrea, 2009; Thompson and Hinz, 2009). Replication fork blockage activates the ataxia telangiectasia and RAD3-related (ATR) kinase (Pichierri and Rosselli, 2004), which phosphorylates members of the FA core complex (Meetei et al., 2003) composed of FANCA, B, C, E, F, G, L, and FAAP100. The activated complex then associates with FANCM-FAAP24, a DNA translocase (Gari et al., 2008), which activates the E3 ligase FANCL that subsequently ubiquitylates FANCD2-FANCI (Thompson and Hinz, 2009). The latter posttranslational modifications license the processing of the blocked replication fork (Figure 1A), which involves pausing of the fork, incision, lesion unhooking, translesion DNA synthesis (TLS), and homologous recombination (HR) (Moldovan and D'Andrea, 2009). FANCJ, a 5′→3′ DNA helicase, appears to be involved in the late stages of ICL repair (Bridge et al., 2005). Its action would give rise to 3′ flaps, preferred substrates of both endonucleases implicated in ICL processing to date, MUS81/EME1 and XPF/ERCC1.

Recently, several laboratories found interaction between FA proteins and polypeptides involved in mismatch repair (Peng et al., 2007; Zhang et al., 2002). Our analysis of the MLH1 interactome (Cannavo et al., 2007) identified FANCJ among the strongest interactors. Another strong MLH1 interactor was KIAA1018, a hypothetical protein predicted (Kinch et al., 2005; Kosinski et al., 2005) to contain a RAD18-like ubiquitin-binding zinc finger near its N terminus and a C-terminal endonuclease domain. Given the importance of ubiquitylation in the FA pathway (Moldovan and D'Andrea, 2009), and the fact that the putative endonuclease domain of KIAA1018 belongs to the same enzyme superfamily as those present in MUS81 and XPF, we asked whether KIAA1018 is related to FA and how mismatch repair (MMR) might be linked to this branch of DNA repair. Hence, we decided to characterize KIAA1018 and to study its role in DNA metabolism. We now show that KIAA1018 is a nuclease involved in the processing of mitomycin C (MMC)- and cisplatin-induced DNA damage, to which it is recruited by ubiquitylated FANCD2.

RESULTS

KIAA1018 Contains Evolutionarily Conserved Zinc Finger and Endonuclease Domains

Analysis of MLH1 and PMS2 interactomes (Cannavo et al., 2007) identified several peptides originating from the human *KIAA1018* open reading frame (ORF), which encodes a polypeptide of 1017

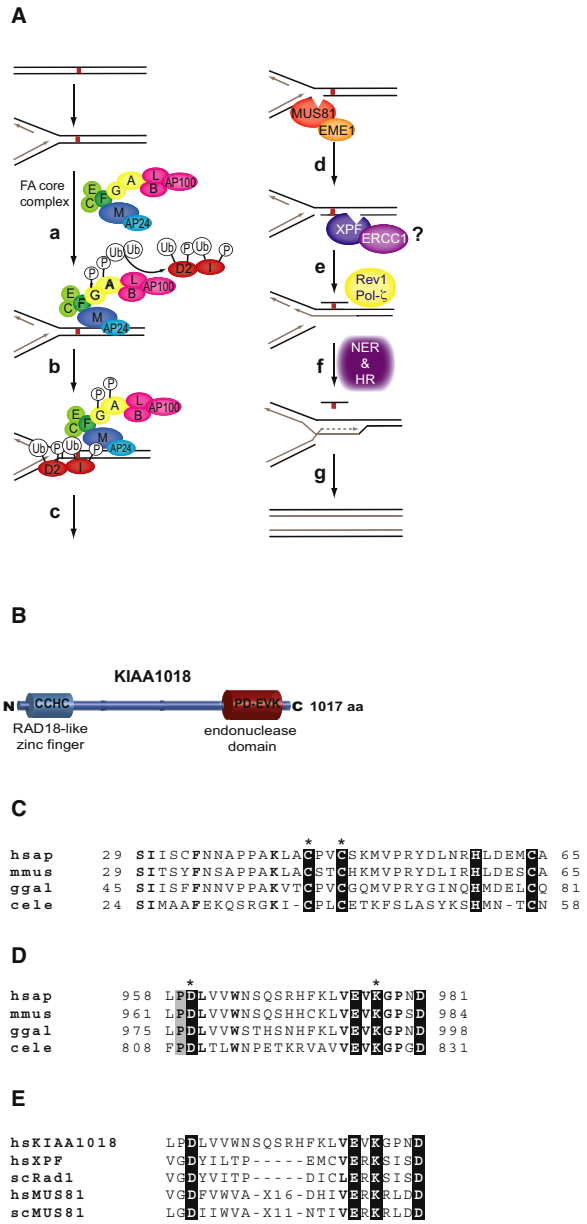

Figure 1. Schematic Representation of the FA Pathway and Evolutionary Conservation of KIAA1018

(A) A consensus model of interstrand crosslink repair (Moldovan and D'Andrea, 2009; Wang, 2007). Upon stalling of the replication fork, the FA core complex is phosphorylated on several subunits by ATR and recruited to the lesion by FANCM/FAAP24. This interaction activates the E3 ligase activity of FANCL (a), which monoubiquitylates the FANCD2/FANCI heterodimer (b). The fork is then cleaved by MUS81 on one side and unhooked by XPF/ERCC1 on the other (c and d). Translesion polymerases then fill the gap opposite the unhooked oligonucleotide (e), which is released by excision repair (f). The collapsed replication fork is then rescued by the HR machinery, including FANCD1 (BRCA2), FANCN (PALB2), and likely also FANCJ (f and g).

(B) KIAA1018 is a polypeptide of 1017 aa, containing a predicted N-terminal RAD18-like CCHC zinc finger and a C-terminal endonuclease domain.

Alignments of the zinc finger (C) and endonuclease (D) domains of KIAA1018 from man, mouse, chicken, and worm are shown.

(E) Alignment of the endonuclease domain of human KIAA1018 with those of human MUS81 and XPF and their yeast orthologs Mus81 and Rad1, respectively. Identical residues are shown in bold. The key residues of the zinc finger and endonuclease motifs are boxed. The numbers indicate aa residues flanking these motifs in the respective *KIAA1018* open reading frames. Asterisks mark aa mutated to alanine (see Results).

amino acids (aa). Its N-terminal region was predicted to contain a RAD18-like CCHC zinc finger, a so-called UBZ domain, present in proteins that bind ubiquitylated polypeptides (Hofmann, 2009). The C-terminal portion of KIAA1018 was suggested to contain an endonuclease domain of the PD-D/E(X)K type (Kinch et al., 2005; Kosinski et al., 2005) (Figure 1B).

Alignment of the aa sequences of human, murine, avian, and *C. elegans* KIAA1018 revealed a high degree of evolutionary conservation, particularly in the UBZ region (Figure 1C) and in the putative endonuclease PD-D/E(X)K motif (Figure 1D), which is found in other DNA repair proteins, such as the bacterial MMR protein MutH, certain restriction enzymes, and, most notably, the eukaryotic MUS81 and XPF/RAD1 endonucleases (Figure 1E).

Depletion of KIAA1018 Sensitizes Human Cells to Interstrand Crosslinking Agents

We asked whether KIAA1018 deficiency sensitizes cells to a particular type of DNA damage. To this end, we knocked down *KIAA1018* mRNA in HEK293 cells by siRNA targeting exon 3 (Figure 2A) and subjected these cells to treatment with several DNA-damaging agents. Compared to wild-type (WT) controls, the KIAA1018 knockdown cells were not significantly sensitized to X-rays (Figure 2B), UV irradiation (Figure 2C), or camptothecin (Figure 2D). In contrast, KIAA1018-deficient cells were hypersensitive to the ICL-inducing agents MMC (Figure 2E) and cisplatin (Figure 2F), similarly to cells deficient in FANCJ (Figures 2A, 2E, and 2F). siRNA targeting exon 5 yielded similar results (data not shown); the above phenotype was thus not caused by an off-site effect of the siRNA.

KIAA1018 Requires Its Putative Nuclease Domain for Activity

We generated HEK293 cell lines stably expressing KIAA1018 N-terminally fused to the green fluorescent protein (GFP). The *GFP-KIAA1018* fusion cDNAs encoded either the WT enzyme or a variant carrying a D960A (DA) mutation in its predicted nuclease active site. The cDNAs also contained silent mutations in the *KIAA1018* ORF, which made the respective mRNAs resistant to knockdown by exon 3 siRNA. As shown in Figure S1A (available online), the selected clones expressed similar levels of the GFP-WT and GFP-DA variants. Treatment of these cells with Luc siRNA did not affect their sensitivity to MMC. When KIAA1018 siRNA was used, the sensitivity of the GFP-WT clone was also unaffected, whereas the GFP-DA clones were sensitized to MMC treatment (Figure 2G). This result confirms that the phenotype induced by the KIAA1018 siRNA was not due to an off-target effect, demonstrates that the GFP-WT fusion

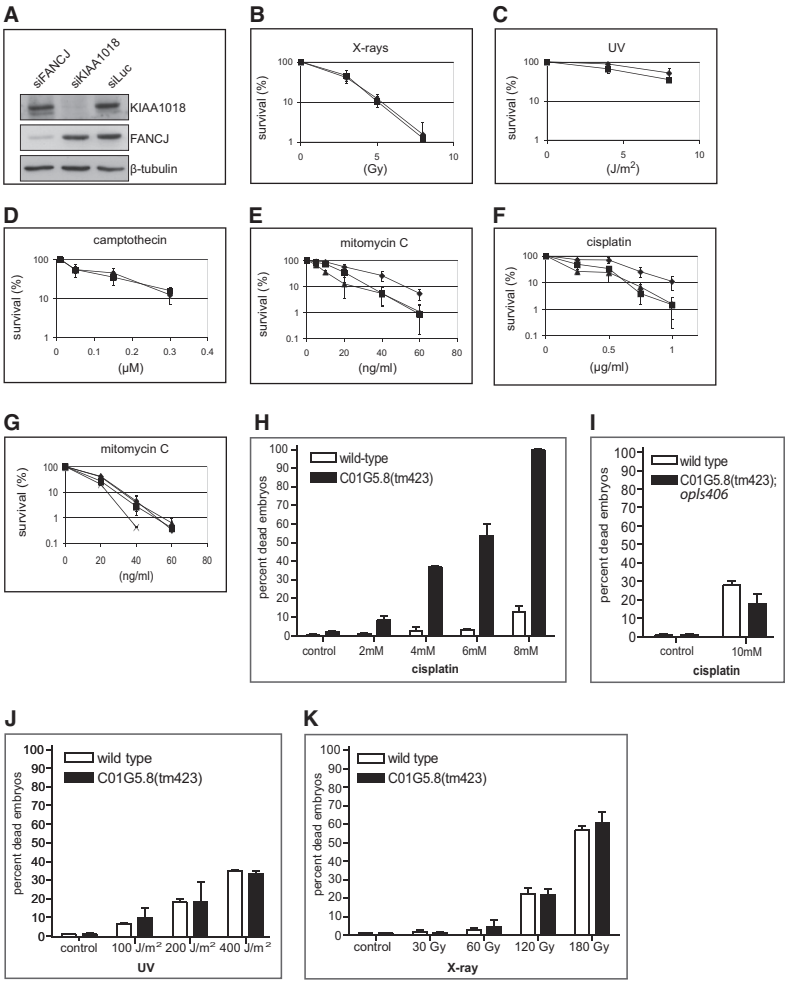

Figure 2. siRNA Knockdown of KIAA1018 Sensitizes Cells to MMC and Cisplatin

(A) Western blot showing efficacy of treatment with the indicated siRNAs. Samples were collected 40 hr after siRNA transfection. siLuc served as negative control and β-tubulin as loading control.

(B–F) Clonogenic survival assays of HEK293 cells treated 40 hr after siRNA-mediated KIAA1018 or FANCJ knockdown. KIAA1018-depleted cells and mock-depleted controls were similarly sensitive to X-rays (B), UV radiation (C), and camptothecin (D). siRNA-mediated knockdown of KIAA1018 or FANCJ sensitized cells to MMC (E) and cisplatin (F). Key: (◆) siLuc; (■) siKIAA1018; (▲) siFANCJ.

(G) Clonogenic survival assay with HEK293 cells stably expressing siRNA-resistant GFP-KIAA1018. Cells expressing WT GFP-KIAA1018 showed similar sensitivity to MMC, irrespective of depletion of endogenous KIAA1018. In contrast, expression of GFP-KIAA1018 D960A resulted in increased sensitivity to MMC after depletion of endogenous KIAA1018. Key: (◆) GFP-KIAA1018 WT + siLuc; (■) GFP-KIAA1018 WT + siKIAA1018; (▲) GFP-KIAA1018 D960A + siLuc; (**X**) GFP-KIAA1018 D960A + siKIAA1018. Graphs represent the results of three independent experiments, each carried out in triplicate. Each data point represents an average ± standard deviation (SD).

(H) Increased embryonic lethality of *C01G5.8 (tm423)* mutant animals in response to cisplatin treatment. (I) Rescue of *C01G5.8(tm423)* mutant phenotype by C01G5.8::gfp expression. (J and K) Embryonic lethality after treatment with UV or IR. Synchronized L4 or *opIs406(*$P_{C01G5.8}$*::C01G5.8::gfp::let-858(3′UTR))* animals were exposed to cisplatin for 24 hr (H and I) and were subsequently allowed to lay eggs for 8 hr. For IR and UV treatments (J and K), synchronized young adult animals were allowed to lay eggs for 6–8 hr 24 hr post-treatment. Embryonic lethality was quantified 24 hr later. Data shown represent the average percent embryonic lethality of 20 adult animals ± SD.

See also Figure S1.

protein is functional, and, most importantly, shows that the nuclease domain is indispensable for KIAA1018 function.

Disruption of the *KIAA1018* Ortholog *C01G5.8* in *C. elegans* Leads to Cisplatin-Induced Embryonic Lethality

KIAA1018 is highly conserved in evolution (Figures 1C and 1D). In order to ascertain that the above-described sensitivity to ICL-inducing agents was not limited to KIAA1018-depleted human cells, we examined the phenotype of *C. elegans* disrupted in the *KIAA1018* ortholog *C01G5.8* (Figure S1B). The *C01G5.8(tm423)* mutant developed similarly to WT (data not shown), which showed that C01G5.8 is not required for normal growth. Cisplatin treatment caused a dramatic increase in embryonic lethality in the *C01G5.8(tm423)* mutants, whereas the viability of WT worms was only slightly impaired (Figure 2H).

We next generated the transgenic *C. elegans* line *opIs406 (*$P_{C01G5.8}$*::C01G5.8::gfp)* (Figure S1C). Like the human ortholog, the nematode GFP fusion protein overexpressed in this line was functional, as it rescued the cisplatin-sensitive phenotype of the *C01G5.8(tm423)* mutants (Figure 2I). Because treatment with ultraviolet (UV) (Figure 2J) or ionizing radiation (IR) (Figure 2K) had a similar effect on both WT and mutant animals, we conclude that C01G5.8 functions in the repair of cisplatin-induced damage during embryonic development. The sensitization to cisplatin of both human cells and *C. elegans* lacking KIAA1018 or its ortholog C01G5.8 suggests that the function of this protein family in the processing of DNA damage is evolutionarily conserved.

KIAA1018/C01G5.8 Localization to Subnuclear Foci Is Enhanced by DNA Damage

As the GFP fusion proteins were functional, we decided to study their localization. In actively proliferating cells, namely embryos (Figures 3A and 3B) and germ cells of the mitotic region (Figures 3C and 3D), we observed both an evenly distributed as well as

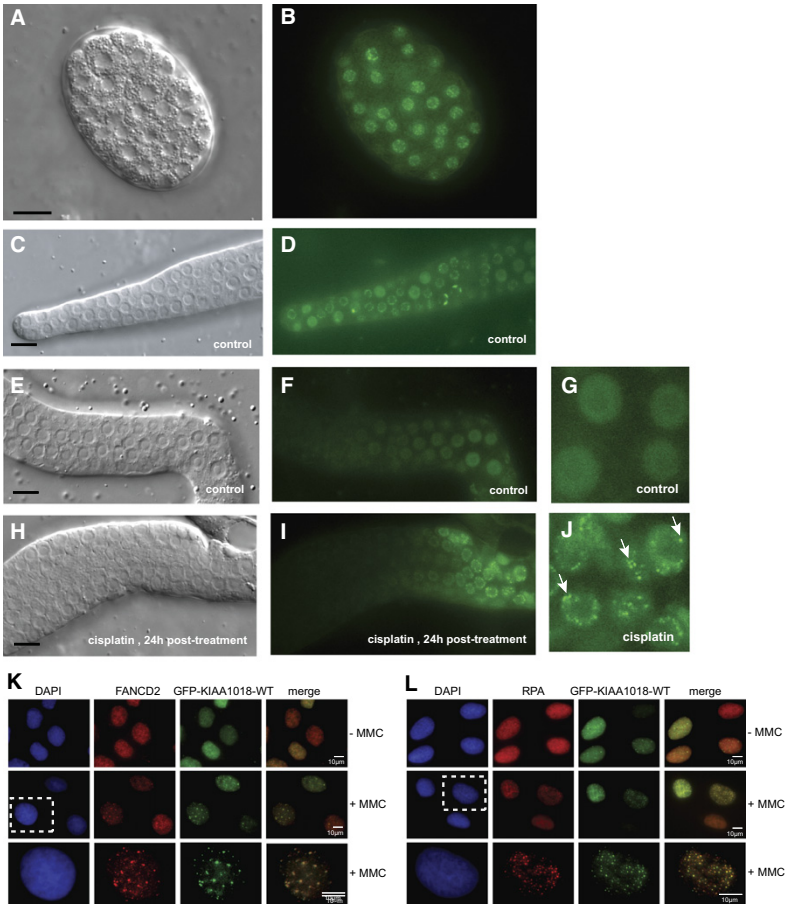

Figure 3. KIAA1018 Is Recruited to Sites of DNA Damage in *C. elegans* and Human Cells

(A) C01G5.8 is a nuclear protein expressed in embryos and in the germline of *C. elegans*. C01G5.8::gfp was detected in the nucleus of embryos (A and B), mitotic germline zone (C and D), and late pachytene stage germ cells (E–J) of the transgenic *opIs406[$P_{C01G5.8}$::C01G5.8::gfp::let-858(3′UTR)]* line. Cisplatin treatment resulted in relocalization of C01G5.8::gfp to distinct foci (arrows) (H–J). Scale bars, 10 μm.

Human GFP-KIAA1018-WT colocalizes with FANCD2 (K) and RPA (L) to MMC-induced foci. U2OS cells stably expressing GFP-KIAA1018-WT were mock-treated or treated with MMC (120 ng/ml). After 20 hr, cells were stained with antibodies against FANCD2 (TexasRed) (K) or RPA (TexasRed) (L).

fociform C01G5.8::gfp pattern. In contrast, in pachytene zone germ cells, which are arrested in prophase of meiosis I, C01G5.8::gfp was evenly distributed (Figures 3E–3G) but formed foci upon cisplatin treatment (Figures 3H–3J).

Aggregation in subnuclear foci is a hallmark of proteins participating in DNA-damage response. As C01G5.8::gfp formed foci in cisplatin-treated cells, we wanted to know whether human KIAA1018 acted similarly. Untreated cells contained a small number of foci of GFP-KIAA1018, FANCD2, and Replication Protein A (RPA, marker of long stretches of single-stranded DNA). Upon cisplatin (data not shown) and MMC treatment, the number of foci rose dramatically, and GFP-KIAA1018 colocalized in them with both FANCD2 (Figure 3K) and RPA (Figure 3L).

FANC Complex Signaling Is Unaffected in KIAA1018-Depleted Cells

Given that sensitivity to ICL-inducing agents is a hallmark of FA cells, and that KIAA1018 colocalizes to DNA-damage foci with FANCD2, we suspected that KIAA1018 might be linked to the FA pathway. We therefore asked whether KIAA1018 deficiency affects activation of the FA complex, which can be detected as monoubiquitylation of FANCD2 and FANCI (Garcia-Higuera et al., 2001; Smogorzewska et al., 2007). As shown in Figure 4A, treatment of HEK293 cells with MMC or hydroxyurea (HU) resulted in substantial FANCD2 ubiquitylation, but this process was unaffected by KIAA1018 knockdown. A similar phenomenon was observed in cells lacking FANCJ (Bridge et al., 2005). Thus, if KIAA1018 were linked to the FA pathway, it would—like FANCJ—act downstream of the FA complex.

Human Cells Lacking FANCD2, KIAA1018, or Both Proteins Display Similar Sensitivities to MMC

Given that GFP-KIAA1018 and FANCD2 colocalize to DNA-damage-induced foci, we asked whether KIAA1018 and FANCD2 were epistatic. We therefore knocked down KIAA1018 and FANCD2, either singly or together, in HEK293 cells (Figure 4B). As shown in Figure 4C, cells lacking both proteins were not appreciably more sensitive to MMC than cells lacking only one of these polypeptides. This suggests that KIAA1018 might be epistatic with the FA proteins, although a stable system is necessary to exclude the possibility of an incomplete knockdown in cells treated with both siRNAs.

The Zinc Finger of KIAA1018 Is Necessary and Sufficient for Targeting the Protein to Sites of DNA Damage

KIAA1018 possesses a UBZ motif close to its N terminus (Figures 1B and 1C). In other polypeptides, this motif has been shown to interact with ubiquitylated polypeptides (Hofmann, 2009). In order to characterize the function of the UBZ of KIAA1018, we expressed in *E. coli* glutathione S-transferase (GST) fused to KIAA1018 aa 1–124 containing either the WT UBZ or a variant in which the UBZ was disrupted by mutating cysteines 44 and 47 to alanines (Figure 1C). As zinc finger domains are also known to bind DNA, we tested these peptides in a mobility shift assay, using a homoduplex 38-mer oligonucleotide. We found no

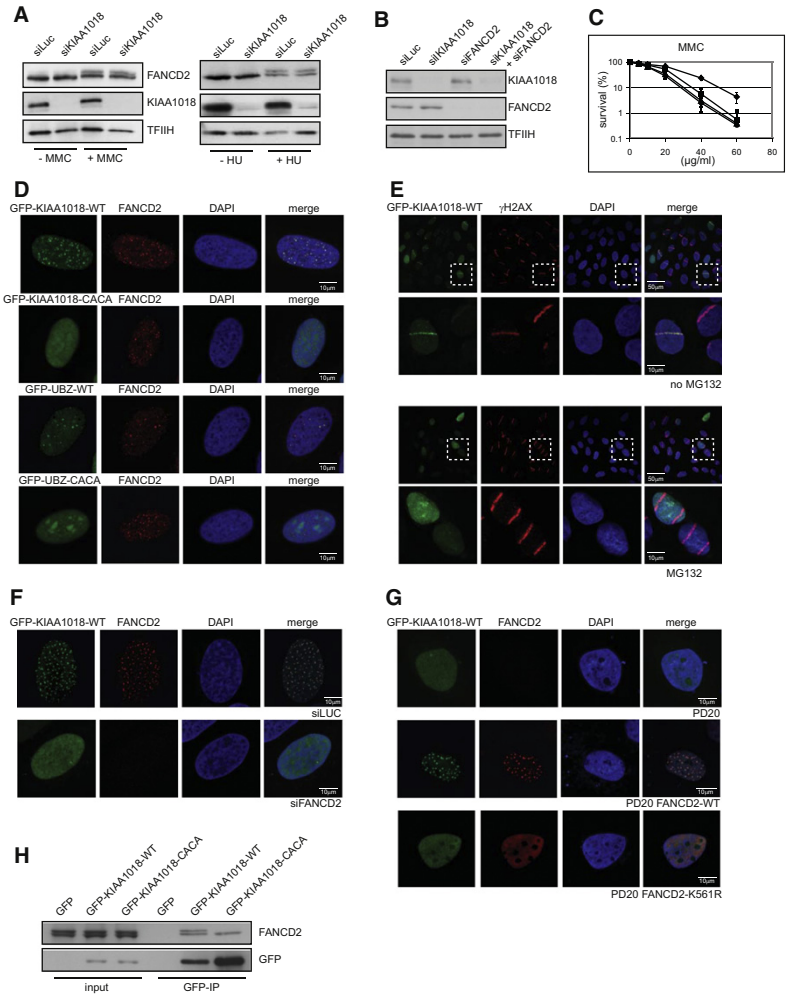

Figure 4. KIAA1018 Localization to MMC-Induced Foci Requires Ubiquitylation and FANCD2

(A) Western blot of extracts of HEK293 cells treated or mock-treated with MMC (20 hr) or HU (16 hr) 40 hr after transfection with the indicated siRNAs. The treatments resulted in substantial monoubiquitylation of FANCD2 in both experiments, which shows that KIAA1018 acts downstream (or independently) of the FA complex. TFIIH served as loading control.

(B) Western blot showing KIAA1018 and FANCD2 levels in HEK293 cells 40 hr after treatment with the respective siRNAs. siLuc served as negative control and TFIIH as loading control.

(C) siRNA-mediated knockdown of KIAA1018 or FANCD2 sensitized cells to MMC to a similar extent as a knockdown of both proteins. The results of three independent experiments are shown, each carried out in triplicate. Each data point represents an average ± SD. Key: (◆) siLuc; (■) siKIAA1018; (▲) siFAND2; (●) siKIAA1018 + siFANCD2.

(D) U2OS cells stably expressing GFP-tagged full-length KIAA1018-WT (top row), full-length zinc finger CACA variant (second row), the N-terminal 124 amino acids of WT KIAA1018 containing the zinc finger (third row), or the corresponding CACA zinc finger fragment (bottom row) were treated with 120 ng/ml MMC for 16 hr before immunostaining with FANCD2 antibody. GFP foci are only detectable in cells transfected with vectors expressing KIAA1018 variants with an intact UBZ domain.

(E) U2OS cells stably expressing GFP-KIAA1018-WT were laser microirradiated and immunostained 2 hr later with an antibody against γ-H2AX. Where indicated, cells were incubated with 20 mM MG132 for 120 min before irradiation. GFP-KIAA1018 fails to be recruited to damage stripes in the absence of ubiquitylation.

(F) U2OS cells stably expressing GFP-KIAA1018-WT were treated with luciferase or FANCD2 siRNAs for 48 hr. Treatment with 120 ng/ml MMC for 16 hr was followed by immunostaining with anti-FANCD2 antibody. GFP-KIAA1018 is not recruited to damage foci in the absence of FANCD2.

(G) PD20 (FA-D2) fibroblasts (top row), PD20 fibroblasts stably expressing FANCD2-WT (middle row), or FANCD2-K561R mutant (bottom row) were transiently transfected with GFP-KIAA1018-WT, treated with 120 ng/ml MMC for 16 hr, and immunostained with anti-FANCD2 antibody. GFP-KIAA1018 only localizes to damage foci in cells expressing the WT FANCD2 protein.

(H) Extracts of HEK293 cells stably expressing GFP-KIAA1018-WT or GFP-KIAA1018-CACA and treated with 120 ng/ml MMC were incubated with anti-GFP antibody and the immunoprecipitate was analyzed with antibodies against GFP or FANCD2. GFP-KIAA1018 interacts preferentially with the monoubiqyitylated form of FANCD2.

See Figure S2 for quantifications.

evidence of the GST-fusions interacting with DNA in this assay, even though the mismatch binding factor MutSα bound to the homoduplex (a poor substrate for this protein) under identical conditions (Figure S2A).

We then studied the MMC response of the GFP-KIAA1018 WT and CACA variants stably expressed in U2OS cells. We generated two additional cell lines expressing solely the N-terminal 124 aa residues encoding either the WT or the mutant UBZ. Expression of these variants in U2OS cells, followed by treatment with MMC, resulted in the formation of foci in cells expressing WT GFP-KIAA1018 and the 124 aa UBZ only. These foci colocalized with those formed by FANCD2. In contrast, both KIAA1018-CACA variants diffused throughout the nucleus and failed to form foci upon MMC treatment, even though FANCD2 foci formed normally (Figure 4D and Figure S2B). siRNA-mediated knockdown of endogenous KIAA1018 in cells expressing the KIAA1018 GFP-UBZ fragment did not alter the targeting to the MMC-induced foci, thus excluding the possibility that GFP-UBZ localizes to the damage sites via association with the endogenous protein (data not shown). This

suggested that the UBZ is necessary and sufficient to target GFP-KIAA1018 to DNA-damage foci generated by MMC treatment.

Recruitment of KIAA1018 to DNA-Damage Foci Is Dependent on FANCD2 Ubiquitylation

We wanted to know whether KIAA1018 targeting to MMC-induced foci was dependent on ubiquitylation, similarly to that described for FANCD2 (Garcia-Higuera et al., 2001). To this end, we pretreated the U2OS cells stably expressing GFP-KIAA1018 with MG132, an inhibitor of the 26S proteasome, which also causes sequestration of ubiquitin in the cytoplasm (Dantuma et al., 2006). We then generated DNA damage by a UV microlaser, which induces a variety of DNA lesions concentrated in micron-thin stripes and causes a substantial perturbation of chromatin structure, which brings about rapid recruitment of the phosphorylated form of the histone variant γ-H2AX. As shown in Figure 4E and Figure S2C, GFP-KIAA1018 and γ-H2AX colocalized in the laser stripes, but the KIAA1018 signal remained diffuse in MG132 pretreated cells. This indicated that KIAA1018 recruitment to DNA damage in chromatin required nuclear ubiquitin.

In the above experiments, we showed that MMC treatment of U2OS cells stably expressing GFP-KIAA1018 induced the formation of KIAA1018 foci (Figures 3K and 3L), that FANCD2 colocalized with GFP-KIAA1018 to these foci (Figure 3K), and that KIAA1018 was recruited to laser-induced stripes in a ubiquitin-dependent manner (Figure 4E). As no KIAA1018 foci were formed in cells in which *FANCD2* mRNA was knocked down with either one of two different siRNAs (Figures 4B and 4F, Figure S2D, and data not shown), we concluded that KIAA1018 recruitment to DNA-damage foci required ubiquitin and FANCD2.

This hypothesis could be further substantiated in the *FANCD2*-mutated cell line PD20, which displayed no MMC-induced foci of GFP-KIAA1018 (Figure 4G, top row; see also Figure S2E). The phenotype of this cell line could be rescued by expression of *FANCD2* cDNA; in the latter cell line, FANCD2 and GFP-KIAA1018 colocalized to MMC-induced foci (Figure 4G, middle row; Figure S2E). In contrast, when the cells were stably transfected with a FANCD2 K561R variant that cannot be ubiquitylated (Garcia-Higuera et al., 2001), both proteins failed to form foci upon MMC treatment (Figure 4G, bottom row; Figure S2E).

The above evidence strongly suggested that KIAA1018 is recruited to MMC-induced foci by monoubiquitylated FANCD2, likely in complex with FANCI. We therefore asked whether KIAA1018 and FANCD2 interact directly. Using anti-GFP antibodies, we immunoprecipitated the GFP-KIAA1018 fusion protein, or its CACA UBZ variant, from extracts of stably transfected, MMC-treated HEK293 cells, and probed the immunoprecipitates for the presence of FANCD2. As shown in Figure 4H, the GFP antibodies pulled down WT GFP-KIAA1018 and both the unmodified and the monoubiquitylated forms of FANCD2. Notably, only the unmodified form was present in the GFP-KIAA1018-CACA pull-down, which shows that KIAA1018 interacts specifically with the monoubiquitylated form of FANCD2 via its UBZ domain.

KIAA1018 Is a Nuclease

As bioinformatic analysis of the *KIAA1018* ORF predicted the protein to be an endonuclease (Kinch et al., 2005; Kosinski et al., 2005), and given that the protein appears to protect cells against ICL-generating substances, we asked whether the protein is indeed a nuclease.

We expressed full-length KIAA1018 in *E. coli* fused to an N-terminal Nus-His-tag (Ermolova et al., 2003) to aid solubility and purified the fusion protein to apparent homogeneity (Figures S3A and S3B). To test for nucleolytic activity, we deployed a nonspecific endonuclease assay (Kadyrov et al., 2007). Incubation of supercoiled plasmid DNA with increasing amounts of the Nus-His-KIAA1018 fusion protein in the presence of manganese and 100 mM KCl gave rise first to open circular, then linear forms (Figure 5A, Figure S3C), showing that KIAA1018 cleaved the substrate endonucleolytically. At the highest concentrations, the linearized DNA was degraded, which suggested that the enzyme is also an exonuclease. The UBZ-CACA variant was similarly active as the WT enzyme, but the two variants carrying mutations in the putative nuclease active site, D960A (DA) and K977A (KA), were severely impaired at equal protein concentrations (Figure 5A and Figures S3A–S3C). The loss of nuclease activity of the latter two variants was apparently not linked to incorrect folding or other structural perturbation, as the proteins were still able to bind DNA in a gel shift assay (Figure S3D).

Most metal-dependent nucleases can be inhibited either by chelating agents or by zinc or calcium. This is also true for KIAA1018, which could be effectively inhibited by EDTA or by zinc chloride (Figure 5B). The enzyme displayed optimal activity at pH 7.2–7.4 and 25 mM KCl in the presence of manganese. When magnesium was used, the endonucleolytic activity was somewhat reduced, but the degradation of DNA was restricted (Figure S3E). Under optimized conditions and when used in large excess, the KA variant possessed residual nuclease activity in the plasmid relaxation assay (Figure S3F). For this reason, we decided to use the WT and the DA variant in the search for specific substrates of KIAA1018.

KIAA1018 Preferentially Cleaves 5′ Flaps and Has Both Exo- and Endonuclease Activities

In the above experiments, to aid solubility we used bacterially expressed KIAA1018 carrying a 55 kDa Nus-His tag. In order to ensure that its activity was unaffected by the tag or by the lack of posttranslational modifications, we expressed KIAA1018 and its DA variant in the baculovirus system. An N-terminal maltose-binding protein (MBP) tag was used to express the protein, but this was removed during purification (Figures S4A and S4B). We tested the untagged enzyme on different oligonucleotide structures resembling intermediates of replication and recombination (Figure S4C). We used magnesium as the divalent ion because proteins of the PD-(D/E)XK nuclease superfamily are all magnesium dependent.

We first used substrates labeled at the 5′ end of the top strand (Figure S4C, f9) and could show that KIAA1018 cleaved them in the following order of preference: 5′ flap > > > splayed arm ≈ 3-way junction (3-WJ) > 3′ flap. The principal products were fragments between 31 and 35 nucleotides in length. As the flap was 30 nucleotides long, this indicated that the enzyme cleaved

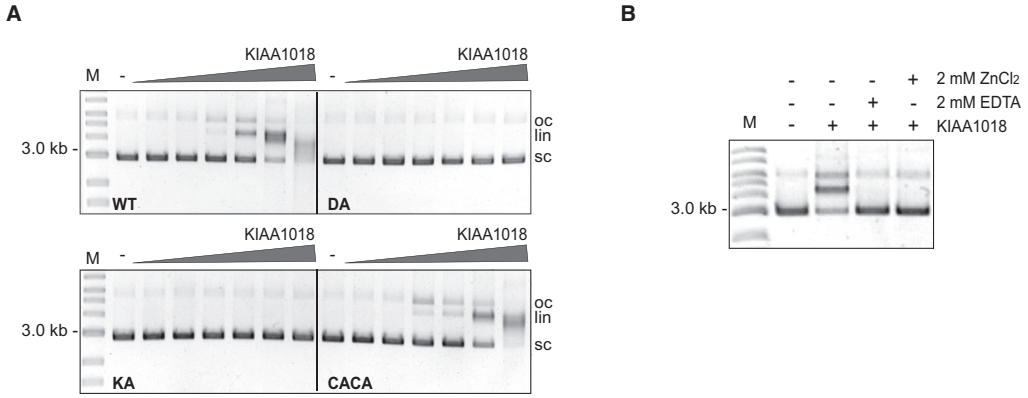

Figure 5. KIAA1018 Is a Nuclease

(A) Twenty fmoles of plasmid DNA were incubated with increasing amounts of bacterially expressed Nus-His-KIAA1018. The WT protein and the CACA mutant converted the supercoiled (sc) DNA first to open-circular (oc) and then to linear (lin) forms, whereas the DA and KA mutants did not. The figure is an image of an ethidium bromide-stained 0.8% agarose gel. M: 1 kb marker (NEB), WT: Nus-His-KIAA1018-WT; DA: Nus-His-KIAA1018 mutant D960A; KA: Nus-His-KIAA1018 mutant K977A; CACA: Nus-His-KIAA1018 mutant C44AC47A; (–) no protein.

(B) Inhibition of KIAA1018 endonuclease activity with 2 mM EDTA or 2 mM $ZnCl_2$. M: 1 kb marker, KIAA1018: WT. Assays were carried out in manganese buffer. See Figure S3 for supplemental information.

the substrates in double-stranded (ds) DNA, 1–5 nucleotides downstream from the junction (Figure 6A and Figure S4C, large arrow). In the reactions containing the 3-WJ, 3′ flap, and, to a small extent, also the splayed arm substrate, we also detected very fast-migrating species, which corresponded in length to 2–4 nucleotides. This suggested that KIAA1018 is also a 5′→3′ exonuclease, as already anticipated from the preliminary assays (Figure 5A). We could confirm this by labeling the same substrates at the 5′ end of the bottom strand (Figure 6A). In these assays, all substrates gave rise to a pentamer fragment. (The exonucleolytic cleavage products differed in length between the substrates labeled in the top or the bottom strands because the latter was one nucleotide longer. See Figure S4C.) This shows that KIAA1018 can generate 5′-recessed ends from blunt-ended substrates and that the enzyme makes the first incision ~4 nucleotides into the ds region on these substrates (Figure S4C, small arrows). Interestingly, although the exonuclease activity of KIAA1018 on ds termini was robust, the 5′ flap substrate was processed to yield predominantly the single-stranded (ss) 31- to 35-mer flap and only small amounts of the rapidly migrating species. This suggested that the enzyme did not degrade the cleaved-off ss flap with appreciable efficiency. We could confirm this by incubating the 5′ flap substrate with increasing amounts of enzyme. As shown in Figure 6B, the amount of free ss flap fragments increased with enzyme concentration, but only a minor increase in the high-mobility species was observed.

Next we labeled the substrates at the 3′ end. As shown in Figure 6C, the 5′ flap substrate gave rise to a series of bands ranging in length from approximately 10–29 nucleotides, which represent products of 5′→3′exonucleolytic degradation of the labeled strand after the flap was cleaved off (Figure 6F). Interestingly, while the 5′-labeled 3-WJ (f9 strand) was cleaved with very low efficiency (Figure 6A), the same substrate labeled at the 3′ end of the same (f9) strand appeared to be endonucleolytically cleaved and then exonucleolytically degraded with efficiency similar to the 5′ flap. By 3′-labeling the 30-mer (f7) of the 3-WJ, we could show that this oligomer was rapidly degraded, creating thus a 5′ flap substrate that was then efficiently processed by KIAA1018 (Figure 6D).

The bacterially expressed KIAA1018 used in comparable amounts (Figure S4B) behaved in these assays similarly in magnesium (data not shown) and in manganese (Figures S4D and S4E). However, although manganese increased KIAA1018′s enzymatic activity, it decreased its specificity.

That the cleaved-off 5′ flap (Figures 6A and 6B) was not further processed by the enzyme is supported by the fact that ssDNA was not appreciably bound by the enzyme in a gel shift assay, whereas linear dsDNA, 5′ flap and 3′ flap substrates were bound with similar efficiencies (Figure S4F).

In an attempt to study the substrate preference of KIAA1018 exonuclease, we incubated the enzyme with several different substrates. As shown in Figure 6E and Figure S4G, KIAA1018 exonuclease activity displayed a clear preference for dsDNA substrates containing a recessed 5′ end, a nick, or a gap. Blunt-ended DNA was processed less efficiently and the worst substrates were ssDNA and ss 5′ overhangs, as anticipated from the stability of the cleaved-off 5′ flap (Figure 6B).

To test whether the substrate specificity of KIAA1018 might be altered by an as-yet-unidentified interacting partner, we immunoprecipitated the enzyme from HEK293 cells stably expressing either FLAG-tagged KIAA1018 WT or the DA variant. The immunoprecipitate of the WT enzyme displayed the same substrate preference as the bacterially expressed and the Sf9-expressed proteins (Figures 6A and 6H, Figure S4D). However, it appeared to be more specific, giving rise to a single product upon incubation with the 5′ flap substrate (cf. product in Figure 6A). This change was not due to MLH1, as coexpression of KIAA1018

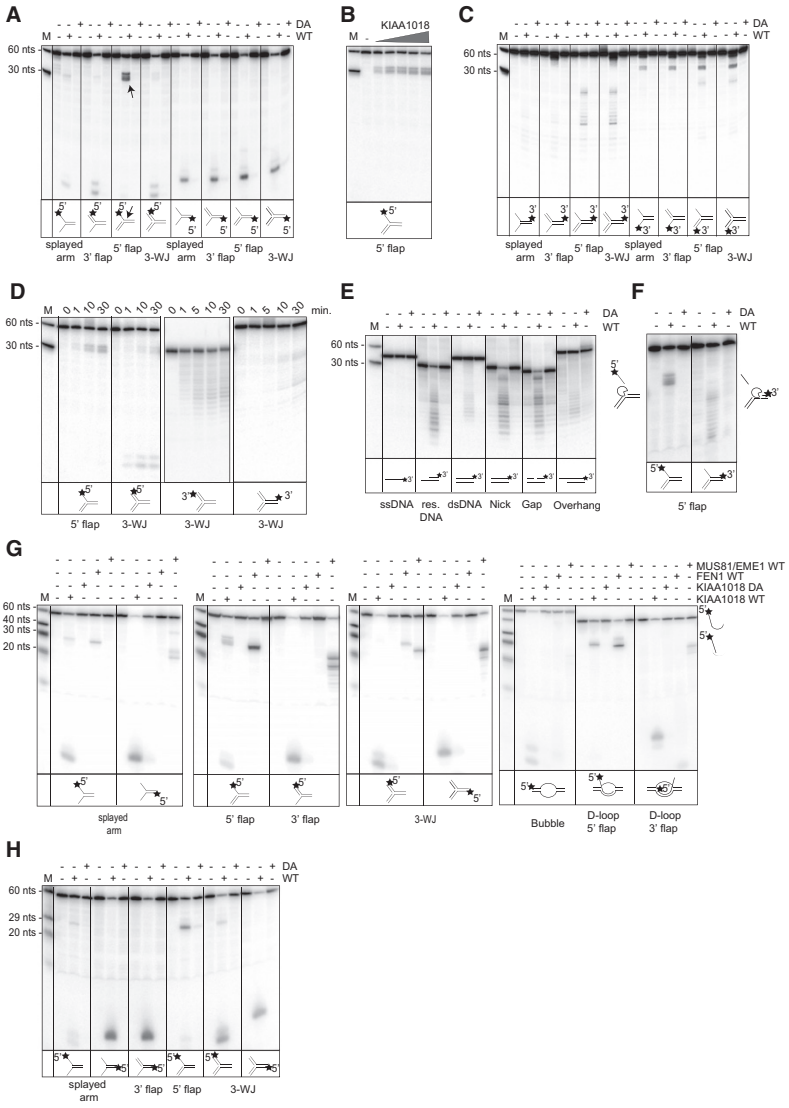

Figure 6. KIAA1018 Exhibits Preference for 5′ Flaps

(A) Sf9-expressed KIAA1018-WT and its DA variant were incubated with the indicated substrates (protein to DNA ratio 10:1). KIAA1018 exhibits a preference for 5′ flaps. Asterisk represents ^{32}P phosphate.

(B) Incubation of WT KIAA1018 (3- to 10-fold excess over DNA) with the 5′ flap substrate for 1 hr at 37°C. The ss product was resistant to KIAA1018 exonuclease.

(C) DNA substrates used in (A) were labeled at the 3′ end (see asterisks) to assess the exonuclease activity of KIAA1018 (10:1 ratio protein to DNA). Following endonucleolytic incision at the flap, KIAA1018 degraded the remaining ds region toward the 3′ terminus of the 5′ flap and 3-WJ (see below).

(D) Time course of KIAA1018 incubation with the indicated substrates (3:1 ratio protein to DNA). Whereas the 5′ flap was cut by KIAA1018 endonucleolytically, the 3-WJ lost its 5′ label due to KIAA1018 exonuclease activity. The 30-mer oligo of the 3-WJ is a good substrate for KIAA1018 exonuclease; its degradation gave rise to a 5′ flap substrate, which was then endonucleolytically cleaved by KIAA1018 (cf. panel A and Figure S4D). Labeling of the 3′ end of the 3-WJ showed also weak 5′→3′ degradation of the top strand.

(E) KIAA1018 exonuclease preferentially degrades dsDNA. Highest activity was observed on recessed, nicked, or gapped DNA substrates (10:1 ratio protein to DNA), whereas ss DNA and 5′ overhangs were poor substrates for KIAA1018.

(F) KIAA1018 incises 5′ flaps and then degrades the remaining strand in a 5′→3′ direction (20:1 ratio protein to DNA). In this experiment, the 5′ flap substrate was labeled either at the 5′ or the 3′ end of the 60-mer oligonucleotide f9 (Figure S4C) as indicated. The structures of the products are shown at the side of the autoradiograph.

(G) Comparison of substrate preference of KIAA1018, FEN1, and MUS81/EME1 (20:1 ratio protein to DNA). FEN1 and KIAA1018 prefer 5′ flaps, whereas MUS81/EME1 prefers 3′ flaps. All proteins were expressed in Sf9 cells.

(H) FLAG-KIAA1018 immunoprecipitated from stably transfected HEK293 cells showed the same specificity as the bacterially and Sf9-expressed recombinant KIAA1018 protein but made a more defined cut at the DNA junction.

All assays shown in this figure were carried out in magnesium. Samples were separated on denaturing 20% polyacrylamide gels for 1 hr at 40V/cm. The radioactive species were visualized by PhosphoImager (Typhoon 9400). M, oligonucleotide markers; WT, KIAA1018-WT; DA, KIAA1018 variant D960A. 3-WJ, 3-way junction. See Figure S4 for supplemental information.

with MLH1 did not affect the outcome of the nuclease assays (data not shown). We are currently analyzing the interactome of KIAA1018 in search for possible partners of this nuclease.

The substrate spectrum of KIAA1018 resembles that of FEN1, which displays preference for 5′ flaps (Harrington and Lieber, 1994). However, unlike KIAA1018, FEN1 made only a single cut, at the end of the ss flap (Figure 6G). In contrast, MUS81/EME1 failed to cleave the 5′ flap substrate but showed a clear preference for 3′ flaps, as reported (Kaliraman et al., 2001). We also included two D loop structures and a bubble in these experiments, as intermediates of recombination, but also as structures that arise transiently during DNA replication and transcription, processes blocked by cisplatin and MMC. Interestingly, the 5′ flaps of the D loop proved to be processed by the KIAA1018 endonuclease activity with similar efficiency to the 5′ flap, whereas only the exonuclease acted on the bubble and the 3′ flap substrates (Figure 6G, right panel).

The DA variant was used in parallel with the WT enzyme in the above assays. As processing of the tested substrates was almost undetectable (Figure 6, Figure S4), we conclude that

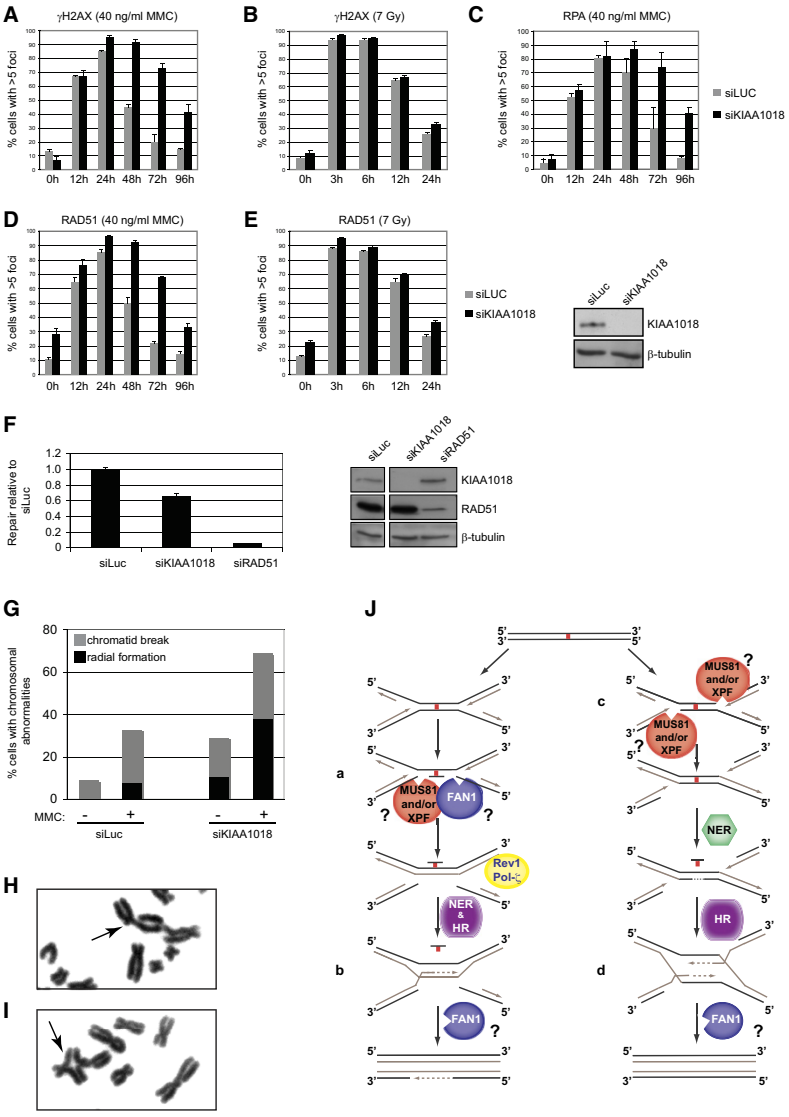

Figure 7. KIAA1018 Is Involved in HR

U2OS cells were treated with Luc or KIAA1018 siRNAs for 40 hr. Treatment with 40 ng/ml MMC (A, C, and D) or irradiation with 7 Gy (B and E) was followed by immunostaining with anti-γH2AX (A and B), anti-RPA (C), and anti-Rad51 (D and E) antibodies at the indicated time points after treatment. Graphs show % cells with more than five foci. In three independent experiments, 50 cells were counted per experiment. Each data point represents an average ± SD. Western blot showing efficiency of treatment with indicated siRNA for (A)–(E).

(F) Depletion of KIAA1018 results in a partial decrease of HR frequency compared to RAD51. HEK293 DR-GFP cells were transfected with siRNA against Luc (control), KIAA1018, and RAD51. Forty hours later, transfection with an I-SceI encoding plasmid or mock transfection were performed, followed by flow cytometric analysis 48 hr later. Approximately 1.1% of transfected cells pretreated with siRNA against Luc expressed GFP. Mock transfection did not result in GFP-positive cells. Graph represents the results of four independent experiments, each carried out in triplicate. Each data point represents an average ± SD.

(G–I) Depletion of KIAA1018 causes genomic instability. (G) Metaphase spreads of siLuc or si-KIAA1018 transfected HEK293 cells treated or not with 25 ng/ml MMC for 20 hr were analyzed for chromatid breaks (H) and radial structures (I). Fifty spreads were analyzed per sample.

(J) Scheme of possible involvement of KIAA1018/FAN1 in the processing of ICLs. See text for details.

both the exo- and the endonuclease activities are inherent to the same active site of KIAA1018, rather than to a contaminant in the purified fractions.

KIAA1018 Is Involved in the Repair of MMC-Induced Double-Strand Breaks

As shown in Figure 1A, processing of ICLs was suggested to involve endonucleolytic cleavage of the blocked replication forks by MUS81/EME1 and/or XPF/ERCC1. These one-ended double-strand breaks (DSBs) can be visualized directly by pulse-field gel electrophoresis (De Silva et al., 2000; Hanada et al., 2006), or indirectly as subnuclear foci of phosphorylated histone H2AX (γ-H2AX) (Niedernhofer et al., 2004; Rothfuss and Grompe, 2004). We wanted to test whether KIAA1018 depletion affected the formation and/or persistence of these DSBs. As shown in Figure 7A, 12 hr after MMC treatment, cells pretreated with KIAA1018 or control siRNAs contained ~6-fold more γ-H2AX foci than untreated controls. These foci reached a maximum at the 24 hr time point and then began to decline. This decline was substantially slower in cells depleted of KIAA1018, such that a considerable number of γ-H2AX foci were still present in the cells at the 96 hr time point. However, the KIAA1018-deficient cells do not appear to have a general defect in DSB repair, as treatment with IR induced similar numbers of γ-H2AX foci in cells pretreated with siRNA against KIAA1018 and Luc control (Figure 7B).

KIAA1018 Deficiency Does Not Affect DSB Resection but Causes Delay in the Disappearance of RPA Foci

Repair of DSBs is accomplished by one of two principal pathways: nonhomologous end-joining (NHEJ) and HR (West, 2003). DSBs arising through the processing of ICLs are thought to be addressed predominantly by HR, whereby one strand of the broken duplex has to be resected in a 5′→3′ direction to generate long stretches of ssDNA. Given that KIAA1018 has

robust exonuclease activity, we wanted to find out whether it might be required for resection. The ssDNA generated during resection is coated first by RPA, and this process can be visualized in the form of RPA foci. As shown in Figure 7C, we observed a substantial increase of RPA foci in MMC-treated cells, but these appeared with similar kinetics in cells pretreated with siRNA against KIAA1018 and Luc. KIAA1018 thus does not appear to be required for DSB resection. However, after 96 hr, the RPA focus number returned nearly to untreated control levels, whereas the siKIAA1018 pretreated cells still displayed numerous foci.

KIAA1018 Is Involved in HR

During HR, RAD51 displaces RPA on the ssDNA to generate filaments that invade homologous sequences on the sister chromatid (West, 2003). We analyzed the formation and disappearance of RAD51 foci in MMC-treated cells, pretreated with siRNA against KIAA1018 or Luc. We observed a 2- to 3-fold increase in RAD51 foci already in untreated cells, but this difference became less prominent in MMC-treated cells at the 12 and 24 hr time points, when the number of foci reached a maximum. However, at later time points, cells depleted of KIAA1018 contained more than twice as many RAD51 foci as the control (Figure 7D). This showed that KIAA1018 is not required for the early HR steps, but rather for their completion. As in the case of γ-H2AX foci (Figure 7B), no appreciable difference in the number of foci or the kinetics of their appearance and disappearance could be seen in the KIAA1018 and Luc siRNA pretreated cells upon irradiation (Figure 7E), which shows that the HR defect is limited to events induced by MMC.

In order to confirm this hypothesis, we deployed the reporter system described by Stark and colleagues (Bennardo et al., 2008), which monitors successful recombination events between two homologous DNA fragments integrated in the genome of HEK293 cells. Both these fragments encode defective *GFP* and one carries an engineered recognition site for the I-SceI endonuclease. Transfection of I-SceI cDNA into these cells leads to cleavage of one of the *GFP* copies. Cells in which the I-SceI-generated DSB is repaired by HR will express GFP. As shown in Figure 7F, HR was almost entirely abolished in cells pretreated with siRNA against RAD51, whereas siRNA against KIAA1018 reduced the efficiency of HR in this system by ~30%. This result confirms that KIAA1018 is involved in HR, but its role in the rescue of DSBs that did not arise as intermediates of ICL processing appears to be minor.

KIAA1018 Deficiency Brings about Genomic Instability

Taken together, the evidence presented above implicates KIAA1018 specifically in the processing of damage induced by ICL-generating agents, which is one of the hallmarks of cells from FA patients. The latter cells also display considerable chromosomal instability (Akkari et al., 2000). Given the phenotypic similarity of FA- and KIAA1018-deficient cells, the dependence of KIAA1018 on FANCD2, and the above DSB repair defect, we examined metaphase chromosome spreads in HEK293 cells depleted either of KIAA1018 or of FANCJ by siRNA. As reported by others (Bridge et al., 2005), we detected a notable increase in chromosomal instability in FANCJ-depleted cells, where several chromosomal aberrations were frequently seen in single cells (data not shown). In KIAA1018-depleted cells, the chromosomal instability increase was much less pronounced. However, we noted an increase in aberrations already in untreated cells, and MMC treatment induced a 2-fold higher number of aberrations in KIAA1018-depleted cells as compared to the control siRNA pretreated cell population. Importantly, the increase in radial chromosome formation was 5-fold higher than in the control (Figures 7G–7I). Depletion of KIAA1018 thus brings about chromosomal instability reminiscent of that seen in cells of FA patients.

DISCUSSION

As predicted by bioinformatic analysis (Kinch et al., 2005; Kosinski et al., 2005), KIAA1018 is indeed a nuclease with both endo- and exonuclease activities (Figure 5, Figure 6, Figure S3, and Figure S4). Due to its association with FANCD2, we propose to name it FAN1 (*F*ANCD2-*a*ssociated *n*uclease 1).

With its preference for 5′ flaps, FAN1 displays an opposite polarity to the two endonucleases implicated in ICL metabolism to date, MUS81/EME1 and XPF/ERCC1, both of which cleave preferentially 3′ flaps (Figure 6G and Ciccia et al., 2008). MUS81/EME1 is believed to initiate ICL repair by cleaving the leading-strand template of the blocked replication fork (Figure 1A, step c) and thus generate a one-ended DSB at the fork. The subsequent "unhooking" of the lesion (Figure 1A, step d) was proposed to involve XPF/ERCC1, but this is incongruent with its preference for 3′ flaps and is thus subject to some controversy (Ciccia et al., 2008). Recently, Walter and colleagues (Raschle et al., 2008) proposed an alternative mechanism of ICL repair, in which processing of the crosslink initiates only when replication forks traveling in opposite directions converge at the ICL (Figure 7J). In this scenario, FAN1 could work in concert with the 3′ flap-specific enzymes to unhook the ICL by cleaving the lagging-strand template (Figure 1A and Figure 7J, intermediate a) and thus help generate the substrate for the TLS polymerases Rev1 and pol-ζ (Raschle et al., 2008), which could later participate in the HR-mediated repair of the DSBs (Figure 7J, intermediate b). FAN1 might be involved also in the resolution of the HR intermediates. Although plausible, this mechanism has two caveats. First, the small size of the plasmid used made it likely that replication forks traveling in opposite directions would reach the ICL almost concurrently. This may not be the case in genomic DNA of higher eukaryotes, where replication origins are far apart. Moreover, ICLs activate a DNA-damage checkpoint that should prevent firing of late (or dormant) origins and thus reduce the chances of two forks colliding. The second caveat concerns the X-structure itself, inasmuch as MUS81/EME1 and/or XPF/ERCC1 could cleave both leading-strand templates of the X to generate two one-sided DSBs and a linear, but crosslinked, intermediate (Figure 7J, structure c). Both termini of this structure could be primer-extended to generate a substrate for excision repair. In this scenario, FAN1 would not be involved in the incision of the blocked fork, although it might participate in the repair of the two one-ended DSBs by HR (Figure 7J, intermediate d).

Data presented in Figure 7 support the involvement of FAN1 downstream from the replication fork cleavage. FAN1 deficiency

affected neither the formation of MMC-induced DSBs, as measured by the appearance of γ-H2AX foci (Figure 7A), nor their resection, as evidenced by RPA and RAD51 foci formation (Figures 7C and 7D respectively). However, it did affect DSB repair. Thus, even though the reduction in HR efficiency as measured by the GFP assay in HEK293 cells (Figure 7F) was only slight, the disappearance of RAD51 foci in vivo was substantially delayed (Figure 7D). Moreover, the chromosomal breaks and radials observed in FAN1-depleted MMC-treated cells strengthened the notion that FAN1 participates in HR and that, in its absence, MMC-induced lesions are processed erroneously, possibly by NHEJ, to give rise to the observed aberrations. Based on the above observations and coupled with evidence showing that repair of DSBs induced by IR was unaffected by FAN1 status, and that FAN1 depletion did not alter the sensitivity of cells to IR and camptothecin (Figures 2B and 2D), as well as methyl methane sulfonate (MMS) and HU (data not shown), we propose that FAN1 is required for the processing of recombination intermediates that arise predominantly during the metabolism of damage induced by ICL-generating agents. The elucidation of the molecular role of FAN1 will have to await the results of studies deploying a defined system, such as that described by the Walter laboratory (Raschle et al., 2008).

Our findings that the recruitment of FAN1 to MMC-induced foci is dependent on FANCD2 ubiquitylation, and that the two proteins appear to physically interact, represent strong evidence in support of an involvement of this nuclease in the FA-dependent pathway of ICL repair. It remains to be seen whether *FAN1* is a *FA* gene. To date, FA patients fall into 13 complementation groups that are linked to mutations in the *FANCA, B, C, D1, D2, E, F, G, I, J, L, M*, and *N* genes. However, several patients are yet to be assigned, and we are in the process of screening the DNA of these individuals for germline mutations in *FAN1*.

EXPERIMENTAL PROCEDURES

cDNA, vectors, antibodies, cell lines, protein purifications, and standard procedures are described in Extended Experimental Procedures.

Immunofluorescence Staining and Laser-Induced Damage

U2OS cells cultured on coverslips were mock-treated or treated with 120 ng/ml MMC and fixed 16 or 20 hr later with 3% formaldehyde/PBS for 15 min at 4°C. Membranes were permeabilized with 0.2% Triton X-100 in PBS for 5 min at 4°C. Samples were blocked with 3% nonfat milk/PBS and incubated with primary antibodies overnight at 4°C and with secondary antibodies for 1 hr at 37°C. DNA was stained with DAPI. Slides were analyzed using an Olympus IX81 or a Zeiss LSM710 confocal microscope (sequential scanning mode).

Ten micromoles of BrdU was added to the cells 24 hr prior to laser microirradiation. Laser stripes were induced with a laser beam (λ = 355 nm) at 50% power using the 40× objective. Cells were fixed 2 hr later.

siRNA Treatments and Cell Survival Assays

HEK293 cells were transfected with siRNAs in 6-well plates at 60% confluency using calcium phosphate. For survival assays, cells were seeded 24 hr after transfection in triplicates in 6-well plates at a density of 400 cells per well. Sixteen hours after seeding, the cells were treated with indicated concentrations of MMC, cisplatin, camptothecin, UV, or IR. Medium was replaced 24 hr (MMC and cisplatin), 1 hr (camptothecin), or directly (UV, IR) after treatment. After 8 days, the cells were fixed and stained with 0.5% crystal violet in 20% ethanol and colonies containing more than 50 cells were counted.

Specific Nuclease Assays

Endonuclease Assays

One nanomole of labeled substrate was incubated with 10 nmole (or as indicated) of KIAA1018 WT or its variants in 25 mM HEPES-KOH (pH 7.4), 25 mM KCl, 1 mM $MnCl_2$ or $MgCl_2$ as indicated, and 0.05 mg/ml BSA for 30 min at 37°C. The reaction was terminated with 0.1% SDS, 14 mM EDTA, and 0.1 mg/ml Proteinase K and incubation at 55°C for 15 min. Loading buffer was added and the samples were separated on a 20% denaturing polyacrylamide gel for 1 hr at 40 V/cm. The gels were dried and the bands were visualized on a PhosphoImager.

Exonuclease Assays

These were carried out as above, using the substrates indicated at the bottom of the panels in Figure 6E and Figure S4G.

Endonuclease Assays with FLAG-KIAA1018 Immunoprecipitate from HEK293 Cells

Stably transfected HEK293 cells expressing 3×FLAG-KIAA1018 were grown on 15 cm dishes with G418 to 80% confluency. The cells were pelleted by centrifugation, washed in PBS, and snap-frozen. The pellets were lysed (50 mM Tris-HCl pH 7.4, 150 mM NaCl, 1% Triton, protease inhibitors) and incubated on ice for 20 min. The lysate was centrifuged and incubated with mouse anti-FLAG M2-Agarose (Sigma) for 2 hr at 4°C on a rotating wheel (300 rpm). Subsequently, the beads were washed twice for 15 min with 500 μl wash buffer (50 mM Tris-HCl pH 7.4, 150 mM NaCl, and 1 μg/ml BSA), then twice for 15 min with 500 μl with elution buffer (62.5 mM HEPES-KOH pH 7.4, 62.5 mM KCl, 5% glycerol, and 1 mM DTT). FLAG-KIAA1018 was eluted with FLAG-peptides (150 ng/μl, Sigma) in a total volume of 70 μl for 30 min at 4°C on a shaker (600 rpm).

Homologous Recombination Assay

This was carried out essentially as described (Bennardo et al., 2008). Details can be found in the Extended Experimental Procedures.

SUPPLEMENTAL INFORMATION

Supplemental Information includes Extended Experimental Procedures and four figures and can be found with this article online at doi:10.1016/j.cell.2010.06.022.

ACKNOWLEDGMENTS

We express our gratitude to John Rouse for the KIAA1018 antibody and for sharing unpublished information, to Milica Enoiu for discussions and for critical reading of the manuscript, Stephanie Felscher for help with evaluation of chromosomal instability, Myriam Marti for help with western blot analyses, Ian Hickson for MUS81/EME1, Ulrich Hübscher for FEN1, Pavel Janscak and Rajakrishnan Kanagaraj for the oligonucleotides, Jordi Surralles for the FANCD2-deficient and WT- or K561R- complemented PD20 cells, Petr Cejka for the Sf9 expression system, and Stefano Ferrari for MG132. We also acknowledge collaborations with Johan de Winter and Hans Joenje and with the group of Shunichi Takeda. The *C01G5.8(tm423)* deletion allele was kindly provided by Dr. Shohei Mitani (Japanese National Bioresource Project). This work was supported by Swiss National Science Foundation grants nr. 3100A0-118158 (J.J.) and 3100A0-128675 (M.H.). The generous support of the Bonizzi-Theler (J.J.) and Ernst Hadorn (M.H.) Foundations is also gratefully acknowledged.

Received: March 3, 2010
Revised: May 29, 2010
Accepted: June 15, 2010
Published: July 8, 2010

REFERENCES

Akkari, Y.M., Bateman, R.L., Reifsteck, C.A., Olson, S.B., and Grompe, M. (2000). DNA replication is required To elicit cellular responses to psoralen-induced DNA interstrand cross-links. Mol. Cell. Biol. *20*, 8283–8289.

Bennardo, N., Cheng, A., Huang, N., and Stark, J.M. (2008). Alternative-NHEJ is a mechanistically distinct pathway of mammalian chromosome break repair. PLoS Genet. *4*, e1000110.

Bridge, W.L., Vandenberg, C.J., Franklin, R.J., and Hiom, K. (2005). The BRIP1 helicase functions independently of BRCA1 in the Fanconi anemia pathway for DNA crosslink repair. Nat. Genet. *37*, 953–957.

Cannavo, E., Gerrits, B., Marra, G., Schlapbach, R., and Jiricny, J. (2007). Characterization of the interactome of the human MutL homologues MLH1, PMS1, and PMS2. J. Biol. Chem. *282*, 2976–2986.

Ciccia, A., McDonald, N., and West, S.C. (2008). Structural and functional relationships of the XPF/MUS81 family of proteins. Annu. Rev. Biochem. *77*, 259–287.

Dantuma, N.P., Groothuis, T.A., Salomons, F.A., and Neefjes, J. (2006). A dynamic ubiquitin equilibrium couples proteasomal activity to chromatin remodeling. J. Cell Biol. *173*, 19–26.

De Silva, I.U., McHugh, P.J., Clingen, P.H., and Hartley, J.A. (2000). Defining the roles of nucleotide excision repair and recombination in the repair of DNA interstrand cross-links in mammalian cells. Mol. Cell. Biol. *20*, 7980–7990.

Ermolova, N.V., Ann Cushman, M., Taybi, T., Condon, S.A., Cushman, J.C., and Chollet, R. (2003). Expression, purification, and initial characterization of a recombinant form of plant PEP-carboxylase kinase from CAM-induced Mesembryanthemum crystallinum with enhanced solubility in Escherichia coli. Protein Expr. Purif. *29*, 123–131.

Garcia-Higuera, I., Taniguchi, T., Ganesan, S., Meyn, M.S., Timmers, C., Hejna, J., Grompe, M., and D'Andrea, A.D. (2001). Interaction of the Fanconi anemia proteins and BRCA1 in a common pathway. Mol. Cell *7*, 249–262.

Gari, K., Decaillet, C., Stasiak, A.Z., Stasiak, A., and Constantinou, A. (2008). The Fanconi anemia protein FANCM can promote branch migration of Holliday junctions and replication forks. Mol. Cell *29*, 141–148.

Hanada, K., Budzowska, M., Modesti, M., Maas, A., Wyman, C., Essers, J., and Kanaar, R. (2006). The structure-specific endonuclease Mus81-Eme1 promotes conversion of interstrand DNA crosslinks into double-strands breaks. EMBO J. *25*, 4921–4932.

Harrington, J.J., and Lieber, M.R. (1994). The characterization of a mammalian DNA structure-specific endonuclease. EMBO J. *13*, 1235–1246.

Hofmann, K. (2009). Ubiquitin-binding domains and their role in the DNA damage response. DNA Repair (Amst.) *8*, 544–556.

Kadyrov, F.A., Holmes, S.F., Arana, M.E., Lukianova, O.A., O'Donnell, M., Kunkel, T.A., and Modrich, P. (2007). Saccharomyces cerevisiae MutLalpha is a mismatch repair endonuclease. J. Biol. Chem. *282*, 37181–37190.

Kaliraman, V., Mullen, J.R., Fricke, W.M., Bastin-Shanower, S.A., and Brill, S.J. (2001). Functional overlap between Sgs1-Top3 and the Mms4-Mus81 endonuclease. Genes Dev. *15*, 2730–2740.

Kinch, L.N., Ginalski, K., Rychlewski, L., and Grishin, N.V. (2005). Identification of novel restriction endonuclease-like fold families among hypothetical proteins. Nucleic Acids Res. *33*, 3598–3605.

Kosinski, J., Feder, M., and Bujnicki, J.M. (2005). The PD-(D/E)XK superfamily revisited: identification of new members among proteins involved in DNA metabolism and functional predictions for domains of (hitherto) unknown function. BMC Bioinformatics *6*, 172.

Meetei, A.R., Sechi, S., Wallisch, M., Yang, D., Young, M.K., Joenje, H., Hoatlin, M.E., and Wang, W. (2003). A multiprotein nuclear complex connects Fanconi anemia and Bloom syndrome. Mol. Cell. Biol. *23*, 3417–3426.

Moldovan, G.L., and D'Andrea, A.D. (2009). How the fanconi anemia pathway guards the genome. Annu. Rev. Genet. *43*, 223–249.

Niedernhofer, L.J., Odijk, H., Budzowska, M., van Drunen, E., Maas, A., Theil, A.F., de Wit, J., Jaspers, N.G., Beverloo, H.B., Hoeijmakers, J.H., et al. (2004). The structure-specific endonuclease Ercc1-Xpf is required to resolve DNA interstrand cross-link-induced double-strand breaks. Mol. Cell. Biol. *24*, 5776–5787.

Peng, M., Litman, R., Xie, J., Sharma, S., Brosh, R.M., Jr., and Cantor, S.B. (2007). The FANCJ/MutLalpha interaction is required for correction of the cross-link response in FA-J cells. EMBO J. *26*, 3238–3249.

Pichierri, P., and Rosselli, F. (2004). The DNA crosslink-induced S-phase checkpoint depends on ATR-CHK1 and ATR-NBS1-FANCD2 pathways. EMBO J. *23*, 1178–1187.

Raschle, M., Knipscheer, P., Enoiu, M., Angelov, T., Sun, J., Griffith, J.D., Ellenberger, T.E., Scharer, O.D., and Walter, J.C. (2008). Mechanism of replication-coupled DNA interstrand crosslink repair. Cell *134*, 969–980.

Rothfuss, A., and Grompe, M. (2004). Repair kinetics of genomic interstrand DNA cross-links: evidence for DNA double-strand break-dependent activation of the Fanconi anemia/BRCA pathway. Mol. Cell. Biol. *24*, 123–134.

Smogorzewska, A., Matsuoka, S., Vinciguerra, P., McDonald, E.R., 3rd, Hurov, K.E., Luo, J., Ballif, B.A., Gygi, S.P., Hofmann, K., D'Andrea, A.D., et al. (2007). Identification of the FANCI protein, a monoubiquitinated FANCD2 paralog required for DNA repair. Cell *129*, 289–301.

Thompson, L.H., and Hinz, J.M. (2009). Cellular and molecular consequences of defective Fanconi anemia proteins in replication-coupled DNA repair: mechanistic insights. Mutat. Res. *668*, 54–72.

Wang, W. (2007). Emergence of a DNA-damage response network consisting of Fanconi anaemia and BRCA proteins. Nat. Rev. Genet. *8*, 735–748.

West, S.C. (2003). Molecular views of recombination proteins and their control. Nat. Rev. Mol. Cell Biol. *4*, 435–445.

Zhang, N., Lu, X., Zhang, X., Peterson, C.A., and Legerski, R.J. (2002). hMutSbeta is required for the recognition and uncoupling of psoralen interstrand cross-links in vitro. Mol. Cell. Biol. *22*, 2388–2397.